

CTV Non-linear Time-History Analyses

Athol J. Carr

**Professor Emeritus, Department of Civil and Natural Resources Engineering,
University of Canterbury**

1.0 Introduction

- 1 I have been engaged by the Royal Commission to undertake a review of the NLTHA modelling and then to facilitate discussions between the panel of experts.
- 2 This report summarises the review of the non-linear time history analyses (NLTHA) used for the CTV building undertaken for Royal Commission.
- 3 The reporting has been undertaken in two parts.
 - The first covers my own initial concerns regarding the modelling and analysis undertaken by Compusoft Ltd (Compusoft) for Clark Hyland.
 - The second part details the discussions between the panel of experts.(see Appendix A).
- 4 The panel of experts comprises:
 - Mr Ashley Smith (Structure Smith Ltd)
 - Mr Derek Bradley/ Dr Barry Davidson/ Mr Tony Stuart. (Compusoft)
 - Professor Emeritus Athol Carr (University of Canterbury)
 - Professor John Mander (Texas A & M University)
 - Professor Robin Shepherd
 - Dr Brendon Bradley (University of Canterbury)
 - Dr Graeme McVerry (GNS Science).

2.0 Initial Concerns with the NLTH Modelling and Analysis

- 5 Clarke Hyland¹ and Compusoft Ltd² prepared reports (herein referred to as the Hyland report and Compusoft report, respectively) detailing the analyses carried out on the CTV building as part of the Department of Building and Housing (DBH) investigation of the building collapse. Following reviews of these reports I identified a number of concerns as to the reliability of the NLTHA results.
- 6 My concerns are listed in the following sections. The Compusoft responses are shown in *italics*.

2.1 Modelling details

- 7 Finite elements were used by Compusoft to model the walls and floors of the CTV building. The accuracy of finite element solutions is dependent on the capabilities of the finite elements used in the model and the refinement of the element mesh.
- 8 The reports indicated that non-linear shell elements were used for the walls of the North Tower and the South wall of the building. No mesh details were provided, particularly for the North tower. The tower would be subject to large overturning moments, torques and shear forces. The overturning moments could also result in large tensile forces which may be further increased by the large vertical accelerations associated with the February 22nd 2011 earthquakes. If details of the mesh of the finite elements were provided, the reader would gain a better idea of the achievable accuracy of the model.
- 9 Compusoft responded with the following statement.
- 10 *For the NLTHA analyses for the DBH, the modelling philosophy undertaken was targeted at realistically representing the overall building performance so that multiple failure hypotheses could be investigated. For this reason it was decided that more useful information could be obtained by investigating trends in the building behaviour rather than having the analysis terminate at the first structural instability.*
- 11 *The model for the walls used a laminated shell element where the reinforcement were modelled as layers of steel surrounded by layers of concrete and the appropriate stress-strain models were used for both the steel and concrete.*
- 12 Compusoft also supplied screen-captured images of the meshes used for the walls and floors to all members of the Panel of Experts. The meshes appear to be sufficiently refined to give reasonable modelling of both walls and floors (see Appendix B of this report).
- 13 The finite element mesh data supplied also has eased the concerns about accuracy of the finite element models. The modelling of the walls on the South side are sufficiently described in the Compusoft report as are the details of the coupling beams between the two walls.

¹ Hyland, CTV Building Collapse, Report prepared for the Department of Building and Housing, 25th January 2012,

² Compusoft Engineering, CTV Building Non-Linear Seismic Analysis Report, February 2012

2.2. Time step

- 14 The Compusoft report did not make any statements about the time-step used in their analyses. The time-step is very important as if the step is too large the analyses may not be able to represent the high frequency response characteristics of the building. This may also be important as many of the vertical modes of vibration in the structure have relatively high frequencies and the high frequency effects are also significant when localised inelastic deformations occur.
- 15 Information should have been provided so that readers could have confidence in the results.
16. *Compusoft responded stating that the time-step is varied automatically in the SAP2000 analyses and I am assured that the time-step reduced to extremely small sizes when required to maintain accuracy of the analyses.*

2.3. Column yield interaction surfaces

- 17 The Hyland report refers to the very high vertical accelerations experienced in the February 22nd 2011 earthquake in their discussion on the behaviour of the columns in the building. The report also notes that the columns were subjected to high compression forces under gravity load conditions, and that they had poor confinement in the likely plastic hinge locations.
- 18 The Compusoft modelling of the columns ignored the effects of varying axial forces in the yield conditions in the column plastic hinges. They only considered a Bending Moment – Bending Moment (M-M) interaction and not the normal column Axial Force - Bending Moment – Bending Moment (P-M-M) interaction. This simplification may not give a true representation if there are significant variations in the column axial forces.
- 19 In general, for structures of the type such as the CTV building, where the floors are relatively flexible and the lateral loads are taken by the walls, the variations in the axial forces due to the lateral shaking would not be significant. In most time-history analyses the vertical accelerations are not taken into account and the axial forces would therefore only vary due to overturning effects in the structure. If the frame was not very tall then these overturning effects would be small. However, in this case, the vertical accelerations are large and these simplifications are not appropriate.
- 20 Compusoft responded with the following statement.
- 21 *It was accepted at early stage that the lateral performance of the building would be dominated by the performance of the walls. Consequently the analyses were set up so that the columns or hinges did not fail or drop load as their rotations would be governed by the wall displacements. Furthermore, on the basis of the overall analysis philosophy columns were not permitted to fail axially. This way information would be available to investigate variations on the original analysis parameters such as concrete strength/strain. As M-M hinges adequately represent the total stiffness of the structure, and are suitable for obtaining the global building response we believe*

that they are suitable for the determination trends in building behaviour. Calculated building drifts will not be significantly affected by inclusion of axial interaction. The use of M-M hinges made the interrogation of the model easier and reduced computation time.

2.4 Beam-column joints

- 22 The structural drawings of the CTV building show no shear or confining steel in the beam-column joints.
- 23 The CompuSoft computational model assumed that the beams and columns intersected at the centre of the joint. The flexibility of the beams and columns continued to the joint intersection point allowing some deformation within the joint. The joints themselves were, in effect, infinitely strong and which meant that the model is not able to represent inelastic behaviour in, or failure of, the beam-column joints.
- 24 Due to the detailing of the joints, inelastic behaviour is to be expected within the joint regions. It is possible that the joints are the weakest parts of the beams and columns. The computation challenge is that there are not a great number of computational models for modelling in-elastic behaviour in joints, particularly for three dimensions beam-column joints.
- 25 Some consideration of the inelastic behaviour of the joints should have been allowed for in the analyses.
- 26 CompuSoft responded with the following statement.
- 27 *We wish to emphasise that the frame elements that form the beam column joint zones were not modelled as being fully rigid. They were modelled however to behave elastically and did not capture panel distortion, although they did accommodate the elastic stiffness of the frames over half the joint zone.*
- 28 *With regard to the modelling of the inelastic behaviour of beam column joints we note that in the research community, there is considerable uncertainty over the performance of beam column joints - particularly for the detailing exhibited in the joints of the CTV building. In addition, there is no routine modelling techniques that adequately captures the performance of 3-D interacting beam column joints, particularly those that are potentially subject to multiple failure types such as the CTV joints. The benefits of including beam-joint strength and stiffness degradation would be:*
- More accurately assessing building displacements and drifts.*
- Accurately assessing local member effects such as column hinging and potential joint failure*
- 29 *With regard to the assessment of displacements, it was evident from the pushover analyses that the response of the CTV building was governed by the walls, with the frames contributing as little as 10% to the overall seismic resistance of the structure. Consequently any stiffness degradation in the joints would have little effect on drifts.*

- 30 *Given the uncertainty over the performance and the difficulties in accurately modelling the performance of the joints, we believed it prudent to assess the joints via post processing. It should be noted that the given the uncertainties discussed, certainty cannot be obtained over the joint performance. Multiple sensitivity analyses, using various modelling approaches would improve understanding of the joint behaviour, however without physical testing the actual performance will remain unknown.*
- 31 *With regard to the assessment of displacements, it was evident from the pushover analyses that the response of the CTV building was governed by the walls, with the frames contributing as little as 10% to the overall seismic resistance of the structure. Consequently any stiffness degradation in the joints would have little effect on drifts.*
- 32 *Given the uncertainty over the performance and the difficulties in accurately modelling the performance of the joints, we believed it prudent to assess the joints via post processing. It should be noted that the given the uncertainties discussed, certainty cannot be obtained over the joint performance. Multiple sensitivity analyses, using various modelling approaches would improve understanding of the joint behaviour, however without physical testing the actual performance will remain unknown.*

2.5 Masonry infill walls

- 33 The witness evidence indicates possible contact between columns and walls; however the structural drawings show a required gap.
- 34 The modelling undertaken by both Hyland and Compusoft of the masonry infill walls in the lower floors on the Western side of the building assumed them to be either fully built-in with ample strength or fully separated from the columns so that there was no interaction between the columns and the infill walls. There were no intermediate computational models for the situation where the walls interact with the frame if the inter-storey deflections exceed the design clearances or construction clearance. In this situation, the walls will affect the behaviour of the frame and may fail in-plane if the imposed forces on the wall exceed its capacity.
- 35 A more realistic model could allow for some gap and gap filling material. The problem will be to determine what is an appropriate clearance and the stiffness of the gap-filling material. This could result in a large number of analysis permutations and even then the most appropriate solution may not be realistic. There will however be no way of knowing which permutation of such a model is the correct one.
- 36 Compusoft responded with the following statement.
- 37 *Given the uncertainty on construction and performance, the approach used was one that would effectively bound the effect that the masonry walls have on the response and performance of the structure.*

2.6 Floor diaphragm connections to tower

- 38 Both the Hyland and Compusoft reports provide little detail regarding the strength connections between the tower and floors apart from that of the drag bars. The report states that the connection for the remainder of the floors is a compression only connection. Was there no connection initially, the failure of an existing connection will give different force distribution than that which will be seen if there is assumed to be no tension capable connection to start with but that fails part way through the analysis.
- 39 The Compusoft model assumed that the connections of the floors to the Tower were such that the drag bar connection was continuous with time. In their analysis the forces in the drag-bars were checked to see if the strength was exceeded by post-processing the results. In their report Compusoft claimed that if the drag bars failed then the analysis failed, and therefore this scenario was in effect not modelled.
- 40 Some analyses should be undertaken to allow the drags bars to fail and try to capture the analysis results in the fractions of a second following the failure of these drag bars. This would help in trying to identify the possible sequence of failure. Maintaining the fixed floor connection may mask other non-linear effects in the structure. If there is no vertical shear connection assumed from the floors to the tower then the vertical loads from the floors are transferred to the columns in gridline 3 (see Figure 3, Hyland report).
- 41 Compusoft responded with the following statements.
- 42 *In the NLTH analysis the failure of the drag bars was explicitly modelled (refer page 21 and 22 of the CTV Building Non-linear seismic analysis report). No post processing was undertaken with regard to the drag bars, and disconnection can be seen in diaphragm actions presented in Figures E13, F12 & 13, G12 & 13, etc.... of our report.*
- 43 *The diaphragms to the toilet area of the north core were modelled as elastic shell elements. This was undertaken as there is considerable uncertainty over the capacity of the floor slab in this area (primarily concerning the contribution of the metal decking to strength and stiffness). In addition, there are many different possible failure planes and mechanisms which would add considerable complexity and would be difficult to model accurately. To adequately assess the performance of the floor slab connection would have required multiple sensitivity analyses, and there would still have been uncertainty on the results. Failure of this section of diaphragm would have lead to uncontrolled drifts and ultimately failure of the frames, so a decision was made to model this section of diaphragm using linear elements with results reported that were suitable for assessment by others. Using this approach the results July 2012 would be available for those investigating the collapse to assess multiple failure planes at each time step in the analysis.*
- 44 *Vertical connection between the drag bars and the north core walls will not have much effect on results as the gravity load transferred will be dependant on the flexibility of the cantilevered section of floor slab, which is considerably more flexible*

than the main beam lines. As the tributary width of floor slab that could be supported by the walls is small the effect on the analysis results will be negligible.

2.7 Damping model

2.7.1 General damping representation

- 45 Damping in most NLTH analyses is a problem. There is no accepted engineering understanding of the mechanism of damping in structures and hence no well defined manner of representing the damping in the analyses.
- 46 If a structure is set in motion then the amplitude of the motion decays with time. This decay phenomenon, referred to as damping, is usually represented by damping models, such as that proposed by Rayleigh³. The usual assumption is viscous damping as this is mathematically convenient. Most design codes assume that the level of damping in building structures is taken as being 5% of critical viscous damping. The approach used for most of the time history analyses conducted in the past 50 years is based on the assumption that the magnitudes of the damping forces are small. If the behaviour of a simple structure is considered with 5% critical viscous damping, the damping forces are about 10% of the inertial and elastic forces in the structure. It is generally assumed that if the damping model in the analysis is not correct, this does not have a great effect on the analysis answers.
- 47 SAP2000 (as used by CompuSoft), along with most other programs used for non-linear time-history structural analyses, uses the Rayleigh damping model.

2.7.2 Rayleigh damping model

- 48 The Rayleigh damping model is convenient as it uses the mass and stiffness properties of the structure which are already available within the analysis. The damping matrix [C] is taken as a proportion of the mass and stiffness matrices [M] and [K] respectively

$$[C] = \alpha[M] + \beta[K]$$

where α and β are chosen to give the required percentage of critical viscous damping at two specified and different frequencies.

- 49 The typical variation of damping with frequency is shown in Figure 1. There are two asymptotes, the one at the damping axis where the frequency tends to zero and the other asymptote increases linearly with frequency. It is this second asymptote that is associated with very high damping in the high modes. These modes are associated with localized deformation modes in the structure and these are activated when inelastic deformations occur in the structure.
- 50 Research by Crisp at the University of Canterbury in 1979⁴ showed the serious inaccuracies inherent in the Rayleigh damping model. It was found that the damping

³ Rayleigh, Lord (1877), *Theory of Sound (two volumes)*, Dover Publications, New York, reissued 1945, second edition.

⁴ Crisp, D.J. (1980) *Damping Models for Inelastic Structures*. Master of Engineering Report, Department of Civil Engineering, University of Canterbury, 1980

actions (forces and moments) in the structure could be greater than the actions in the structural members, having a disproportionate effect on the results of the analysis.

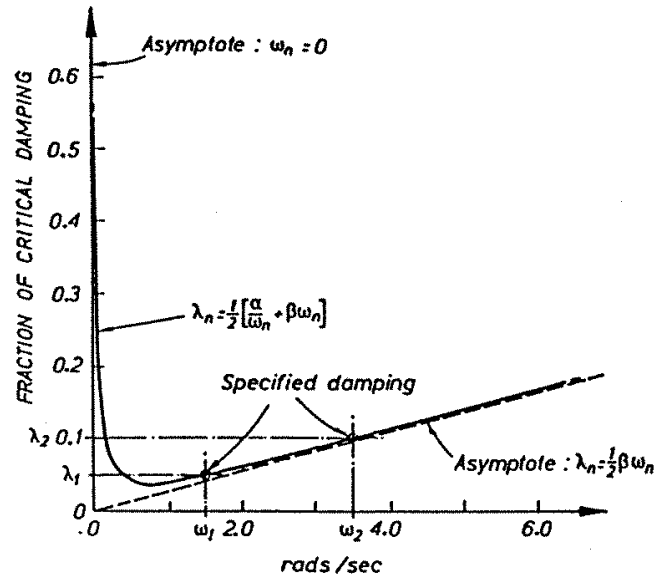


Figure 1. Rayleigh Damping Model

- 51 It was found that these unrealistically high damping actions were of short duration and only occurred when inelastic deformations were starting or ending. Crisp showed that as the damping in the high modes was reduced the damping actions reduced. When the damping in the high modes was reduced to the same 5% as was used in the lower modes the damping forces reduced to a similar magnitude to those seen in an elastic structure.

2.7.3 Alternative damping models

- 52 Many users of the inelastic time history analysis program Ruaumoko⁵ have attempted to avoid using the Rayleigh damping model. Where users still wish to use the Rayleigh damping model it is suggested that great care be used in selecting the frequencies where the damping is specified. This program has the ability to use new damping models^{6,7,8} to assign the same damping ratio, say 5%, across all frequencies of free-vibration.
- 53 As an example, the responses of a 12 storey reinforced concrete frame using different damping models is shown in Figure 2. The modeller using Ruaumoko has a

⁵ Carr, Athol J. (1981) *Ruaumoko*, User manuals. Department of Civil Engineering, University of Canterbury: 1981,-2012. See www.ruaumoko.co.nz

⁶ Wilson, E.L. and Penzien, J. (1972) Evaluation of Orthogonal Damping Matrices, *Int. J. Numerical Methods in Engg.*, Vol. 4, 1972, pp 5–10.

⁷ Carr, A.J. (1997) Damping Models for Inelastic Analyses. *Proc. Asia-Pacific Vibration Conference '97*, Kyongju, Korea, Nov. 1997: 42–8.

⁸ Carr, Athol J. (2005) Damping Models for Time-history Structural Analyses. *Proc. 11th Asia-Pacific Vibration Conference APVC-05*, Langkawi, Malaysia, November 25-27 2005. pp287-293.

choice of using either the initial elastic stiffness or the time-varying tangent stiffness. The damping matrix may be used as either a tangent damping matrix or a secant damping matrix. The tangent matrix provides the changes in the damping actions as a function of the changes in velocity within each time-step whereas the secant matrix

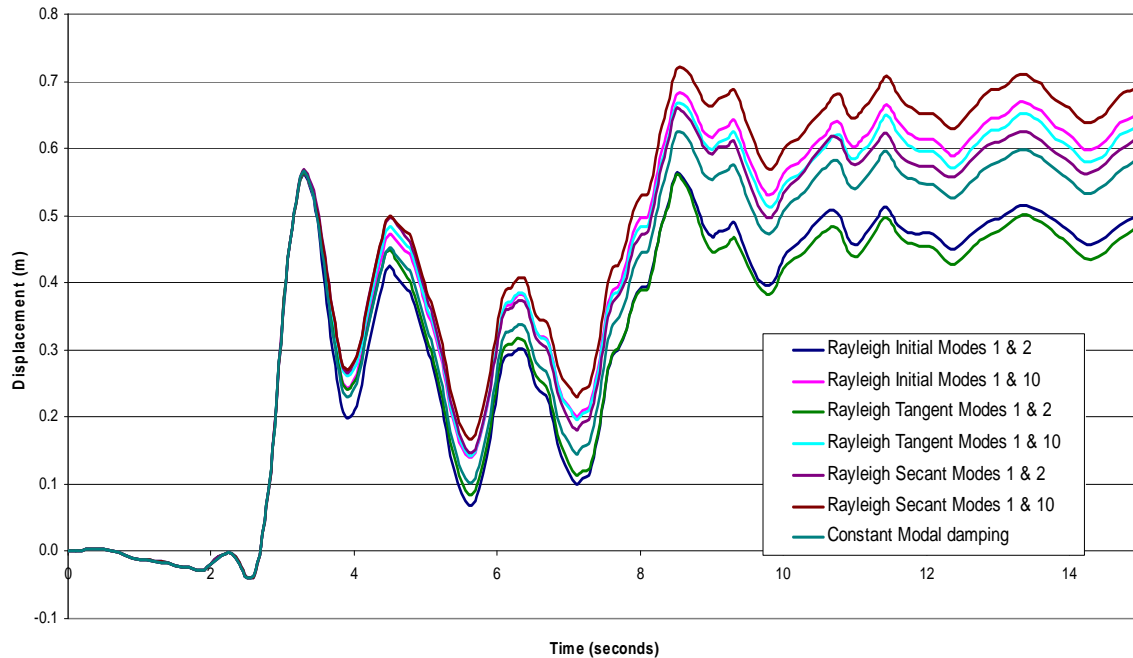


Figure 2 Effects of Varying Damping Models – Which Solution Do We Want?

gives the damping actions as a function of the velocities. The results are shown for several different versions of the Rayleigh damping model as well as that for the Wilson-Penzien uniform damping model.

2.7.4 Compusoft damping models

- 54 The damping models used for the CTV analyses have tried to get a realistic compromise within the limitations of the initial stiffness Rayleigh damping model. The damping was specified at natural periods of free-vibration of 1.29 seconds and 0.05 seconds respectively. These are effectively at mode 1 and somewhere about mode 90. The problem is that for all frequencies between mode 1 and mode 90 the amount of viscous damping is less than 5% of critical viscous damping and reduces to approximately 2% at the minimum point (see Figure 3). This reduction of the damping ratio could imply an increase of the displacement responses of those lowly damped modes of the structure by the order of 40%. For the lateral displacements of the towers this will be of minor concern as the first mode will dominate the lateral displacements. However, the effects of the lower damping will affect some of the localized vertical floor modes.

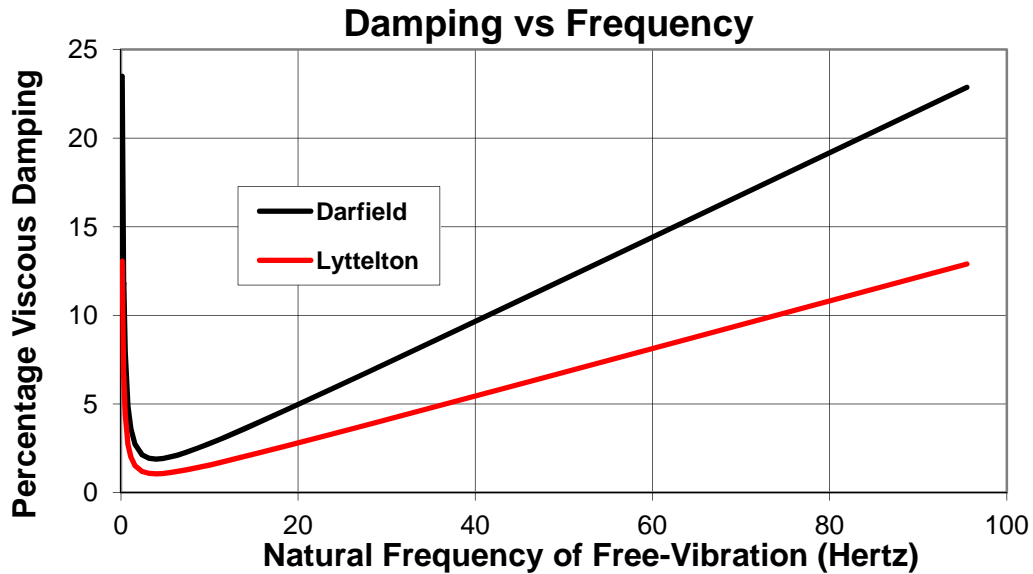


Figure 3 Damping versus Frequency (small frequency range)

- 55 Figure 4 shows that for the case where 5% critical viscous damping is specified for the analyses that all modes with frequencies greater than about 400Hz are supercritically damped (damping greater than 100%). This means that these modes do not vibrate. In my experience in 40 years of non-linear time-history analyses, that depending on the complexity or refinement of the computational model, most structures have their highest modes with frequencies of the order of 6000 Hz.

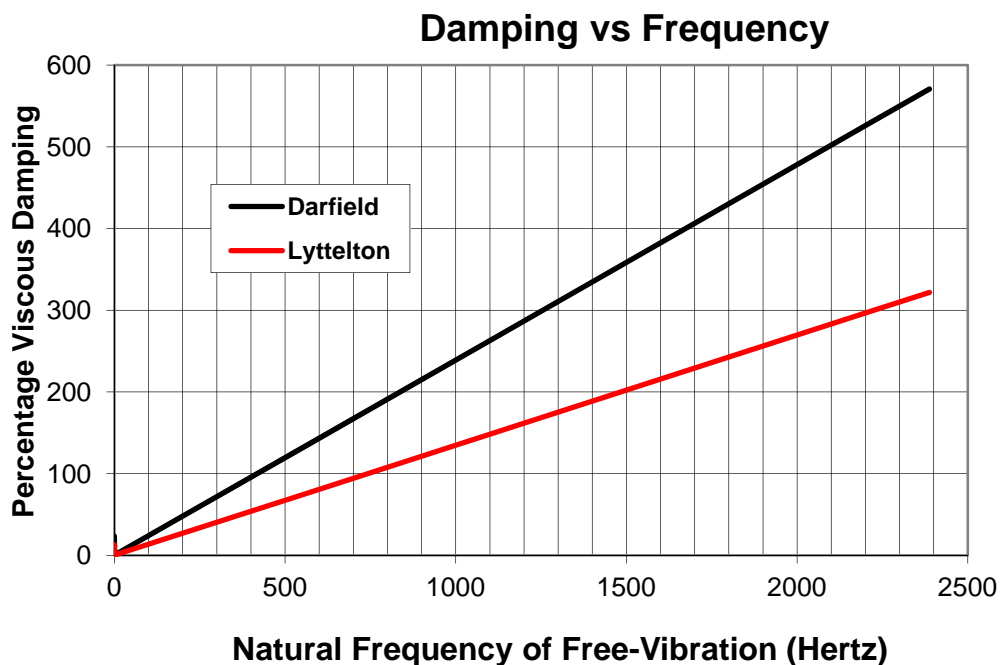


Figure 4 Damping versus Frequency (large frequency range)

CTV Non-linear Time-History Analyses Report

- 56 If the damping properties remain constant with time, i.e. the damping matrix [C] is invariant with time, then in a non-linear structure when yielding of the members occurs the ratio of the effective damping increases. To partially counter this effect the modeller could use the current tangent stiffness of the structure as the stiffness matrix in the Rayleigh damping matrix. This is not possible in SAP2000. Compusoft have attempted to achieve a measure of countering the extra damping associated with the Rayleigh damping model for the CTV building. They realised that the CTV building was likely to be highly non-linear in the February 2012 earthquake analysis. Their model selected a lower level of viscous damping, (2.8% of critical viscous damping) at the frequencies used to set up the Rayleigh damping model. As can be seen in Figures 3 and 4 this gives very low levels of damping associated with the modes with natural periods between 1.29 and 0.05 seconds (0.77 and 20Hz respectively). This low level of damping may result in larger than realistic responses. The responses that should diminish with time are not doing so at the rate expected.
- 57 Compusoft responded with the following statement.
- 58 *Compusoft Engineering acknowledge that the damping model used in the original analysis could produce damping levels that would be considered to be slightly lower than desirable for vertical modes of vibration..*

Telephone Conference: 10am (NZ Standard time) 25th May 2012

Buddle Findlay Offices, 245 St Asaph Street, Christchurch

59 **Attendees:**

Ashey Smith, Derek Bradley, Barry Davidson and Tony Stuart – Auckland,
 Brendon Bradley and Athol Carr – Christchurch,
 Graeme McVerry, - (GNS) Lower Hutt,
 John Mander – Texas, USA,
 Robin Shepherd – California, USA.

60 **Major Points.**

- 1 **Analysis Data:** Will Alan Reay have access to the analysis data? Athol Carr to enquire.
- 2 **Column Hinges:** These should have an Axial Force-Moment-Moment interaction instead of the Moment-Moment interaction in the present analyses. This is important with the high axial forces in the columns under gravity loading and with the effects of vertical accelerations.
- 3 **Column and Beam Strengths:** General agreement that the column strengths used in analyses are acceptable.
- 4 **Beam-Column Joints:** The beam-column joints were modelled as rigid whereas they may, in fact, be weaker than the columns or beams that frame into them. The joint flexibility and strength limitations should be modelled.
- 5 **Masonry Infill:** This was modelled as two extreme situations: one with no contact and the other with full contact. Could do an analysis with a gapped contact. This is not considered as important as items 2 and 4 above.
- 6 **Wall Modelling:** Rocking on base foundation beams is allowed for in the computational model and the wall modelling was acceptable to participants in the conference.
- 7 **Beam models:** The models used are considered as acceptable.
- 8 **Floors:**
 - a. General model. This is considered as acceptable.
 - b. Flexural stiffness. This should be considered as variable. In the centres of the spans the degree of cracking will be less and the stiffness will be greater whereas near the beam supports the negative moments will introduce a lower stiffness. The flexural stiffness effects could be important under vertical accelerations. A suggestion was made to use a grillage model for the flexural effects in the floor together with a membrane element to transfer diaphragm shear.
- 9 **Beam-Pull-out Effects:** Allowance could be made for full or partial connection to beams to columns on exterior frames (Column lines 2 and 3) as there is minimal seating.
- 10 **Earthquake excitations:**

- a. Frequency components. There was some initial discussion about the effects of high frequency and low frequency contributions to the ground motions recorded in the February earthquakes. It was recommended that the excitation suite should include the ground motions recorded at the Resthaven station.
 - b. Sequential earthquake analysis. There is a strong recommendation to not treat the September and February earthquake as separate events (i.e starting each analysis using the same stiffnesses and strengths) as has been done in the analyses reported. It was felt that for at least one of the records, the September record should be run followed by a period of free-vibration to allow the motion of the structure to settle, and then follow with the February earthquake. This means that for the February earthquake the model starts with the structure already possessing the stiffness degradation from the September earthquake. It is recommended that the Christchurch Cathedral College ground motion record be used for this extended analysis.
- 11 Damping: The program SAP2000 only possesses the Initial Stiffness Rayleigh Damping model. For the September earthquake 5% critical viscous damping was assumed for natural periods of free-vibration close to mode 1 and mode 90 of the frame. To attempt to allow for tangent stiffness damping for the February earthquake a lower amount of 2.8% critical viscous damping was specified at these two frequencies to compensate for the reduced stiffness. This Rayleigh Damping model has damping of a lower amount, down to about 1.8% of critical viscous damping, for the modes in between. This will give larger displacements for the responses of these modes. For the sway modes the difference in displacements may not be significant as with the short (6 storey) walls the higher modes will have a small displacement contribution. This may not be true for the accelerations associated with these modes. However, a large number of the intervening modes of free-vibration are vertical modes and the lower damping associated with these modes may be a problem in getting reliable vertical response in the structure. A further consequence of the Rayleigh Damping model is that modes with natural periods of free-vibration less than about 0.0015 seconds will be super-critically damped. This may have a significant effect on inelastic deformations in the structure.
- The sequential September-February sequential earthquake analysis would eliminate the need for a reduction of damping used for the February earthquakes.

61 Conference concluded at approximately 12:00pm NZ Standard time.

Follow-up post Teleconference.

- 62 Following the teleconference the experts submitted further information with respect to the behaviour of the columns and the joints.
- 63 There were two follow-up documents from Barry Davidson (Compusoft) and one from Prof. John Mander:

COMPUSOFT

E N G I N E E R I N G

PO Box 9493, Newmarket, Auckland, New Zealand.
Telephone: +64 9 522 1456 Website: www.compusoftengineering.com

28th May 2012

Professor Athol Carr
Canterbury Earthquakes Royal Commission,
PO Box 14503 Christchurch Mail Centre 8544,
Christchurch.

Subject: CTV Analysis

Dear Prof. Carr,

During and following our telephone meeting on Friday 25th May 2012, it became apparent to me that not all members of that meeting were aware of the processes around the CTV nonlinear time history analyses. I think now is a good time to clarify some of the issues to you and the other members of the nonlinear analysis review group.

During the telephone conference there was some criticism regarding the overall process undertaken in the CTV investigation. It should be known that Compusoft Engineering Ltd. acted in a sub consulting role throughout providing the nonlinear time history analysis. The investigation was commissioned and managed by the DBH via StructureSmith and the DBH Expert Panel. While Compusoft Engineering Ltd contributed to the details of modelling, and advising on the SAP2000 capabilities, they had no control over the overall process.

During the telephone conference there was some criticism regarding the complexity and or extent of the models. It should be noted that there were significant time constraints imposed on all parties and these had a direct impact on the allowable complexity of the model developed by Compusoft Engineering Ltd. The overall analysis model was developed in consultation with StructureSmith, Hyland Consultants and the Expert Panel with consideration of these constraints. A significant number of inputs to the analysis model were dictated by these people.

Up until now we have been responding to requests from the Royal Commission for clarification of various aspects of the analyses that we carried out for StructureSmith and DBH, as an extension to our initial contract.

Our understanding from the Royal Commission Direction dated 18 May 2012 and from the telephone meeting on 25 May 2012 is that we are now working under a new regime, where

May 2012

some changes to the model may be made, and further analyses run to investigate the items discussed by Alan Reay's representatives.

We strongly feel that it would be appropriate for the DBH expert panel to have a representative involved in the current discussions about proposed changes to the model, particularly as all inputs will be subject to critical interrogation/inspection by others. Our preference would be for Nigel Priestley to be involved, since he was closely involved in critiquing the existing model and so will be aware of the implications of further changes.

We are currently working through the items that were discussed during the telephone meeting, to see how we can incorporate some of the additional features that were requested. CompuSoft is willing to make changes to the model, however prior to making these changes we will require specifics on all discussed parameters, including documentation supporting the chosen parameters.

Sincerely,



Barry Davidson
Engineering Director

cc Marcus Elliot – Canterbury Earthquakes Royal Commission
Ashley Smith – StructureSmith
David Hopkins – Department of Building & Housing

COMPUSOFT
ENGINEERING

PO Box 9493, Newmarket, Auckland, New Zealand.
Telephone: +64 9 522 1456 Website: www.compusoftengineering.com

31st May 2012

Professor Athol Carr
Canterbury Earthquakes Royal Commission,
PO Box 14503, Christchurch Mail Centre,
Christchurch 8544.

Subject: Further analysis of the CTV building

Please find below our responses to the items raised in your summary of the telephone conference that took place on 25th May 2012.

1. Analysis Data

CEL takes no exception to the release of any raw analysis results to ARCL electronic format (e.g. Microsoft Excel or Microsoft Access database) provided that the same information is provided to StructureSmith, Hyland Consultants, and members of the DBH Expert Panel.

The analysis model has been well documented in the CEL report and also issued in *.pdf format to all parties. Discussion regarding the release of a complete working analysis model to ARCL is ongoing between CEL and the Royal Commission.

2. Column Hinges

CEL is investigating the efforts of implementing P-M-M interacting hinges into the model to more accurately represent the nonlinear behaviour of the columns.

3. Column and Beam Strengths

These will be unchanged in the analysis for all elements.

4. Beam - Column Joints

The incorporation of inelastic behaviour in the beam-column joint zone will constitute a significant change to the analysis model and could take a significant time to implement and test. For this to progress we would require guidance from experts acting for ARCL and members of the DBH expert panel.

5. Masonry Infill

The effects of the masonry have been bounded in the previous analyses by considering both full interaction (i.e. no gap) and zero interaction (i.e. a 'large' gap.) If it is deemed appropriate to incorporate a gap – interaction, a suitable description of the mechanism and appropriate backbone curve would need to be identified and agreed to by the panel for inclusion into the model.

6. Wall Modelling

No changes to the wall model are considered necessary.

7. Beam Models

No changes to the beam model are considered necessary.

8. Floors

There was noted to be some concern relating to floor stiffness with respect to plate actions. In the previous analyses the sensitivity of the column actions to variations in slab plate stiffness was explored by considering variations to the linear bending stiffness of the slab elements.

In order to accurately include the effects of the differing slab stiffness when subject to sagging and hogging deformation, a non-linear plate response of the slab would be required to be included in the analysis model. Agreement on the hysteretic curves would be required.

9. Beam Pull out Effects

Compusoft Engineering Ltd consider that the inclusion of beam pullout effects would add significant complexity to the analysis model.

May 2012

10. Earthquake Excitations

The REHS record can be included in future analysis runs should it be deemed appropriate.

An analysis that includes a sequence of ground motions such as September then February, can be proceeded with if the panel recommend this procedure.

11. Damping

Should it be considered necessary the previous damping models could be revised. We would welcome any suggestions to the damping models assumed in the analyses. Sincerely,



Barry Davidson
Engineering Director

Follow up remarks to the telephone conference 25th May 2012

These remarks are intended to be constructive in order to seek a reasonable pathway to the truth. To do that one should be aware that the original documents prepared for the DBH were written, in part, in the spirit of whether the building conformed to the codes of the day. In that work, much reference has also been made to the NZSEE (1996) document on assessment of buildings. As a co-author of that particular piece of work, it should be emphasized that its intent is to give a fair, albeit conservative, assessment of the state of a structure in order to identify critical weaknesses. It is contended therefore, that these state-of-the-NZ-practice recommendations may not be particularly useful; instead state-of-the-art knowledge should be used wherever possible.

This document first elaborates, where considered necessary, on the summary *Major Points* as documented by Professor Carr following the telephone conference. It then goes on to describe some remaining gaps that should also be seriously considered.

Discussion on the major points:

1. Dr Reay should have access to the data, he is an expert the dynamics of structures in his own right. In addition, Mr. Doug Latham and Mr. Urmson should also be deemed experts, if necessary. In striving for the truth all experts that have studied the CTV building at length should be utilized; the argument of commercial sensitivity is frivolous and without merit. Moreover, Mr. Urmson has a masters on this very topic, and prior to the earthquake commenced the work at Texas A&M on SAP2000 analysis on the NZ *Redbook* building. I was his advisor. That work subsequently showed that that textbook-designed exemplar structure would not survive the 2/22 event—like the IRD building across the street from the CTV, the Redbook building would also need to be razed.
2. Because the previous computational analysis did not apply correct modeling of the columns, as evidenced from a cursory examination of the inadmissible results plotted in Fig. 15 of Hyland's report, the results are of little (if any) value. Moreover, the conclusions are essentially worthless as one cannot confidently claim they have not arrived at a false-positive result. While it is vital to have the correct axial load-bimoment dependent interaction surface, it is also important that the hysteretic models for the column be calibrated accordingly. There is no reason to use a concrete compression strain limit of 0.004, this is more likely to be 0.008 for that class of 1980's concrete; this has been demonstrated in the modeling of concrete structural elements

constructed with Christchurch concrete during the 80's era (Mander, 1983). Coupled with this is the need to appropriately model the falling branch of the buckled reinforcement. Again, for guidance on this matter, one could use by interpolation the stress-strain results for tests that were done by Mander (1983) with support to diameter (s/d_b) ratios of 10 and 15. Both of these aspects are also important in the modeling of the correct post-peak representation of the column behavior—particularly where very high axial loads are concerned.

3. My thinking was that there was general agreement that the approach to modeling the columns was on the right track, and the concrete strength used was apparently specified +2.5MPa. At the time, and for the immediate future these values should suffice. But based on mounting evidence now to hand, the Central Lab tests, along with the subsequent inferences by Hyland are quite faulty. Therefore, it should be noted that some selective reruns of the analyses will need to be done to ascertain any changes in behavior when higher strengths are used, say specified plus x% where x is yet to be determined. It should also be noted, that the strength of the columns, particularly at each floor-slab level, should be based on the beam strength; this comment relates to the next point.
4. There is no forensic evidence that the lap splices slipped; and there is little evidence of hinging within the clear length of the columns—there is clear forensic evidence that the hinging coupled with shear effects have taken place within the joints. This hinge-type yielding was evidently concentrated over a very short length in the vicinity of the floor slab, and also the soffit of the beams. It will be interesting to see what the concrete/analysis experts use to model the joints accordingly. Also note, the Priestley et al (1997) recommendations used in the post-processing to detune the strength of the joints in compression to $0.5f'_c$ (= 12.5 MPa , or an axial load of 1570 kN) are clearly incorrect. Those recommendations were based on work done on bridge piers which by comparison have very light axial loads. The average axial load on the columns was often well above 1600kN, even in the first substantial (September) earthquake, and survived. Therefore, an appropriate joint model needs to be proposed. I comment on this further in the next section.
5. It is agreed that strictly a gapped element should be used to accommodate the gaps as specified on the construction drawings. Project ATC-43 has provided recommendations on how to do this (FEMA 307, 1998).

6. OK
7. This relates back to the comments in 2 and 4 above. Because the interior beams were stronger than the columns, beam hinging is unlikely. Any hinging would likely be the weaker positive beam hinges; it would be slight and concentrated at the face of the joint. In the case of the exterior joints, it is likely that both positive and negative beam hinges occur. Moreover, sudden failure is possible as noted in 9 below.
8. I doubt that there is evidence that the stiffness would vary. Reinforced slabs are inevitably cracked throughout. The lever arms are typically large ($j > 0.9$), and the stiffness in the order of $E I_{eff} = 0.1 E I_g$. The amount of cracking will not be less in the mid-span region, if anything cracking will increase, and possibly even lead to a central east-west positive (sagging) yield-line in each bay due to high vertical acceleration response. The main point is that all surviving eyewitnesses attest to the fact that the building was considerably more vibration-prone after the September event. What most likely happened then (and this could be confirmed with the proposed end-on-end analyses), is the initial fixed-fixed support condition at the supports was affected through slab-steel (mesh) yielding, effectively making the slabs vibrate in a pin-pin end-condition. This would lead to floor deflection amplifications of up to 5 times the case of full fixity (the undamaged condition). These larger vibrations were evidently noticed by most occupants; for example, trucks driving by would vertically excite the ground and this could easily be felt within the CTV structure. As the floor's concurrent ability to transmit in-plane compressive loads along with large downward gravity-enhanced (vertical motion) displacements in the north-south direction would be impaired, it should be stressed that any future analyses attempt to capture this out-of-plane floor vibration coupled with in-plane buckling capability. It is expected that in the limit, a slab in-plane buckling failure might ensue, which in turn may overload and collapse the columns.
9. The importance of this point cannot be overstated. The behavior of this junction may also have been a key trigger mechanism in the failure of the structure. For example, a connection-seat failure along line A would lead to the overloading on the columns in line B and thereby column instability with a subsequent implosion. Again this is not helped by the high vertical ground motions.
10. The starting point for this analysis is to rerun the CBGS as an end-on-end continuous run and compare the results to those previously obtained. For this parametric

variation, only the ground motion run approach can be changed and nothing else—that is the original model, in spite of its acknowledged shortcomings be retained for the analysis. Then, ***all*** four agreed upon motions (CHHC, CBGS, CCCC and REHS) should be rerun with combined continuous end-on-end motions, along with all the above mentioned structural analysis enhancements. Recent work by Bradley has shown that it is not so much the average that is important, but the spread of results too—this can only be achieved once all four are run.

11. In spite of the remarks about damping, there seems little evidence of amplifications arising from higher mode effects. Perhaps, what is important is to ensure the vertical mode is captured well. Floor systems tend to be lively with low damping, but this should be rechecked.

Remaining Gaps

When engineers carry out earthquake response NLTHA their natural instinct is to look for a classic horizontal inertial type side-sway or soft storey mechanism. Although the Hyland report suggests this did indeed happen, there is little, if any, forensic evidence that this happened with CTV. There is, however, plenty of evidence (both forensic and from eyewitnesses) to suggest this is more of a gravity-dominated event. The building did not just topple. It is evident the building came straight down, and it is my theory it was a stability failure of both the floor slabs in the N-S direction along with pull-out of the beam connections. But the question remains: why? If correctly modeled, this analysis should illuminate what really happened.

From the above remarks related to the telephone conference it is evident some serious shortcomings exist in the present computational models—every effort needs to be made to rectify these, specifically:

- No axial load-moment interaction
- No softening of the beam-column joints (note that a simple strength hierarchy analysis show these become fuses and inhibit the column hinges from fully forming)
- No pull-out (unseating) capability of the exterior E-W beam connections
- It is also not clear to me whether the slabs (specifically in the NS direction) can handle nonlinear behavior in terms of combined in-plane (NS) axial load and out-of-plane bending adequately to capture the possibility of out-of-plane buckling.

The second and third items above will be the most challenging to model. This is an area I have recently been doing a lot of research for TxDOT. One promising method is to use

compatibility-based truss models applied in SAP 2000 (Scott et al, 2012). An example of how the CTV beam-column joints in the E-W direction could be modeled is presented in figure 1. The key is in appropriately sizing the arch and its strength, which also has to be successively detuned as the transverse principal strain increases during loading. Properly done good results are obtainable.

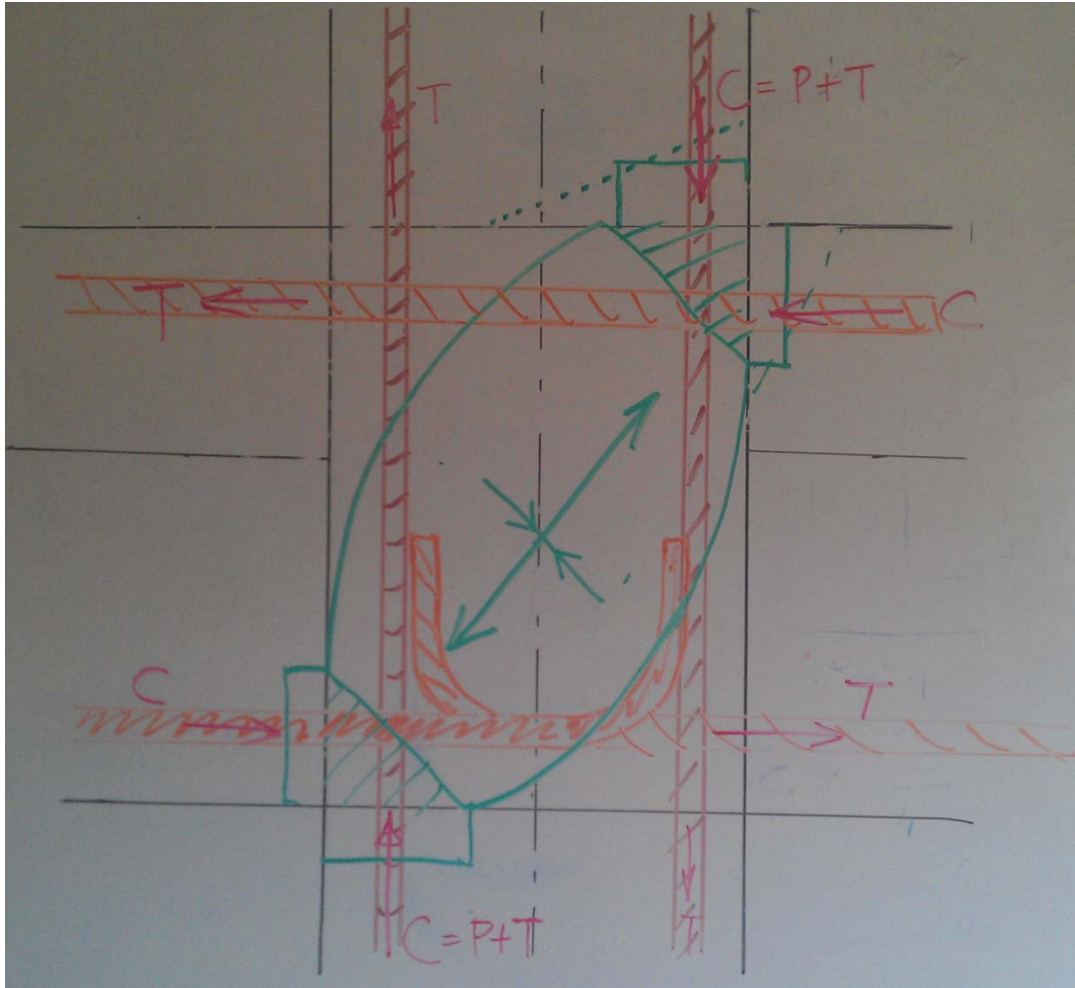


Fig. 1. Truss model showing joint modeled by a diagonal arch.

For clarity the sketch only shows an active arch for clockwise column moment input.

John B Mander

College Station, TX

10:00 pm 5/28/12

References

FEMA 307 (1998) "Evaluation of Earthquake Damaged Concrete and Masonry Wall Buildings." Federal Emergency Management Agency, Washington DC.

<http://www.fema.gov/library/viewRecord.do?id=1652>

Mander, J.B., (1983) "The seismic design of bridge piers," PhD thesis, University of Canterbury,

<http://ir.canterbury.ac.nz/handle/10092/1197>

NZSEE (2006) *Assessment and Improvement of the Structural Performance of Buildings in Earthquakes*. New Zealand Society for Earthquake Engineering, Wellington, New Zealand, 400pp.

Priestley, M J N (1997) *Displacement-Based Seismic Assessment of Reinforced Concrete Buildings*. Journal of Earthquake Engineering. 1(1): pp.157-192.

Scott, R.M., Mander, J.B., and Bracci, J.M., (2012) "Compatibility strut and tie modeling: Part I—Formulation," ACI Structural Journal, *in press*

Scott, R.M., Mander, J.B., and Bracci, J.M., (2012) "Compatibility strut and tie modeling: Part II—Modeling," ACI Structural Journal, *in press*

- 64 The Royal Commission declined to allow Alan Reay Consulting Ltd. (ARCL) access to the SAP2000.s2k data set although they were provided with a .pdf version of the data. This would enable ACRL to see what the computational model included but not directly be able to use the data to run their own analyses with their licensed version of SAP2000.
- 65 Compusoft advised that their solution to providing the Axial Force-Moment-Moment (P-M-M) Column Yield interaction would be to use a fibre (or filament) type model for the column plastic hinges. This fibre model would use the concrete stress-strain laws for the concrete and the steel stress-strain law for the steel instead of using an hysteresis rule, such as that of Takeda, to represent the moment-rotation properties of the plastic hinge.
- 66 There has been a considerable interchange of ideas and comment about the computational modelling of the beam-column joints, in particular between Professor John Mander, Derek Bradley (Compusoft) and Ashley Smith (StructureSmith). Many suggestions about the inelastic behaviour and ideas for modelling were discussed in a series of email exchanges. What was proposed at the teleconference was to model the joint behaviour by adjusting the column yield behaviour at the plastic hinge just above the joint to match that of the joint, as the joint was considered to be the weaker of the two components. It was considered that although there is an effect of the magnitude of the column axial force on the strength of the joint, its modelling in the joint behaviour is uncertain and for the present time it was considered that taking the axial force as constant across the joint was a satisfactory solution.
- 67 There was little further discussion on the masonry infill in the lower storeys of the West wall as the panel had decided that the two limit cases was sufficient in the time left for further analyses.
- 68 The modelling of the floors still needed some input. Professor Mander suggested that the floor flexural stiffness could be as low as 10% of the gross floor stiffness.
- 69 The beam pull-out from the exterior joints on the West side of the building required estimates of the pull-out strength and rotational deformation limits, to determine when the pull-out could be expected to be likely to occur. These still had not been provided but could be inferred from the discussions of the beam-column joint behaviour.
- 70 Following the questions about the excitations, it had been agreed that the Resthaven accelerograms were to be used. Initially the existing data sets would be used to see what differences in the responses were likely. It was also agreed that an analysis would be conducted starting with the September earthquake, followed by a period of free vibration and then the February earthquake. This would give an analysis where the February earthquake would be applied to an already damaged structure giving results which would more likely match what happened to the actual building. There was still the question as to how long the analyses should be, the starting times, the finishing times and such for both the September and February records.
- 71 Compusoft agreed to look at the damping models, in particular at the reduced damping for the February analyses. Whatever was done, it would be a compromise

that had to be achieved within the limitations of the only damping model available in the SAP2000 program, namely Rayleigh damping using the initial elastic stiffness.

CTV ANALYSES VIDEO CONFERENCE 8th JUNE 2012-06-07**Brief Summary of Results****72 Expert Panel Attending: 9.00 am to 11:15 am**

- Athol Carr (chair) (Christchurch)
- Robin Shepherd (California, USA, telephone connection only)
- John Mander (Texas, USA)
- Barry Davidson (Auckland)
- Brendon Bradley (Christchurch)
- Graeme McVerry (Lower Hutt)
- Ashley Smith (Auckland)
- Derek Bradley (Auckland)
- Tony Stuart (Auckland)

73 Ground Motion Questions.

- The only other ground motion record contemplated is the Resthaven record. Dr Bradley has argued that the high frequency content is not significantly different from the other sites, but the response spectra for the vertical component are more significant. The question is what else would we learn from adding another record to the suite, possibly letting us draw the conclusions from four slightly different records rather than current three records. We do not want an average response but drawing the conclusions from the variations in the sets of responses is what is needed.

General agreement that the Resthaven record should be included in the suite of CBD records. It was initially suggested that the existing data set be used to gauge the differences in the response with that for the other 3 records.

- Running the Cathedral College record for the September earthquake and then February earthquake would be very useful, we have the structure is a possibly degraded state from the September event when the February record arrives and the subterfuge of reducing the damping for the second analysis will not be required. Taking 2.8% damping versus 5% damping could increase the responses by the order of 50%. We are stuck with Rayleigh damping but just let us use it sensibly.

General agreement that the CCC record be run for both earthquakes. Suggested that 40 seconds of the September record be run, then restart with the Christchurch record. SAP2000 has a re-start option which retains the state at the end of the earlier run so do not need to generate a long record with the two motions with a period of free-vibration in-between. A suggestion by Prof. Shepherd that if time is available that all four ground motions be run in this way.

Structural Modelling Questions.

- **Columns yield interaction**, Compusoft is already setting up the data to provide and Axial-Force/Moment/Moment yield interaction.
Full agreement. Suggestion by Profs. Shepherd and Mander that there is now test evidence that the concrete strength is nearer 1.5 times the specified 28 day strength rather than that used by Compusoft of the 28 day strength + 2.5 MPa. Profs. Shepherd and Mander may be able to supply the report to Compusoft, otherwise use the currently assumed strengths for the revised analyses.
- **Beam/column joints**, How are these to be modelled, nothing in SAP2000 to do this easily and no world consensus as yet on modelling joints, particularly in 3D. Can the effects be done by playing with the column yield actions if the joints are weaker than the columns and beams? Can the joints be checked in a post-processing manner?
After considerable discussion it was agreed that the easiest manner of modelling the behaviour of the beam column joints is to reduce the strengths of the column plastic hinges just about the joint (except for the base of the ground floor columns) to a possible 2/3 of the column strength. Prof. Mander to provide suggested strengths to Compusoft.
- **Floor trampolining effects**. The trampolining effect, and its consequential effects on the column axial loads may be significant. This is already allowed for in the Compusoft model but possibly the flexural stiffnesses of the floors may need to be modified to allow for flexural cracking. My estimate using approximately 40% of flexural stiffness gives a trampolining frequency of about 5.5 Hz and vertical deflections at the centre of the 7.5 m floor spans of +/- 13mm for the REHS vertical motion ,
 Prof. Carr does not agree with Prof. Mander's arguments about floor buckling, the in-plane forces (normal and shear) are not that great and the floor is not that thin. The out-of-plane displacements are small compared with the floor thickness. *Prof. Mander countered that the effective thickness in the compression zone might be rather small. This was not pursued any further.*
In general these trampolining effects are already incorporated in the Compusoft model and maybe apart from possibly reducing the flexural floor stiffness, no further action is required.
- **Beam pull-out at end columns** - can this be checked from post-processing. Or should it (can it) be included within the computational model
Regarded as important in the model but would require considerable addition to the current model. The decision was to model this as a plastic hinge at the beam ends with a rapid degradation of strength once a given plastic rotation is reached. This approach requires only a small modification to the data set. Prof. Mander is to suggest plastic rotation limits.

75 **Other points raised in the conference**

- i) **Who will pay for the extra analyses.** Prof. Carr is to find out the answer from the Royal Commission and report to the panel of experts.*
- ii) **5% damping in the Rayleigh Damping model** This is satisfactory as modelled using the current frequencies to determine the Rayleigh **Alpha** and **Beta**.*
- iii) **Interaction of Infill walls.** The Compusoft models have considered only two limiting cases, full clearance and no clearance. The panel agrees that this is sufficient as any attempt to model partial separation introduces too many parameters, particularly within the time constraints..*
- iv) **Alternative Computer Analyses.** Prof. Shepherd commented that it was pity that an alternative solution could not be carried out with an alternative non-linear time-history analyse program to the SAP2000 used in the Compusoft analyses. Different programs work in different ways, have different modelling options and so may give solutions that differ in various aspects. Many members of the panel concurred but accepted that this is not possible in the time or with the man-power available.*
- v) **Best Solution.** The panel agreed that the behaviour of buildings in the Christchurch Earthquakes will be the subject of world-wide engineering research over the coming decade. It is not possible in the time given and the data available at present to obtain what might be considered as the “correct” or “perfect” solution for the analyses for the Royal Commission. However, the aim with the present analyses is to obtain a solution which gives the best understanding of the behaviour of the CTV building and from this provide the most likely scenario for the failure mechanism.
This future research, with the provision of better material information and better computational models may help show what really happened.*

Athol Carr

76 **Email discussion following the Videoconference on the following issues.**

Interpretations from the Video Conference

Barry Davidson, Derek Bradley and Tony Stuart prepared some notes and suggestions following the videoconference.

- 77 They have one comment on their notes about Floor trampoline effects. The notes finished that section with the statement: "In general these trampoline effects are already incorporated in the Compusoft model and maybe apart from possibly reducing the flexural stiffness, no further action is required.
- 78 Their recollections were that we agreed further analysis may be required to test the sensitivity of varying floor stiffness and damping.
- 79 Regarding floor stiffness, the parameters used in the Compusoft model are explained in sections 5.7 and 11.3 of the Compusoft report. They recalled John Mander's comment that he felt the floor positive bending stiffness may actually be greater, up to 80% gross, because of the contribution of the decking. However they are not sure what John thinks about the negative bending stiffness assumed by Compusoft, which is just as important. What we need to do is agree on a sensible range of floor bending stiffness values, negative and positive, to adequately bound the vertical earthquake effects on columns.
- 80 Regarding damping, they thought that the panel agreed that 2% would be a reasonable estimate for the floor damping for the February event which is higher than the (approximately) 1% used in the current model.
- 81 Barry Davidson sent the Compusoft Interpretation of the conclusions from the videoconference

COMPUSOFT

ENGINEERING

PO Box 9493, Newmarket, Auckland, New Zealand.
Telephone: +64 9 522 1456 Website: www.compusoftengineering.com

8th June 2012

Professor Athol Carr
Canterbury Earthquakes Royal Commission,
PO Box 14503, Christchurch Mail Centre,
Christchurch 8544.

Subject: Compusoft interpretation of meeting held 8th June 2012

The following are our recollections from the videoconference meeting held this morning. They are intended to assist in resolving the agreed way forward as quickly as possible and are probably not complete. The *italicised* bullet points identify our thoughts and comments on what was discussed.

1. Summary of discussion

1. Column PMM interaction.

PMM interaction of the column hinges is to be incorporated into the model. One point of interest amongst members of the panel appears to be the effect the column lap splice located immediately above slab level will have on the performance of the column hinge. It is considered that the presence of the lap splice will result in a much shorter plastic hinge region, and will be partially located within the depth of the beam-column joint (which consists of lower strength concrete). In an attempt to consider this behaviour it is proposed that the hinge located at the base of the column exhibits a degrading backbone curve.

- *Compusoft comment: PMM interaction to be incorporated via a fibre based hinge. Hinge hysteretic behaviour for hinge at base of column to be modified such that it exhibits degradation. The backbone curve and hysteresis rules for*

the lower hinge in columns to be provided by others for inclusion in the model.

2. Modelling of the Beam – Column joint zone.

The three dimensional inelastic behaviour of the panel zone is not to be incorporated explicitly into the model. Our understanding is that the effect of any inelastic behaviour of the panel zone is instead considered by way of the modified column hinge located at the base of the column (as discussed above).

- *Compusoft comment: We note that the panel zone behaviour is not to be incorporated explicitly in the model and as such would suggest its performance be assessed via post-processing as per previous.*

3. Beam pull-out.

Beam pull-out to be considered by way of a modified moment-rotation backbone curve for beam flexural hinges.

- *Compusoft comment: The backbone curve and locations for the affected beams to be provided by others for inclusion in the model.*

4. Concrete strength

There is a report that is not yet available that proposes that the concrete strength is greater than what was used in the initial analyses. Some requests were made that analyses be undertaken considering the unconfined compressive strength of all concrete be taken as 1.5 times the specified strength.

- *Compusoft comment: Confirmation of concrete stress/strain behaviour to be provided by others for incorporation into the model.*

5. Floor vibration and resulting inertia effects.

The floor elements are to be modified to consider an alternative effective linear stiffness for plate actions. The buckling of floor elements is not to be considered in the analysis.

- *Compusoft comment: The effective (linear elastic) flexural stiffness of the floor elements **to be provided for** inclusion in the model.*

6. Ground motion.

Certain members of the panel requested that all analyses are to be run in a sequential manner such that any strength or stiffness degradation present as a result of the September event is included in the February response. The REHS records are to be included in future analyses and also run for existing model. All records are to be run in a truncated format.

- *Compusoft comment: Compusoft understand that the priority will be running the CCCC record in a sequential manner with others being undertaken should it be deemed necessary. A clear prioritised workflow that presents exactly which records are to be considered along with suitable start and end times for each record should be provided.*

7. Masonry.

All future analyses are to consider the masonry to be sufficiently separated such that no interaction is possible (for any level of drift).

- *Compusoft comment: Analyses to assume that masonry walls do not provide any vertical support to the beams at levels 2 & 3 irrespective of beam deformation.*

8. Damping.

Damping parameters used in the previous analyses for the September event is deemed to be acceptable. Damping levels for the February event to be reviewed due to concerns relating to the low levels of damping that are present for vertical floor modes.

- *Compusoft comment: Damping parameters to be provided by others for inclusion in model. It should be noted that in SAP2000 we can run sequential analyses with different Rayleigh damping coefficients for each analysis.*

June 2012

2. Additional Comments

1. Outputs.

The quantity of output data is immense for these analyses.

- *Compusoft comment: The output items of interest are to be listed for inclusion into a formal report to be issued by Compusoft.*

Yours sincerely,

• 

Barry Davidson
Engineering Director

Drag-Bar Strengths.

82 On the 10th June 2012 BECA consulting engineers provided the Royal Commission with their estimates of the strength of the drag- bars that were added in the early 1990s to strengthen the connection between the floors and the tower in the upper storeys. These strengths are lower than the ones computed earlier and used for the Compusoft analyses. This information was forwarded to the panel of experts for consideration. (see **BULMAD249.0431.pdf**)

83 The table of interest is Table 1 on page 10 and should be compared with the values used in the Compusoft report on page 266. The values for the connection strengths provided in the BECA report are lower at all floors than those used in the analyses to date. If the new values are accepted then the structural model should be updated before the new analyses are carried out. If the new values are not accepted then there should be good grounds for doing so.

Comment by Professor Robin Shepherd.

84 He could not see any reason why the further runs should not be undertaken using the BECA values for the connections.

Comment by Ashley Smith.

85 1. One reason why the BECA values are lower than those on page 266 of the Hyland/Smith report is that BECA have used characteristic material strengths and not expected, or nominal material strengths (as found from testing by Hyland).

86 2. As noted by BECA there is considerable uncertainty in the estimation of these tensile capacities.

87 3. Hyland calculated the values on page 266 of the Hyland/Smith report, based on Fib 2011. I calculated similar values, by less rigorous methods, referring to the Ramset resource book. I considered these to be upper bound values.

88 4. Regarding the modelling of the drag bar connection tensile capacities, whichever values we decide are appropriate, the situation modelled is not realistic in any case because we have not modelled the potential failure of the slab diaphragm connection 4/C to C/D. The expected strength of this slab connection is somewhat uncertain, because; we know that mesh can be brittle, we don't know how much the metal deck contributes and because we must consider in-plane tension, bending and shear actions and also out-of-plane actions simultaneously.

89 5. It is not feasible to model total diaphragm disconnection if we want the analysis to run to the end of the record.

90 6. Taking into account the above uncertainties and modelling limitations I would be just as happy to remove the limits on drag bar tensile capacity from the model (i.e. to leave the drag bars connected) and to review their likelihood of failure by post-processing, as we have with all the other potential failure mechanisms.

Comments from Dr Hyland

- 91 The Drag Bars were found from the physical evidence not to have failed prior to collapse initiating in the Line 2 and 3 columns. Heyworth supports this conclusion. Analysis in the BCR and by Clifton showed that they were the weakest link of the slab to the North Core for diaphragm actions. They therefore provide a good basis to benchmark or calibrate the performance of the CTV Building immediately prior to collapse. However again some of the DBH Panel refused to concede that collapse had not initiated prior to Drag Bar failure.'

Comments from Professor Nigel Priestley

- 92 The BECA report indicates that probable strength of the drag bars is less than used in the original analyses. Has this report been repudiated?

Concrete Strength.

Comments from Athol Carr.

- 93 My understanding from the meeting was that the strength used are those in the current models unless the report from the US with the 1.5 28 day strength is received and accepted.

Comment by Ashley Smith.

- 94 Regarding column concrete strengths - can Profs Mander and Shepherd confirm which test report they were referring to during the video conference of 8 June when they suggested the following:

- 95 That that there is now test evidence that the concrete strength is nearer 1.5 times the specified 28 day strength rather than that used by Compusoft of the 28 day strength + 2.5 MPa. Profs. Shepherd and Mander may be able to supply the report to Compusoft, otherwise use the currently assumed strengths for the revised analyses.

- 96 It assumed it may have been included in Douglas Haavik's evidence and report **WIT.HAAVIK.0001.5**, which I have now read on the RC secure website. From the Key extracts from Haavik's conclusions and executive summary I cannot see how the above statements by Haavik can be interpreted as verifying column concrete strengths being nearer to 1.5 x specified strength. Perhaps Profs Mander and Shepherd were referring to other evidence?

Comment by John Mander.

- 97 It is in my evidence **WIT.MANDER.0001(1).pdf**

Comments from Ashley Smith

- 98 Having now read John Mander's evidence my understanding of the various opinions about the CTV building column concrete strengths is (in simple terms) as follows:

Hyland – Mean 29.6 MPa

Mackechnie – Review of Hyland test results, average 30 MPa, but this may be low because of micro-cracking. Noted that other structures investigated by the RC had core strengths significantly higher than design strength.

Haavik – Range from 2.7% to 55.8% higher than Hyland

Mander – CTL core tests – median strength 1.5 x specified strength

Dhakal column tests provisional results above 25MPa, with size effect possibly in the order 0.85. Therefore estimate $1.5 \times 0.85 = 1.28$ x specified strength?

CCANZ - Significantly higher than Hyland, but further testing required to make definitive conclusions regarding concrete strengths.

- 99 No doubt the above will be debated further by the concrete experts during the RC hearing. In the meantime, for the purposes of progressing the NTHA my suggestion would be for Compusoft to continue initially with the current 'specified strength + 2.5 MPa' to test the other parameters we have been considering, and to then do a comparative analysis (perhaps one EQ record only) with specified strength x say 1.3 to test the sensitivity of results. I would be happy to hear comments from others.

Comments by John Mander.

- 100 2 scanned extracts

This series of tests and examinations can best be viewed as a prototype for a full-scale test program to determine the condition of the CTV Building's concrete prior to the 22 September 2010 earthquake. The number of samples is not enough to draw definitive conclusions. One conclusion that can be drawn rather easily is that samples in this test program from the same column remnants as the Hyland Materials Report in each case produced higher concrete core compressive strength test results than their Hyland counterparts. The measured strength (corrected for l/d) increase ranged from a low of 2.7

This report details the criticisms of the "Hyland Materials Report" and gives results of the current test program, which showed compressive strengths with increases ranging from 2.7 % up to 55.8 % for the same columns in the "Hyland Materials Report". It is likely that none of the current compressive strength test results was below the specified strength at the time of original placement.

Comments by Ashley Smith.

- 101 I am conscious that concrete strengths will be debated further by the concrete experts in the upcoming hearing, but that will be too late for the further NTHA that has been requested. In the meantime I recommend that we use 1.3 x specified concrete strength throughout, i.e. for all elements. This will determine the expected overall response of the building as well as the expected capacities of the various elements, including the columns and the joints in particular. We should then also consider what changes would result from potential variations to these expected concrete strengths.
- 102 I have copied my email of 12 June below, which sets out my understanding of the various opinions and test results we have to hand of column concrete strengths. In addition I note that Hyland's compression tests on the north core wall (which was the one element that did not collapse, and also did not suffer significant damage) averaged 35.5 MPa = 1.42 x specified strength. Note also that Compusoft currently have 33.5 MPa = 1.34 x specified strength in the NTHA model for the shear walls which control the overall response.
- 103 I hope that John and others agree that the recommended '1.3 x' is a sensible 'middle ground' given the variation of opinion and test results that we have to hand. The above recommendation is made without prejudice in order for us to be able to progress the analysis.

Comments from Nigel Priestley.

- 104 I have not seen the reasons why these have been so drastically changed from the CTV report values, but I presume that Clark and Ashley agree with the changes?

Column Plastic Hinge Modelling.

Comments from Athol Carr to Compusoft.

- 105 I was not aware that the P-M-M interaction would be provided by a fibre model (at computational cost), does the program have the capability of using a straight P-M-M yield surface.
- 106 Note that John thinks that as the column action is controlled by the joints. Further, if the joints are really the weak link then again John's comments on only using a simple M-M interaction for the columns would in general be rather like your current computational model. If the joints cannot put a yield moment into the columns the columns will remain largely elastic. The columns can effectively be modelled with an average axial load model, then the P-M-M interaction in the columns may not be very important. The base of the ground floor columns may still need the P-M-M interaction.

Comments by John Mander.

- 107 I have some questions about what SAP can actually do. I was surprised that they want to use a fiber model, I doubt that it is helpful.
- 108 Moreover, if we can do away with using fiber models and just use a more realistic lumped plasticity model that in effect mimics the weak joints, the program should run more speedily.
- 109 The shear capacities assigned to the joints in the lower stories for the joints are compression critical. The values proposed by Compusoft are a nonsense, and demonstrably wrong! First it should be noted that the joints have only a vertical capacity of some 2300 kN in axial compression. Clearly this cannot be so, as from the previous [mostly incorrect] work there were axial forces over 3200kN being registered. If proposed joint capacities are true, then the structure would have probably fallen down on capping out the upper stories during construction. Moreover, it would not have even survived the Darfield event, but it did!
- 110 This leads to the folly of using a fiber model. There is no point in using such a model if the columns will be mostly elastic, there was sufficient forensic evidence to prove that to be the case; it was the joints that were munted, but not on Darfield event. Again I have shown how the theories appear when plotted in figure 1 attached. Essentially, there is no axial load variation for the joints if one uses the industry standard of FEMA 356. This markedly simplifies the analysis, As such in an earlier email to me soliciting my opinion Professor Carr gave his and I quote: "Hi John, I would appreciate your comments. I think just modifying the column properties, as you suggest, will be easier. Regards, Athol." Obviously Prof. Carr is put in a difficult position chairing this committee, as he evidently does not want to be seen to be "paddling his own canoe", well I don't mind putting my oar in and say that he is right!

Comments from Nigel Priestley.

- 111 Interesting that John Mander believes that BC joint behaviour precludes ability of columns to yield, but wants an ϵ_{cu} of 0.008.
- 112 Lap splice performance: The figure you show was based on circular columns with low axial load levels, and rather close spacing of vertical reinforcement. I would expect the curves would be conservative for columns with higher axial load. However, the degradation of the lap splice requires several cycles of inelastic response with compression strains exceeding 0.002 followed by high tensile strains. Also, the experimental data were based on tests where the lap splice was typically located in a region where the moment for the full splice length exceeded about $0.8 M_{max}$. This condition would not exist in the CTV columns. Further, the column remnants do not appear to display lap splice failure. I think you could ignore this possibility.
- 113 Column P-M-M response: As I have previously stated, I don't see much point in the added complexity of the proposed P-M-M analysis of the columns. The displacement response of the building will not be significantly influenced by any changes in the column stiffness resulting from the modelling changes, since the stiffness of the walls will still dominate. In view of the approximations still inherent in a fibre model, there seems little to be gained.
- 114 On the other hand, the fibre modelling MUST be compared with conventional line-element modelling of a fixed-end case to ensure that the fibre element is working correctly. Some issues that need to be addressed:
- Plastic hinge length should include strain penetration, but this must not be located EXTERNAL to the beam/column interface, or the locations of the gauss points at which moment is calculated will be incorrect.
 - Shear deformation: how is this to be included? Normally fibre models cannot simulate shear deformation. If this is not included, there is no point, in my view, in the fibre modelling.
 - Because of the high axial loads, portions of the column will remain un-cracked under seismic response. It appears that the modelling is to include only one set of fibres (the plastic hinge length) with elastic behaviour above. If this is the case the accuracy could be insufficient given the very low plastic displacement capacity. If more fibre sections are planned, this needs to be clarified in the report.
 - The way in which spalling and cyclic loading is to be handled needs to be clarified.
 - Plastic hinge length. 200mm is reasonable top and bottom, though even when based on strain penetration, I would expect the plastic hinge length to be smaller at the base than at the top. However, fibre modelling normally has a linear strain distribution over the fibre length. If this is the case, then the length of the fibres needs to be 400mm, not 200mm, since the 200mm is based on constant strain over the plastic hinge length.
- 115 In addition, it is unclear to me what model is to be used for concrete fibres under repeated loading. This is stated as Takeda, but so far as I am aware, Takeda hysteresis is only used for modelling inelastic response of line elements, not for response of pure concrete fibres, which are strongly asymmetric, and display little energy absorption.

Comment from Brendon Bradley.

- 116 I echo the comments of Carr, Priestley, Mander regarding the use of fibre-discretized modelling of the columns. The marginal increase in the accuracy of modelling pure flexure is more than offset by the inability to account for flexure-shear interaction for these columns, which are unlikely flexure critical. Furthermore, the computational cost of this modelling choice is leading to problematic choices when considering other features (analysis duration etc). I would advocate the use of 1D line elements as also suggested by others.

Comment from Derek Bradley.

- 117 CompuSoft is responsible for the implementation of the analysis and we have chosen to use a fibre based approach to model the column hinges. The fibre based hinge approach has been incorporated into the model and tested. We can confirm that the approach used produces a faster solution, more accurate results and has the additional benefit of providing more information for the purposes of interrogation. We note that P-M-M interaction in the columns was deemed to be necessary by ARCL's representatives up until recently. The significance of the column hinges will clearly be affected by the choice of the yield capacity of the beam-column joint. For some level of beam-column joint yield capacity the columns will become an issue. If indeed there is little hinging as has been suggested then these should not be adding significantly to the solution times.
- 118 We note that there has been some comments regarding the performance and effectiveness over our fibre-based approach to the column hinges. These have already been incorporated in the model and I can confirm that the approach that we are using is more robust, faster, is more accurate, and will produce more useful information with which the results can be interrogated than a lumped plasticity approach. We see no benefit in reverting to a M-M hinge model.

Masonry In-fill Panels

Comment from Athol Carr.

- 119 As far as I understand from the meeting the two limit cases, no contact and full contact cover the requirements to everyone's satisfaction

Comments from Dr Hyland:

- 120 I am concerned that the NTHA Panel is not addressing the fundamental issues of calibration of the NTHA to the observed physical damage.
- 121 This matter was also a significant cause of contention during the development of the BCR with refusal of some of the DBH Panel to allow consideration of scaling of input motions and full contact of the infill masonry on Line A with the frame. The results in the BCR have to therefore be interpreted in the light that they were not calibrated to actual observed damage and the results should not be considered an absolute measure of reality. The inability to even allow exploration of these matters has limited the usefulness of the NTHA in my view.
- 122 Some of the DBH Panel would also not concede that the masonry infill wall had not been visibly damaged prior to the February Aftershock and should be considered in modelling as masonry confined by the surround concrete beams and columns. In fact eyewitnesses did not report any visible damage when preparing it for recladding in the two days before the collapse. They testify that there were no obvious gaps between the masonry and the columns on the outside face, close fit of the blocks to the undersides of the concrete beams and some intermittent gaps in the mortar to the underside of the beams. Video evidence is consistent with their testimony. This is covered in detail in the BCR.
- 123 The actual response of the building based on witness testimony and collapse evidence appears to have been consistent with this masonry having affected the structural behaviour. For example tenants recall the building responding in an east west motion during aftershocks. Windows on the south and east faces were damaged in the September Earthquake and a window on one of those faces in December Aftershock. The North Core was found to have a lean after the February Aftershock and collapse that increased above Level 3 on the North east end of the North Core.
- 124 The properties however required by the DBH Panel to be used for the masonry infill were for a soft flexural yielding mode of failure that degraded in stiffness and strength to zero at the critical drift ranges of around 1%. The collapse evidence shows some panels that fractured in shear.
- 125 The Drag Bars were found from the physical evidence not to have failed prior to collapse initiating in the Line 2 and 3 columns. Heyworth supports this conclusion. Analysis in the BCR and by Clifton showed that they were the weakest link of the slab to the North Core for diaphragm actions. They therefore provide a good basis to benchmark or calibrate the performance of the CTV Building immediately prior to collapse. However again some of the DBH Panel refused to concede that collapse had not initiated prior to Drag Bar failure.'

- 126 This seems to be proposing that the analyses are run with progressively increasing ground accelerations to find out at what level the wall contributes to the structure response. The analyses to date have considered two cases, full contact and no contact. The ideal, and if we had an idea of what clearance there was and or the stiffness of the contact material, would be to include gap springs but this would also require some strength limitation modelling of the masonry infill. The masonry would not normally have a good bond to the beams above and the top course was not grouted. There was supposed to be some gap at the columns and how many parameter studies would be required to cover the possible permutations. As far as I can tell the analyses that have been done meet the requirements of the DBH panel of experts. If this is not so I would like to be so informed.

Comment by Athol Carr

- 127 This seems to be proposing that the analyses are run with progressively increasing ground accelerations to find out at what level the wall contributes to the structure response. The analyses to date have considered two cases, full contact and no contact. The ideal, and if we had an idea of what clearance there was and or the stiffness of the contact material, would be to include gap springs but this would also require some strength limitation modelling of the masonry infill. The masonry would not normally have a good bond to the beams above and the top course was not grouted. There was supposed to be some gap at the columns and how many parameter studies would be required to cover the possible permutations. As far as I can tell the analyses that have been carried out meet the requirements of the DBH panel of experts. If this is not so I would like to be so informed.

- 128 No further comment has been received from the Expert Panel.

Comment from Athol Carr to Marcus Elliot of the Royal Commission.

- 129 With respect to the comments by Clarke Hyland. These seem to be differences of opinion between him and the DBH Expert Panel. The problem with the masonry panels is that there is a gap, how wide was it in fact, how stiff was the filling, if the gap was not there and if it was undamaged in September then it almost implies that either the forces were small or that there was a gap which prevented the columns loading the masonry. Trying to cover the analyses would lead to a large number of parameter studies to get a range of possible responses. The ERSA analyses were only possible to cover full contact or no contact though a soft connection could be tried. However, the ERSA is elastic and cannot model a closing gap type analysis. For the NLTHA they used to same two cases, full contact and no contact. A gapped contact could be used, but what gap to use, and then strength limitations etc would be required for the masonry panels. The panels were inserted after the frame is built so the top course of blocks could not be filled and the contact with the beam above would have little strength. The ends of the panels to the columns is another story, what gap, what stiffness does the stuff in between have and at what force does the panel fail, in-plane or out-of-plane. As stated before, this could introduce a large number of contestable parameters and subsequent analyses. The expert panel that I am facilitating has discussed the panels and agreed that the two limit cases, full contact and no contact will suffice. Given the next decade someone may do some investigation as to the possible effects.

Floor Diaphragm modelling

Comment from John Mander

- 130 Regarding the slab, some extra work will be needed to calculate the softened properties of the cracked concrete, and as you will appreciate, that is not a simple heuristic rule. And even the joint shear capacity will require extra work. Previously, I had only calculated the solution for a few critical locations.

Comment from Athol Carr to John Mander.

- 131 I think that we could reduce the flexural stiffness of the floor on the elements along the beams, not so critical in mid-span.

Comment from John Mander.

- 132 I agree about the stiffness of the floor beams. Some rough calculations showed about $EI_{\text{eff}} = 0.1 EI_g$ at the support
- 133 Regarding the slab, some extra work will be needed to calculate the softened properties of the cracked concrete, and as you will appreciate, that is not a simple heuristic rule.
- 134 As yet, I haven't thoroughly gone over the slab stiffness, but based on some provisional analyses, it's about $EI = 0.1EI_{\text{gross}}$

Slab summary.

	EI_{cr} / EI_g	
	Bonded	Unbonded
-ve moment / support	0.049	0.190
+ve moment / midspan	0.236	0.0256

Note: $EI_g = 18720 \text{ kN-m}^2$

For convenience, assume $EI_{cr} = 0.1 EI_g$ throughout.

Comments by Athol Carr.

- 135 You indicate that for the slab flexural stiffness, a suggestion of $0.1 I_g$ but what is I_g , does it include topping (I would assume it does) but does it also include the Traydek etc. (actually Dimond Hibond, see ER not Traydek)

Response from John Mander.

- 136 I do not have the properties for the Traydek so it is only for the concrete-rebar composite system only. I will redo these but only if someone will supply the Traydek as mm^2/m and perhaps the I_{xx} and depth properties otherwise we essentially assume that that the deck has peeled off.

Comments from Nigel Priestley.

- 137 Floor elements: I wonder if the floor stiffness values of $0.1 I_{g\text{gross}}$ are appropriate. The slab reinforcement level is such that cracks will be very infrequent (ultimate capacity is, I believe less than cracking capacity, and hence tension stiffening will be extreme. Again there seem to be too many debatable changes being made to the analysis to have confidence in the results.
- 138 As noted, I believe that $0.1 I_{g\text{gross}}$ is much too low as it doesn't consider tension stiffening. If the results indicate sensitivity to the floor stiffness, the new results will be suspect.

Earthquake Records (Inclusion of Resthaven accelerograms)

Comment from Athol Carr.

139 As far as ground record, my understanding from the meeting was that REHS is to included, at least one run with existing data and possible included in the new analyses. For the sequential September –February analysis, CCCC accelerograms at the moment, the rest, if and only if time permits. This last aspect was a comment from Robin Shepherd.

140 The Expert Panel was advised of the release of the Geotechnical Advice Addendum 2 from Tim Sinclair to the NTHA review group for information. This covers, amongst other issues the recommendation to include the REHS record as an upper bound, which we have already agreed within the NTHA review group. Note: The version attached is slightly different to that uploaded on the Royal Commission website (there were some formatting errors in the figures on the website version, which will be corrected and reloaded by T&T to match that attached). (see **WIT.SINCLAIR.0002**)

Comment from Graeme McVerry

141 This is in line with the addition of the REHS records to the suite.

Earthquake Records (Duration of analyses)

Comments from Athol Carr.

142 We are trying to resolve the duration issues, 50 seconds or so might require of the order of 10 days! The durations data require only the changing of two numbers, the other modelling issues will take some time to set so urgency is important. When I get the results of some indicative duration analyses I will share them for comment.

From Athol Carr to Barry Davidson.

143 I have used the verification data set used for Ruaumoko as part of the Spectra calculations. This is a 1 second natural period single degree of freedom system with a bi-linear hysteresis. I have run with the September and February CCCC_N26W records. the analysis for September was 50 seconds long and 40 for the February records and if my calculations are right the first 5 seconds are truncated off both of the GNS records.

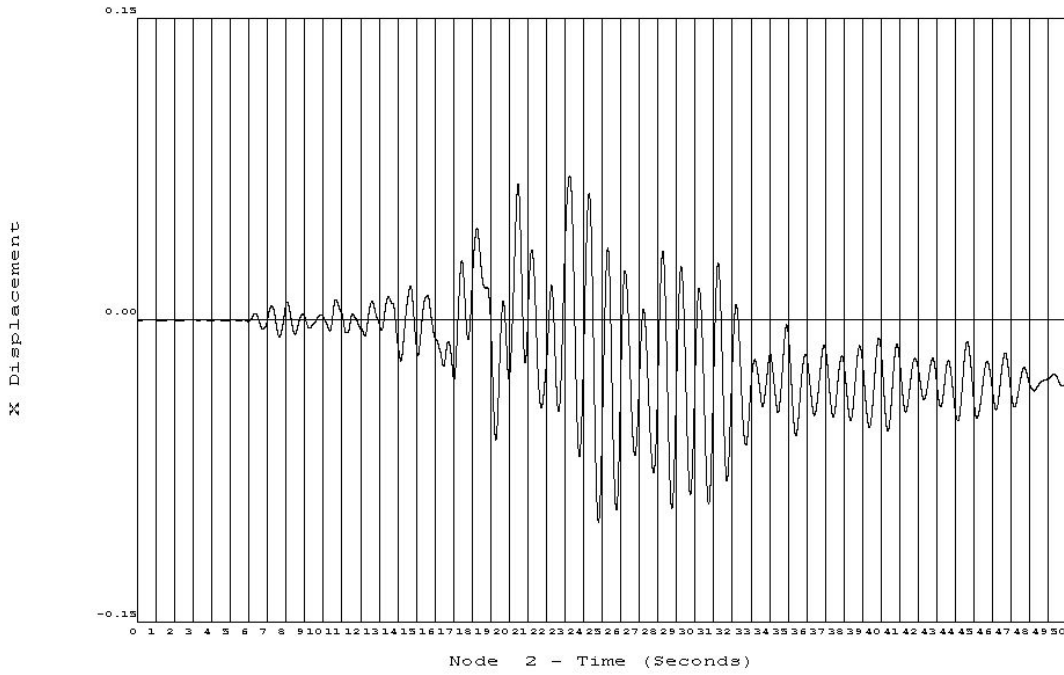
144 Looking at the September response one could almost start the analysis at 15 seconds into the record and might be able to say cut it off at 35 seconds (20 seconds of the record though really should take a bit more of the record)'

145 Looking at the February response one could almost start the analysis at 6 seconds into the record and might be able to say cut it off at 26 seconds (again about 20 seconds of the record though really should take a bit more of the record)

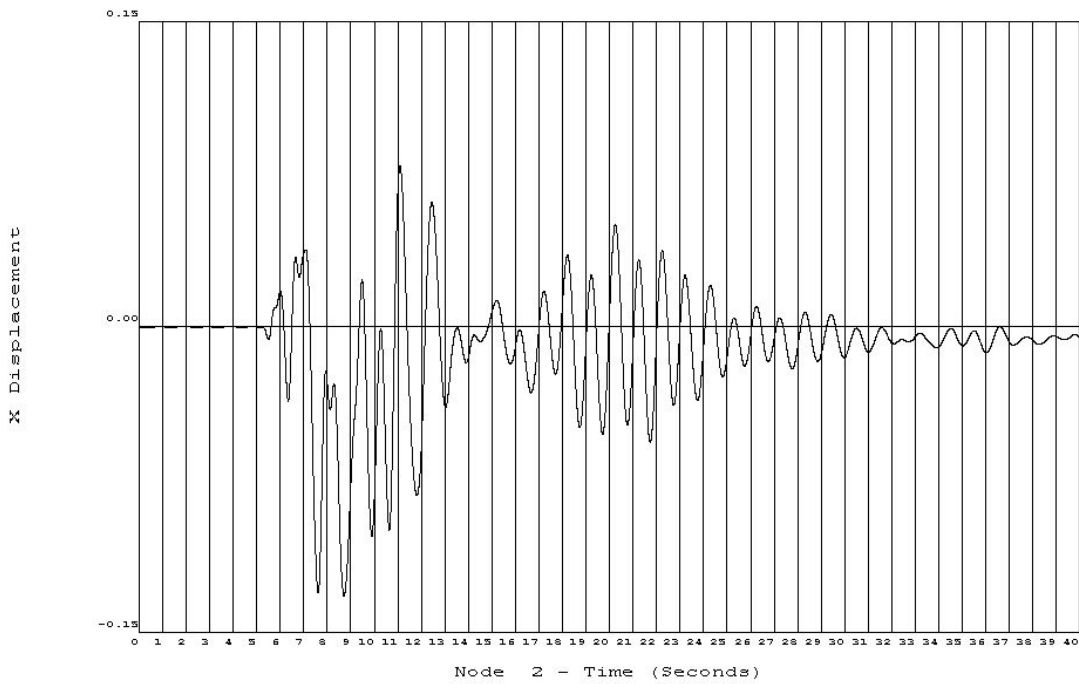
146 I examined the analyses for another building in Christchurch, 6 storeys, about 1.2 second period but very torsional response, modes 1 3 4 6 7 and 11 were torsional modes, 2 and 5 were the first two translational modes in the other direction and lots of vertical modes starting at about mode 8. I only have used the Christchurch Botanic Gardens results for the February records and for that there are about 20 seconds of strong response. I have added the floor displacement and rotation plots to show what I mean.

147 I am not sure how much this helps in terms of the suggested accelerograms for your analyses.

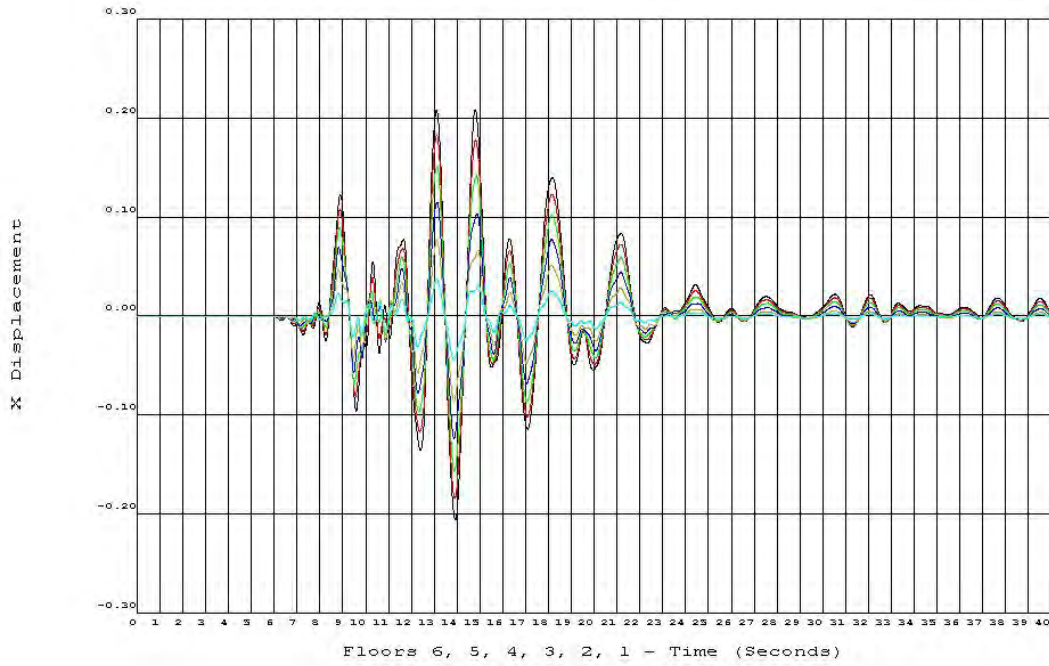
148 The composite plot for Grand Chancellor using the Resthaven S88E accelerograms with 50 seconds of the September record, 10 seconds free vibration, 15 seconds of the Boxing day record, 10 seconds of free vibration and then 50 seconds of the February record is also attached for interest. This building starts out with a 2.8 seconds natural period of free-vibration.



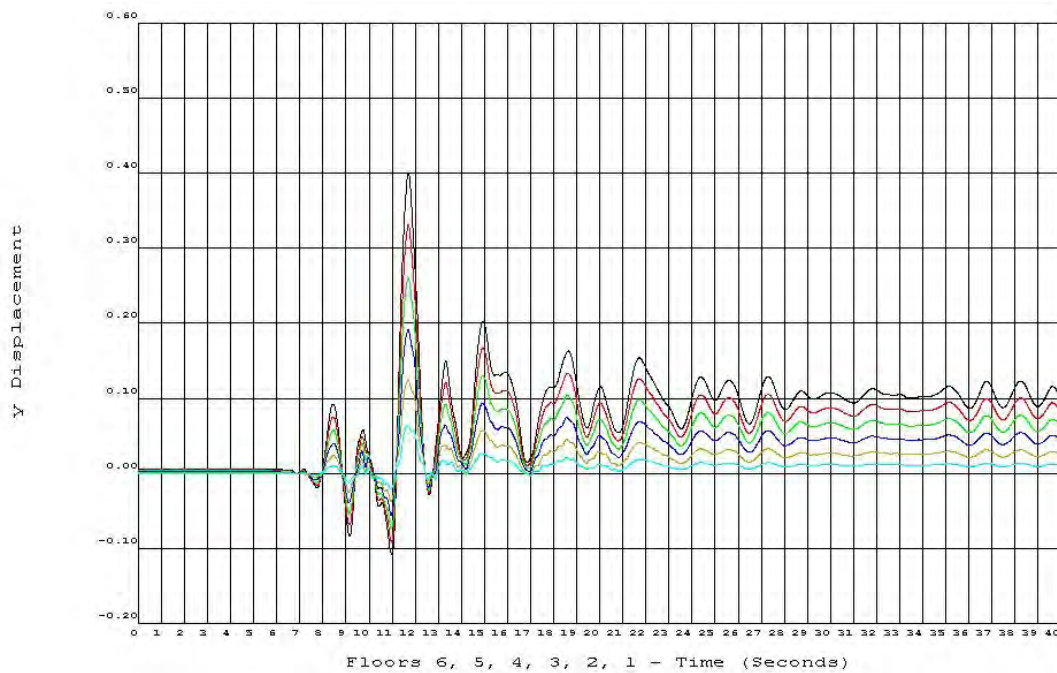
Response of non-linear SDOF building to the September excitation



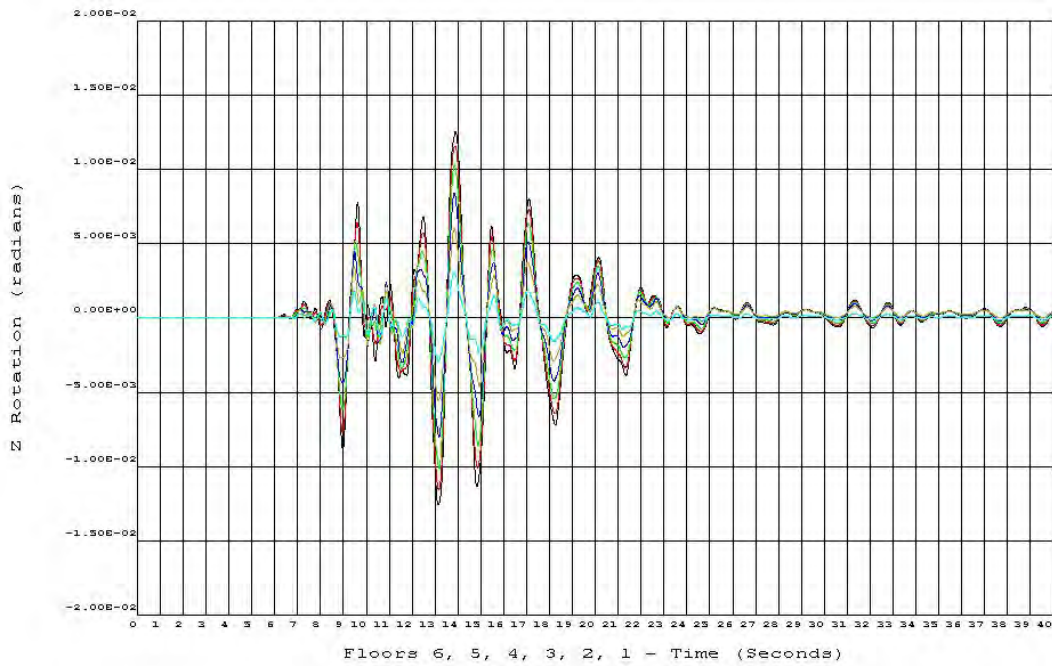
Response of non-linear SDOF building to the February excitation



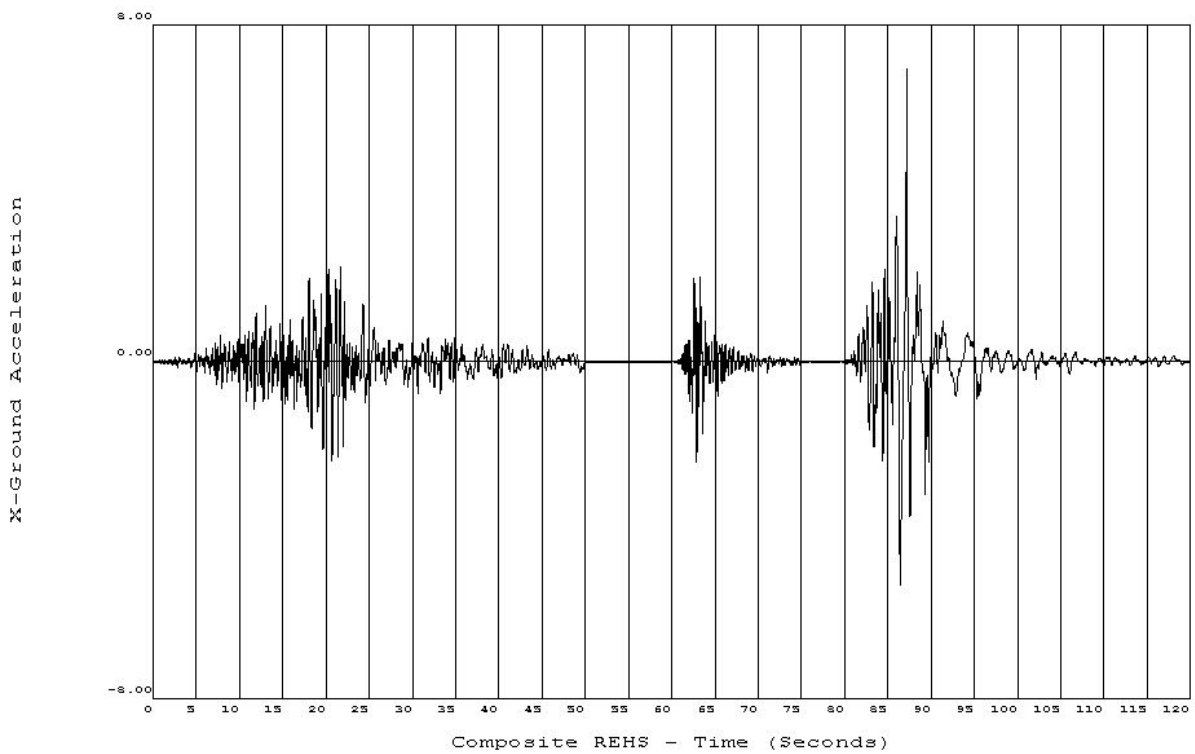
X-direction Displacement of the 6 floors in 6 Storey building - Botanic Gardens record.



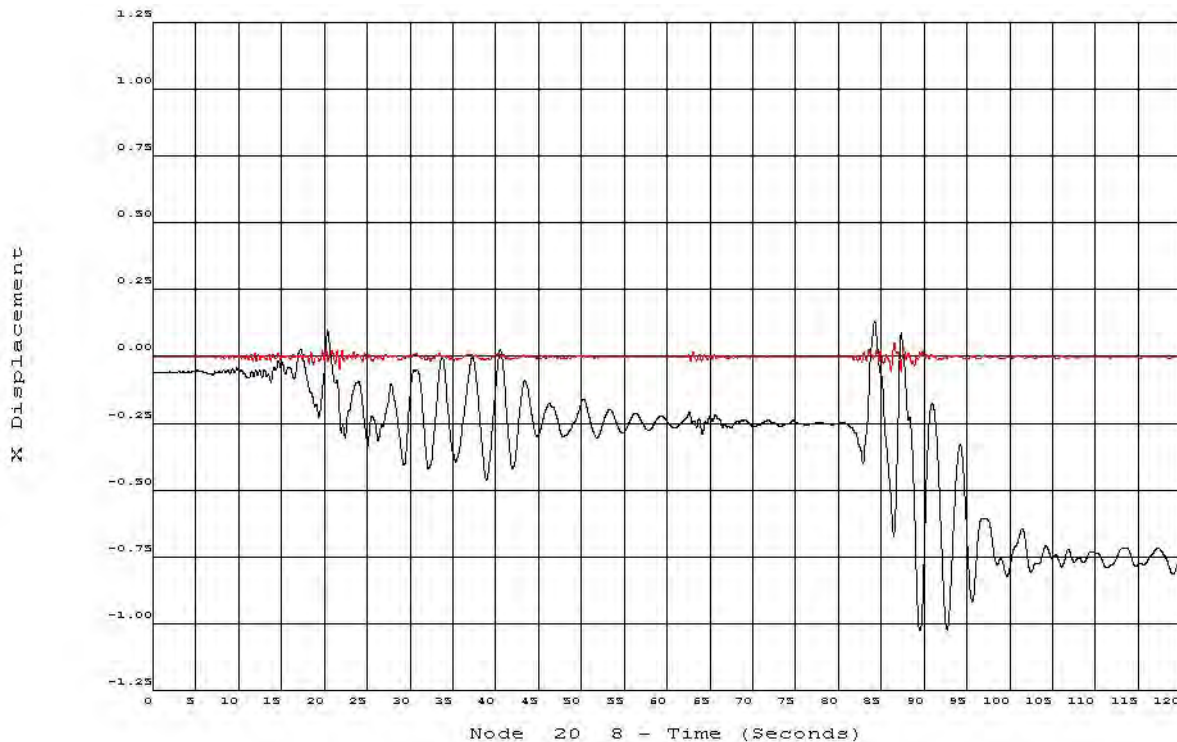
Y-direction Displacement of the 6 floors in 6 Storey building - Botanic Gardens record



Z direction Rotation of the 6 floors in 6 Storey building - Botanic Gardens record



Composite record of the September, Boxing Day and February REHS accelerograms.



Response of levels 8 and 26 of building to the Composite REHS accelerogram.

Comments from Graeme McVerry.

- 149 I have looked at the proposed start and finish times of the various analysis runs. They look reasonably consistent with the durations that I indicated in my comments on Thursday. I assume that the extra 25 seconds on the CBGS February run is to catch any action during the low-amplitude ground motions after the main excitation has died away.
- 150 For the CCCC September record, long-period components are apparent in the input records out to about 60s at velocities of about 50mm/s. The strong input lasts up to about 40s.
- 151 I suspect that both these durations are longer than you would like.
- 152 The input looks insignificant until about 10s, but I have seen comments in papers about record processing that when acausal filtering is used in the ground-motion processing the whole of the early part of the record has to be retained. I presume this is to handle the sorts of features you see in the early part of the February CCCC ground displacement plots.
- 153 Perhaps one strategy would be to run a series of simple one degree-of-freedom oscillators tuned to the peaks of the spectra, and see how long their significant response lasts, to see the duration required for the real run.
- 154 For the February records, it looks as though the ground-motions are virtually over after 30s, but with quite strong ground displacements up to only a few seconds before this. Probably from time 10s to time 30s is required to catch the long-period

response to these records, although the strongest response probably occurs by time 20s.

- 155 I understood during the video conference that Athol had done an extended-duration run for another damaged Christchurch building using a February input motion. That may give the best guidance as to how long the excitation needs to be run.

Comments from Brendon Bradley.

- 156 Regarding ground motion durations:

- 157 The assessment of required input duration should not be based on the intensity of acceleration, but the amplitude of the response with time. A simple way to assess this in advance is to examine the response history of an elastic SDOF of period approximately equal to that of the structure (i.e. $T=1-1.5s$). Based on this I found:

- At least 50 seconds of the Darfield eq-induced ground motion is needed
- At least 25 seconds of the Christchurch eq-induced ground motion is needed.

- 158 I wont specify the start time, in order to avoid a mistake in the interpretation of Compusoft's version of the GeoNet files. The start time must be before the start of the P-wave arrival (i.e. before the acceleration amplitudes change from the background noise level).

- 159 I don't support the consideration of beginning the analysis after the start of the ground motion (i.e. after the arrival of the P-waves at the site). The result of this would be that the initial conditions of the response can be significantly changed, leading to a different response during the strong portion of the ground motion.

- 160 It seems that we are spending more (human) time arguing about how much analysis time it is possible to cut off than the computational time it will take to run the full analysis. Given that the computer can be run overnight without the need for someone to sit beside it there should be conservatism to consider more rather than less (personally I would just consider the full record given that the algorithm convergence is presumably happening without the need for iteration during the initial and final parts of the ground motion).

Comment from Robin Shepherd.

- 161 I fully agree with Brendon's view.

Comment from John Mander.

- 162 Maybe if you used fibre models but with elastic beams and lumped plasticity in columns it will considerable faster!

Comment from Athol Carr following telephone call to John Mander.

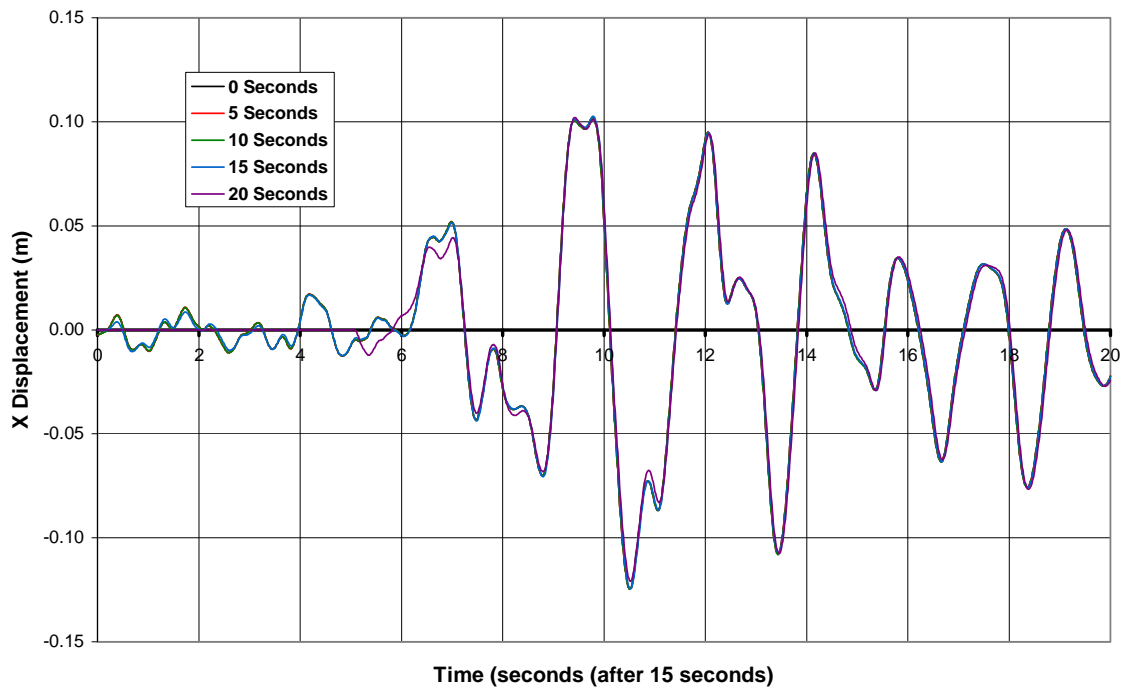
- 163 John also agrees that the very beginning of the earthquake record is not that important in a relative displacement analysis (as most engineering THA use). In traditional engineering analyses we NEVER had the beginning of the record and for 50 years or so this did not worry anyone. The beginning of the record would be important in a total displacement formulation (i.e. for travelling wave models in long

bridges which are easier to set up in a total displacement formulation). Also as we are using analyses which do not have any modelling effects related to significant accumulative damage model, as long as the analyses transverse the major structural responses the duration should be long enough. I am running some comparative analyses, should be complete in about an hour, to see what effects of different starting points will have. I will pass this to all as soon as I have finished.

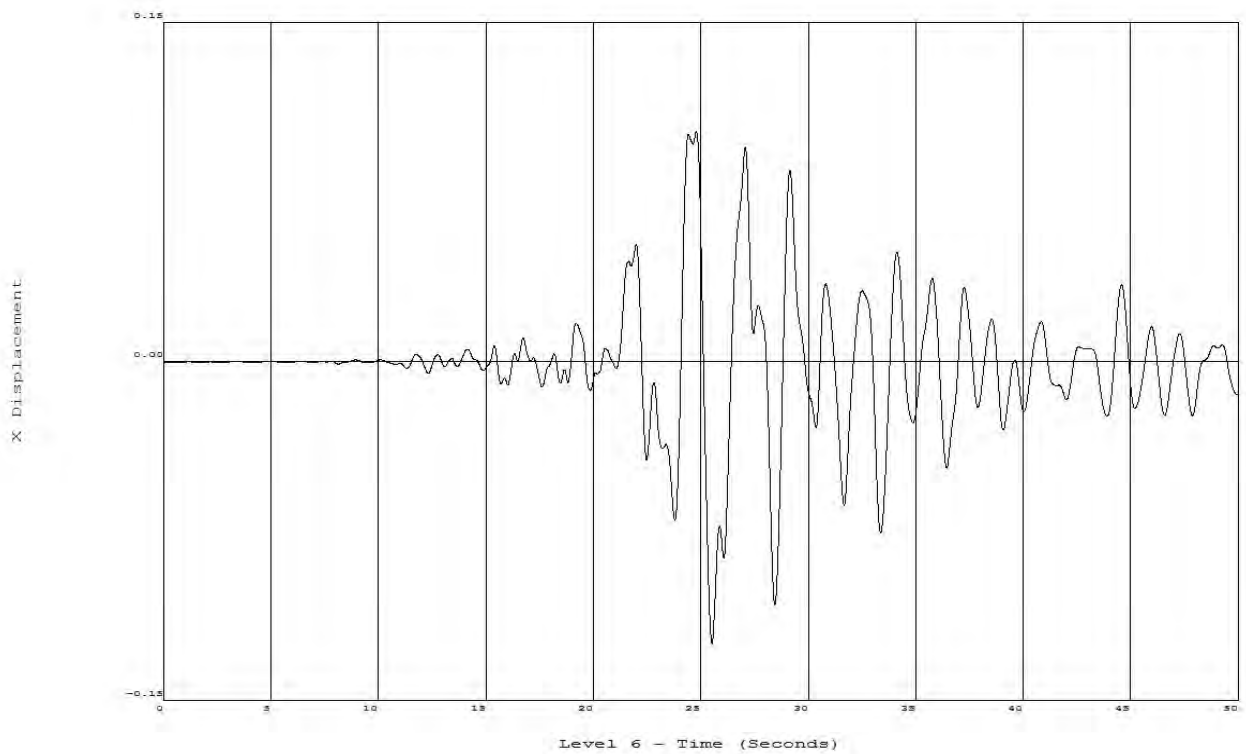
Comment from Athol Carr.

- 164 I show the effects of the choice of truncation of the start of the CCCC September ground motion on the response of a 6 storey building. This building has a natural period in the x direction (largely torsional) of about 1.3 seconds and in the y direction (no rotation) of about 1 second. As seen the initial part of the ground motion has little effect on the response. For almost 50 years we have never had the initial parts of the records at all, the instrument had to be triggered. I have also shown the response for the whole 50 seconds of the analysis and from that, if we are interested in the peak responses, then again we do not need to use all the record. The whole records would be on some use if we were looking at accumulated damage but the models we are using do not have a means of measuring this.
- 165 The analysis used all three components of the input motion, the y direction peaks with a slightly greater displacement but again the effects of ignoring the start of the records is minor.
- 166 I look forward to comments from the panel.
- 167 This is for the CCCC September analysis plotting the results from 15 seconds to 35 seconds from the start of the GNS acceleration record with different start points (as indicated) into the record. The peak responses and the responses in general are not noticeably affected by the omission of the initial part of the record. It might be noted that the first 10 seconds of the record is largely noise but the 20 second start omits quite a part of the initial motion.

Comparisons for Different Starting Times



Results for a 6 storey building with natural period of free vibration of 1.3 seconds in the X direction and 1.1 second in the Y direction.



Response for the 50 second ground motion.

Comment from Athol Carr to Marcus Elliot of the Royal Commission.

- 168 I have had some response about the duration of the records to use. There were suggestions that we should run the whole record including the arrival of the P-wave. For virtually all computer analyses over the past 50 years we have never had the arrival of the P-wave on the records. The old instruments had to be triggered so the beginning of the record was missing. Further, traditional engineering NLTHA practice has been to stop the analyses after the major part of the shaking has passed. The exception is if we have models that compute damage indices etc. where the number of cycles and accumulated damage, energy dissipation are computed or where the engineer wants to know the residual displacements in the structure, then the longer duration of the analysis is important.

Comment from Athol Carr.

- 169 Virtually all structural analysis programs compute relative-to-the-ground structural displacements and therefore the small accelerations occurring before the strong motion starts has little effect. If one has analyses that use total displacement formulations, i.e. when there multiple support inputs, then the starting parts of the records are much more important.

CTV Non-linear Time-History Analyses Report

Damping,

Comment from Athol Carr to Compusoft.

- 170 I am happy with the 5% damping model you are using, it has its problems in the lower frequencies in having less damping and in the high frequencies, having too much damping. What you have is a compromise. I am not sure what level of equivalent structural ductility you are indicating in the February event but a structure ductility of 4 would imply about a halving of the frequencies and for which the secant stiffness would be about a quarter of the original. The tangent stiffness could be a lot less than this but in a tangent stiffness Rayleigh damping model only the stiffness changes, i.e. relative change in the Rayleigh Beta and not in Alpha.

Comment from Nigel Priestley.

- 171 I haven't been a party to discussions on the changes, but I infer from the letter that the values of period at which 5% damping applies have been chosen to result in an effective 3.3% damping at the fundamental mode, and that this is based on predicted ductility. If so, I'm OK with it. Please confirm.

Beam Pull-out at Exterior Columns.

Comment from John Mander.

- 172 I'll have to take a look at +ve beam rotation/pullout, but any suggestions, let me know.

Comment from Nigel Priestley.

- 173 No comment.

Beam-Column Joints.

Comment from Athol Carr

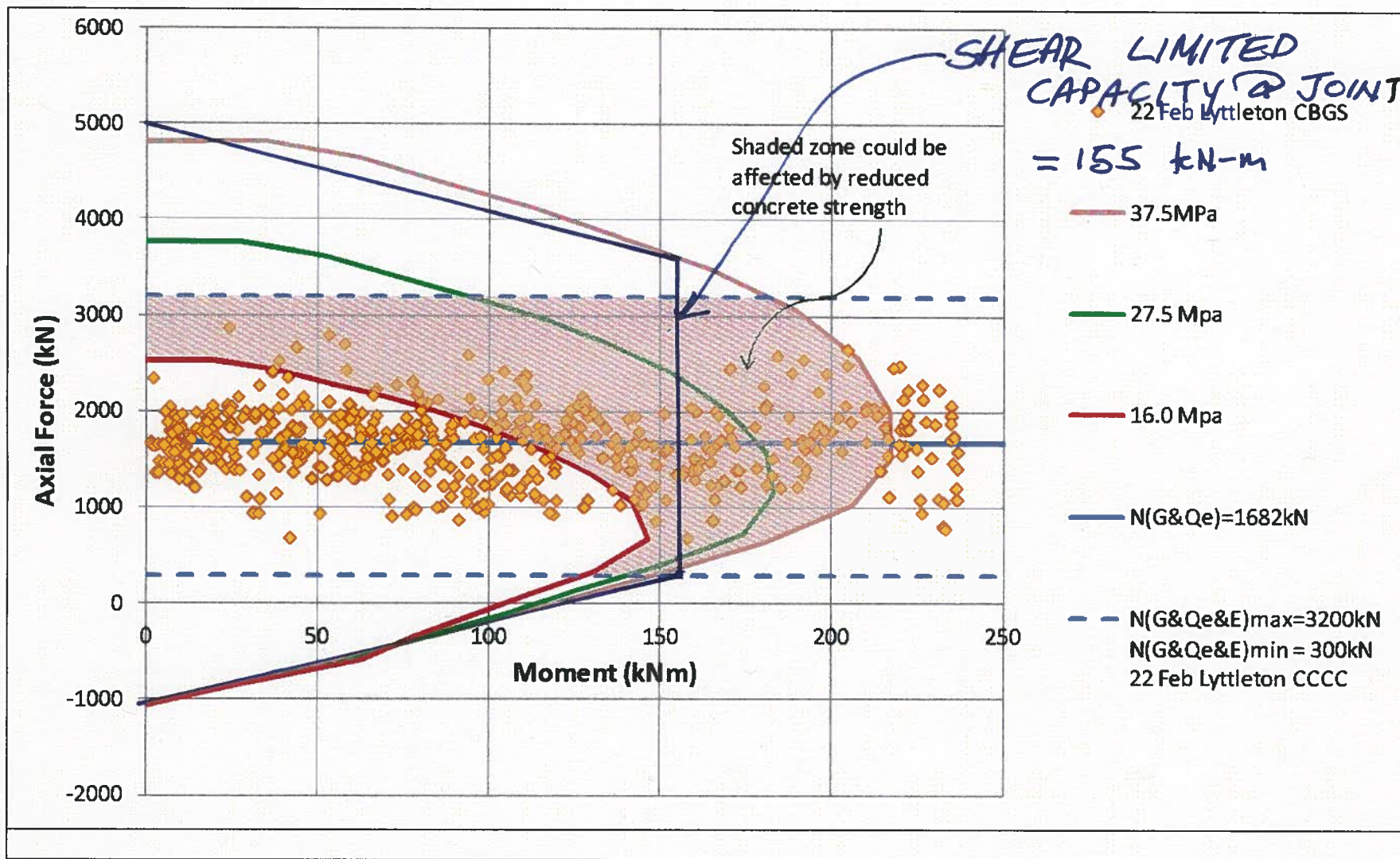
- 174 The agreement was that the joint behaviour will be modelled as a modified column-base plastic hinge.

Comment from Athol Carr to John Mander.

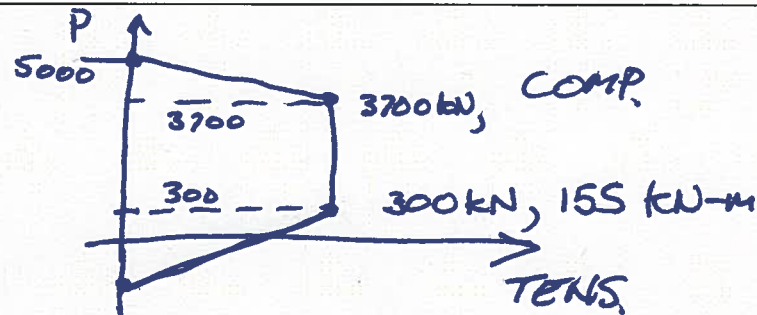
- 175 We probably cannot look at every joint but may do with a suitable strength of a typical, or critical joints, and at least get them near right. The strengths look as if we should use 1.5 design strengths. We do not have a decade to dot every i or cross every t. We need to get the analyses underway.

Comment from John Mander

- 176 As you know I consider $f'_c = 1.5 f'_c$ [specified] = 37.5 MPa for all joints, beams, slabs and upper columns.
- 177 Even the joint shear capacity will require extra work. Previously, I had only calculated the solution for a few critical locations.
- 178 I have some questions about what SAP can actually do. I was surprised that they want to use a fiber model, I doubt that it is helpful.
- 179 What I am seeing in my calculations is that there is a CONSTANT moment capacity at the joints limited by shear (~155kNm) over all the moment range for axial loads of 300 to about 3300kN. See provisional solution attached.
- 180 This makes it really easy to model; just a beam model would suffice, as axial variable axial load interaction is no longer needed. In fact, because they previously did not see axial loads below 300 kN, we could just specify a blanket capacity regardless of axial load.



Simplified final joint-moment capacity
PROVISIONAL
(calcs to follow).



Comment from Barry Davidson

181 Our proposal to proceed is attached.

COMPUSOFT

ENGINEERING

PO Box 9493, Newmarket, Auckland, New Zealand.
Telephone: +64 9 522 1456 Website: www.compusoftengineering.com

15th June 2012

Professor Athol Carr
Canterbury Earthquakes Royal Commission,
PO Box 14503, Christchurch Mail Centre,
Christchurch 8544.

Subject: Beam Column Joint Model

There has been much comment on the modelling of the beam-column joint. It is difficult to develop a suitable analytical model for the beam-column joint detailed in the CTV building that appropriately provides interaction with the axial force in the joint. Compusoft would like to promote the use of a simplified mechanism whereby a nonlinear element is incorporated to the model that connects the beams to the columns. This nonlinear element would provide for moment vs rotation behaviour with appropriate backbone and hysteretic form that would allow for strength and stiffness degradation of the joint. An overview of the model is presented in Figure 1 below.

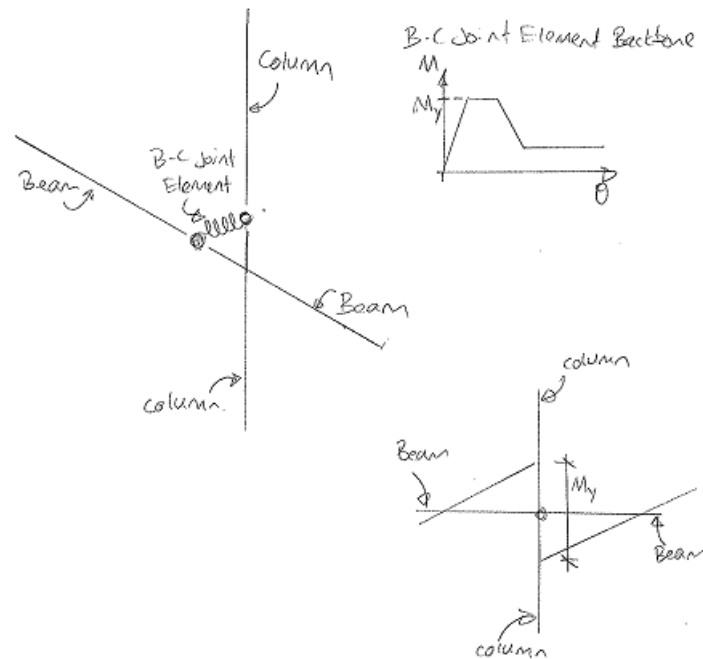


Figure 1: proposed beam-column joint model

In this model the backbone curve would be derived with consideration of the joint axial load that is present for the gravity combination (which would vary across the building). Whilst this model would not accommodate axial-moment interaction as a result of earthquake induced actions, it would consider the average joint stress throughout the earthquake, which we feel is acceptable given the level of uncertainty in the mechanism.

Recent suggestions have promoted using FEMA 356 methodology to consider the behaviour of the beam-column joint. We have concerns that the FEMA 356/ASCE-41 beam-column joint model is both empirical and conservative. Our view on the conservatism of the model is supported by review of recent comprehensive research on the subject both internationally and in New Zealand (Hassan et al. 2010; Moehle et al. 2006; Weng Yuen 2010).

Compusoft would promote that the yield capacity of the beam-column joint (denoted as ' M_y ' in Figure 1) be derived following similar principles as undertaken previously (refer Appendix B of Compusoft Report 11033-0). There is clearly significant uncertainty (and debate) regarding the deformation capacity of the beam-column joint. To alleviate this uncertainty a bilinear model could be considered with the deformation demands assessed via post-processing of results.

We feel that this approach would provide a suitable analytical model of the beam-column joint, and provide reasonable confidence in the overall structural behaviour.

Yours sincerely,



Tony Stuart
Structural Engineer

References

- Hassan, W. M., Park, S., Lopez, R. R., Mosalam, K. M., and Moehle, J. P. (2010). "Seismic Response of Older-Type Reinforced Concrete Corner Joints." *Ninth U.S. National and 10th Canadian Conference on Earthquake Engineering*, Toronto, Canada.
- Moehle, J. P., Lehman, D., and Lowes, L. N. (2006). "Beam-Column Connections." *PEER/EERI Seminar on Nonductile Concrete*, Accessed at: peer.berkeley.edu/research/powerpoint/non_ductile_concrete/Joints - Moehle c.ppt (Jun. 15, 2012).
- Weng Yuen, K. (2010). *Selective Weakening and Post-Tensioning for the Seismic Retrofit of Non-Ductile RC Frames*. The University of Canterbury, Christchurch, New Zealand, 672p.

Comment from Derek Bradley.

- 182 With regard to John's comment about the joint capacities being independent of axial load, we propose the following model for the beam column joints. Any comments would be appreciated.

Comment from Barry Davidson.

- 183 Please see the attached letter from Compusoft requesting action and supporting our suggested procedure to obtain data as described earlier.

COMPUSOFT

E N G I N E E R I N G

PO Box 9493, Newmarket, Auckland, New Zealand.
Telephone: +64 9 522 1456 Website: www.compusoftengineering.com

15th June 2012

Professor Athol Carr
Canterbury Earthquakes Royal Commission,
PO Box 14503, Christchurch Mail Centre,
Christchurch 8544.

Subject: Information Flow

Compusoft is concerned at the lack of response to its request for information relating to revisions to the NLTH analysis, and the perception of some panel members regarding the capabilities of SAP2000, and the analysis progress to date.

The NLTH analyses are being adjusted and re-run due to ARCL concerns over some of the analysis parameters in the original analysis. ARCL's representatives have requested and promoted that certain element behaviour be examined. Compusoft has no problem in refining the model to investigate the concerns of ARCL, however we note that in order for us to progress these analyses we require the previously requested input data to be provided by ARCL's representatives. No relevant information has been provided to date.

Furthermore it seems that more time has been spent discussing the analysis methodology rather than the provision of essential input information. Compusoft is responsible for incorporating element performance into the analysis model as they are best placed to do so. We suggest that the desired performance of each element be developed by ARCL's representatives without mind to how it will be implemented - Compusoft will provide guidance on that.

There seems to be an impression that Compusoft have been waiting on confirmation of payment prior to commencing work. We would like to confirm that this is not the case and in fact, Compusoft has been working on refining the analysis for several weeks. During this

June 2012

time we have been developing, implementing, and testing several items that ARCL's representatives wished to be examined more thoroughly. Not the least of which is P-M-M column interaction, which we have now been informed is no longer required despite this being identified as a weakness in the original analysis by ARCL's representatives.

The document that we sent to you yesterday was to promote an efficient way of getting the information previously requested. We requested that ARCL's representatives fill in the missing information rather than discuss the various inputs via e-mail correspondence. The analysis model needs to be adjusted and run as a matter of urgency.

We note that whilst we have not seen Professor Manders calculation on beam column joint capacity, the initial findings that joint capacity is essentially independent of joint axial load is contrary to the test data and research that we have seen to date. Professor Manders calculations may be based upon recent research and understanding of these types of joints that we have not had access to. However we believe that given the difference between what we previously understood, and information presented to us, we believe it would be prudent to have this information independently reviewed prior to implementation in the analysis model.

Yours sincerely,



Barry Davidson
Engineering Director

Comment from John Mander.

- 184 I've done some stuff for the concrete part of the analysis. The numbers changed a little from yesterday's provisional results for the joint-shear moment detuning. The good news, I believe is that fiber-elements are NOT needed, just a regular Takeda model with lumped plasticity will do the trick.

Response to CompuSoft Letter of 14 June.

by J. B. Mander.

The plastic hinge should be based on

- (1.2) "yield penetration arising from the interface of the lap upwards ($\sim 6db$) and downwards ($\sim 6db$). This amounts to

$$l_p = 2 \times 4400 \epsilon_y db$$

$$l_p = 2 \times 4400 \times \frac{448}{205000} \times 20 = 192 \text{ mm.}$$

which seems about right, take as

$$\boxed{l_p = 200 \text{ mm} = 0.15 h_c}$$

- (1.1) As above use $l_p = 200 \text{ mm}$

BEAM COLUMN JOINT ZONES.

All concrete take as 1.5 f_c specified for joints, same as floor \Rightarrow

$$f_c = 25 \times 1.5 = 37.5 \text{ MPa}$$

$$\sqrt{f'_c \text{ MPa}} = \sqrt{37.5} = \underline{6.124 \text{ MPa}}$$

Area of joint limited from column $A_j = \frac{\pi}{4} \times 0.4^2 = 0.1257 \text{ m}^2$
(its actually square through beam).

According to FEMA 356

$$V_n = \gamma \sqrt{f'_c \text{ psi}} A_j \quad (\text{Eq 6-5})$$

where $\gamma = 10$ in psi units (table 6-10 FEMA-356)

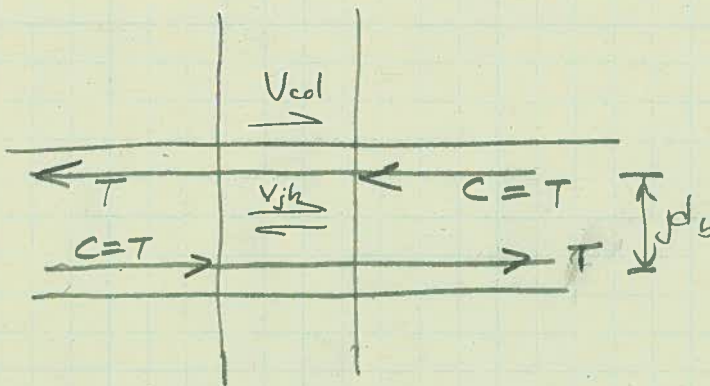
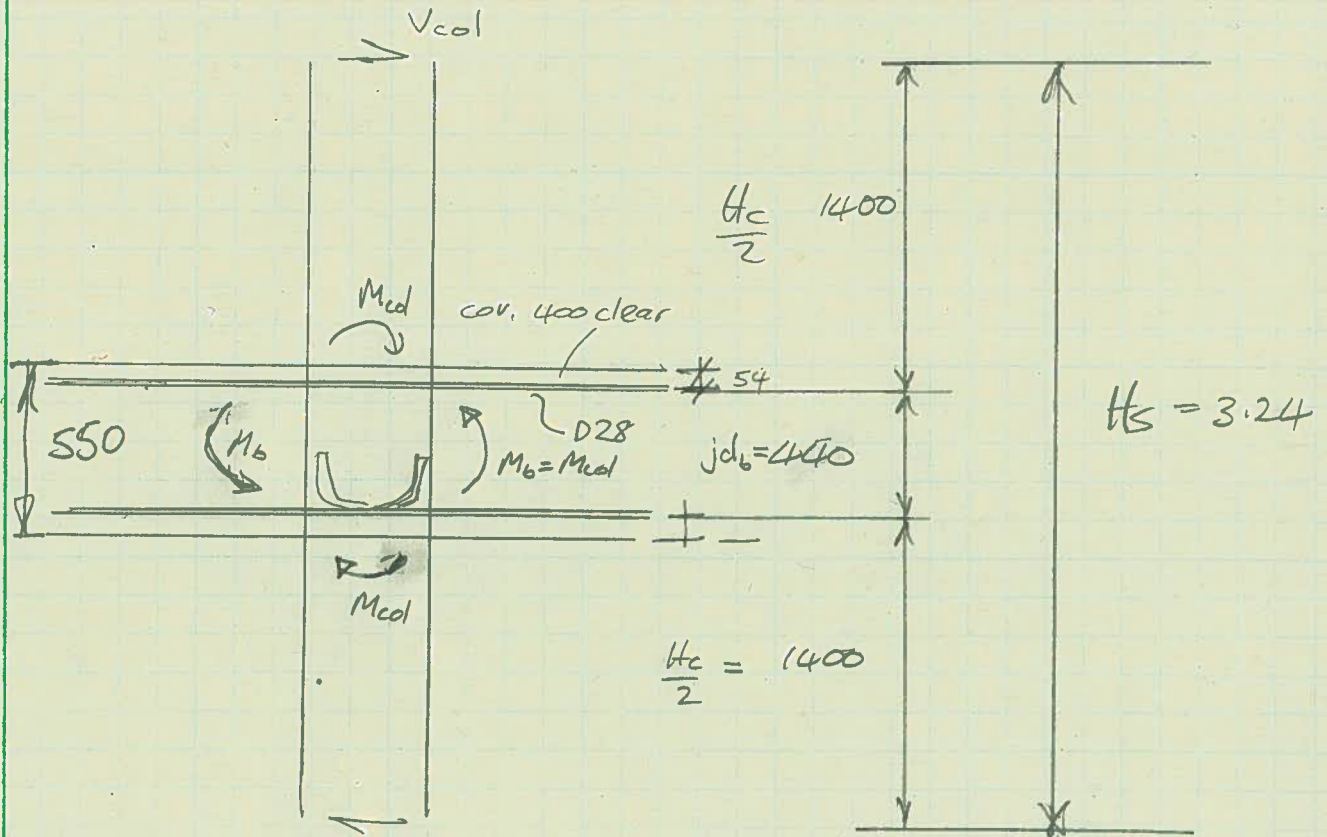
$$\therefore \gamma (\text{MPa}) = \gamma_{\text{psi}} / 12 = 10/12$$

$$\therefore V_n = \frac{10}{12} \sqrt{f_c \text{ MPa}} A_j \quad \text{N}$$

$$V_n = \frac{10}{12} \sqrt{37.5} \times 125.7 = \underline{640 \text{ kN}}$$

Exterior joint with transverse beams $\gamma = 8$ psi

$$\therefore \text{Exterior vs interior} = \underline{80\% \text{ capacity.}}$$



$$V_{jh} = 2T - V_{col}$$

$$\text{but } T = M_b = M_{col} / j_{db} = \left(V_{col} \frac{H_c}{2} \right) / j_{db}$$

$$\therefore 2T = V_{col} \frac{H_c}{j_{db}}$$

$$V_{jh} = V_{col} \left(\frac{H_c}{j_{db}} - 1 \right)$$

$$\text{but } H_c = H_s - j_d$$

$$\therefore V_{jh} = V_{col} \left(\frac{H_s - j_d - j_d}{j_{db}} \right) \Rightarrow V_{col} = V_{jh} / \left(\frac{H_s}{j_{db}} - 2 \right)$$

And thus $M_{col} = V_{col} \frac{H_c}{2}$

$$M_{col} = \frac{V_{jh} H_c / 2}{2 \left(\frac{H_s}{jcb} - 2 \right)}$$

$$M_{cd} = \frac{V_{jh} 4400}{2 \left(\frac{3240}{440} - 2 \right)} \quad \text{kN-m}$$

$$M_{col} = 0.261 V_{jh} \quad \text{kN-m}$$

∴ Joint shear limiting moment capacity

$$M_{col} = 0.261 \times 640 \text{ kN-m}$$

$$M_{cd} = 166 \text{ kN-m} \quad \text{INTERIOR JOINTS}$$

Exterior Joints

$$M_{cd} = 0.8 \times 166 = 133 \text{ kN-m}$$

This is in E-W direction

$$\therefore \sum M_b < 2 \times 133 = 266 \text{ kN-m} = 2M_{cd}$$

Beams: $f_y = 448 \text{ MPa}$

Top steel 4-D28 = 2463 $T = 1103 \text{ kN}$

Bottom steel 2-D28 $\Rightarrow T = 552 \text{ kN}$

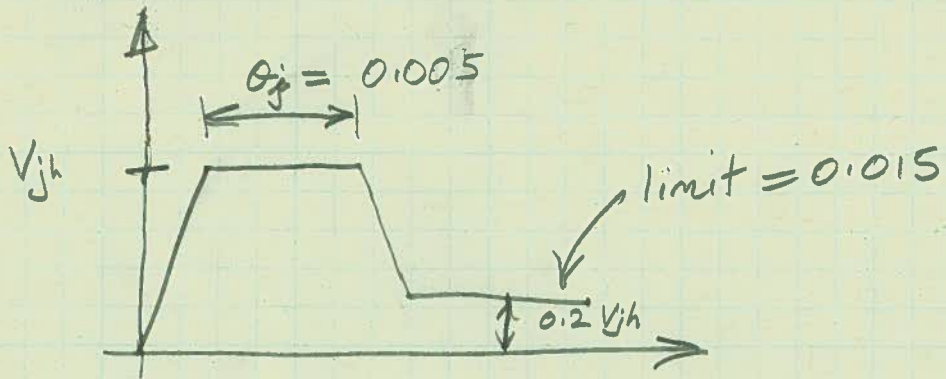
Topst. $M' = T' j d = 1103 \times 0.44 = 486 \text{ kNm}$

bot.st. $M = T j d = 552 \times 0.44 = 243 \text{ kN-m}$

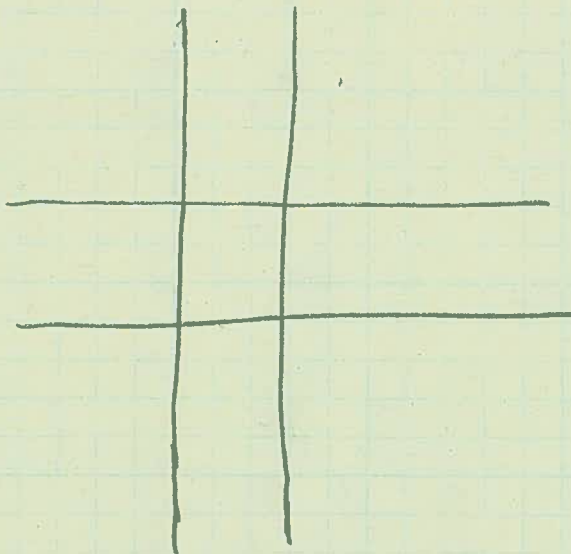
For sway with +ve moments bottom bars pull out
 $M_b = 243 < 266$ beam hinging occurs.
 For sway with -ve M column " "
 $M_s = 486 > 2M_{col} = 266$

Rotations on joints
Interior

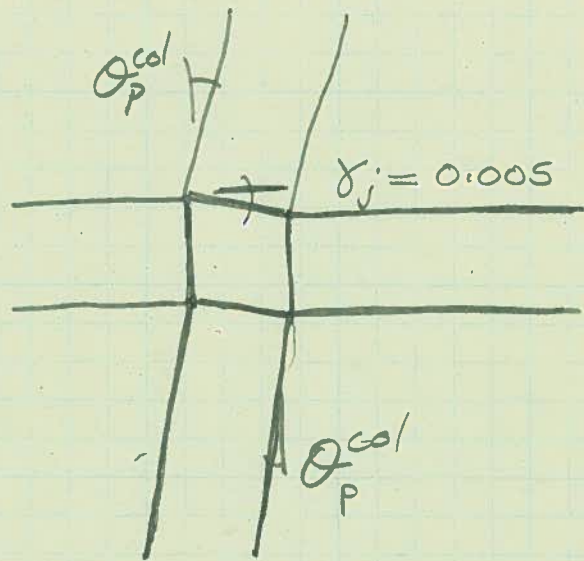
Table 6-9 FEMA 356.



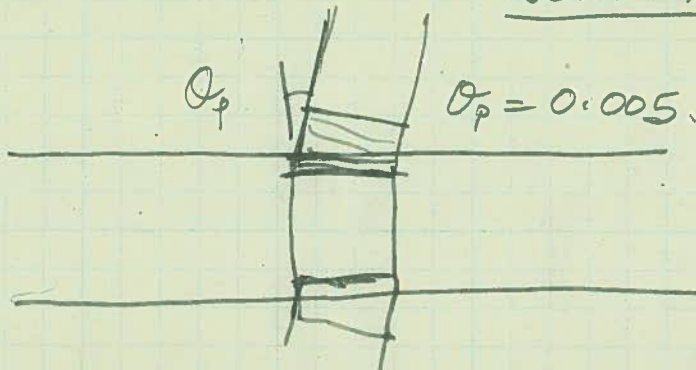
Converting this into a beam column joint hinge



B-C Joint.



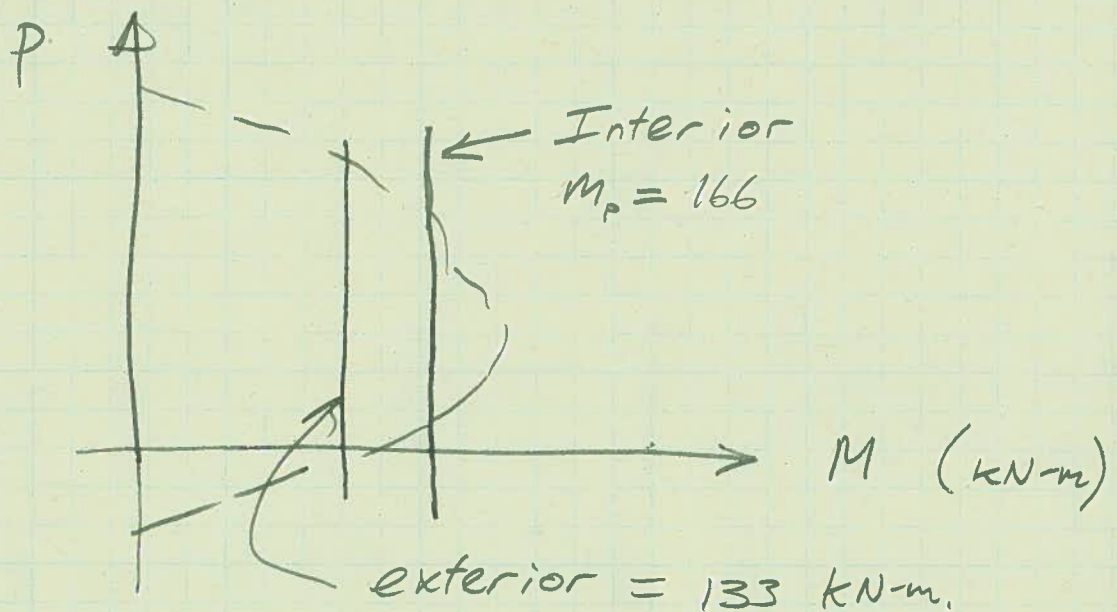
Joint Distortion



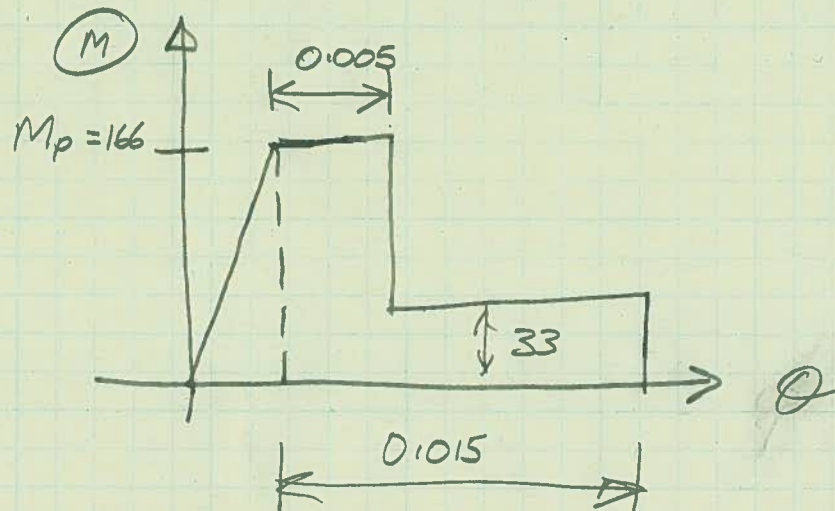
SAP 2000 Modeling

Summary for column properties

Because joint capacity according to FEMA 356 is invariant with axial load (according to Table 6-9) then columns can be modeled just like beams with Takeda and

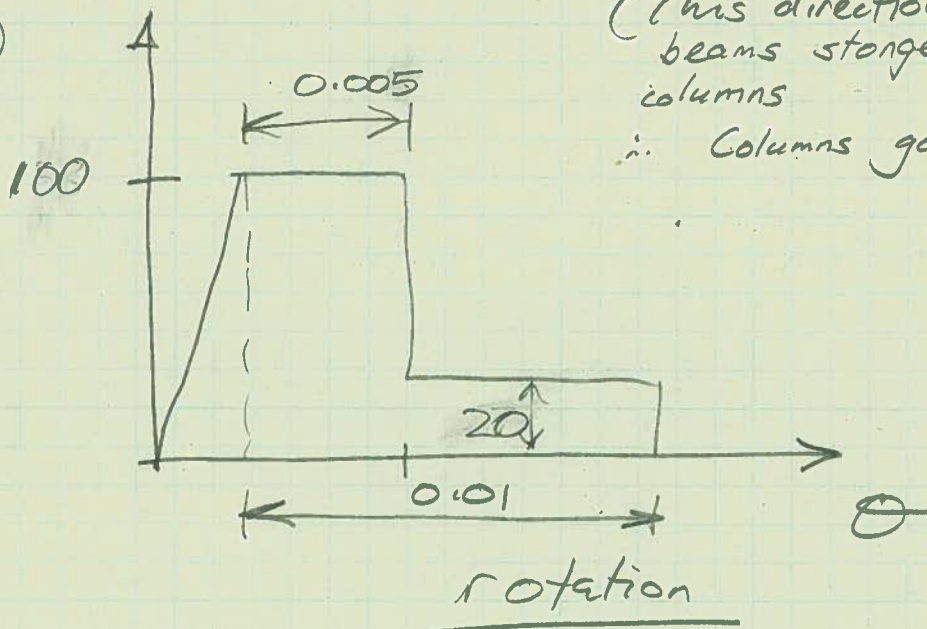


Columns E-W interior



Columns N-S Exterior.

(M)



(This direction
beams stronger than
columns
 \therefore Columns govern).

$$\gamma_j = 6 \quad \text{c.f.} \quad \gamma_j = 10 \quad \text{Interior}$$

Exterior joint
w/o transverse
beams

$$M = 166$$

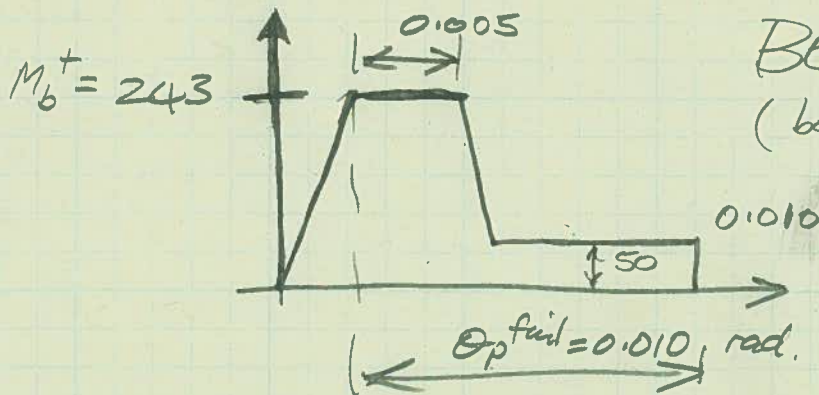
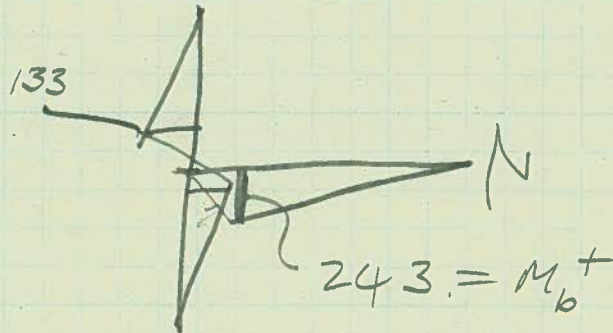
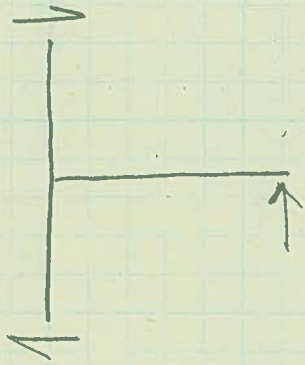
$$M = \frac{6}{10} = 100$$

Columns @ Exterior line A.

$$M_{col} = +133 \quad \text{kN-m}$$

$\Sigma M_{col} = 266$ so set these as usual

$$M_b = 243$$



BEAM Moment
(bottom-bar pullout effect)

Assumed to be governed by joint

Analysts to check axial load in lower columns along line (A) and line (F)

If $P > 0.4 f_c A_g$

$$P \geq 0.4 \times 37.5 \times (\frac{\pi}{4} \times 400^2) = 1885 \text{ kN}$$

IF $P > 1885 \text{ kN}$ THEN : \rightarrow

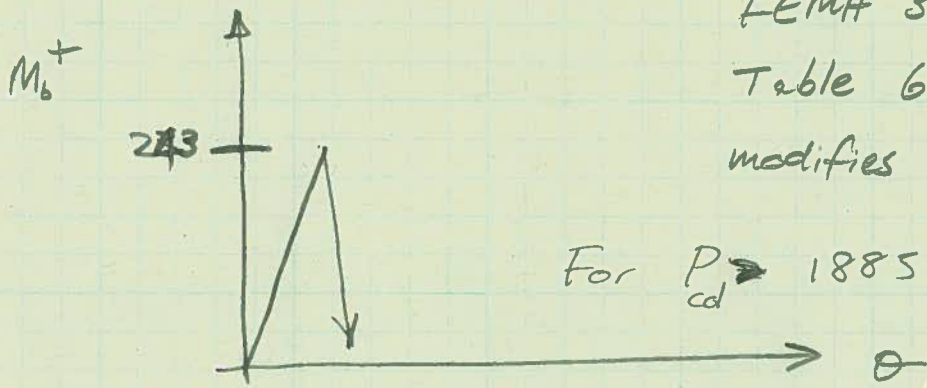
Joint is brittle, model as follows.

(Note this may not be a problem because tributary bay areas are small).

FEMA 356

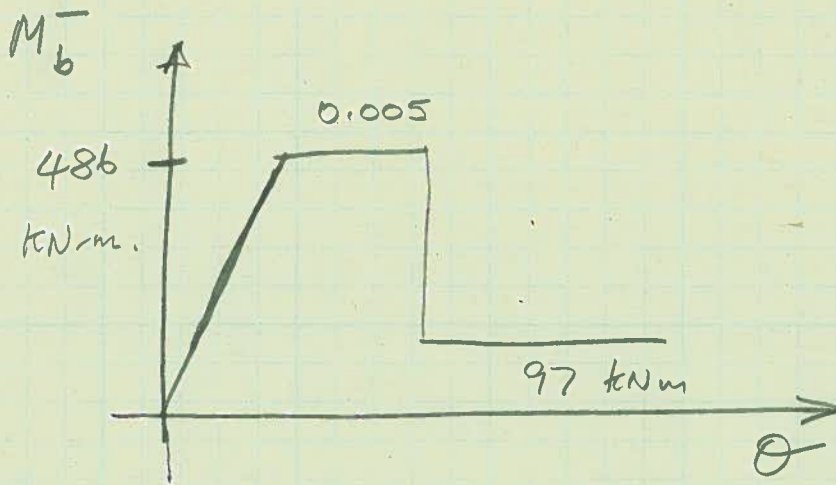
Table 6-9 ii

modifies accordingly.



Elastic behavior only

Negative Moment Effect of Joints at Line (A) and (F)



Because $M_b^- \geq \sum M_{col}$
 $486 > 2 \times 166 = 332 \text{ kN-m}$

Negative beam hinging is unlikely.

Nevertheless, model it much like a joint.

⑤ CONCRETE STRENGTH

Use $f'_c \text{ expected} = 1.5 f'_c$

Everywhere.

Comment from Athol Carr following request from Barry Davidson above.

- 185 I presume John implies that the axial force interaction is not important for the joint hinges (as column hinges at the bases of the columns) but does this also cover the other column hinges as this seems to require the use of fibre models in SAP2000. Maybe if the real yield is in the joints then maybe the columns are NOT a problem and simpler column hinging models for the columns are ok. Would this be a reasonable assumption?

Comments from John Mander.

- 186 The columns are limited by joint shear. Using FEMA 356 this is invariant with axial load, so that it means that you can use a beam model based on Takeda-this will be considerable faster. I have modelled the joints as lumped plasticity (=200mm long) at column ends. You can set the column axial stiffness (it should be proportional to the average axial load) as constant and for the interior connections you may speed things up by keeping the beams elastic.

Comment from Tony Stuart.

- 187 Please find attached our proposed methodology for modelling of the beam-column joint for your review and comment.

Subject: Development of a model for beam-column joints of the CTV building
CEL Reference 12026.03 Revision 0
Author: Nicholas Brooke

1. Introduction

Discussions regarding proposed alterations and enhancements to the CTV Building non-linear analysis model have made it clear that a key enhancement desired by members of the Royal Commission Expert Panel is implementation of non-linear beam-column joint behaviour. This is considered critical due to the highly deficient nature of the beam-column joints, and their resulting potential to fail prior to the occurrence of either beam or column hinging.

Realistic non-linear modelling of deficient concrete beam-column joints is unfortunately not a trivial exercise. Several factors make it difficult to accurately model the joints of the CTV building. These include:

- The response of deficient joint is still a highly active research topic;
- There are fundamental international disagreements regarding the mechanics and behaviour of concrete beam-column joints;
- Simple models of deficient beam-column joints available in the literature are typically intended for assessment of existing structures, and are thus considered to be unduly conservative for forensic engineering purposes;
- Rigorous joint models available in the literature are not suitable for implementation in commercial finite element software, particularly for a model containing multiple beam-column joints such as that of the CTV building.

This document presents discussion related to the adopted model for the CTV beam-column joints. This discussion is divided into a number of topics. Discussion of some these topics includes non-comprehensive review of relevant literature where this has been used as the basis for defining the beam-column joint model.

2. Implementation

A number of methods can be used to incorporate beam-column joint response within a structural finite element model. The method adopted by CompuSoft Engineering Limited for the CTV structural model is to develop a non-linear rotational spring representing the beam-column joint shear stress-shear strain response, with this spring located at the node representing the intersection of beams and columns at the beam-column joint. The moment applied to the joint can be related to the shear stress in the joint based on the geometry of the structure. Details of the calculations defining this relationship are presented in Appendix A.

The rotational spring used to model the joints has the following features:

- Independent, non-interacting properties for orthogonal axes of loading.
- No moment-axial load interaction.
- A moment-rotation backbone curve based on the joint shear stress-shear strain backbone curve described in the following sections and the calculations presented in Appendix A.
- Hysteretic response based on a “Pivot” hysteresis model (Dowell et al. 1998).

Review of relevant literature has shown that there is significant disagreement between sources with regards to both the peak strength of deficient beam-column joints, and also the force-deformation relationship that is appropriate for deficient joints. This document considers these two issues separately, first considering an appropriate backbone curve defining the relationship between joint deformation and relative or normalised strength, and then considering the peak strength expected from a beam-column joint.

3. Definition of relative stress vs deformation backbone curve

In this section an appropriate backbone curve relating joint deformation to joint stress is discussed and then defined. In order to clarify the discussion, the backbone curve is defined initially based on relative joint stress, with a relative joint stress of 1.0 being taken as equal to the maximum joint shear strength.

Figure 1 shows a number of backbone curves for the relative stress-strain response of deficient beam-column joints. As indicated, these curves have been drawn from a wide

variety of sources. It is evident from the plot that there is considerable variance between the postulated curves. Brief details of each curve are as follows:

- The FEMA 356/ASCE 41 curve is taken from a widely used U.S. document outlining procedures for assessment of existing buildings.
- The curve recommended by Park (2010) was based on testing of four exterior beam-column joints. The deformation at peak stress is determined based on joint geometry.
- The curve proposed by Weng Yuen (2010) is for exterior joints, and is a modification of similar curves published widely by other researchers.
- Sharma et al. (2011) specified in the paper that “the plot of principal tensile stress vs. joint shear deformation ... seems appropriate”, but did not show supporting experimental data. Review of the referenced data (Clyde et al. 2000; Pantelides et al. 2002) suggests that the adopted curve was a “lower bound” appropriate for assessment but less so for prediction.
- Birely et al. (2012) provided no data regarding the descending branch of the backbone curve. They calibrated their curve against data from interior beam-column joint tests.

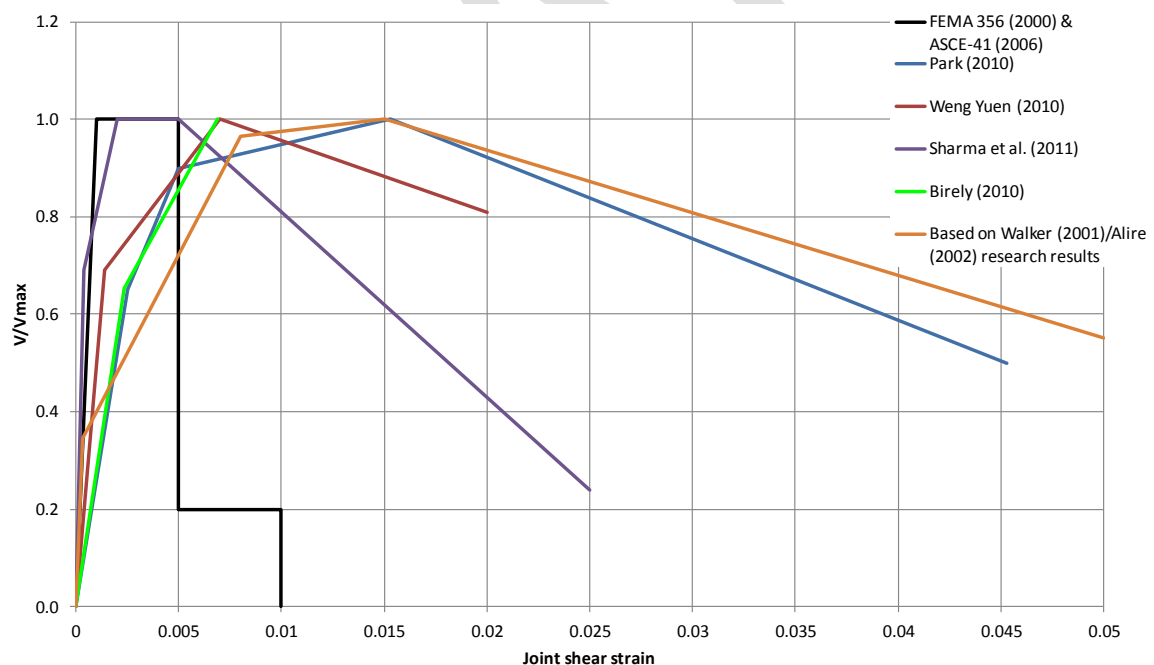


Figure 1: Backbone curves from various sources (Alire 2002; ASCE 2006; Birely et al. 2012; S. Park 2010; Sharma et al. 2011; Walker 2001; Weng Yuen 2010)

- The final curve plotted was developed by Compusoft Engineering Limited based on review of data presented by Walker (2001) and Alire (2002). It represents an approximate average of the stress-deformation response measured during 11 tests on interior beam-column joints. Data from these 11 tests is shown in Figure 2.

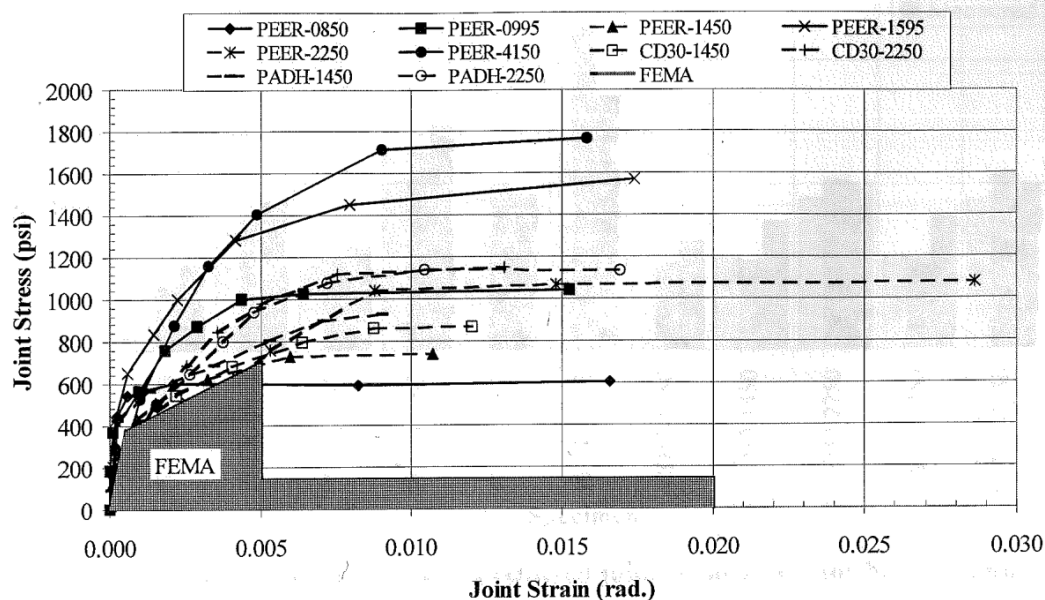


Figure 6.18: Joint shear stress-joint shear strain data with the FEMA model.

Figure 2: Joint shear stress vs strain until 3% drift for tests by Walker (2001) and Alire (2002) of interior unreinforced joints with axial load of $\approx 0.1A_g f_c$

It is clear from consideration of the data presented in Figure 1 that the backbone curve presented in FEMA 356/ASCE 41 is significantly conservative. Further evidence supporting this statement can be seen in Figure 3, which shows the stress-deformation response of further deficient beam-column joints. Similarly, it seems that the curve proposed by Sharma et al. (2011) is unduly conservative for forensic purposes. A backbone curve based on consideration of the remaining four backbone curves has been developed and is presented in Figure 4. It can be seen that is curve is similar to the curve presented by Weng Yuen (2010).

Members of the Royal Commission Expert Panel have stated to Compusoft Engineering Limited that the provision of any “plasticity” in the backbone curve for the beam-column joints is unrealistic, as any such plasticity is a result of yielding of beams and/or columns. Thus it is their opinion that strength decay should begin immediately following the development of peak joint strength, particularly if the joint is not strong enough to sustain

yielding of the framing members. Compusoft Engineering Limited does not believe that this view is correct. Figure 5 shows experimental behaviour of specimen PEER-4150 (Alire 2002; D. E. Lehman et al. 2004) with the proposed backbone curve overlaid. This joint was designed so that the joint shear strength should be exceeded prior to significant yielding of either beams or columns, with this being found to be the case during testing. Despite this it is evident that the stress resisted by the joint core remained essentially constant until quite large deformations were reached. In comparison, the proposed backbone curve appears to underestimate the ability of the joint core to resist stresses at large deformations.

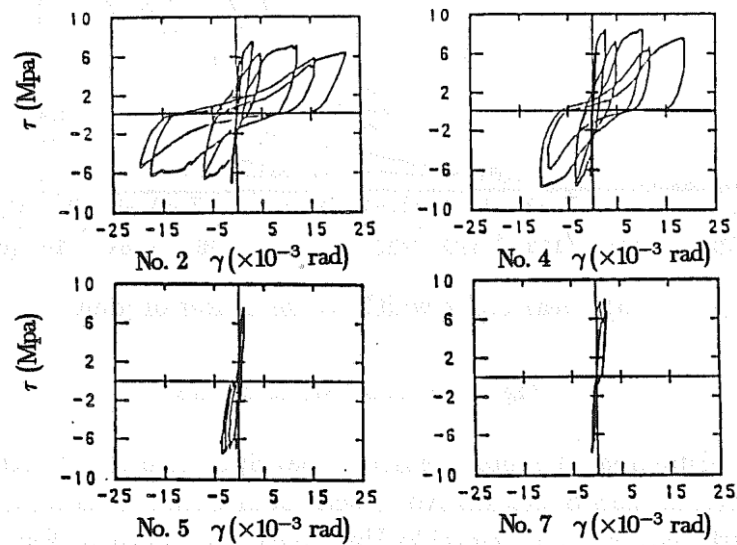


Figure 3: Joint shear stress-deformation response of deficient beam-column joints (from Kurose 1987)

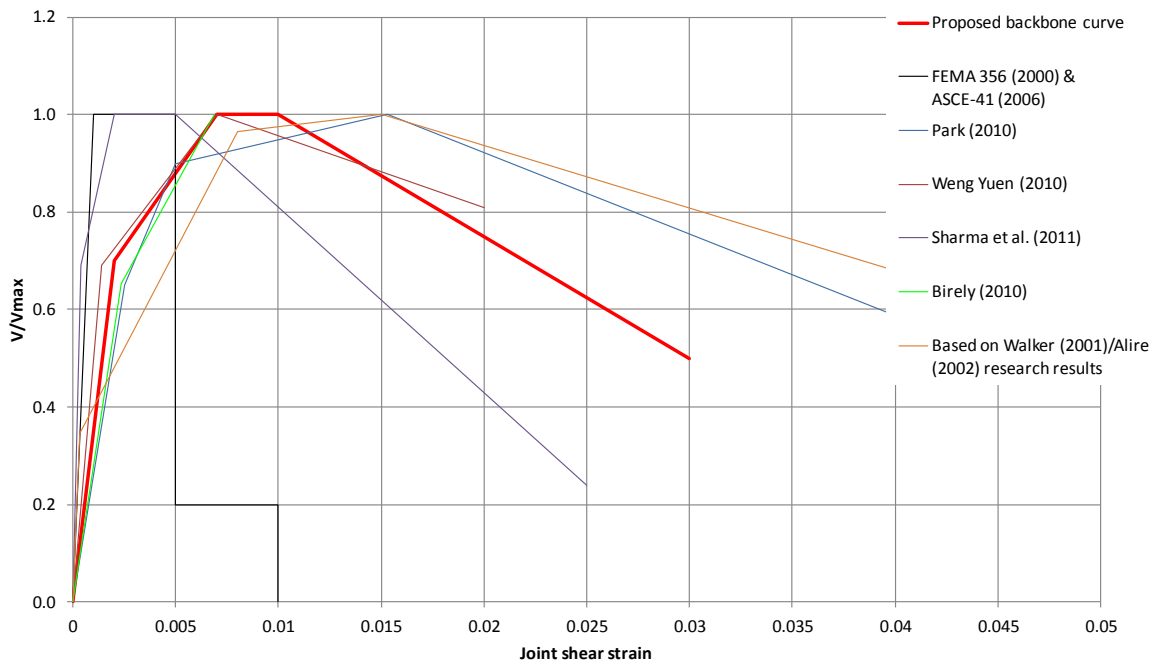


Figure 4: Proposed backbone curve for joint deformation

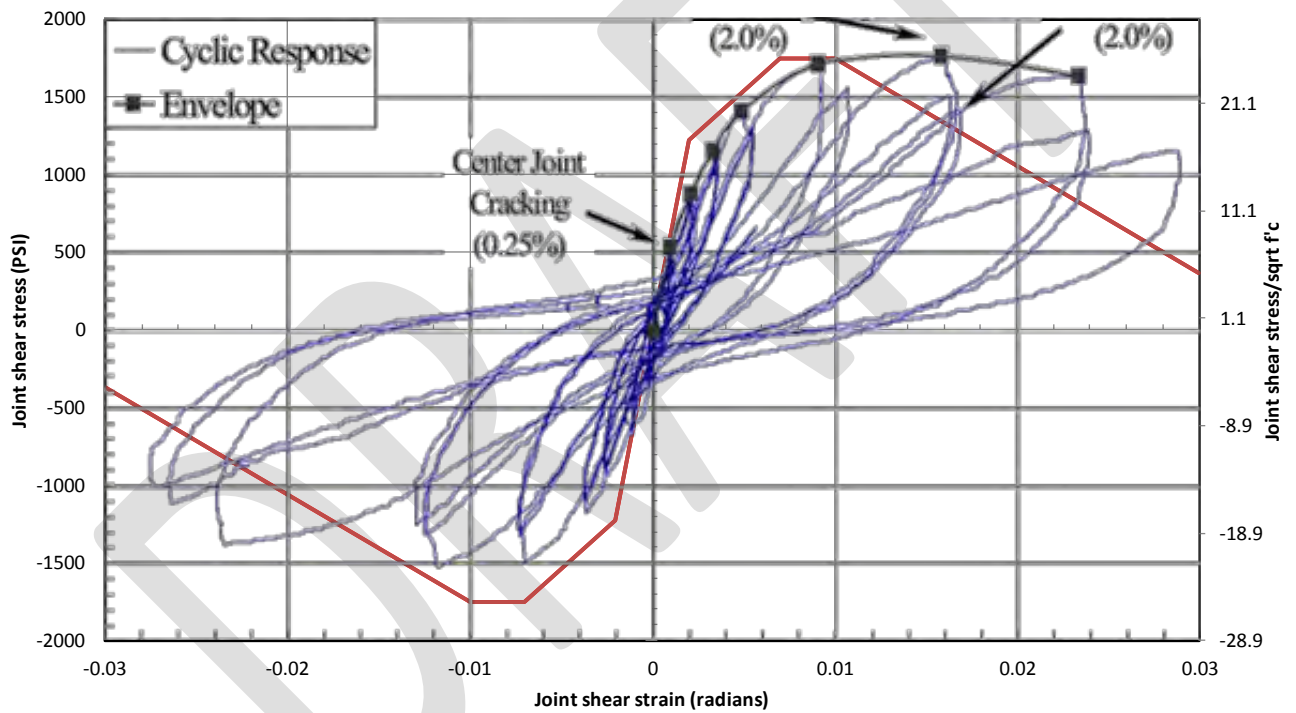


Figure 5: Comparison of PEER-4150 (Alire 2002; D. E. Lehman et al. 2004) against proposed backbone curve

4. Definition of maximum joint shear strength

Two proposals for joint shear strength have been considered. These correspond broadly to the methods used in New Zealand and the U.S.A. for determination of deficient joint core strength.

The New Zealand method for determining joint core strength is based on checking that limiting values of joint principal tension and compression stresses are not exceeded (Hakuto et al. 2000; NZSEE 2006; Priestley 1997; Weng Yuen 2010). The limits on the principal stresses are dependent on joint detailing, and whether the joint is of the interior or exterior kind. The method inherently leads to joint shear strength being dependent on column axial load.

In U.S. practice, joint shear strength is typically assumed to be independent of column axial load. The limiting joint shear stress is assumed to be proportional to the square root of concrete compressive strength. The constant relating joint shear strength and square root compressive strength is typically referred to as γ , and its value is dependent on the type of joint (interior/exterior) and the presence of members framing into the joint on the orthogonal axes. Refinements of this method have recently been proposed by Park (2010), who suggested that joint aspect ratio affected shear strength.

Figure 6 shows a comparison of the joint shear strength coefficient for interior joints according to U.S. practice, New Zealand practice, and with modification to U.S. practice based on the work of Park (2010). Figure 7 shows similar data for exterior joints. It is clear that there is a marked difference between these strengths for interior joints. Compusoft Engineering Limited intend to undertake further research to determine which of the two approaches is more accurate for interior joints. It is notable that Lehman et al. (2004) and Moehle (2006) have noted that the strengths given by ASCE 41 can be conservative by a factor of two, with coefficients as high as 25 being observed for interior joints. These observations may support the method used in NZ practice as being more realistic.

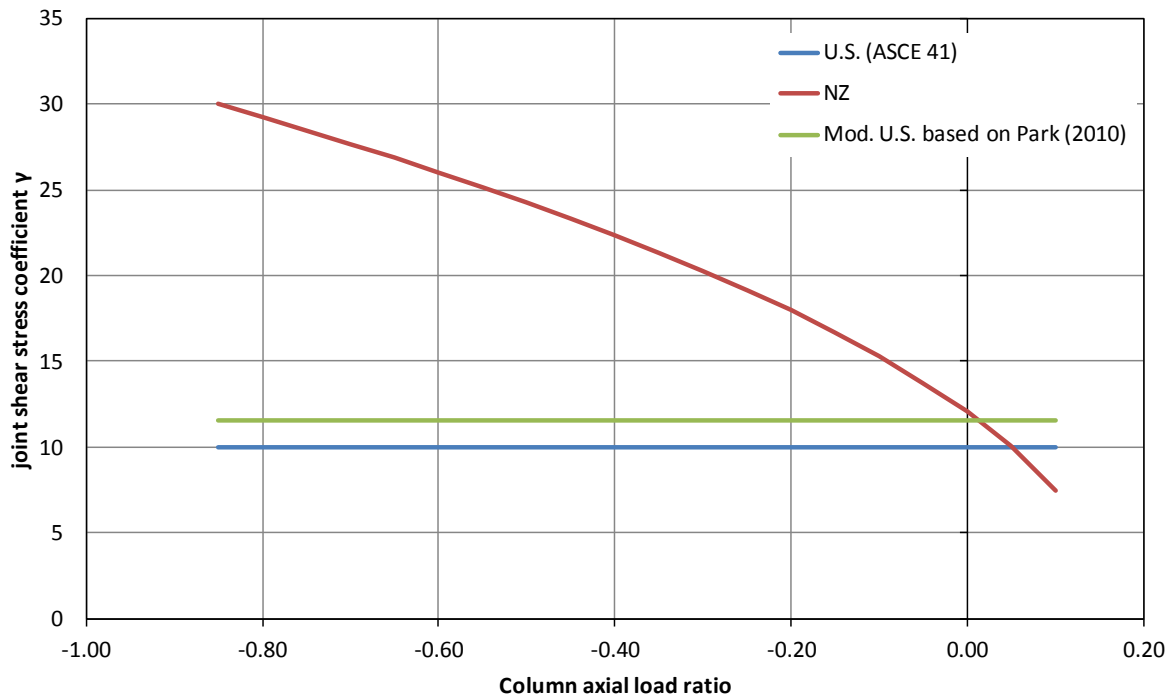


Figure 6: Column axial load ratio against joint shear strength coefficient for interior joints

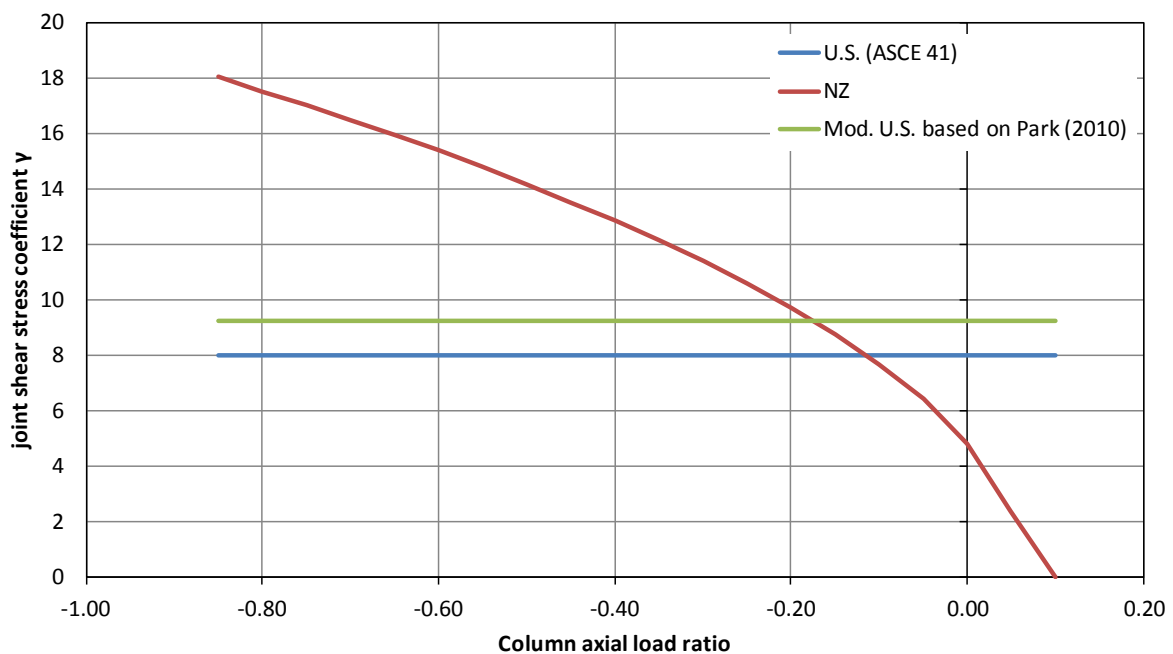


Figure 7: Column axial load ratio against joint shear strength coefficient for exterior joints

A further complexity is added to definition of the strength of deficient beam-column joints because it is acknowledged in the literature that the strength is not in fact a unique value dependent only on joint core properties (dimensions, concrete strength etc.). Rather, the

strength is also dependent on the plastic deformation of the members framing into the beam-column joint (Hakuto et al. 2000; D. E. Lehman et al. 2004; Priestley 1997).

5. Conclusions

6. References

- Alire, D. A. (2002). *Seismic Evaluation of Existing Unconfined Reinforced Concrete Beam-Column Joints*. University of Washington, Seattle, Washington, 306p.
- ASCE. (2006). *ASCE 41-06 Seismic Rehabilitation of Existing Buildings*. American Society of Civil Engineers, Reston, Virginia, 411p.
- Birely, A., Lowes, L. N., and Lehman, D. E. (2012). "A Model for the Practical Nonlinear Analysis of Reinforced-Concrete Frames Including Joint Flexibility." *Engineering Structures*, 34, pp.455–465.
- Clyde, C., Pantelides, C. P., and Reaveley, L. D. (2000). *Performance-Based Evaluation of Exterior Reinforced Concrete Building Joints for Seismic Excitation*. Pacific Earthquake Engineering Research Center, Berkeley, California, 50p.
- Dowell, R. K., Seible, F., and Wilson, E. L. (1998). "Pivot Hysteresis Model for Reinforced Concrete Members." *ACI Structural Journal*, 95(5), pp.607–616.
- Hakuto, S., Park, R., and Tanaka, H. (2000). "Seismic Load Tests on Interior and Exterior Beam-Column Joints with Substandard Reinforcing Details." *ACI Structural Journal*, 97(1), pp.11–25.
- Kurose, Y. (1987). *Recent Studies on Reinforced Concrete Beam-Column Joints in Japan*. Phil M. Ferguson Structural Engineering Laboratory, The University of Texas, Austin, Texas, 164p.
- Lehman, D. E., Stanton, J. F., Anderson, M., Alire, D. A., and Walker, S. G. (2004). "Seismic Performance of Older Beam-Column Joints." *13th World Conference on Earthquake Engineering*, Vancouver, Canada.
- Moehle, J. P., Lehman, D., and Lowes, L. N. (2006). "Beam-Column Connections." *PEER/EERI Seminar on Nonductile Concrete*, Accessed at: peer.berkeley.edu/research/powerpoint/non_ductile_concrete/Joints - Moehle c.ppt (Jun. 15, 2012).
- NZSEE. (2006). *Assessment and Improvement of the Structural Performance of Buildings in Earthquakes*. New Zealand Society for Earthquake Engineering, Wellington, New Zealand, ~400p.
- Pantelides, C. P., Hansen, J., and Nadauld, J. (2002). *Performance-Based Evaluation of Exterior Reinforced Concrete Building Joints for Seismic Excitation*. Pacific Earthquake Engineering Research Center, Berkeley, California, 103p.
- Park, S. (2010). *Experimental and Analytical Studies on Old Reinforced Concrete Buildings with Seismically Vulnerable Beam-Column Joints*. University of California, Berkeley, 260p.
- Priestley, M. J. N. (1997). "Displacement-Based Seismic Assessment of Reinforced Concrete Buildings." *Journal of Earthquake Engineering*, 1(1), pp.157–192.

- Sharma, A., Eligehausen, R., and Reddy, G. R. (2011). "A New Model to Simulate Joint Shear Behaviour of Poorly Detailed Beam-Column Connections in RC Structures Under Seismic Loads, Part 1: Exterior Joints." *Engineering Structures*, 33, pp.1034–1051.
- Walker, S. G. (2001). *Seismic Performance of Existing Reinforced Concrete Beam-Column Joints*. University of Washington, Seattle, Washington, 326p.
- Weng Yuen, K. (2010). *Selective Weakening and Post-Tensioning for the Seismic Retrofit of Non-Ductile RC Frames*. The University of Canterbury, Christchurch, New Zealand, 672p.

DRAFT

Appendix A Calculations showing basis for relating joint moment to shear stress for modelling purposes

COMPUSOFT
ENGINEERING

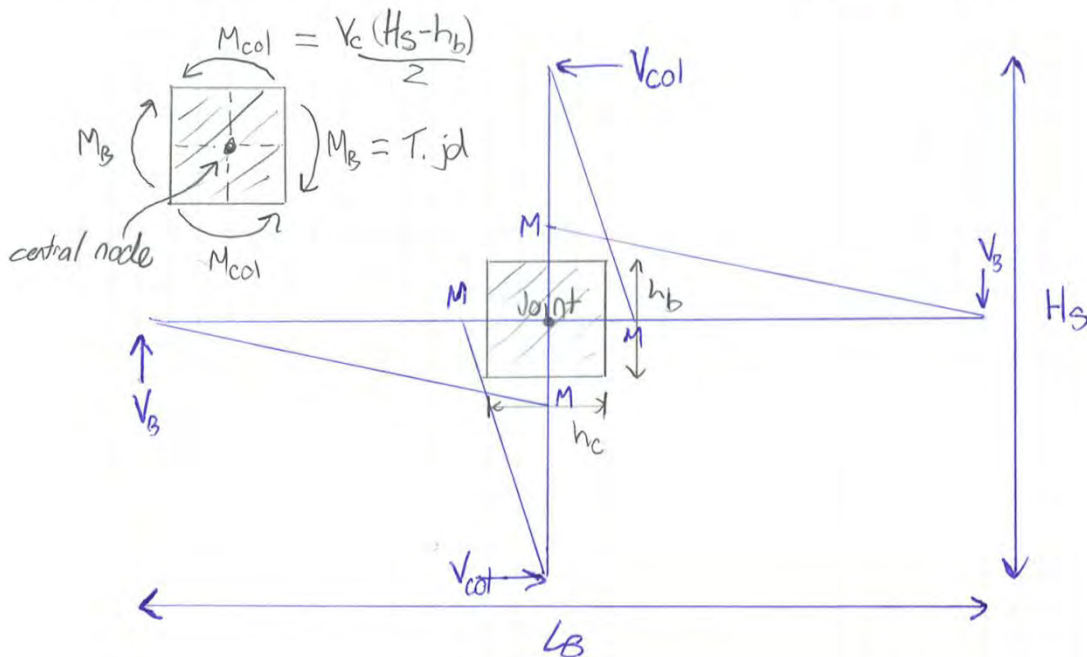
Project: CTV Joints

Date: 19/06 Page: 1

CALCULATIONS

Section: _____

By: NJB Checked: _____



Report joint capacity as moment resistance at central node
- ie '2M'

Joint capacities based on principal stresses are calculated
as V_{jh} (horizontal joint shear capacity)

First consider conversion between:

$$V_{jh} = 2T - V_{col}$$

$$T = \frac{M_B}{j_d} = \frac{M_{col} \cdot H_s}{j_d \cdot L_b} \cdot \frac{L_b - h_c}{H_s - h_b} = \frac{V_{col} H_s (L_b - h_c)}{2 j_d L_b}$$

$$\therefore V_{jh} = V_{col} \left(\frac{H_s (L_b - h_c)}{L_b j_d} - 1 \right)$$

COMPUSOFT
ENGINEERING

Project: CTV Joints Date: 19/06 Page: 2

CALCULATIONS

Section: _____ By: NJB Checked: _____

$$\text{Now, } 2M = V_{col} H_s$$

$$\text{substituting } V_{col} = \frac{2M}{H_s}$$

$$V_{jh} = \frac{2M}{H_s} \left(\frac{H_s}{L_B} \left(\frac{L_B - h_c}{j_d} - 1 \right) \right)$$

$$2M = \frac{V_{jh}}{\frac{L_B - h_c}{L_B j_d} - \frac{1}{H_s}}$$

For CEL example plots, dimensions taken were:

$$L_B = 7000 \text{ mm} \quad H_s = 3240 \text{ mm}$$

$$h_c = 400 \text{ mm} \quad j_d = 445 \text{ mm}$$

$$\text{therefore } 2M = 0.553 V_{jh} \quad (\text{KN-M})$$

DRAFT

Comment from Athol Carr to John Mander.

188 I think just modifying the column properties, as you suggest, will be easier.

Comment from Athol Carr to Tony Stuart.

189 This was one of the solutions that I thought might be usable early on but was a bit more unhappy in it's use for 3D joints. Most of the joints are effectively 2D, so then ok. However, John's suggestions for the modified column behaviour would offer a simpler solution, particularly as it is only modifying the current column yield properties.

Comment from John Mander.

190 This email is in response to the Compusoft regarding the NLTHA. Their letter, of the 15/6/12, was on the subject of beam column joints, and primarily in response to my proposal.

191 In their letter Compusoft mount a counter proposal, ostensibly because of the FEMA-based method I proposed was too conservative. It is not stated by how much this is too conservative, nor what a better model was and how that superior reality check is measured back to tests.

192 I am fully aware that what I proposed is mildly conservative, and would welcome a constructive alternative. But I fear what has been proposed by Compusoft has no guarantee of being in better shape, because no details have been proposed as to what would be the parameters used in their alternative model. In fact, I doubt that any other alternative would be measurably better [read less conservative by x%] because there is actually a paucity of viable data to use and calibrate accordingly. I spent much of yesterday dealing with this issue. And a thorough scour of the literature showed me there were at best about 3 specimens that may be relevant--from the 1960's no less, details from a different era and all for exterior joints. In fact most experimental tests on unreinforced beam-column joints have no axial loads, and certainly all less than $P=0.2 f'_c A_g$.

193 Those results for high axial loads were in decent agreement with my FEMA-based proposal; that is they were not conservative. But it should be noted that the results were for exterior joints, and it is the interior joints in the CTV Building that are more shear critical and mostly above $P=0.4 f'_c A_g$, especially in the lower stories.

194 Beam columns joint behaviour is actually a topic I am working on with my graduate students presently. We are using advanced compatibility based truss models, and to take care of the complex book keeping using SAP 2000 in a quasi static fashion to re-predict our experimental results. Good agreement has been obtained for large scale bridge bent tests we have recently completed in our labs, but the axial load levels are low, $P_e < 0.1 f'_c A_g$.

195 I have spent some time with my students over the past weeks try to model this for the CTV beam-column assemblages, it is an extremely tricky proposition as numerically the model can become unstable. It takes about 4 hours to run for about 50 degrees

- of freedom, and this is statically. The method is still very much in the research lab phase.
- 196 However, yesterday I sat down and did a lot of analyses, using a slightly simpler form to find just the joint capacities [not the complete force-deformation /hysteretic behaviour] based on just using some rational mechanics. The method is about a 2-generation advancement on Collins' MCFT, and incorporates compression softening of the principal compression diagonal in a joint, based on the concurrent transverse tensile strains. The results are promising, but they are tentative, they also check out well with the more comprehensive cyclic inelastic strut and tie modelling using SAP2000.
- 197 I have then converted the answers into equivalent column-end moments, and compared the results with the maximum bending moments from found using a full moment curvature analysis for concrete with $f'_c = 37.5$ MPa [specified + 50% for the joint concrete is the same for the entire building] .
- 198 The results are attached.
- 199 Although I am moderately confident in my own analysis, I do not expect others to be at this time. I wouldn't agree to it if someone else gave it to me and said just trust me on this, because where is the experimental validation. It is for this reason we must stick with what is considered to be best practice in the industry. It is agreed that the developers of FEMA 356 concede that improvements need to be made, but there is no new viable data, especially for high axial loads to use.
- 200 In their previous work, Compusoft was excessively un-conservative in their column modelling and thus even more so by not modelling the joints at all. It is for this reason that some mild conservatism may be the correct way to go for the joints. If we get wholesale failure, and don't believe the outcomes, we could perhaps try increasing the answers by some 20percent to gauge the sensitivity of behaviour to joint shear. In fact, this is indeed the correct approach to investigate what really did cause the CTV failure.
- 201 To me the main attraction of modelling the joints with a blanket capacity [the green line in fig. 1 attached] means the analysis can proceed more quickly.
- 202 I consider we should do it that way, where the clumsy very-slow-to-run fiber models are NOT used and a more robust lumped plasticity model is used instead that does not need moment axial load interaction [at least in the E-W direction]. In this way, time permitting we can explore other factors, such as the influence of the west wall infills. This too is a very tricky subject, and should not be thrown in as a last minute curved ball. We certainly should come back to it however.

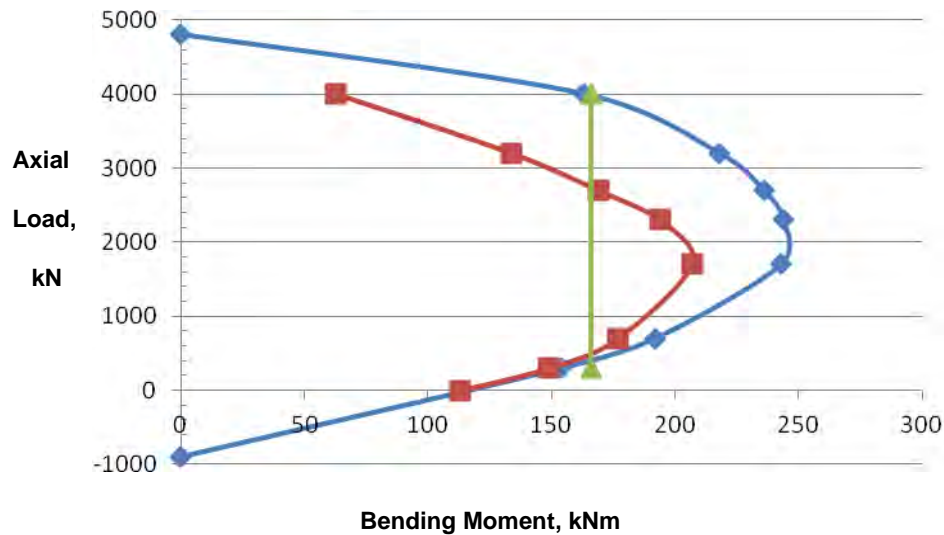


Figure 1. Axial load interaction diagram for the joint concrete in the CTV Building.

- The outer blue curve shows the strength based on flexural bending
- The inner red curve shows the computed strength based on an advanced compatibility strut and tie analysis which incorporates the tensile strain softening of the joint concrete
- The vertical green line is the proposed interior joint strength as given in FEMA 356.

Comment from Derek Bradley.

203 We have attempted to revise our letter outlining what we intend to do so that the analysis can be progressed.

COMPUSOFT

ENGINEERING

PO Box 9493, Newmarket, Auckland, New Zealand.
Telephone: +64 9 522 1456 Website: www.compusoftengineering.com

18th June 2012

Professor Athol Carr
Canterbury Earthquakes Royal Commission,
PO Box 14503, Christchurch Mail Centre,
Christchurch 8544.

Subject: Summary of input parameters for SAP2000 analysis model

The following is a list detailing Compusoft's understanding of the alterations required to the existing analysis model. The development of this information has been based upon all recent correspondence. Should any part not represent the thoughts of a panel member then please forward your interpretation along with supporting documentation.

Note the intent is to commence running the analyses within the next 48 hours, so ALL information is required by lunchtime tomorrow (NZ time) so that it can be incorporated into the model in time. If we do not get a response with regard to each of these items it will be assumed that no party member has any problems or issues with any of the proposals discussed below. With that in mind please comment ASAP. It would be of assistance if this document is marked up with any amendments required and returned to us. Once all comments are in we would appreciate your directive to Compusoft on the parameters to be adopted.

1. Column PMM interaction.

PMM interaction of the column hinges is to be incorporated into the model via a fibre based model. In this model the column section is discretised into a series of concrete and steel fibres with applicable hysteretic form (Takeda and kinematic respectively).

1.1. Lower Hinges

The lower hinges (with the exception of the ground floor column) are to be reduced in length due to the effect of the bar laps just above the floor level, and are to be based upon the concrete material properties of the beam column joint. The hinge length adopted for these locations is as below:

- Lower column plastic hinge length, $L_p = 200$ mm

1.2. Upper Hinges

The upper hinges are to be placed at the underside of the beams. These hinges are to consider the concrete and reinforcement properties present in the beam-column joint. The length of these hinges is to be taken as considered for the Lower hinges.

- Upper column plastic hinge length $L_p = 200$ mm

2. Modelling of the Beam – Column Joint Zone

The beam-column joint is to be modelled via the incorporation of a nonlinear element that connects the beams to the columns. This nonlinear element will provide for moment vs rotation behaviour with the backbone taken as bilinear. The yield strength of the joint will be determined following the methodology presented in Appendix B of the Compusoft Non-Linear Seismic Analysis Report (ref 11033-0). Figure 1 and Figure 2 below present the joint yield moment profiles for an interior and exterior joint. The axial force used in the derivation of the joint yield moment will correspond to that which is present for the gravity combination (which will vary across the building). As the beam curvature ductility's are expected to be low the joints will be based upon $\mu\phi = 0$.

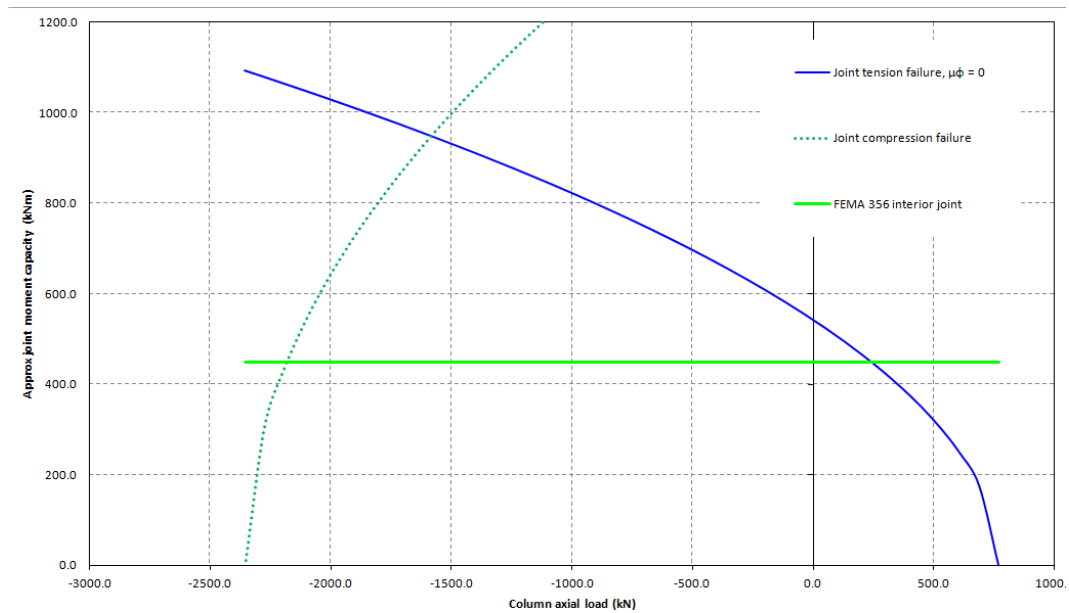


Figure 1: Interior beam-column joint yield capacity

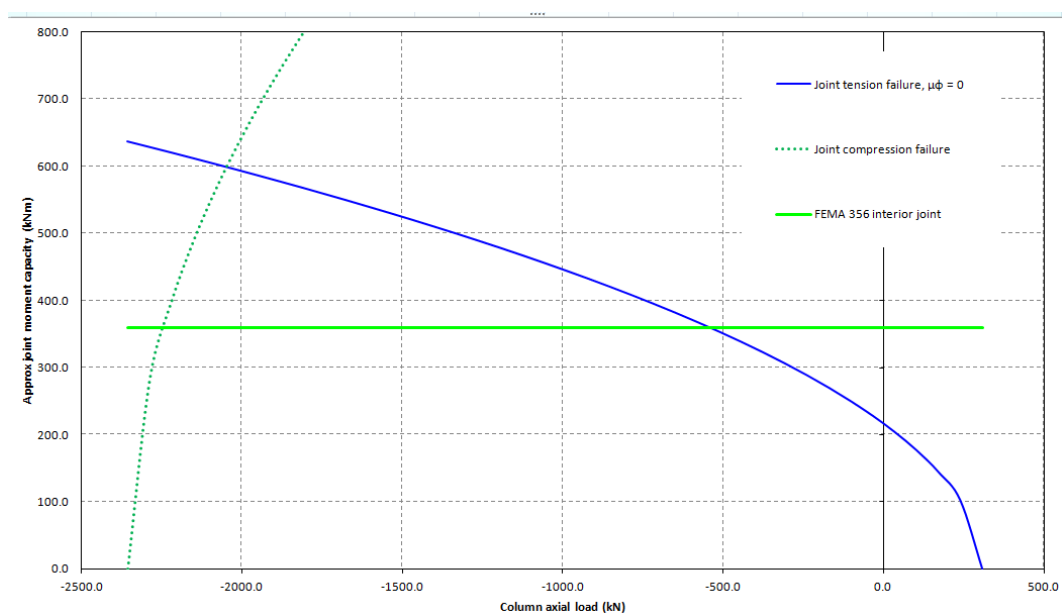


Figure 2: Exterior beam-column joint yield capacity

The performance assessment of the beam-column joint is then to be undertaken via post-processing. Compusoft will provide beam-column joint results suitable for assessment purposes by others.

We acknowledge that there is significant uncertainty (and debate) regarding the yield strength of the beam-column joint. With this in mind it may be prudent to undertake additional sensitivity analyses considering variations to the adopted yield strengths.

3. Beam pull-out.

It was understood that the effect of the bar pullout was to be represented via an adjusted moment-rotation backbone curve for the affected beam flexural hinges. At this time no suitable backbone curve has been promoted and as such will not be considered in these analyses.

4. Concrete strength

All concrete strengths are to be revised to consider $f'_{c,expected} = 1.5 * f'_{c,specified}$. The concrete strengths and strain parameters are summarised in Table 1 below.

Table 1: Concrete stress-strain parameters

Material	f'_c (MPa)	E_c (GPa)
PC Beams	37.5	27.2
Ground beams	30	25.1
Columns L1 - L2	52.5	31
Columns L2 - L3	45	29.2
Columns L3 - Roof	37.5	27.2
Floor Slabs	37.5	27.2
Shear Walls	37.5	27.2
Beam-Column Joints	37.5	27.2

Notes: 1. $\epsilon_{co} = 0.002$ throughout.
2. $\epsilon_{cu} = 0.006$ throughout.

5. Floor behaviour.

5.1. Adjacent to beams

The floor elements adjacent to all beams on grids 1, 2, 3 and 4 are modelled as nonlinear layered shell elements considering the geometry, concrete and reinforcement content present at the beam face (and neglecting the profiled metal decking). This will allow the stiffness

and strength of the floor elements at these locations to be considered explicitly in the model. The strength of the floor beyond the line of starter bars has not been modelled and should be considered via post processing.

5.2. In floor span

Linear elastic shell elements will be used to model the floor elements in the span. The floor elements in the span are considered with $EI_{eff} = 0.1 * EI_{gross}$ (where $EI_{gross} = 18720 \text{ kNm}^2/\text{m}$).

5.3. Drag Bars

Drag bars will be modelled as outlined in Table 5 of the Compusoft Non-Linear Seismic Analysis Report (ref 11033-0).

6. Ground motion.

To investigate the effects of cumulative damage on the structure, two of the records will be run in a sequential manner. For the records of interest this will allow the damage state arising from previous events to be included. All four records will also be run for the Lyttelton event without taking into account any damage that may have occurred as the result of previous events. Figure 3 below presents the two analysis sequences being considered and Table 2 below presents a summary list of the time history analyses that are to be undertaken for each record.

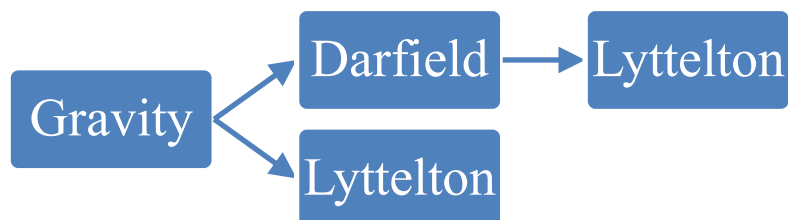


Figure 3: Time history analysis sequence

Table 2: Analysis run summary

Record	Event	Starting stress state	Start Time (sec)	Finish Time (sec)
CCCC	Darfield	Gravity	10	50
CCCC	Lyttelton	Darfield	10	25
CBGS	Darfield	Gravity	10	50
CBGS	Lyttelton	Darfield	10	25
CCCC	Lyttelton	Gravity	10	25
CBGS	Lyttelton	Gravity	10	50
CHHC	Lyttelton	Gravity	10	25
REHS	Lyttelton	Gravity	10	25

- Notes:
1. The starting stress state refers to the starting point for the analysis case such that initial damage is incorporated. Note that where applicable a zero record will be inserted to ensure that all motion has ceased prior to the next event.
 2. Start and Finish times are with reference to the GNS records. Note that the GNS records commence at T = -5 seconds.

7. Masonry.

Masonry interaction will NOT be modelled. It is to be assumed that beams along GL A support the weight of the masonry with no propping effects that may reduce column axial loads.

8. Damping.

8.1. For September (Darfield) Analyses

The damping model will be the same as used for the DBH series of analyses for the September (Darfield Event), i.e. Rayleigh damping with 5% @ 1.29 sec and 5% @ 0.05 sec.

8.2. For February (Lyttelton) Analyses

The proposed damping model for the February (Lyttelton) analyses is as follows;

	Period, T (sec)	Frequency, ω (rad/s)	Damping, ξ
First	0.25	25.13	0.020
Second	1.29	4.87	0.033

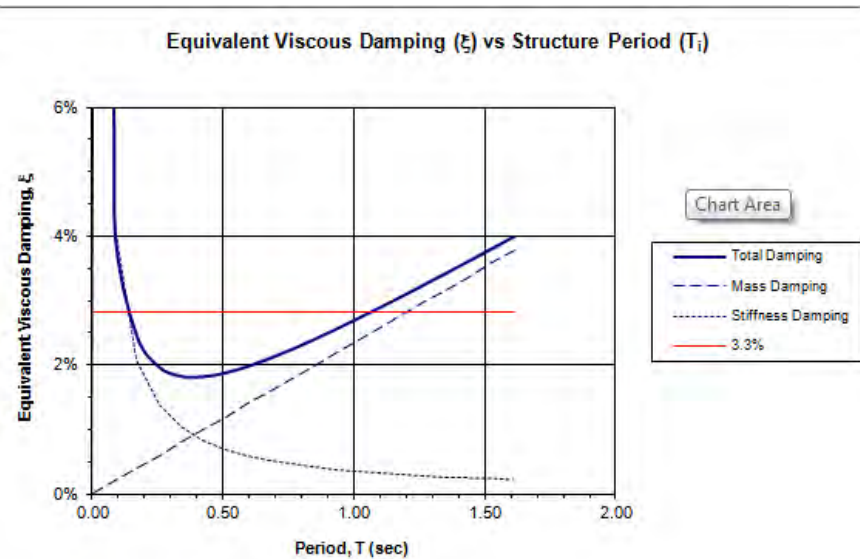


Figure 4: Damping parameters to be used for the Lyttelton event.

9. Outputs.

A full analysis report for the CTV building will be produced with content being similar to that undertaken previously (refer Compusoft Non-Linear Seismic Analysis Report 11033-00).

We will endeavour to obtain any additional results that people require, but note that post processing of results is time consuming and insufficient time is available to process all results for all records. Please set out (in order of priority) which results you would like to see and in what format.

Yours sincerely,



Derek Bradley

Comments from John Mander.

- 204 I am totally unsatisfied with this proposal and it must not proceed yet until we know the outcome is likely to be on the right track.
- 205 As far as I can tell the problems that remain are as follows:
- 206 1. The shear capacities assigned to the joints in the lower stories for the joints are compression critical. The values proposed by Compusoft are a nonsense, and demonstrably wrong! First it should be noted that the joints ostensibly have only a vertical capacity of some 2300 kN in axial compression. Clearly this cannot be so, as from the previous [mostly incorrect] work there were axial forces over 3200kN being registered. If proposed joint capacities are true, then the structure would have probably fallen down on capping out the upper stories during construction. Moreover, it would not have even survived the Darfield event, but it did!
- 207 2. This leads to the folly of using a fiber model. There is no point in using such a model if the columns will be mostly elastic, there was sufficient forensic evidence to prove that to be the case; it was the joints that were munted, but not on Darfield event. Again I have shown how the theories appear when plotted in figure 1 attached. Essentially, there is no axial load variation for the joints if one uses the industry standard of FEMA 356. This markedly simplifies the analysis, As such in an earlier email to me soliciting my opinion Professor Carr gave his and I quote: "Hi John, I would appreciate your comments. I think just modifying the column properties, as you suggest, will be easier. Regards, Athol." Obviously Prof. Carr is put in a difficult position chairing this committee, as he evidently does not want to be seen to be "paddling his own canoe", well I don't mind putting my oar in and say that he is right!
- 208 3. It appears there is a significant multiplier on the Compusoft calculated joint capacities and especially when compared to what I had previously computed. One of the 2 of us is in serious error. So Compusoft need to put up their calculations for scrutiny. The main problem is that Compusoft's results are on the outside of even the interaction diagram in Figure 15 of the H-S Report [see figure 2 attached]. If that were true, then we could say we had a strong joint-weak column. Again, a cursory glance of the beam-column-joint reinforcing details will tell a domain-expert this cannot be the case.
- 209 4. And finally the most serious concern of all. It is totally unacceptable to re-do the analyses, and not model the joint directly. Not including the softening effects and not including cyclic effects which capture degradation etc. Compusoft propose: "The performance assessment of the beam-column joint is then to be undertaken via post-processing. Compusoft will provide beam-column joint results suitable for assessment purposes by others." This seems to indicate we are in for more inadmissible results, just as were previously presented in Figure 15. What I believe this is saying, is Compusoft will model the building and its behaviour will be governed by column response and we are using a Rolls Royce to take you there. And after the ride, we'll look back and tell you if the joint demands exceeded their capacities. Now this might be an ok thing to do in a design practice environment, as it leads the designer in the right direction to make the appropriate fixes. But for a forensic analysis, such as this, the poor performance, warts and all, must be carried through to its logical conclusion--the failure. Showing the joint shear peak responses on a diagram like figure 15 in the old H-S Report is basically what Compusoft are saying

they will do. That was part and parcel of such post-processing in the original ground, which also let the cat out of the bag demonstrating to the world this was a faulty process and result. This must not happen again. The performance assessment needs to be a results-oriented outcome--failure of the structure [which admittedly may mean the program crashes through numerical instability]. By not using a direct approach it only shows a speculative outcome.

- 210 5. so we come back to point 2 above. The single blanket axial load-independent joint capacity is the most constructive way to go for now. If the structure crashes early, say in the Darfield event, then we apparently got it wrong, but a simple fix is to then progressively increase the joint strength. Remember, without the Roll Royce column modelling sophistication [and employing Elms' principle of consistent crudeness], the analyses will fly through much faster. By increasing the joint capacity by say 20 percent, a rerun will indicate the sensitivity to this parameter.

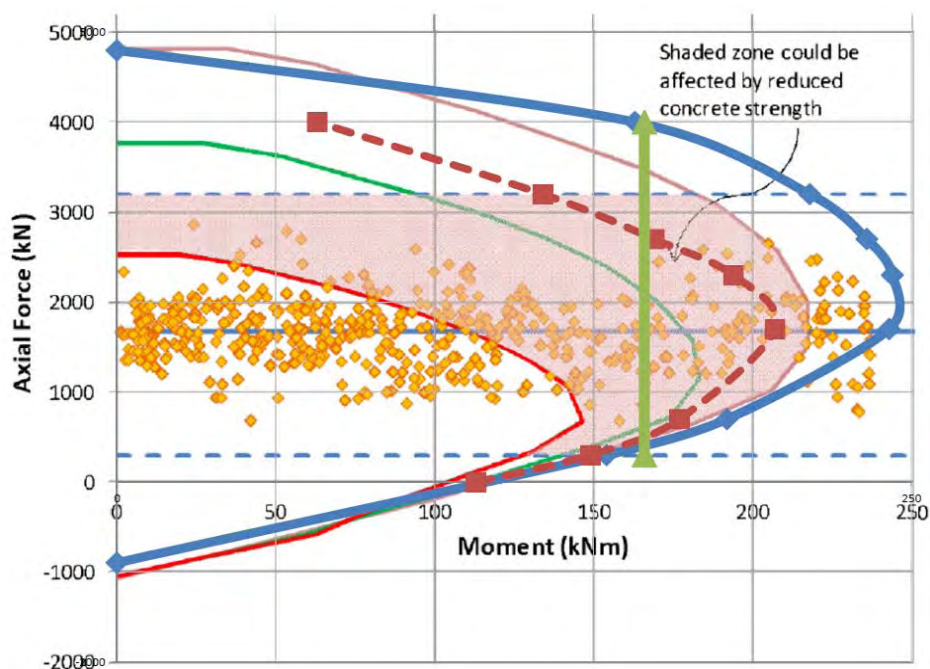


Figure 1. Axial load interaction diagram for the joint concrete in the CTV Building.

- The thick outer blue curve shows the strength based on flexural bending
- The thick inner red dashed curve shows the computed strength based on an advanced compatibility strut and tie analysis which incorporates the tensile strain softening of the joint concrete
- The thick vertical green line is the proposed interior joint strength as given in FEMA 356.
- The other lines and data points are from an over-plot of Figure 15 of the H-S Report.

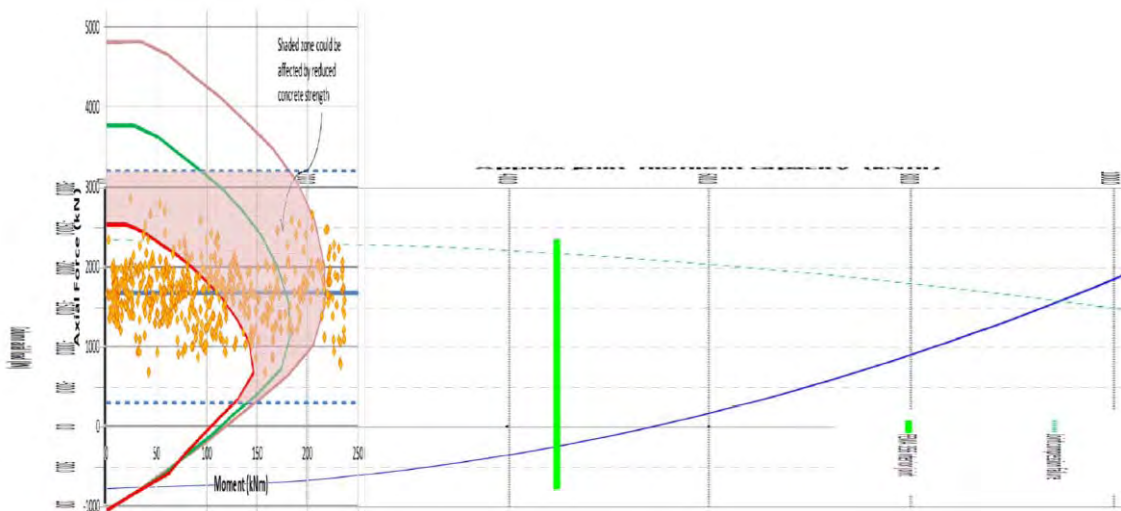


Figure 2. Axial load interaction diagram for the joint concrete in the CTV Building.

- The pink region along with the yellow dots are the [inadmissible] results that go beyond the failure surface of the interaction diagram from the original Compusoft analyses [this is a squashed up version of fig. 15 from the H-S Report..
- The green vertical line is what Compusoft presently claim is a “conservative” joint capacity as per FEMA 356 [note it seems markedly off-scale]
- The lower blue curve is the tensile cracking capacity of the joint, as presently claimed by Compusoft.
- And the upper green dashed curved is the Compusoft predicted compressions capacity of the beam column joints based on $f'_c = 37.5$ MPa.

Comment from Athol Carr

- 211 We have to have a model on which there is pretty well full agreement. The proper joint model is essential, including the strength degradation as well as the stiffness degradation, picking problems up by post-processing is not satisfactory as the loss of stiffness, and strength of the joints is required if the model is to show the effects on the rest of the structure. If the analysis fails as the joints fail then this indicates what probably happened in the earthquake. If the members are to remain, then the transfer of the actions to other members may be masked. If the joints are the critical members then the P-M-M column modelling is not so important, they never get to the critical stage (maybe base ground floor as an exception).

Comment from Brendon Bradley.

- 212 I agree with the comments from Prof. Mander, followed by Prof. Carr. In order for the analyses to be informative/admissible, they must seek to simulate the potential failure mechanisms which can eventuate. Post-processing of results to infer possible failure is not acceptable in forensic analyses, in my opinion.

Comment from Derek Bradley.

- 213 It appears as if Professor Mander has misunderstood some of our points, which we would like to clarify. In addition CompuSoft disagrees with a number of comments and have the following response.

214 Point 1.

- 215 The axial load carrying capacity in compression presented in Figures 1 & 2 of our letter is based upon limiting the compression strut to $0.5f_c'$. We are aware that this is conservative for high axial loads with low bending moments. The proposal is to determine the joint yield moment capacity based on the axial force arising from the gravity combination only (which can be considered to be approximately the average throughout the course of an earthquake). It should be noted that the maximum axial compressive force in any column for the gravity load combination is below the level at which this criteria would govern. We are trying to capture the most likely performance of the joint to best represent the performance of the building.

- 216 We take exception to the statement that the previous work was mostly incorrect, and believe that given the uncertainties in input data, it adequately represents the response and trends of the building behaviour, and is suitable for the terms of reference of the investigation.

217 Point 2.

- 218 In our opinion FEMA 356 is an assessment guide and NOT industry standard for the forensic examination of collapses. It is known to under-represent joint capacity and does not consider the effects of axial load. CompuSoft have been criticised for simplifying aspects of the original analysis only to have alternative approaches offered that have the same level of uncertainty. We acknowledge that there is significant uncertainty surrounding the yield capacity of the joints and for this reason have proposed that several scenarios be considered. Using the proposed implementation of joint behaviour in SAP2000 this is an easy change to facilitate.

219 Point 3.

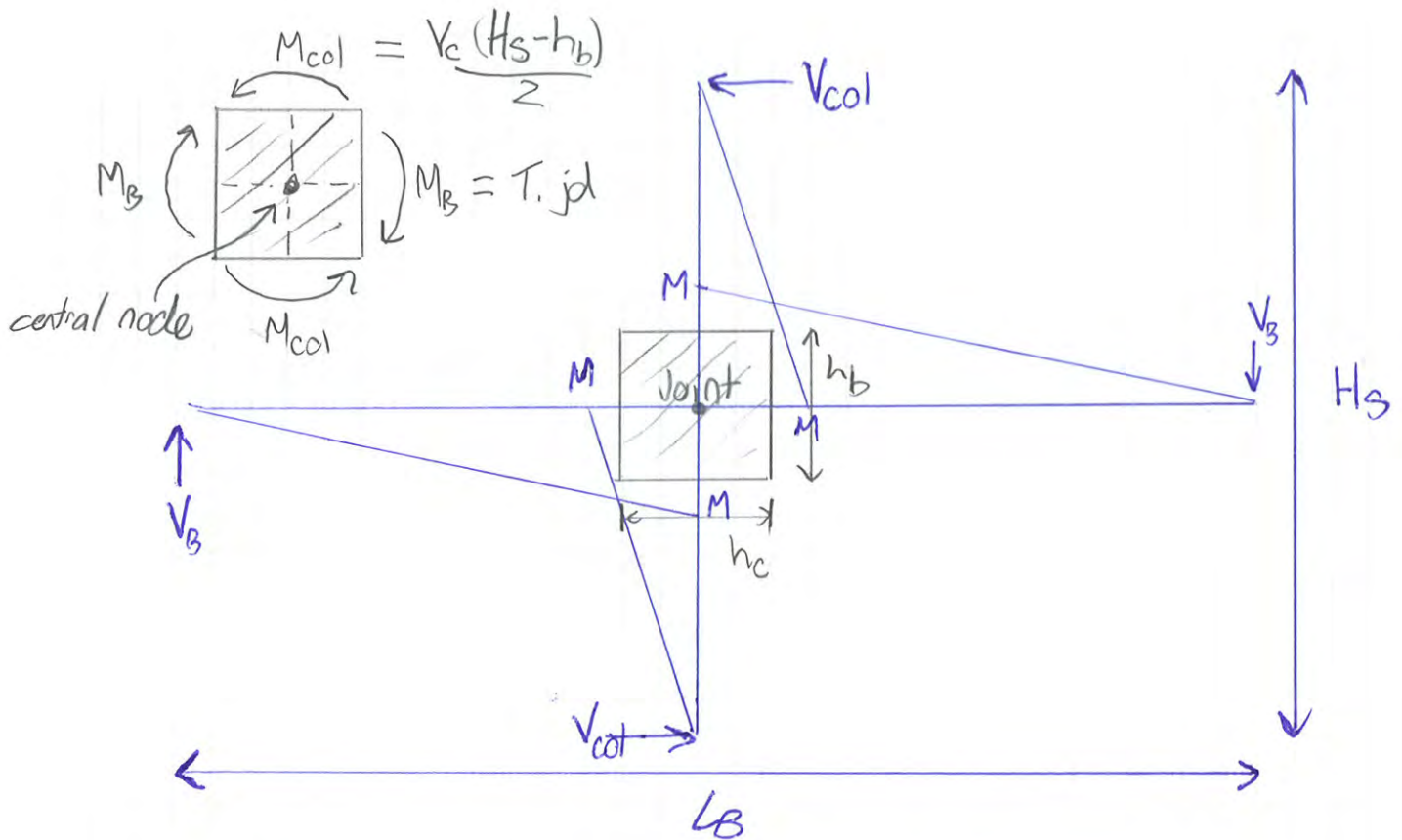
- 220 We have attached our calculations. There could be some confusion in that Figures 1 & 2 of our letter presents the capacity of the joint (i.e. the total moment transferred between the beams and columns), not that attributed to an individual beam or column.

221 Point 4.

- 222 There is little data available presenting the performance of poorly reinforced beam-column joints, however the test results that we have seen indicate that the FEMA

guidance is excessively conservative (i.e. would produce smaller than actual joint capacities). Degrading joint capacity can be incorporated, however incorporating excessively conservative backbone curves (from FEMA 356) could potentially produce incorrect results and over represent damage in the joints. Again, because there is significant uncertainty we have promoted that multiple scenarios be investigated. We had proposed a bi-linear approach as this will improve stability and allow the investigation of collapse hierarchies, which we believe is a pragmatic solution to this problem.

- 223 We are happy to incorporate strength degradation of the joint however believe that this should be based upon more accurate knowledge of the joint performance and then bounded with a sensitivity analysis. Compusoft will forward an alternate backbone curve for the beam-column joints shortly. As with our response to Item 2, we would promote that two scenarios are investigated to represent a reasonable bound of the joint capacity.
- 224 In addition we totally dispute the claim that the results of the previous analysis were 'inadmissible'. The reason the Figure 15 has points plotted outside of the P-M curve is due to isotropic hardening of the M-M hinge in the SAP analysis. It is important to note that these data points occur AFTER the building was considered to have collapsed, and the increase in moment capacity is of a few percent - which would not materially effect the response of the frames as (which only contribute 10-15% to the seismic resistance of the building).
- 225 Point 5.
- 226 Using a blanket 'conservative' joint capacity is contrary to the sentiments of item 4. In addition, ensuring numerical instability in models can be counter-productive and lead to lengthy delays in troubleshooting models and verifying results.



Report joint capacity as moment resistance at central node
 - i.e. '2M'

Joint capacities based on principal stresses are calculated
 as V_{jh} (horizontal joint shear capacity)

first consider conversion between:

$$V_{jh} = 2T - V_{col}$$

$$T = \frac{M_B}{jd} = \frac{M_{col} \cdot H_s}{jd \cdot L_b} \cdot \frac{L_b - h_c}{H_s - h_b} = \frac{V_{col} H_s (L_b - h_c)}{2jd L_b}$$

from top left

$$\therefore V_{jh} = V_{col} \left(\frac{H_s (L_b - h_c)}{L_b \cdot jd} - 1 \right)$$

$$\text{Now, } 2M = V_{col} H_s$$

$$\text{substituting } V_{col} = \frac{2M}{H_s}$$

$$V_{jh} = \frac{2M}{H_s} \left(\frac{H_s}{L_B} \frac{(L_B - h_c)}{j d} - 1 \right)$$

$$2M = \frac{V_{jh}}{\frac{L_B - h_c}{L_B j d} - \frac{1}{H_s}}$$

For CEL example plots, dimensions taken were:

$$L_B = 7000 \text{ mm} \quad H_s = 3240 \text{ mm}$$

$$h_c = 400 \text{ mm} \quad j d = 445 \text{ mm}$$

$$\text{therefore } 2M = 0.553 V_{jh} \quad (\text{KN-M})$$

Considering joint shear strength, V_{jh} , based on principal stress limits

$$V_{jh_{max}} = \left(\sigma_p \sqrt{1 - \frac{\sigma_a}{\sigma_p}} \right) A_{jh}$$

where σ_p is a permissible principal stress limit,

$$\text{either } \sigma_t = k \sqrt{f_c} \quad \text{for tension}$$

where k is dependent on joint type

$$\text{or } \sigma_c = -0.5 f_c$$

and σ_a is column axial stress, i.e.

$$\sigma_a = \frac{N_{col}}{A_{col}}$$

Noting compression stresses are taken as negative.

For CTV joint, column area is different to effective joint area

$$A_{col} = \frac{400^2 \pi}{4} = 125664 \text{ mm}^2$$

$$A_{jh} = 400^2 = 160000 \text{ mm}^2$$

Taking, for example, $f'_c = 37.5 \text{ MPa}$, and

$$N_{col} = -1000 \text{ kN (in compression)}$$

$$\text{and } K = 1.0 \text{ (interior joint, } \mu_b = 1.0)$$

$$\sigma_a = -\frac{1000 \times 10^3}{125664} = -8 \text{ MPa}$$

$$\sigma_t = 1\sqrt{37.5} = 6.1 \text{ MPa}$$

$$\sigma_c = -0.5 \times 37.5 = -18.7 \text{ MPa}$$

$V_{jh \text{ max}}$ is lesser of limit for tension or compression

$$\begin{aligned} \text{Compression: } V_{jh \text{ max } c} &= \left(-18.7 \sqrt{1 - \frac{-8}{-18.7}} \right) 160000 \\ &= 2276 \text{ kN} \end{aligned}$$

$$\begin{aligned} \text{Tension } V_{jh \text{ max } t} &= \left(6.1 \sqrt{1 - \frac{-8}{6.1}} \right) 160000 \\ &= 1481 \text{ kN} \end{aligned}$$

$$\therefore V_{jh \text{ max}} = \min(V_{jh \text{ max } c}, V_{jh \text{ max } t}) = 1481 \text{ kN}$$

Converting to equivalent joint moment capacity

$$2M = 0.553 V_{jh} = 819 \text{ kNm}$$

↗ page 2.

cf. CEL plot.

Comment from John Mander.

- 227 I really would like to see your alternative backbone curves. They are important in the overall scheme of things.
- 228 In short, though 2 things you may want to make a quick response on. I still think that this is all messed up, and its largely a perspective thing. Basically using $k = 1$ is inadmissible WITHIN a weak joint [it is not even feasible to get a concrete tensile strength that high, this is merely an empirical surrogate for other things]. Note that for the peak tensile strength of concrete $k = 0.5$, and $k = 0.35$ more like an average WITHIN a joint. And for compression you can use 0.85 peak and about 0.7 f_c average max WITHIN the joint. You need to remember that Priestly's stuff was all based on hinging deterioration OUTSIDE the joint that is deteriorated BECAUSE of the joint--that is nothing like what we have with CTV where the joint is just plain weak!!!.
- 229 My figure 1 curve is correct, verified by 2 contrasting theories, the straight line is intended to be a simple compromise to get a firm understanding of the sensitivity of the joints on the overall response. Note the more exacting of the two possibilities is not dissimilar to yours in shape, it just that the scale is more appropriate. I think your stress method may work, if more reasonable values are used. And your results need to be presented as per one end moment, not two. That said, I feel that a simplified method is still worth considering to focus on the shear as a starting point, and then move to more complexity.
- 230 And BTW, its ok to take exception to my comments I think that's cool, but that wont alter the facts in black and white [no actually in yellow and pink] for the world to see--figure 1 below!

Unreinforced Joint Strength

FEMA 356 specifies the following:

$$V_j = \gamma \sqrt{f'_c} b h$$

joint geometry	γ
	4
	6
	8
	10
	12

- No new data. Probably still valid.
- Assuming bars are anchored in joint, strength limited by strength of framing members, with upper bound of $\gamma \approx 15$. For $15 \geq \gamma \geq 4$, joint failure may occur after inelastic response. For $\gamma \leq 4$, joint unlikely to fail.
- Assuming bars are anchored in joint, strength limited by strength of framing members, with upper bound of $\gamma \approx 25$. For $25 \geq \gamma \geq 8$, joint failure may occur after inelastic response. For $\gamma \leq 8$, joint unlikely to fail.

Fig 1. – taken from previously referenced Jack Moehle presentation

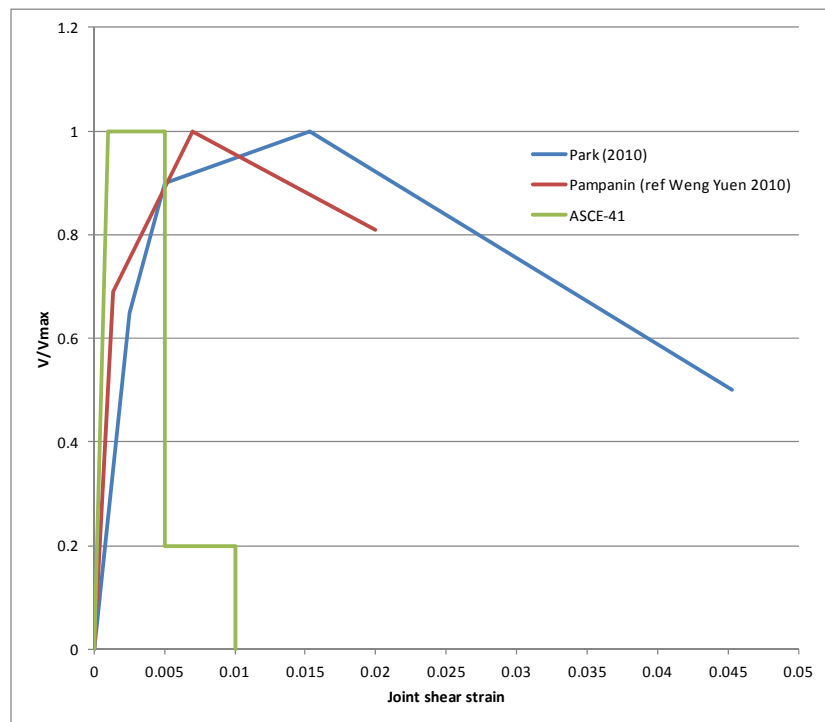


Fig 2. – comparison of joint shear stress-deformation backbone curves

Comment from Athol Carr.

- 231 The proper joint model is essential, including the strength degradation as well as the stiffness gradation, picking problems up by post-processing is not satisfactory as the loss of stiffness, and strength of the joints is required if the model is to show the effects on the rest of the structure. If the analysis fails as the joints fail then this indicates what probably happened in the earthquake. If the members are to remain, then the transfer of the actions to other members may be masked. If the joints are the critical members then the P-M-M column modelling is not so important, they never get to the critical stage (maybe base ground floor as an exception).

Comment from Ashley Smith.

- 232 The other comment that I wanted to make is that the various proposals we have seen for modelling beam-column joint failure all appear to require us to predetermine the limiting column moment, or beam moment that will initiate joint failure. In other words, we do not have an independent formulation of the beam-column joint capacity to test in the analysis, to see whether columns or joints fail first. Rather, depending on the input data, we will have predetermined the failure sequence. Given the variance we currently have between the various parties about the likely joint strength parameters, I am concerned about the potential to 'tailor' the joint strength inputs so as to achieve a particular result. At the very least we will need to test the sensitivity.

Comment from John Mander.

- 233 Everyone keeps saying that FEMA 356 is very conservative--well it is for joints WITH transverse reinforcing, but only mildly so with no joint steel. As shown in my own solution, that was created independently in two completely different mechanics-based methods [one an adaption of the MCFT, the other based on strut and tie] to get the curved red solution in my fig 1, it is not that different from the FEMA 356 [green line] which leads to a quick and easy implementation. I know either would be really easy to implement in Ruaumoko. Having worked somewhat with SAP 2000 recently, I realize it is clunky to say the least, but I thought this would have been doable without going around using Compusoft's obtuse pathway.
- 234 Thus the biggest concern remains, Compusoft seem intent on "post-processing". This will not work, moreover, as you know, you cannot preset the "failure surface " based on an average axial load. This is what has got them in hot water over the last debacle that leads to the infamous Fig 15. The program needs to be run such that the "yield surface" is a moving target that is checked at each time-step, and dependent on axial load.

Comments from Nigel Priestley

- 235 Beam/Column Joint Modelling: Again the complexity of the detailing (particularly the beam bent-up bars) makes refined modeling of the joint difficult. However, I support the use of the NZSEE recommendations over the FEMA 356 recommendations, which are conservative and insensitive to axial load, despite ample evidence from experiments that axial load level is critical, especially for joints with little or no transverse reinforcement.
- 236 There does not seem to be any discussion in the compusoft letter about the joint deformation associated with the envelope characteristic. When (if) the joint reaches capacity it will soften remarkably, and the proposed strength and stiffness envelopes will be inappropriate. How is this behavior under repeated loading to be handled?
- 237 It will be apparent from the above that I see little merit in adopting the FEMA 356 provisions for assessing the beam column joints because of their coarseness and lack of consideration of axial load level. It should also be noted that the calculations presented by Mander appear to be based on a beam hinging mechanism, with reinforcement providing the compression force, whereas I understand that the columns are critical. In this case, the beam compression force is provided by concrete compression, and a direct diagonal strut can be developed to carry the compression forces across the joint.
- 238 New Zealand (under Bob Park's and Tom Paulay's guidance) has always attempted to understand joint performance, while the Americans have preferred simple empirical approaches that have not correlated well with experimental results.
- 239 Note that compression field theory also supports the use of joint strength related to axial load level, and hence principal stress levels, as do experiments of unconfined joints in Europe.

Comment from John Mander.

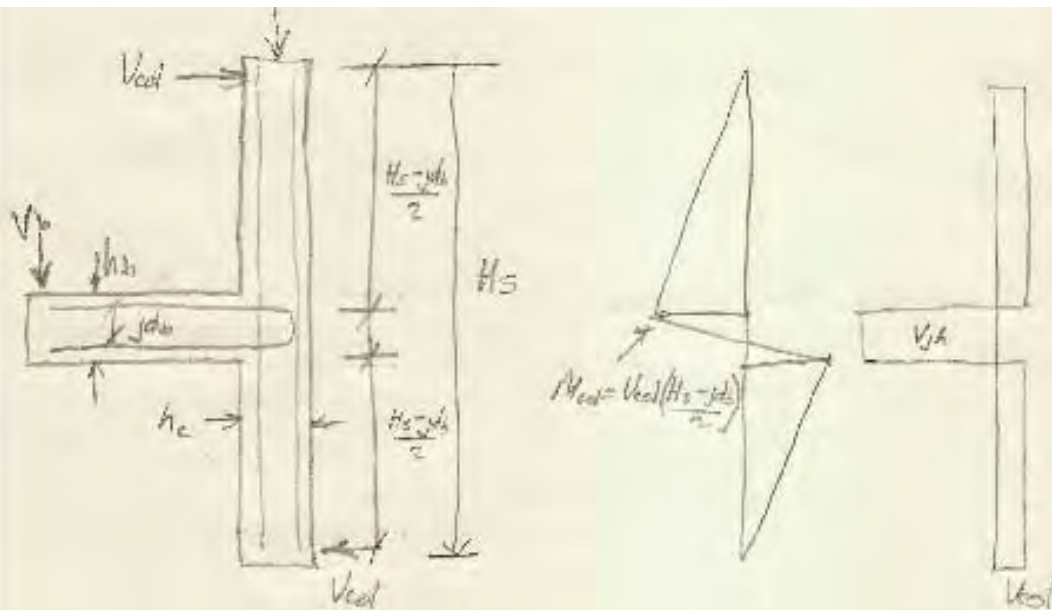
- 240 Following the feed-back I've done some searching, and some further analysis.
- 241 Compusoft are right, some good stuff has come from the Berkeley shop recently. Some of the stuff they mention, has not seen the light of day in the peer reviewed literature, that should therefore be disregarded. But there remains one really good paper by Park and Mosalam which is actually hot off the press. A copy of the paper is attached.
- 242 I feel really good about this paper as it uses a mostly a fundamental approach, with some calibration back to an extensive database. It is quite similar to the fundamental approach I developed previously and presented in my thick red dashed curve in fig. 1 of my previous missive. And btw, this was NOT based on the beam being critical, as one critic previously wrongly claimed!
- 243 The Park paper is strictly for exterior columns, but our interior columns would apply here too [as per fig 1a].
- 244 The authors use a combination of all the best knowledge presented by others, and then develop a mechanics based solution. A couple of experimentally defined parameters remain, but they do a solid job on calibrating them.
- 245 The solution is calibrated for different beam-to-column aspect ratios, naturally this is pretty important because previous formulations essentially assume the joint-strut is 45-degrees, which for the CTV building it is not.
- 246 When applying the results as attached in the scan file, I find the equivalent COLUMN end moment to be $M_p = 154 \text{ kNm}$.
- 247 This is strangely similar to my previous FEMA 356 result of $M = 166 \text{ kNm}$ for interior and 133 kNm for the exterior.
- 248 The similarity is because the capacity would be some 20% stronger than FEMA 356, but this additional strength is offset by the fact that in EQ 9, the $\cos(\theta)$ value detunes the strength due to the aspect ratio of the joint, tall joints are weaker [no surprise there].
- 249 It should be noted that the Park paper is calibrated and thus limited to axial loads of about $P = 0.2 f'c A_g$. It turns out this is indeed mostly OK for all the exterior columns in the CTV Building. And of course the good thing is the strength is invariant with axial load over this range. So this means we should limit our column capacities to this at the joints. And the columns remain essentially elastic, which means we do not need to model them as fiber elements, as others have very rightly pointed out.
- 250 But what of the interior columns in the E-W direction along line 2 and 3?
- 251 Everyone claims, including me [see my thick red dashed line again], that axial load must have some effect. Its intuitive, isn't it?
- 252 Well maybe. Park and Mosalam in section 2.4 of their paper mount an argument on this too. After arguing with themselves, they come to the conclusion like this, and I paraphrase: "Well shucks, this is complicated, and too hard for our brains, and we

don't have any experimental results to fall back on to prove otherwise, let's just park it and talk about where we do have heaps of results, but they are so all over the map we don't need to worry." See figure 5 which is related to this line of thinking.

- 253 My own thoughts are these. One would think that as the axial load increases, it should be somewhat beneficial in providing more shear resistance [as per the Mohr's circle stress analysis formulations imply, like Compusoft have been touting]. I too fell into this trap for 5 minutes. But the reality is this. As the axial load increases, and if the column is WEAKER than the beam, then the eccentricity reduces such that $e = M/P$. As the eccentricity decreases, the strut angle in the joint must increase, so the corner to corner strut angle becomes

$$\theta = \text{atan} [(j_d_beam) / (2e)] = \text{atan} [((j_d_beam) * P / (2M)]$$

- 254 And as theta increases, cosine [theta] as in Eq 9 of the P&M paper decreases along with the shear capacity.
- 255 So the angle change has an offsetting effect. This is why it is not surprising to see more or less a constant flat surface in experimental results plotted in Fig 5 of the P&M paper where $\Gamma_n \sim 1.0$ [MPa units]
- 256 Accordingly, it is my suggestion that in order to move forward we need to take the bull by the horns and adopt something for gamma for the interior beam-columns joints.
- 257 The beauty of adopting a uniform joint capacity over a wide range of axial loads is we can model the beams as elastic, the columns as mostly elastic with what amounts to a constant capacity fuse at each end [the joint restricted capacity].
- 258 This also obviates the need for using a fiber model that others have rightly pointed out must not be used. And the most attractive point of all, no post-processing of what the joint does will be needed, as it drives the outcome directly.(see papers by Park and Mosalam, Appendix C)



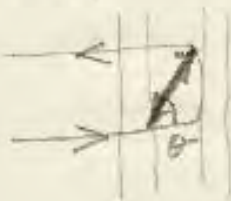
$$V_{jh} = \frac{2 M_{col}}{j d_b} = \frac{2 V_{col} (H_s - j d_b / 2)}{j d_b} \quad \text{(BMD)}$$

$$V_{jh} = V_{col} \left(\frac{H_s}{j d_b} - 1 \right) = \sigma_j b_j h_c \sqrt{f_c}$$

$$M_{col} = V_{jh} \frac{j d_b}{2} = b_j h_c \frac{j d_b}{2} \sqrt{f_c} \sigma_j$$

$$M_{col} = 0.4 \times 0.4 \times \frac{440}{2} \sqrt{37.5} \sigma_j = 215 \sigma_j \text{ kN-m}$$

Upper bound solution: $\gamma_{max} = 1.9 \frac{\cos \theta}{1.31 + 0.085 h_b / h_c}$



$$\theta = \tan^{-1} \frac{440}{280} = 57.5^\circ$$

$$\cos \theta = 0.537$$

$$\gamma_{max} = \frac{1.9 \times 0.537}{1.31 + 0.085 \times 550 / 400} = 0.715$$

because joint (beam) is over-reinforced $SI > 0.97$

$$\therefore \gamma_{max} = 0.715 \Rightarrow \underline{M_{col} = 154 \text{ kN-m}}$$

Comment from Derek Bradley.

259 We will look though this. In the interim though, do you have any thoughts on the backbone curve we sent through? We note that the blue backbone curve was derived from the same research as the paper you mention below. We have compared the recommended curve against other data and have found that it is broad agreement (see attached).

260 In addition, do you have any comment on the stress/strain profile for the concrete? You mentioned that some of the concrete you had tested had shown ultimate strains of up to 0.008, however we have proposed 0.006 as being more of a probable ultimate strain. Comments would be appreciated. Comments on the stress/strain profile would also be appreciated.

Comment from John Mander

261 I found another paper by the same authors who appear to be doing a bit of double dipping on this topic.

262 Regarding the force-deformation they do make a good point.

263 There are two types of joints:

264 BJ, where the beam yields first in flexure and then the joint goes later; this leads to tri-linear behavior.

265 J: where the joint is weaker than both the beams and the columns [as in the CTV Building], the behavior is bilinear shear-brittle. However, the \$64,000 question is: what is the post-peak slope?

266 I will do some more digging. Some of the references you cite are promising, some are not because they have not been through an independent peer review process. But I'll look further afield as well.

(see *ACI Moselam –Joints.pdf*)

Comment from Derek Bradley.

267 Do you have any comment on the concrete stress/strain?

Comment from John Mander.

268 I'm not sure why you need to know this, unless you are using fiber models, which as already several have said is not kosher. But if you must know, there is an ambiguity in what the failure strain is and it depends on the context.

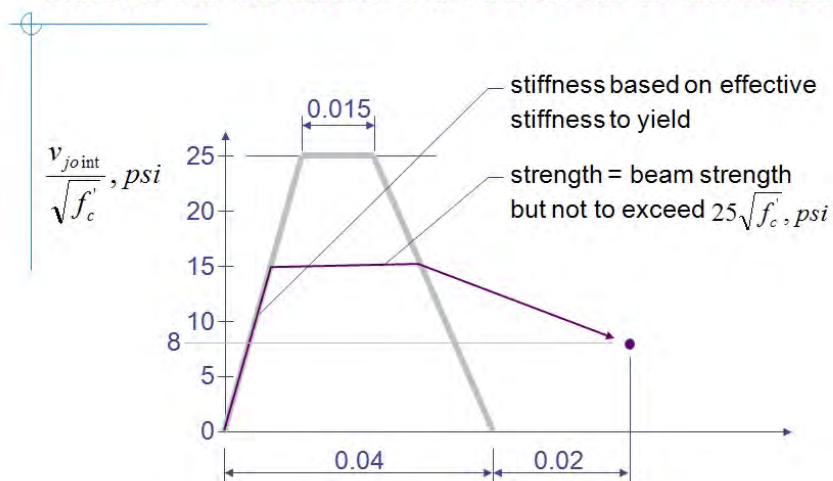
269 The lowest you will see is for pure compression tests and this can be as small as 0.004 under dynamic conditions. But this is never really seen, unless in a large-scale lab test.

- 270 For flexure a higher value is needed. Interestingly, the thicker the cover, with less transverse steel the stain is much larger, and as much as 0.009 to 0.01.
- 271 For flexure, such as the CTV columns with moderately thick cover, 0.0085 is about right.
- 272 See table 1 in attached paper. (see ASCE2011 Mahdu & Mander – Appendix C)

Comment from Derek Bradley.

- 273 We have been doing some more digging of our own, and have found a couple more interesting papers related to the (cyclic) stress-strain behaviour of joints. We've attached three of them to this email.
- 274 The Cellik paper is probably less interesting, and certainly less clear in its presentation, but we felt there might be value in sending it as it provides further support for the Walker/Alire data having been considered by other researchers and accepted as valid.
- 275 We will be working over the next couple of hours to develop backbone curves based on the Anderson paper, and will send these through when completed. However, given the time constraints we would appreciate your comments (at least initial thoughts) today.

Suggested envelope relation *interior connections with continuous beam bars*



Backbone. cf J.Moehle

(See Cellik and Ellingwood.pdf, Lehman et al 13WCEE, Anderson Joint Model.pdf – see Appendix C)

Comment from John Mander

- 276 I have attached some figures from an early paper by Nigel Priestley on the topic.
- 277 If you read the paper, at the time it was somewhat speculative and indicative needing more results to calibrate. Well more than a decade has gone by, and not much new stuff has turned up.
- 278 Most of the tests as far as I can tell, have stronger columns than beams. In fact, all the detailing was fine EXCEPT for the joints, and in spite of this, few, if any have a constructive model.
- 279 If you look at the results carefully, then you can generally see something like Fig 18 exists; fig 16 is a simplified version of fig. 18.
- 280 I really think we need to keep this envelop elegantly simple [like my latest stress-strain models] as they are more versatile in a general sense. And I feel fig 18 fits the bill accordingly.
- 281 Regardless of the peak [which we seem to almost have some agreement on], that can be the plateau on the left, and then all we need to do is assign two more coordinates, one will be around 0.02 to 0.04 radians, at y% of the peak, and another at an ultimate rotation with zero capacity. Here if we wanted to have a residual capacity, which would probably be the right thing to do, we should just assign a very large value for the ultimate rotation.
- 282 We do need to remember that the CTV columns are critical components and not the beams, this makes everything brittle like in Fig 16/18. The initial slope is really the flexural behavior, while the post-peak behavior is the joint only.
- 283 I would suggest
the mid-point be made [0.03rad, 50%]
and at ultimate [0.1rad, 0.0]

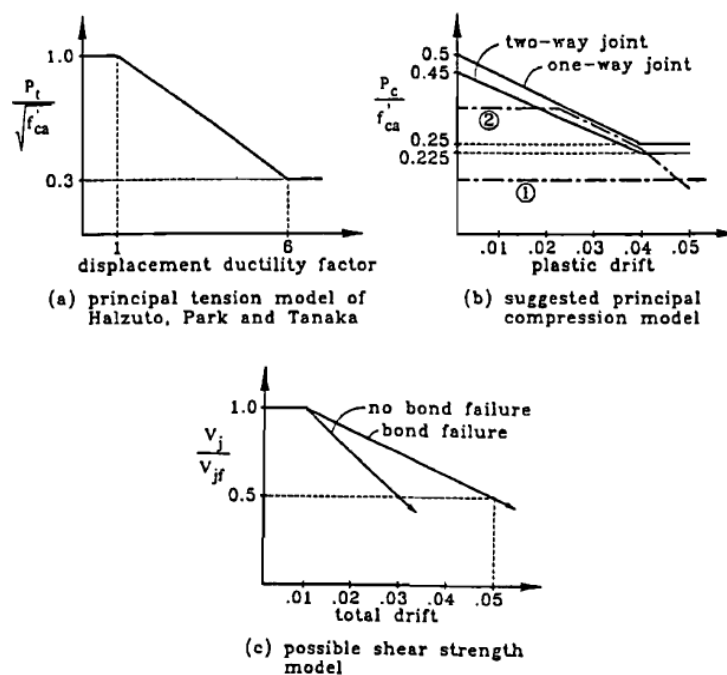


Fig. 16. Possible failure models for interior beam-column joints.

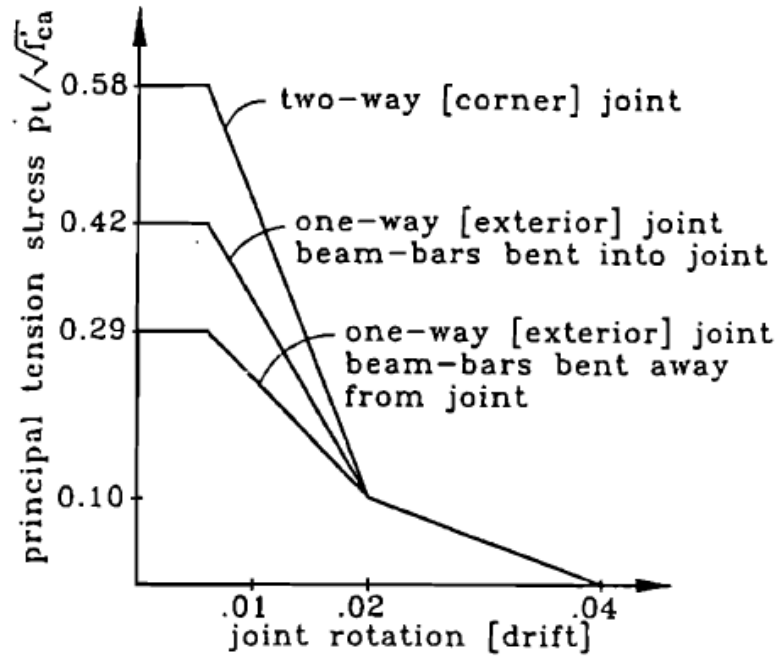
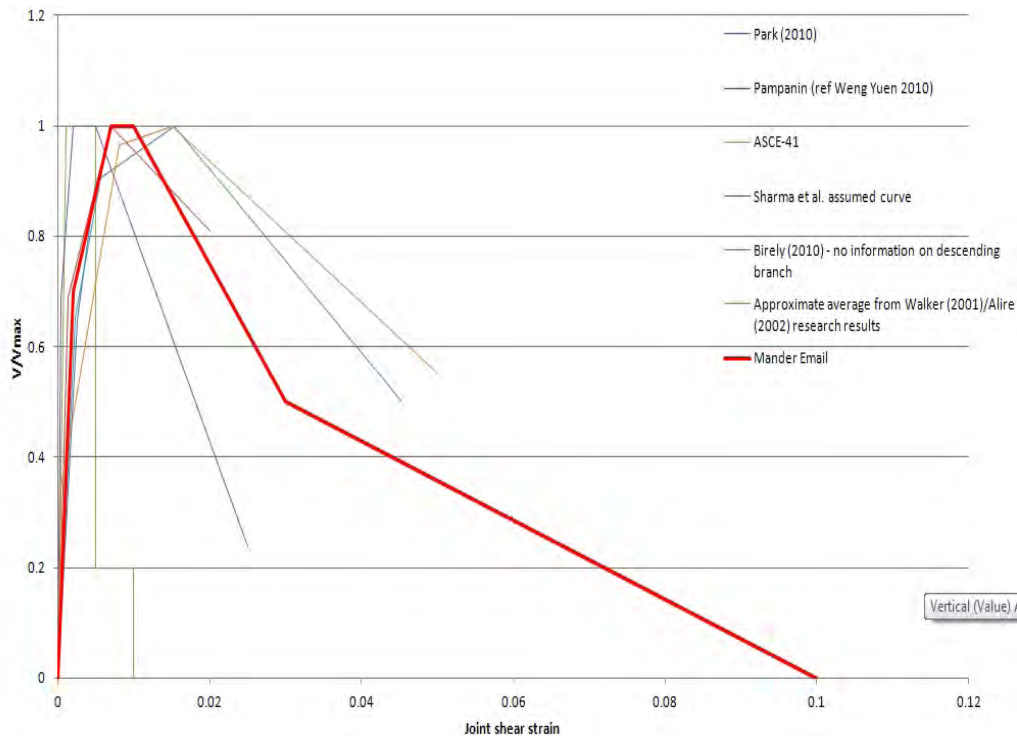


Fig. 18. Suggested strength degradation model for exterior and corner joints.

From Priestley (1997), J. EQ.Eng, 1(1),157-192

Comment from Derek Bradley

- 284 Attached is an image that shows our interpretation of the numbers you put in your last email. You will note we have added an initial elastic branch to the curve - this is defined by the points (0,0), (0.002,0.7), and (0.007,1). This has been added based on consideration of the previously shown backbones (i.e. we think it is realistic to represent elastic shear deformation of the joint core), and to aid modelling stability. The remainder of the curve is (0.01,1), (0.03,0.5) and (0.1,0) as per your email. If you agree, we will use this curve for all joints in the model, with strengths based on the outcome of current discussion.



Comment from John Mander.

285 This very close but not quite like I envisage it.

286 What I have in mind is there is a natural strength hierarchy. For low levels of lateral load, column and beam flexure govern up until the joint "cracks", then the displacement is within the lumped "hinge", which is really a surrogate for the joint rotation. If loading is in the forward direction then the hinge governs by softening. If the displacement reverses, there is a combination of elastic-plastic hysteretic behaviour, as per the hysteretic rule, which presumably would be the Takeda model in SAP 20000. So it should just go straight up [column], peak, and then straight down [joint]. Also presently you are showing it going up in a bi-linear fashion, but in that I suspect you mean the joint is bi-linear. But that need not be the case, the joint remains essentially rigid until it "cracks and immediately softens. Remember the top plateau is only for when you also have beam yielding, which in effect slowly commences the joint softening. What we have is a more sudden death.

287 Might I suggest you try putting a small sub-assembly together and run it through its paces under a couple of cycles to see that it captures the correct behaviour.

Comments from Nigel Priestley in response to models proposed by Derek Bradley

(see *Compusoft 12026.xx Beam-ColumnJoint Discussion*) and (see *ASCE211Madhu-Mander-1.pdf in Appendix C*)

288 Strain penetration: Your fibre model is different, from what I am familiar with, which would have a linear strain profile along the fibre length, with 2 gauss points within the fibre length. The characteristic moment is defined at the gauss point closest to the member end, and should coincide with it, ideally.

- 289 Spalling: I have previously suggested that a maximum compression strain of perhaps 0.007 might be sustainable at the beam/column interface, as a result of confinement of the column concrete provided by the beam and slab. This level of compression strain has been recorded in columns immediately above a rigid foundation. However, considering the seating of precast beams on the column top, and the generally poor detailing of the joints, the level of confinement provided by a rigid foundation could not occur in the CTV columns (except perhaps at foundation level). Further because of the high compression level in the columns, the compression strains will continue at high levels for longer than the usual distance from the column ends. In regions separated from the column ends, spalling will not be inhibited by adjacent-member confinement, and might initiate at strains as low as 0.0025.
- 290 My view is that the 0.004 you used was probably the correct value. Certainly you should not use more than 0.006, which I view to be non-conservative. I also note that the total deformation of the columns is not increased significantly when the compression strain is increased to 0.007.
- 291 Takeda model for concrete: I'm still uncertain about this. Can you sketch the typical hysteretic response?
- 292 Beam Column Joint Modelling: I agree with your assessment. Presumably John Mander has also seen your reasoning?
- Comments from Nigel Priestley on the Compusoft Beam-Column Joint Model.*
- 293 I think Nicholas has done an excellent job of presenting the different available models for joint shear stress/strain behaviour of unreinforced joints. I agree with the conclusions in the report for both strength and deformation capacity. I can add that an unreinforced exterior corner joint I tested in the late 1990's under variable axial load (including quite high levels) did not degrade rapidly as would be predicted by the FEMA356 approach. Unfortunately The data are confidential and embargoed by Court.
- 294 The problems I see are related to Appendix A, and the assumptions inherent in the calculations presented. These assume that the Column shears are equal above and below the joint, and that beam moments are also equal (and opposite) on either side of the joint. These will not generally be the case, particularly when the beams have not yielded, and the columns are also still in the "elastic" phase of response. Gravity moments in the beams will have a very significant influence on response, meaning that moments on either side of the joint will differ significantly.
- 295 Further, there is a big difference between the joint transfer mechanism when the beams compression force (which provides 50% of the 2T part of the equation) is primarily provided by concrete compression rather than by compression force in previously yielded reinforcement. When the latter condition exists, and the beam moments are both at yield capacity, then the Equation in App A is correct, but when the beam compression force is primarily provided by concrete compression, a diagonal strut carries that portion of the shear diagonally through the joint, rather than

by bond. It is difficult to model the changing conditions in a numeric model, and I don't have confidence that acceptable answers will result from the proposed model.

- 296 Having said that, I think the model could be improved by using the average of the column shear above and below the joint instead of the shear above the joint, and note that my argument about the diagonal strut carrying part of the joint shear means that the model will yield conservatively low strength if neither the beams and columns are yielding.

Response from Nic Brooke (Compusoft) to Nigel Priestley

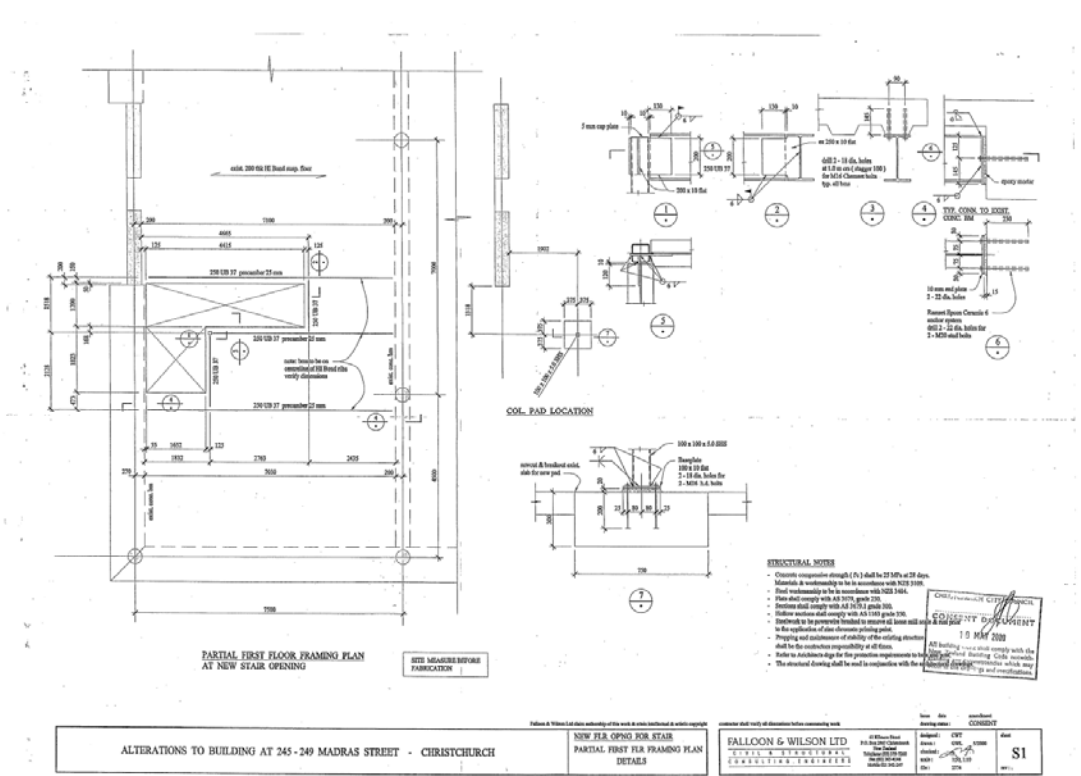
- 297 Thank you for the kind comments about the report, and the useful information also. I believe I came across mention of the corner joint test you referred to - Jack Moehle makes mention in a couple of documents of a test you conducted in relation to the Royal Palms building.
- 298 We are in full agreement about the issues inherent in the Appendix A calculations, and the probability that the results generated will be questionable. Within the time and software limitations imposed, it is unfortunately not realistic to implement the joint degradation in a more rigorous manner.

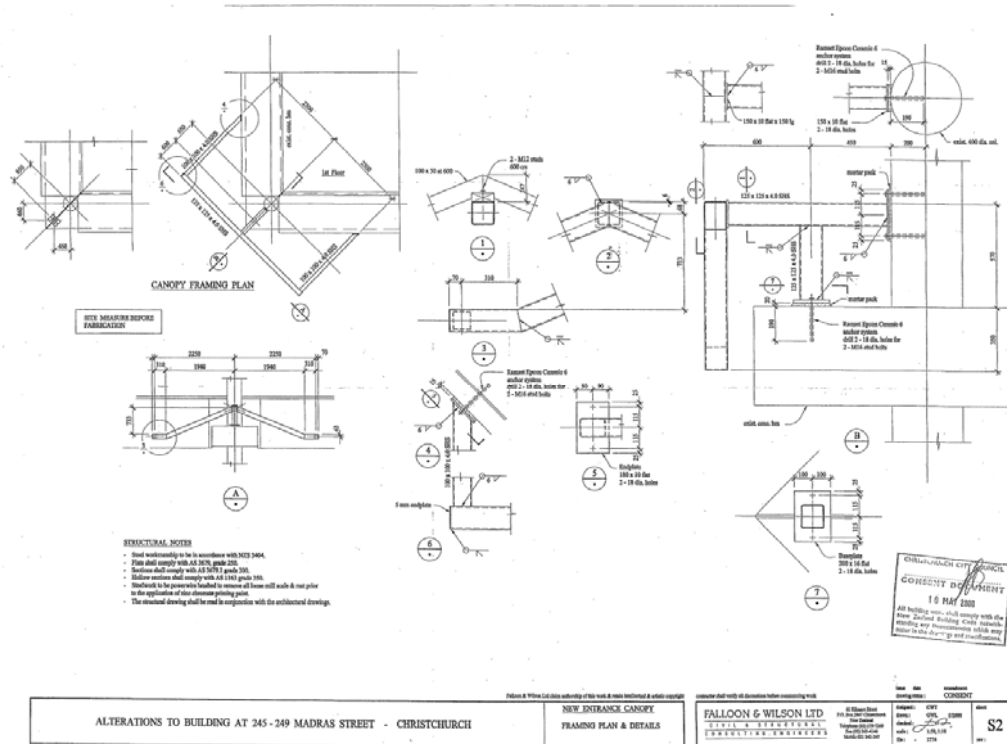
Analysis Procedures.

- 299 Allowing the analyses to progress beyond potential failure and then post-processing the results to determine if failures leading to collapse is very useful in the assessment of buildings and may fill a purpose in the CTV analyses in trying to determine the likelihood, due to uncertainties in the strengths of components, of one failure mechanism being only slightly more likely than another failure mechanism in the structure. However, in the study of the CTV building analyses models must also be used where failure of members or components is allowed. If the analysis fails at a certain time in the analysis then it is likely to mean that the structure may also fail at that time. It is hoped, that up to the point of analysis failure, the results of the analysis are available to the analysts.

Other Issues (Internal Stair Case).

- 300 Buddle-Findlay passed the following drawings to the expert panel. While loathe to complicate what is already a complicated and well-advanced process, it has recently come to our attention that CTV installed an internal staircase between levels 1 and 2 of the CTV building in 2000.
- 301 Can you tell us whether this staircase is modelled in the Compusoft NTHA model? If not, it seems to us that this is a critical feature of the building that ought to be accounted for in the modelling. Could you please circulate this email or a summary of it amongst the panel and invite comment?





Comment from Derek Bradley.

302 I can confirm that the floor penetration for this stair has been accounted for in the model.

Other Issues: (Earthquake excitations between 4th September 2010 and 22nd February 2011).

This email from Willie Palmer was passed to Athol Carr by the Royal Commission.

NLTHA Issue

- 303 Noting that the earthquake events listed in paragraphs 4.1.2 and 4.1.3 of the draft directions (4 September 2010 and 22 February 2011), these events are far better included in the NLTHA panel analysis, which I understand they are. However, those two earthquake events alone would seem to be inadequate. Between 4 September 2010 and 22 February 2011 there were many additional earthquakes of a magnitude in the range of the Boxing Day earthquake (4.91) or higher. All of these earthquakes had the potential to contribute to the cumulative fatigue initiated by the first 4 September 2010 earthquake at 4.35am. In fact many of the aftershocks of such magnitude occurred on the same day (4 September) and immediately following days, along with other dates prior to 22 February.
- 304 By way of example I **enclose** a list of the major earthquakes of magnitude 5 and above (plus the Boxing Day earthquake) in the relevant period. This list is compiled from: <http://www.geonet.org.nz/canterbury-quakes/significant.html> . For the list in question currently very few of the records are available on the GeoNet ftp site. Therefore, it is not possible for me to indicate the peak ground accelerations across the city without access to these records. No doubt this information is readily available to those more familiar with use of the records than me. The GeoNet reference numbers are included in the attached pdf. However, in the context of a magnitude 7.1 earthquake on 4 September 2010 at 4.35am, causing damage arguably at design level to the CTV Building, the list illustrates that there are other material earthquakes that need to be taken into account in any NLTHA analysis.
- 305 Action required
- 306 Accordingly, on behalf of ARCL we suggest that the NLTHA expert analysis should include modelling of the significant earthquake events between 4.35am on 4 September 2010 and 22 February 2011 so that the cumulative fatigue effect can be considered. Working from the attached list obviously more data from GNS will need to be obtained as to the PGAs and responses. I am copying this email to Professor Carr so that he is aware of this request.
- 307 Again, I am happy to discuss any of the above and look forward to your response.

Comment by Athol Carr

- 308 This is outside the DBH brief which only specified considering the September and February events. Considering that the computational models have not used any cumulative damage modelling this would require an enormous amount of post-processing. Such assessments would also require running all analyses for the full duration if we are measuring cyclic information. The number of earthquake records that would have to be processed to get them in the form suitable for NLTHA is considerable if the attached list is used.

GeoNet Reference Number	Date (local time)	Magnitude
3366155	Sat, Sep 4 2010 4:56 am	5.3
3366230	Sat, Sep 4 2010 7:56 am	5.2
3366310	Sat, Sep 4 2010 11:12 am	5.3
3366313	Sat, Sep 4 2010 11:14 am	5.3
3366452	Sat, Sep 4 2010 4:55 pm	5.4
3367742	Mon, Sep 6 2010 11:24 pm	5.2
3367749	Mon, Sep 6 2010 11:40 pm	5.4
3367832	Tue, Sep 7 2010 3:24 am	5.4
3368445	Wed, Sep 8 2010 7:49 am	5.1
3382676	Mon, Oct 4 2010 10:21 pm	5.0
3388384	Wed, Oct 13 2010 4:42 pm	5.0
3391440	Tue, Oct 19 2010 11:32 am	5.0
	Sun, Dec 26 2011 10:30 am	4.9
3450113	Thu, Jan 20 2011 6:03 am	5.1

This list is compiled from the GeoNet webpage (<http://www.geonet.org.nz/canterbury-quakes/significant.html>) and do not represent all of the aftershocks between September 4, 2010 and February 22, 2011.

CTV Non-linear Time-History Analyses Report

Comment by Barry Davidson.

- 309 It is possible to run these analyses to assess the cumulative damage, although we note that this would take weeks of analysis time and then a number of weeks to post-process the results.
- 310 Whilst we are happy assist in anyway, it is our professional opinion that the additional analyses would add little benefit to the understanding of 'why' the CTV Building fell down i.e. the identification of the critical elements that initiated the collapse, and a possible failure sequence. There is little evidence that "fatigue" would have contributed to any failure. Current NLTH analyses indicate that the Darfield event was not sufficient to cause collapse, and the Lyttelton event would have caused collapse assuming that the building was in **an** undamaged state at the commencement of the EQ.
- 311 We would recommend that the refined NLTH analyses be undertaken for the Darfield record and the damaged state be reviewed, along with the expected change in building response post earthquake. Assessments could then be made by reviewing the spectral accelerations for the following records (in comparison to Darfield's). This would allow quick assessment to be made on the likely effect (if any) that these EQ's would have on elemental damage.

Comments from Athol Carr to Marcus Elliot of the Royal Commission.

- 312 On the issue of looking at all earthquakes greater than magnitude 5 in the period from 4 September to 22 February I have had only a response from Barry Davidson. I agree with his comments. The magnitude 5+ earthquakes are about two orders of magnitude less than the September event, i.e energy release 30+ to 900 times less. The general comment is that the September earthquake would not cause the CTV building to fail (I use that word as collapse implies that it literally falls) and in fact it was standing after the event. The analyses indicate that the building would collapse in the February earthquake even if the building was undamaged (not brand new as the drag bars were not there in 1987) in any previous event. The comment was that, yes the analyses could be done, it would probably take weeks and further even more weeks to interpret the data. The general comment was that they could, if desired, be done for the September and February events, look at the damage caused by the September earthquake and then look at the response spectra for the other events and see if they would give any significant response to the structure. Most of the events quoted were in the Darfield-Greendale area and were thence some distance from Christchurch. The exception is the Boxing Day event. Here the epicentral distance is small. My experience on the analyses of the Grand Chancellor building is that the Boxing Day earthquake generated sizable floor accelerations in the building but that the displacements were minimal, almost down at the noise level. It seemed to have its major effects on the very short natural period URM structures that had not been damaged in the September earthquake due to effects of different principal excitation directions).

Appendix A. Panel of Experts to Consider NLTHA for CTV Building.

**ORDER AS TO DIRECTIONS IN RELATION TO
NON-LINEAR TIME HISTORY ANALYSIS EVIDENCE**

1. The Royal Commission directs that the expert witnesses whose evidence will relate to Non-Linear Time History Analysis (NTHA) of the response the CTV Building are to confer.
2. These witnesses are:
 - 2.1. Ashley Smith.
 - 2.2. Derek Bradley/Barry Davidson/ Tony Stuart.
 - 2.3. Athol Carr.
 - 2.4. Professor John Mander.
 - 2.5. Professor Robin Shepherd.
 - 2.6. Brendon Bradley.
 - 2.7. A representative of GNS Science.
3. The Royal Commission appoints Professor Athol Carr as a facilitator with authority to take the steps necessary to achieve the purposes of this order.
4. The purposes of the experts conferring are:
 - 4.1. To endeavour to reach agreement on the input data to be used to conduct a NTHA of the response of the CTV Building which provides the most reliable model of the response of the Building to the earthquakes at 4.35am on 4 September 2010 and 12.51pm on 22 February 2011.
 - 4.2. Where agreement cannot be reached on the inputs, to identify:
 - 4.2.1. The inputs which cannot be agreed.
 - 4.2.2. The reasons for the disagreement.
 - 4.3. To produce NTHA results which provide the most reliable model of the response of the Building to the earthquakes at 4.35 am on 4 September 2010 and 12.51pm on 22 February 2011, and which can then be analysed and interpreted. In this respect:

- 4.3.1. Compusoft has already conducted a NTHA of the response of the CTV Building ('the Compusoft NTHA').
 - 4.3.2. The experts are to consider whether the Compusoft NTHA provides the most reliable model of the response of the Building to the earthquakes at 4.35am on 4 September 2010 and 12.51pm on 22 February 2011.
 - 4.3.3. If the experts cannot agree about whether the Compusoft NTHA provides the most reliable model, the experts are to identify the reasons for their disagreement.
- 4.4. If the experts do not reach agreement that the Compusoft NTHA provides the most reliable model of the response of the Building to the earthquakes at 4.35am on 4 September 2010 and 12.51pm on 22 February 2011, a further NTHA is to be carried out. In this case:
 - 4.4.1. The experts are to agree on the inputs to be used. If agreement is not reached, they are to identify their reasons for disagreement.
 - 4.4.2. If agreement is not reached, or in the opinion of the facilitator is not likely to be reached, the facilitator is to report to the Royal Commission on the areas of disagreement and their significance so that the Commission can consider whether any further orders are required.
5. These directions apply to NTHA input data and NTHA results, but not to any evidence relating to subsequent interpretation of NTHA results, which shall be a matter for individual parties to address.
6. The experts are to take all necessary steps to achieve the purposes described above, including:
 - 6.1. All input data used in the Compusoft NTHA and any other NTHA are to be made available to every other expert.
 - 6.2. The data is to be provided in a form suitable for use in an alternative model.
7. The input data used in the Compusoft NTHA:
 - 7.1. Is confidential to the persons listed in paragraph 2 of this order.
 - 7.2. Must not be used by any expert for any purpose other than those described in these directions.

- 7.3. May be disclosed to any party's legal advisors, but those advisors must not disclose it to their client or any other person.
- 7.4. Must be returned to CompuSoft following the conclusion of the CTV hearing.
- 7.5. Must not be copied or retained.
8. All other information shared between experts:
 - 8.1. Remains confidential to the parties, their legal advisors and the experts except where it is included in the joint report.
 - 8.2. Must not be used by any expert for any purpose other than those described in these directions.
 - 8.3. Must be returned to the provider following the conclusion of the CTV hearing.
 - 8.4. Must not be copied or retained.
9. The experts are to produce a joint report for the Royal Commission which identifies the following:
 - 9.1. All areas of agreement.
 - 9.2. All areas of disagreement, including the reasons for the disagreement.
 - 9.3. The results of any further NTHA/s.
10. The experts are to comply with the Code of Conduct for Expert Witnesses set out in schedule 4 to the High Court Rules. In particular the experts are to:
 - 10.1. Attempt to reach agreement about the matters set out above.
 - 10.2. Exercise independent and professional judgement and not to act on the instructions or directions of any person to withhold or avoid agreement.
11. The joint report is to be provided to the Royal Commission by 18 June 2012. If the date cannot be met, the Royal Commission is to be advised immediately this becomes apparent.
12. The provisions of Practice Note No 2 in relation to the filing of briefs of evidence no longer apply in relation to evidence from the experts listed above relating to NTHA input data and NTHA results.
13. The Royal Commission reserves the right to alter these directions.

14. Any matters of dispute about the processes to be followed must be raised with the Royal Commission forthwith.
15. The experts may be required to participate in a 'hot tub' in the course of the CTV hearing during which they will be called upon to give evidence and answer questions about the matters set out in these directions.
16. These directions are made in the exercise of powers of the Chair of the Royal Commission as a Judge of the High Court of New Zealand under section 13 of the Commissions of Inquiry Act 1908.

Dated: 18 May 2012



The Honourable Justice Cooper

Chair of the Royal Commission

A Judge of the High Court of New Zealand

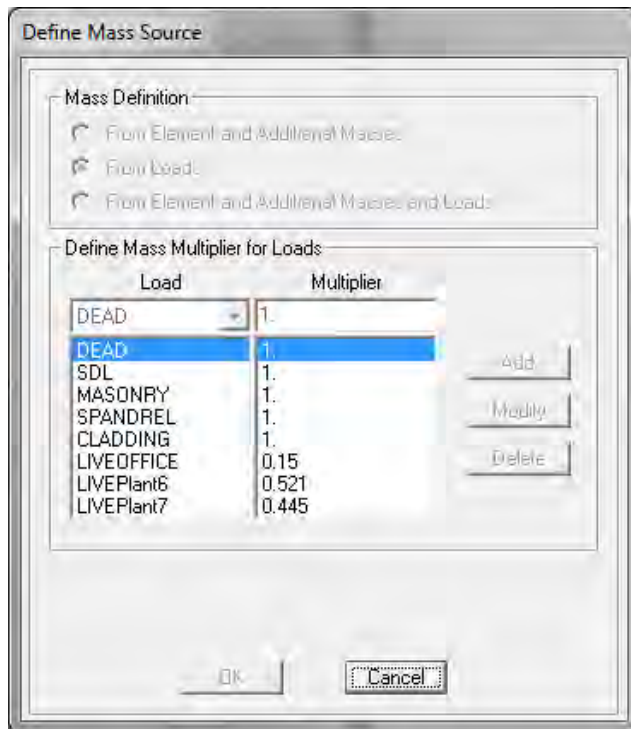
Appendix B.

SAP2000 Screen Plots of CTV NLTHA Model Documentation and Meshing Details

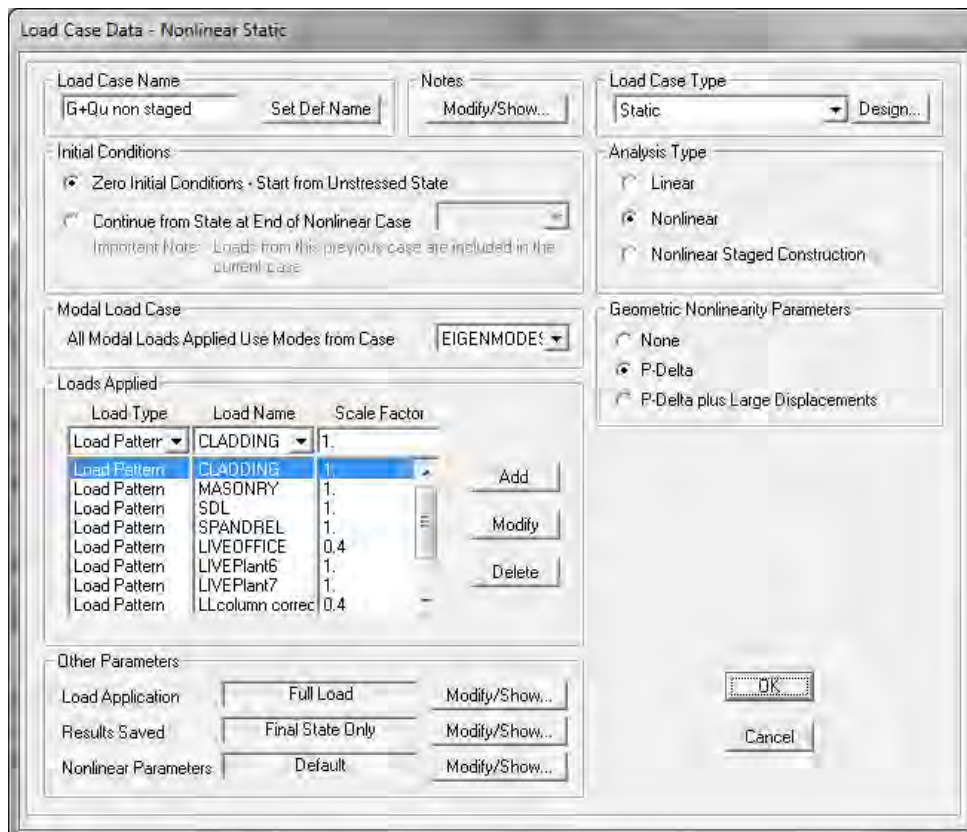
1. Analysis Cases.
2. Column Hinges
3. Foundations
4. Meshing
5. Miscellaneous Links.
6. Sample Beam Hinges
7. Wall Properties.

Analysis Cases & Mass Source

Dynamic mass source:



Gravity precursor case for the time history runs:



Lyttelton CBGS TH analysis case:

Load Case Data - Nonlinear Direct Integration History

Load Case Name: CBGS110221u1u2u3 Set Def Name Modify/Show... Notes: Modify/Show... Load Case Type: Time History Design...

Initial Conditions:

Zero Initial Conditions - Start from Unstressed State

Continue from State at End of Nonlinear Case G+Qu non sta

Important Note: Loads from this previous case are included in the current case.

Analysis Type: Linear Nonlinear

Time History Type: Modal Direct Integration

Model Load Case: Use Modes from Case: EIGENMODES

Geometric Nonlinearity Parameters:

None P-Delta P-Delta plus Large Displacements

Loads Applied

Load Type	Load Name	Function	Scale Factor	Time Factor	Arrival Time	Coord Sys	Angle
Accel	U1	N00E_20	9.81	1.	-16.5	GLOBAL	0.
Accel	U1	N00E_20110	9.81	1.	-16.5	GLOBAL	0.
Accel	U2	N90E_20110	9.81	1.	-16.5	GLOBAL	0.
Accel	U3	Vert_2011022	9.81	1.	-16.5	GLOBAL	0.

Show Advanced Load Parameters Add Modify Delete

Time Step Data:

Number of Output Time Steps:

Output Time Step Size:

Time History Motion Type:

Transient Periodic

Other Parameters:

Damping: Proportional Damping Modify/Show...

Time Integration: Hilber-Hughes-Taylor Modify/Show...

Nonlinear Parameters: Default Modify/Show...

OK Cancel

Non-linear case parameters are listed below

Mass and Stiffness Proportional Damping

Damping Coefficients

	Mass Proportional Coefficient	Stiffness Proportional Coefficient
<input type="radio"/> Direct Specification		
<input checked="" type="radio"/> Specify Damping by Period	0.2626	4.290E-04
<input type="radio"/> Specify Damping by Frequency		

	Period	Frequency	Damping
First	1.29		0.028
Second	0.05		0.028

Recalculate Coefficients

OK Cancel

Time Integration Parameters

Method

<input type="radio"/> Newmark	Gamma	
	Beta	
<input type="radio"/> Wilson	Theta	
<input type="radio"/> Collocation	Gamma	
	Beta	
	Theta	
<input checked="" type="radio"/> Hilber - Hughes - Taylor	Gamma	0.5
	Beta	0.25
	Alpha	0
<input type="radio"/> Chung and Hulbert	Gamma	
	Beta	
	Alpha	
	Alpha-m	

OK Cancel

Nonlinear Parameters

Material Nonlinearity Parameters

- Plane Element Tension/Compression Only
- Plane Element Hinge
- Cable Element Tension Only
- Link Gap/Hash/Spring Nonlinear Properties
- Link Diver Nonlinear Properties
- Time Dependent Material Properties

Solution Control

Maximum Substep Size	0
Minimum Substep Size	0
Maximum Constant-Stiff Iterations per Step	10
Maximum Newton-Raphson Iter. per Step	40
Iteration Convergence Tolerance (Relative)	1.000E-04
Use Event-to-event Stepping	Yes
Event Lumping Tolerance (Relative)	0.01
Max Line Searches per Iteration	20
Line-search Acceptance Tol. (Relative)	0.1
Line-search Step Factor	1.618

Reset To Defaults

OK Cancel

Lyttelton CCC TH analysis case:

Load Case Data - Nonlinear Direct Integration History

Load Case Name: Notes:

Load Case Type:

Initial Conditions:

Zero Initial Conditions - Start from Unstressed State

Continue from State at End of Nonlinear Case

Important Note: Loads from this previous case are included in the current case.

Model Load Case:

Geometric Nonlinearity Parameters:

None

P-Delta

P-Delta plus Large Displacements

Analysis Type: Linear Nonlinear

Time History Type: Modal Direct Integration

Loads Applied

Load Type	Load Name	Function	Scale Factor	Time Factor	Arrival Time	Coord Sys	Angle
Accel	U1	N00E_20	9.81	1.	-15.04	GLOBAL	0.
Accel	U1	N00E_201102	9.81	1.	-15.04	GLOBAL	0.
Accel	U2	N90E_201102	9.81	1.	-15.04	GLOBAL	0.
Accel	U3	Vert_2011022	9.81	1.	-15.04	GLOBAL	0.

Show Advanced Load Parameters

Time Step Data:

Number of Output Time Steps:

Output Time Step Size:

Time History Motion Type: Transient Periodic

Other Parameters:

Damping:

Time Integration:

Nonlinear Parameters:

Mass and Stiffness Proportional Damping

Damping Coefficients:

Direct Specification

Specify Damping by Period

Specify Damping by Frequency

	Mass Proportional Coefficient	Stiffness Proportional Coefficient
	<input type="text" value="0.2626"/>	<input type="text" value="4.290E-04"/>

	Period	Frequency	Damping
First	<input type="text" value="1.29"/>	<input type="text"/>	<input type="text" value="0.028"/>
Second	<input type="text" value="0.05"/>	<input type="text"/>	<input type="text" value="0.028"/>

Lyttelton CHHC TH analysis case:

Load Case Data - Nonlinear Direct Integration History

Load Case Name: CHHC110221u1u2u3 Set Def Name Notes: Modify/Show... Load Case Type: Time History Design...

Initial Conditions:
 Zero Initial Conditions - Start from Unstressed State
 Continue from State at End of Nonlinear Case G+Qu non sta
Important Note: Loads from this previous case are included in the current case.

Analysis Type:
 Linear
 Nonlinear
 Time History Type:
 Modal
 Direct Integration

Model Load Case:
 Use Modes from Case: EIGENMODES

Geometric Nonlinearity Parameters:
 None
 P-Delta
 P-Delta plus Large Displacements

Loads Applied

Load Type	Load Name	Function	Scale Factor	Time Factor	Arrival Time	Coord Sys	Angle
Accel	U1	N00E_20	9.81	1.	-16.	GLOBAL	0.
Accel	U1	N00E_201102	9.81	1.	-16.	GLOBAL	0.
Accel	U2	N90E_201102	9.81	1.	-16.	GLOBAL	0.
Accel	U3	Vert_2011022	9.81	1.	-16.	GLOBAL	0.

Show Advanced Load Parameters Add Modify Delete

Time Step Data:
 Number of Output Time Steps: 560
 Output Time Step Size: 0.02

Time History Motion Type:
 Transient
 Periodic

Other Parameters:
 Damping: Proportional Damping Modify/Show...
 Time Integration: Hilber-Hughes-Taylor Modify/Show...
 Nonlinear Parameters: Default Modify/Show...

OK Cancel

Mass and Stiffness Proportional Damping

Damping Coefficients:

Direct Specification
 Specify Damping by Period
 Specify Damping by Frequency

	Mass Proportional Coefficient	Stiffness Proportional Coefficient
	0.2626	4.290E-04

	Period	Frequency	Damping
First	1.29		0.028
Second	0.05		0.028

Recalculate Coefficients

OK Cancel

Darfield CBGS TH analysis case:

Load Case Data - Nonlinear Direct Integration History

Load Case Name: Notes:

Load Case Type:

Initial Conditions:

Zero Initial Conditions - Start from Unstressed State

Continue from State at End of Nonlinear Case

Important Note: Loads from this previous case are included in the current case.

Model Load Case:

Analysis Type: Linear Nonlinear

Time History Type: Modal Direct Integration

Geometric Nonlinearity Parameters:

None P-Delta P-Delta plus Large Displacements

Loads Applied

Load Type	Load Name	Function	Scale Factor	Time Factor	Arrival Time	Coord Sys	Angle
Accel	U1	N00E_20	9.81	1.	-28.9	GLOBAL	0.
Accel	U1	N00E_201009	9.81	1.	-28.9	GLOBAL	0.
Accel	U2	N90E_201009	9.81	1.	-28.9	GLOBAL	0.
Accel	U3	Vert_201009C	9.81	1.	-28.9	GLOBAL	0.

Show Advanced Load Parameters

Time Step Data:

Number of Output Time Steps:

Output Time Step Size:

Time History Motion Type: Transient Periodic

Other Parameters:

Damping:

Time Integration:

Nonlinear Parameters:

Mass and Stiffness Proportional Damping

Damping Coefficients:

Direct Specification

Specify Damping by Period

Specify Damping by Frequency

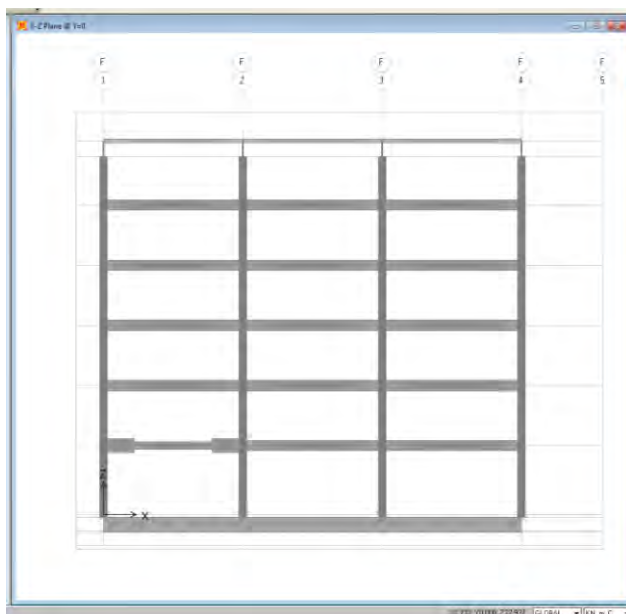
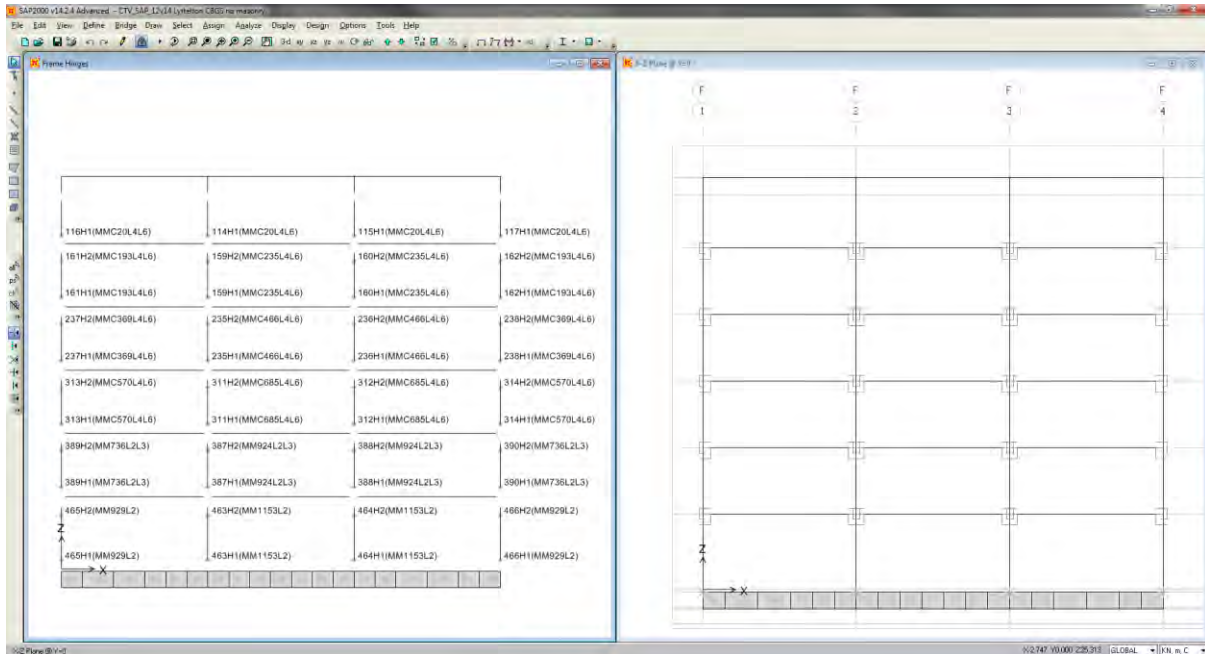
	Period	Frequency	Damping	
First	<input type="text" value="1.29"/>	<input type="text"/>	<input type="text" value="0.05"/>	<input type="button" value="Recalculate Coefficients"/>
Second	<input type="text" value="0.05"/>	<input type="text"/>	<input type="text" value="0.05"/>	

Mass Proportional Coefficient:

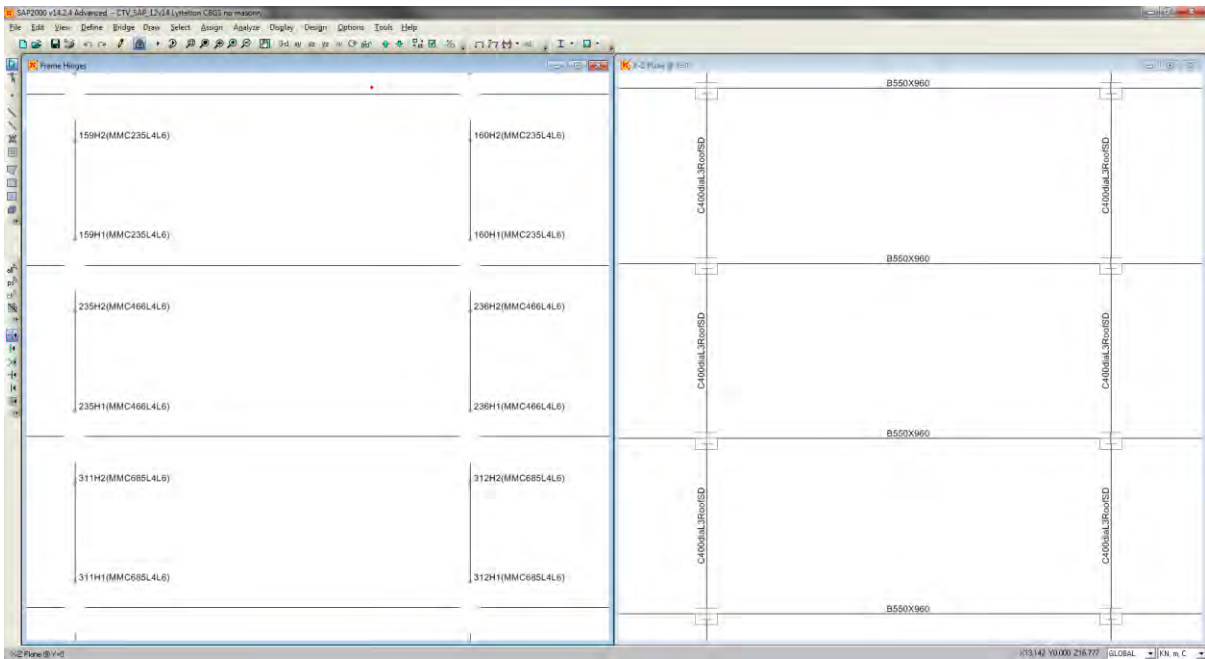
Stiffness Proportional Coefficient:

GL F column hinges

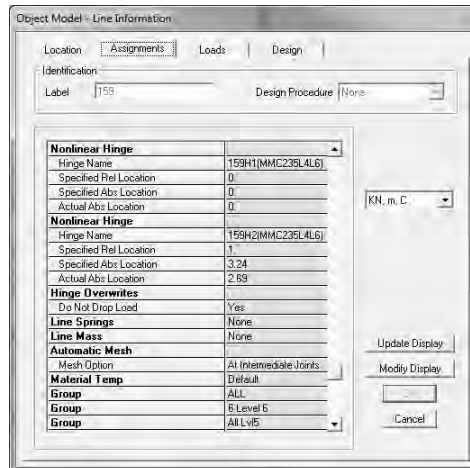
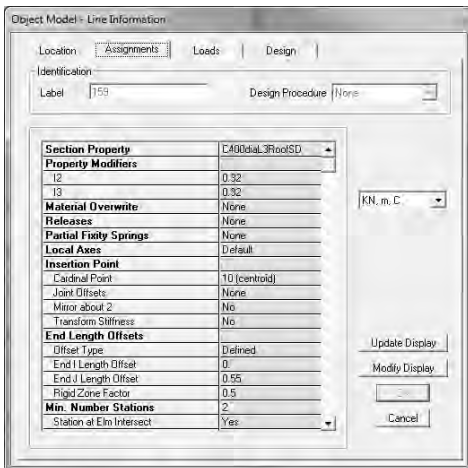
Note: Hinge naming convention is MMC466L4L6 i.e. '**MMC**' = MM hinge, '**466**' = Axial gravity load used to determine hinge property (G+Qu), '**L4L6**' = floor levels for which hinge values are valid i.e. columns above level 3 (this relates to the concrete strength used to determine hinge properties).



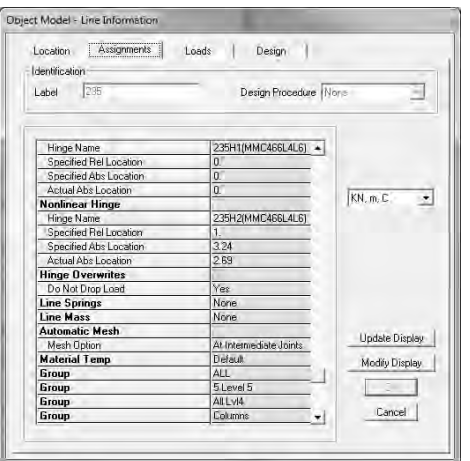
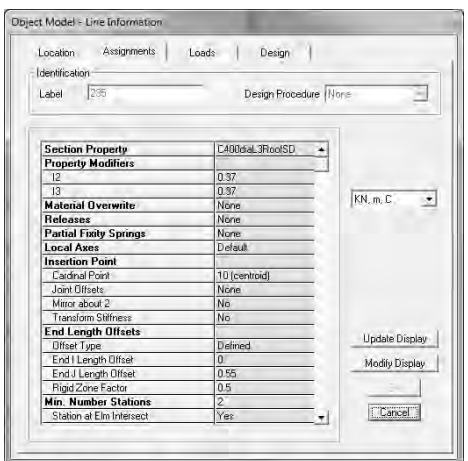
Frame F GL 2 & 3 levels 3-4, 4-5, & 5-6 section properties and hinges



Column F2 level 5-6 hinge assignments



Column F2 level 4-5 hinge assignments



Hinge MMC466L4L6 material properties and moment curvature information

SD Section Data

Section Name: C400diaL3RoofSD
 Section Notes: Modify/Show Notes...

Base Material: + 276MPaConcConfined

Design Type:
 No Check/Design
 General Steel Section
 Concrete Column

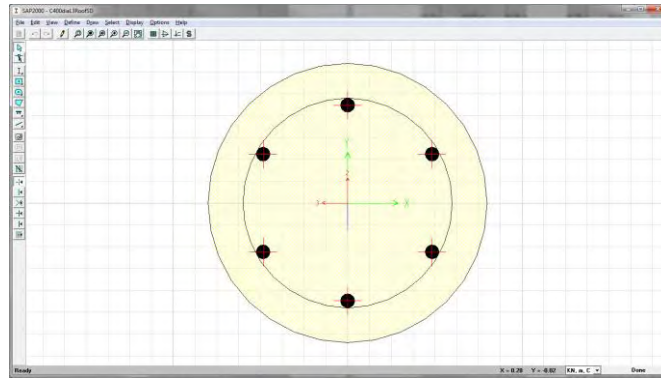
Concrete Column Check/Design:
 Reinforcement to be Checked
 Reinforcement to be Designed

Define/Edit/Show Section:
 Section Designer...

Section Properties: Properties...
 Property Modifiers: Set Modifiers...

Display Color:

DK Cancel



Material Property Data

Material Name: 276MPaConcConfined
 Material Type: Concrete
 Symmetry Type: Isotropic

Modulus of Elasticity: E = 24300000
 Weight and Mass: Weight per Unit Volume: 24, Mass per Unit Volume: 0
 Units: KN, m, C

Poisson's Ratio: U = 0.2
 Coeff of Thermal Expansion: A = 0.000000

Shear Modulus: G = 10223333

Advanced Material Property Data:

Nonlinear Material Data

Material Name: 276MPaConcConfined
 Material Type: Concrete

Hysteresis Type: Tgholds
 Drucker-Prager Parameters: Friction Angle: 0, Dilatational Angle: 0
 Units: KN, m, C

Stress-Strain Curve Definition Options:
 Parametric
 User Defined

User Stress-Strain Curve Data:
 Number of Points in Stress-Strain Curve: 13

	Strain	Stress	Point ID
1	7.455E-03	16163.28	
2	6.212E-03	19182.48	E
3	5.202E-03	21611.39	
4	-3.783E-03	25738.85	
5	-2.364E-03	28605.77	C
6	-1.852E-03	27913.41	
7	-1.419E-03	25261.76	
8	-9.458E-04	19767.54	
9	4.728E-04	-11039.59	
10	2.364E-04	-5687.03	
11	0	0	A
12	1.346E-04	0	B
13	1.481E-03	0	E

Order Rows Show Plot

Material Property Data

Material Name: 380MPaReinf Expected
 Material Type: Rebar
 Symmetry Type: Uniaxial

Modulus of Elasticity: E1 = 200500000
 Weight and Mass: Weight per Unit Volume: 0, Mass per Unit Volume: 0
 Units: KN, m, C

Poisson's Ratio: U12 = 0
 Coeff of Thermal Expansion: A1 = 1.170E-05

Shear Modulus: G12 = 0

Other Properties for Rebar Materials:
 Minimum Yield Stress, Fy: 449000
 Minimum Tensile Stress, Fu: 603000
 Expected Yield Stress, Fye: 449000
 Expected Tensile Stress, Fue: 603000

Advanced Material Property Data:

Nonlinear Material Data

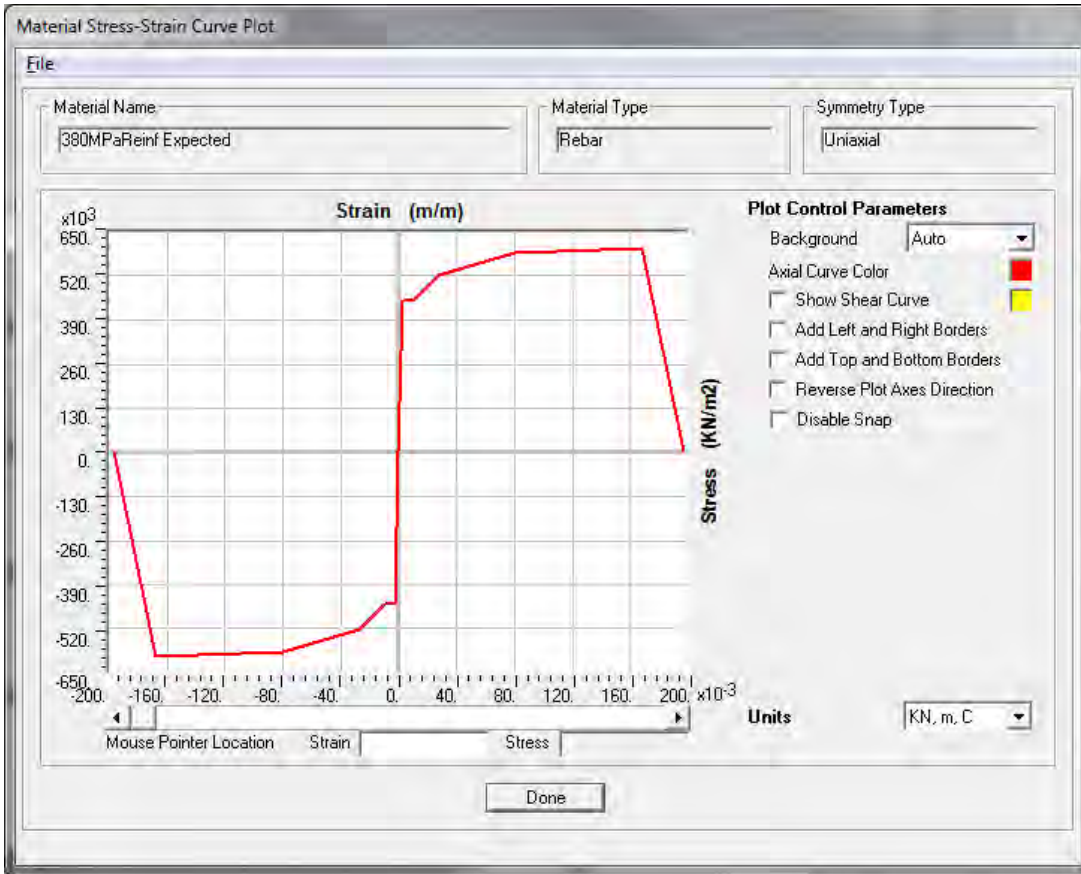
Material Name: 380MPaReinf Expected
 Material Type: Rebar

Hysteresis Type: Kinematic
 Drucker-Prager Parameters: Friction Angle: , Dilatational Angle:
 Units: KN, m, C

Stress-Strain Curve Definition Options:
 Parametric
 User Defined

Parametric Strain Data:
 Strain At Onset of Strain Hardening: 9.700E-03
 Ultimate Strain Capacity: 0.168
 Final Slope (Multiplier on E): 0.1
 Use Caltrans Default Controlling Strain Values (Bar Size Dependent)

Show Stress-Strain Plot

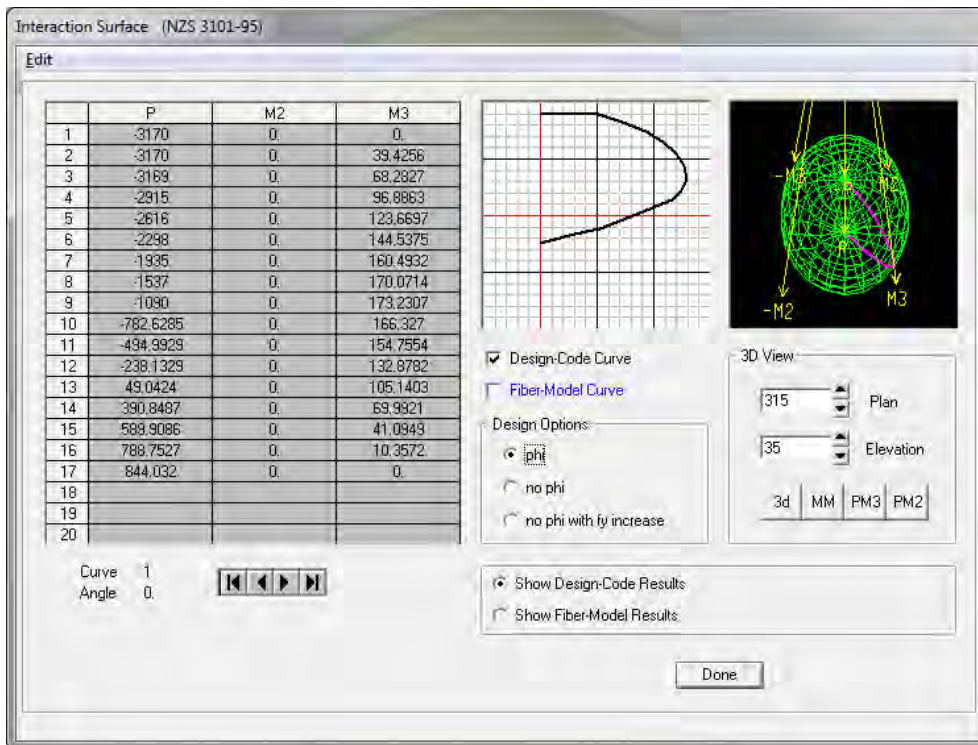


Moment Curvature Curve Details (Exact Integration)

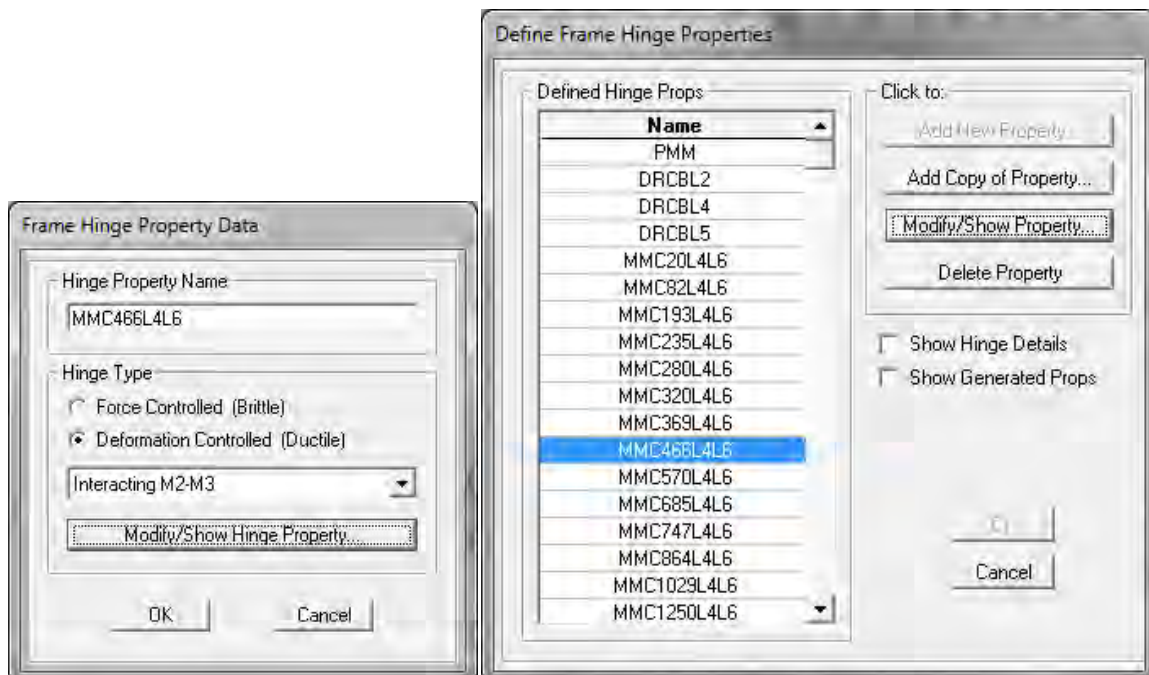
File

Concrete Strain	Neutral Axis	Steel Strain	Tendon Strain	Concrete Compression	Steel Compression	Steel Tension	Prestress Force	Net Force	Curvature	Moment
-1.394E-04	0.	-1.394E-04	0.	-412.3982	-53.8395	0.	0.	-466.2377	0	4.437E-15
-1.546E-04	-1.8214	-1.288E-04	0.	-412.183	-53.8114	0.	0.	-465.9944	0.0000785	2.5386
-1.776E-04	-0.7286	-1.128E-04	0.	-412.1881	-53.8121	0.	0.	-466.0001	0.0001912	6.3464
-2.082E-04	-0.4048	-9.114E-05	0.	-412.188	-53.812	0.	0.	-466.	0.0003442	11.4235
-2.464E-04	-0.2602	-6.436E-05	0.	-412.1768	-53.812	0.	0.	-465.9888	0.0005355	17.7677
-2.923E-04	-0.1821	-3.224E-05	0.	-411.9432	-53.8134	0.	0.	-465.7566	0.000765	25.2563
-3.436E-04	-0.1327	7.514E-06	0.	-413.0902	-53.4206	0.4837	0.	-466.0271	0.001033	32.4515
-3.979E-04	-0.0973	5.722E-05	0.	-415.8501	-53.9676	3.6833	0.	-466.1344	0.001339	38.7164
-4.550E-04	-0.0703	1.172E-04	0.	-420.4911	-53.2711	7.5452	0.	-466.217	0.001683	44.3391
-5.151E-04	-0.0494	1.872E-04	0.	-426.8439	-56.921	17.531	0.	-466.2339	0.002065	49.6429
-5.785E-04	-0.0327	2.668E-04	0.	-434.8695	-60.5081	29.1101	0.	-466.2676	0.002486	54.6816
-6.455E-04	-0.0192	3.558E-04	0.	-444.428	-63.9951	42.168	0.	-466.2551	0.002945	59.607
-7.162E-04	-8.061E-03	4.542E-04	0.	-455.5064	-67.4021	56.6847	0.	-466.2237	0.003442	64.5537
-7.907E-04	1.228E-03	5.618E-04	0.	-468.0794	-70.7515	72.6376	0.	-466.1933	0.003978	69.6061
-8.690E-04	9.074E-03	6.785E-04	0.	-482.1148	-74.0594	90.0108	0.	-466.1634	0.004552	74.8216
-9.513E-04	0.0158	8.043E-04	0.	-497.5842	-77.3419	108.7683	0.	-466.1378	0.005164	80.2412
-1.038E-03	0.0215	9.388E-04	0.	-514.381	-80.6646	128.9042	0.	-466.1415	0.005814	85.8469
-1.129E-03	0.0263	1.081E-03	0.	-532.2473	-84.138	150.2481	0.	-466.1372	0.006502	91.5789
-1.226E-03	0.0304	1.232E-03	0.	-551.0884	-87.8088	172.7734	0.	-466.1238	0.007229	97.4447
-1.328E-03	0.0339	1.390E-03	0.	-570.861	-91.7016	196.4554	0.	-466.1071	0.007994	103.475
-1.435E-03	0.0369	1.556E-03	0.	-591.5426	-95.8301	221.2805	0.	-466.0921	0.008797	109.6915
-1.547E-03	0.0395	1.730E-03	0.	-613.0313	-100.251	247.1919	0.	-466.0964	0.009639	116.0727
-1.666E-03	0.0416	1.910E-03	0.	-635.1195	-105.0634	274.0906	0.	-466.0924	0.0105	122.5646
-1.791E-03	0.0434	2.097E-03	0.	-657.678	-110.3256	301.9181	0.	-466.0855	0.0114	129.1574
-1.916E-03	0.0454	2.297E-03	0.	-675.9335	-114.7998	324.721	0.	-466.0124	0.0124	134.4057
-2.042E-03	0.0475	2.510E-03	0.	-690.6375	-118.5826	343.11	0.	-466.1101	0.0134	138.4756
-2.174E-03	0.0493	2.729E-03	0.	-705.455	-122.7207	362.0665	0.	-466.1092	0.0144	142.5426
-2.311E-03	0.0508	2.955E-03	0.	-720.3737	-127.2763	381.5489	0.	-466.1011	0.0155	146.6131
-2.456E-03	0.0521	3.188E-03	0.	-735.3619	-132.271	401.5428	0.	-466.0901	0.0166	150.695
-2.607E-03	0.0531	3.427E-03	0.	-750.2798	-137.799	421.9854	0.	-466.0934	0.0177	154.7592
-2.735E-03	0.0555	3.702E-03	0.	-749.9578	-138.1636	422.016	0.	-466.1053	0.0189	155.4298
-2.868E-03	0.0577	3.986E-03	0.	-749.6697	-138.5707	422.016	0.	-466.2244	0.0202	156.0319
-3.004E-03	0.0597	4.278E-03	0.	-749.2244	-138.9589	422.016	0.	-466.1672	0.0214	156.5535
-3.145E-03	0.0616	4.579E-03	0.	-748.7537	-139.4028	422.016	0.	-466.1404	0.0227	157.0221
-3.291E-03	0.0632	4.889E-03	0.	-748.228	-139.9134	422.016	0.	-466.1253	0.0241	157.4435
-3.441E-03	0.0647	5.207E-03	0.	-747.637	-140.4858	422.016	0.	-466.1089	0.0254	157.8244
-3.595E-03	0.0661	5.534E-03	0.	-746.996	-141.1222	422.016	0.	-466.1022	0.0269	158.1737
-3.754E-03	0.0674	5.870E-03	0.	-746.2667	-141.8439	422.016	0.	-466.0946	0.0283	158.4919
-3.916E-03	0.0686	6.214E-03	0.	-745.3088	-142.5775	422.016	0.	-465.8703	0.0298	158.7831
-4.088E-03	0.0695	6.563E-03	0.	-745.3521	-142.6994	422.016	0.	-466.0355	0.0313	158.9658
-4.274E-03	0.0701	6.910E-03	0.	-747.684	-140.672	422.2821	0.	-466.0739	0.0329	158.9031
-4.467E-03	0.0705	7.263E-03	0.	-749.6814	-140.672	424.3697	0.	-465.9837	0.0345	158.7867
-4.666E-03	0.0709	7.623E-03	0.	-751.5765	-140.672	426.2408	0.	-466.0077	0.0361	158.6362
-4.872E-03	0.0712	7.989E-03	0.	-753.2416	-140.672	427.8965	0.	-466.0171	0.0378	158.4381
-5.085E-03	0.0714	8.362E-03	0.	-754.665	-140.672	429.316	0.	-466.021	0.0395	158.1936
-5.304E-03	0.0716	8.740E-03	0.	-755.8316	-140.672	430.481	0.	-466.0226	0.0413	157.9035
-5.531E-03	0.0717	9.125E-03	0.	-756.7349	-140.672	431.3848	0.	-466.0221	0.0431	157.5716

OK



Hinge MMC466L4L6 definition



Frame Hinge Property Data for MMC466L4L6 - Interacting M2-M3

Hinge Specification Type

Moment - Rotation

Moment - Curvature

Hinge Length:

Relative Length

Scale Factor for Curvature (SF)

SF is Equal to Yield Curvature (Steel Objects Only)

User SF:

Load Carrying Capacity Beyond Point E

Drops To Zero Is Extrapolated

Symmetry Condition

Moment Curvature Dependence is Circular

Moment Curvature Dependence is Doubly Symmetric about M2 and M3

Moment Curvature Dependence has No Symmetry

Requirements for Specified Symmetry Condition

1. Specify curve at angle of 0°.

Axial Forces for Moment Curvature Curves

Number of Axial Forces:

[Modify/Show Axial Force Values...](#)

Curve Angles for Moment Curvature Curves

Number of Angles:

[Modify/Show Angles...](#)

[Modify/Show Moment Curvature Curve Data...](#)

[Modify/Show M2-M3 Interaction Surface Data...](#)

OK Cancel

Moment Rotation Data for MMC466L4L6 - Interacting M2-M3

Edit

Select Curve

Axial Force: Angle: Curve #1:

Units:

Moment Curvature Data for Selected Curve

Point	Moment/Yield Mom	Curvature/SF
A	0.	0.
B	1.	0.
C	1.072	0.0172
D	1.072	0.34
E	0.2	0.4

Note: Yield moment is defined by interaction curve.

[Copy Curve Data](#) [Paste Curve Data](#)

Current Curve - Curve #1
Force #1; Angle #1

3-D Surface

Acceptance Criteria (Plastic Deformation / SF)

Immediate Occupancy:

Life Safety:

Collapse Prevention:

Show Acceptance Points on Current Curve

3D View

Plan: Elevation: Aperture:

Axial Force:

Hide Backbone Lines

Show Acceptance Criteria

Show Thickened Lines

Highlight Current Curve

3D CC MC3 MC2

Moment Curvature Information

Symmetry Condition:

Number of Axial Force Values:

Number of Angles:

Total Number of Curves:

Angle Is Moment About

0 degrees = About Positive M2 Axis

90 degrees = About Positive M3 Axis

180 degrees = About Negative M2 Axis

270 degrees = About Negative M3 Axis

OK Cancel

M2-M3 Interaction Curve Definition for MMC466L4L6

Edit

User Interaction Curve Options:

Circular Symmetry

Doubly Symmetric about M2 and M3

No Symmetry

Number of MM Definition Points:

Scale Factors:

	M2	M3
	<input type="text" value="148.5"/>	<input type="text" value="152.3"/>

Include Scale Factors in Plot

Interaction Curve Requirements - Doubly Symmetric:

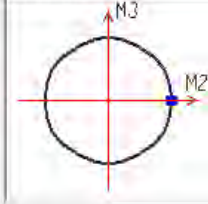
1. A minimum of 3 M2-M3 points are specified.
2. First point has $M2 > 0$ and $M3 = 0$.
3. Then all intermediate points have $M2 > 0$ and $M3 > 0$.
4. Last point has $M2 = 0$ and $M3 > 0$.
5. As the point number increases, $M3$ should increase and $M2$ should decrease.
6. The M2-M3 interaction curve must be convex (no dimples in surface).



Interaction Curve Data (P = 0.1)

Point	M2	M3
1	1	0
2	0.974	0.272
3	0.888	0.5
4	0.729	0.686
5	0.5	0.845
6	0.245	0.959
7	0	1

Interaction Curve Plot:



Highlight Current Point

M2:

M3:

Hinge MM1150L2L3 definition

Frame Hinge Property Data

Hinge Property Name:

Hinge Type:

Force Controlled (Brittle)

Deformation Controlled (Ductile)

Frame Hinge Property Data for MM1150L2L3 - Interacting M2-M3

Hinge Specification Type <input type="radio"/> Moment - Rotation <input checked="" type="radio"/> Moment - Curvature Hinge Length <input type="text" value="0.29"/> <input type="checkbox"/> Relative Length		Scale Factor for Curvature (SF) <input type="radio"/> SF is Equal to Yield Curvature (Steel Objects Only) <input checked="" type="radio"/> User SF <input type="text" value="1.."/>	
		Load Carrying Capacity Beyond Point E <input checked="" type="radio"/> Drops To Zero <input type="radio"/> Is Extrapolated	
Symmetry Condition <input checked="" type="checkbox"/> Moment Curvature Dependence is Circular <input type="checkbox"/> Moment Curvature Dependence is Doubly Symmetric about M2 and M3 <input type="checkbox"/> Moment Curvature Dependence has No Symmetry			
Requirements for Specified Symmetry Condition 1. Specify curve at angle of 0°.			
Axial Forces for Moment Curvature Curves Number of Axial Forces <input type="text" value="N.A."/> <input type="button" value="Modify/Show/Hide Basic Data..."/>		Curve Angles for Moment Curvature Curves Number of Angles <input type="text" value="1"/> <input type="button" value="Modify/Show Angles..."/>	
<input type="button" value="Modify/Show Moment Curvature Curve Data..."/> <input type="button" value="Modify/Show M2-M3 Interaction Surface Data..."/>			
<input type="button" value="OK"/>		<input type="button" value="Cancel"/>	

M2-M3 Interaction Curve Definition for MM1150L2L3

Edit

User Interaction Curve Options

Circular Symmetry
 Doubly Symmetric about M2 and M3
 No Symmetry

Number of MM Definition Points:

Scale Factors

M2	M3
191.9	189.8

Include Scale Factors in Plot KN, m, C

Interaction Curve Requirements - Doubly Symmetric

1. A minimum of 3 M2-M3 points are specified.
2. First point has $M2 > 0$ and $M3 = 0$.
3. Then all intermediate points have $M2 > 0$ and $M3 > 0$.
4. Last point has $M2 = 0$ and $M3 > 0$.
5. As the point number increases, $M3$ should increase and $M2$ should decrease.
6. The M2-M3 interaction curve must be convex (no dimples in surface).

Interaction Curve Data (P = 0)

Point	M2	M3
1	1	0
2	0.96	0.262
3	0.857	0.5
4	0.704	0.709
5	0.5	0.877
6	0.256	0.972
7	0	1

Interaction Curve Plot

Highlight Current Point

M2:
M3:

Moment Rotation Data for MM1150L2L3 - Interacting M2-M3

Edit

Select Curve

Axial Force: Angle: Curve #1:

Units: KN, m, C

Moment Curvature Data for Selected Curve

Point	Moment/Yield Mom	Curvature/SF
A	0	0
B	1	0
C	1.07	7.200E-03
D	1.07	0.3
E	0.2	0.4

Note: Yield moment is defined by interaction curve.

3-D Surface

Acceptance Criteria (Plastic Deformation / SF)

Immediate Occupancy	3.000E-03
Life Safety	0.012
Collapse Prevention	0.015

Show Acceptance Points on Current Curve

3D View

Plan: Elevation: Aperture:

Axial Force:

Hide Backbone Lines
 Show Acceptance Criteria
 Show Thickened Lines
 Highlight Current Curve

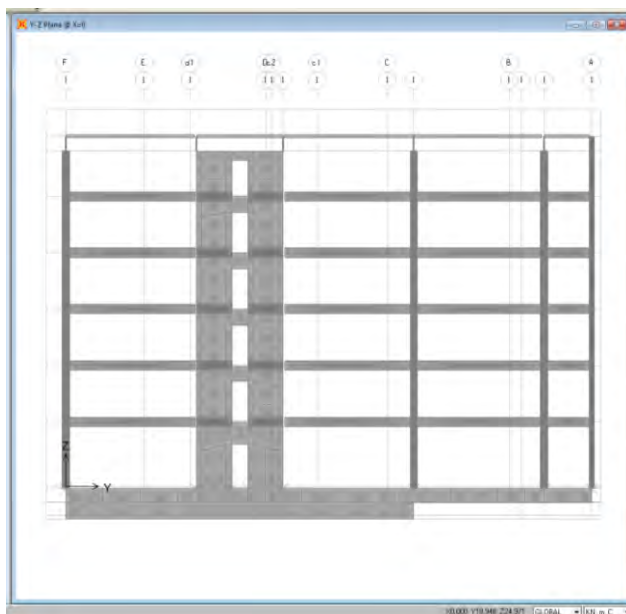
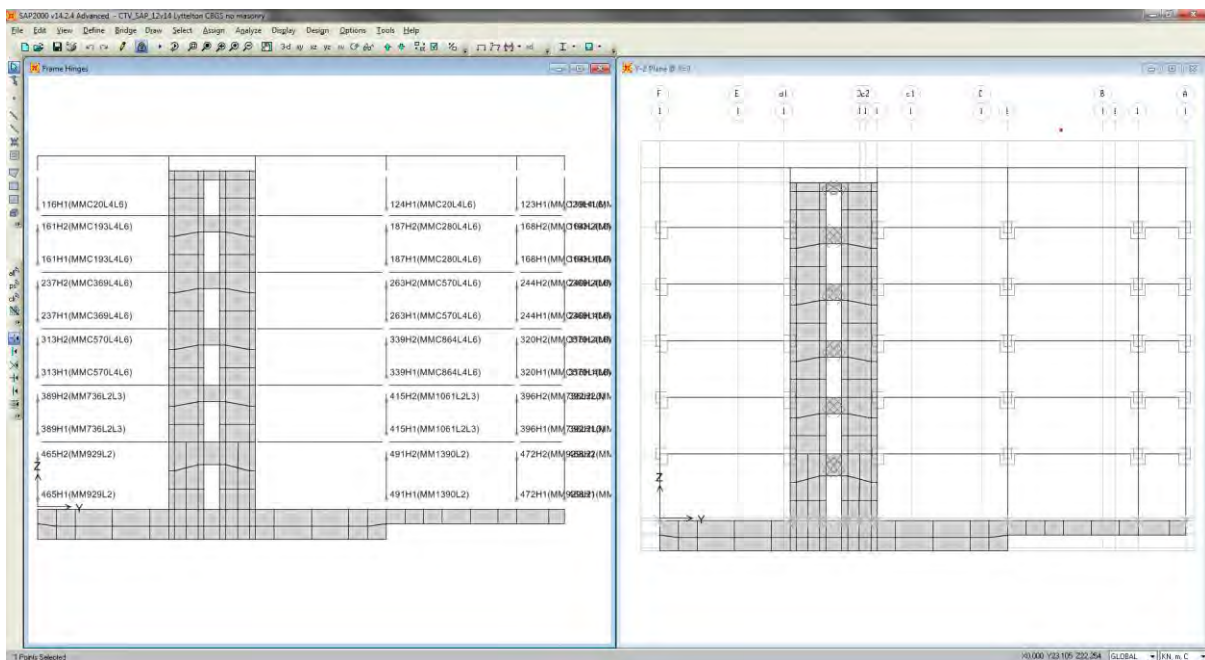
Moment Curvature Information

Symmetry Condition:
Number of Axial Force Values:
Number of Angles:
Total Number of Curves:

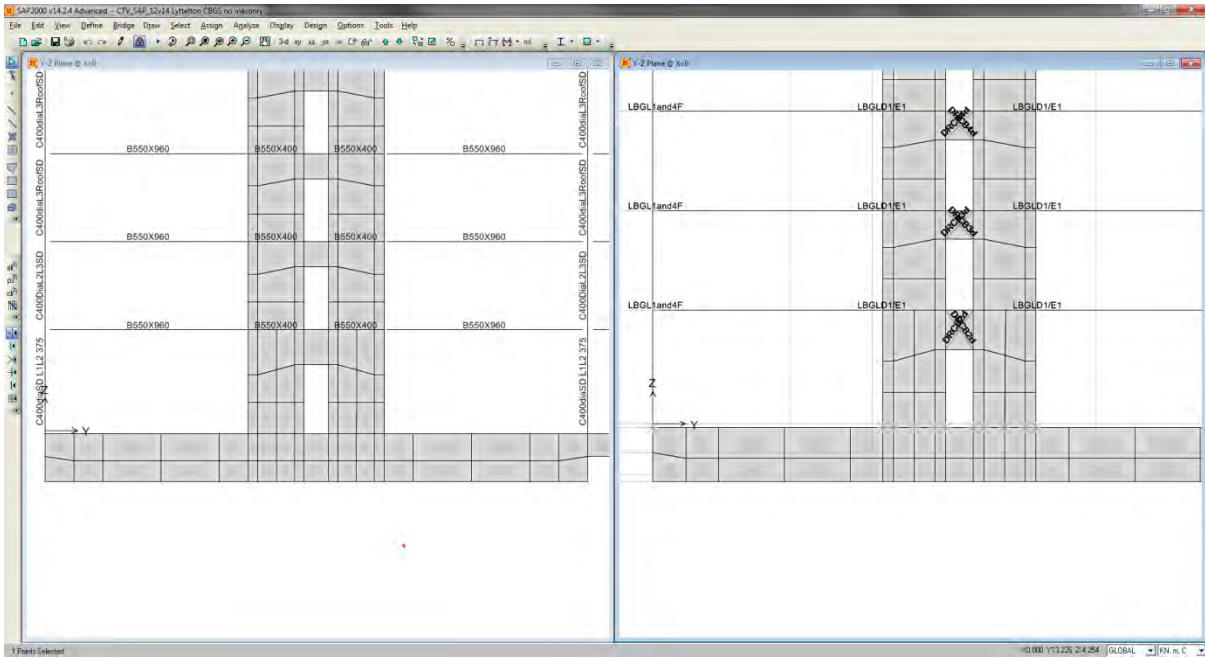
Angle Is Moment About

0 degrees = About Positive M2 Axis
90 degrees = About Positive M3 Axis
180 degrees = About Negative M2 Axis
270 degrees = About Negative M3 Axis

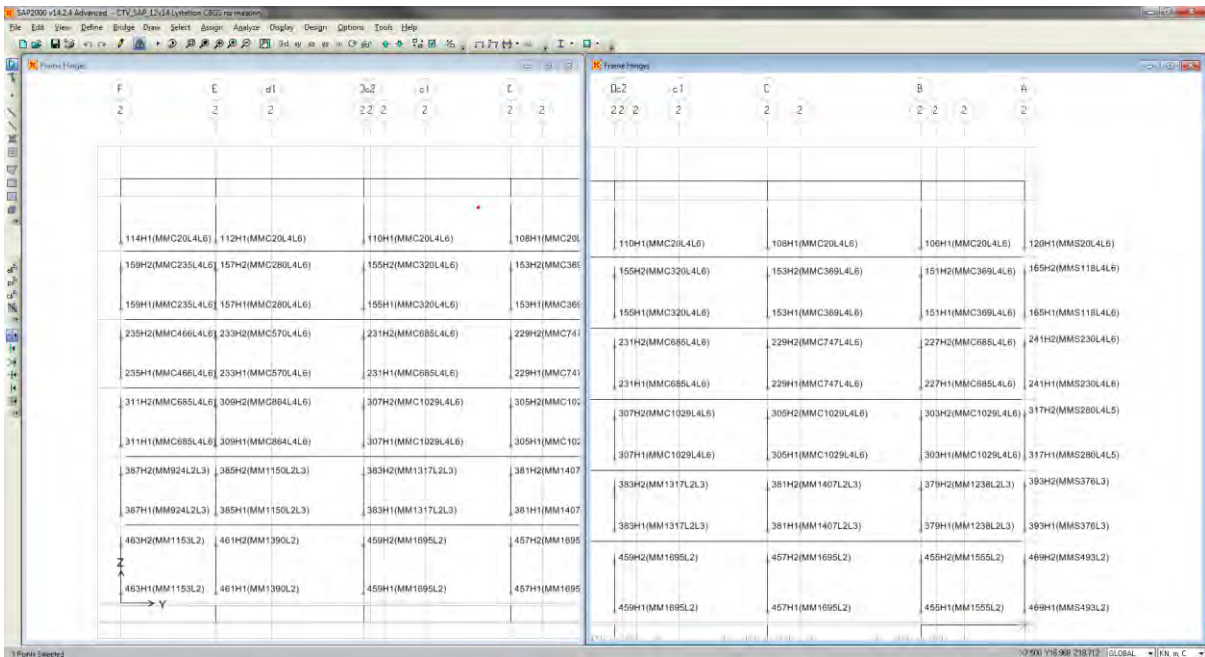
GL 1 column hinges



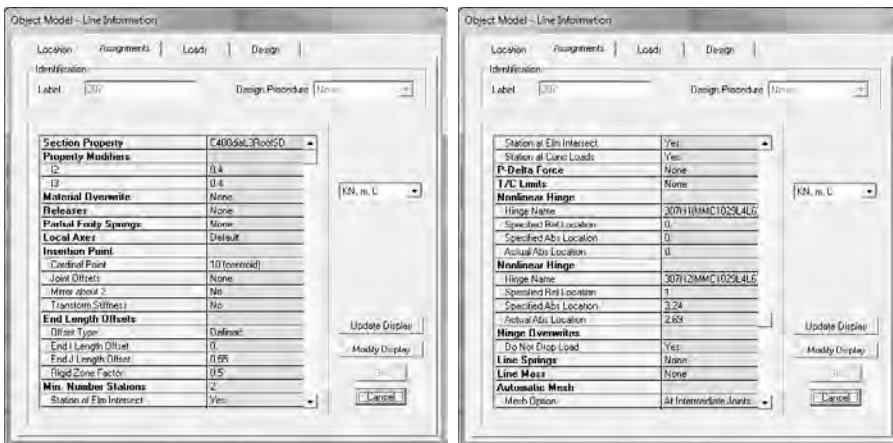
GL 1 (levels 2-4, GL C to F shown)material properties



GL 2 column hinges (GL 3 is similar)



Column D2 level 3-4 hinge assignments



Column D2 level 3-4 hinge assignments



Hinge MM1695L2 material properties and moment curvature information

SD Section Data

Section Name: C400dieSD L1L2 375
 Section Notes: Modify/Show Notes...

Base Material: 375MPaConcConf

Design Type: No Check/Design
 General Steel Section
 Concrete Column

Economic Column Check/Design:
 Flex/Reserve) to Be Checked
 Flex/Reserve) to Be Designed

Define/Edit/Show Section
 Section Designer

Section Properties: Properties...
 Property Modifiers: Set Modifiers...

Display Color:

OK Cancel

Material Property Data

Material Name: 375MPaConcConf
 Material Type: Concrete
 Symmetry Type: Isotropic

Modulus of Elasticity E: 29280000
 Weight and Mass: Weight per Unit Volume: 24, Mass per Unit Volume: 0, Units: KN, m, C

Poisson's Ratio U: 0.2

Coeff of Thermal Expansion A: 3.900E-06

Shear Modulus G: 11345833

Other Properties for Concrete Materials:
 Specified Concrete Compressive Strength, f_c: 37500
 Lightweight Concrete
 Shear Strength Reduction Factor:

Advanced Material Property Data:
 Nonlinear Material Data...
 Material Damping Properties...
 Time Dependent Properties...
 Thermal Properties...

OK Cancel

Nonlinear Material Data

Material Name: 375MPaConcConf
 Material Type: Concrete

Hysteresis Type: Takeda
 Drucker-Prager Parameters: Friction Angle: 0, Dilatational Angle: 0, Units: KN, m, C

Stress-Strain Curve Definition Options:
 Parameters
 User Defined

User Stress-Strain Curve Data:
 Number of Points in Stress-Strain Curve: 12

	Strain	Stress	Point ID
1	-7.106E-03	-18556.17	E
2	-5.922E-03	-18781.18	
3	-4.992E-03	-23036.59	
4	-3.631E-03	-31842.9	
5	-2.269E-03	-38509.3	
6	-1.819E-03	-37045.3	
7	-1.361E-03	-32075.8	
8	-9.077E-04	-23469.05	
9	-4.538E-04	-12254.37	
10	-2.269E-04	-6170.61	
11	0.	0.	A
12	1.000E-04	0.	B

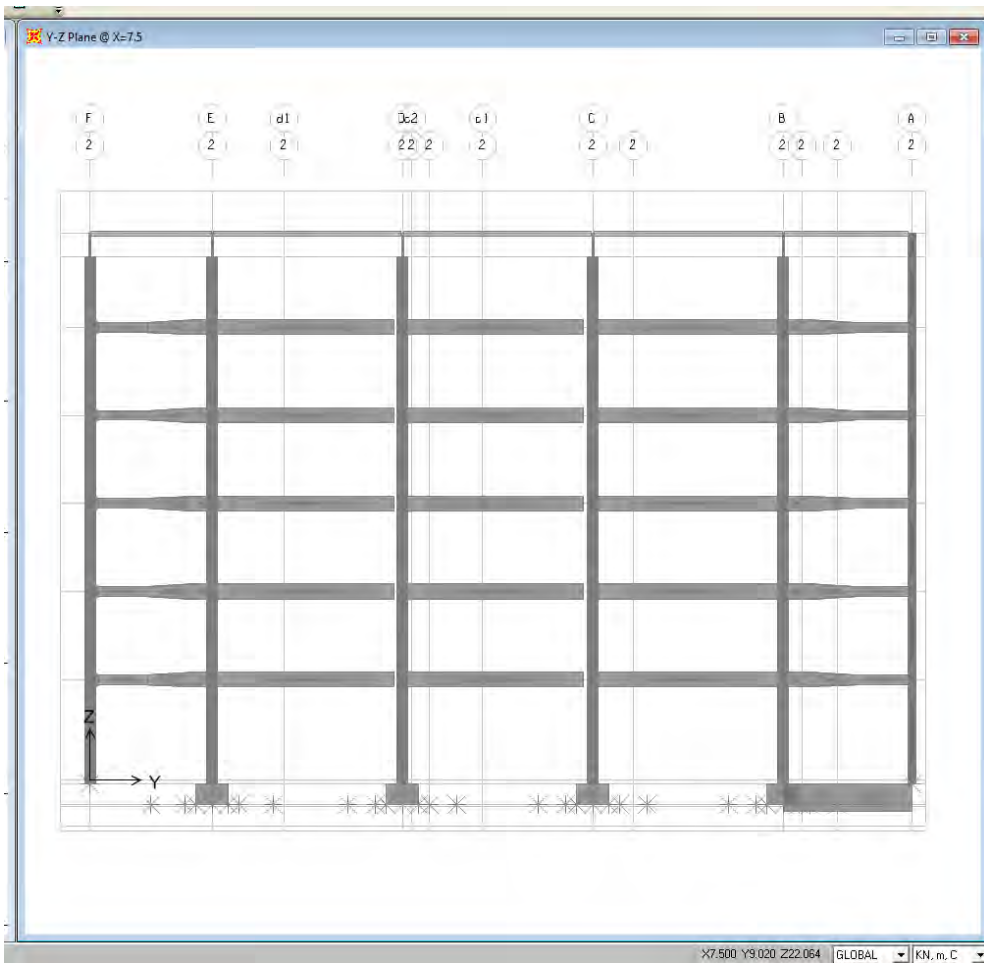
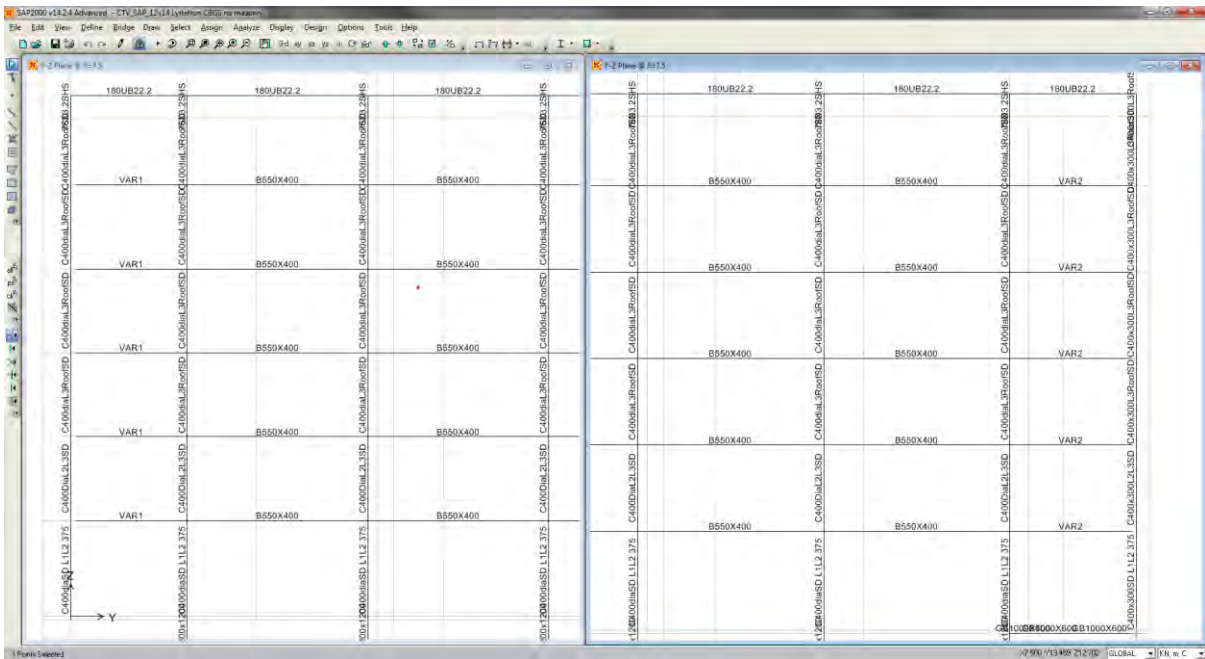
Order Flows Show Plot... OK Cancel

Moment Curvature Curve Details (Exact Integration)

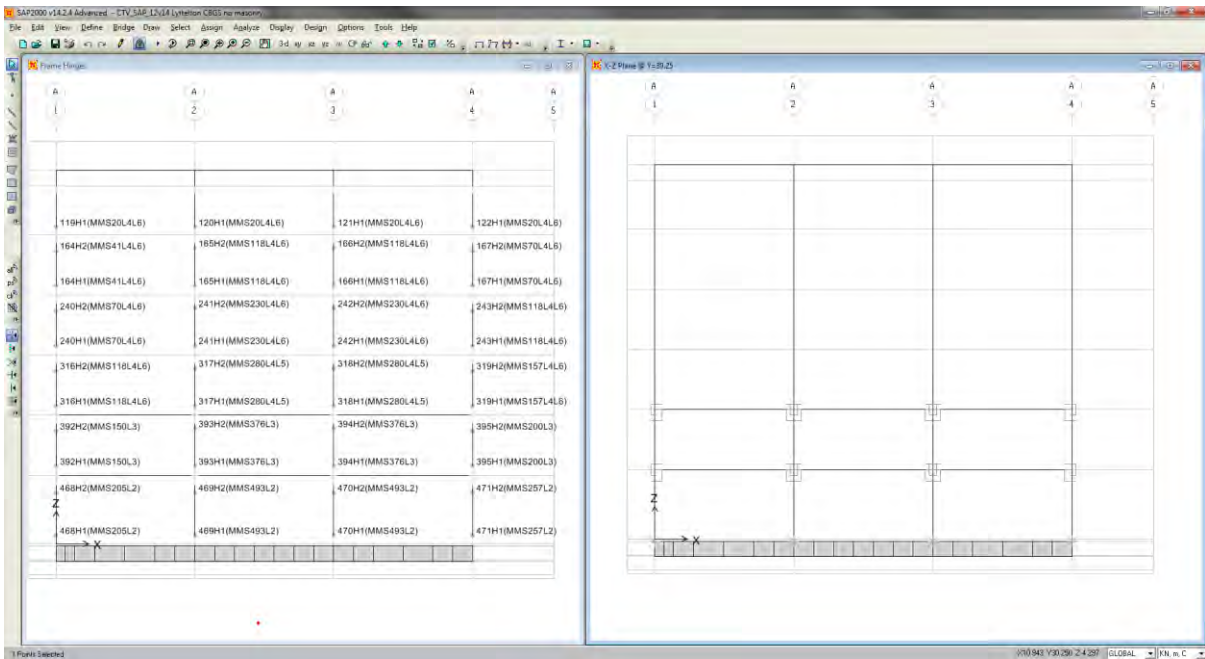
Concrete Strain	Neutral Axis	Steel Strain	Tendon Strain	Concrete Compression	Steel Compression	Steel Tension	Prestress Force	Net Force	Curvature	Moment
-4.618E-04	0	-4.618E-04	0	-1517	-178.3479	0	0	-1695	0	1.312E-14
-4.815E-04	-4.6771	-4.479E-04	0	-1517	-178.3435	0	0	-1695	0.0009887	3.4503
5.173E-04	-1.8716	-4.374E-04	0	-1517	-178.4128	0	0	-1695	0.003488	8.6871
-5.540E-04	-1.9403	-4.600E-04	0	-1517	-178.5067	0	0	-1695	0.004443	15.6277
-6.037E-04	-0.9692	-3.657E-04	0	-1516	-178.6246	0	0	-1695	0.006911	24.329
-6.893E-04	-0.4888	-3.248E-04	0	-1516	-178.7685	0	0	-1695	0.009873	34.7707
-7.299E-04	-0.3478	-2.787E-04	0	-1516	-179.937	0	0	-1695	0.01333	46.9527
-8.089E-04	-0.2068	-2.208E-04	0	-1516	-178.1758	0	0	-1695	0.01726	60.8481
-8.960E-04	-0.214	-1.603E-04	0	-1515	-179.5305	0	0	-1695	0.02172	76.8147
-9.905E-04	-0.1746	-9.214E-05	0	-1515	-179.7267	0	0	-1695	0.02666	94.0274
-1.104E-03	-0.1441	-1.323E-05	0	-1516	-178.6665	0	0	-1695	0.03209	109.8894
-1.218E-03	-0.1199	7.844E-05	0	-1519	-180.824	4.8205	0	-1695	0.03801	123.8671
-1.333E-03	-0.1	1.777E-04	0	-1524	-183.9439	11.4364	0	-1695	0.04443	135.9646
-1.448E-03	-0.0803	2.910E-04	0	-1530	-183.9507	18.7287	0	-1695	0.05134	147.2093
-1.561E-03	-0.0591	4.165E-04	0	-1538	-184.267	27.4875	0	-1695	0.05874	157.9478
-1.713E-03	-0.057	5.530E-04	0	-1548	-193.489	46.7367	0	-1695	0.06604	168.0675
-1.852E-03	-0.0488	6.995E-04	0	-1560	-203.0565	67.4708	0	-1695	0.07503	177.5179
-1.998E-03	-0.0381	8.530E-04	0	-1572	-212.9895	89.541	0	-1695	0.08592	186.832
-2.143E-03	-0.3397	1.009E-03	0	-1585	-223.5058	112.8273	0	-1695	0.0993	193.6882
-2.317E-03	-0.0248	1.191E-03	0	-1597	-234.92	136.6849	0	-1695	0.1163	206.7371
-2.482E-03	-0.0195	1.360E-03	0	-1610	-247.3939	161.8795	0	-1695	0.1314	220.0774
-2.679E-03	-0.0154	1.558E-03	0	-1621	-261.1126	187.3087	0	-1695	0.154	232.8202
-2.876E-03	-0.012	1.738E-03	0	-1632	-276.1496	213.1969	0	-1695	0.179	247.6698
-3.089E-03	-0.3668	1.899E-03	0	-1643	-291.481	239.3351	0	-1695	0.2148	262.1612
-3.326E-03	-0.0048	2.111E-03	0	-1658	-300.8059	264.2697	0	-1695	0.256	278.0554
-3.566E-03	-6.367E-03	2.309E-03	0	-1667	-310.5267	282.211	0	-1695	0.3173	295.9781
-3.820E-03	-5.264E-03	2.507E-03	0	-1670	-320.9971	299.7732	0	-1695	0.386	326.4041
-4.097E-03	-4.343E-03	2.709E-03	0	-1699	-333.5844	308.1182	0	-1695	0.462	353.2319
-4.419E-03	-3.262E-03	2.905E-03	0	-1690	-351.0995	318.4151	0	-1695	0.5214	376.8445
-4.786E-03	-2.726E-03	3.079E-03	0	-1649	-369.9924	324.294	0	-1695	0.6299	392.355
-5.137E-03	-0.0102	3.171E-03	0	-1631	-393.0233	328.7345	0	-1695	0.8244	401.4560
-5.561E-03	-0.0115	3.344E-03	0	-1610	-413.531	336.690	0	-1695	0.926	396.6909
-6.032E-03	-0.0146	3.487E-03	0	-1611	-422.016	337.8318	0	-1695	0.9276	388.4318
-6.559E-03	-0.0166	3.629E-03	0	-1615	-422.016	342.4062	0	-1695	0.9293	384.0177
-6.878E-03	-0.0214	3.682E-03	0	-1606	-422.016	334.8548	0	-1695	0.9311	373.0524
-7.334E-03	-0.0234	3.822E-03	0	-1610	-422.016	337.6541	0	-1695	0.9328	368.6248

OK

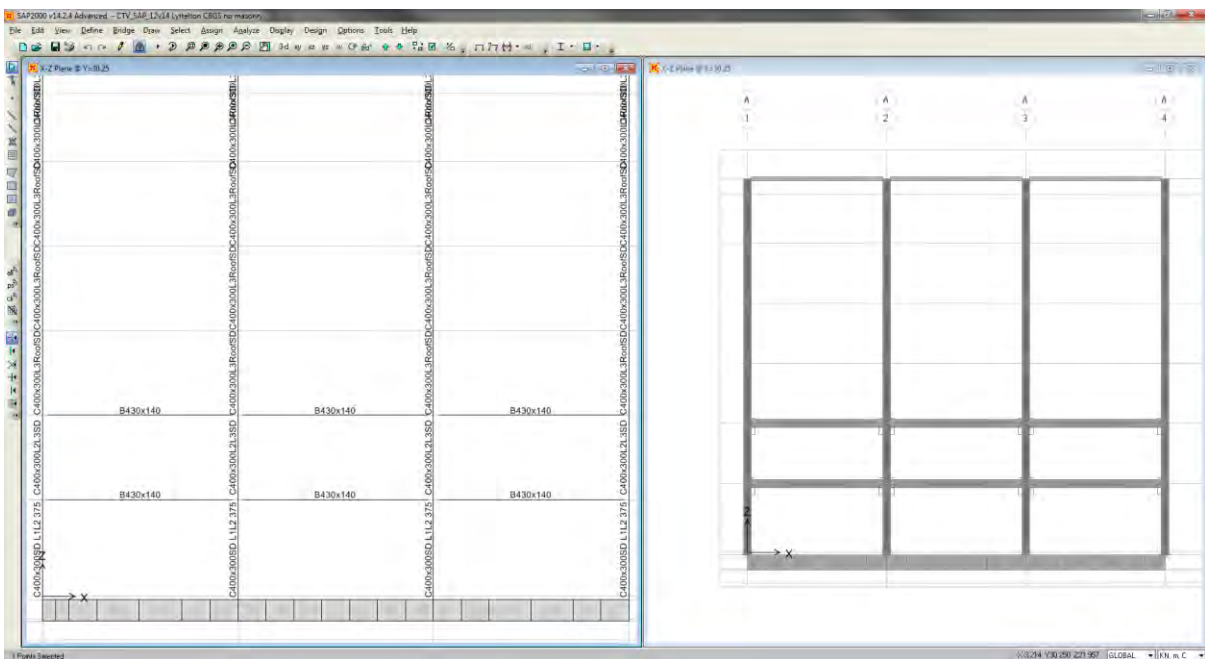
GL 2 frame sections (GL 3 is similar)



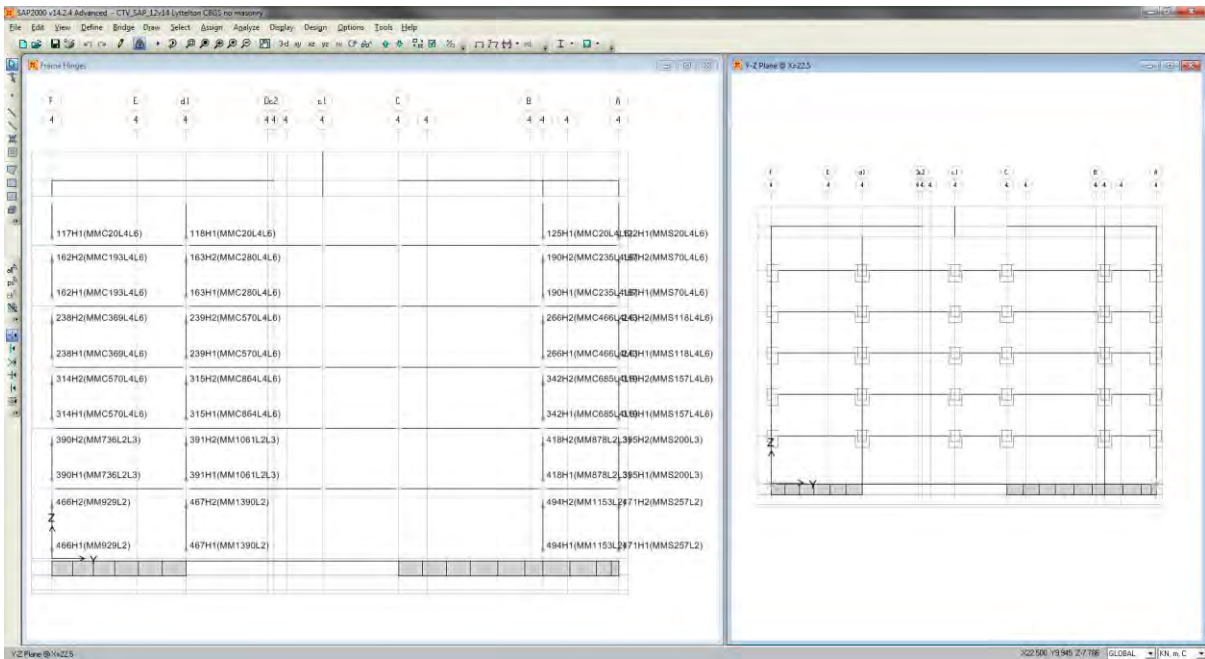
GL A column hinges



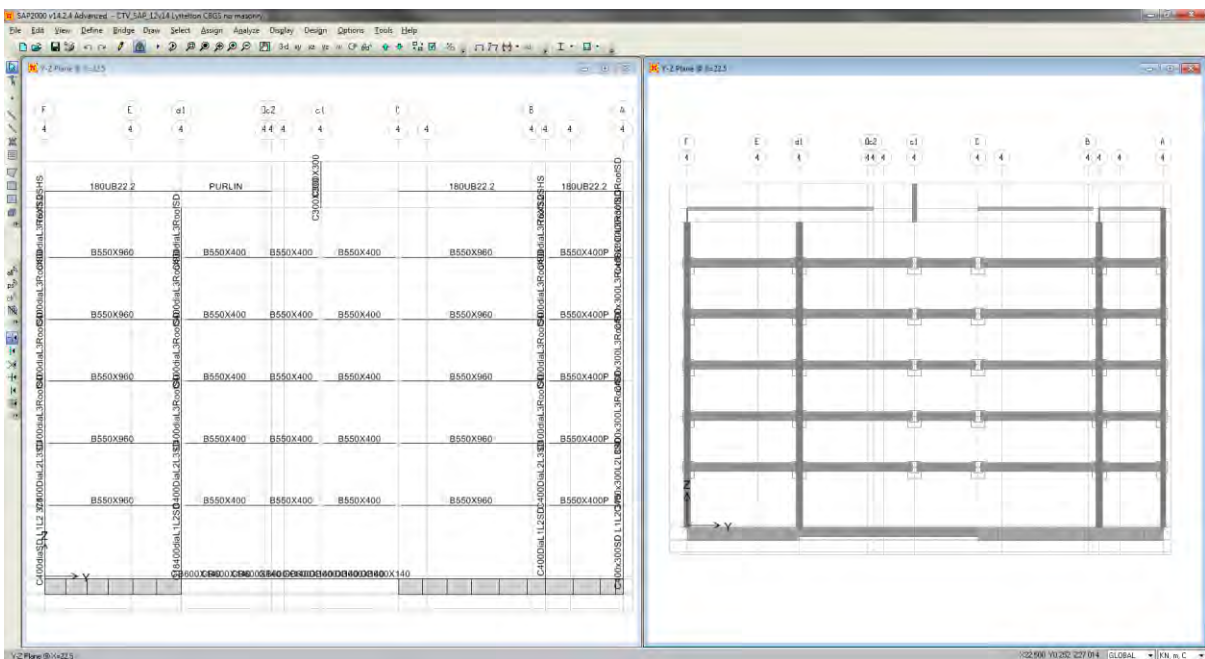
GL A frame sections



GL 4 column hinges

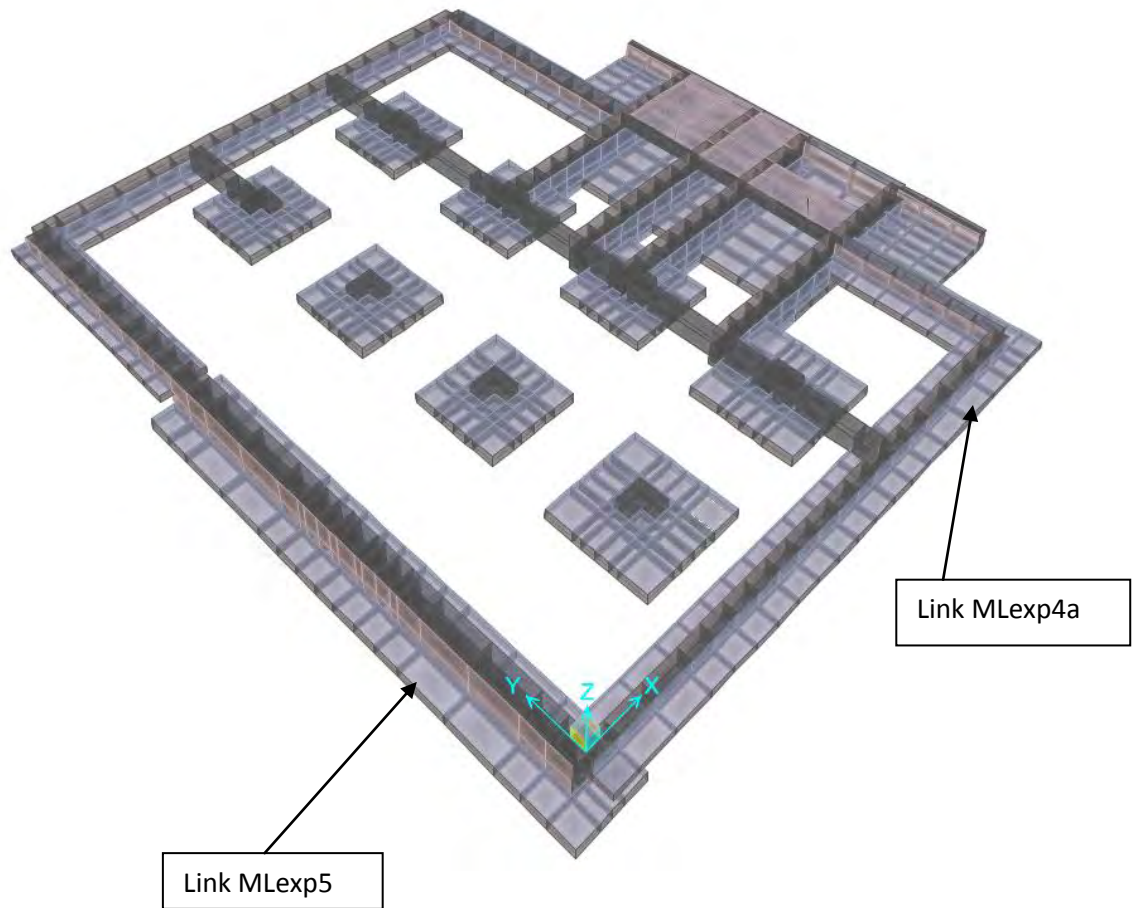


GL 4 frame sections



Foundation links

Note that these have been applied as area springs to the u/s of the foundations. The spring is assigned as a multi-linear link. Compressive spring values have been assigned as per Table 3 and Figure 7 of our analysis report. Examples as follows;



Link MPexp4a

Shell assignment:

Object Model - Area Information

Location Assignments Loads

Identification

Label 2154

Section Property	
Section Name	GB0.35mFlange
Section Type	Shell (Shell-Thin)
Property Modifiers	
r11	0.23
Material Overwrite	None
Thickness Overwrite	None
Joint Offset Overwrite	None
Local Axes	Default
Area Spring	
Spring Type	Link Property
Link Property	MLexp4a
Link 1-Axis Orientation	Normal To Face
Face	Bottom
Normal Orientation	Inward
Axis 2 Angle	0.
Area Mass	None
Automatic Area Mesh	None
Auto Edge Constraint	Yes
Material Temp	Default

KN, m, C

Update Display

Modify Display

Cancel

Link definition

Link/Support Property Data

Link/Support Type MultiLinear Elastic

Property Name MLexp4a Set Default Name

Property Notes Modify/Show...

Total Mass and Weight

Mass	0.	Rotational Inertia 1	0.
Weight	0.	Rotational Inertia 2	0.
		Rotational Inertia 3	0.

Factors For Line, Area and Solid Springs

Property is Defined for This Length In a Line Spring 1

Property is Defined for This Area In Area and Solid Springs 1

Directional Properties

Direction	Fixed	NonLinear	Properties
<input checked="" type="checkbox"/> U1	<input type="checkbox"/>	<input checked="" type="checkbox"/>	Modify/Show for U1...
<input type="checkbox"/> U2	<input type="checkbox"/>	<input type="checkbox"/>	Modify/Show for U2...
<input type="checkbox"/> U3	<input type="checkbox"/>	<input type="checkbox"/>	Modify/Show for U3...
<input type="checkbox"/> R1	<input type="checkbox"/>	<input type="checkbox"/>	Modify/Show for R1...
<input type="checkbox"/> R2	<input type="checkbox"/>	<input type="checkbox"/>	Modify/Show for R2...
<input type="checkbox"/> R3	<input type="checkbox"/>	<input type="checkbox"/>	Modify/Show for R3...

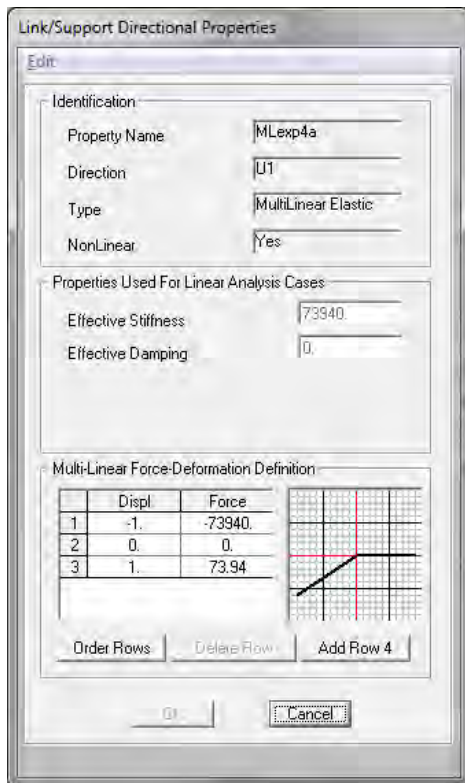
Fix All Clear All

P-Delta Parameters

Advanced...

0.1

Cancel



Link MLexp5

Shell assignment:



Link definition

Link/Support Property Data

Link/Support Type: MultiLinear Elastic

Property Name: MLexp5 Set Default Name

Property Notes: Modify/Show...

Total Mass and Weight

Mass	0	Rotational Inertia 1	0
Weight	0	Rotational Inertia 2	0
		Rotational Inertia 3	0

Factors For Line, Area and Solid Springs

Property is Defined for This Length In a Line Spring: 1

Property is Defined for This Area In Area and Solid Springs: 1

Directional Properties

Direction	Fixed	NonLinear	Properties
<input checked="" type="checkbox"/> U1	<input type="checkbox"/>	<input checked="" type="checkbox"/>	Modify/Show for U1...
<input type="checkbox"/> U2	<input type="checkbox"/>	<input type="checkbox"/>	Modify/Show for U2...
<input type="checkbox"/> U3	<input type="checkbox"/>	<input type="checkbox"/>	Modify/Show for U3...
<input type="checkbox"/> R1	<input type="checkbox"/>	<input type="checkbox"/>	Modify/Show for R1...
<input type="checkbox"/> R2	<input type="checkbox"/>	<input type="checkbox"/>	Modify/Show for R2...
<input type="checkbox"/> R3	<input type="checkbox"/>	<input type="checkbox"/>	Modify/Show for R3...

Fix All Clear All

P-Delta Parameters

Advanced...

0 Cancel

Link/Support Directional Properties

Edit

Identification

Property Name: MLexp5

Direction: U1

Type: MultiLinear Elastic

NonLinear: Yes

Properties Used For Linear Analysis Cases

Effective Stiffness: 104350

Effective Damping: 0

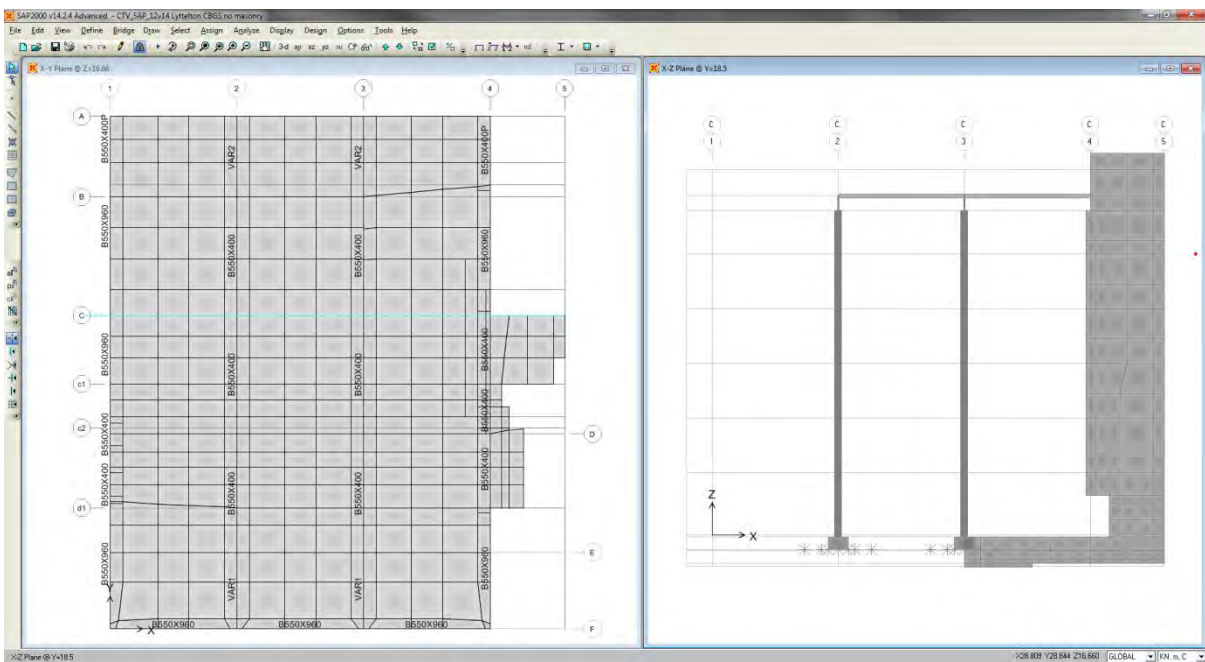
Multi-Linear Force-Deformation Definition

	Displ	Force
1	-1	-104350
2	0	0
3	1	10435

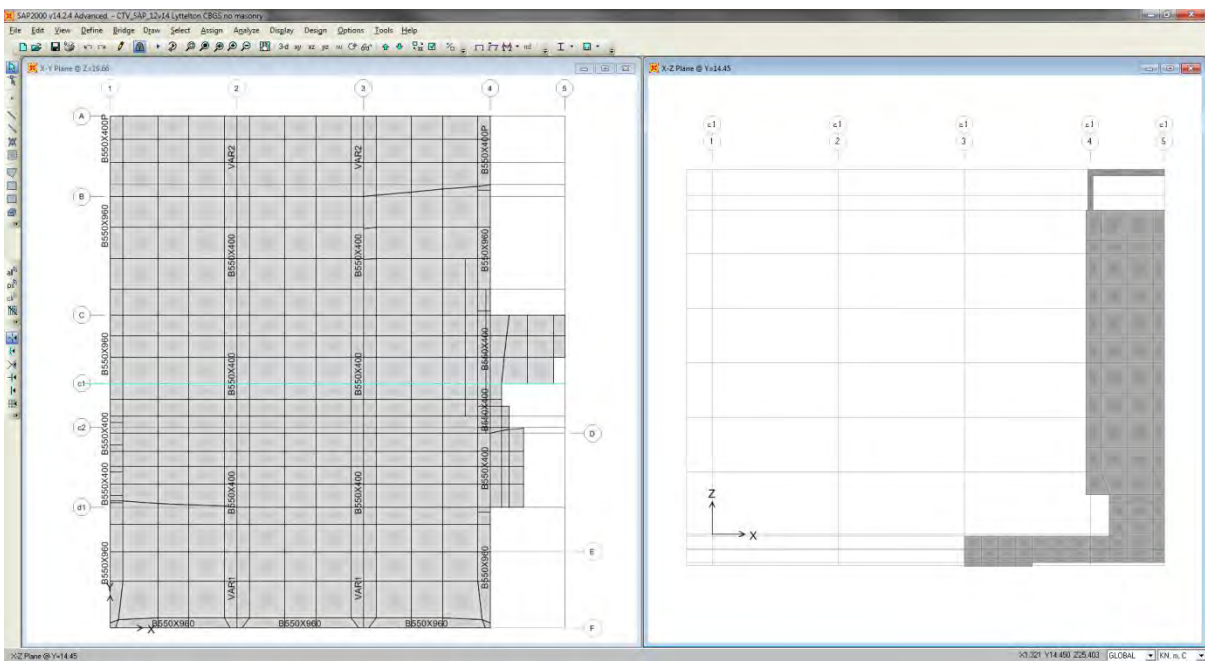
Order Rows Delete Row Add Row 4

0 Cancel

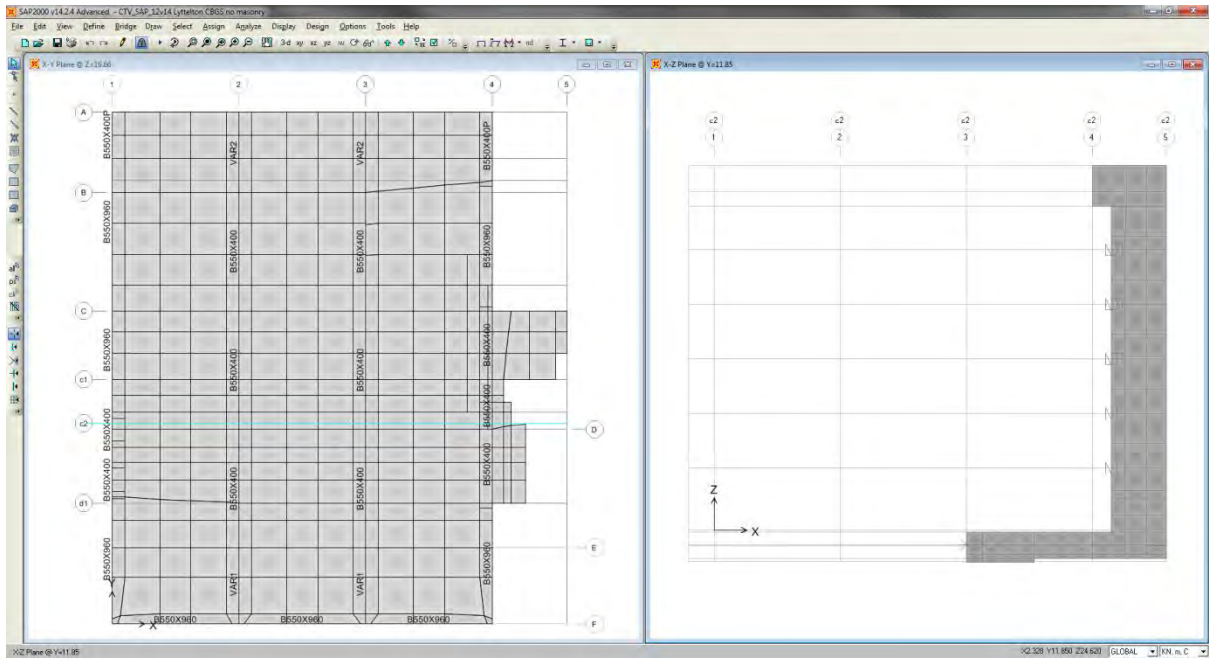
Typical floor meshing and meshing on GL C wall



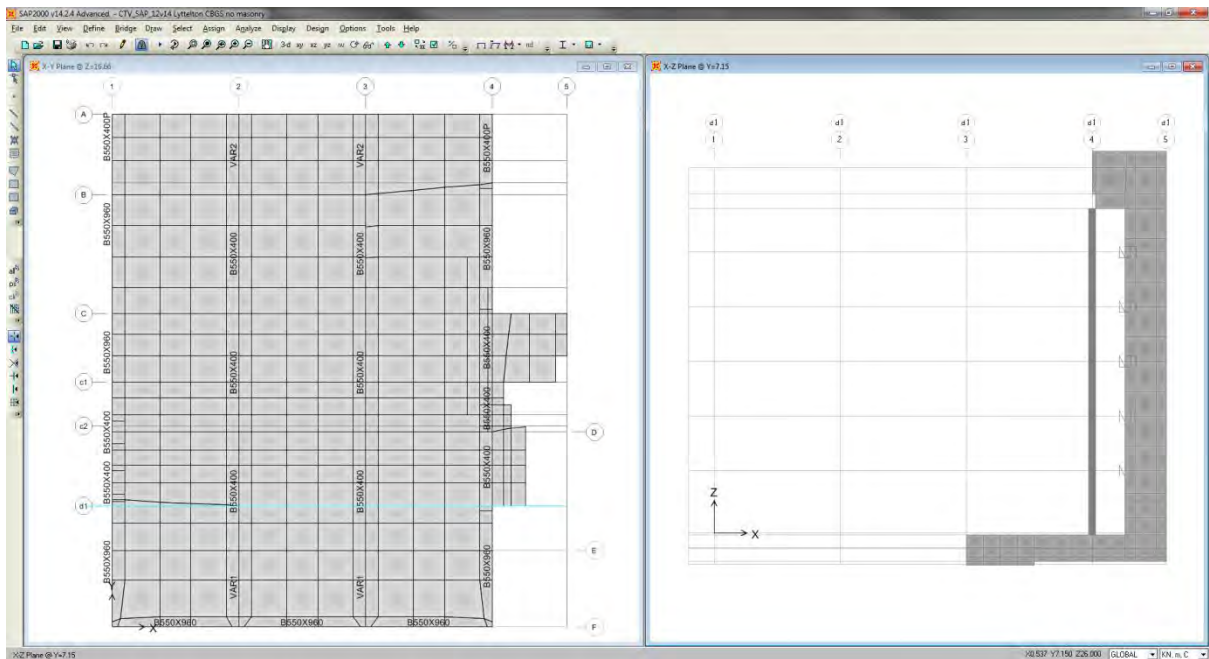
Typical floor meshing and meshing on GL C1 wall



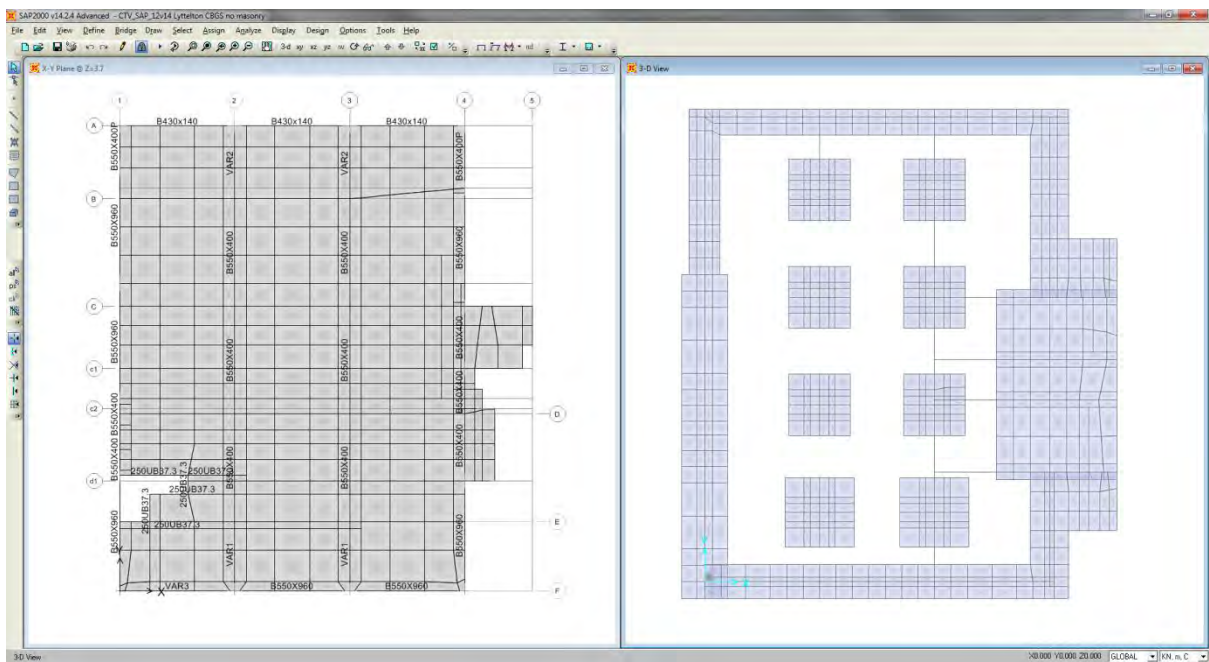
Typical floor meshing and meshing on GL D wall



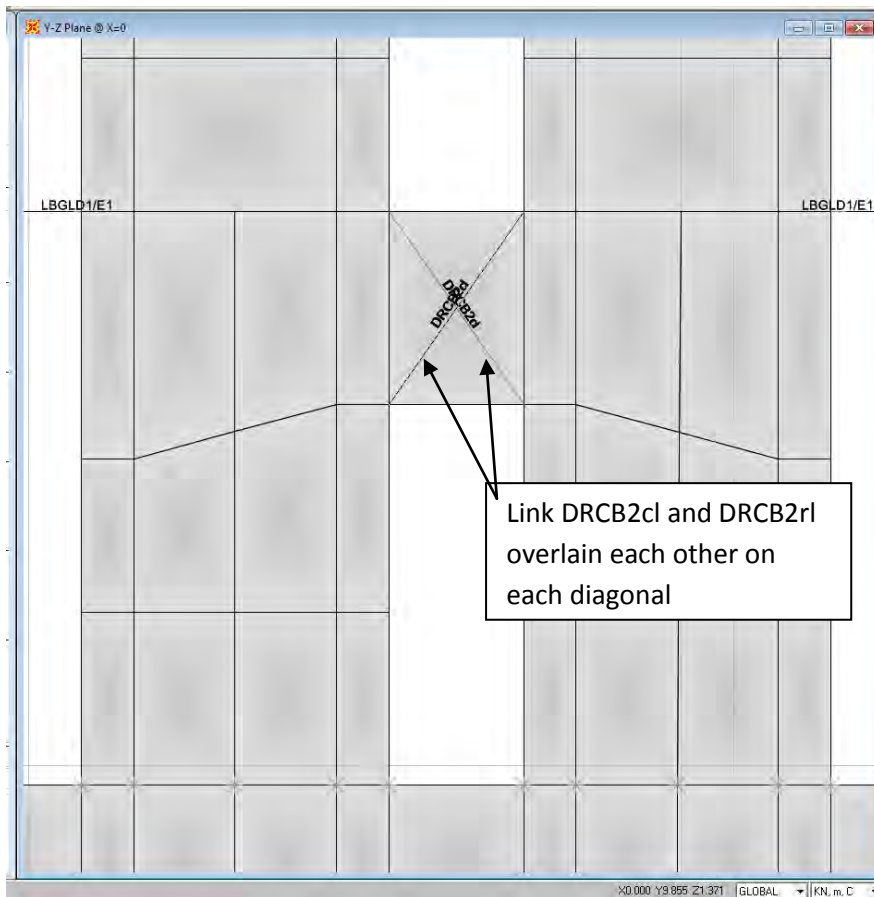
Typical floor meshing and meshing on GL D/E wall



Level 2 meshing and foundation meshing



Coupled shear wall (south wall) diagonal reinforcement links



Link/Support Property Data

Link/Support Type:

Property Name:

Property Notes:

Total Mass and Weight

Mass	<input type="text" value="0"/>	Rotational Inertia 1	<input type="text" value="0"/>
Weight	<input type="text" value="0"/>	Rotational Inertia 2	<input type="text" value="0"/>
		Rotational Inertia 3	<input type="text" value="0"/>

Factors For Line, Area and Solid Springs

Property is Defined for This Length In a Line Spring:

Property is Defined for This Area In Area and Solid Springs:

Directional Properties

Direction	Fixed	NonLinear	Properties
<input checked="" type="checkbox"/> U1	<input type="checkbox"/>	<input checked="" type="checkbox"/>	<input type="button" value="Modify/Show for U1..."/>
<input type="checkbox"/> U2	<input type="checkbox"/>	<input type="checkbox"/>	<input type="button" value="Modify/Show for U2..."/>
<input type="checkbox"/> U3	<input type="checkbox"/>	<input type="checkbox"/>	<input type="button" value="Modify/Show for U3..."/>
<input type="checkbox"/> R1	<input type="checkbox"/>	<input type="checkbox"/>	<input type="button" value="Modify/Show for R1..."/>
<input type="checkbox"/> R2	<input type="checkbox"/>	<input type="checkbox"/>	<input type="button" value="Modify/Show for R2..."/>
<input type="checkbox"/> R3	<input type="checkbox"/>	<input type="checkbox"/>	<input type="button" value="Modify/Show for R3..."/>

P-Delta Parameters

Concrete link properties

Link/Support Directional Properties

Edit

Identification

Property Name: DRCB2cl

Direction: U1

Type: MultiLinear Plastic

NonLinear: Yes

Hysteresis Type And Parameters

Hysteresis Type: Takeda

No Parameters Are Required For This Hysteresis Type

Properties Used For Linear Analysis Cases

Effective Stiffness: 296202

Effective Damping: 0

Multi-Linear Force-Deformation Definition

	Displ	Force
1	-0.0406	-163.56
2	-0.0293	-219.01
3	-0.0218	-284.78
4	-0.0143	-405.13
5	-4.200E-03	-716.68

Order Rows Delete Row Add Row 10

Hysteresis Definition Sketch

MultiLinear Plastic - Takeda

OK Cancel

Link/Support Directional Properties

Edit

Identification

Property Name: DRCB2cl

Direction: U1

Type: MultiLinear Plastic

NonLinear: Yes

Hysteresis Type And Parameters

Hysteresis Type: Takeda

No Parameters Are Required For This Hysteresis Type

Properties Used For Linear Analysis Cases

Effective Stiffness: 296202

Effective Damping: 0

Multi-Linear Force-Deformation Definition

	Displ	Force
6	-3.361E-03	-700.18
7	-2.520E-03	-636.33
8	0	0
9	2.255E-03	0

Order Rows Delete Row Add Row 10

Hysteresis Definition Sketch

MultiLinear Plastic - Takeda

OK Cancel

Link/Support Property Data

Link/Support Type:

Property Name:

Property Notes:

Total Mass and Weight

Mass: Rotational Inertia 1:

Weight: Rotational Inertia 2:

Rotational Inertia 3:

Factors For Line, Area and Solid Springs

Property is Defined for This Length In a Line Spring:

Property is Defined for This Area In Area and Solid Springs:

Directional Properties

Direction	Fixed	NonLinear	Properties
<input checked="" type="checkbox"/> U1	<input type="checkbox"/>	<input checked="" type="checkbox"/>	<input type="button" value="Modify/Show for U1..."/>
<input type="checkbox"/> U2	<input type="checkbox"/>	<input type="checkbox"/>	<input type="button" value="Modify/Show for U2..."/>
<input type="checkbox"/> U3	<input type="checkbox"/>	<input type="checkbox"/>	<input type="button" value="Modify/Show for U3..."/>
<input type="checkbox"/> R1	<input type="checkbox"/>	<input type="checkbox"/>	<input type="button" value="Modify/Show for R1..."/>
<input type="checkbox"/> R2	<input type="checkbox"/>	<input type="checkbox"/>	<input type="button" value="Modify/Show for R2..."/>
<input type="checkbox"/> R3	<input type="checkbox"/>	<input type="checkbox"/>	<input type="button" value="Modify/Show for R3..."/>

P-Delta Parameters

Reinforcement link information

Link/Support Directional Properties

Edit

Identification

Property Name: DRCB2I
 Direction: U1
 Type: MultiLinear Plastic
 NonLinear: Yes

Hysteresis Type And Parameters

Hysteresis Type: Pivot
 α_1 : 10 β_1 : 0.9 η : 0
 α_2 : 10 β_2 : 0.9

Properties Used For Linear Analysis Cases

Effective Stiffness: 285761
 Effective Damping: 0

Multi-Linear Force-Deformation Definition

	Displ	Force
1	-0.5	-222.16
2	-0.39	-222.16
3	-0.3746	-1110.82
4	-0.1884	-1081.82
5	-2.776E-03	-791.36

Order Rows Delete Row Add Row 12

Hysteresis Definition Sketch

Multilinear Plastic - Pivot

OK Cancel

Link/Support Directional Properties

Edit

Identification

Property Name: DRCB2I
 Direction: U1
 Type: MultiLinear Plastic
 NonLinear: Yes

Hysteresis Type And Parameters

Hysteresis Type: Pivot
 α_1 : 10 β_1 : 0.9 η : 0
 α_2 : 10 β_2 : 0.9

Properties Used For Linear Analysis Cases

Effective Stiffness: 285761
 Effective Damping: 0

Multi-Linear Force-Deformation Definition

	Displ	Force
6	0	0
7	2.776E-03	791.36
8	0.1884	1081.82
9	0.3746	1110.82
10	0.39	222.16

Order Rows Delete Row Add Row 12

Hysteresis Definition Sketch

Multilinear Plastic - Pivot

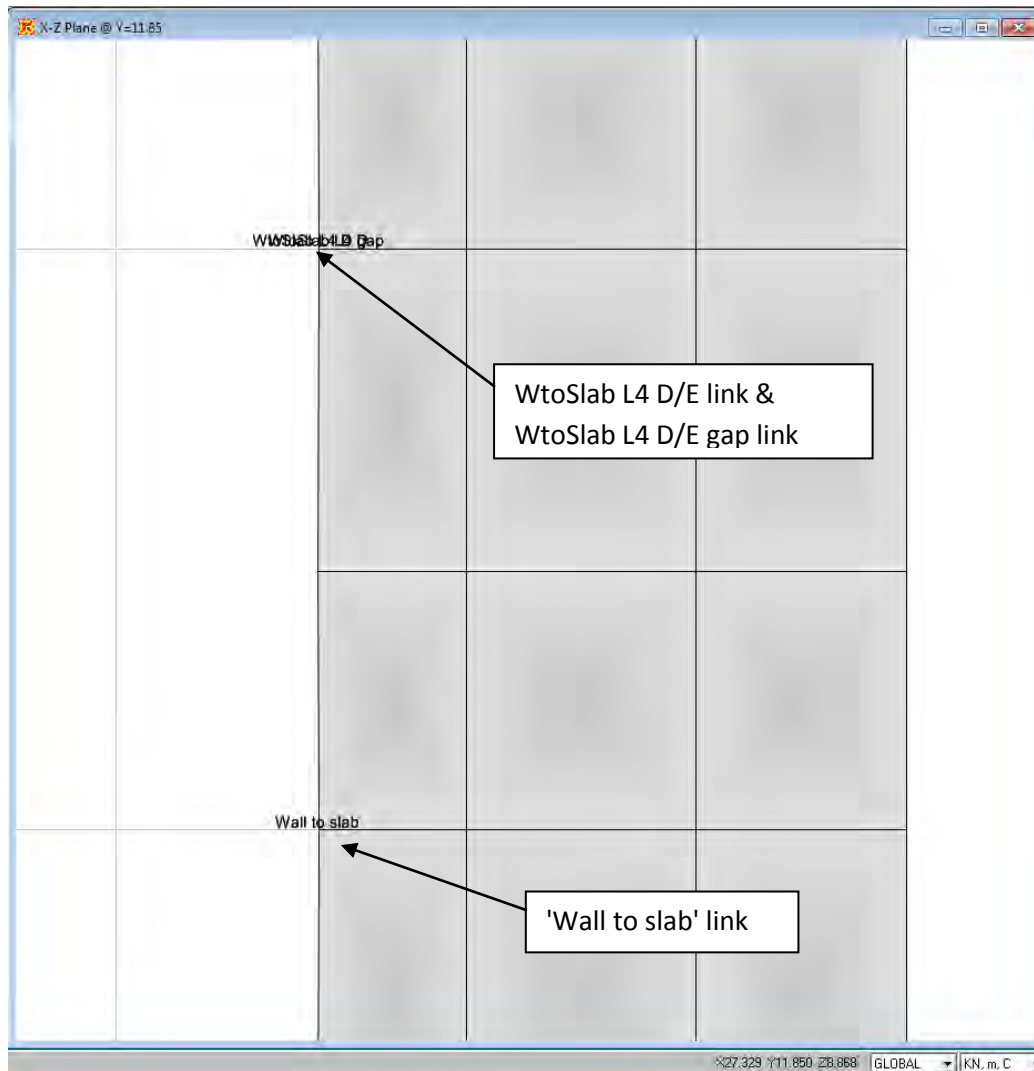
OK Cancel

Wall D and Wall D/E on north core link (lift shaft walls)

Levels 3 and 4 of wall D/E shown.

Note: Gap elements only are installed at levels 2 and 3 for walls D & D/E.

Gap and multi-linear plastic links are overlain on levels 4, 5, & 6 for walls D & D/E



L2 & L3 gap element

Link/Support Property Data

Link/Support Type:

Property Name:

Property Notes:

Total Mass and Weight

Mass: Rotational Inertia 1:

Weight: Rotational Inertia 2:

Rotational Inertia 3:

Factors For Line, Area and Solid Springs

Property is Defined for This Length In a Line Spring:

Property is Defined for This Area In Area and Solid Springs:

Directional Properties

Direction	Fixed	NonLinear	Properties
<input checked="" type="checkbox"/> U1	<input type="checkbox"/>	<input checked="" type="checkbox"/>	<input type="button" value="Modify/Show for U1..."/>
<input type="checkbox"/> U2	<input type="checkbox"/>	<input type="checkbox"/>	<input type="button" value="Modify/Show for U2..."/>
<input type="checkbox"/> U3	<input type="checkbox"/>	<input type="checkbox"/>	<input type="button" value="Modify/Show for U3..."/>
<input type="checkbox"/> R1	<input type="checkbox"/>	<input type="checkbox"/>	<input type="button" value="Modify/Show for R1..."/>
<input type="checkbox"/> R2	<input type="checkbox"/>	<input type="checkbox"/>	<input type="button" value="Modify/Show for R2..."/>
<input type="checkbox"/> R3	<input type="checkbox"/>	<input type="checkbox"/>	<input type="button" value="Modify/Show for R3..."/>

P-Delta Parameters

Link/Support Directional Properties

Identification

Property Name:

Direction:

Type:

NonLinear:

Properties Used For Linear Analysis Cases

Effective Stiffness:

Effective Damping:

Properties Used For Nonlinear Analysis Cases

Stiffness:

Open:

L4 Links (note L5 & L6 are similar)

Link/Support Property Data

Link/Support Type: MultiLinear Plastic

Property Name: WtoSlab L4 D Set Default Name

Property Notes Modify/Show...

Total Mass and Weight

Mass	<input type="text" value="0"/>	Rotational Inertia 1	<input type="text" value="0"/>
Weight	<input type="text" value="0"/>	Rotational Inertia 2	<input type="text" value="0"/>
		Rotational Inertia 3	<input type="text" value="0"/>

Factors For Line, Area and Solid Springs

Property is Defined for This Length In a Line Spring

Property is Defined for This Area In Area and Solid Springs

Directional Properties

Direction	Fixed	NonLinear	Properties
<input checked="" type="checkbox"/> U1	<input type="checkbox"/>	<input checked="" type="checkbox"/>	<input type="button" value="Modify/Show for U1..."/>
<input type="checkbox"/> U2	<input type="checkbox"/>	<input type="checkbox"/>	<input type="button" value="Modify/Show for U2..."/>
<input type="checkbox"/> U3	<input type="checkbox"/>	<input type="checkbox"/>	<input type="button" value="Modify/Show for U3..."/>
<input type="checkbox"/> R1	<input type="checkbox"/>	<input type="checkbox"/>	<input type="button" value="Modify/Show for R1..."/>
<input type="checkbox"/> R2	<input type="checkbox"/>	<input type="checkbox"/>	<input type="button" value="Modify/Show for R2..."/>
<input type="checkbox"/> R3	<input type="checkbox"/>	<input type="checkbox"/>	<input type="button" value="Modify/Show for R3..."/>

P-Delta Parameters

Link/Support Directional Properties

Edit

Identification

Property Name: WtoSlab L4 D

Direction: U1

Type: MultiLinear Plastic

NonLinear: Yes

Hysteresis Type And Parameters

Hysteresis Type: Takeda

No Parameters Are Required For This Hysteresis Type

Properties Used For Linear Analysis Cases

Effective Stiffness: 1000000

Effective Damping: 0

Multi-Linear Force-Deformation Definition

	Displ	Force
1	-1.	0.
2	0.	0.
3	2.310E-03	320.
4	0.01	3.
5	0.02	0.

Order Rows Delete Row Add Row 7

Hysteresis Definition Sketch

MultiLinear Plastic - Takeda

OK Cancel

Link/Support Directional Properties

Edit

Identification

Property Name: WtoSlab L4 D

Direction: U1

Type: MultiLinear Plastic

NonLinear: Yes

Hysteresis Type And Parameters

Hysteresis Type: Takeda

No Parameters Are Required For This Hysteresis Type

Properties Used For Linear Analysis Cases

Effective Stiffness: 1000000

Effective Damping: 0

Multi-Linear Force-Deformation Definition

	Displ	Force
3	2.310E-03	320.
4	0.01	3.
5	0.02	0.
6	0.15	0.

Order Rows Delete Row Add Row 7

Hysteresis Definition Sketch

MultiLinear Plastic - Takeda

OK Cancel

Link/Support Property Data

Link/Support Type:

Property Name:

Property Notes:

Total Mass and Weight

Mass: Rotational Inertia 1:

Weight: Rotational Inertia 2:

Rotational Inertia 3:

Factors For Line, Area and Solid Springs

Property is Defined for This Length In a Line Spring:

Property is Defined for This Area In Area and Solid Springs:

Directional Properties

Direction	Fixed	NonLinear	Properties
<input checked="" type="checkbox"/> U1	<input type="checkbox"/>	<input checked="" type="checkbox"/>	<input type="button" value="Modify/Show for U1..."/>
<input type="checkbox"/> U2	<input type="checkbox"/>	<input type="checkbox"/>	<input type="button" value="Modify/Show for U2..."/>
<input type="checkbox"/> U3	<input type="checkbox"/>	<input type="checkbox"/>	<input type="button" value="Modify/Show for U3..."/>
<input type="checkbox"/> R1	<input type="checkbox"/>	<input type="checkbox"/>	<input type="button" value="Modify/Show for R1..."/>
<input type="checkbox"/> R2	<input type="checkbox"/>	<input type="checkbox"/>	<input type="button" value="Modify/Show for R2..."/>
<input type="checkbox"/> R3	<input type="checkbox"/>	<input type="checkbox"/>	<input type="button" value="Modify/Show for R3..."/>

P-Delta Parameters

Link/Support Directional Properties

Identification

Property Name:

Direction:

Type:

NonLinear:

Properties Used For Linear Analysis Cases

Effective Stiffness:

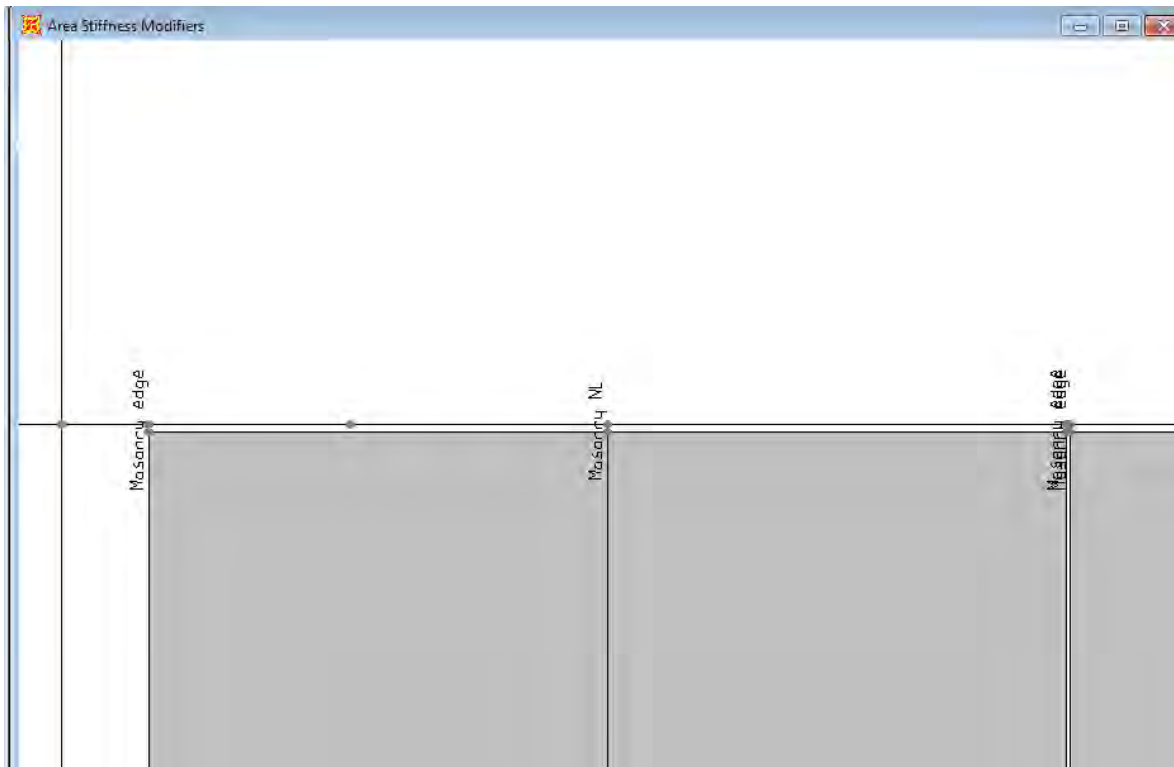
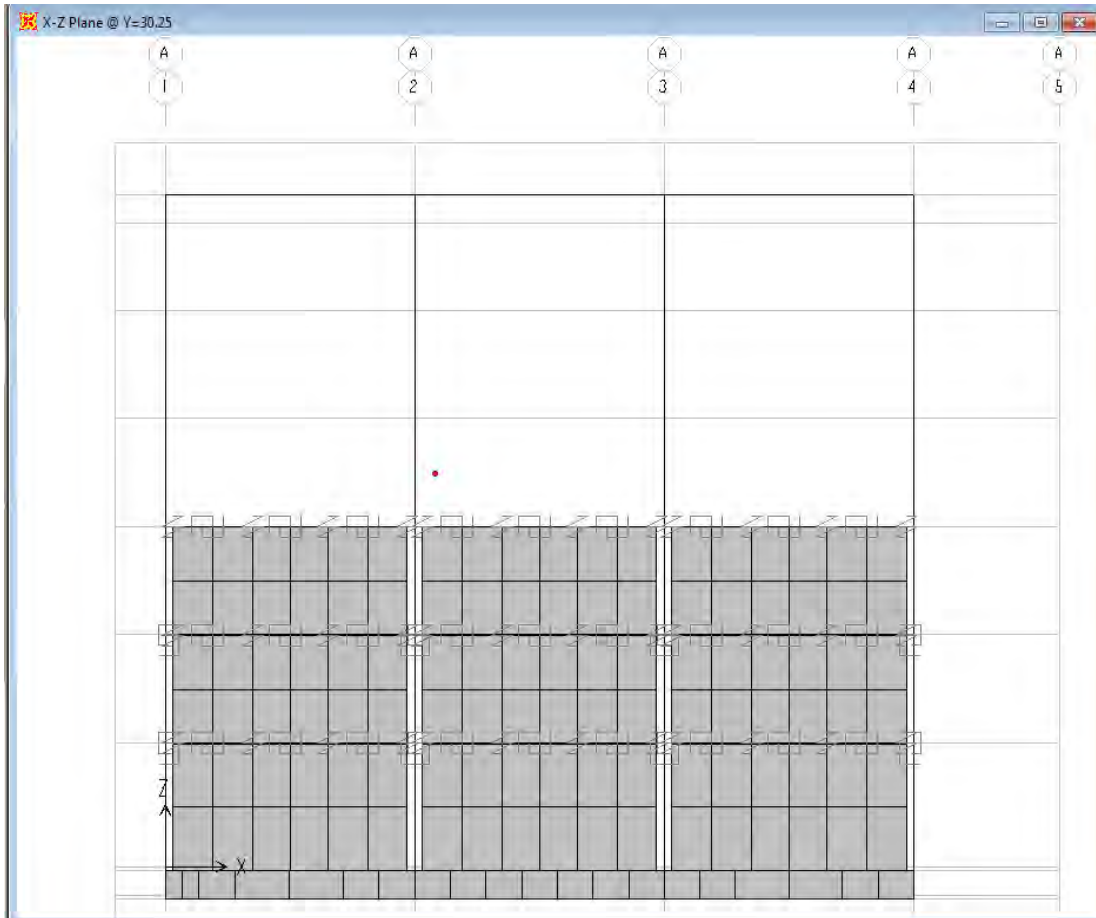
Effective Damping:

Properties Used For Nonlinear Analysis Cases

Stiffness:

Open:

Masonry Model (Model B) Links



Link/Support Property Data

Link/Support Type:

Property Name:

Property Notes:

Total Mass and Weight

Mass: Rotational Inertia 1:

Weight: Rotational Inertia 2:

Rotational Inertia 3:

Factors For Line, Area and Solid Springs

Property is Defined for This Length In a Line Spring:

Property is Defined for This Area In Area and Solid Springs:

Directional Properties

Direction	Fixed	NonLinear	Properties
<input type="checkbox"/> U1	<input type="checkbox"/>	<input type="checkbox"/>	<input type="button" value="Modify/Show for U1"/>
<input checked="" type="checkbox"/> U2	<input type="checkbox"/>	<input checked="" type="checkbox"/>	<input type="button" value="Modify/Show for U2.."/>
<input type="checkbox"/> U3	<input type="checkbox"/>	<input type="checkbox"/>	<input type="button" value="Modify/Show for U3.."/>
<input type="checkbox"/> R1	<input type="checkbox"/>	<input type="checkbox"/>	<input type="button" value="Modify/Show for R1"/>
<input type="checkbox"/> R2	<input type="checkbox"/>	<input type="checkbox"/>	<input type="button" value="Modify/Show for R2.."/>
<input type="checkbox"/> R3	<input type="checkbox"/>	<input type="checkbox"/>	<input type="button" value="Modify/Show for R3.."/>

P-Delta Parameters

Link/Support Directional Properties

Edit

Identification

Property Name:

Direction:

Type:

NonLinear: Yes

Hysteresis Type And Parameters

Hysteresis Type:

No Parameters Are Required For This Hysteresis Type

Properties Used For Linear Analysis Cases

Effective Stiffness:

Effective Damping:

Shear Deformation Location

Distance from End-J:

Multi-Linear Force-Deformation Definition

	Displ	Force
1	-0.15	-2.
2	-0.1	-100.
3	-3.300E-03	-100.
4	0.	0.
5	3.300E-03	100.

Hysteresis Definition Sketch

MultiLinear Plastic - Takeda

Link/Support Property Data

Link/Support Type:

Property Name:

Property Notes:

Total Mass and Weight

Mass	<input type="text" value="0"/>	Rotational Inertia 1	<input type="text" value="0"/>
Weight	<input type="text" value="0"/>	Rotational Inertia 2	<input type="text" value="0"/>
		Rotational Inertia 3	<input type="text" value="0"/>

Factors For Line, Area and Solid Springs

Property is Defined for This Length In a Line Spring:

Property is Defined for This Area In Area and Solid Springs:

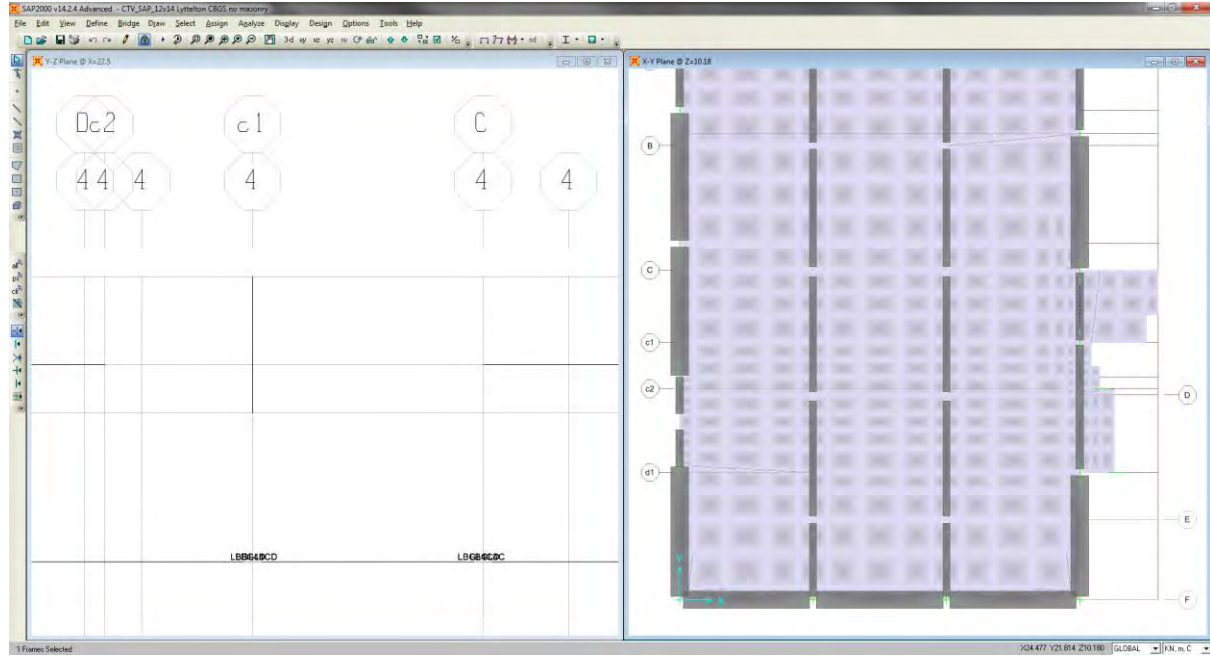
Directional Properties:

Direction	Fixed	Properties
<input type="checkbox"/> LR	<input type="checkbox"/>	<input type="button" value="Modify/Show for All"/>
<input type="checkbox"/> LL	<input type="checkbox"/>	
<input checked="" type="checkbox"/> UL	<input checked="" type="checkbox"/>	
<input type="checkbox"/> RL	<input type="checkbox"/>	
<input type="checkbox"/> RR	<input type="checkbox"/>	
<input type="checkbox"/> RB	<input type="checkbox"/>	
<input type="checkbox"/> RB	<input type="checkbox"/>	

P-Delta Parameters:

Beam Hinges (these have been input as a non-linear link)

Beam on GL 4 spanning between GL C and D.



Link/Support Property Data

Link/Support Type:

Property Name:

Property Notes:

Total Mass and Weight

Mass	<input type="text" value="0"/>	Rotational Inertia 1	<input type="text" value="0"/>
Weight	<input type="text" value="0"/>	Rotational Inertia 2	<input type="text" value="0"/>
		Rotational Inertia 3	<input type="text" value="0"/>

Factors For Line, Area and Solid Springs

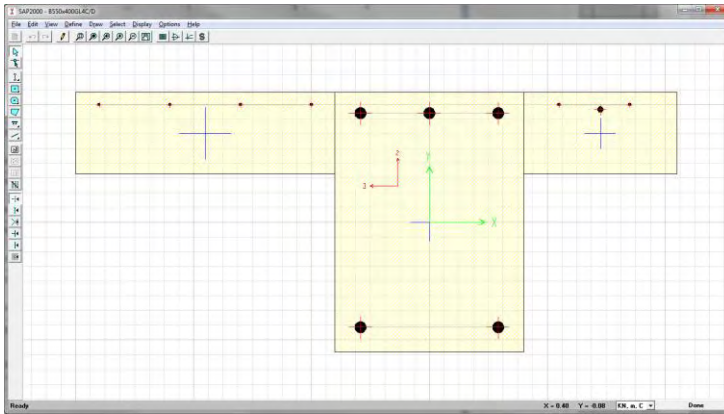
Property is Defined for This Length In a Line Spring:

Property is Defined for This Area In Area and Solid Springs:

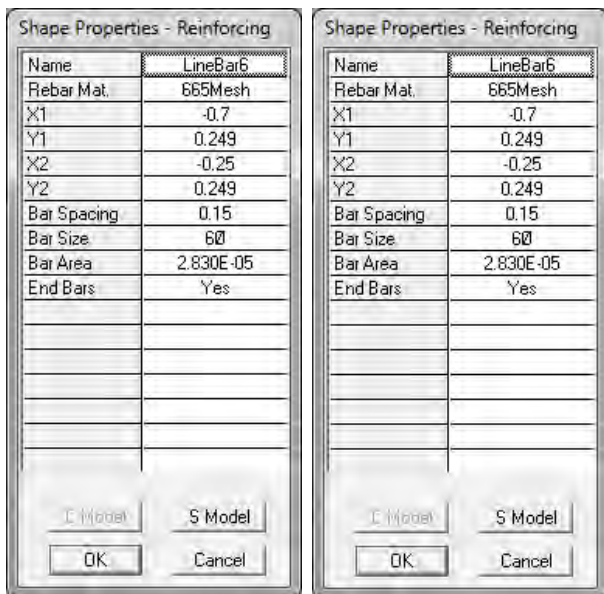
Directional Properties

Direction	Fixed	NonLinear	Properties
<input checked="" type="checkbox"/> U1	<input type="checkbox"/>	<input type="checkbox"/>	<input type="button" value="Modify/Show for U1..."/>
<input checked="" type="checkbox"/> U2	<input type="checkbox"/>	<input type="checkbox"/>	<input type="button" value="Modify/Show for U2..."/>
<input checked="" type="checkbox"/> U3	<input type="checkbox"/>	<input type="checkbox"/>	<input type="button" value="Modify/Show for U3..."/>
<input checked="" type="checkbox"/> R1	<input type="checkbox"/>	<input type="checkbox"/>	<input type="button" value="Modify/Show for R1..."/>
<input checked="" type="checkbox"/> R2	<input type="checkbox"/>	<input type="checkbox"/>	<input type="button" value="Modify/Show for R2..."/>
<input checked="" type="checkbox"/> R3	<input type="checkbox"/>	<input checked="" type="checkbox"/>	<input type="button" value="Modify/Show for R3..."/>

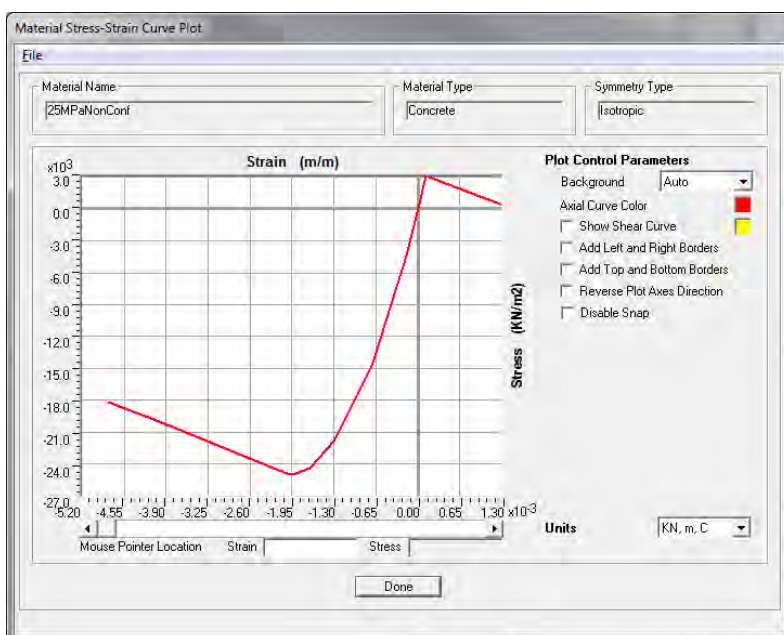
P-Delta Parameters



Reinforcement details (note 664mesh has been miss-labelled as 665 mesh)



Concrete stress-strain plot



Mesh reinforcement information

Material Property Data

Material Name: 665Mesh | Material Type: Rebar | Symmetry Type: Uniaxial

Modulus of Elasticity: E1 = 2.009×10^5 | Units: KN, m, C

Poisson's Ratio: U12 = 0

Coeff of Thermal Expansion: A1 = 1.170×10^{-5}

Shear Modulus: G12 = 0

Weight and Mass: Weight per Unit Volume: 0 | Mass per Unit Volume: 0

Other Properties for Rebar Materials:

Minimum Yield Stress, Fy	615000
Minimum Tensile Stress, Fu	665000
Expected Yield Stress, Fye	615000
Expected Tensile Stress, Fue	665000

Advanced Material Property Data:
 Nonlinear Material Data... | Material Damping Properties...
 Time Dependent Properties... | Thermal Properties...

Nonlinear Material Data

Material Name: 665Mesh | Material Type: Rebar

Hysteresis Type: Kinematic | Units: KN, m, C

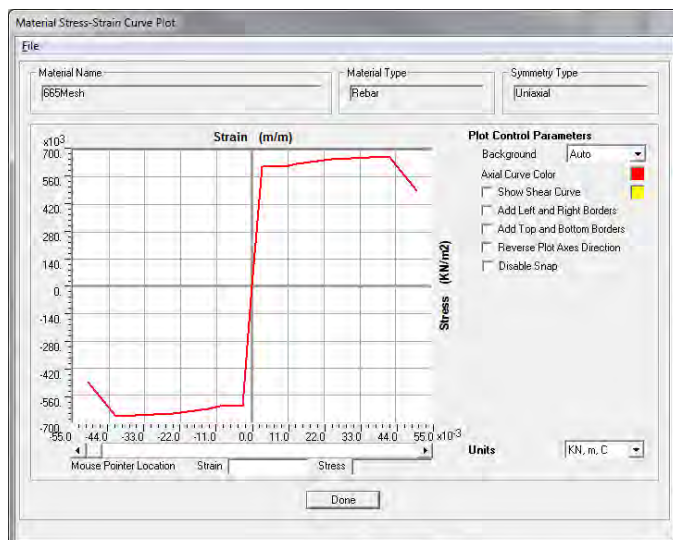
Stress-Strain Curve Definition Options: Parametric (selected) | Park | Convert To User Defined

Parametric Strain Data:

Strain At Onset of Strain Hardening	0.01
Ultimate Strain Capacity	0.042
Final Slope (Multiplier on E)	-0.1

Use Caltrans Default Controlling Strain Values (Bar Size Dependent)

Show Stress-Strain Plot...



Reinforcement information

Nonlinear Material Data

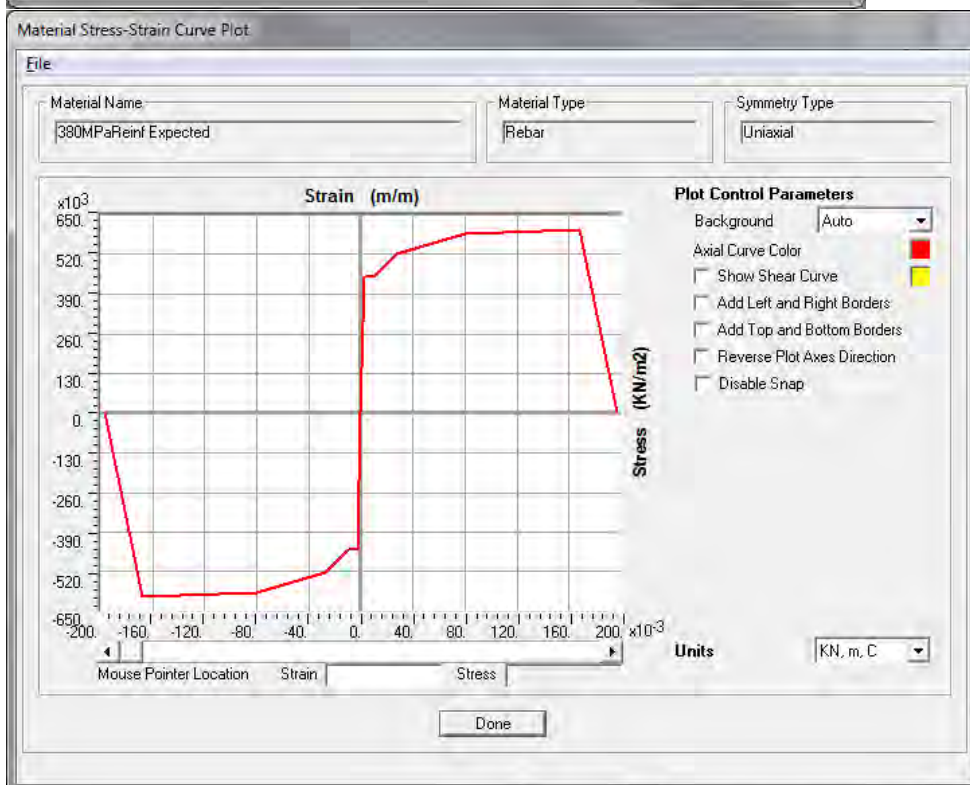
Edit

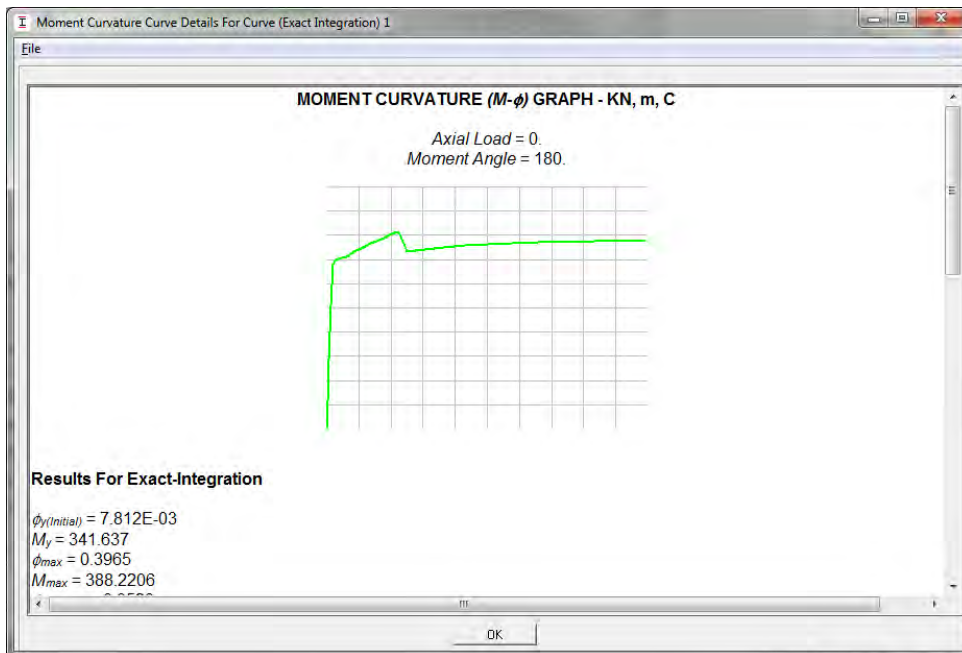
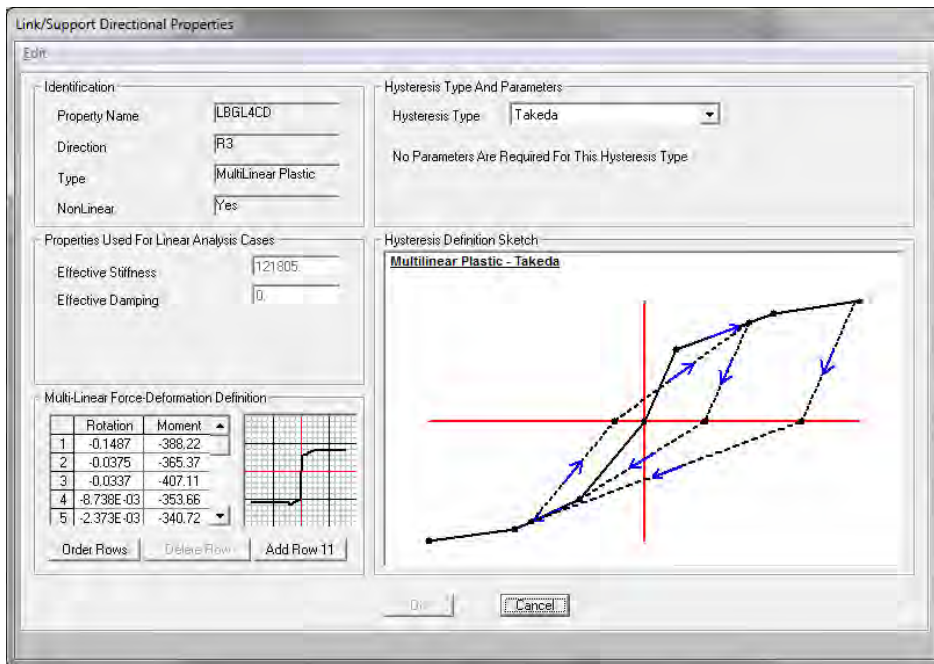
Material Name: 380MPaReinf Expected Material Type: Rebar

Hysteresis Type: Kinematic Friction Angle: Dilatational Angle: Units: KN, m, C

Stress-Strain Curve Definition Options:
 Parametric Park User Defined

Parametric Strain Data:
 Strain At Onset of Strain Hardening: 9.700E-03
 Ultimate Strain Capacity: 0.168
 Final Slope (Multiplier on E): -0.1
 Use Caltrans Default Controlling Strain Values (Bar Size Dependent)





Moment Curvature Curve Details For Curve (Exact Integration) 1

Strain	Axis	Strain	Strain	Compression	Compression	Tension	Force	Net Force	Curvature	Moment
0.	0.	0.	0.	0.	0.	0.	0.	0.	0	0.
-1.581E-04	0.2023	3.961E-04	0.	-108.7264	-19.1289	127.6441	0.	-0.2111	0.001058	58.5737
-4.017E-04	0.1999	9.839E-04	0.	-267.2299	-48.9969	316.9807	0.	0.7539	0.002644	144.5056
-7.364E-04	0.1971	1.758E-03	0.	-471.613	-90.6837	562.7094	0.	0.4127	0.004759	256.1914
-1.067E-03	0.2077	2.813E-03	0.	-616.0905	-126.4597	742.336	0.	-0.2143	0.007404	340.7204
-1.296E-03	0.2292	4.246E-03	0.	-610.4708	-138.459	748.7595	0.	-0.1702	0.0106	347.8453
-1.534E-03	0.2444	5.948E-03	0.	-602.0054	-146.7899	748.7595	0.	-0.0358	0.0143	350.5353
-1.789E-03	0.2552	7.910E-03	0.	-596.2469	-153.2798	748.7595	0.	-0.7671	0.0185	352.5746
-2.066E-03	0.263	0.0101	0.	-590.5006	-158.8169	748.8714	0.	-0.4461	0.0233	353.6642
-2.396E-03	0.2679	0.0126	0.	-591.8894	-169.0625	760.8407	0.	-0.1112	0.0286	359.5398
-2.769E-03	0.2713	0.0152	0.	-591.7789	-182.1419	773.9574	0.	0.0366	0.0344	365.6011
-3.182E-03	0.2737	0.0182	0.	-589.5192	-197.5119	787.8028	0.	0.7716	0.0407	371.5702
-3.647E-03	0.2752	0.0213	0.	-585.1036	-217.4678	802.4059	0.	-0.1655	0.0476	378.1022
-4.203E-03	0.2754	0.0246	0.	-568.3091	-249.1649	818.1641	0.	0.6901	0.055	383.5441
-4.891E-03	0.2741	0.0281	0.	-534.7857	-300.2403	834.6947	0.	-0.3313	0.0629	388.6147
-5.583E-03	0.2736	0.0318	0.	-506.0312	-347.0321	852.2552	0.	-0.8082	0.0714	394.9562
-6.282E-03	0.2737	0.0358	0.	-480.7026	-389.9848	870.947	0.	0.2596	0.0804	401.9733
-7.529E-03	0.2681	0.0396	0.	-482.9001	-405.3504	888.0196	0.	-0.231	0.0899	407.105
-7.221E-03	0.2796	0.0452	0.	-418.5186	-375.4151	794.594	0.	0.6603	0.0999	365.3749
-7.914E-03	0.2802	0.05	0.	-400.9628	-401.9607	802.2482	0.	-0.6754	0.1105	368.8557
-9.188E-03	0.2763	0.0545	0.	-404.4571	-405.3504	809.391	0.	-0.4165	0.1216	370.5131

OK

Link/Support Directional Properties

Edit

Identification

Property Name: LBGL4CD

Direction: R3

Type: MultiLinear Plastic

NonLinear: Yes

Hysteresis Type And Parameters

Hysteresis Type: Takeda

No Parameters Are Required For This Hysteresis Type

Properties Used For Linear Analysis Cases

Effective Stiffness: 121805

Effective Damping: 0

Multi-Linear Force-Deformation Definition

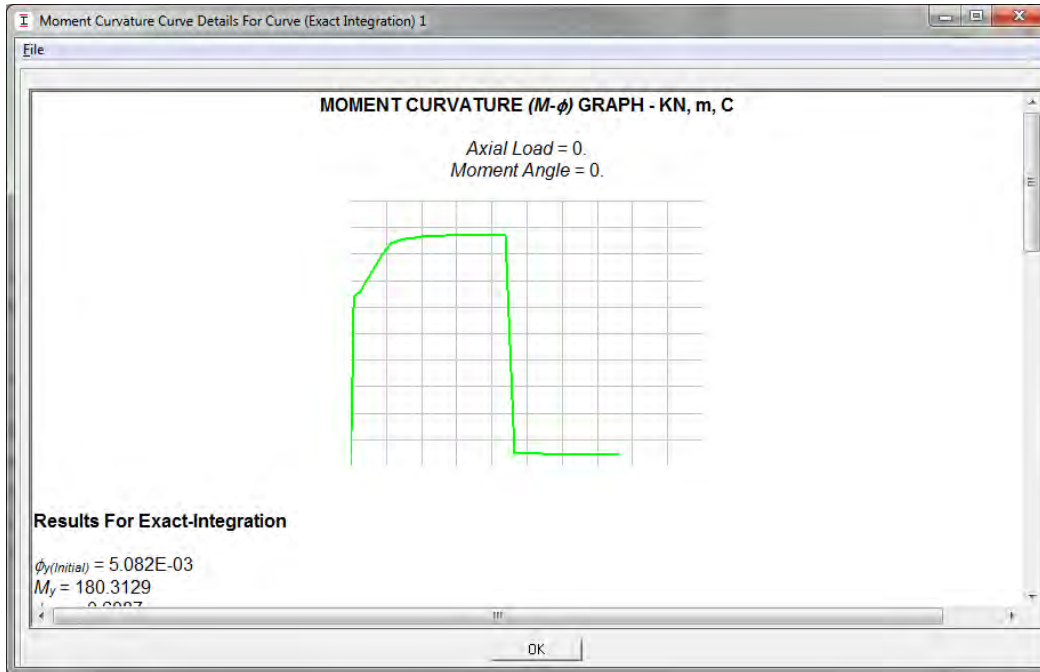
	Rotation	Moment
6	0.	0.
7	1.928E-03	192.89
8	8.738E-03	199.14
9	0.0337	251.6
10	0.1319	261.13

Order Rows | Delete Row | Add Row 11

Hysteresis Definition Sketch

Multilinear Plastic - Takeda

OK | Cancel



Moment Curvature Curve Details For Curve (Exact Integration) 1

File

Concrete Strain	Neutral Axis	Steel Strain	Tendon Strain	Concrete Compression	Steel Compression	Steel Tension	Prestress Force	Net Force	Curvature	Moment
0.	0.	0.	0.	0.	0.	0.	0.	0.	0	0.
-7.336E-05	0.1289	4.534E-04	0.	-74.9364	-9.8622	84.0991	0.	-0.6994	0.001058	39.9112
-1.827E-04	0.1291	1.134E-03	0.	-185.9431	-24.4241	210.3754	0.	8.186E-03	0.002644	99.5512
-3.330E-04	0.1283	2.037E-03	0.	-332.5605	-45.3425	377.9149	0.	0.0118	0.004759	178.5642
-4.385E-04	0.139	3.249E-03	0.	-361.4475	-43.7981	405.3504	0.	0.1048	0.007404	192.8856
-5.366E-04	0.1475	4.731E-03	0.	-372.8692	-32.36	405.3504	0.	0.1213	0.0106	194.2054
-6.409E-04	0.1533	6.470E-03	0.	-389.6482	-15.6184	405.3504	0.	0.0838	0.0143	195.3878
-7.541E-04	0.1575	8.464E-03	0.	-410.8843	-11.4876	422.3911	0.	0.0192	0.0185	196.5769
-8.783E-04	0.1605	0.0107	0.	-438.2724	-10.397	449.1716	0.	0.5022	0.0233	199.138
-1.017E-03	0.1626	0.0132	0.	-473.5258	-9.5124	483.1301	0.	0.0919	0.0286	204.009
-1.172E-03	0.1641	0.0159	0.	-511.0704	-9.6499	520.5803	0.	-0.14	0.0344	209.1426
-1.346E-03	0.1652	0.0189	0.	-550.2542	-9.956	560.0718	0.	-0.1385	0.0407	214.5362
-1.539E-03	0.1659	0.0222	0.	-591.2605	-10.4277	601.6302	0.	-0.058	0.0476	220.2614
-1.753E-03	0.1664	0.0256	0.	-633.3417	-11.1579	644.4447	0.	-0.0548	0.055	226.3005
-1.993E-03	0.1666	0.0294	0.	-674.8171	-12.3069	687.1137	0.	-0.0102	0.0629	232.543
-2.261E-03	0.1665	0.0333	0.	-714.5869	-13.9971	728.5687	0.	-0.0152	0.0714	238.9554
-2.564E-03	0.1663	0.0375	0.	-751.1104	-16.3795	767.4904	0.	4.637E-04	0.0804	245.4594
-2.900E-03	0.166	0.0419	0.	-783.5863	-19.4423	802.9146	0.	-0.1139	0.0899	251.6027
-3.259E-03	0.1656	0.0465	0.	-808.2775	-22.8248	830.5024	0.	-0.5999	0.0999	253.9772
-3.653E-03	0.1652	0.0514	0.	-827.5922	-26.9574	854.5799	0.	0.0303	0.1105	256.04
-4.106E-03	0.1645	0.0565	0.	-835.2757	-32.6746	867.9039	0.	-0.0464	0.1216	257.6723
-4.669E-03	0.1632	0.0617	0.	-813.9243	-41.7119	855.4185	0.	-0.2177	0.1333	257.8441
-5.246E-03	0.1622	0.0672	0.	-794.3638	-50.8771	845.6152	0.	0.3744	0.1454	258.4046
-5.844E-03	0.1613	0.0729	0.	-776.5507	-63.448	839.9701	0.	-0.0286	0.1581	259.5285
-6.451E-03	0.1606	0.0789	0.	-759.7815	-75.6277	835.335	0.	-0.0742	0.1713	259.5276
-7.076E-03	0.16	0.0851	0.	-744.5999	-87.9033	832.3298	0.	-0.1734	0.1851	259.7492
-7.719E-03	0.1595	0.0916	0.	-730.7037	-100.3344	830.7287	0.	-0.3095	0.1994	260.1764
-8.381E-03	0.1591	0.0983	0.	-717.943	-112.9335	830.4729	0.	-0.4036	0.2142	260.7678

OK

Beam on GL 1 spanning into the south wall .

Link/Support Property Data

Link/Support Type: MultiLinear Plastic

Property Name: LBGLD1/E1 Set Default Name

Property Notes: Modify/Show...

Total Mass and Weight

Mass: 0 Rotational Inertia 1: 0

Weight: 0 Rotational Inertia 2: 0

Rotational Inertia 3: 0

Factors For Line, Area and Solid Springs

Property is Defined for This Length In a Line Spring: 1

Property is Defined for This Area In Area and Solid Springs: 1

Directional Properties

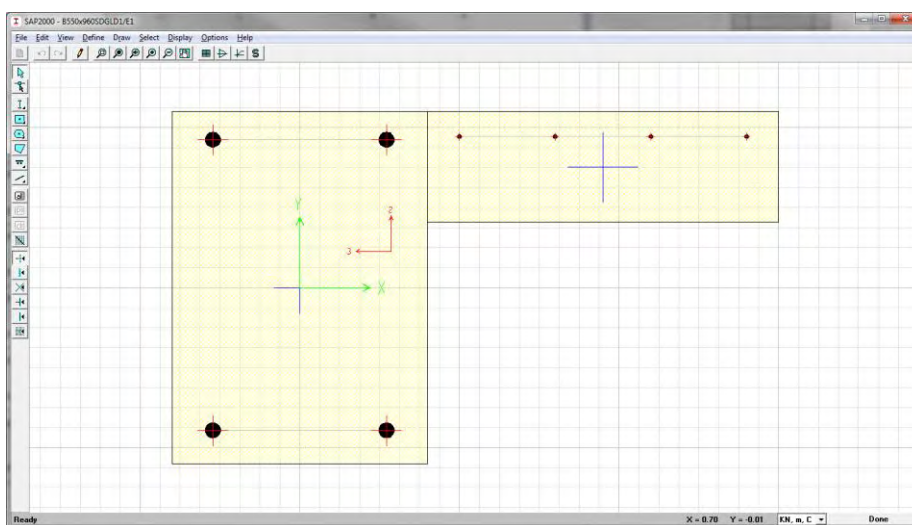
Direction	Fixed	NonLinear	Properties
U1	<input type="checkbox"/>	<input type="checkbox"/>	Modify/Show for U1...
U2	<input type="checkbox"/>	<input type="checkbox"/>	Modify/Show for U2...
U3	<input type="checkbox"/>	<input type="checkbox"/>	Modify/Show for U3...
R1	<input type="checkbox"/>	<input type="checkbox"/>	Modify/Show for R1...
R2	<input type="checkbox"/>	<input type="checkbox"/>	Modify/Show for R2...
R3	<input type="checkbox"/>	<input checked="" type="checkbox"/>	Modify/Show for R3...

Fix All Clear All

P-Delta Parameters

Advanced...

Cancel



Link/Support Directional Properties

Edit

Identification

Property Name: LBGLD1/E1

Direction: R3

Type: MultiLinear Plastic

NonLinear: Yes

Hysteresis Type And Parameters

Hysteresis Type: Takeda

No Parameters Are Required For This Hysteresis Type

Properties Used For Linear Analysis Cases

Effective Stiffness: 75232.98

Effective Damping: 0.

Multi-Linear Force-Deformation Definition

	Rotation	Moment
1	-0.177	-251.74
2	-0.0483	-235.94
3	-0.0436	-266.84
4	-0.0101	-226.79
5	-2.874E-03	-219.5

Order Rows Delete Row Add Row 11

Hysteresis Definition Sketch

MultiLinear Plastic - Takeda

OK Cancel

Link/Support Directional Properties

Edit

Identification

Property Name: LBGLD1/E1

Direction: R3

Type: MultiLinear Plastic

NonLinear: Yes

Hysteresis Type And Parameters

Hysteresis Type: Takeda

No Parameters Are Required For This Hysteresis Type

Properties Used For Linear Analysis Cases

Effective Stiffness: 75232.98

Effective Damping: 0.

Multi-Linear Force-Deformation Definition

	Rotation	Moment
6	0.	0.
7	2.578E-03	191.02
8	0.0101	195.54
9	0.0436	245.82
10	0.1798	255.79

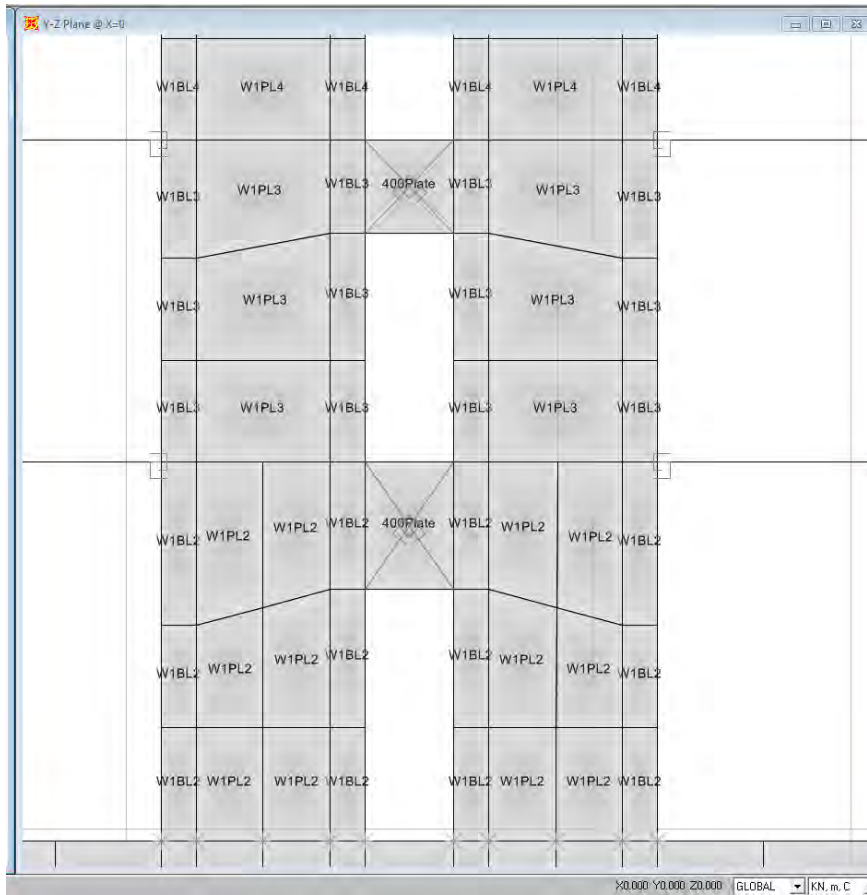
Order Rows Delete Row Add Row 11

Hysteresis Definition Sketch

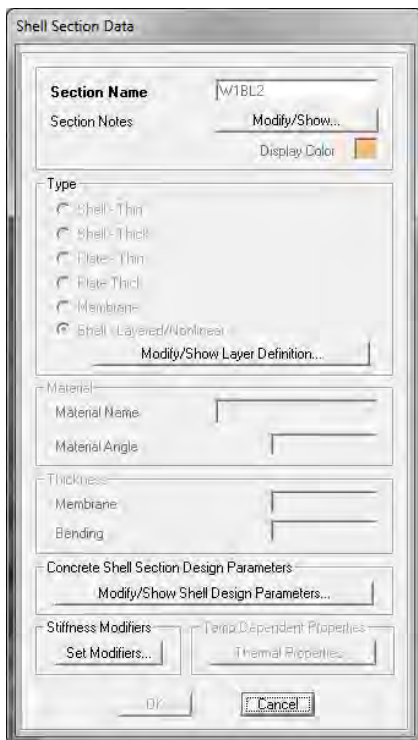
MultiLinear Plastic - Takeda

OK Cancel

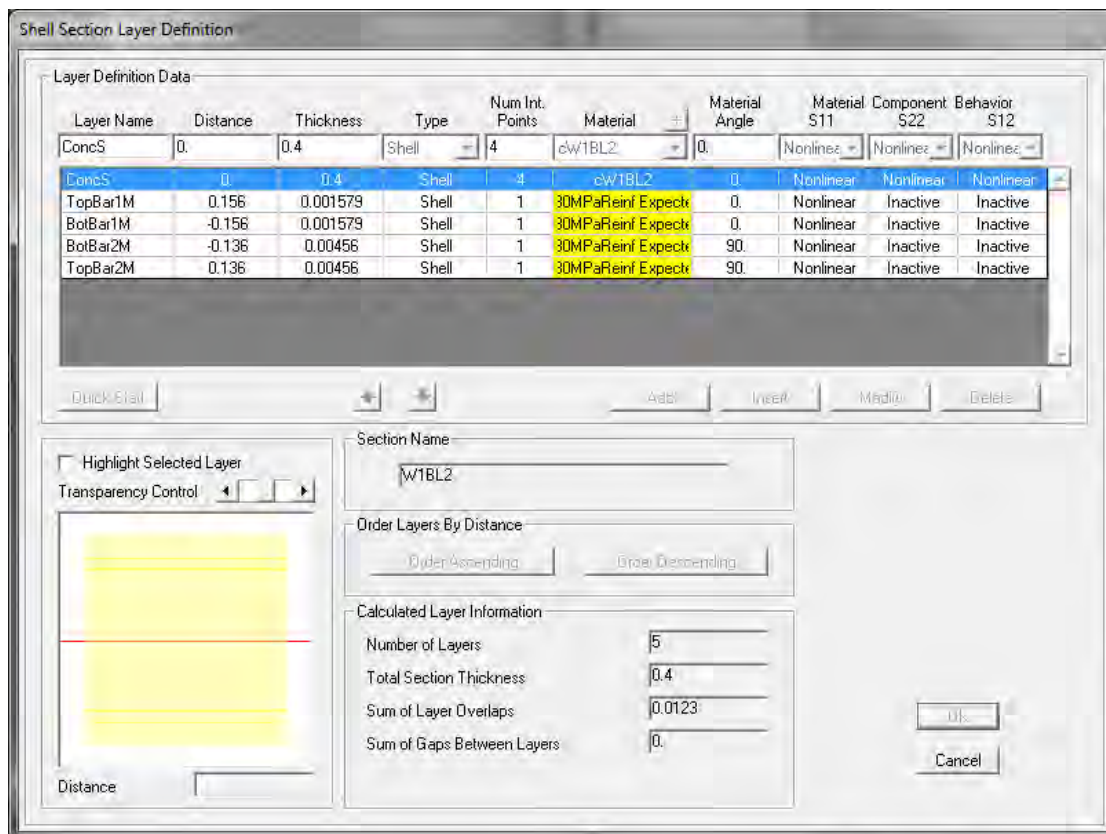
Southern Shear Wall



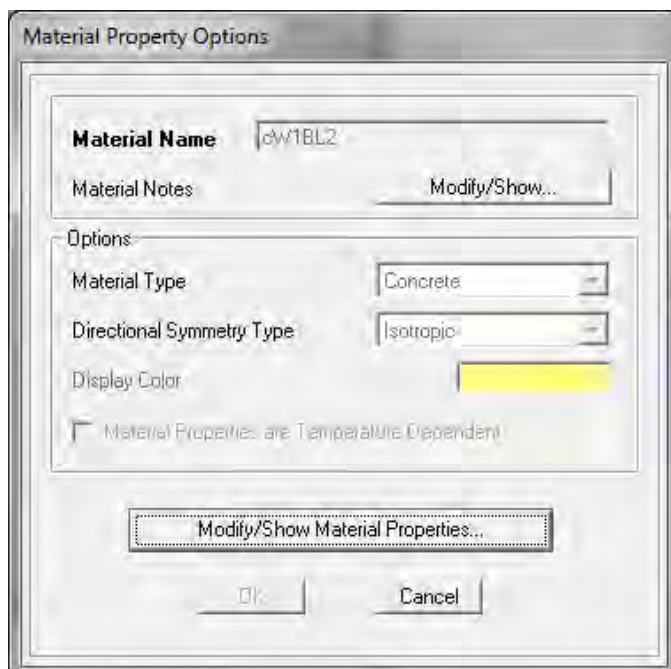
Wall end shell definition at base of wall



Non-linear layers shell definition



Shell concrete properties for end shell



Material Property Data

Material Name: cW1BL2 Material Type: Concrete Symmetry Type: Isotropic

Modulus of Elasticity: E = 27200000

Poisson's Ratio: ν = 0.2

Coeff of Thermal Expansion: α = 9.900E-06

Shear Modulus: G = 11150000

Weight and Mass: Weight per Unit Volume: 24 Mass per Unit Volume: 0 Units: KN, m, C

Other Properties for Concrete Materials: Specified Concrete Compressive Strength, f_c: 33500

Lightweight Concrete
Shear Strength Reduction Factor: []

Advanced Material Property Data:
 Nonlinear Material Data... Material Damping Properties...
 Time Dependent Properties... Thermal Properties...

[] [Cancel]

End shell non-linear material definition - determined using confined concrete and Mander confined concrete model

Nonlinear Material Data

Material Name: cW1BL2 Material Type: Concrete

Hysteresis Type: Takeda Drucker-Prager Parameters: Friction Angle: 0 Dilatational Angle: 0 Units: KN, m, C

Stress-Strain Curve Definition Options:
 Parametric User Defined Convert To User Defined

User Stress-Strain Curve Data
 Number of Points in Stress-Strain Curve: 24

	Strain	Stress	Point ID
1	-0.0457	0	
2	-0.0393	-17761.95	-E
3	-0.0387	-17889.61	
4	-0.0363	-18523.58	
5	-0.0338	-19223.18	
6	-0.0313	-20000.03	
7	-0.0288	-20868.77	
8	-0.0264	-21847.97	
9	-0.0239	-22961.61	
10	-0.0214	-24241	
11	-0.019	-25727.46	
12	-0.0165	-27475.81	
13	-0.014	-29557.57	

[] [Cancel]

Reinforcement properties for walls

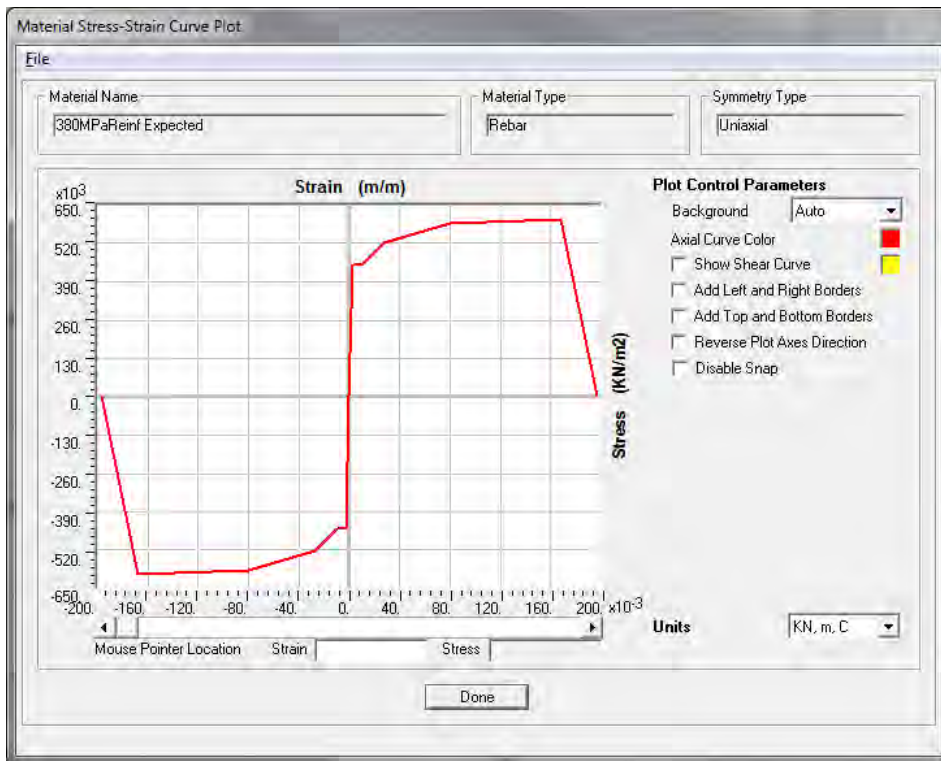
Material Property Data

Material Name 380MPaReinf Expected	Material Type Rebar	Symmetry Type Uniaxial
Modulus of Elasticity E1 2.050E+08	Weight and Mass Weight per Unit Volume 0 Mass per Unit Volume 0	Units KN, m, C
Poisson's Ratio U12 0	Other Properties for Rebar Materials	
Coeff of Thermal Expansion A1 1.170E-05	Minimum Yield Stress, Fy	448000
Shear Modulus G12 0	Minimum Tensile Stress, Fu	603000
	Expected Yield Stress, Fye	448000
	Expected Tensile Stress, Fue	603000
Advanced Material Property Data		
Nonlinear Material Data...		Material Damping Properties...
Time Dependent Properties...		Thermal Properties...
<input type="button" value="OK"/> <input type="button" value="Cancel"/>		

Nonlinear Material Data

Edit

Material Name 380MPaReinf Expected	Material Type Rebar	
Hysteresis Type Kinematic	Drucker-Prager Parameters Friction Angle Dilatational Angle	Units KN, m, C
Stress-Strain Curve Definition Options		
<input checked="" type="radio"/> Parametric	Park	<input type="button" value="Convert To User Defined"/>
<input type="radio"/> User Defined		
Parametric Strain Data		
Strain At Onset of Strain Hardening	9.700E-03	
Ultimate Strain Capacity	0.168	
Final Slope (Multiplier on E)	-0.1	
<input type="checkbox"/> Use Caltrans Default Controlling Strain Values (Bar Size Dependent)		
<input type="button" value="Show Stress-Strain Plot..."/>		
<input type="button" value="OK"/> <input type="button" value="Cancel"/>		



South wall mid section of wall at base

Shell Section Data

Section Name: W1FL2

Section Notes: [Modify/Show...](#)

Display Color: ■

Type

- Shell - Thin
- Shell - Thick
- Plate - Thin
- Plate - Thick
- Membrane
- Shell (Layered/Nonlinear)
 - [Modify/Show Layer Definition...](#)

Material

Material Name:

Material Angle:

Thickness

Membrane:

Bending:

Concrete Shell Section Design Parameters

[Modify/Show Shell Design Parameters...](#)

Stiffness Modifiers

[Set Modifiers...](#) Temp. Dependent Properties

[Thermal Properties...](#)

OK [Cancel](#)

Shell Section Layer Definition

Layer Definition Data

Layer Name	Distance	Thickness	Type	Num Int. Points	Material	Material Angle	Material S11	Material S22	Behavior S12
ConcS	0.	0.4	Shell	4	cw/PL2-7	0.	Nonlinear	Nonlinear	Nonlinear
BotBar1M	-0.156	0.000566	Shell	1	30MPaReinf Expect	0.	Nonlinear	Inactive	Inactive
TopBar1M	0.156	0.000566	Shell	1	30MPaReinf Expect	0.	Nonlinear	Inactive	Inactive
BotBar2M	-0.136	0.000447	Shell	1	30MPaReinf Expect	90.	Nonlinear	Inactive	Inactive
TopBar2M	0.136	0.000447	Shell	1	30MPaReinf Expect	90.	Nonlinear	Inactive	Inactive

Highlight Selected Layer
 Transparency Control:

Section Name:

Order Layers By Distance:

Calculated Layer Information:

Number of Layers	<input type="text" value="5"/>
Total Section Thickness	<input type="text" value="0.4"/>
Sum of Layer Overlaps	<input type="text" value="2.026E-03"/>
Sum of Gaps Between Layers	<input type="text" value="0."/>

Material Property Data

Material Name:

Material Type:

Symmetry Type:

Modulus of Elasticity: E

Poisson's Ratio: ν

Coeff of Thermal Expansion: α

Shear Modulus: G

Weight and Mass:

Weight per Unit Volume:

Mass per Unit Volume:

Units:

Other Properties for Concrete Materials:

Specified Concrete Compressive Strength, f_c:

Lightweight Concrete

Shear Strength Reduction Factor:

Advanced Material Property Data:

Non-linear stress strain information for shell

Nonlinear Material Data

Edit

Material Name: cWPL2-7 Material Type: Concrete

Hysteresis Type: Takeda Drucker-Prager Parameters: Friction Angle: 0 Dilatational Angle: 0 Units: KN, m, C

Stress-Strain Curve Definition Options:
 Parametric User Defined Convert To User Defined

User Stress-Strain Curve Data

Number of Points in Stress-Strain Curve: 8

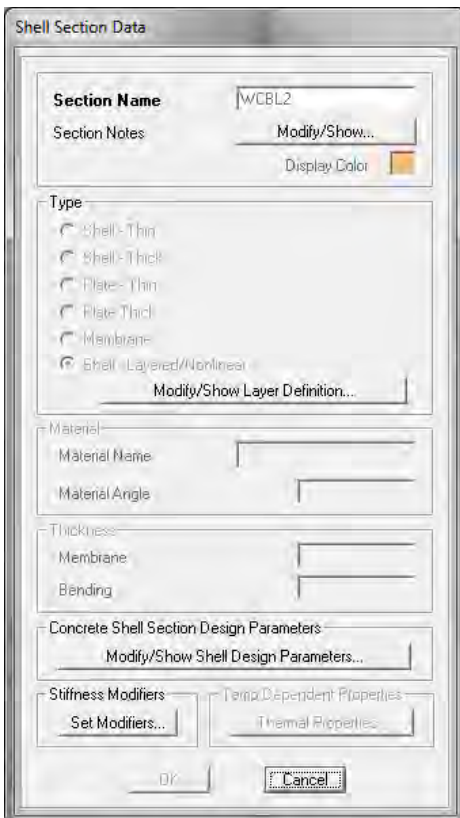
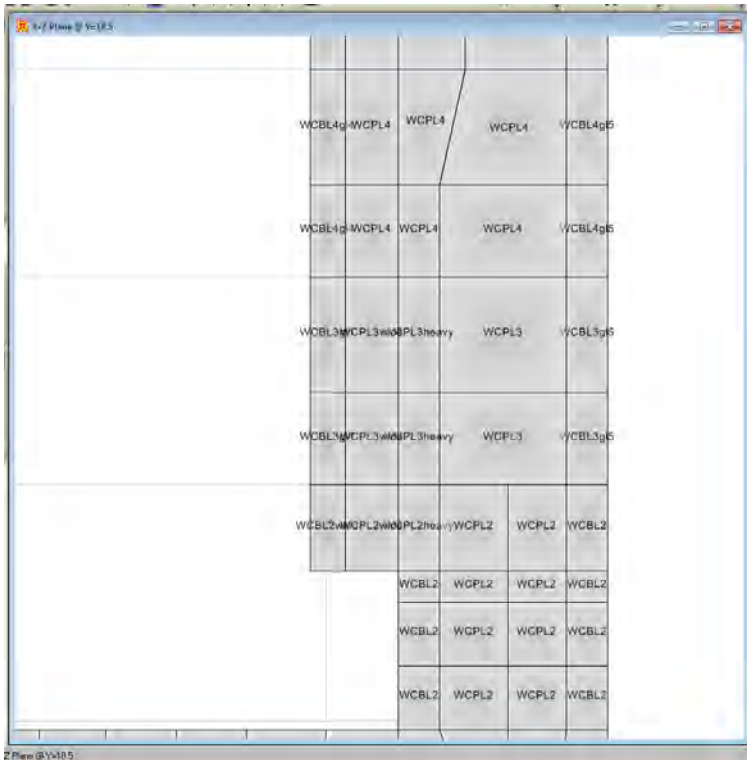
	Strain	Stress	Point ID
1	-4.000E-03	-23109.83	-E
2	-3.024E-03	-29242.03	
3	-2.000E-03	-33500.	-C
4	-1.568E-03	-32085.4	
5	-9.760E-04	-24390.51	
6	-2.000E-04	-5509.8	
7	0.	0.	A
8	1.000E-04	0.	B

Order Rows

Show Plot...

Cancel

North Core wall on GL C



Shell Section Layer Definition

Layer Definition Data

Layer Name	Distance	Thickness	Type	Num Int. Points	Material	Material Angle	Material S11	Material S22	Behavior S12
ConcM	0.	0.3	Membrane	1	cWCBL2	0.	Nonlinear	Nonlinear	Nonlinear
ConcM	0.	0.3	Membrane	1	cWCBL2	0.	Nonlinear	Nonlinear	Nonlinear
TopBar1M	0.	0.004442	Membrane	1	30MPaReinf Expect	0.	Nonlinear	Inactive	Inactive
TopBar2M	0.	0.012818	Membrane	1	30MPaReinf Expect	90.	Nonlinear	Inactive	Inactive
ConcP	0.	0.211	Plate	2	cWCBL2	0.	Linear	Linear	Linear

Quick Edit Add Insert Modify Delete

Highlight Selected Layer
Transparency Control

Section Name: WCBL2

Order Layers By Distance
Order Ascending Order Descending

Calculated Layer Information

Number of Layers	4
Total Section Thickness	0.3
Sum of Layer Overlaps	0.25
Sum of Gaps Between Layers	0.

Distance

OK Cancel

Material Property Data

Material Name: cWCBL2

Material Type: Concrete

Symmetry Type: Isotropic

Modulus of Elasticity: E = 37800000

Weight and Mass: Weight per Unit Volume = 24, Mass per Unit Volume = 0

Units: KN, m, C

Poisson's Ratio: ν = 0.2

Coeff of Thermal Expansion: α = 9.900E-06

Shear Modulus: G = 11500000

Other Properties for Concrete Materials

Specified Concrete Compressive Strength, f_c : 33500

Lightweight Concrete

Shear Strength Reduction Factor:

Advanced Material Property Data

Nonlinear Material Data... Material Damping Properties...
Time Dependent Properties... Thermal Properties...

OK Cancel

Nonlinear Material Data

Edit

Material Name: Material Type:

Hysteresis Type: Drucker-Prager Parameters: Friction Angle: Dilatational Angle: Units:

Stress-Strain Curve Definition Options: Parametric User Defined Convert To User Defined

User Stress-Strain Curve Data

Number of Points in Stress-Strain Curve:

	Strain	Stress	Point ID
1	-0.0681	-8783.49	
2	-0.0568	-40113.1	E
3	-0.0555	-40338.9	
4	-0.0503	-41416.	
5	-0.0451	-42620.5	
6	-0.0399	-43979.2	
7	-0.0347	-45526.2	
8	-0.0295	-47303.	
9	-0.0243	-49355.1	
10	-0.0191	-51705.9	
11	-0.0139	-54226.5	
12	-8.679E-03	-55874.2	-C
13	-6.943E-03	-55431.2	

Order Rows Show Plot...

OK Cancel

Shell Section Data

Section Name: Modify/Show...

Section Notes: Display Color

Type: Shell-Thin Shell-Thick Plate-Thin Plate-Thick Membrane Shell-Layered/Nonlinear Modify/Show Layer Definition...

Material: Material Name Material Angle

Thickness: Membrane Bending

Concrete Shell Section Design Parameters: Modify/Show Shell Design Parameters...

Stiffness Modifiers: Set Modifiers... Temp-Dependent Properties Thermal Properties

OK Cancel

Shell Section Layer Definition

Layer Definition Data

Layer Name	Distance	Thickness	Type	Num Int. Points	Material	Material Angle	Material S11	Component S22	Behavior S12
ConcM	0.	0.3	Membrane	1	cWPL2.7	0.	Nonlinear	Nonlinear	Nonlinear
ConcM	0.	0.3	Membrane	1	cWPL2.7	0.	Nonlinear	Nonlinear	Nonlinear
TopBar1M	0.	0.002011	Membrane	1	30MPaReinf Expect	0.	Nonlinear	Inactive	Inactive
TopBar2M	0.	0.000916	Membrane	1	30MPaReinf Expect	90.	Nonlinear	Inactive	Inactive
ConcP	0.	0.18	Plate	2	cWPL2.7	0.	Linear	Linear	Linear

Click/Exit + * Add Incr Mod Delete

Highlight Selected Layer

Transparency Control:

Distance:

Section Name:

Order Layers By Distance: Order Ascending Order Descending

Calculated Layer Information:

Number of Layers:

Total Section Thickness:

Sum of Layer Overlaps:

Sum of Gaps Between Layers:

OK Cancel

Appendix C.

Papers Submitted to Aid Discussion on Modelling

1. Park, S. and Mosalam, K.M.. Analytical Model for Predicting Shear Strength of Unreinforced Exterior Beam-Column Joints, ACI Structural Journal. March-April 2012, p149-160.
2. Anderson, M, Lehman, D, and Stanton, J. A cyclic shear stress–strain model for joints without transverse reinforcement. Engineering Structures 30 (2008) 941–954.
3. Karthik, M.M. and Mander, J.B. Stress-Block Parameters for Unconfined and Confined Concrete Based on a Unified Stress-Strain Model. Journal of Structural Engineering, ASCE, February 2011, p270-273.
4. Celik, O.C. and Ellingwood, B.R., Modeling Beam-Column Joints in Fragility Assessment of Gravity Load Designed Reinforced Concrete Frames, Journal of Earthquake Engineering, 12:,2008, p357–381.
5. Lehman, D., Stanton, J., Anderson, M. Aire, D. and Walker, S. Seismic Performance of Older Beam-Column Joints. 13th World Conference on Earthquake Engineering, Vancouver, B.C., Canada, August 1-6, 2004, Paper No. 1464.
6. Paulay, T. and Williams, R.L. The analysis and Design of and the Evaluation of Design Actions for Reinforced Concrete Ductile Shear Wall Structures. Bull. NZ Soc. For Earthquake Engineering, Vol 13, No 2, June 1980, p108-143.
7. Park, S. and Mosalam, K.M.. Parameters for shear strength prediction of exterior beam–column joints without transverse reinforcement, Engineering Structures, 36 (2012) 198–209

Title no. 109-S14

Analytical Model for Predicting Shear Strength of Unreinforced Exterior Beam-Column Joints

by Sangjoon Park and Khalid M. Mosalam

This paper presents an analytical model to predict the shear strength of reinforced concrete (RC) exterior beam-column joints without transverse reinforcement (denoted as unreinforced) in the joint region. Several existing analytical models developed for reinforced beam-column joints have shown limited success in assessing the shear strength of unreinforced joints due to an inapplicable shear-transfer mechanism. A new shear-strength model is proposed based on a mechanism consisting of two inclined struts in the joint. The proposed model is validated by the accurate prediction of the shear strength of many tests from published literature. The proposed model accounts for the variation of joint shear strength with the joint aspect ratio and the beam reinforcement ratio, using truss analogy and the deterioration of bond resistance, respectively. Finally, the joint moment-rotation relationship is estimated using the proposed model, and simulations are successfully performed for two published tests.

Keywords: beam-column joint; inclined strut; reinforced concrete; shear-strength model.

INTRODUCTION

There has been significant effort to better assess the shear strength of reinforced concrete (RC) beam-column joints without transverse reinforcement in the joint region (referred to hereafter as “unreinforced joints”), which are commonly observed in older-type RC buildings designed without or with little consideration for seismic forces. Several existing analytical models attempted to predict the shear strength of unreinforced joints based on the average principal tensile stress limit or the strut-and-tie (SAT) approach using the average stress equilibrium and strain compatibility.¹⁻⁴ The existing models have a conceptual limitation, however, because these average equilibrium and compatibility equations are not suitable to reflect the behavior of unreinforced joints in which the joint shear failure is typically localized. In particular, the tensile strains of the beam and column longitudinal reinforcement cannot represent average strains in the horizontal and vertical directions in the unreinforced joint panel.² Additionally, the accuracy of the SAT approach is highly dependent on estimating the diagonal strut area because the joint shear strength is very sensitive to this estimated area.⁵

From an extensive literature review, the analytical joint strength model developed in this study is motivated by the following observations. First, the unreinforced exterior joints having the same concrete strength and geometry fail in shear at different levels of joint shear stress demand, which is determined by the beam’s longitudinal reinforcement ratio and its strength. This is an important observation considering that the unreinforced exterior joint resembles an unconfined concrete cuboid with seemingly unique strength. Second, in the case of joint shear failure following beam reinforcement yielding, the shear strength of unreinforced

exterior joints decreases due to yield penetration into the joint region. To obtain the reduced shear strength, three modification methods are adopted in the existing models: 1) directly reducing the joint shear strength by a ductility factor^{6,7}; 2) reducing the area of the diagonal strut by a ductility factor⁸; and 3) reducing the applied joint shear force in the average joint stress equilibrium equation by a ductility factor.⁴ The relationship between the reduction of joint shear strength and the ductility factor is empirically proposed in these models. The ductility factor is relatively uncertain and includes the deformation of other members in addition to the joint distortion. Therefore, the empirically proposed relationships cannot be accurately generalized.

The proposed analytical model is developed to fulfill the following objectives:

1. The new approach uses a consistent procedure to predict two different types of joint shear failure—that is, without beam reinforcement yielding (denoted as J type) or with beam reinforcement yielding (denoted as BJ type)—without the need for ductility factors.
2. The solution procedures are suitable for practical applications.
3. The new approach does not require the estimation of the diagonal strut area A_{str} .
4. The new approach can be used to establish an envelope of the joint shear stress-strain relationship that can be transformed to the moment-rotation relationship of a rotational spring representing the joint region. This objective is essential for simulating beam-column joints in the structural analysis of nonductile RC frames.

RESEARCH SIGNIFICANCE

An analytical model is proposed to predict the shear strength of unreinforced exterior beam-column joints based on a new SAT approach. The proposed model addresses the variation of joint shear strength for different joint aspect ratios and beam longitudinal reinforcement ratios without the use of a ductility factor, as in existing models. Based on the findings from the evaluations of previous tests using the proposed model, a simplified model is developed for practical engineering applications. The proposed model is used to provide a constitutive relationship for a rotational spring to represent the flexibility of beam-column joints in the seismic evaluation of nonductile RC frames.

ACI Structural Journal, V. 109, No. 2, March-April 2012.

MS No. S-2009-317.R4 received October 29, 2010, and reviewed under Institute publication policies. Copyright © 2012, American Concrete Institute. All rights reserved, including the making of copies unless permission is obtained from the copyright proprietors. Pertinent discussion including author’s closure, if any, will be published in the January-February 2013 *ACI Structural Journal* if the discussion is received by September 1, 2012.

ACI member **Sangjoon Park** is a Postdoctoral Researcher of Civil and Environmental Engineering at the University of California, Berkeley, CA. He received his BS and MS from Seoul National University, Seoul, South Korea, and his PhD from the University of California, Berkeley. His research interests include analytical and experimental study of the behavior of reinforced concrete structures subjected to earthquake loads.

ACI member **Khalid M. Mosalam** is a Professor and Vice Chair of Civil and Environmental Engineering at the University of California, Berkeley. He received his BS and MS from Cairo University, Giza, Egypt, and his PhD from Cornell University, Ithaca, NY. His research interests include experimental, computational, and hybrid simulation research related to concrete, masonry, and wood structures subjected to extreme loads.

DEVELOPMENT OF ANALYTICAL MODEL Assumptions

Tests by Wong⁴ show that the joint shear strength for the detail of the beam reinforcement hook bent away from the joint region is less than that for the beam reinforcement hook bent into the joint region, as shown in Fig. 1. This reduction is related to the lack of a well-confined diagonal strut crossing the corners of the joint panel when the joint material, geometry, and beam longitudinal bars are identical for both details. The comparison between the two details in Fig. 1 motivates an idea that the horizontal joint shear force is resisted by two inclined struts in the joint region and their contributions are affected by the manner in which the beam longitudinal tension reinforcing bars are anchored into the joint region.

In the proposed model, two inclined struts are first assumed to resist the horizontal joint shear force (Fig. 2) in parallel, where the horizontal joint shear force is resisted by the sum of the two horizontal components of the two struts. Strut ST1 is developed by the 90-degree hook of the beam reinforcement, whereas Strut ST2 is developed by the bond resistance of the concrete surrounding the beam reinforcement. In this study, the only considered anchorage detail of

beam longitudinal bars is the 90-degree hooks on the top and bottom bars bent into the joint region. Presumably, the fraction of each strut in this detail can be determined by the level of beam reinforcement tensile stress, which is related to the bond resistance, as discussed in the following.

The second assumption is that the joint shear failure is initiated adjacent to the node of Strut ST1 on the side where no beam is framing into the joint—that is, the top left node in Fig. 2. This assumption is supported by two facts: 1) this node anchors one tie (C-C-T node); and 2) the crack width is greatest at this node. Hence, such crack morphology reduces the strength of the nodal zone, which can be estimated using a softening concrete constitutive model. This crack pattern is observed in published tests of unreinforced exterior joints with or without one lateral beam. Therefore, the proposed model is applicable to these two critical types of unreinforced exterior joints because the shear strength of exterior joints, with lateral beams on both sides, increases significantly compared with these two types.⁹

Park and Mosalam¹⁰ suggested that the principal tensile strain, at the shear failure of unreinforced exterior beam-column joints, can be expressed as follows

$$\epsilon_1 = 0.003 + 0.0005(h_b/h_c) \quad (1)$$

where h_b is the height of the beam cross section; and h_c is the height of the column cross section in the loading direction. The proposed principal tensile strain was compared to the joint shear strains measured in tests from the literature.¹⁰ To express the joint shear strength in terms of the square root of the concrete standard compressive strength ($\sqrt{f'_c}$) and consider the simplicity of a linear reduction (in the denominator) of the compressive strength with the increase of the principal tensile strain, a softening concrete model suggested

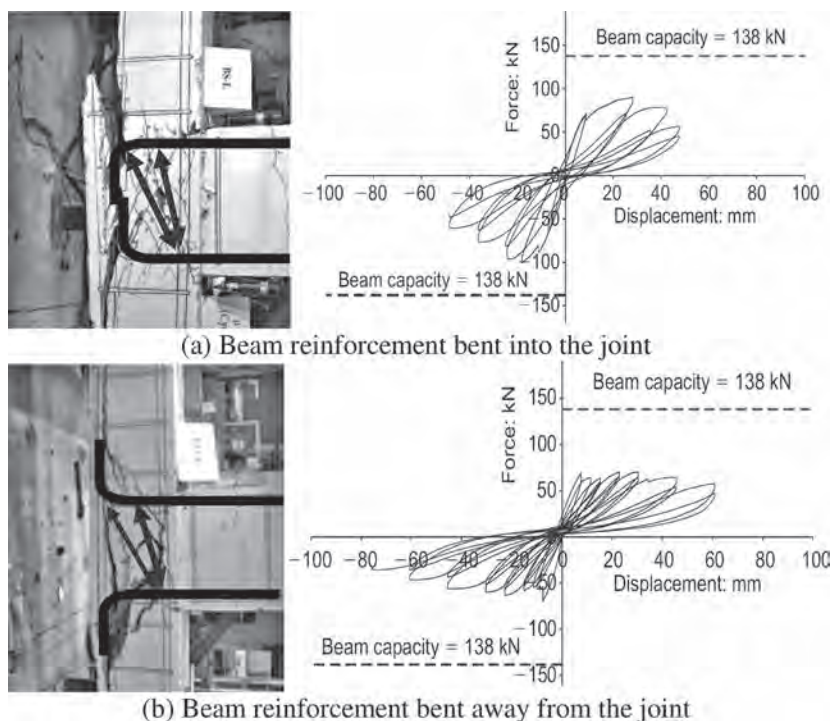


Fig. 1—Different contribution of diagonal strut to joint shear strength.⁴
(Note: 1 mm = 0.0394 in.; 1 kN = 0.2248 kips.)

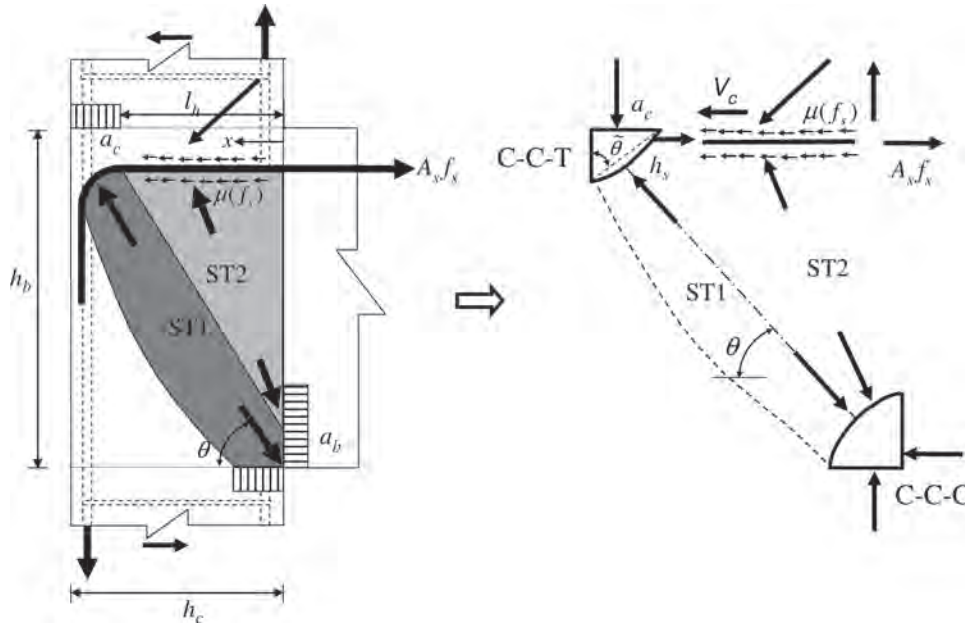


Fig. 2—Assumed SAT model in exterior beam-column joints.

by Vollum¹¹ is adopted to develop a relevant model for the concrete panel of the unreinforced joints—that is

$$\sigma = \frac{a_1 \sqrt{f'_c}}{0.8 + 170 \epsilon_1} \quad (2)$$

where σ is the strain-softening concrete compressive strength; and a_1 is a constant with values of 71.3 psi (5.9 MPa). It is worth mentioning that Eq. (2) is almost identical to the softening concrete model proposed by Zhang and Hsu¹² in Eq. (3) for $0.003 \leq \epsilon_1 \leq 0.004$

$$\sigma = \frac{\tilde{a}_1 \sqrt{f'_c}}{\sqrt{1 + 250 \epsilon_1}} \quad (3)$$

where \tilde{a}_1 is a constant with values of 69.9 psi (5.8 MPa). The Zhang and Hsu¹² model was verified by their tests and has been adopted by other researchers.^{2,4}

Equilibrium

In Fig. 3, the beam flexural moment and column shear force at the joint right and top faces are presented as follows

$$M_b = V_b \times L = A_s f_s \times jd_b \quad (4)$$

$$V_c = \frac{L + h_c/2}{H} V_b \quad (5)$$

where V_b and V_c are the beam and column shear forces, respectively; L is the length from the beam inflection point to the column face; H is the height between the upper and lower column inflection points; A_s and f_s are the area and stress of the beam tensile reinforcement, respectively; d_b is the effective depth of the beam; and jd_b indicates the internal moment

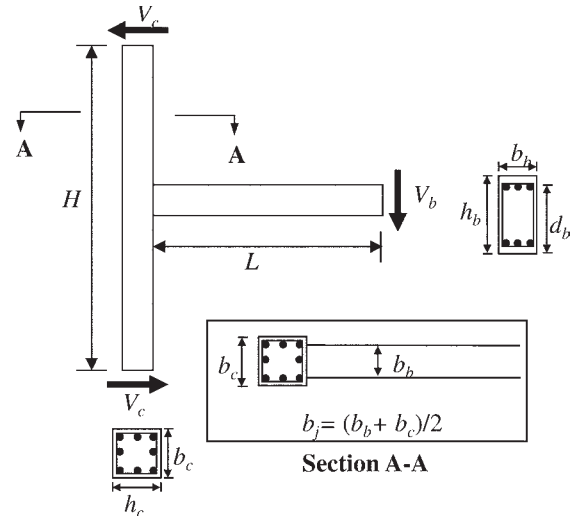


Fig. 3—Global equilibrium in exterior beam-column joint.

arm of the beam cross section at the beam-joint interface (typically $jd_b = 0.875d_b$ at yielding). Accordingly, the horizontal shear force of the joint panel is calculated as follows

$$V_{jh} = A_s f_s - V_c = A_s f_s \left(1 - \frac{L + h_c/2}{H} \frac{jd_b}{L} \right) \quad (6)$$

Considering that the effective depth of the beam is close to 90% of the total height in practical beam cross sections, the following approximation can be made

$$jd_b \approx 0.8h_b \Rightarrow \frac{L + h_c/2}{H} \frac{jd_b}{L} = \frac{L + h_c/2}{L} \frac{0.8h_b}{H} \approx 0.85 \frac{h_b}{H} \quad (7)$$

The horizontal joint shear force equation, Eq. (6), can be simplified using Eq. (7) as follows

$$V_{jh} \approx A_s f_s \left(1 - 0.85 \frac{h_b}{H} \right) \quad (8)$$

On the other hand, the horizontal joint shear force is decomposed as follows

$$V_{jh} = V_{jh,ST1} + V_{jh,ST2} \quad (9)$$

$$V_{jh,ST1} = A_s f_s - n\pi\phi_b \int_0^{l_h} \mu(f_s) dx \quad (10)$$

$$V_{jh,ST2} = n\pi\phi_b \int_0^{l_h} \mu(f_s) dx - V_c \quad (11)$$

where n is the number of beam longitudinal bars in tension with diameter ϕ_b . Note that $\mu(f_s)$ is the bond stress distribution along the beam bar (Fig. 2) as a function of the tensile stress of the bar f_s , which varies with the distance x —that is, $f_s = f_s(x)$. The x -axis and distance l_h are depicted in Fig. 2. Vollum¹¹ and Hwang and Lee² approximated the horizontal projection of the width of the diagonal Strut ST1 using Eq. (12a) and (12b), respectively.

$$a_c = 0.4h_c \quad (12a)$$

$$a_c = \left(0.25 + 0.85 \frac{P}{f_c h_c b_c} \right) h_c \quad (12b)$$

where P is the column axial load (positive if compression). Therefore, the horizontal projection of the inclined Strut ST2 can be obtained as follows

$$l_h = h_c - a_c \quad (13)$$

In this study, the horizontal projection l_h is investigated in the subsequent section by varying it from $0.6h_c$ corresponding to Eq. (12a) to $0.75h_c$ corresponding to Eq. (12b), with the conservative assumption of $P = 0$.

The column shear force is included in the equilibrium of the inclined Strut ST2 (Eq. (11)) instead of the equilibrium of the diagonal Strut ST1 (Eq. (10)) because most of the column shear force is resisted by the middle portion of the column cross section due to flexural cracks forming at both sides of the rectangular column cross section under reversed cyclic loading. In addition, the vertical component of Strut ST2 is equilibrated by an inclined strut in the column, as shown in Fig. 2, where the horizontal components of Strut ST2 and the inclined strut in the column are assumed to be presented by $V_{jh,ST2}$ in Eq. (11).

Fraction factor

The shear forces of Struts ST1 and ST2 can be expressed using a fraction factor α as follows

$$V_{jh,ST1} = \alpha V_{jh} \quad (14)$$

$$V_{jh,ST2} = (1 - \alpha)V_{jh} \quad (15)$$

This fraction factor is expressed as a function of the tensile stress of the beam reinforcement because it is related to the bond deterioration of this reinforcement. Obviously, the fraction factor increases as the bond strength deteriorates because the Strut ST1 contribution is dominant after bond failure occurs.¹³ In the proposed model, the bi-uniform bond strength model proposed by Lehman and Moehle¹⁴ is extended to tri-uniform and is adopted to represent the trilinear behavior of the reinforcing steel. The bond strength in elastic beam tensile reinforcement, μ_E , is $12\sqrt{f'_c}$ psi^{0.5} ($1.0\sqrt{f'_c}$ MPa^{0.5}) and that in inelastic beam tensile reinforcement, μ_Y , is $0.5\mu_E$. The residual bond strength μ_R is selected from the CEB-FIP Model Code¹⁵ as $0.15\mu_E$. In this study, the effects of cover depth and bar spacing on bond strength are not explicitly accounted for within the joint region. However, these effects are implicitly considered by expressing the bond stress distribution along the beam bar, $\mu(f_s)$ in Fig. 2, as a function of the tensile stress of the bar f_s .

The fraction factor α is derived from the trilinear stress-strain model of the reinforcing steel, as shown in Fig. 4. It is assumed that the beam longitudinal bars follow the standard hooked-bar details and, thus, Strut ST1 can carry the joint shear force (illustrated as a spring in Fig. 4) without anchorage bearing failure. From Eq. (8), (10), and (14), α is derived as follows

$$A_s f_s - n\pi\phi_b \int_0^{l_h} \mu(f_s) dx = \alpha A_s f_s \left(1 - 0.85 \frac{h_b}{H} \right) \Rightarrow \quad (16)$$

$$\alpha = \frac{H}{H - 0.85h_b} \left(1 - \frac{4}{\phi_b} \frac{\int_0^{l_h} \mu(f_s) dx}{f_s} \right)$$

where $A_s = n\pi\phi_b^2/4$ is used in Eq. (16). The assumed breaking points of the beam longitudinal bar stress (f_o , f_p , and f_r) and intermediate values of the fraction factor (α_1 and α_2) are derived in the following subsections.

Derivation of f_o —The contribution of Strut ST1 is negligible as long as the bond strength of Strut ST2 is able to resist all the horizontal shear force. The tensile stress of beam reinforcement at this point, f_o in Fig. 4, is given by

$$f_o = \frac{4}{\phi_b} \mu_E l_h \quad (17)$$

Derivation of α_1 —The fraction factor α_1 corresponds to the onset of yielding of beam reinforcement at the column face. Therefore

$$\alpha_1 = \frac{H}{H - 0.85h_b} \left(1 - \frac{4}{\phi_b} \frac{\mu_E}{f_y} l_h \right) \quad (18)$$

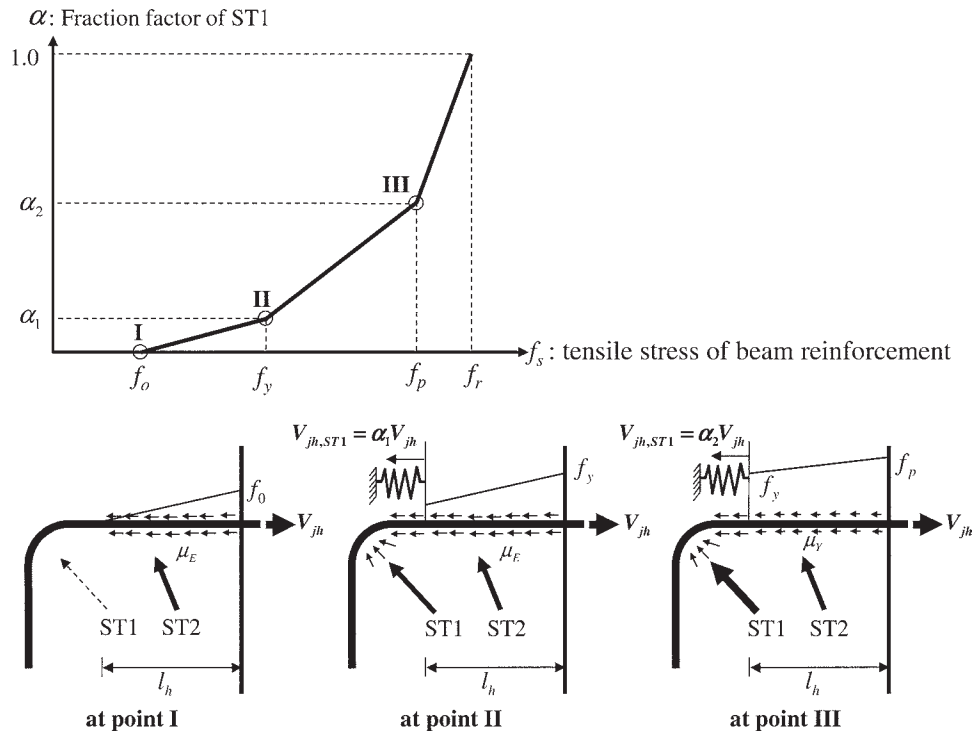


Fig. 4—Trilinear relationship of fraction factor.

Derivation of f_p and f_r —The tensile stress f_p is defined when the beam reinforcement yielding propagates over the width of Strut ST2. Therefore, the bond strength of concrete surrounding the beam longitudinal bars is equal to μ_y over the entire length l_h . Accordingly, referring to Fig. 4, one obtains the following

$$f_p = f_y + \frac{4}{\phi_b} \mu_y l_h \quad (19)$$

The tensile stress f_r corresponding to $\alpha = 1.0$ is expressed implicitly using Eq. (16) because the bond distribution cannot be explicitly defined at $\alpha = 1.0$. The tensile stress f_p can be equated to f_r if α_2 corresponding to f_p is equal to 1.0 (Fig. 4). Therefore, the tensile stress value of the beam reinforcement, f_r , corresponding to $\alpha = 1.0$, is expressed as follows

$$f_r = \frac{4}{\phi_b} \frac{H}{0.85h_b} \int_0^{l_h} \mu(f_r) dx \geq f_p \quad (20)$$

Derivation of α_2 —The fraction factor α_2 is defined when the tensile stress of the beam longitudinal reinforcement at the column face reaches f_p . Therefore

$$\alpha_2 = \frac{H}{H - 0.85h_b} \left(1 - \frac{4}{\phi_b} \frac{\mu_y}{f_y + \frac{4}{\phi_b} \mu_y l_h} l_h \right) \leq 1.0 \quad (21)$$

Definition of joint shear failure

The beam-column joint shear strength V_n is defined as the horizontal joint shear force when the horizontal shear force resisted by Strut ST1 reaches its shear capacity. It is

not necessary to estimate the strength of Strut ST2 in the proposed model. Based on the assumed SAT model, the horizontal shear capacity of Strut ST1 ($V_{jh,ST1,max}$) is obtained as follows

$$V_{jh,ST1,max} = c_0 D \cos \theta, \quad D = \sigma b_j h_s, \quad (22)$$

and $\theta = \tan^{-1}(h_b/h_c)$

where c_0 is a constant to be determined from the experimental data; and $b_j = (b_b + b_c)/2$. Note that b_b and b_c are the respective widths of the beam and column cross sections. The strut width h_s can be related to h_c from the geometry of the C-C-T node (Fig. 2) as follows

$$h_s \sin \tilde{\theta} = a_c = s h_c \quad (23)$$

where $\tilde{\theta}$ is the angle of the C-C-T node; and s is a constant. For reference, Hwang and Lee² assumed $\sin \tilde{\theta} = 1$ for developing a joint shear strength model. Substituting Eq. (1), (2), and (23) into Eq. (22), one obtains

$$V_{jh,ST1,max} = \bar{c} \frac{b_j h_c \sqrt{f'_c} \cos \theta}{1.31 + 0.085 \left(\frac{h_b}{h_c} \right)}, \quad \theta = \tan^{-1} \left(\frac{h_b}{h_c} \right) \quad (24)$$

where \bar{c} is a constant encompassing the effects of c_0 , a_1 , s , and $\sin \tilde{\theta}$. The shear capacity of Strut ST1 can be estimated as the minimum joint shear strength at which ST1 takes all the horizontal joint shear force—that is, the fraction factor is equal to 1.0 in Eq. (14). From Hakuto et al.,⁶ the horizontal joint shear force $\gamma b_j h_c \sqrt{f'_c}$ (where $\gamma = 4 \text{ psi}^{0.5}$ [0.33 MPa^{0.5}]) is taken as the minimum joint shear strength to trigger the

joint shear failure for the studied joint aspect ratio $h_b/h_c = 500/460 \approx 1.1$ —that is, $\theta = \pi/3.8$ rad. Applying this suggestion to define the constant \bar{c} , one obtains

$$\bar{c} \frac{\cos(\pi/3.8)}{1.31 + 0.085 \times 1.1} = \gamma \Rightarrow \bar{c} = 2.07\gamma \quad (25)$$

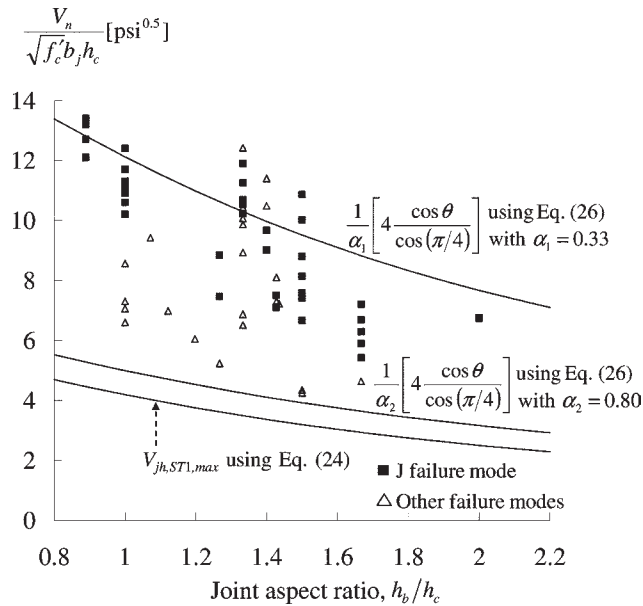


Fig. 5—Upper and lower limits of joint shear strength from experimental database. (Note: $1.0 \text{ psi}^{0.5} = 0.083 \text{ MPa}^{0.5}$.)

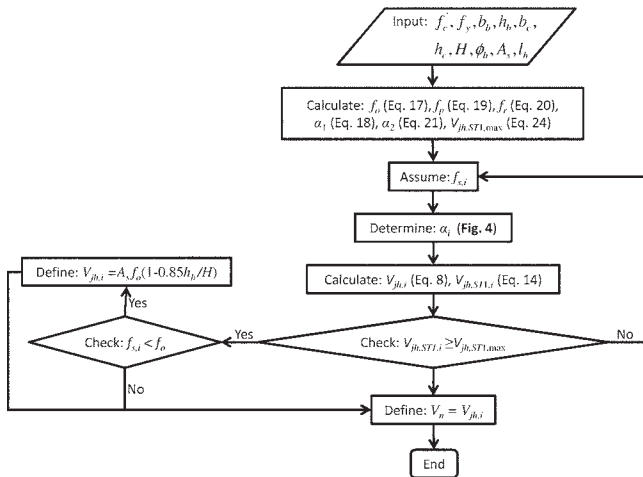


Fig. 6—Solution algorithm of proposed analytical model.

Using Eq. (24) with the value of \bar{c} from Eq. (25), the shear capacity of Strut ST1 becomes $4.2b_j h_c \sqrt{f'_c} \text{ psi}^{0.5}$ ($0.35 \sqrt{f'_c} \text{ MPa}^{0.5}$) for a joint aspect ratio $h_b/h_c = 1.0$. The estimated shear capacity of Strut ST1 is compared with the lower limit of joint shear strength observed in the collected experimental database as detailed by Park and Mosalam,¹⁰ as shown in Fig. 5. The selected shear capacity of Strut ST1 is slightly less than the observed lower limit of joint shear strength, indicating that Strut ST2 must have had little contribution to the joint shear resistance. Accordingly, the joint shear strength is calculated by an iterative procedure using the algorithm illustrated in Fig. 6.

VERIFICATION OF PROPOSED MODEL

The test results of unreinforced exterior joint specimens from the database, as detailed by Park and Mosalam,¹⁰ are compared to the predictions by the proposed model in Table 1. The proposed model predicts the joint shear strengths of the database with a mean value of 0.99 for the ratio between the test results and model predictions and a corresponding coefficient of variation (COV) of 14%, as shown in Table 1. The predictions are made with $l_h = 0.65h_c$, which is obtained from Table 2, indicating that the analytical predictions are acceptable for the listed values of l_h and better correlated with the experimental results for $l_h = 0.65h_c$. In Fig. 7, the evaluation results using the proposed model are compared with those from two existing analytical strength models proposed by Hwang and Lee² and Tsonos,³ where better accuracy of the proposed model is clearly demonstrated. It should be noted that these two existing models were developed for reinforced exterior joints based on a mechanistic approach and modified to predict the shear strength of unreinforced exterior joints. Moreover, the proposed model accurately predicts the beam reinforcement yielding and consequent lower shear strength for the BJ failure type (joint shear failure with beam yielding) of the specimens in the database,¹⁰ as shown in Table 1, where the yielding is indicated as Y (beam reinforcement yielding).

SIMPLIFIED STRENGTH MODEL

From the evaluation of the literature data set in Table 1, it is found that the contribution of Strut ST1—that is, fraction factor α —is bounded between 0.31 and 0.77 for the J (joint

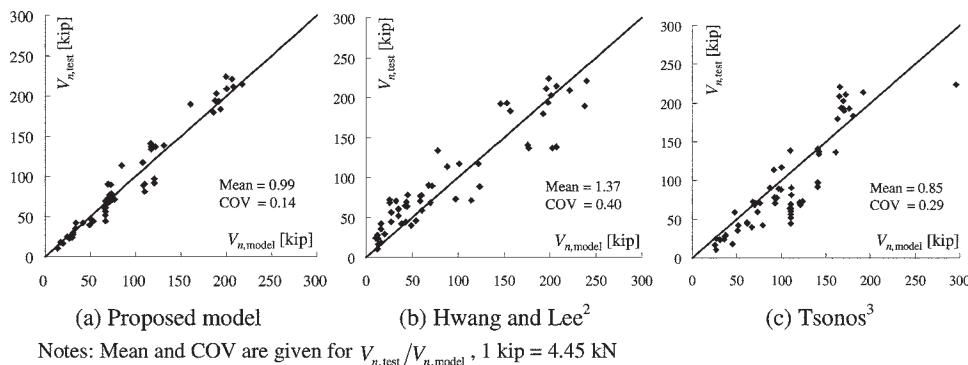


Fig. 7—Comparison of evaluation results with two existing analytical models.

Table 1—Verification of proposed analytical model

Reference	Specimen	f'_c , ksi	$f_{y,beams}$, ksi	$V_{n,test}$, kips	$f_{s,model}$, ksi	$V_{n,model}$, kips (α , %)	Failure type ^a	$V_{n,test}/V_{n,model}$
16, 17	V	3.30	51.0	138.4	37.6	130.8 (31.1)	J	1.06
	7	5.70	51.0	189.7	46.1	160.2 (33.4)	BJ	1.18
18	OT0	9.76	63.1	224.1	73.5(Y [†])	199.4 (48.2)	BJ	1.12
19	SP1	4.46	50.3	140.9	45.2	116.5 (40.6)	BJ	1.21
	SP2	4.51	50.6	136.9	45.5	117.2 (40.6)	BJ	1.17
	SP5	4.63	50.4	136.7	47.3	121.7 (44.0)	BJ	1.12
4	BS-L	4.48	75.4	70.9	56.7	71.1 (39.2)	J	1.00
	BS-U	4.50	75.4	76.7	56.8	71.2 (39.3)	J	1.08
	BS-L-LS	4.58	75.4	77.5	57.2	71.7 (39.4)	J	1.08
	BS-L-300	4.94	75.4	113.5	64.0	84.7 (45.5)	BJ	1.34
	BS-L-600	5.28	75.4	63.8	55.9	66.3 (35.8)	J	0.96
	BS-L-V2T20	4.73	75.4	89.7	57.8	72.5 (39.6)	J	1.24
	BS-L-V4T10	4.10	75.4	90.6	55.0	69.0 (38.7)	J	1.31
	JA-NN03	6.50	75.4	68.4	80.9 (Y)	68.9 (53.3)	BJ	0.99
	JA-NN15	6.67	75.4	73.1	81.6 (Y)	69.5 (53.6)	BJ	1.05
	JB-NN03	6.87	75.4	71.3	86.5 (Y)	76.3 (59.5)	BJ	0.93
20	02	6.70	65.9	213.9	61.8	217.3 (36.4)	J	0.98
	06	5.94	65.9	211.4	59.1	207.8 (35.9)	J	1.02
	04	5.37	65.9	208.9	57.0	200.2 (35.4)	J	1.04
	05	5.82	65.9	220.9	58.7	206.3 (35.8)	J	1.07
21	01	4.79	66.5	193.2	53.7	191.7 (38.9)	J	1.01
	02	4.38	66.5	179.6	52.1	185.7 (38.4)	J	0.97
	03	4.93	66.5	183.4	54.3	193.6 (39.1)	J	0.95
	04	4.58	66.5	202.7	52.9	188.7 (38.6)	J	1.07
	05	4.60	66.5	192.6	52.9	188.9 (38.7)	J	1.02
	06	4.50	66.5	193.9	52.5	187.4 (38.5)	J	1.03
22	BCJ1	4.93	104.4	68.8	69.0	71.0 (32.2)	J	0.97
	BCJ3	4.79	104.4	72.4	68.2	70.2 (32.0)	J	1.03
	BCJ5	5.51	104.4	70.6	71.8	73.9 (32.7)	J	0.96
	BCJ6	5.08	104.4	70.8	69.7	71.7 (32.3)	J	0.99
23	C4ALN0	6.15	75.7	24.8	44.8	24.8 (32.2)	P	1.00
	C4ALH0	15.08	75.7	42.3	61.0	33.9 (37.0)	P	1.25
	C6LN0	7.40	75.7	23.4	47.6	26.4 (33.2)	J	0.89
	C6LH0	14.65	75.7	35.4	60.4	33.5 (36.9)	J	1.06

^aJ is joint shear failure without beam yielding; BJ is joint shear failure with beam yielding; CF is column failure; BF is beam failure; P is pullout failure; and A is anchorage failure.
[†]Y is beam reinforcement yielding.

Notes: 1 ksi = 6.90 MPa; 1 kip = 4.45 kN.

shear failure without beam yielding) and BJ types of failure, respectively. This observation and the joint aspect ratio effect are used to simplify the analytical model for practical engineering applications. As shown in Fig. 8, the ratio of joint shear strength between two different joint aspect ratios is close to the ratio of the cosine values for the two inclination angles of Strut ST1 with the horizontal. For the joint aspect ratio $h_b/h_c = 1.0$ (that is, $\theta = \pi/4$ rad), the shear stress capacity of ST1, $\gamma_{ST1}\sqrt{f'_c}$, is assumed to be $4\sqrt{f'_c}$ psi^{0.5} ($0.33\sqrt{f'_c}$ MPa^{0.5}), which is typically adopted as the concrete

tensile strength. Using Eq. (14), the joint shear strength is defined as follows

$$V_n = \frac{1}{\alpha} V_{jh,ST1,max} = \frac{1}{\alpha} \gamma_{ST1} \sqrt{f'_c} b_j h_c \frac{\cos \theta}{\cos(\pi/4)} \quad (26)$$

Using Eq. (26), the upper and lower limits of the joint shear strength are plotted in Fig. 5 for the fraction factors $\alpha_1 = 0.33$ and $\alpha_2 = 0.80$, respectively, which are close to

Table 1 (cont.)—Verification of proposed analytical model

Reference	Specimen	f'_c , ksi	$f_{y,beam}$, ksi	$V_{n,test}$, kips	$f_{s,model}$, ksi	$V_{n,model}$, kips (α , %)	Failure type*	$V_{n,test}/V_{n,model}$
24	4a	5.66	82.7	44.6	55.8	66.7 (42.4)	CF	0.67
	4b	5.66	82.7	52.2	55.1	66.7 (42.4)	J	0.78
	4c	5.66	82.7	64.3	55.1	66.7 (42.4)	J	0.96
	4d	5.66	82.7	56.8	55.1	66.7 (42.4)	J	0.85
	4e	5.66	82.7	60.5	55.1	66.7 (42.4)	J	0.91
	4f	5.66	82.7	69.2	55.1	66.7 (42.4)	J	1.04
25	U40L	3.52	56.1	59.8	47.9	66.1 (42.4)	J	0.91
	U20L	3.87	56.1	42.4	60.6 (Y)	41.8 (70.3)	A	1.02
	B101	4.63	56.8	78.3	53.1	73.3 (43.9)	J	1.07
26	T-1	4.47	61.6	117.0	63.2 (Y)	107.8 (40.4)	BJ	1.08
	T-2	4.47	61.6	117.0	63.2 (Y)	107.8 (40.4)	BJ	1.08
27	EX-2	7.61	75.4	39.6	67.3	49.2 (45.4)	BJ	0.80
28	SP1-NS	3.74	45.7	81.4	48.3 (Y)	109.5 (33.9)	CF	0.74
	SP1-EW	3.74	45.7	90.4	48.3 (Y)	109.5 (33.9)	CF	0.83
	SP2-NS	5.02	45.7	91.7	53.0 (Y)	120.3 (35.7)	J	0.76
	SP2-EW	5.02	45.7	96.9	53.0 (Y)	120.3 (35.7)	J	0.81
29	Model 5	3.84	55.8	16.2	54.9	19.9 (45.7)	BJ	0.81
30	RC-1	2.81	46.9	29.3	55.0 (Y)	30.8 (43.7)	BJ	0.95
31	A0	4.58	84.1	18.2	95.7 (Y)	17.5 (77.0)	BJ	1.04
	B0	4.58	84.1	44.4	97.4 (Y)	53.4 (49.6)	BJ	0.83
	C0	4.58	84.1	45.9	88.0 (Y)	51.2 (51.7)	BJ	0.90
32	RCNH1	4.35	76.1	10.9	78.7 (Y)	14.2 (57.6)	BF	0.77
33	T0	4.44	61.6	88.4	63.0 (Y)	108.1 (40.2)	BJ	0.82
34	C-1	2.83	84.8	24.4	49.2	28.3 (37.3)	J	0.86
	C-2	3.44	84.8	24.2	52.4	30.2 (38.6)	J	0.80
	T-C	3.57	84.8	28.1	53.1	30.6 (38.8)	J	0.92
35	ED1	4.51	50.6	134.1	45.5	117.2 (40.6)	BJ	1.14
							Mean	0.99
							COV	0.14

*J is joint shear failure without beam yielding; BJ is joint shear failure with beam yielding; CF is column failure; BF is beam failure; P is pullout failure; and A is anchorage failure.
[†]Y is beam reinforcement yielding.

Notes: 1 ksi = 6.90 MPa; 1 kip = 4.45 kN.

Table 2—Statistics of evaluation results for investigated values of l_h

l_h		$0.6h_c$	$0.65h_c$	$0.7h_c$	$0.75h_c$
$V_{n,test}/$	Mean	1.020	0.989	0.959	0.931
$V_{n,model}$	Coefficient of variation	0.144	0.143	0.143	0.142

the minimum and maximum fraction factors (0.31 and 0.77, respectively) observed in the evaluation of the database using the analytical model. Then, the fraction factor is replaced by a new strength factor k as follows

$$k = \frac{1}{\alpha} \frac{\gamma_{ST1}}{\gamma_{ext}} \quad (27)$$

where γ_{ext} is equal to 12.0 psi^{0.5} (1.0 MPa^{0.5}), which corresponds to the upper limit of the normalized joint shear strength for the joint aspect ratio $h_b/h_c = 1.0$ in Fig. 5. The strength factor k is bounded between 0.4 and 1.0 by the maximum and minimum fraction factors, respectively. As the fraction factor varies with the tensile stress of the beam reinforcement, variation of this strength factor is determined by the following joint shear index, which is derived from Eq. (8), assuming that beam reinforcement yields

$$SI_j = \frac{A_s f_y}{b_j h_c \sqrt{f'_c}} \left(1 - 0.85 \frac{h_b}{H} \right) \quad (28)$$

The joint shear index represents the joint shear demand at the onset of yielding of the beam longitudinal tension bars. In other words, joint shear failure occurs at a lower tensile

stress of beam longitudinal bars if the joint shear index is larger. Accordingly, the joint shear index is inversely proportional to the tensile stress of the beam longitudinal bars at the onset of joint shear failure. The simplified joint shear strength model is proposed as follows

$$V_n = k \left[\gamma_{ext} \sqrt{f'_c} b_j h_c \frac{\cos \theta}{\cos(\pi/4)} \right] \quad (29a)$$

$$k = 0.4 + 0.6 \left[\frac{SI_j - X_1}{X_2 - X_1} \right] \leq 1.0, \quad (29b)$$

$$X_1 = \gamma_{ST1} \frac{\cos \theta}{\cos(\pi/4)} \text{ and } X_2 = \gamma_{ext} \frac{\cos \theta}{\cos(\pi/4)}$$

The strength factor in the simplified model (Fig. 9) is comparable to a strength degradation factor in the model proposed by Park.⁷ The benefit of the simplified model is that an iterative solver is not needed and that the joint shear index parameter can be easily determined.

ENVELOPE OF JOINT SHEAR STRESS-STRAIN RELATIONSHIP

The proposed analytical model predicts the joint shear strength based on the tensile stress of the beam longitudinal reinforcement under the assumption that the principal tensile strain is predefined by the joint aspect ratio. Therefore, the proposed model can provide the envelope of the joint shear stress-strain relationship, which can be transformed into the moment-rotation relationship of an equivalent rotational spring element of the joint region. From strain compatibility and Eq. (8), the joint shear strain and horizontal shear stress are as follows

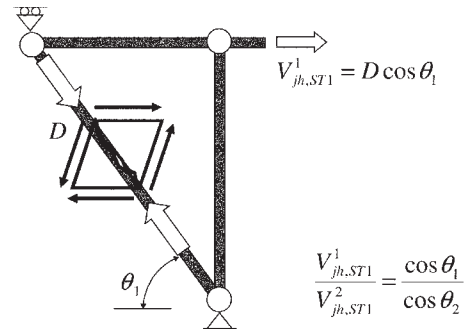
$$\gamma_{xy} = \sqrt{4 \left(\epsilon_1 - \frac{\epsilon_a}{2} \right)^2 - \epsilon_a^2} \quad (30)$$

$$v_{jh} \approx \frac{A_s f_s}{b_j h_c} \left(1 - 0.85 \frac{h_b}{H} \right) \quad (31)$$

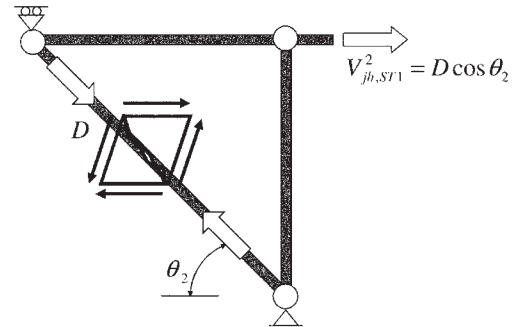
where ϵ_a is the compressive (negative) strain from the column in the vertical direction. In most tests, the compressive strain ϵ_a is negligible because the applied column axial load ratio is low—for example, $P/A_g f'_c = P/h_c b_c f'_c \leq 0.2$.¹⁰ Therefore, the shear strain γ_{xy} at the joint failure becomes twice the principal tensile strain ϵ_1 , which is obtained from Eq. (1).

In the J failure type, the joint shear stress-strain relationship is assumed to be linear before joint shear failure, whereas in the BJ failure type, the joint shear stress-strain relationship is assumed to be bilinear, as shown in Fig. 10. Knowing the RC frame and joint dimensions, the moment-rotation relationship of the rotational spring is obtained from the shear stress and strain of the joint as follows

$$M_j = v_{jh} b_j h_c / \lambda, \lambda = \frac{2L}{(2L + h_c) j d_b} - \frac{1}{H} \quad (32)$$



(a) High joint aspect ratio



(b) Low joint aspect ratio

Fig. 8—Consideration of joint aspect ratio effect in simplified model.

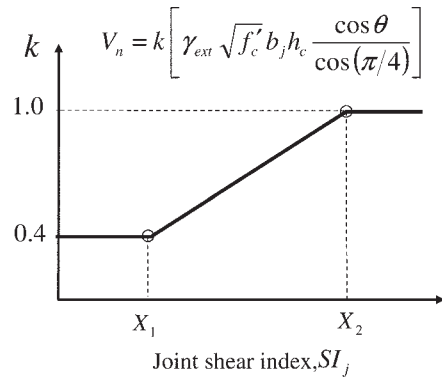


Fig. 9—Consideration of beam reinforcement ratio effect in simplified model.

$$\theta_j = \gamma_{xy} + \Delta_{slip} / (d_b - c) \quad (33)$$

where M_j is the moment of the joint panel at the center of the panel; θ_j is the joint rotation; Δ_{slip} is the relative movement of the beam reinforcement with respect to the perimeter of the joint panel; and c is the depth of the neutral axis measured from the extreme compression fiber, as illustrated in Fig. 11. The denominator λ in Eq. (32) makes use of Eq. (4) and (5), representing the global equilibrium in Fig. 3. The total rotation of the joint spring is the sum of the joint shear strain and the slip rotation (Fig. 10), where the slip is defined as follows

$$\Delta_{slip} = \int_0^{l_s} \epsilon_s(x) dx + \Delta_h \quad (34)$$

where l_s is the straight lead length of the beam longitudinal bar; ϵ_s is the beam longitudinal bar strain within the joint

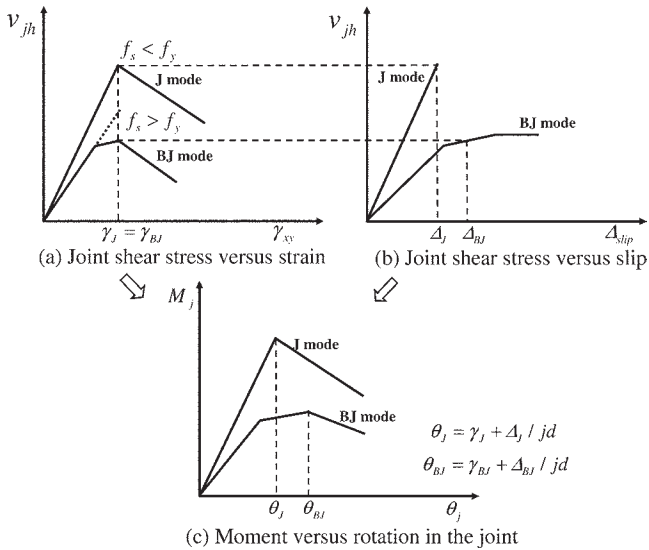


Fig. 10—Relationship of joint moment rotation and its decomposition.

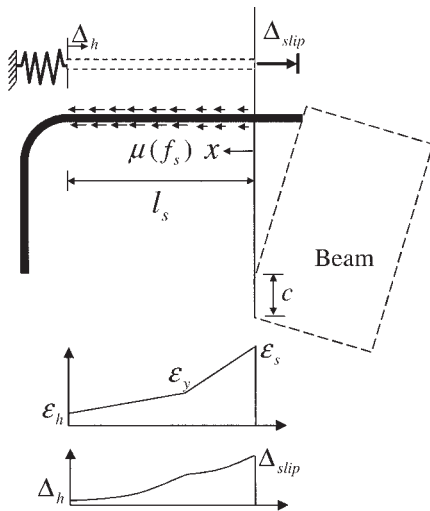
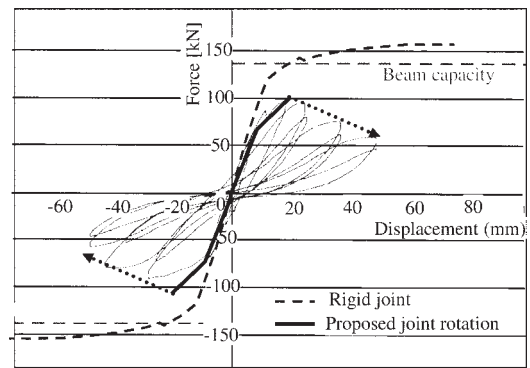


Fig. 11—Slip of hooked bar of beam.

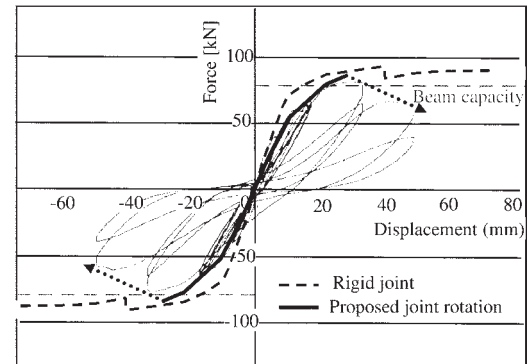
region; and Δ_h is the slip at the end of the straight lead (refer to Fig. 11), which is estimated using existing slip models from the literature.³⁶⁻³⁸

Simulations are performed on the two tests by Wong⁴ using OpenSees.³⁹ The specimens are modeled with two different idealizations: 1) considering the one-dimensional beam and column elements intersecting at the joint (rigid joint); and 2) similar to the first but the joint region is modeled with a rotational spring and joint offsets. A zero-length rotational spring is used to implement the proposed joint moment-rotation relationship, and the joint offset option is used to rigidly connect the center of the joint with the column and beam faces.

The test results of the two specimens representing the J and BJ failure types are compared with the analytical simulations in Fig. 12(a) and (b), respectively. The shear strengths and corresponding deformation of the two specimens are accurately predicted by the proposed model. The initial stiffness of the joint shear stress-strain relationship is taken as twice the secant stiffness to the yield point because high stiffness is expected up to the initiation of the diagonal joint cracking.⁴⁰ The post-failure behavior of the joint, which is not



(a) J failure (BS-L)



(b) BJ failure (JA-NN03)

Fig. 12—Simulation of two specimens from Wong⁴ using proposed analytical model. (Note: 1 mm = 0.0394 in.; 1 kN = 0.2248 kips.)

part of this study, is qualitatively represented by the dotted lines in Fig. 12. The initial stiffness and post-failure behavior will be investigated in a future extension of this study.

CONCLUSIONS

An analytical shear strength model for unreinforced exterior beam-column joints is developed based on two inclined strut mechanisms in the joint region. The two inclined struts are assumed to resist the horizontal joint shear force in parallel, and the fraction of each strut contribution is formulated using the bond resistance of the concrete surrounding the beam's longitudinal tensile reinforcement within the joint region. The proposed model is validated by comparisons with the results of a large database of unreinforced exterior beam-column joint tests from published literature. For practical engineering applications, a simplified model is also developed from the proposed analytical model. Finally, the relationship of moment-rotation in the joint region is derived from the proposed analytical model and successfully simulates the responses of two published tests. For an accurate simulation of older-type ductile RC building frames containing unreinforced joints, the developed joint moment-rotation relationship is recommended for use in the seismic evaluation of these frames.

ACKNOWLEDGMENTS

This study is supported primarily by the National Science Foundation (NSF) Award No. 0618804 (J. P. Moehle, PI) through the Pacific Earthquake Engineering Research Center (PEER). Any opinions, findings, and conclusions or recommendations expressed in this paper are those of the authors and do not necessarily reflect those of NSF or PEER.

NOTATION

a_c	= horizontal projection of width of diagonal Strut ST1
b_b	= width of beam cross section
b_c	= width of column cross section
d_b	= effective depth of beam cross section
H	= height between upper and lower column inflection points
h_b	= total height of beam cross section
h_c	= total height of column cross section
L	= length from beam inflection point to column face
l_h	= horizontal projection of width of diagonal Strut ST2
M_j	= moment in joint panel
α	= fraction factor of diagonal Strut ST1
Δ_{slip}	= relative movement of beam reinforcement with respect to perimeter of joint
ϵ_1	= principal tensile strain of joint panel (tension positive)
ϕ_b	= beam longitudinal bar diameter
γ_{xy}	= shear strain of joint panel
θ	= angle of joint diagonal, $\theta = \tan^{-1}(h_b/h_c)$
θ_j	= joint rotation

REFERENCES

- Priestley, M. J. N., "Displacement-Based Seismic Assessment of Reinforced Concrete Buildings," *Journal of Earthquake Engineering*, V. 1, No. 1, Jan. 1997, pp. 157-192.
- Hwang, S. J., and Lee, H. J., "Analytical Model for Predicting Shear Strength of Exterior Reinforced Concrete Beam-Column Joints for Seismic Resistance," *ACI Structural Journal*, V. 96, No. 5, Sept.-Oct. 1999, pp. 846-858.
- Tsonos, A. G., "Cyclic Load Behavior of Reinforced Concrete Beam-Column Subassemblages of Modern Structures," *ACI Structural Journal*, V. 104, No. 4, July-Aug. 2007, pp. 468-478.
- Wong, H. F., "Shear Strength and Seismic Performance of Non-Seismically Designed Reinforced Concrete Beam-Column Joints," PhD dissertation, Hong Kong University of Science and Technology, Kowloon, Hong Kong, China, 2005, 341 pp.
- Hwang, S. J., and Lee, H. J., "Strength Prediction for Discontinuity Regions by Softened Strut-and-Tie Model," *Journal of Structural Engineering*, ASCE, V. 128, No. 12, Dec. 2002, pp. 1519-1526.
- Hakuto, S.; Park, R.; and Tanaka, H., "Seismic Load Tests on Interior and Exterior Beam-Column Joints with Substandard Reinforcing Details," *ACI Structural Journal*, V. 97, No. 1, Jan.-Feb. 2000, pp. 11-25.
- Park, R., "A Static Force-Based Procedure for the Seismic Assessment of Existing Reinforced Concrete Moment Resisting Frames," *Bulletin of the New Zealand National Society for Earthquake Engineering*, V. 30, No. 3, 1997, pp. 213-226.
- Hwang, S. J.; Wang, K. C.; and Lee, H. J., "Designing and Retrofitting Strategy of Reinforced Concrete Beam-Column Joints," *Proceedings of SINO-UK Joint Workshop on Deep Excavations and Earthquake Resistance Design of Structures*, H. D. Lin, ed., Taipei, Taiwan, 2001.
- Zhang, L., and Jirsa, J. O., "A Study of Shear Behavior of Reinforced Concrete Beam-Column Joints," *PMFSEL Report No. 82-1*, the University of Texas at Austin, Austin, TX, 1982, 118 pp.
- Park, S., and Mosalam, K. M., "Shear Strength Models of Exterior Beam-Column Joints without Transverse Reinforcement," *PEER Report 2009/106*, University of California, Berkeley, Berkeley, CA, 2009, 87 pp.
- Vollum, R. L., "Design and Analysis of Exterior Beam Column Connections," PhD dissertation, Imperial College of Science Technology and Medicine, University of London, London, UK, 1998, 603 pp.
- Zhang, L. X., and Hsu, T. C., "Behavior and Analysis of 100 MPa Concrete Membrane Elements," *Journal of Structural Engineering*, ASCE, V. 124, No. 1, Jan. 1998, pp. 24-34.
- Booth, E., and Fenwick, R., *Concrete Structures in Earthquake Regions: Design and Analysis*, Longman Scientific and Technical, Harlow, UK, 1994, 368 pp.
- Lehman, D. E., and Moehle, J. P., "Seismic Performance of Well-Confined Concrete Bridge Columns," *PEER Report 1998/01*, University of California, Berkeley, Berkeley, CA, Dec. 2000, 295 pp.
- Comité Euro-International du Béton, "CEB-FIP Model Code 1990," *Bulletin d'Information No. 213/214*, Thomas Telford, London, UK, 1993, 437 pp.
- Hanson, N. W., and Conner, H. W., "Seismic Resistance of Reinforced Concrete Beam-Column Joints," *Journal of the Structural Division*, ASCE, V. 93, No. ST5, Oct. 1967, pp. 533-560.
- Hanson, N. W., and Conner, H. W., "Tests of Reinforced Concrete Beam-Column Joints under Simulated Seismic Loading," *PCA Research and Development Bulletin*, Portland Cement Association, Skokie, IL, 1972, 11 pp.
- Hwang, S. J.; Lee, H. J.; Liao, T. F.; Wang, K. C.; and Tsai, H. H., "Role of Hoops on Shear Strength of Reinforced Concrete Beam-Column Joints," *ACI Structural Journal*, V. 102, No. 3, May-June 2005, pp. 445-453.
- Uzumeri, S. M., "Strength and Ductility of Cast-in-Place Beam-Column Joints," *Reinforced Concrete Structures in Seismic Zones*, SP-53, N. Hawkins and D. Mitchell, eds., American Concrete Institute, Farmington Hills, MI, 1977, pp. 293-350.
- Clyde, C.; Pantelides, C. P.; and Reaveley, L. D., "Performance-Based Evaluation of Exterior Reinforced Concrete Building Joints for Seismic Excitation," *PEER Report 2000/05*, July 2000, 50 pp.
- Pantelides, C. P.; Hansen, J.; Nadauld, J.; and Reaveley, L. D., "Assessment of Reinforced Concrete Building Exterior Joints with Substandard Details," *PEER Report 2002/18*, May 2002, 103 pp.
- Ortiz, I. R., "Strut-and-Tie Modeling of Reinforced Concrete Short Beams and Beam-Column Joints," PhD dissertation, University of Westminster, London, UK, 1993, 208 pp.
- Scott, R. H., and Hamil, S. J., "Connection Zone Strain in the Reinforced Concrete Beam-Column Connections," *Proceedings of the 11th International Conference on Experimental Mechanics*, Oxford, UK, 1998, pp. 65-69.
- Parker, D. E., and Bullman, P. J. M., "Shear Strength within Reinforced Concrete Beam-Column Joints," *The Structural Engineer*, V. 75, No. 4, Feb. 1997, pp. 53-57.
- Kanada, K.; Kondo, G.; Fujii, S.; and Morita, S., "Relation between Beam Bar Anchorage and Shear Resistance at Exterior Beam-Column Joints," *Transaction of the Japan Concrete Institute*, V. 6, 1984, pp. 433-440.
- Ghobarah, A., and Said, A., "Seismic Rehabilitation of Beam-Column Joints Using FRP Laminates," *Journal of Earthquake Engineering*, V. 5, No. 1, Jan. 2001, pp. 113-129.
- Sarsam, K. F., and Phipps, M. E., "The Shear Design of In-Situ Reinforced Concrete Beam-Column Joints Subjected to Monotonic Loading," *Magazine of Concrete Research*, V. 37, No. 130, Mar. 1985, pp. 16-28.
- Engindeniz, M., "Repair and Strengthening of Pre-1970 Reinforced Concrete Corner Beam-Column Joints Using CFRP Composites," PhD dissertation, Georgia Institute of Technology, Atlanta, GA, 2008, 358 pp.
- Woo, S. W., "Seismic Performance of RC Frames in a Low to Moderate Seismicity Region," PhD dissertation, Korea University, Seoul, South Korea, 2003, 256 pp.
- Liu, C., "Seismic Behavior of Beam-Column Joint Assemblies Reinforced with Steel Fibers," master's of engineering thesis, University of Canterbury, Christchurch, New Zealand, 2006, 195 pp.
- Karayannis, C. G.; Chaliouris, C. E.; and Sirkelis, G. M., "Local Retrofit of Exterior RC Beam-Column Joints Using Thin RC Jackets—An Experimental Study," *Earthquake Engineering and Structural Dynamics*, V. 37, 2008, pp. 727-746.
- Gencoglu, M., and Eren, I., "An Experimental Study on the Effect of Steel Fiber Reinforced Concrete on the Behavior of the Exterior Beam-Column Joints Subjected to Reversal Cyclic Loading," *Turkish Journal of Engineering & Environmental Science*, V. 26, 2002, pp. 493-502.
- El-Amoury, T., and Ghobarah, A., "Seismic Rehabilitation of Beam-Column Joints Using GFRP Sheets," *Engineering Structures*, V. 24, No. 11, Nov. 2002, pp. 1397-1407.
- Antonopoulos, C. P., and Triantafyllou, T. C., "Experimental Investigation of FRP-Strengthened RC Beam-Column Joints," *Journal of Composites for Construction*, ASCE, V. 7, No. 1, Feb. 2003, pp. 39-49.
- Sagbas, G., "Nonlinear Finite Element Analysis of Beam-Column Subassemblies," master's of applied science thesis, University of Toronto, Toronto, ON, Canada, 2007, 182 pp.
- Alsawat, J. M., and Saatçioğlu, M., "Reinforcement Anchorage Slip under Monotonic Loading," *Journal of Structural Engineering*, ASCE, V. 118, No. 9, Sept. 1992, pp. 2421-2438.
- Monti, G.; Spacone, E.; and Filippou, F. C., "Model for Anchored Reinforcing Bars under Seismic Excitations," *Report UCB/EERC-93/08*, University of California, Berkeley, Berkeley, CA, 1993, 91 pp.
- Soroushian, P.; Obaseki, K.; Nagi, M.; and Rojas, M. C., "Pullout Behavior of Hooked Bars in Exterior Beam-Column Connections," *ACI Structural Journal*, V. 85, No. 3, May-June 1988, pp. 269-276.
- OpenSees, "Open System for Earthquake Simulation," PEER, University of California, Berkeley, Berkeley, CA, 2010. (<http://opensees.berkeley.edu>)
- Kim, J., and LaFave, J. M., "Key Influence Parameters for the Joint Shear Behavior of Reinforced Concrete (RC) Beam-Column Connections," *Engineering Structures*, No. 29, 2007, pp. 2523-2539.

NOTES:



A cyclic shear stress–strain model for joints without transverse reinforcement

Meredith Anderson^a, Dawn Lehman^{b,*}, John Stanton^b

^a Reid Jones Christoffersen, Ltd., Vancouver, Canada

^b Civil and Environmental Engineering, University of Washington, Seattle, WA 98195, United States

Received 11 April 2006; received in revised form 31 January 2007; accepted 2 February 2007

Available online 30 July 2007

Abstract

In many older reinforced concrete frames, the joints contain no transverse reinforcement. Under seismic loading, those joints may suffer damage and deform, and thereby contribute significantly to the displacements of the frame, which significantly impacts its performance. However, engineers typically ignore joint deformations in seismic analyses, largely due to the lack of appropriate analytical models and reliable data against which to verify them. To improve the simulation of two-dimensional response of frames with joints without transverse reinforcement, a constitutive model was developed for the shear deformations of the joint. The model replicates cyclic degradation in strength and modulus, and energy dissipation of the branch curves. It was calibrated using measured data from tests on joints without transverse reinforcement that were subjected to a range of displacement histories and joint shear stress demands. The model has a general form, and is supplemented by recommendations for the values of the model parameters, which are expressed as functions of the joint geometry and material properties. An independent data set was used to validate the proposed model.

© 2008 Published by Elsevier Ltd

Keywords: Earthquake engineering; Performance-based seismic design; Beam–column joints; Seismic analysis; Retrofit

1. Introduction

Reinforced concrete frame buildings built prior to the 1970s typically contain reinforcing details that do not lead to ductile response. Such frames are referred to as non-ductile. The lack of ductility is associated with many potential damage modes, including column shear, column axial load, slip of spliced or embedded rebar, and joint shear. The study reported here addresses only joint shear.

Joints in reinforced concrete frames that are subjected to lateral loading may experience high shear stresses. In current seismic design, limits on joint shear stresses play a dominant role in determining the column size, but this was not always the case. Prior to the pioneering experiments of Hanson and Connor [11], codes did not specify limits on the joint shear stress or require joint transverse reinforcement. As a result, older joints may be subjected to shear stresses that are larger,

and vary more, than those in modern joints, yet they typically contain no transverse reinforcement. This combination of high demand and poor detailing increases their vulnerability.

The mid-1970s saw the adoption into codes of prescriptive rules for seismic design that closely resemble those in force today. However, many existing buildings were constructed before that time and the robustness of their seismic performance is therefore open to question. Although definitive data on the numbers of non-ductile concrete buildings are lacking, some estimates exist. For example, the California Seismic Safety Commission estimates that there are 40,000 such buildings in California, which suggests that simulation models specific to this type of building are needed for their seismic evaluation.

Previous experimental research has focused largely on measures to improve the seismic response of beam–column joints. As a result, almost all of the experimental specimens have included transverse reinforcement and the test results have concentrated on strength. Furthermore, the imposed displacement histories have almost all consisted of monotonically increasing drift cycles (e.g., [7,8,14,16]).

* Corresponding author. Tel.: +1 206 632 6860.

E-mail address: delehman@u.washington.edu (D. Lehman).

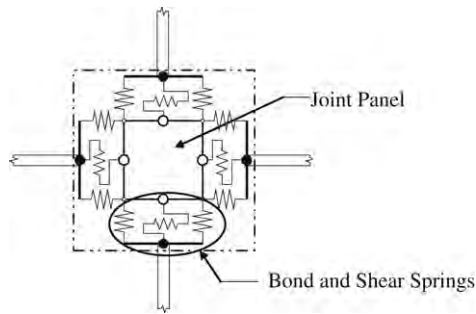


Fig. 1. Macro-element joint model (adapted from Mitra and Lowes (2006)).

However, two recent series of tests have been conducted on joints without transverse reinforcement and also focused on quantifying joint flexibility and damage [2,22]. Those studies showed that even moderate cracking reduces the apparent shear modulus of the joint to a value that is well below the theoretical uncracked level, and that the resulting joint deformations contribute significantly to the overall frame deformations [3].

In the experiments, the specimens consisted of cruciform beam–column sub-assemblages, as shown in Fig. 1. Comparison of tests with and without transverse reinforcement indicates that the transverse reinforcement influences the cyclic response of the joint. In particular, the drift capacity corresponding to any given post-peak strength is increased and it slows the degradation of strength and stiffness.

Perhaps surprisingly, the peak load achieved in the tests appears to be little affected by the presence or amount of transverse reinforcement, but rather is controlled by the flexural strength of the beams (for a weak-beam/strong-column test specimen) [17,18,22]. However, once the beam bars have yielded, the joint suffers more and more damage, and its shear strength diminishes, with cycling, causing the proportion of the total displacement that is attributable to joint shear deformation to increase. For example, in the tests [2,22], the contribution of the joint deformation to the total displacement reached 50% by a drift ratio of 3% drift ratio in all specimens, and by a drift ratio of only 1% in the specimen with the highest joint shear stress demand. The two primary exceptions to this pattern of degrading strength are provided by beams that are very weak or very strong compared with the joint. In the former case, the joint experiences such a low shear stress that it never suffers damage beyond fine cracking, while in the latter the beams remain elastic and the system strength is indeed controlled by the joint shear strength, even under monotonic load [2].

For the range of joint shear stress demands found in the field [18], the beam strength typically lies in the middle range for which the joint behavior is characterized by a continuous reduction in capacity with cycling. Therefore dynamic simulation of older buildings requires a joint model capable of replicating this degrading cyclic response. A simulation model based on a fixed value of strength is not sufficient.

Practicing engineers usually ignore joint shear deformations in their analyses because including them complicates the analysis and reliable joint models are not readily available. Consequently, the frame displacements are underestimated.

Accurate simulation of the joint behavior is important for several additional reasons. First, the joint flexibility is important because it increases the drift demand, which may lead to more non-structural damage and to structural instability through P-delta effects. Second, joint shear is the dominant failure mode in many frames, and it can only be predicted by using a representative model of the joint behavior. It has been argued that global displacement, such as roof drift, is the most important indicator of performance and that it can be predicted by ignoring joint behavior and empirically modifying the stiffnesses of other elements, such as the columns. However, damage occurs due to local, not global, behavior, so such an approach makes prediction of damage difficult. Furthermore, the value of the modifier depends on the demand, the stiffnesses of the adjacent elements and the damage state of the joint, which varies throughout the load history. Therefore, analysis based on a fixed stiffness modifier is not likely to represent the true response.

A small number of researchers have developed analytical models to simulate the response of joints, and most of them have used the joint shear stress and strain as the characterizing variables. Kunnath [13] developed an empirically-based, five-parameter model that reflects the primary response characteristics of joints subjected to cyclic loading, such as stiffness and strength degradation. Ghobarah and Biddah [10] constructed a simpler model in which the stress–strain response was based on the softened truss theory, which is appropriate for joints with well-distributed transverse reinforcement. Lowes and Altoontash [15] developed a macro-element model of the entire joint (similar to that shown in Fig. 1), including slip and inelastic action of the beam bars within the joint and simulating the joint shear response using the modified compression-field theory to represent the shear response of the joint panel, which was deemed appropriate for modern joints with transverse reinforcement and limited joint shear stress demands [15]. The constitutive properties of most joint shear models were calibrated using experimental data from cyclic shear panel tests and validated using experimental joint shear data. In almost all cases, the test specimens used for validation were subjected to cyclic deformation histories bounded by a monotonically increasing envelope curve (e.g., [10,15,17]).

In general, these models are capable of simulating joints that meet the current code requirements for transverse reinforcement, because they were developed from tests that contained it. However, they are less able to represent the more complex joint degradation associated with the lack of transverse reinforcement. Similarly, the fact that they were developed from load histories that consist of symmetric cycles contained within a monotonically increasing envelope means that they lack the rules necessary to replicate other load histories, such as the more random ones associated with real earthquakes. These require, for example, rules that describe response to a small displacement cycle following a large one.

The proposed constitutive model was developed to simulate the degrading shear stress–strain behavior of joints containing no transverse reinforcement, and to replicate response to a wide range of cyclic deformation histories. The ability to simulate

the cyclic response of the joint response was critical since, as described previously, currently available models are not able to do so [3,17]. For example, Lowes and Altoontash [15] as well as studies by others (as documented in [17]) show that using the modified compression field theory to simulate the joint shear stress–strain response is accurate only for joints with moderate to high joint transverse reinforcement ratios. As a result, Mitra and Lowes [17] developed a joint model which assumes that the joint shear load is transferred via a single strut and the strut constitutive model is based on a confined concrete stress–strain model. However, the results indicate that even with this improvement, the model is not capable of replicating the full response of joints without transverse reinforcement with different joint shear stress demands, load histories, and concrete strengths.

Development of a model specifically appropriate for simulation of joints in older, non-ductile reinforced concrete frames is warranted. Specifically, a joint shear constitutive model for the panel element shown in Fig. 1 is required. It addresses only the shear stress–strain behavior of the panel itself, so the constitutive model for the bars and the bond between the bars and the concrete of the panel must be modeled separately. The research reported here was undertaken to develop such a model for a joint without transverse reinforcement. The proposed model was based on test data from Walker [22] and Alire [2]. Walker [22] used a rich array of displacement histories, including some with highly asymmetric patterns and others with many cycles of constant amplitude displacement, in addition to the more common symmetric, increasing-amplitude cycles. Alire [2] studied a wide range of joint shear stress demands. The sections that follow describe the most important trends in the experimental response, and the development, calibration, and validation of the model.

The model specifically simulated the joint shear stress–strain response or the panel component of a macro-element joint model, such as shown in Fig. 1. Therefore, reliable local joint measurements, such as those made using the joint panel instrumentation shown in Fig. 4(a) and (b), were needed to calibrate and validate the model. The model was developed using some of the data from the Alire and Walker studies. It was validated using the remaining Alire–Walker data that had not been used during the development. This procedure was adopted because data from other tests of joints without transverse reinforcement were not available in a suitable form and sufficiently detailed. Finally, the model was tested against a dataset obtained from a test on a joint with little transverse reinforcement [14]. It constituted data that was independent and available and represented the required conditions as closely as possible.

2. Measured response

To develop an appropriate constitutive model for the joint shear stress–strain response of older joints, the local joint shear response measured during the tests was analyzed and reduced to the primary aspects of the monotonic and cyclic response [22, 2]. Particular attention was paid to the degradation in strength

Table 1

Target and actual joint shear stresses for Walker–Alire test series

	Specimen	Target			Measured	
		v_j/f'_c	f'_c	$v_j/\sqrt{f'_c}$	\bar{f}'_c	$v_j/\sqrt{\bar{f}'_c}$
Series 1	SCDH-1450	0.14	34.5	0.82	31.8	0.91
	SCDH-2250	0.22	34.5	1.29	38.4	1.20
	CD15-1450	0.14	34.5	0.82	29.8	0.96
	CD30-1450	0.14	34.5	0.82	42.6	0.94
	CD30-2250	0.22	34.5	1.29	38.2	1.29
	PADH-1450	0.14	34.5	0.82	42.9	0.98
	PADH-2250	0.22	34.5	1.29	36.3	1.31
Series 2	SCDH-0850	0.08	34.5	0.47	35.0	0.71
	SCDH-0995	0.09	65.5	0.73	60.4	0.91
	SCDH-1595	0.15	65.5	1.21	61.5	1.38
	SCDH-4150	0.41	34.5	2.41	33.0	2.08

SCDH = Standard Cyclic Displacement History (Fig. 2(a)), CD15 and CD30 = Constant Displacement to 1.5% and 3% Drift, respectively (Fig. 2(b) and (c)), and PADH = Pulse Asymmetric Displacement History (Fig. 2(d)).

and average shear modulus caused by the different cyclic strain histories. Here average joint shear strain refers to the value measured over the central region of the joint, and the average shear modulus is obtained from that strain using the joint instrumentation shown in Fig. 4(a) and (b) and the average shear stress computed from the shear force divided by the total joint area. The measured area roughly corresponds to the area simulated by the joint shear panel, as shown in Fig. 1.

The experimental studies were developed to establish the influence of the displacement history, joint shear stress demand, and material properties (in particular, concrete strength) on the joint performance. The values of the primary study variables are summarized in Table 1, and the test specimens, setup, and displacement histories are illustrated in Figs. 2 and 3. The Standard Cyclic Displacement History (SCDH) used sets of three cycles, each of which had a larger amplitude than the last. This history was used as a standard to facilitate comparison with tests by other investigators, many of whom have used similar histories. The Constant Displacement histories (CD15 and CD30) were intended to simulate the effects of long-duration earthquakes, while the Pulse Asymmetric Displacement History (PADH) was chosen to represent the effects of a near-fault earthquake. These latter two provided a rich source of behavioral information, typically not available from other test programs, on which to base rules for the analytical model.

The naming system for the test specimens consisted of four alphanumeric symbols, followed by a dash and four numbers. The four symbols define the displacement history (SCDH, PADH, CD15 or CD30). The first two numbers after the dash indicate the joint shear stress demand as a fraction of the concrete strength, measured in percent, and the last two numbers indicate the target concrete strength in hundreds of psi. For example, the demand in specimen SCDH-0850 was $0.08f'_c$, and the target concrete strength was 5000 psi (35 MPa).

The joint shear stresses were chosen to span the full range of expected behavior types. The lowest (Specimen SCDH-0850) was intended to lead to beam hinging rather than joint shear failure, while the highest (Specimen SCDH-4150) was intended to cause failure in joint shear prior to beam-bar yielding. Fig. 4

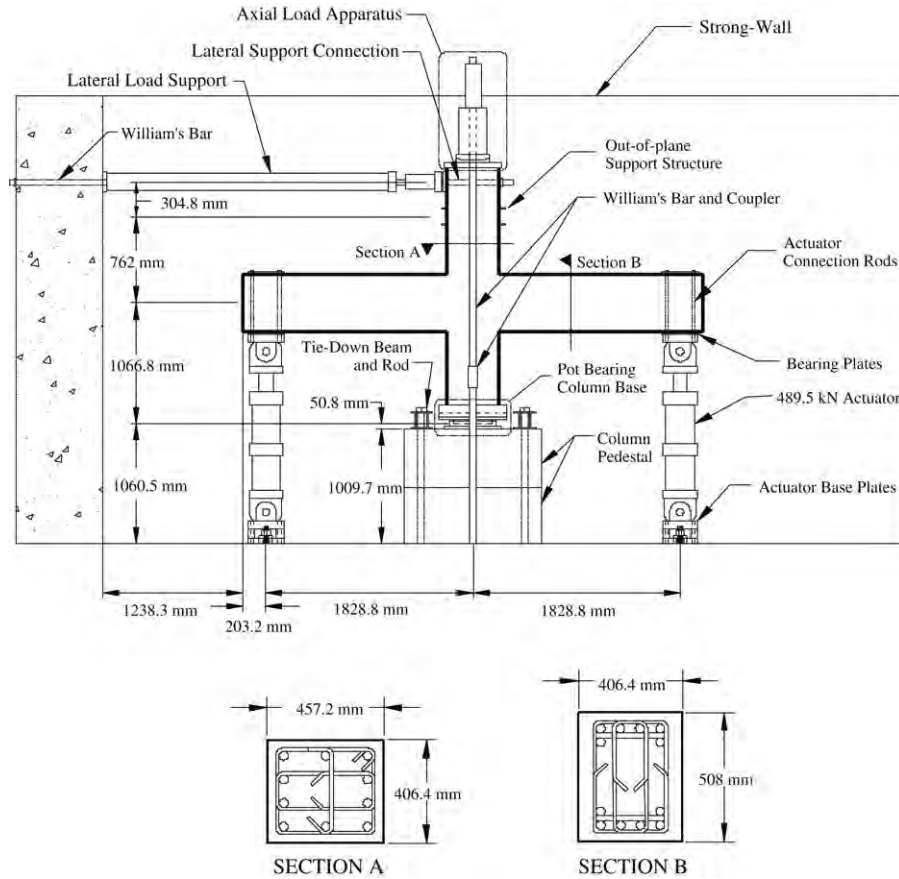


Fig. 2. Setup and specimen dimensions for joint tests [22,2].

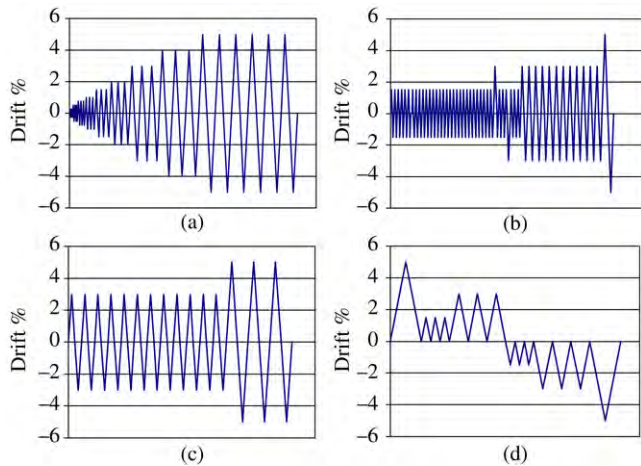


Fig. 3. Displacement histories: (a) SCDH, (b) CD15, (c) CD30, (d) PADH.

shows the range of end damage states for three specimens with different joint shear stress demands. As indicated by the photograph, the goal of achieving the range of behavior was approximately met in the tests. The different material properties were included primarily to study the relationship between joint shear resistance and concrete strength. Additional information about the test programs can be found in the reference documents [2,22].

In the following discussion, the sign convention is that a positive path (envelope or branch curve) is one along which the

average strain velocity (i.e. the differential of strain with respect to time) is positive (strain is becoming more positive), while a positive reversal point is one at which the strain acceleration is positive (i.e. response changes from a negative path to a positive one). The test results revealed the following key behavioral characteristics.

- The peak load and mode of failure depended on the joint shear stress demand and displacement history. This finding contrasts sharply with provisions in codes. For example, Section 21.5.3 of ACI 318-02 and Section 6.5.2.3 of FEMA 356 give equations for joint shear capacities that depend on the dimensions and the concrete strength [1,9] as well as the joint transverse reinforcement ratio [9]. The implication is that the joint will fail in shear if the joint shear stress demand exceeds this capacity, but otherwise beam hinging will be the controlling failure mechanism and the joint will remain undamaged. However, in the tests by Walker and Alire, the joint was badly damaged regardless of shear stress demand, and the peak load was controlled by the beam-bar strength and the specimen geometry, and not by the joint shear capacity defined by ACI 318-02 or FEMA 356. (For example in Specimen 0850, although the nominal joint shear stress was approximately half the ACI allowable value for an interior joint, the joint sustained considerable damage after many cycles). This suggests that joint capacity is not a single number, but rather that joint shear failure is a phenomenon analogous to fatigue, whereby at any demand

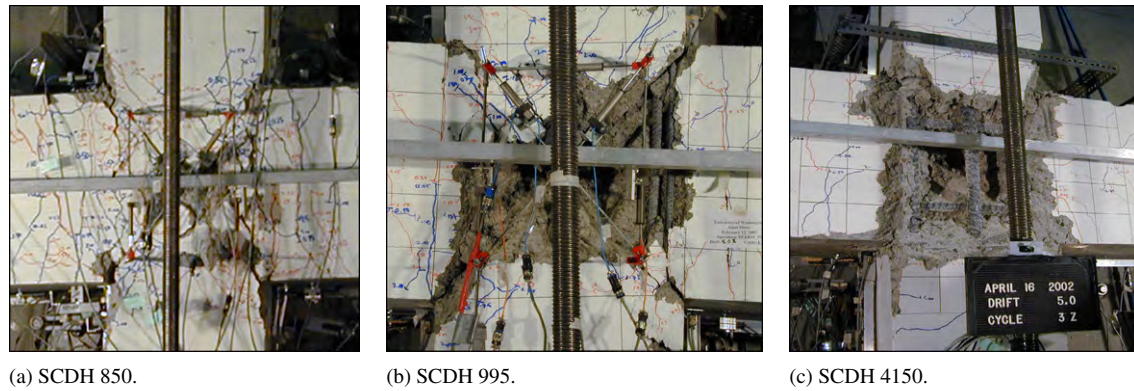


Fig. 4. End damage states for joints with different shear stress demands.

above a certain threshold, failure will occur eventually but only after a number of cycles that depends on the intensity of the demand. Only in the specimen with the highest joint shear demand (Specimen SCDH-4150) was the peak lateral load reached just as the beam bars yielded; the resistance exhibited by this joint is therefore believed to be an upper bound on the joint shear strength. In the specimen with the lowest demand (Specimen SCDH-0850), extensive beam hinging preceded the joint shear failure, and the resistance of this joint is believed to approximate the endurance limit.

- The shape of the shear stress–strain envelope differs for different joint shear stress demands. The degree and severity of damage and post-peak degradation depends on the joint shear stress demand.
- The joint stress–strain relationship can be divided into three major regions. They can be seen most easily in Fig. 9, which illustrates the model. However, the trends that are idealized in the model can also be seen in the data measured in the tests. In the first region, the joint cracking is not visible and its stress–strain response is linearly elastic. In the second, the joint is cracked and the strain–strain law is hysteretic but non-degrading. In the third, the relationship is hysteretic and degrades. The second and third regimes start after threshold strain values have been reached.
- Test data illustrating the third region is shown in Fig. 6. Once the threshold strain of approximately 0.006 rad has been passed, even a small increase in joint shear strain results in degradation of the response, manifested as pinching of the hysteresis loop. This behavior is demonstrated in the joint stress–strain response shown in Fig. 6 by the difference in the two labeled negative branch curves. Curve 1 follows a strain reversal that is less than the threshold strain and shows no pinching, while Curve 2 exceeds the threshold strain and exhibits a more pinched response.
- Provided the threshold strain has been passed, an increase in shear strain beyond the current maximum reversal value results in significant degradation of strength and modulus of the branch curve in the direction of the strain of interest. An example of this behavior is shown in Fig. 7. The shear modulus and strength of the negative branch curve labeled 2 is degraded relative to the modulus and strength of the negative branch curve labeled 1; this degradation results

from the larger reversal strain of Curve 2 relative to Curve 1. However, the properties (strength and modulus) of Curve 3 are the same as Curve 2 because, in this case, the maximum reversal strain resulting from Curve 2, was not exceeded by the reversal resulting from Curve 3.

- Cycling at an approximately constant deformation amplitude causes a gradual change in both damage and resistance, as shown in Fig. 8. This occurs because if the strain does not increase, the pre-existing cracks merely close and no new concrete is crushed. In the figure, the peak strain in each cycle increases slightly because the beam displacement, and not the joint shear strain, was used to control the magnitude of the imposed displacements. Thus the joint concrete incurred a small amount of additional damage with each cycle. The beam bars remained elastic and their stiffness, therefore, remained constant. But with each cycle, the secant stiffness of the joint dropped so the joint accounted for an increasingly large proportion of the total deformation and the joint shear strain increased a little. Only when the displacement exceeded the current maximum value did the resistance increase again and the damage accumulation speed up.

A number of constitutive models are available in structural analysis software (e.g., IDARC [12], *Ruaumoko* [6]), several of which can model stiffness degradation and pinching. The program *Ruaumoko* [6] contains one of the richest libraries of constitutive laws, and was used to simulate the joint shear response of the experimental specimens [3]. Based on careful evaluation of the models and the specimen behavior, the constitutive model by Stewart et al. [21] was deemed to be the most appropriate to represent the response of a joint without transverse reinforcement. The constitutive model uses several parameters to define a trilinear backbone curve and branch curves that include pinching, a fixed unloading stiffness and degrading reloading stiffness. Using data from the measured joint shear curves, values for each of these parameters were estimated. Fig. 5 shows typical results. The model performs quite well with the SCDH load history (Fig. 5(a)), but replicates poorly the response of the specimen subjected to the CD30 history (Fig. 5(b)). This occurs because the degradation rules are a function of ductility demand or number of cycles, but not both. The test results show that the available degradation

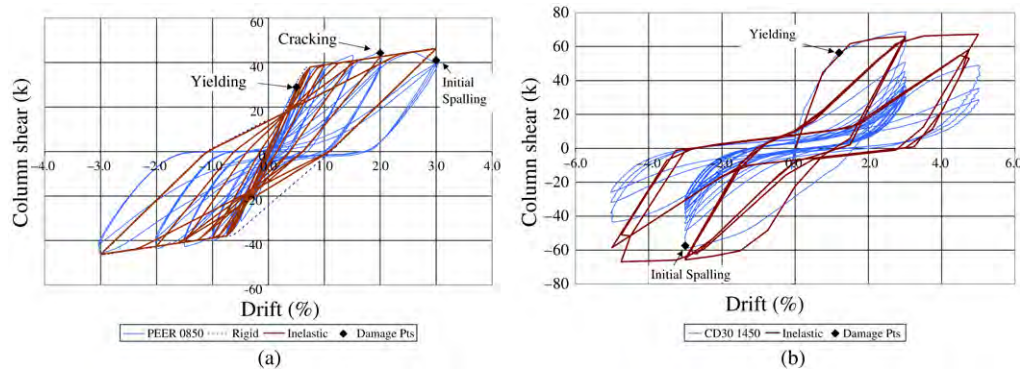


Fig. 5. Measured and predicted response with existing software for specimens: (a) SCDH-0850, (PEER 0850), (b) CD30-1450.

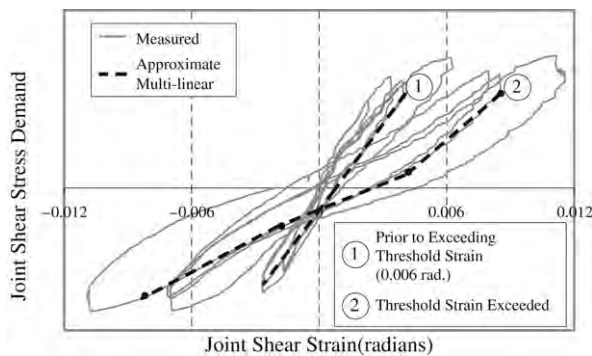


Fig. 6. Degradation and pinching in branch curves after exceeding threshold strain.

rules are adequate if the amplitudes of successive cycles exceed those of the previous ones, as is the case for the SCDH history, but they fail to replicate the response if the new cycle is equal to or smaller than the previous one. These results indicate that acceptable replication of the measured response is not possible with the hysteretic models currently available in existing commercial software [4]. This finding is partly a consequence of the wide variety of displacement histories used in the tests, which revealed behaviors that did not occur in the tests on which earlier models were based.

3. Model development

Simulation of a non-ductile reinforced concrete frame requires a model capable of capturing the cyclic degradation of a joint without transverse reinforcement. To develop this capability, the results of the experimental testing were used to develop and validate a constitutive model for joint shear response. The initial motivation was to simulate the observed strength and stiffness degradation under constant amplitude cyclic loading, which had proved impossible with available software, but the goal was soon expanded to include responses to the three very different types of displacement history used in the tests. This required a relatively complex set of rules.

The key components of the model, illustrated in Fig. 9, are:

- A trilinear envelope to represent the monotonic response and the envelope to the cyclic response. The points at which the segments of the curve meet are referred to as breakpoints.

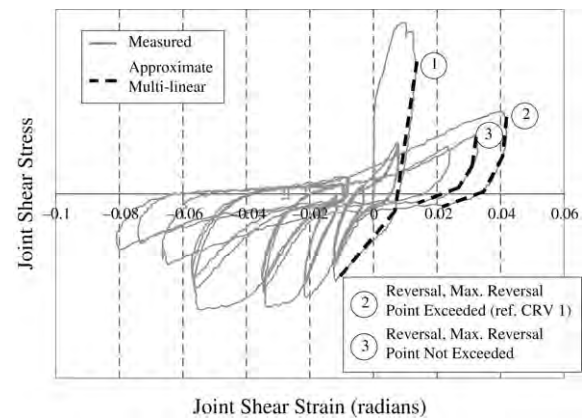


Fig. 7. Example of degradation that depends on maximum reversal strain.

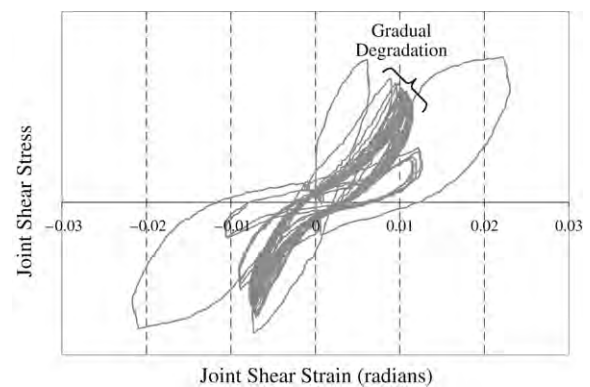


Fig. 8. Example of gradual degradation resulting from constant amplitude history.

- Multi-linear branch curves, including non-degrading and degrading curves, to define the loading path between a reversal and the return to the envelope in the opposite direction.

The degree of nonlinearity and degradation in the branch curves depends on the magnitude of the maximum reversal strain (in the direction of interest), the joint shear stress demand, and, in some cases, the previous joint shear strain demand. Therefore, a different set of rules was developed for each of three regions, which are defined by the breakpoints in the envelope curve. However, in all cases, the complete path along the new branch curve can be determined as soon as a reversal

Table 2
Segments of joint shear stress–strain path

Component	Sgmt	Tangent modulus	Endpoint stress	Endpoint strain
Envelope	$e01$	$G_{e01} = v_{e1}/\gamma_{e1}$	Input parameter	Input parameter
	$e12$	$G_{e12} = (v_{e2} - v_{e1})/(\gamma_{e2} - \gamma_{e1})$	Input parameter	Input parameter
	$e23$	$G_{e23} = \rho_{G,e23} * G_{e02}$	Large default value may be used	
Non-degrading branch curves	$b01$	$G_{b01} = \rho_{G,b01} * G_{e02}^{opp}$	$v_{b1} = \rho_{v,b1} * v_{b0}$	
	$b12$	$G_{b12} = (v_{e1} - v_{b1})/(\gamma_{e1} - \gamma_{b1})$	$v_{b1} = v_{e1}$	$\gamma_{b1} = \gamma_{e1}$
	$b24$	$G_{b24} = G_{e12}$	$v_{b4} = v_{e2}$	$\gamma_{b4} = \gamma_{e2}$
Degrading branch curves	$b01$	$G_{b01} = \rho_{G,b01} * G_{e02}^{opp}$	$v_{b1} = \rho_{v,b1} * v_{b0}$	$\gamma_{b1} = (v_{b1} - v_{b0})/G_{b01} + \gamma_{b1}$
	$b12$	$G_{b12} = \rho_{G,b12} * G_{maxrev}^{opp}$	Intercept with segment 23	
	$b23$	$G_{b23} = \alpha_{G,b23} * G_{e02}^{opp}$	Intercept with segment 23 and the stress axis intercept: $v_{int} = \alpha_{v,int} * v_{e2}$	
	$b34$	$G_{b34} = \alpha_{G,b34} * \beta_{G,b34} * G_{maxrev}$	$v_{b4} = \alpha_{v,b4} * v_{e2}$	$\gamma_{b4} = v_{b4}/G_{b34}$
	$b4b0$	$G_{b45} = G_{e23} = \rho_{G,e23} * G_{e02}$	$v_{b1} = v_{e1}$	$\gamma_{b1} = \gamma_{e1}$

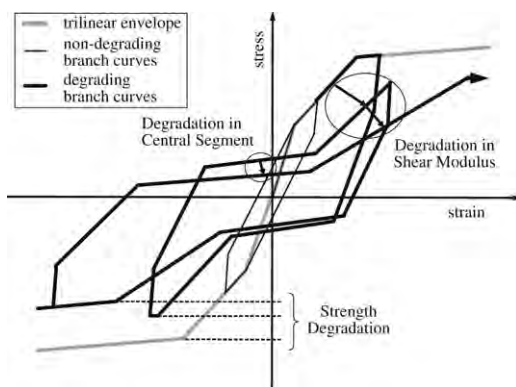


Fig. 9. Overview of joint shear constitutive model.

point is detected, because the parameters of each segment of the branch curves depend only on the properties of the envelope and the coordinates of the maximum reversal point.

In the first region, when the maximum strain is less than the first breakpoint of the envelope curve, the response is linearly elastic and remains on the envelope curve, which in this region is simply a straight line through the origin. In the second region, where the maximum strain reached lies between the second breakpoints of the positive and negative envelope curves, the cyclic response follows branch curves between the envelopes, and is hysteretic but not degrading. An example of such a branch curve is shown with a narrow black line in Fig. 9. In the third region, when the maximum strain exceeds the second breakpoint of the envelope curve, the response defined by the branch curves is both hysteretic and degrading. Two consecutive loops of this type are shown as heavy black lines in Fig. 9. Cycling causes the slopes of the loading curves to decrease (degradation in the tangent shear modulus). It also results in the branch curves' dropping below the envelope curve. Degradation in the strength and modulus are also apparent in the central segment of the curve, as it passes through zero strain. This behavior is caused by cracks that remain open, so the concrete particles are not in contact and little force can be transmitted internally. This is sometimes referred to as pinching, because the mid-region of the loop is narrower than the outer regions. The result is a region

encompassing zero strain where the resistance is small, and reduced loop area and energy dissipation.

4. Model operation

The rules that define the envelope and branch curves are summarized in the equations provided in Table 2. Their bases and the way that they operate are described in the following sections. However, the nomenclature used is described first, because familiarity with it helps to understand the operation of the model.

4.1. Nomenclature

A consistent naming system was developed for the input (user-specified) and internal model variables. Here, input parameters are in bold italics and internal variables are in italics. The notation system consists of main variables and subscripts. The main variable refers to the type of parameter (e.g., v , γ and G for stress, strain and modulus, respectively). The primary subscript identifies the corresponding line segment or point. Calculation of the branch curve segments requires constant or degradation dimensionless coefficients, which are indicated by Greek symbols (ρ , α and β). In them, the primary subscript refers to the main variable that they modify. Where necessary, a secondary subscript is used for the coefficients to identify the corresponding line segment or point, and a superscript of +, −, or opp is used to indicate the path direction (positive, negative or opposite to the current direction, respectively).

The points defining the envelope are named sequentially from $e0$ to $e3$ with $e0$ indicating the origin (Fig. 10). A similar naming scheme, using $b0$ through $b5$, is used for the points that define the branch curves (Figs. 11 and 12). The point $b0$ is the reversal point. Note that point $b3$ is not used in the non-degrading branch curves.

Stresses, strains and moduli are primary variables. Pairs of stresses and strains, suitably subscripted, define fixed points on the envelope and branch curves. For example, the stress at the second breakpoint on the envelope, point $e2$, is v_{e2} . The names of the corresponding tangent shear moduli are defined using the points that define the line segments, and contain the numbers

Table 3
Degradation parameters

Segment	Variable	Strain ratio	Multiplier
b23	$\alpha_{G,b23}$	$1/s_{\maxrev,e2} = \gamma_{e2}/\gamma_{\maxrev}$	G_{e02}^{opp}
	$\alpha_{v,int}$	$s_{\maxrev,e2} = \gamma_{\maxrev}/\gamma_{e2}$	v_{e2}
b34	$\alpha_{G,b34}$	$sb_{0,\maxrev} = \gamma_{b0}/\gamma_{\maxrev}$	G_{\maxrev}
	$\beta_{G,b34}$	$s_{\maxrev,opp,\maxrev} = \gamma_{\maxrev}^{opp}/\gamma_{\maxrev}$	G_{\maxrev}
	$\alpha_{v,b4}$	$s_{\maxrev,e2} * \beta_{v,b4}(\gamma_{\maxrev}/\gamma_{e2}) * \beta_{v,\beta4}$	v_{e2}
	$\beta_{v,\beta4}$	$s_{\maxrev,e2}^{opp} = \gamma_{\maxrev}^{opp}/\gamma_{e2}^{opp}$	$\alpha_{v,b4}$

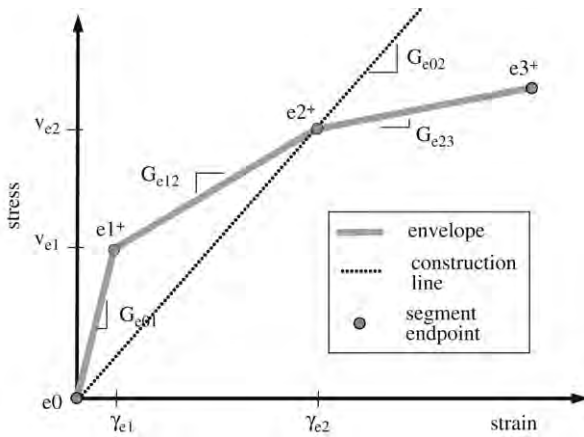


Fig. 10. Envelope segments (positive envelope shown).

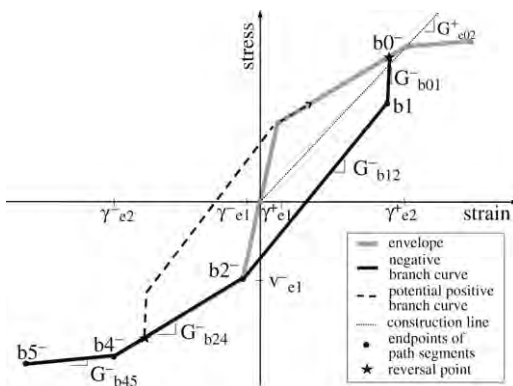


Fig. 11. Non-degrading branch curves.

of the starting and ending points of the segment. The tangent modulus (or slope) of the segment is either calculated from its endpoint stress and strain values (e.g., for G_{e12}) or using an equation given in Table 2 (e.g., for G_{e23}). A secant modulus is the slope of a line beginning at the origin (e.g., G_{e02}^+ shown in Fig. 9). For example, the tangent modulus G_{b12}^- in Fig. 11 is the slope between points b1 and b2 of a branch curve for which the strain direction is negative. Table 2 shows that its value is determined from the secant modulus G_{e02}^+ . That is, G_{b12}^- is given by the product $\rho_{G,b12} * G_{e02}^{opp}$, where $\rho_{G,b12}$ is a dimensionless coefficient and G_{e02}^{opp} is the secant modulus from the origin to point e2 on the envelope in the opposite direction. The only exceptions to the subscript convention are those that refer to the secant modulus to the maximum reversal point, G_{\maxrev} , and the stress-axis intercept, v_{int} .

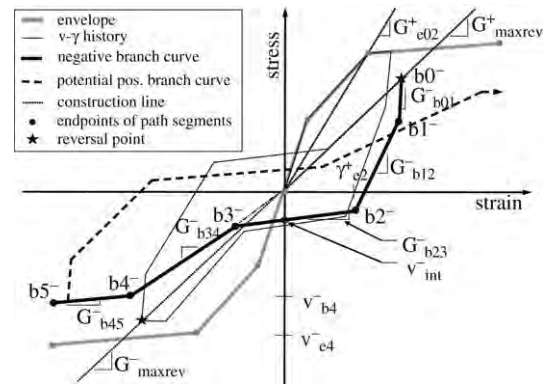


Fig. 12. Degrading branch curves.

Constant and degrading coefficients, called ρ and α (or β) respectively, are used in determining many of the tangent modulus and strength values. Each coefficient has a pair of subscripts that refer to the resultant parameter. For example, G_{e23} is calculated as the product of the constant coefficient $\rho_{G,e23}$ and the secant modulus G_{e02} . The degrading coefficients are functions of a normalized strain history, and are described in some detail below. Coefficients α and β define degradation due to strain effects in the same and opposite loading directions, respectively.

Strain ratios, designated as s , are used to determine the values of the degradation coefficients. Table 3 indicates the strain ratio that is used to determine each degrading coefficient. The primary and secondary subscripts on s refer to the strains in the numerator and denominator of the strain ratio, respectively. For example, $s_{\maxrev,e2}$ is the ratio of the strain at the maximum reversal point, γ_{\maxrev} , to the strain at point e2 on the envelope, γ_{e2} . A third subscript is used to distinguish the values of the strain ratios and degradation parameters at breakpoints in the α - s or β - s functions. For example, the first breakpoint of the function for the modulus degradation parameter $\alpha_{G,b34}$ is the point $(s_{\maxrev,e2,1}, \alpha_{G,b34,1})$. The recommended input values for the corresponding strain ratios and degrading coefficients are provided in Table 4. A general discussion of the recommended values is presented in the section on calibration; a more detailed description is available in a reference report [3].

4.2. Trilinear monotonic response and cyclic envelope

The trilinear curve used to model the monotonic response and envelope to the cyclic response is shown in Fig. 10. The

Table 4
Recommended expressions for input parameters

Group	Name	Description	Value	Limits
Envelope	v_{e1}^a	Stress at point $e1$	$0.48\sqrt{f'_c}$ (Mpa)	–
	γ_{e1}	Strain at point $e1$	0.00043	–
	v_{e2}^a	Stress at point $e2$	$0.95 * c_j * \sqrt{f'_c}$ (Mpa)	–
	γ_{e2}	Strain at point $e2$	0.006	–
	$\rho_{G,e23}$	Constant modulus ratio	0.015	–
Segment $b01$	$\rho_{G,b01}$	Constant modulus ratio	20	–
	$\rho_{v,b1}$	Constant modulus ratio	0.65	–
Segment $b12$	$\rho_{G,b12}$	Constant modulus ratio	$2.41c_j + 0.59$ (MPa)	$2 < \rho_{G,b12} \leq 3.5$
Segment $b23$	$\alpha_{v,int}$	Constant ratio $\alpha_{v,int}$ for all $s_{maxrev,e2}$	0.10	–
	$\alpha_{G,b23,1}$	$\alpha_{G,b23}$ at $s_{maxrev,e2,1}$	0.087	–
	$\alpha_{G,b23,2}$	$\alpha_{G,b23}$ for $s_{maxrev,e2} \geq s_{maxrev,e2,2}$	0.006	–
	$s_{maxrev,e2,1}$	Strain ratios at the breakpoints of the $\alpha_{v,int}$ & $\alpha_{G,b23}$ degradation functions	2.85	–
	$s_{maxrev,e2,2}$		8.1	–
Segment $b34$ stiffness degradation	$\alpha_{G,b34,2}$	$\alpha_{G,b34}$ when $s_{b0,maxrev} = s_{b0,maxrev,2}$	0.88	–
	$\alpha_{G,b34,3}$	$\alpha_{G,b34}$ when $s_{b0,maxrev} > s_{b0,maxrev,3}$	0.74	–
	$s_{b0,maxrev,1}$	First breakpoint of $\alpha_{G,b34}$ curve	1 ^b	–
	$s_{b0,maxrev,2}$	Second breakpoint of $\alpha_{G,b34}$ curve	1.03	–
	$s_{b0,maxrev,3}$	Third breakpoint of $\alpha_{G,b34}$ curve	1.85	–
	$\beta_{G,b34,1}$	$\beta_{G,b34}$ at $s_{maxrev_opp,maxrev,1}$	1 ^b	–
	$\beta_{G,b34,2}$	$\beta_{G,b34}$ at $s_{maxrev_opp,maxrev,2}$	0.27	–
	$s_{maxrev_opp,maxrev,1}$	First breakpoint of the $\beta_{G,b34}$ curve	1.69	–
	$s_{maxrev_opp,maxrev,2}$	Second breakpoint of the $\beta_{G,b34}$ curve	4.11	–
	Segment $b34$ strength degradation	$\alpha_{v,b4,1}$	$\alpha_{v,b4}$ when $s_{maxrev,e2} = s_{maxrev,e2,1}$	1.0
$\alpha_{v,b4,2}$		$\alpha_{v,b4}$ when $s_{maxrev,e2} = s_{maxrev,e2,2}$	$-0.47c_j + 1.15$ (MPa)	$0.5 \geq \alpha_{v,b4,2} \leq 1$
$s_{maxrev,e2,1}$		First breakpoint of $\alpha_{v,b4}$ curve	$s_{\alpha,b4,2} - 10(1 - \alpha_{b,b4,2})$	≥ 1
$s_{maxrev,e2,2}$		Second breakpoint of $\alpha_{v,b4}$ curve	$\alpha_{v,b4,2}/0.086$	–
$s_{maxrev,e2,3}$		Third breakpoint of $\alpha_{v,b4}$ curve	20	$> s_{maxrev,e2,2}$
$\beta_{v,b4,1}$		$\beta_{v,b4}$ when $s_{maxrev,e2}^{opp} = s_{maxrev,e2,1}^{opp}$	1 ^b	–
$\beta_{v,b4,2}$		$\beta_{v,b4}$ when $s_{maxrev,e2}^{opp} \geq s_{maxrev,e2,2}^{opp}$	0.68	–
$s_{maxrev,e2,1}^{opp}$		First breakpoint of $\beta_{v,b4}$ curve	1 ^b	–
$s_{maxrev,e2,2}^{opp}$		Second breakpoint of $\beta_{v,b4}$ curve	2.07	–

c_j is the joint shear stress coefficient.

^a Parameter may have separate positive and negative input values.

^b Default value of this parameter is used.

curve is defined by pairs of stress and strain input parameters (e.g. v_{e2} and γ_{e2}) and their recommended values are provided in Table 4. Most are self-explanatory, but the fixed stress point, v_{e2} , is given by $0.95 c_j \sqrt{f'_c}$ (MPa), where c_j is the shear stress coefficient of the joint, defined by the maximum joint shear stress that can be induced by the beam bars divided by $\sqrt{f'_c}$. (Note that $c_j < 2.4$ because data are not available for joints without transverse reinforcement that have been tested to shear stresses higher than this.) In calculating the joint shear stress, the beam bars are assumed to be stressed to 1.25 times their nominal yield strength. Because the full monotonic response was not determined experimentally, an arbitrarily large strain value, γ_{e3} , is used to define the endpoint of segment $e23$. The corresponding stress is obtained from the known starting point (γ_{e2} , v_{e2}), slope (G_{e23}) and ending strain, γ_{e3} , of that segment of the curve. Table 2 provides the value for G_{e23} .

4.3. Non-degrading branch curves

Non-degrading branch curves are constructed when the maximum reversal strain lies between γ_{e1} and γ_{e2} , as shown in Fig. 11. (Note that these strain limits may be different for positive and negative loading). In the figure, three line types are to differentiate the model components. The trilinear envelope is shown using thick grey lines (consistent with Fig. 10.) A negative stress–strain path is shown from reversal point $b0^-$ and includes all possible points on the path. A potential positive path resulting from a positive reversal point is also shown (dashed line) to indicate a full nonlinear, non-degrading cycle. The potential positive path results from a reversal point that does not exceed the threshold strain, γ_{e2}^- . Therefore both paths use the non-degrading branch curve rules described in the following paragraph and the equations provided in Table 2.

Once a reversal point has been detected, all of the segment parameters of the new potential stress–strain path are calculated, using the variables and coefficients in Table 2. The first segment is defined by the reversal point stress and strain and the modulus G_{b01} . The value of G_{b01} is relatively large, and is the product of a constant coefficient, $\rho_{G,b01}$, and G_{e02}^{opp} , the secant modulus for segment $e02$ of the opposite-direction envelope (in the figure G_{e02}^+ is shown because the branch curve is a negative one). The stress at the endpoint of the segment, v_{b1} , is the product of a constant coefficient, $\rho_{v,b1}$, and the stress at the reversal point, v_{b0} . Segment $b12$ is defined by its endpoints. It starts at point $b1$, defined above, and ends at point $b2$, which is located at point $e2^-$ on the negative envelope. The remaining segments, $b24$ and $b45$, lie on the envelope.

4.4. Degrading branch curves

A degrading branch curve exists if the maximum reversal strain has exceeded the threshold strain, γ_{e2} . The complexity in the branch curves depends on the value of the reversal strain. The simplest case occurs when a positive reversal (i.e. a loading direction change from negative to positive) occurs at a positive strain, in which case the path rejoins the envelope as directly as possible. The most complex path results from a maximum reversal strain exceeding γ_{e2} (Fig. 12 and Table 2), where the path is multi-linear and the modulus and the strength degrade with cycling. The degradation depends primarily on the magnitude of the current strain demand relative to a threshold strain, but also on the magnitude of the peak strain in the direction opposite to the loading direction. Fig. 7 illustrates the reduction in strength and modulus in the positive direction due to negative strain excursions. Smith [20] gives full details of all possible paths.

Fig. 12 shows a negative branch curve resulting from a large negative strain reversal. This curve is emphasized using a thick line; the prior stress–strain history is shown using a thin line. The branch curve consists of five segments, which extend from point $b0^-$ (reversal point) to point $b5^-$. Equations and rules that define the endpoint and tangent modulus of each segment are provided in Table 2. Some of the segment properties depend on the strain at, and/or the secant modulus to, the maximum reversal point reached so far, γ_{maxrev} and G_{maxrev} respectively. Therefore, these two variables must be updated when the strain reversal exceeds the current maximum strain reversal. This updating is done separately in each direction.

The following provides a description of each segment of a nonlinear degrading branch curve, as shown in Fig. 12 and defined in Table 2. The rules for segment $b01$ are identical to those used for non-degrading branch curves, described previously. The strength and tangent modulus of the remaining segments degrade. The tangent modulus of segment $b12$, G_{b12} , is the product of the constant coefficient $\rho_{G,b12}$ and the secant modulus to the maximum reversal point of the opposite-direction envelope, $G_{\text{maxrev}}^{\text{opp}}$. The stress and strain of the endpoint $b2$ are defined by the intersection with segment $b23$.

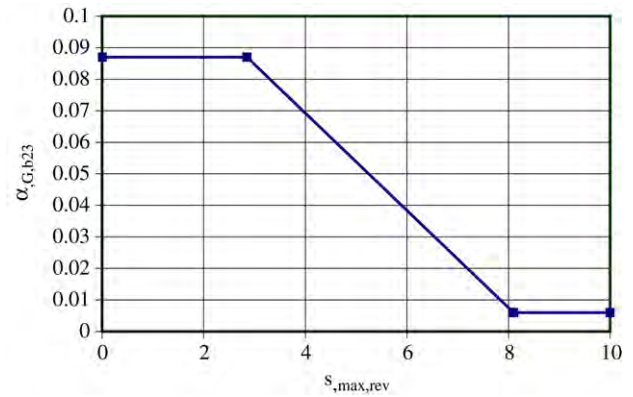


Fig. 13. Example of relation for stiffness degradation parameter.

The position and slope of segment $b23$, the central segment of the branch curve shown in the figure, are determined by the tangent modulus of the segment, G_{b23} , and stress intercept, v_{int} . Fig. 12 shows an example of the decrease in the modulus and strength of segment $b23^-$ resulting from a reversal strain in the second cycle that is larger than that of the first. In the constitutive model, the degraded modulus is defined as the product of the degrading coefficient $\alpha_{G,b23}$ and the secant modulus G_{e02}^{opp} , as indicated in Table 2. The stress intercept, v_{int} , is the product of the degrading coefficient $\alpha_{v,\text{int}}$ and stress v_{e2}^{opp} . These degrading coefficients are functions of ratios of strain relative to the maximum reversal strain. Values for the breakpoints in those relations are given in Table 4. For clarification, Fig. 13 shows the relationship between the stiffness degradation parameter, $\alpha_{G,b23}$ (used to calculate the modulus G_{b23}) and $s_{\text{max,rev}}$; details of other relationships are given in [3,19].

Segment $b34$ is defined by the tangent modulus G_{b34} and the constraint that the segment projects through the origin. The stress v_{b3} at point $b3$ is defined by the intercept with segment $b23$. The stress, v_{b4} , at the endpoint $b4$ is defined separately. Both the tangent modulus G_{b34} and the stress v_{b4} depend on the peak strain demands in both the current and opposite directions (Table 3). The degradation in the tangent modulus of the segment is expressed as the product of the two coefficients, $\alpha_{G,b34}$ and $\beta_{G,b34}$, and the secant modulus G_{maxrev} , as indicated in the equation in Table 2. The experimental data show that the degradation in this secant modulus is inversely proportional to the maximum strain ratio [3]. Therefore, the degrading coefficient $\alpha_{G,b34}$ depends on the inverse of the strain ratio $s_{b0,\text{maxrev}}$, i.e., $1/s_{b0,\text{maxrev}} = \gamma_{\text{maxrev}}/\gamma_{b0}$, as indicated in Table 3. The second degrading coefficient, $\beta_{G,b34}$, accounts for the degradation that occurs when the cyclic strain demands are highly asymmetric, as illustrated in Fig. 7.

Strength degradation of the joint shear stress curves was observed at large strain demands, as indicated in Fig. 7. Therefore v_{b4} is determined as the product of a degrading coefficient $\alpha_{v,b4}$ and the stress, v_{e2} . If no strength degradation is applied, the breakpoint lies on the intersection of a line with a slope of G_{b34} and the trilinear envelope. The coefficient $\alpha_{v,b4}$ degrades as a function of the strain ratio $s_{\text{maxrev},e2} = \gamma_{\text{maxrev}}/\gamma_{e2}$; breakpoint values for the trilinear function are

provided in Table 4. In addition, the strength degradation of v_{b4} is more marked in the direction opposite to that of the first excursion beyond the threshold strain, γ_{e2} . To model this behavior, the strength degradation parameter $\alpha_{v,b4}$ may be reduced using the coefficient $\beta_{v,b4}$. The coefficient $\beta_{v,b4}$ depends on the strain ratio $s_{\maxrev,e2}^{opp}$ which depends on strains in the opposite direction (as indicated by the *opp* superscript). This degrading coefficient is applied only once, when $s_{\maxrev,e2}^{opp}$ first exceeds 1.0. Therefore, $\beta_{v,b4}$ is considered a modifier on $\alpha_{v,b4}$ rather than directly on the stress v_{b4} . It is important to note that this degradation only affects response in one direction; for the other direction, the unmodified relationship is used.

The final segment of the branch curve is segment $b45$ which extends from point $b4$ and has a tangent modulus equal to that of segment $e23$. Equations for these parameters are provided in Table 2.

5. Model calibration

The experimental test data from Walker [22] and Alire [2] were used to calibrate the proposed constitutive model since they constitute one of the few data sets for joints without transverse reinforcement. This section describes the calibration procedure. For each input parameter, recommended values are proposed and provided in Table 4. Additional discussion of the implementation of the model can be found in the reference documents [3,20].

The parameters that were calibrated fell into one of four categories:

- (1) Fixed input parameters that define the envelope curve (e.g. γ_{e02} , G_{e02}).
- (2) Fixed coefficients, ρ , that define the ratio between an instantaneous branch curve segment property (such as G_{b01}) and a fixed property (such as G_{e02}^{opp}).
- (3) Degrading coefficients α that define the effects on a variable of cycling in the current direction and the corresponding strain ratios at the breakpoints in the α - s function.
- (4) Degrading coefficients β that define the effects on a variable of cycling in the opposite direction and the corresponding strain ratios at the breakpoints in the β - s function.

The fixed input quantities (categories 1 and 2, above) were chosen to be either constants or functions of the joint properties, such as dimensions, concrete strength or shear stress demand. The α and β coefficients were typically found to depend on the previous strain history. In each case it was necessary to identify the characteristic of that history that best described the dependence, and then to obtain a numerical relationship.

The calibration procedure was as follows. (Equations and further details of the error measures used are provided in [3].)

- (1) Identify the governing parameters for each model component (as described above).
- (2) Use trends in the measured data to establish initial estimates of the input values (e.g. γ_{e02}) and parameter relationships (e.g., the relationship between α_{Gb34} and the relevant strain ratio).

- (3) Minimize a local error measure to determine the best-fit equation and corresponding values for each model parameter. For example, a trilinear relationship was chosen to relate $\alpha_{G,b34}$ to the strain ratio $s_{bo,\maxrev}$. Each test series was treated separately and best-fit values were found for breakpoints that defined the multi-linear relationship. The error that was minimized in this operation was the difference between the measured and predicted values of $\alpha_{G,b34}$. Individual results were obtained for each test series, because the parameter value might depend on the joint properties. For example, the monotonic response (or envelope) curve depends on the joint shear stress demand but is independent of the displacement history. Therefore, all of the specimens within a test series (e.g., Test Series 1450) were used to develop a single best-fit calibration equation.
- (4) A global error measure was then minimized to refine the best-fit estimate. A weighted root-mean squared error measure was developed and calculated as the sum of the normalized squared differences between the measured and predicted stresses for each point in the joint shear strain history. Because small differences in the predicted initial stiffness can result in large relative differences in the predicted and measured stresses, each stress difference was weighted by the ratio of the initial and minimum secant shear moduli for the strain of interest, e.g., G_{01} to G_{\maxrev} . This permitted a more even weighting of the initial and latter stresses. The parameters were given initial values obtained from Step 3, and were then adjusted systematically to minimize this weighted root mean squared error.
- (5) The best-fit equations were then combined to develop a single recommended equation for each model parameter. For each parameter, the values obtained from each test individually were then averaged and used as starting values. The best fit value was the one that minimized the global root mean squared error measure for all of the tests.

The following discussion summarizes the resulting values for the recommended equations for each model component. The recommended values and equations for calculating each input parameter are provided in Table 4. Additional details may be found in [3].

The breakpoints on the envelope are determined by shear stress (v) and strain (γ) input values at points $e1$ and $e2$, respectively, which represent significant changes in the measured curve. The secant modulus to the first breakpoint (G_{e01}) is approximately half of the elastic shear modulus. While a value of 100% of the elastic shear modulus might be expected, the experimental data show clearly that the value is significantly smaller. This reduction is likely caused by internal; micro-cracking, although the cause of it is not known for certain. Restrained shrinkage provides a possible explanation, because the beam and column bars provide a relatively rigid frame around the joint region and would inhibit its contraction. No shrinkage cracks were observed on the faces of the joints prior to testing, but micro-cracks could nonetheless have been present but not detected.

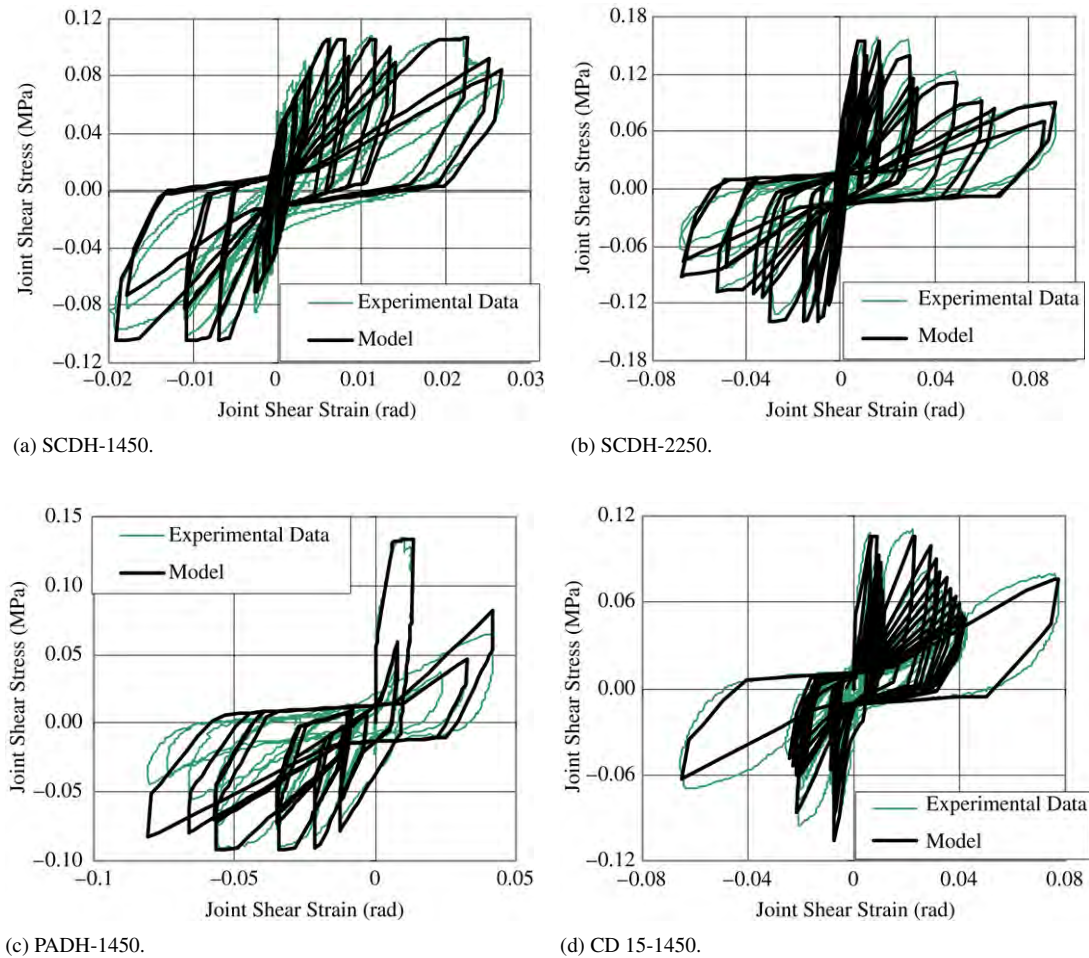


Fig. 14. Measured and predicted joint shear response for selected specimens.

The first breakpoint stress, v_{e1} , is $0.48\sqrt{f'_c}$ MPa. The second breakpoint stress, v_{e2} , is 95% of the theoretical peak joint shear stress demand ($0.95c_j\sqrt{f'_c}$) with an upper bound of $2.4\sqrt{f'_c}$ MPa where c_j is the joint shear stress coefficient. The threshold strain γ_{e2} is 0.006 rad. For the third segment, the recommended value of the modulus ratio $\rho_{G,e23}$ is 0.015, i.e., the tangent modulus of the third segment of the envelope is 1.5% of the secant modulus to the second breakpoint on the envelope (G_{e02}).

Table 4 also provides the input values for the non-degrading coefficients, ρ , and for the relationships between the degrading coefficients α and β and the strain ratios on which they depend. These relations are multilinear. Further discussion regarding the development of these relationships is detailed in [3].

6. Model validation

The experimental data [2,22] were compared to the response predicted by the constitutive model using the equations in Table 4. These data are the same as those used to develop and calibrate the model, so on that basis the fit might be expected to be good. However, the combined data sets contained joint shear stress demands that covered a range of 5 to 1, two different concrete strengths and four radically different cyclic displacement histories, and so the task of developing a single

model to fit all the data was not trivial. The results are illustrated in Fig. 14(a)–(d).

Fig. 14(a) shows the measured and predicted responses of Specimen SCDH-1450 which represents an average level of joint shear stress demand, approximately equal to the ACI limit. Specimen SCDH-2250 (Fig. 14(b)) represents a larger joint shear stress demand, which may sometimes be found in older construction [18]. The model captures the measured response well in both cases, and the degradation in response caused by the higher joint shear stress, in both the measured and predicted response, is clear.

Anderson [3] found that, while other constitutive models may be able to replicate response to standard symmetric deformation histories, unconventional histories provide a greater challenge. In some cases, those models lack rules to govern response under some of the circumstances that might arise. By contrast, the proposed model is capable of modeling response to a wide range of shear strain histories, which represents a significant advance. To illustrate this capability, the measured and predicted responses of specimens PADH-1450 and CD15-1450 are shown in Fig. 14(c) and (d) respectively. The model is capable of predicting both the slow degradation exhibited by the constant displacement loading of CD15-1450 and the response to the highly asymmetric loading of PADH-

1450. The predicted strength and shear moduli of the negative stress–strain curves of the final cycles of the PADH-1450 are larger than the measured values. However, these cycles result from displacement cycles to 4% and 5% drift that were applied following a cycle to 5% drift in the opposite direction, so they represent extreme behavior. It is also worth noting that the peak measured joint shear strain (8%) was larger than the corresponding column drift ratio (5%), indicating that the joint damage was severe and that the measured data were becoming questionable, which likely resulted from damage to the joint concrete in which the instruments were embedded. The modeling predicted the measured response well during the large drift pulse and in the lower shear strain cycles that follow it, which was judged to be more useful in practice.

Independent experimental data were sought for objective validation of the model. However, no recorded shear stress–strain data could be found for joints without transverse reinforcement. Although previous tests on joints without transverse reinforcement have been conducted, e.g. [5], the local shear stress–strain response data were not available and therefore could not be used in this research study. Furthermore, the reinforcement details in those test specimens contained many different deficiencies, any one of which could have controlled the failure mode. This characteristic would render them unsuitable for validating a model of the joint alone, even if the joint strain data were available. The closest available were data from a lightly reinforced specimen tested by Leon [14]. Although the test specimen did include transverse reinforcement, use of the data was deemed appropriate because (1) the specimen's joint shear stress data were available and (2) the amount and spacing of transverse reinforcement was such that its impact on the response was expected to be minimal. The specimens had a peak joint shear stress demand of approximately $1.25\sqrt{f'_c}$ MPa ($15\sqrt{f'_c}$ psi) and a relatively low volumetric joint reinforcement ratio (0.6%, or approximately one third of the amount required by Chapter 21 of CI 318-05). The model input was based on the values and equations provided in Table 4 and on the specimen properties. Fig. 15 shows the measured and predicted responses of the specimen. The model predicts the cyclic response well, including the pinching of the response and the degradation in the strength and modulus.

7. Summary and conclusions

7.1. Summary

A constitutive model for shear stress and strain in beam–column joints without transverse reinforcement was developed to improve the simulation, and therefore the performance assessment, of non-ductile reinforced concrete frame buildings. Under cyclic loading, these joints may exhibit significant strength and stiffness degradation. Currently available constitutive models are not capable of accurately simulating this degradation. Using available experimental data, a constitutive model that explicitly accounts for the effects of the cyclic strain history was developed. The model is capable

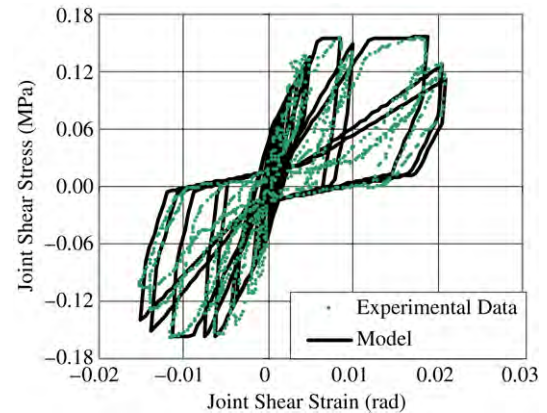


Fig. 15. Measured and predicted response of specimen BCJ2 [14].

of predicting accurately the cyclic response of the joint for a wide range of displacement histories, joint shear stress demands and concrete strengths. The model was validated using an independent data set.

The model includes an envelope curve to model the monotonic response, and non-degrading and degrading branch curves. A series of equations was developed for each component of the model. These equations were calibrated using experimental data and were then simplified for general application of the model.

To properly model the cyclic response, degradation in the strength and shear modulus was explicitly included in the branch curves. The degradation equations are updated using only a single point of the previous strain history (e.g., the maximum reversal strain to date) rather than the entire strain history. In that respect, the model provides a reasonably simple method of accounting for cyclic degradation that avoids complexities like counting cycles or tracking energy.

7.2. Conclusions

Based on the research, the following conclusions were drawn about the response of, and modeling requirements for beam–column joints without transverse reinforcement.

- At low joint shear strain demands, the response is linearly elastic with a shear modulus of approximately half of the elastic shear modulus.
- Cycles below a threshold strain level do not induce degradation in the response.
- For cycles that exceed the threshold strain, the cyclic degradation depends on the strain history. Modeling this degradation requires tracking the strain history variables, including the maximum and reversal strains, but does not require counting cycles or computing energy.
- Degradation in the modulus of the branch curves of the cyclic response results from an increase in the strain demand beyond the previous maximum and depends on the cyclic strain demand history.
- Degradation in the modulus and strength of the central segment of the degrading branch curves depends on the maximum strain demand and is not affected by cycling.

- During asymmetric cycling, the response in one direction is influenced by the half cycles in the opposite direction, if the threshold strain level is exceeded.
- The joint shear stress demand influences the degree of strength degradation as well as the stress–strain breakpoints that characterize the envelope curve.
- Degradation in the tangent modulus of each segment of the branch curves, including the pinching response, is not affected by the joint shear stress demand.

The proposed model provides a rational mechanism for including joint shear deformations in a cyclic analysis of the in-plane response of a non-ductile reinforced concrete frame. It replicates well the response of tests that used a wide range of variables, but a frame model that incorporates it requires more degrees of freedom than a simple, centerline model. In some cases, a simpler numerical model is preferable and attempts are being made to create a centerline model that uses effective stiffnesses to replicate as best as possible the additional frame displacement resulting from deformation of the beam–column joint.

Acknowledgements

The research was supported by NSF under Award Number EEC-9701568 through the PEER center and the Valle Scholarship program at the University of Washington. This support is gratefully acknowledged. The authors would also like to thank Steve Smith for his assistance in refining the model nomenclature and operation.

References

- [1] ACI Committee 318. Building code requirements for structural concrete (ACI 318-02) and commentary (ACI 318R-02). Farmington Hills (MI): ACI; 2002. p. 443.
- [2] Alire Daniel A. Seismic evaluation of existing unconfined reinforced concrete beam–column joints. MSCE thesis. Department of Civil and Environmental Engineering, University of Washington; 2002. p. 291.
- [3] Anderson MA. Analytical modeling of existing reinforced concrete beam–column joints. MSCE thesis. Department of Civil and Environmental Engineering, University of Washington; 2003. p. 308.
- [4] Anderson MA, Smith S, Lehman DE, Stanton JF. Development and calibration of a joint shear stress–strain model for reinforced concrete beam–column joints. Report no. SM 04-02. Seattle (WA): Department of Civil Engineering, University of Washington; 2004.
- [5] Beres A, White RN, Gergely P. Seismic behavior of reinforced concrete frame structures with nonductile details: Part I — Summary of experimental findings of full scale beam–column joint tests. Report NCEER-92-0024. NCEER, State University of New York at Buffalo; 1992.
- [6] Carr AJ. Ruaumoko: The Maori God of volcanoes and earthquakes, 2-dimensional version. New Zealand: University of Canterbury; 2002.
- [7] Durrani AJ, Wight JK. Behavior of interior beam-to-column connection under earthquake-type loading. ACI J 1985;82(3):343–9. Title no. 82–30, Farmington Hills (MI): ACI.
- [8] Ehsani MR, Wight JK. Exterior R/C beam-to-column connections subjected to earthquake-type loading. ACI J 1985;82(4):492–9. Title no. 82–43, Farmington Hills (MI): ACI.
- [9] FEMA 356. Prestandard and commentary for the seismic rehabilitation of buildings. Prepared by the American Society of Civil Engineers, Washington (DC): Federal Emergency Management Agency; 2000. FEMA Publication No. 356.
- [10] Ghobarah A, Biddah A. Dynamic analysis of reinforced concrete frames including joint shear deformation. Engineering Structures 1999;21: 971–87.
- [11] Hanson N, Connor H. Seismic resistance of reinforced concrete beam–column joints. Proc ASCE, J Struct Div 1967;93(ST5):533–60.
- [12] Kunnath SK. IDARC. Inelastic damage analysis of RC Frames shear-wall structures. Computer program. <http://civil.eng.buffalo.edu/idarc2d50/>.
- [13] Kunnath SK. Macromodel-based nonlinear analysis of reinforced concrete structures. In: Structural engineering worldwide. Oxford (England): Elsevier Science; 1998. Paper no. T101-5 [computer file].
- [14] Leon RT. Shear strength and hysteretic behavior of interior beam–column joints. ACI Str J 1990;87(1):3–11.
- [15] Lowes LN, Altoontash A. Modeling reinforced concrete beam–column joints subjected to cyclic loading. ASCE J Struct Eng 2003;129(12): 1686–97; ASCE J Struct Eng 2005;131:993 [Discussion].
- [16] Meinheit DF, Jirsa JO. Shear strength of RC beam–column connections. Proc ASCE, J Struct Div 1981;107(ST11).
- [17] Mitra N, Lowes LN. Evaluation, calibration and verification of a reinforced concrete beam–column joint model. J Struct Eng ASCE [submitted for publication].
- [18] Mosier WG. Seismic assessment of reinforced concrete beam–column joints. MSCE thesis. Dept. of Civil and Environmental Engineering, University of Washington; 2000. p. 218.
- [19] Prakash V, Powell GH, Campbell SD. 1993. DRAIN 2DX. <http://nisee.berkeley.edu/elibrary/getdoc?id=DRAIN2DXZIP>.
- [20] Smith S. Models for the performance evaluation of older reinforced concrete beam–column joints. MSCE thesis. Dept. of Civil and Environmental Engineering, University of Washington; 2004.
- [21] Stewart WG, Dean JA, Carr AJ. The seismic behaviour of plywood sheathed shearwalls. Bull New Zealand N Soc Earthquake Eng 1986; 19(1):48–62.
- [22] Walker SG. Seismic performance of existing reinforced concrete beam–column joints. MSCE thesis. Dept. of Civil and Environmental Engineering, University of Washington; 2001. p. 300.

Table 1. Default Values of the Parameters Used

Parameter	Unconfined ($K=1$) (compression)	Confined ($K>1$) (compression)	Tension
Peak stress	f'_c	$f'_{cc}=Kf'_c$	$f'_t=0.625\sqrt{f'_c(\text{MPa})}$; $f'_t=7.5\sqrt{f'_c(\text{psi})}$
Peak strain	$\epsilon_{co}=0.0015+f'_c(\text{MPa})/70,000^a$; $\epsilon_{co}=0.0015+f'_c(\text{psi})/10^7$	$\epsilon_{cc}=\epsilon_{co}[1+5(K-1)]^b$	$\epsilon_{ct}=0.1\epsilon_{co}$
Ultimate stress	$f_{c1}=12\text{ MPa}=1.74\text{ ksi}^a$	$f_{cu}=12+f'_c(K-1)^c$	$f_{t1}=f'_t/3^d$
Ultimate strain	$\epsilon_{c1}=0.0036^a$	$\epsilon_{cu}=5\epsilon_{cc}^c$	$\epsilon_{t1}=2\epsilon_u/9^d$
Failure strain ^e	$\epsilon_{sp}=0.012-0.0001f'_c(\text{MPa})$; $\epsilon_{sp}=0.012-7\times 10^{-7}f'_c(\text{psi})$	$\epsilon_f=0.004+\epsilon_{cu}$	$\epsilon_u=18 G_f/(5f'_t h)^d$

^aBased on predicted stress-strain relation of normal-weight concrete (Collins and Mitchell 1994).

^bMander et al. (1988a,b).

^cBased on reevaluation of data from Mander et al. (1988a) and Li et al. (2000).

^dRots et al. (1985), where G_f =fracture energy= $h\times$ area under stress-strain softening diagram, and h =crack band width.

^eFailure stress=0 for all cases.

these are the peak strength (ϵ_{co}, f'_c), at the termination of the postpeak branch (ϵ_{c1}, f_{c1}), and the failure strain ($\epsilon_{sp}, 0$). Similarly, for confined concrete the corresponding principal control coordinates are (ϵ_{cc}, f'_{cc}), (ϵ_{cu}, f_{cu}), and ($\epsilon_f, 0$). Using these coordinates as commencement and termination points, the proposed stress-strain model has three branches—an initial power curve up to the peak stress, followed by a bilinear relation in the postpeak region. The expressions representing concrete stresses as a function of strain are

$$0 \leq x < 1; \quad f_c = Kf'_c(1 - |1 - x|^n) \quad (1)$$

$$1 \leq x < x_u; \quad f_c = Kf'_c - \left(\frac{Kf'_c - f_{cu}}{x_u - 1} \right) (x - 1) \quad (2)$$

$$x_u \leq x < x_f; \quad f_c = f_{cu} \left(\frac{x - x_f}{x_u - x_f} \right) \quad (3)$$

in which f_{cu} =stress corresponding to hoop fracture strain ϵ_{cu} ; K =confinement ratio and for confined concrete ($K>1$); x =normalized strain, where $x=\epsilon_c/\epsilon_{cc}$; $x_u=\epsilon_{cu}/\epsilon_{cc}$; and $x_f=\epsilon_f/\epsilon_{cc}$, where ϵ_{cc} and ϵ_f =strain at maximum confined strength of concrete $f'_{cc}=Kf'_c$ and final failure strain of confined concrete, respectively; and $n=E_c\epsilon_{co}/f'_c$ and $n=E_c\epsilon_{cc}/f'_{cc}$ for unconfined and confined concrete, respectively, where $E_c=5,000\sqrt{f'_c(\text{MPa})}=60,000\sqrt{f'_c(\text{psi})}$ =concrete modulus. For unconfined concrete ($K=1$), $\epsilon_{cc}=\epsilon_{co}$, $\epsilon_{cu}=\epsilon_{c1}$, $\epsilon_f=\epsilon_{sp}$, and $f_{cu}=f_{c1}$ in all of the above equations [refer to Fig. 1(b)].

In the present widely used Mander model (Mander et al. 1988b), the governing stress-strain relation lacks the necessary control over the slope of the postpeak branch. This is particularly the case for high-strength concrete as pointed out by Li et al. (2001). It is for this reason and also the ease of algebraic manipulation the above equations are proposed. Proposed default values for the parameters in Eqs. (1)–(3) are defined in Table 1. The expression for f_{cu} was calibrated using data from full-scale experimental results of Mander et al. (1988a) and Li et al. (2000) and adjusted to essentially conform to the widely used original Mander model.

For the stress-strain model of unconfined concrete in tension, the same model as described above for unconfined concrete in compression can be used by replacing the terms (ϵ_{to}, f'_t), (ϵ_{t1}, f_{t1}), and ($\epsilon_u, 0$) for their corresponding terms in compression. Measured values or as a good approximation the values from Table 1 may be used.

In the analysis of moments and axial loads, two different models of the stress-strain performance of the reinforcing steel may be adopted. For nominal design capacities, an elastoplastic model is

customarily adopted to provide a dependable estimate for design. For “exact” analysis of existing reinforced concrete members, a realistic stress-strain model should be adopted using expected values of the control parameters. Fig. 1(c) represents such a model and is conveniently cast in the form of a single equation as follows:

$$f_s = \frac{E_s \epsilon_s}{\left\{ 1 + \left| \frac{E_s \epsilon_s}{f_y} \right|^{20} \right\}^{0.05}} + (f_{su} - f_y) \left[1 - \frac{|\epsilon_{su} - \epsilon_s|^P}{\{ |\epsilon_{su} - \epsilon_{sh}|^{20P} + |\epsilon_{su} - \epsilon_s|^{20P} \}^{0.05}} \right] \quad (4)$$

where

$$P = \frac{E_{sh}(\epsilon_{su} - \epsilon_{sh})}{(f_{su} - f_y)} \quad (5)$$

in which f_s , ϵ_s =stress and strain in steel; E_s and E_{sh} =Young's modulus of elasticity and strain hardening modulus, respectively; f_y and f_{su} =yield strength and ultimate strength of reinforcing steel; and ϵ_{sh} and ϵ_{su} =strain hardening strain and ultimate strain, respectively.

Equivalent Rectangular Stress-Block Parameters

Stress-block parameters can be easily derived using Eqs. (1)–(3) for a wide range of maximum strains as shown in Fig. 2. The force in concrete (C_c) for a known value of maximum strain can be expressed in terms of equivalent stress-block parameters α and β such that $C_c = \alpha f'_c \beta c b$, where c =depth to the neutral axis from the top concrete fiber in compression and b =breadth of the section as shown in Fig. 1(a). The stress-block parameters can be found from taking the first and second moments of area of the stress-strain relations which lead to the following results:

$$\alpha \beta = \frac{\int_0^{\epsilon_c} f_c d\epsilon_c}{f'_c \epsilon_c} \quad (6)$$

and

$$\beta = 2 - 2 \frac{\int_0^{\epsilon_c} f_c \epsilon_c d\epsilon_c}{\epsilon_c \int_0^{\epsilon_c} f_c d\epsilon_c} \quad (7)$$

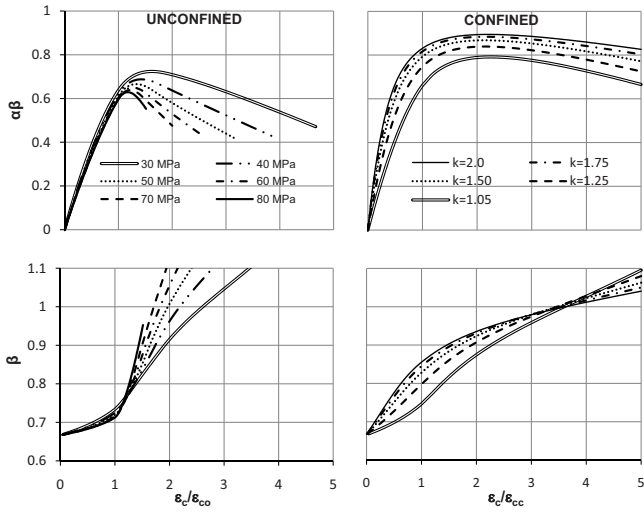


Fig. 2. Stress-block parameters for unconfined and confined concrete

Carrying out the integration in Eqs. (6) and (7) using the stress-strain relations (1)–(3) gives the stress-block relations as follows:

1. For $0 \leq x < 1$

$$\alpha\beta = 1 + \frac{(1-x)^{n+1} - 1}{x(n+1)} \quad (8)$$

$$\beta = 2 - \frac{2}{x^2\alpha\beta} \left[\frac{x^2}{2} + \frac{x(1-x)^{n+1}}{(n+1)} + \frac{(1-x)^{n+2} - 1}{(n+1)(n+2)} \right] \quad (9)$$

2. For $1 \leq x < x_u$

$$\alpha\beta = \frac{A_1}{x} - \frac{x-1}{x(x_u-1)} \left[A_2 - x_u + \frac{x}{2} \left(1 - \frac{f_{cu}}{Kf'_c} \right) \right] \quad (10)$$

$$\beta = 2 - \frac{1}{x^2\alpha\beta} \left[B_1 + (x^2 - 1) - \left(1 - \frac{f_{cu}}{Kf'_c} \right) \left(\frac{2x^3 - 3x^2 + 1}{3(x_u - 1)} \right) \right] \quad (11)$$

3. For $x_u \leq x < x_f$

$$\alpha\beta = \frac{A_1}{x} + A_2 \left(\frac{x_u - 1}{x} \right) + \frac{f_{cu}}{Kf'_c} \left(\frac{(x - x_u)(x + x_u - 2x_f)}{2x(x_u - x_f)} \right) \quad (12)$$

$$\beta = 2 - \frac{1}{x^2\alpha\beta} \left[B_1 + B_2 + B_3 + \frac{f_{cu}}{Kf'_c} \left(\frac{3x_f x_u^2 - 2x_u^3 + x^2(2x - 3x_f)}{3(x_u - x_f)} \right) \right] \quad (13)$$

4. For $x \geq x_f$

$$\alpha\beta = \frac{A_1}{x} + A_2 \left(\frac{x_u - 1}{x} \right) + \frac{f_{cu}}{Kf'_c} \left(\frac{x_f - x_u}{2x} \right) \quad (14)$$

$$\beta = 2 - \frac{B_1 + B_2 + B_3 + B_4}{x^2\alpha\beta} \quad (15)$$

In the above, the following coefficients are used:

$$A_1 = \frac{n}{(n+1)} \quad (16)$$

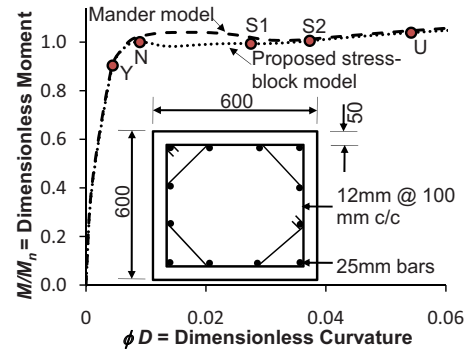


Fig. 3. Comparison of moment-curvature results

$$A_2 = \frac{1}{2} \left(1 + \frac{f_{cu}}{Kf'_c} \right) \quad (17)$$

$$B_1 = \frac{n(n+3)}{(n+1)(n+2)} \quad (18)$$

$$B_2 = (x_u^2 - 1) \quad (19)$$

$$B_3 = \left(\frac{f_{cu}}{Kf'_c} - 1 \right) \left(\frac{2x_u^3 - 3x_u^2 + 1}{3(x_u - 1)} \right) \quad (20)$$

$$B_4 = \frac{f_{cu}}{Kf'_c} \left(\frac{3x_f x_u^2 - 2x_u^3 - x_f^3}{3(x_u - x_f)} \right) \quad (21)$$

The stress-block parameters for unconfined and confined concrete are shown in Fig. 2. Note that calculation of the strength enhancement factor (K) should be performed in accordance with any acceptable concrete model, for example, Mander et al. (1988b) and Li et al. (2001).

Numerical Example

An example of the proposed stress-block approach for generating moment-curvature results for a square column with the following properties is performed. The section properties are breadth and height=600 mm, clear cover=50 mm to the hoops of diameter $d_s=12$ mm, and stirrup spacing $s=100$ mm containing 12 symmetrically placed longitudinal rebars of diameter $d_b=25$ mm. Concrete properties are [refer to Fig. 1(b)] $f'_c=30$ MPa, $\epsilon_{co}=0.0019$, $\epsilon_{sp}=0.009$, $f'_{cc}=45$ MPa, $\epsilon_{cc}=0.00675$, and $E_c=27387$ MPa (the above parameters were calculated using the expressions presented earlier). The longitudinal reinforcing steel properties are [refer to Fig. 1(c)] $f_y=430$ MPa, $E_s=200,000$ MPa, $f_u=650$ MPa, $\epsilon_u=0.12$, $\epsilon_{sh}=0.008$, and $E_{sh}=8,000$ MPa. The axial load on the column is 2,000 kN $=0.185f'_cA_g$.

In the hand computations for the example considered above, for a value of $K=1.5$, and at the first yield strain of steel ϵ_y (“Y” in Fig. 3), the values of the stress blocks were $\alpha=0.828$ and $\beta=0.724$ for unconfined concrete and $\alpha=0.470$ and $\beta=0.702$ for confined concrete. Hand computations were also performed at the following values of the strain: strain at the extreme cover concrete fiber $\epsilon_{max}=0.003$ and ϵ_{sp} (“N” and “S1,” respectively in Fig. 3) and strain at the extreme confined concrete fiber $\epsilon_{max}=\epsilon_{sp}$ and $2\epsilon_{cc}$ (“S2” and “U,” respectively, in Fig. 3). In order to implement the iterative computational procedure to obtain the moment-

curvature relation, a computer program was also developed. A comparison of the stress-block analysis results is presented in Fig. 3.

The differences noted in the moment-curvature results between the proposed model and the classic model of Mander et al. (1988b) are ascribed to differences in modeling the falling branch of the cover concrete of the latter. The hand computations performed using the constitutive equations for the stress-block parameters give an accurate match with the computational moment-curvature results.

Closing Remarks

The proposed analytic stress-strain relation represents well the behavior of both normal strength and high-strength concrete in their unconfined and confined states. The stress-strain relations can be easily inverted to represent the strain as a function of stress. More importantly, the stress-strain model can also be conveniently integrated in order to obtain the stress-block parameters. The stress-block parameters were used in hand computations to obtain points on the moment-curvature relation and these results agree well with a computational fiber analysis. The approach makes it possible to rapidly perform “spot checks” by hand analysis to verify computational results, a necessary step in any formal structural design verification.

References

- ACI Committee 318. (2005). “Building code requirements for structural concrete (318-05) and commentary.” *ACI 318R-05*, Farmington Hills, Mich.
- Collins, M. P., and Mitchell, D. (1994). *Prestressed concrete structures*, Prentice-Hall, Englewood Cliffs, N.J.
- Li, B., Park, R., and Tanaka, H. (2000). “Constitutive behavior of high-strength concrete under dynamic loads.” *ACI Struct. J.*, 97(4), 619–629.
- Li, B., Park, R., and Tanaka, H. (2001). “Stress-strain behavior of high-strength concrete confined by ultra-high and normal-strength transverse reinforcements.” *ACI Struct. J.*, 98(3), 395–406.
- Mander, J. B., Priestley, M. J. N., and Park, R. (1988a). “Observed stress-strain behavior of confined concrete.” *J. Struct. Eng.*, 114(8), 1827–1849.
- Mander, J. B., Priestley, M. J. N., and Park, R. (1988b). “Theoretical stress-strain model of confined concrete.” *J. Struct. Eng.*, 114(8), 1804–1826.
- Park, R., and Paulay, T. (1975). *Reinforced concrete structures*, Wiley, New York.
- Rots, J. G., Nauta, P., Kusters, G. M. A., and Blaauwendraad, J. (1985). “Smearred crack approach and fracture localization in concrete.” *Heron*, 30(1), 1–48.
- Whitney, C. S. (1942). “Plastic theory of reinforced concrete design.” *Proc., ASCE, Transactions ASCE*, Vol. 107, ASCE, New York, 251–326.

This article was downloaded by: [University of Auckland Library]

On: 21 June 2012, At: 14:48

Publisher: Taylor & Francis

Informa Ltd Registered in England and Wales Registered Number: 1072954 Registered office: Mortimer House, 37-41 Mortimer Street, London W1T 3JH, UK



Journal of Earthquake Engineering

Publication details, including instructions for authors and subscription information:

<http://www.tandfonline.com/loi/ueqe20>

Modeling Beam-Column Joints in Fragility Assessment of Gravity Load Designed Reinforced Concrete Frames

Ozan Cem Celik ^a & Bruce R. Ellingwood ^a

^a School of Civil and Environmental Engineering, Georgia Institute of Technology, Atlanta, Georgia, USA

Available online: 04 Apr 2008

To cite this article: Ozan Cem Celik & Bruce R. Ellingwood (2008): Modeling Beam-Column Joints in Fragility Assessment of Gravity Load Designed Reinforced Concrete Frames, Journal of Earthquake Engineering, 12:3, 357-381

To link to this article: <http://dx.doi.org/10.1080/13632460701457215>

PLEASE SCROLL DOWN FOR ARTICLE

Full terms and conditions of use: <http://www.tandfonline.com/page/terms-and-conditions>

This article may be used for research, teaching, and private study purposes. Any substantial or systematic reproduction, redistribution, reselling, loan, sub-licensing, systematic supply, or distribution in any form to anyone is expressly forbidden.

The publisher does not give any warranty express or implied or make any representation that the contents will be complete or accurate or up to date. The accuracy of any instructions, formulae, and drug doses should be independently verified with primary sources. The publisher shall not be liable for any loss, actions, claims, proceedings, demand, or costs or damages whatsoever or howsoever caused arising directly or indirectly in connection with or arising out of the use of this material.

Modeling Beam-Column Joints in Fragility Assessment of Gravity Load Designed Reinforced Concrete Frames

OZAN CEM CELIK and BRUCE R. ELLINGWOOD

School of Civil and Environmental Engineering, Georgia Institute
 of Technology, Atlanta, Georgia, USA

Reinforced concrete (RC) frame structures customarily have been designed in regions of low-to-moderate seismicity with little or no consideration of their seismic resistance. The move toward performance-based seismic engineering requires accurate reliability-based structural analysis models of gravity load designed (GLD) RC frames for predicting their behavior under seismic effects and for developing seismic fragilities that can be used as a basis for risk-informed decision-making. This analytical approach requires particular attention to the modeling of beam-column joints, where GLD frames differ significantly from their counterparts in high-seismic areas. This article focuses on modeling shear and bond-slip behavior of beam-column joints for purposes of seismic fragility analysis of GLD RC frames. The joint panel constitutive parameters are defined to replicate the experimental joint shear stress-strain relationships, while the effect of bond-slip is taken into account through a reduced envelope for the joint shear stress-strain relationship. The joint model is validated using two full-scale experimental RC beam-column joint test series. A fragility assessment of an existing three-story GLD RC frame reveals the importance of modeling shear, anchorage, and bond-slip in joints of GLD frames accurately when performing seismic risk assessments of buildings.

Keywords Beam-column Joints; Building Frames; Concrete, Reinforced; Earthquake Engineering; Engineering Mechanics; Fragility; Reinforcement Anchorage; Bond-slip; Shear Stress

1. Introduction

In the Central and Eastern United States (CEUS), reinforced concrete (RC) frame structures traditionally have been designed using detailing provisions of ACI Standard 318 for the gravity load combination $1.4D + 1.7L$ with little or no consideration of seismic resistance [Hoffmann *et al.*, 1992]. In the event of an earthquake in this region, the expected deficiency in seismic performance of gravity load designed (GLD) RC frames has been widely attributed to reinforcing details that are typical in this type of construction. In one study, Beres *et al.* [1992] reviewed detailing manuals (ACI 315) and design codes (ACI 318) from the past five decades. Based on this review and consultation with practicing structural engineers, the following problematic reinforcing details that are typical in GLD RC frames were identified: (1) little or no transverse shear reinforcement is provided within the beam-column joints; (2) beam bottom reinforcement is terminated within the beam-column joints with a short embedment length; (3) columns have bending moment capacities close to or less than those of the joining beams, promoting column-sidesway or soft-story mechanisms; (4) the longitudinal reinforcement ratio is seldom more than 2% in

Received 19 April 2006; accepted 24 April 2007.

Address correspondence to Bruce R. Ellingwood, School of Civil and Environmental Engineering, Georgia Institute of Technology, Atlanta, GA 30332-0355, USA; E-mail: ellingwood@gatech.edu

columns; (5) there is minimal transverse reinforcement to provide shear resistance and confinement; (6) lightly confined lapped splices of column reinforcement are placed in potential plastic hinge zones just above the floor levels; and (7) construction joints are placed below and above the beam-column joints.

Finite element-based structural models of GLD RC frames must incorporate the critical details in predicting the response of such frames under earthquake loading. The need for such models is becoming apparent with the move toward performance-based seismic engineering and the use of seismic fragility assessment in decision-making [Wen and Ellingwood, 2005]. Previous research [Pessiki *et al.*, 1990; Beres *et al.*, 1992, 1996; Bracci *et al.*, 1992a,b, 1995; Hoffmann *et al.*, 1992; Kunnath *et al.*, 1995a,b] on the seismic performance of such frames has revealed that: (1) the first four details listed above are critical in making such frames vulnerable to seismic demands; (2) the lack of adequate transverse reinforcement has only a marginal effect on performance (confinement of the concrete core by transverse reinforcement can be taken into account through confined concrete models such as the modified Kent and Park model [Park *et al.*, 1982] in fiber models); and (3) previous tests have not pointed to lapped splices and construction joints as a source of poor behavior. Of the nonductile reinforcing details that make GLD RC frames vulnerable to seismic demands (i.e., the first four of the nonductile reinforcing details listed above), the latter two are reflected explicitly in existing finite element platforms. However, additional modeling is required to capture the inadequate joint shear capacity that results from a lack of transverse shear reinforcement and the insufficient positive beam bar anchorage, in the finite element model.

This article focuses on modeling shear and bond-slip behavior of the beam-column joints in GLD RC frames for purposes of modeling seismic fragilities and predicting damage state probabilities. Following a review of the literature on models for simulating the RC beam-column joint response, a joint model is developed that is based on the experimental determination of joint panel shear stress-strain relationship. The panel zone constitutive parameters are defined to replicate the experimental joint shear stress-strain relationships, eliminating the need for further calibration, while the effect of bond-slip is taken into account through a reduced envelope for the joint shear stress-strain relationship. The application of the modeling scheme is validated on two full-scale experimental RC beam-column joint test series. A fragility analysis of a three-story GLD RC frame in which the proposed beam-column joint model is employed demonstrates the importance of modeling shear and bond-slip behavior in joints when performing seismic risk assessments of GLD frames.

2. Review of Beam-Column Joint Modeling in GLD RC Frames

Beam-column joint behavior is governed by shear and bond-slip in GLD RC frames. The typical practice of providing little or no joint shear reinforcement leads to shear deformations in the panel zone that may be substantial. This practice also leads to joint shear failure that can restrict the utilization of the flexural capacities of the joining beams and columns. Moreover, the common practice of terminating the beam bottom reinforcement within the joints makes the bottom reinforcement prone to pullout under a seismic excitation. Insufficient beam bottom bar anchorage precludes the formation of bond stresses necessary to develop the yield stress in the beam bottom reinforcement. Thus, the positive beam moment capacity cannot be utilized. Models of RC beam-column joint response that have been proposed in the literature are reviewed in the following.

Hoffmann *et al.* [1992] and Kunnath *et al.* [1995a] modified the flexural capacities of the beams and columns of GLD RC frames to model insufficient positive beam bar

anchorage and inadequate joint shear capacity implicitly. To account for insufficient positive beam bar anchorage, the pullout moment capacity of the beam was approximated as the ratio of the embedment length to the required development length per ACI 318–89 [ACI Committee 318, 1989] multiplied by the yield moment of the section. This approximation required that the yield strength of the discontinuous steel be reduced by the ratio of the actual to the required anchorage length. To model inadequate joint shear capacity, the flexural capacities of the beams and columns framing into the joint were reduced to a level that would induce shear failure of the joint. The proposed procedure was utilized in inelastic dynamic time history analyses of typical three-, six-, and nine-story GLD RC frames, which revealed that they are susceptible to damage from joint shear failures and weak column-strong beam effects leading to soft-story collapses.

Alath and Kunnath [1995] modeled the joint shear deformation with a rotational spring model with degrading hysteresis. The finite size of the joint panel was taken into account by introducing rigid links (see Fig. 1(a)). The envelope to the shear stress-strain relationship was determined empirically, whereas the cyclic response was captured with a hysteretic model that was calibrated to experimental cyclic response. The model was validated through a comparison of simulated and experimental response of a typical GLD RC frame interior beam-column joint subassembly.

Biddah and Ghobarah [1999] modeled the joint shear and bond-slip deformations with separate rotational springs (see Fig. 1(b)). The shear stress-strain relationship of the joint was simulated using a tri-linear idealization based on a softening truss model [Hsu, 1988], while the cyclic response of the joint was captured with a hysteresis relationship with no pinching effect. The bond-slip deformation was simulated with a bilinear model based on previous analytical and experimental data. The cyclic response of the bond-slip spring was captured with a hysteresis relationship that accounts for pinching effects. The model was validated using experimental data on exterior joints of ductile and nonductile frames. Ghobarah and Biddah [1999] utilized this joint element in performing dynamic analyses of three- and nine-story GLD RC buildings, designed to be typical of office buildings constructed during the 1960's in North America and containing the nonductile reinforcing details identified above. The authors compared the dynamic response of three- and nine-story frames modeled with joint elements to the response of similar frames with rigid joints when subjected to strong motion records scaled to represent earthquakes capable of producing minor, moderate, and severe damage. The comparisons revealed that accounting for joint shear and bond-slip deformations in modeling results in significantly larger drifts, particularly for the nine-story frame.

Youssef and Ghobarah [2001] proposed a joint element (see Fig. 1(c)) in which two diagonal translational springs connecting the opposite corners of the panel zone simulate the joint shear deformation; 12 translational springs located at the panel zone interface simulate all other modes of inelastic behavior (e.g., bond-slip, concrete crushing)—elastic elements were used for the joining elements. The model was validated using experimental test results of ductile and nonductile exterior beam-column joints. This model requires a large number of translational springs and a separate constitutive model for each spring, which may not be available and restricts its applicability.

Lowes and Altoontash [2003] proposed a 4-node 12-degree-of-freedom (DOF) joint element (see Fig. 1(d)) that explicitly represents three types of inelastic mechanisms of beam-column joints under reversed cyclic loading. Eight zero-length translational springs simulate the bond-slip response of beam and column longitudinal reinforcement; a panel zone component with a zero-length rotational spring simulates the shear deformation of the joint; and four zero-length shear springs simulate the interface-shear deformations. Because experimental research that reports bond-slip data of full-scale frames or beam-column joint

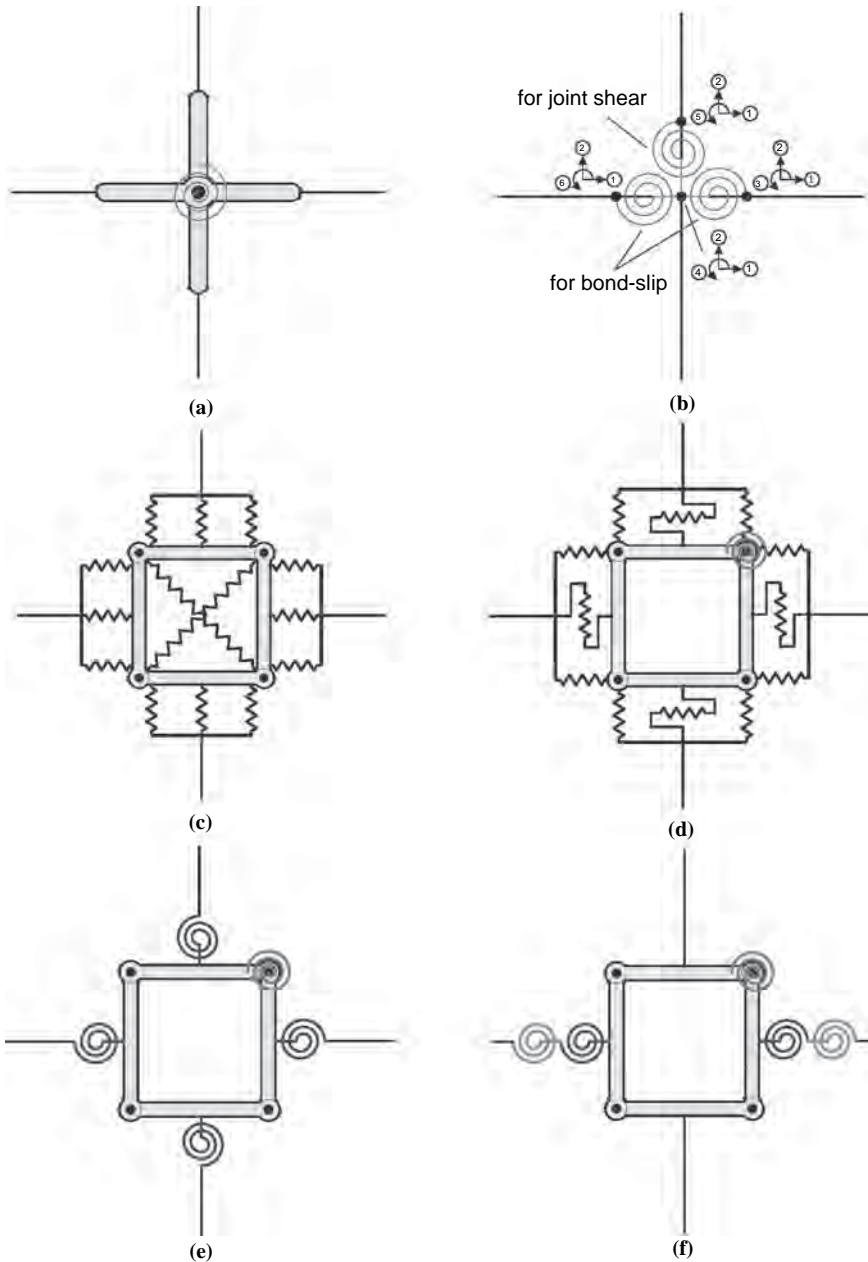


FIGURE 1 Existing beam-column joint models: (a) Alath and Kunnath [1995], (b) Bidadah and Ghobarah [1999], (c) Youssef and Ghobarah [2001], (d) Lowes and Altoontash [2003], (e) Altoontash [2004], and (f) Shin and LaFave [2004].

subassemblies is scarce, the envelope and cyclic response of the bar stress versus slip deformation relationship were developed from tests of anchorage-zone specimens and assumptions about the bond stress distribution within the joint. To define the envelope to the shear stress-strain relationship of the panel zone, the modified-compression field theory (MCFT) [Vecchio and Collins, 1986] was utilized. The cyclic response of the panel zone

was modeled by a highly pinched hysteresis relationship, deduced from experimental data provided by Stevens *et al.* [1991]. A relatively stiff elastic load-deformation response was assumed for the interface-shear components. Lowes *et al.* [2004] later attempted to model the interface-shear based on experimental data; this later effort also predicted a stiff elastic response for the interface-shear.

Mitra and Lowes [2004] subsequently evaluated the model proposed earlier by Lowes and Altoontash [2003] by comparing the simulated response with the experimental response of beam-column joint subassemblies. The experimental data included specimens with at least a minimal amount of transverse reinforcement in the panel zone, which is consistent with the intended use of the model. Joints with no transverse reinforcement, a reinforcing detail typical in GLD RC frames, were excluded from this study. Mitra and Lowes noted that in joints with low amounts of transverse reinforcement, shear is transferred primarily through a compression strut, a mechanism, which is stronger and stiffer than predicted by the MCFT.

Altoontash [2004] simplified the model proposed by Lowes and Altoontash [2003] by introducing a model consisting of four zero-length rotational springs located at beam- and column-joint interfaces, which simulate the member-end rotations due to bond-slip behavior, while the panel zone component with a rotational spring remains to simulate the shear deformation of the joint (see Fig. 1(e)). The constitutive relationship (i.e., the envelope and the cyclic response) for the panel zone from Lowes and Altoontash [2003] was retained, enabling the calculation of constitutive parameters based on material properties, joint geometry, joint reinforcing steel ratio, and axial load. However, calibration of constitutive parameters was still required for joints with no transverse reinforcement to overcome the limitation of the MCFT for such joints. Altoontash [2004] adapted the constitutive model developed for the translational bond-slip springs in Lowes and Altoontash [2003] in a fiber section analysis to derive the constitutive model for the member-end rotational springs, but noted that detailed information on bond-slip response is needed. Furthermore, the development length was assumed to be adequate to prevent complete pullout, which is not necessarily true for bottom reinforcement in beams of GLD RC frames. The validation studies include RC interior beam-column joint tests [Walker, 2001] and a two-story RC frame.

Shin and LaFave [2004] represented the joint by rigid elements located along the edges of the panel zone and rotational springs embedded in one of the four hinges linking adjacent rigid elements (see Fig. 1(f)). The envelope to the joint shear stress-strain response was approximated by the MCFT, whereas experimental data were used to calibrate the cyclic response. Two rotational springs (in series) located at beam-joint interfaces simulate the member-end rotations due to bond-slip behavior of the beam longitudinal reinforcement and plastic hinge rotations due to inelastic behavior of the beam separately. The constitutive parameters for bond-slip deformation were based on a previous study reported by the authors. A comparison of the predictions from this model to results of an RC interior joint test showed good agreement. The proposed joint model is intended for RC beam-column joints of ductile moment frames designed and detailed following modern seismic code requirements.

LaFave and Shin [2005] discussed the use of the MCFT in defining the envelope to the shear stress-strain relationship of the panel zone. The authors collected from the literature experimental joint shear stress and strain data of 50 RC interior joint subassemblies that failed in joint shear. The envelope responses to the experimental data typically follow a quad-linear curve that connects three key points (corresponding to joint shear cracking, reinforcement yielding, and joint shear strength) starting from the origin and has a degrading slope once past the joint shear strength. For each of the experimental subassemblies,

the authors applied the MCFT as described by Lowes and Altoontash [2003] to determine the ordinates of the envelope points, particularly the maximum joint shear stress (i.e., joint shear strength). Comparison of the ratio of analytical (MCFT) to experimental maximum joint shear stress versus the ratio of transverse joint shear reinforcement provided to that required by ACI 318–02 [ACI Committee 318, 2002] revealed that the MCFT approach consistently underestimates the joint shear strength for joints that do not satisfy the joint reinforcement requirement per ACI 318–02. Hence, the MCFT may be inappropriate for modeling GLD RC frames, which have little or no joint transverse shear reinforcement.

3. Modeling Joint Behavior in Finite Element Analysis

Moment transferred through the rotational spring that simulates joint shear deformations constitutes the basic input for most of the modeling schemes discussed above. In this study, the moment-rotation relationship is derived from the experimental determination of joint shear stress and strain. The effect of bond-slip on joint behavior is taken into account through a modification proposed for the joint shear stress-strain relationship.

3.1. Experimental Determination of Joint Shear Stress and Strain

Joint shear stress is defined herein as the horizontal force transferred at the mid-height of a horizontal section of a beam-column joint divided by the joint area. A typical interior beam-column joint test setup for the experimental determination of joint shear stress is shown in Fig. 2(a). The test setup includes half-lengths of the joining beams and columns, based on the assumption that the points of inflection in the joining beams and columns under seismic loading lie at their midpoints. From the free body diagram of the joint panel in Fig. 2(b), with the beam moments at the joint face represented through tension and compression couples, and noting that there is no axial load on the beams, the joint shear is

$$V_{jh} = T_b^L + T_b^R - V_c \quad (1)$$

where T_b^L and T_b^R are the tension forces acting on the left and right faces of the panel (i.e., the tension forces in the left and right beam longitudinal reinforcement), respectively, and V_c is the column shear force. The column shear can be measured easily by a load cell that

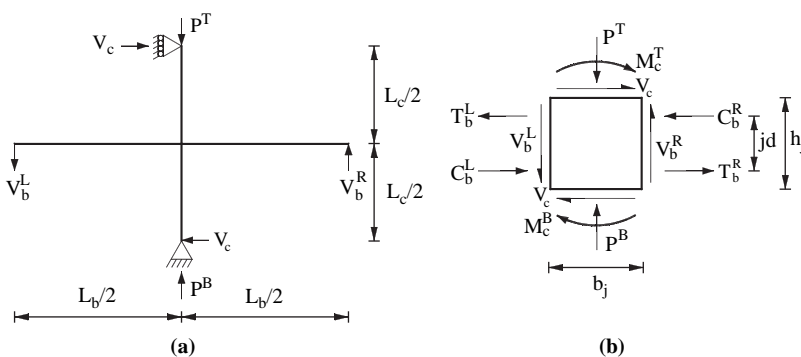


FIGURE 2 The free body diagrams of (a) a typical interior beam-column joint test setup and (b) its joint panel.

is attached at the column top or can be calculated using the equilibrium of forces given the beam-end actuator forces. The tension forces, T_b^L and T_b^R , can be calculated from strain gage measurements, which requires a constitutive model that can accurately predict the stress in the steel. This approach is seldom used due to its impracticality and difficulty [Shiohara, 2001]. Instead, the tension forces, T_b^L and T_b^R , are expressed in terms of the beam moments at the joint face, M_b^L and M_b^R , and the internal moment arm, jd , which is assumed constant throughout the test (superscripts L and R refer to left and right, respectively). The joint shear can then be rewritten as

$$V_{jh} = \frac{M_b^L}{jd} + \frac{M_b^R}{jd} - V_c. \quad (2)$$

If the beam moments at the joint face and the column shear are calculated from the applied shear forces on the left and right beams, V_b^L and V_b^R , then the joint shear is

$$V_{jh} = (V_b^L + V_b^R) \cdot \left[\frac{L_b - b_j}{2jd} - \frac{L_b}{2L_c} \right] \quad (3)$$

where L_b is the total length of the left and right beams, b_j is the width of the joint panel, and L_c is the total length of the top and bottom columns. Then, the joint shear stress is given by

$$\tau_{jh} = \frac{V_{jh}}{A_{jh}} \quad (4)$$

in which A_{jh} is the joint area, which can be calculated, for example, using Sec. 21.5.3 of ACI 318-05 [ACI Committee 318, 2005]. Joint shear stress is usually normalized by either $\sqrt{f'_c}$ or f'_c

$$\bar{\tau}_{jh} = \frac{\tau_{jh}}{\sqrt{f'_c}} \quad (5a)$$

$$\bar{\tau}_{jh} = \frac{\tau_{jh}}{f'_c} \quad (5b)$$

where f'_c is the concrete compressive strength. Both Eqs. (5a) and (5b) have been used in the literature; the first suggests that the joint shear strength is proportional to the concrete tensile (or splitting) strength, whereas the second implies that the shear strength is proportional to the compressive strength [Walker, 2001].

Joint shear strain, γ_j , is defined as the change in the angle between the two initially perpendicular edges of the panel zone.

3.2. Moment-Rotation Relationship of the Panel Zone

Consider the scissors model [Alath and Kunnath, 1995] representation of the joint panel in Fig. 2(b), with the free body forces in Fig. 3. The moment at the rotational spring expressed in terms of the shear forces on the beams is

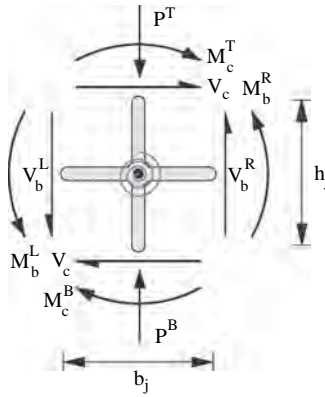


FIGURE 3 The free body diagram of the scissors model.

$$M_j = (V_b^L + V_b^R) \frac{L_b}{2}. \quad (6)$$

If Eq. (3) is substituted into Eq. (4) and the resulting equation is solved for the sum of the shear forces on the beams and substituted into Eq. (6), then the moment transferred through the rotational spring can be expressed in terms of the joint shear stress and sectional dimensions:

$$M_j = \tau_{jh} A_{jh} \frac{1}{\frac{1-b_j/L_b}{jd} - \frac{1}{L_c}}. \quad (7)$$

The relative rotation of the two rigid links that constitutes the scissors model represents the change in the angle between the two adjacent edges of the panel zone. Hence, the rotation of the rotational spring equals the joint shear strain:

$$\theta_j = \gamma_j. \quad (8)$$

Equations (7) and (8) can be used to convert the $\tau_{jh} - \gamma_j$ relationship into the $M_j - \theta_j$ relationship for the scissors model that Alath and Kunnath [1995] proposed. The formulations that include all possible joint configurations (i.e., interior and exterior joints, and interior and exterior top floor joints) to convert the joint shear stress, τ_{jh} , into the moment transferred through the rotational spring, M_j , are given in Appendix A for all the models used later in the analysis.

3.3. Panel Zone Constitutive Model

To implement the constitutive relationship for the panel zone in a finite element-based structural analysis platform, one must define a backbone curve for the envelope and a hysteresis rule for the cyclic response. Previous experimental research on the seismic performance of the beam-column joints that have no transverse reinforcement in the panel zone

[e.g., Beres *et al.*, 1996; Walker, 2001; Alire, 2002; Pantelides *et al.*, 2002] has revealed that the joint shear stress-strain response typically has a degrading envelope and a highly pinched hysteresis. Hence, a constitutive model that has a multi-linear envelope exhibiting degradation and a tri-linear unloading-reloading path representing a pinched hysteresis (see Fig. 4) is implemented in this study. This model was proposed by Lowes and Altoontash [2003], but its control points are defined herein. The envelope (positive or negative) consists of a quad-linear curve that connects four key points starting from the origin and a constant segment that follows the fourth point. The hysteresis rule is defined by a tri-linear unloading-reloading path: (1) the model unloads with the initial stiffness until the force reaches a fraction of the strength; (2) thereafter, points to the pinching point that is defined as a fraction of the maximum previous deformation and the corresponding force; and (3) upon reaching the pinching point, aims to the peak point.

3.4. The Effect of Bond-Slip on the Joint Shear Stress

The typical practice of terminating the beam bottom reinforcement within the beam-column joints with a short embedment length results in bond-slip and a reduced positive beam moment capacity, as explained above. This in turn reduces the joint shear (stress) as can be seen in Eq. (2). The joint shear stress-strain relationship, if symmetric (i.e., has the same positive and negative envelope) owing to the identical beams to the left and right of the joint, preserves its symmetric nature for interior joints. However, it does not remain symmetric for exterior joints, even if symmetric when only the joint shear deformations are considered. The constitutive model selected for the panel zone (see Fig. 4) is sufficiently flexible that it can also represent the anti-symmetric joint shear stress-strain envelope. Bond-slip due to insufficient anchorage of the beam bottom reinforcement can be taken into account by utilizing such a constitutive model with a reduced envelope (only the positive envelope is reduced for exterior joints). Experimental studies suggest that bond-slip causes additional rotation at the beam-ends (at the joint face). However, it has been argued [Leon, 1989] that this additional rotation measured in laboratory tests is largely due to the lack of horizontal restraint at the ends of the beams away from the joint in typical beam-column joint specimens. Hoffmann *et al.* [1992] noted during tests of continuous indeterminate frames that the bar slip is very small and usually difficult to detect visually. Hence, the additional rotation at the beam-ends (apart from the additional joint rotation, which is accounted for) due to bond-slip is neglected.

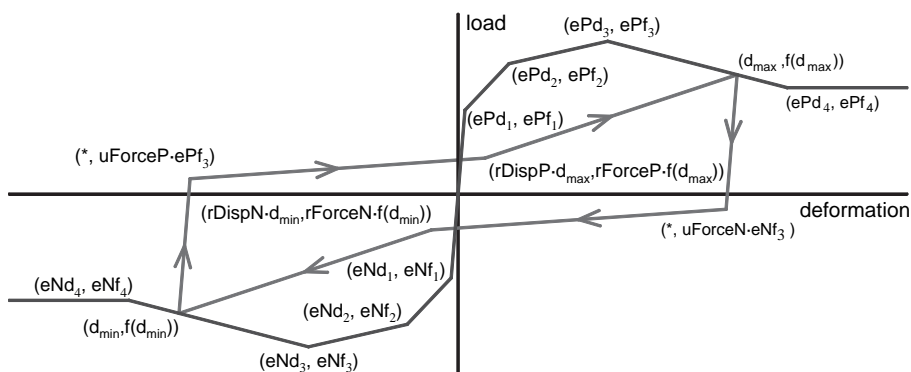


FIGURE 4 The constitutive model proposed by Lowes and Altoontash [2003].

4. Validation of Joint Model by Experimental Tests

To validate the joint model described above for finite element analysis of GLD RC frames, two experimental programs involving RC beam-column test specimens that have no transverse shear reinforcement in the panel zone are considered [Walker, 2001; Pantelides *et al.*, 2002]. These test programs considered interior and exterior joints, respectively. Information about the experimental tests highlighting important details required in the joint modeling process is summarized below. The performance of four different representations of the beam-column joints in reproducing experimental force-drift behavior is assessed.

4.1. Walker [2001] — Interior Beam-Column Joints

Walker [2001] tested seven RC interior beam-column joints, representative of joints in frames constructed prior to 1970, under reversed cyclic loading. Two test series were carried out to study the influence of joint shear stress demand and displacement history on the seismic response. The first series consisted of four nominally identical specimens with a target joint shear stress of $0.14f'_c$ ($0.82\sqrt{f'_c}$ MPa; $9.9\sqrt{f'_c}$ psi), while the second series consisted of three nominally identical specimens with a target joint shear stress of $0.22f'_c$ ($1.29\sqrt{f'_c}$ MPa; $15.6\sqrt{f'_c}$ psi). The two levels of joint shear stress represent the averages of the joint shear stress demands in RC buildings constructed prior to 1967 and between 1967 and 1979, respectively. Four displacement histories (designated PEER, CD15, CD30, and PADH) were used in testing the specimens. The specimens were identified with the name of the applied displacement history and a two-digit extension representing the target joint shear stress (e.g., PEER-14).

None of these specimens had any transverse shear reinforcement in the panel zone. To study the specific influence of this deficient reinforcing detail, other problematic reinforcing details typical in GLD RC frames were not considered in Walker's tests. In particular, the beam bottom bars were continuous; the strong column-weak beam criterion was satisfied (the column-to-beam moment capacity ratio was kept between 1.5 and 1.8); and the transverse shear reinforcement for beams and columns were designed to satisfy the requirements of ACI 318–99 [ACI Committee 318, 1999].

For designing the specimens, the concrete compressive strength was assumed to be 34 MPa (5,000 psi), whereas the steel yield strength was assumed to be 462 MPa (67,000 psi). The axial load applied on the column was $0.1f'_cA_g$ (641 kN; 144 kips) where A_g is the gross area of the column section. Figure 5 shows the steel layouts for the Test Series 14 and Test Series 22, as well the support conditions and the loading points.

4.2. Pantelides *et al.* [2002] — Exterior Beam-Column Joints

Pantelides *et al.* [2002] tested six RC exterior beam-column joints, representative of joints in frames constructed prior to 1970, under reversed cyclic loading. They studied the influence of beam bottom bar anchorage and column axial load level on the seismic response. Anchorage of the beam bottom bars was provided by three different reinforcing details. In two specimens, the beam bottom bars were extended 150 mm (6 in) into the joint, which is the typical practice in GLD RC frames. In another two specimens, the beam bottom bars were extended all the way (360 mm; 14 in) into the joint. In the last two specimens, the beam bottom bars were bent up into the joint with a 180° hook. Two levels of axial load ($0.10f'_cA_g$ and $0.25f'_cA_g$) were studied for each of the three details.

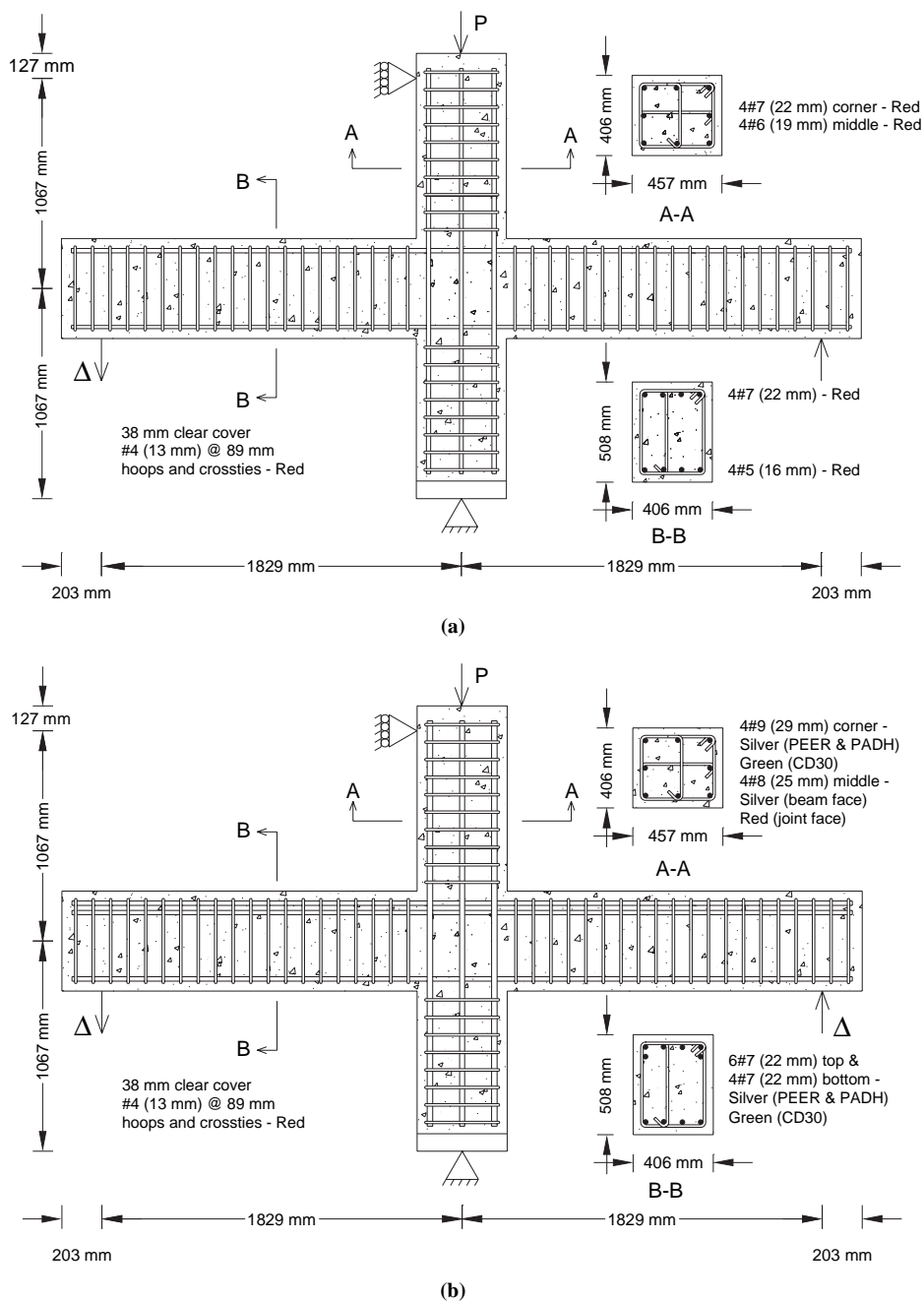


FIGURE 5 The steel layouts for the Walker [2001] specimens: (a) Test Series 14 and (b) Test Series 22 [1 in = 25.4 mm].

All six specimens were nominally identical except for the beam bottom bar anchorage detailing. Figure 6 shows the steel layout for Test Units #1 and #2, along with the support conditions and the loading point. For designing the specimens, it was assumed that the concrete had a compressive strength of 28 MPa (4,000 psi) and Grade 60 reinforcement

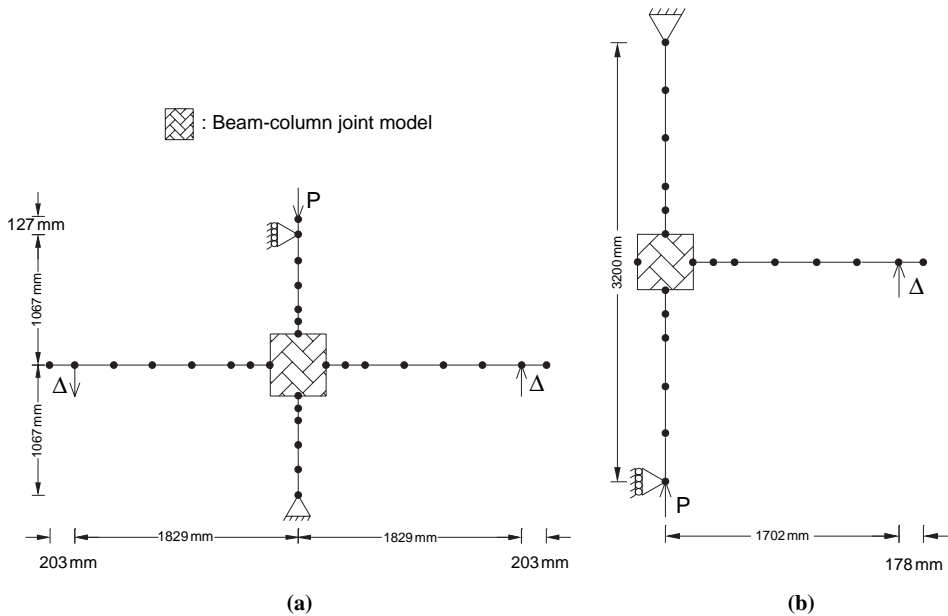


FIGURE 7 The OpenSees models of (a) the Walker [2001] and (b) the Pantelides *et al.* [2002] specimens [1 in = 25.4 mm].

minimum design values, were incorporated into the finite element models. Cover and core concrete properties were calculated using the modified Kent and Park model [Park *et al.*, 1982], while steel properties were represented through a bilinear steel model with strain hardening in the range of 1–2%, based on material tests [Walker, 2001; Pantelides *et al.*, 2002]. Concrete cover loss was taken into account in all cases.

Four different representations of the beam-column joints were considered. The candidate representations were the conventional rigid joint model (i.e., centerline model), the scissors model without rigid end zones (i.e., single rotational spring), the scissors model with rigid end zones [Alath and Kunnath, 1995], and the model proposed by Altoontash [2004], which already has been implemented in OpenSees by its developers as the *Joint2D* element. The conventional rigid joint assumption was included to differentiate the improvements that the other models might offer. A snapshot of all four models is given in Fig. 8.

Both Walker [2001] and Pantelides *et al.* [2002] identified performance levels corresponding to particular joint damage states (e.g., joint cracking, beam yielding, concrete spalling). These performance levels, which were reported in terms of $\bar{\tau}_{jh}$ and γ_j among other performance parameters, formed the basis for setting the four key points required to define the backbone of the shear stress-strain relationships. These four points ($\bar{\tau}_{jh}, \gamma_j$) for each specimen considered in this article are given in Appendix B. Table B1 presents the values of $\bar{\tau}_{jh}$ and γ_j with corresponding damage states for the Walker [2001] specimens, while Table B2 presents those for the Pantelides *et al.* [2002] specimens. It was possible to pick the values of $\bar{\tau}_{jh}$ and γ_j that represent the experimental envelopes more accurately for the Pantelides *et al.* [2002] specimens since $\bar{\tau}_{jh}$ and γ_j were reported for each loading cycle rather than at particular damage states. The internal moment arm values used in calculating the experimental joint shear stress for the Test Series 14 and Test Series 22

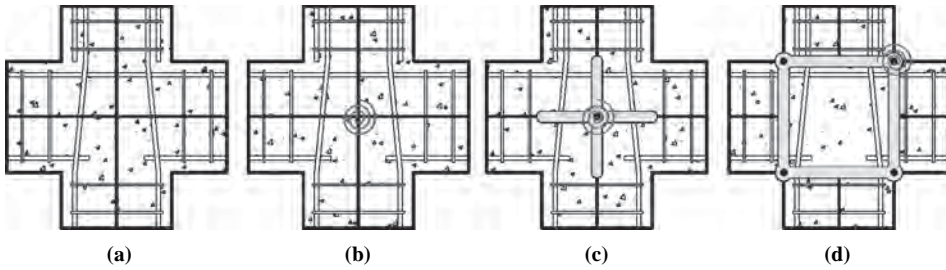


FIGURE 8 The snapshot of all the models used in Sec. 4.3: (a) the conventional rigid joint model; (b) the scissors model without rigid end zones; (c) the scissors model with rigid end zones; and (d) the *Joint2D* model.

(of Walker [2001]) were 411 mm (16.2 in) and 378 mm (14.9 in), respectively, while that for the Pantelides *et al.* [2002] specimens was identified as 303 mm (11.9 in). The $M_f-\theta_j$ relationships were represented through the constitutive model given in Fig. 4, which had already been implemented in OpenSees as the *Pinching4* material. The hysteresis rules were defined through simple definitions of the unloading and pinching points, as given in Sec. 3.3. The following parameters were used in setting the hysteresis rules:

$$uForceP = uForceN = -0.10 \quad (9a)$$

$$rForceP = rDispP = rForceN = rDispN = 0.15. \quad (9b)$$

4.4. Comparisons of Predictions with Experimental Responses

Finite element models were developed for all seven specimens tested by Walker [2001] and for the first four specimens tested by Pantelides *et al.* [2002]. Test Units #5 and #6 (of Pantelides *et al.* [2002]) were not considered because their experimental force-drift responses were similar to those of Test Units #3 and #4, respectively. Only comparisons of predictions with experimental responses for Specimens PEER-14 and PEER-22 (of Walker [2001]) and Test Units #1 and #3 (of Pantelides *et al.* [2002]) are presented in this article. Figures 9–12 compare the simulated force-drift responses with the experimental counterparts for the four specimens. Each figure shows distinct comparisons of the analytical responses from the four joint models with the experimental response. The conventional rigid joint model is inadequate in all cases for reproducing the highly pinched experimental responses, which are characteristic of shear-dominated behaviors [Stevens *et al.*, 1991]. Thus, the importance of accounting for joint shear and bond-slip in modeling of GLD RC frames is clear, and significant improvements to the rigid joint response from all other models are evident from Figs. 9–12. Thus, the following comparisons and conclusions pertain to all joint models except the rigid joint model.

The envelopes to the simulated force-drift responses of the Walker [2001] specimens showed good agreement with the experimental data (see Figs. 9 and 10). The discrepancies that exist between the simulated and experimental envelopes are attributed to how the backbone of joint shear stress-strain relationships was defined, as the performance points $(\bar{\tau}_{jh}, \gamma_j)$ corresponding to particular damage states do not necessarily replicate the experimental shear stress-strain envelope. The degradation in backbone curves was captured.

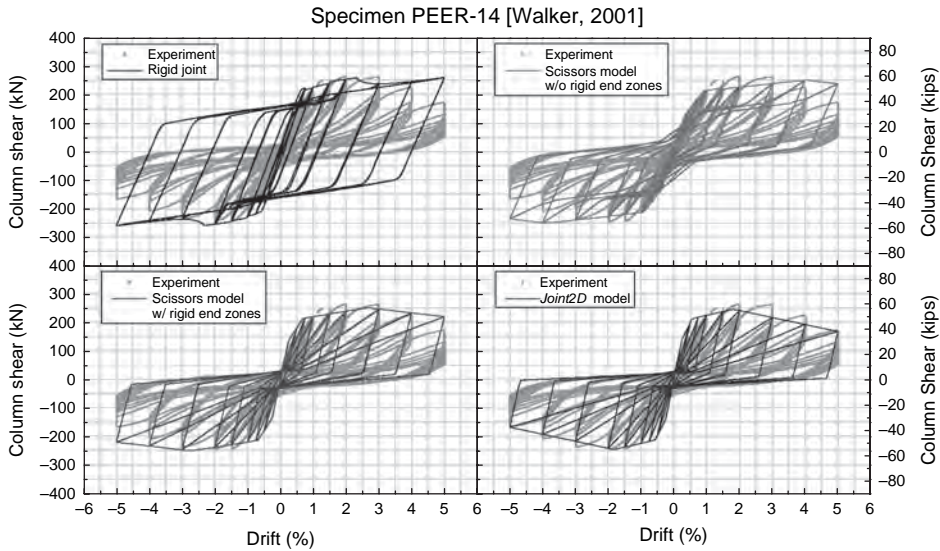


FIGURE 9 The comparisons of the simulated force-drift responses with the experimental response for the Walker [2001] Specimen PEER-14.

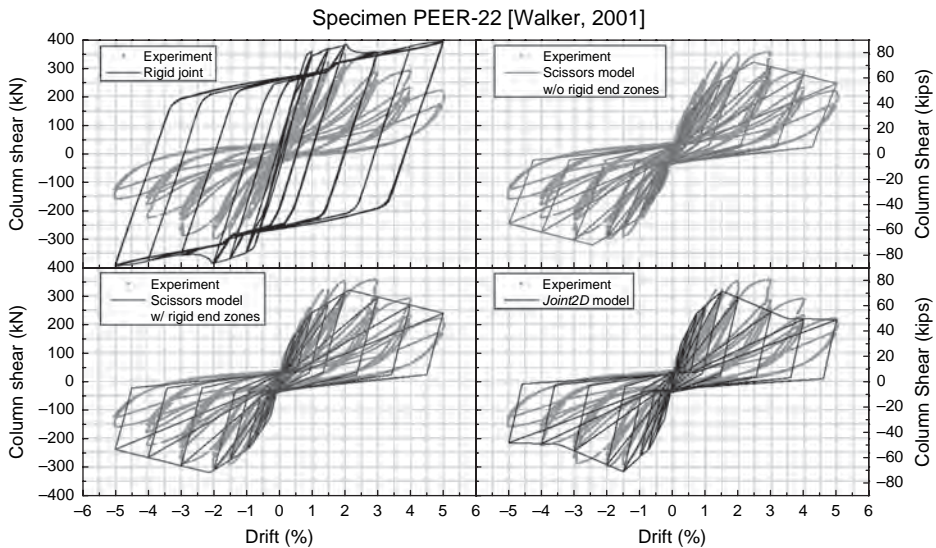


FIGURE 10 The comparisons of the simulated force-drift responses with the experimental response for the Walker [2001] Specimen PEER-22.

The simulated cyclic responses were also in good agreement with the experimental data (see Figs. 9 and 10). Hysteretic energy dissipated during the experimental loading cycles was represented well and the pinching point was captured quite well except for one case with the scissors model without rigid end zones (i.e., Specimen PEER-14).

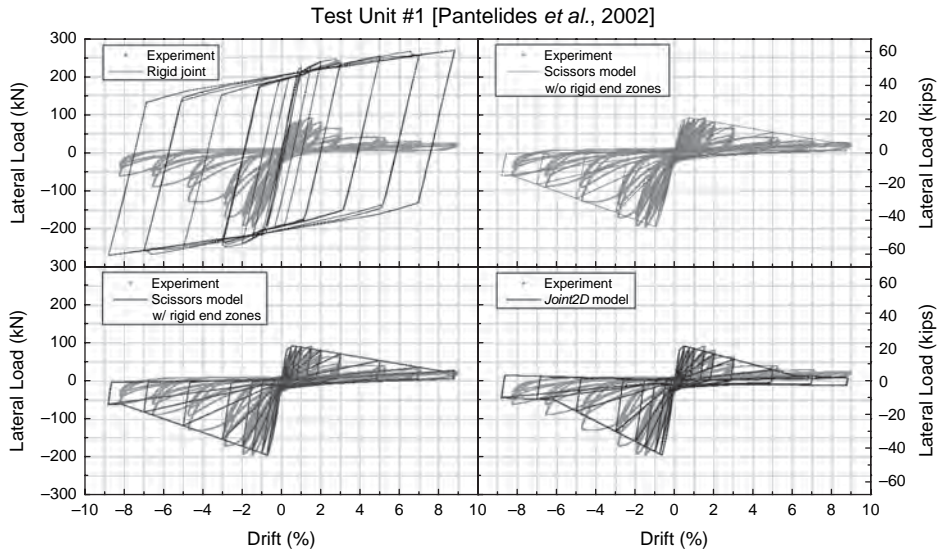


FIGURE 11 The comparisons of the simulated force-drift responses with the experimental response for the Pantelides *et al.* [2002] Test Unit #1.

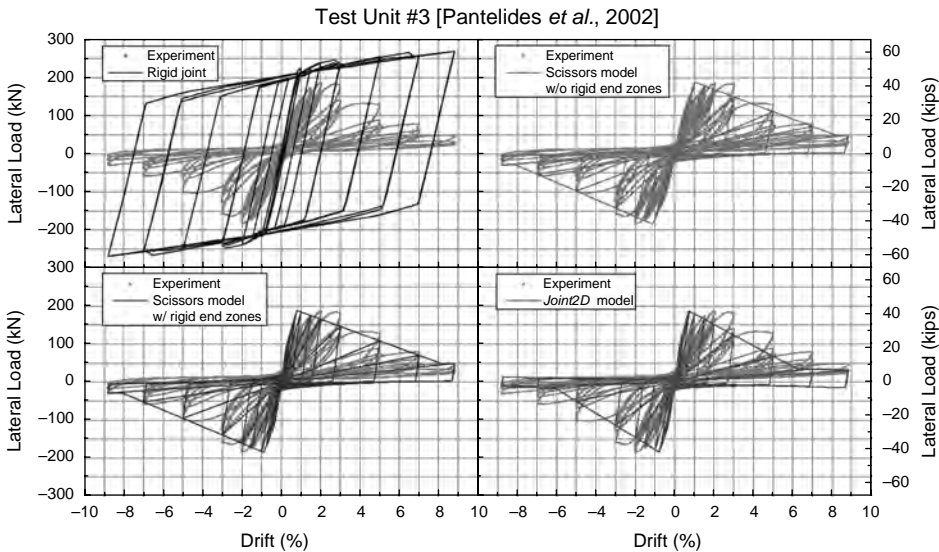


FIGURE 12 The comparisons of the simulated force-drift responses with the experimental response for the Pantelides *et al.* [2002] Test Unit #3.

The Pantelides *et al.* [2002] test series included specimens with discontinuous beam bottom bars, which enabled the model to be tested for its ability to simulate bond-slip in addition to joint shear. The experimental response of Test Unit #3 was essentially symmetric (see Fig. 12) and the beam section was symmetric. This indicates that a development length of 360 mm (14 in) provided adequate anchorage to the beam bottom bars and

prevented bond-slip. The experimental response of Test Unit #1, however, was unsymmetric (see Fig. 11). Every other parameter except the beam bottom bar anchorage was the same for Test Units #1 and #3, so the differences between the corresponding experimental responses (see Figs. 11 and 12) can only be due to the bond-slip behavior resulting from insufficient positive beam bar anchorage. As noted previously, this bond-slip resulted in reduced positive force-drift envelopes. All simulated force-drift responses of the Pantelides *et al.* [2002] specimens (see Figs. 11 and 12) correlate well with the experimental data. The effect of bond-slip in Test Unit #1 was captured (see Fig. 11). The overall response and the hysteretic energy dissipated during the experimental loading cycles were represented well for all specimens.

5. Fragility Assessment of Existing GLD RC Frames

Experimental data to define the backbone curves for the joint shear stress-strain relationships are not available for general configurations of GLD frame joints. Nor is there a theoretical tool for this purpose (e.g., the MCFT has been shown to be inadequate to predict the panel shear stress-strain behavior of GLD RC frame joints [LaFave and Shin, 2005]). Since the fragility assessment of existing GLD frames requires a constitutive relationship for the panel zone for each beam-column joint in the actual frame, the coordinates of the four key points (see Fig. 4) that define the panel zone backbone for a general beam-column joint in a frame are derived below.

5.1. Defining the Backbone of the Panel Zone

Experimental studies (see Table 1) of typical details of GLD RC frame beam-column joints suggest that the four key points of the backbone curve for the panel zone (see Fig. 4) correspond to joint shear cracking, reinforcement yielding, joint shear strength/adjoining beam or column capacity, and residual joint strength, respectively.

Joint shear stresses corresponding to the shear cracking of the panel zone were reported to be in the range of $0.21 - 0.69\sqrt{f'_c}$ MPa ($2.5 - 8.3\sqrt{f'_c}$ psi), increasing with higher axial loads. Uzumeri [1977] showed that the following ACI equation (*cf.* Eq. (5a)) predicts the cracking shear (in $\sqrt{\text{psi}}$ units) well for beam-column joints with no shear reinforcement:

$$(\bar{\tau}_{jh})_{cr} = 3.5\sqrt{1 + 0.002(N_u/A_{jh})} \quad (10)$$

where N_u is the axial load (N_u/A_{jh} in psi). This equation, when used to estimate the experimental cracking shear stresses reported in Table 1, resulted in comparable values, and therefore, was used to define the ordinate of the first point on the backbone.

If the shear failure of the joint does not occur before the adjoining beams/columns reach their ultimate capacity then the second and the third points on the backbone correspond to yield and ultimate capacities of the beams/columns (for GLD RC frames [e.g., Walker, 2001]). The columns reach their ultimate capacity if the design is a weak column-strong beam, and conversely if the design is a strong column-weak beam. In either case, section analyses were carried out to determine the yield and ultimate moment capacities, which were used to calculate the ordinates of the second and the third points on the backbone, as given in Appendix C. The positive yield moment capacities of the beams were scaled by a factor α , which was reported to vary between 0.4 and 0.7 in previous experimental

TABLE 1 Experimental database utilized in defining the backbone of the panel zone for GLD RC beam-column joints

Reference	Joint Reinf.	Beam Bottom Bar	Axial Load ($f_c A_g$)	$(\bar{\tau}_{jh})_{cr}$ ($\sqrt{\text{psi}}$) *	$(\bar{\tau}_{jh})_{max}$ ($\sqrt{\text{psi}}$) *	$(\gamma_j)_{cr}$ (10^{-3} rad)	$(\gamma_j)_y$ (10^{-3} rad)	$(\gamma_j)_{max}$ (10^{-3} rad)	$(\gamma_j)_{res}$ (10^{-3} rad)	α
Exterior Joints										
Uzumeri [1977]	No	Cont.	0.39	7.6	10.7–11.3					
Beres <i>et al.</i> [1992]	No	Disc.	0.11		5.0–7.5					
	Yes	Disc.	0.11		8.5–9.5					
	No	Disc.	0.39		7.0–9.0					
Pantelides <i>et al.</i> [2002]	No	Disc.	0.10	3.8	5.2	0.40		3.5	>23	0.47
			0.25	5.8	7.0					0.66
	No	Disc. [†]	0.10	5.6	10.9	0.47		2.0		
Leon [1990]	No	Cont.	0.10	2.5–3.1	10.2–10.4	0.13		3.3–4.3	>55	1.0
			0.25	4.7–4.9	11.1–11.7	0.34		2.3–3.1	>32	0.94
	Yes	Disc. to Cont.	0	5.6–7.3						
Interior Joints										
Leon [1990]	Yes	Disc. to Cont.	0	5.6–7.3						
Pessiki <i>et al.</i> [1990] / Beres <i>et al.</i> [1992]	No	Disc.	0.11	7.4	9.0–11.1					0.50
			0.39	7.7–7.9	10.5–12.0					0.50–0.70
Walker [2001]	No	Cont.	0.39	6.3–8.2	12.7–13.4					
	Yes	Cont.	0.39	7.8–8.3	11.8–13.6					
	No*	Cont.	0.10	4.1–5.6	8.7–10.2	0.25–0.46	3.3–4.1	9.9–22	42–76	
Shin and LaFave [2004] [‡]	No [†]	Cont.	0.10	4.0–5.2	13.2–14.8	0.34–1.3	5.6–6.3	17–18	50–74	
	Yes	Cont.	0.10			≈0.5	2–10	10–30	30–50	

* $10\sqrt{\text{psi}} = 0.83\sqrt{\text{MPa}}$.[†]Data presented are for the negative backbone.*[†]Data presented are for the Test Series 14 and 22, respectively.[‡]Data are from a collection of 26 interior beam-column joint tests from the literature.

tests (see Table 1), to account for bond-slip. The positive ultimate capacities of the beams then were set equal to the scaled positive yield capacities of the beams.

The ordinate of the fourth point was assumed equal to that of the first point on the backbone, as previous experimental research has revealed that strength degradation occurs once the peak point is attained on the backbone curves of beam-column joints that are typical of GLD construction.

The abscissas of the four key points were based on the available experimental data (see Table 1); these joint shear strains $(\gamma_j)_{cr}, (\gamma_j)_y, (\gamma_j)_{max}, (\gamma_j)_{res}$ typically fall within the following ranges: 0.0001–0.0013, 0.002–0.010, 0.01–0.03, and 0.03–0.10 radians.

Based on the previous experimental research that reported joint shear strength $(\bar{\tau}_{jh})_{max}$ (see Table 1), the ordinates of the points on the backbone were reduced so as not to exceed $(\bar{\tau}_{jh})_{max}$, when the shear failure of the joint occurs before beams or columns reach their capacities. The joint shear strength falls within the following ranges: 0.42–0.62 $\sqrt{\text{MPa}}$ (5.0–7.5 $\sqrt{\text{psi}}$) for the positive backbone and 0.83–1.00 $\sqrt{\text{MPa}}$ (10.0–12.0 $\sqrt{\text{psi}}$) for the negative backbone; of exterior beam-column joints, while that for the interior beam-column joints falls within the 0.75–1.00 $\sqrt{\text{MPa}}$ (9.0–12.0 $\sqrt{\text{psi}}$) range.

5.2. Fragility Analysis of a Three-Story GLD RC Frame

A three-story GLD RC frame typical of building construction in the CEUS [Hoffmann *et al.*, 1992] was considered for demonstrating seismic fragility assessment using the finite element model of the frame that incorporates the new beam-column joint model (adapted to the scissors model with rigid end zones). The lower bound values of joint shear strength (identified above) were utilized together with the following joint shear strains: 0.0005, 0.005, 0.02, and 0.08, and a bond-slip factor $\alpha = 0.5$ in defining the backbone curves of the panel zones for beam-column joints in the frame. The seismic demand on the frame was assessed through nonlinear dynamic time history analyses utilizing synthetic ground motions generated for Memphis, TN [Wen and Wu, 2001].

The GLD RC frame considered is a weak column-strong beam design, and its expected failure mode is a soft-story collapse. The soft-story behavior produces very high interstory drifts in the first story of the frame with rigid joints (conventional rigid joint model with rigid end zones)^a. The first story of the frame with the proposed joint model also sustains large deformations, but the upper stories experience drifts that are larger than those in the rigid-joint frame. Thus, the roof drifts in the frame with the proposed joint model are higher due to the increased flexibility of the frame, but the maximum interstory drifts are less than those in the rigid-joint frame. This behavior is reflected in Fig. 13(a), which illustrates the seismic demand (measured in terms of maximum interstory drift θ_{max} versus spectral acceleration at the fundamental period of the frame $S_d(T_1)$). Since the rigid joint assumption precludes any damage at the joint, it is not realistic in the presence of weak column-strong beam behavior and exaggerates the soft-story effect. On the other hand, the rigid joint assumption is plausible for frames designed for seismic effects according to modern building code provisions. Concurrent analyses of a comparable strong column-weak beam frame^b, depicted in Fig. 13(b), revealed that the proposed joint model leads to maximum interstory drifts that are larger than those obtained using a rigid

^aEigenvalue analyses yielded fundamental periods of 1.07 s when the finite element model of the three-story frame incorporated the new joint model and 1.00 s when rigid joint was assumed.

^bFirst three stories of a nine-story GLD RC frame [Hoffmann *et al.*, 1992], which are identical to those of the three-story frame considered in here except the columns, were considered as the comparable strong column-weak beam frame.

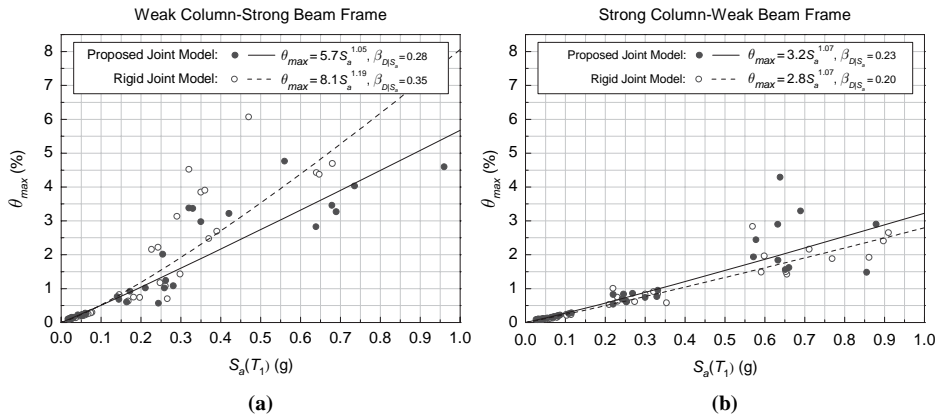


FIGURE 13 The seismic demand on (a) the three-story GLD RC frame and (b) the comparable strong column-weak beam frame.

joint model. Should such a frame contain deficient beam-column joints, the damage at those joints, combined with damage localized at the ends of the beams, would worsen the overall behavior of the frame.

Seismic fragility curves for the three-story GLD RC frame incorporating the proposed joint model were derived for three commonly used performance levels (immediate occupancy (IO), structural damage (SD), and collapse prevention (CP), associated with interstory drifts of 0.25%, 2%, and 4.0%, respectively), as presented in Ellingwood *et al.* [2007]. These seismic fragilities are illustrated in Fig. 14; they reflect the uncertainty due to record-to-record variability in the seismic demand analysis, which is known to be the most important source of uncertainty in fragility assessment [Wen and Ellingwood, 2005], as well as uncertainties in capacity and modeling [Ellingwood *et al.*, 2007]. These comparisons reveal the importance of modeling the joints in GLD RC frames in performing seismic risk assessments of such frames in regions of low-to-moderate seismicity.

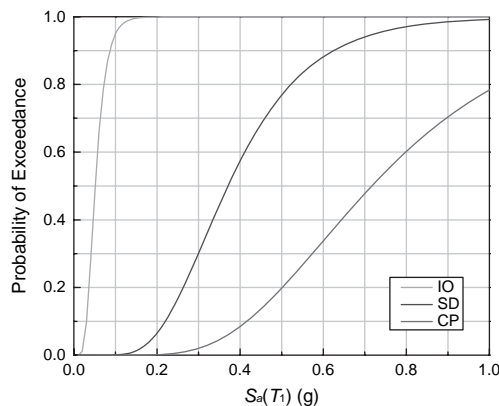


FIGURE 14 The seismic fragilities of the three-story GLD RC frame.

6. Conclusion

A beam-column joint model that accounts for shear and bond-slip in the joints of GLD RC frames was presented in this article, following a review and critical appraisal of existing models developed for this purpose. The experimental determination of joint shear stress and strain formed the basis for the modeling approach. The envelope to the panel zone shear stress-strain relationship was defined through a quad-linear curve that replicates the experimental backbone, whereas the cyclic response was captured through a pinched hysteresis model. Bond-slip was taken into account through a reduced envelope for the joint shear stress-strain relationship.

The beam-column joint model was validated using the results from two full-scale experimental RC beam-column joint test series. Four different beam-column joint representations were considered. It was found that the conventional rigid joint model was inadequate for simulating the highly pinched experimental responses, which revealed the importance of accounting for joint shear and bond-slip in modeling of GLD RC frames. All other models led to significant improvements over the conventional rigid joint assumption. Overall, the scissors model with rigid end zones was sufficiently accurate in predicting the experimental beam-column joint responses for simulating the seismic response of GLD RC frames for purposes of fragility assessment and performance-based earthquake engineering.

Application of the proposed beam-column joint model, with the formulation for defining the backbone of the panel zone, for fragility assessment of a three-story GLD RC frame revealed the importance of modeling the joints in GLD frames in performing seismic risk assessments.

Acknowledgments

This research was supported by the National Science Foundation under grant EEC-9701785 to the Mid-America Earthquake Center. This support is gratefully acknowledged. However, the views expressed are solely those of the authors and may not represent the position of either the MAE Center or NSF. The authors also thank Professor Dawn E. Lehman of the University of Washington, who graciously shared a number of graduate theses and other publications.

References

- ACI Committee 318 [1989] *Building code requirements for reinforced concrete (ACI 318-89) and commentary (ACI 318R-89)*, American Concrete Institute, Detroit, Michigan.
- ACI Committee 318 [1999] *Building code requirements for structural concrete (318-99) and commentary (318R-99)*, American Concrete Institute, Farmington Hills, Michigan.
- ACI Committee 318 [2002] *Building code requirements for structural concrete (ACI 318-02) and commentary (ACI 318R-02)*, American Concrete Institute, Farmington Hills, Michigan.
- ACI Committee 318 [2005] *Building code requirements for structural concrete (ACI 318-05) and commentary (ACI 318R-05)*, American Concrete Institute, Farmington Hills, Michigan.
- ACI-ASCE Committee 352 [1991] *Recommendations for design of beam-column joints in monolithic reinforced concrete structures (ACI 352R-91)*, American Concrete Institute, Farmington Hills, Michigan.
- Alath, S. and Kunnath, S. K. [1995] "Modeling inelastic shear deformations in rc beam-column joints," *Engineering Mechanics Proceedings of 10th Conference*, May 21–24, University of Colorado at Boulder, Boulder, Colorado, ASCE, New York, **2**, 822–825.

- Alire, D. A. [2002] "Seismic evaluation of existing unconfined reinforced concrete beam-column joints," M.Sc. Thesis, Department of Civil and Environmental Engineering, University of Washington, Seattle, Washington.
- Altoontash, A. [2004] "Simulation and damage models for performance assessment of reinforced concrete beam-column joints," PhD Dissertation, Department of Civil and Environment Engineering, Stanford University, Stanford, California.
- Beres, A., White, R. N., and Gergely, P. [1992] "Seismic behavior of reinforced concrete frame structures with nonductile details: Part I — Summary of experimental findings of full scale beam-column joint tests," *Technical Report NCEER-92-0024*, National Center for Earthquake Engineering Research, State University of New York at Buffalo, Buffalo, New York.
- Beres, A., Pessiki, S. P., White, R. N., and Gergerly, P. [1996] "Implications of experiments on the seismic behavior of gravity load designed RC beam-to-column connections," *Earthquake Spectra* **12**(2), 185–198.
- Biddah, A. and Ghobarah, A. [1999] "Modelling of shear deformation and bond slip in reinforced concrete joints," *Structural Engineering and Mechanics* **7**(4), 413–432.
- Bracci, J. M., Reinhorn, A. M., and Mander, J. B. [1992a] "Seismic resistance of reinforced concrete frame structures designed only for gravity loads: Part I — Design and properties of a one-third scale model structure," *Technical Report NCEER-92-0027*, National Center for Earthquake Engineering Research, State University of New York at Buffalo, Buffalo, New York.
- Bracci, J. M., Reinhorn, A. M. and Mander, J. B. [1992b] "Seismic resistance of reinforced concrete frame structures designed only for gravity loads: Part III — Experimental performance and analytical study of a structural model," *Technical Report NCEER-92-0029*, National Center for Earthquake Engineering Research, State University of New York at Buffalo, Buffalo, New York.
- Bracci, J. M., Reinhorn, A. M., and Mander, J. B. [1995] "Seismic resistance of reinforced concrete frame structures designed for gravity loads: performance of structural system," *ACI Structural Journal* **92**(5), 597–609.
- Ellingwood, B. R., Celik, O. C., and Kinali, K. [2007] "Fragility assessment of building structural systems in Mid-America," *Earthquake Engineering and Structural Dynamics*, Special Issue on Seismic Reliability Analysis of Structures, **36**(3), 1935–1952.
- Ghobarah, A. and Biddah, A. [1999] "Dynamic analysis of reinforced concrete frames including joint shear deformation," *Engineering Structures* **21**, 971–987.
- Hoffmann, G. W., Kunnath, S. K., Reinhorn, A. M., and Mander, J. B. [1992] "Gravity-load-designed reinforced concrete buildings: Seismic evaluation of existing construction and detailing strategies for improved seismic resistance," *Technical Report NCEER-92-0016*, National Center for Earthquake Engineering Research, State University of New York at Buffalo, Buffalo, New York.
- Hsu, T. T. C. [1988] "Softened truss model theory for shear and torsion," *ACI Structural Journal* **85**(6), 624–634.
- Kunnath, S. K., Hoffmann, G., Reinhorn, A. M., and Mander, J. B. [1995a] "Gravity-load-designed reinforced concrete buildings — Part I: Seismic evaluation of existing construction," *ACI Structural Journal* **92**(3), 343–354.
- Kunnath, S. K., Hoffmann, G., Reinhorn, A. M., and Mander, J. B. [1995b] "Gravity load-designed reinforced concrete buildings — Part II: Evaluation of detailing enhancements," *ACI Structural Journal* **92**(4), 470–478.
- LaFave, J. M. and Shin, M. [2005] "Discussion of 'Modeling reinforced-concrete beam-column joints subjected to cyclic loading,' by Lowes, L. N. and Altoontash, A.," *ASCE Journal of Structural Engineering* **131**(6), 992–993.
- Leon, R. T. [1989] "Interior joints with variable anchorage lengths," *ASCE Journal of Structural Engineering* **115**(9), 2261–2275.
- Leon, R. T. [1990] "Shear strength and hysteretic behavior of interior beam-column joints," *ACI Structural Journal* **87**(1), 3–11.
- Lowes, L. N. and Altoontash, A. [2003] "Modeling reinforced-concrete beam-column joints subjected to cyclic loading," *ASCE Journal of Structural Engineering* **129**(12), 1686–1697.
- Lowes, L. N., Mitra, N., and Altoontash, A. [2004] "A beam-column joint model for simulating the earthquake response of reinforced concrete frames," *PEER 2003/10*, Pacific Earthquake Engineering Research Center, University of California, Berkeley.

- McKenna, F. and Fenves, G. L. [2006] "Open System for Earthquake Engineering Simulation (OpenSees) User Manual," University of California, Berkeley <http://opensees.berkeley.edu>.
- Mitra, N. and Lowes, L. N. [2004] "Evaluation and advancement of a reinforced concrete beam-column joint model," *Proceedings of the Thirteenth World Conference on Earthquake Engineering*, August 1–6, 2004, Vancouver, B.C., Canada, Paper No. 1001.
- Pantelides, C. P., Hansen, J., Nadauld, J., and Reaveley, L. D. [2002] "Assessment of reinforced concrete building exterior joints with substandard details," *PEER 2002/18*, Pacific Earthquake Engineering Research Center, University of California, Berkeley.
- Park, R., Priestley, M. J. N., and Gill, W. D. [1982] "Ductility of square-confined concrete columns," *ASCE Journal of the Structural Division* **108**(ST4), 929–950.
- Pessiki, S. P., Conley, C. H., Gergely, P., and White, R. N. [1990] "Seismic behavior of lightly-reinforced concrete column and beam-column joint details," *Technical Report NCEER-90-0014*, National Center for Earthquake Engineering Research, State University of New York at Buffalo, Buffalo, New York.
- Shin, M. and LaFave, J. M. [2004] "Testing and modeling for cyclic joint shear deformations in rc beam-column connections," *Proceedings of the Thirteenth World Conference on Earthquake Engineering*, August 1–6, 2004, Vancouver, B.C., Canada, Paper No. 0301.
- Shiohara, H. [2001] "New model for shear failure of rc interior beam-column connections," *ASCE Journal of Structural Engineering* **127**(2), 152–160.
- Stevens, N. J., Uzumeri, S. M., and Collins, M. P. [1991] "Reinforced concrete subjected to reversed cyclic shear — Experiments and constitutive model," *ACI Structural Journal* **88**(2), 135–146.
- Uzumeri, S. M. [1977] "Strength and ductility of cast-in-place beam-column joints," *Reinforced Concrete Structures in Seismic Zones*, Publication SP 53–12, American Concrete Institute, Detroit, Michigan, 293–350.
- Vecchio, F. J. and Collins, M. P. [1986] "The modified-compression field theory for reinforced-concrete elements subjected to shear," *Journal of the American Concrete Institute* **83**(2), 219–231.
- Walker, S. G. [2001] "Seismic performance of existing reinforced concrete beam-column joints," MSc Thesis, Department of Civil and Environmental Engineering, University of Washington, Seattle, Washington.
- Wen, Y. K. and Wu, C. L. [2001] "Uniform hazard ground motions for Mid-America cities," *Earthquake Spectra* **17**(2), 359–384.
- Wen, Y. K. and Ellingwood, B. R. [2005] "The role of fragility assessment in consequence-based engineering," *Earthquake Spectra* **21**(3), 861–877.
- Youssef, M. and Ghobarah, A. [2001] "Modelling of rc beam-column joints and structural walls," *Journal of Earthquake Engineering* **5**(1), 93–111.

Appendix A

TABLE A1 The formulations to convert the joint shear stress into the moment transferred through the rotational spring

Joint Model	Interior and Exterior Joints	Interior and Exterior Top Floor Joints
Scissors Model with and without Rigid End Zones	$M_j = \tau_{jh} A_{jh} \frac{1}{\lambda} *$	$M_j = \tau_{jh} A_{jh} \frac{1}{\lambda'} *$
Joint2D [†]	$M_j = \tau_{jh} A_{jh} \frac{\eta}{\lambda} *$	$M_j = \tau_{jh} A_{jh} \frac{\eta}{\lambda'} *$

* $\lambda = \frac{1-b_j/L_b}{jd} - \frac{1}{L_c}$, $\lambda' = \frac{1-b_j/L_b}{jd} - \frac{2}{L_r}$, $\eta = 1 - h_j/L_c - b_j/L_b$, where h_j is the height of the joint panel.

[†]The constraint equations that relate the external DOFs to the internal DOFs of the joint element were utilized to derive the moment transferred through the rotational spring based on the initial undeformed configuration of the joint element.

Appendix B

TABLE B1 The performance points used in defining the backbone of the shear stress-strain relationships for the Walker [2001] specimens

Specimen	Damage State	$\bar{\tau}_{jh}$ ($\sqrt{\text{psi}}$)*	γ_j (10^{-3} rad)
PEER-14	Joint Cracking	5.6	0.46
	Beam Yielding	8.7	3.4
	Concrete Spalling	10.2	22
	20% Reduction in Strength	7.1	80 [†]
PEER-22	Joint Cracking	5.2	1.3
	Beam Yielding	9.7	6.3
	Concrete Spalling	13.2	17
	20% Reduction in Strength	9.5	50

*The definition complies with Eq. (5a) [$10\sqrt{\text{psi}} = 0.83\sqrt{\text{MPa}}$].

[†]The value was assumed due to the lack of data.

TABLE B2 The performance points used in defining the backbone of the shear stress-strain relationships for the Pantelides *et al.* [2002] specimens

Specimen	Positive Envelope		Negative Envelope	
	$\bar{\tau}_{jh}$ ($\sqrt{\text{psi}}$)*	γ_j (10^{-3} rad)	$\bar{\tau}_{jh}$ ($\sqrt{\text{psi}}$)*	γ_j (10^{-3} rad)
Test Unit #1	3.8	0.385	5.8	0.455
	4.6	0.824	8.8	1.12
	5.2	3.52	10.9	1.96
	1.5	80 [†]	3.4	80 [†]
Test Unit #3	3.2	0.141	2.6	0.239
	5.1	0.272	6.3	0.948
	10.4	3.28	10.2	4.29
	2.7	80 [†]	1.6	80 [†]

*The definition complies with Eq. (5a) [$10\sqrt{\text{psi}} = 0.83\sqrt{\text{MPa}}$].

[†]The value was assumed due to the lack of data.

Appendix C

The moments transferred through the joint (i.e., the rotational spring) when the adjoining beams/columns reach their yield and ultimate capacities are given below for the scissors models:

$$(M_j^{+,-})^{y,u} = \min \left[\frac{(M_C^B)^{y,u} + (M_C^T)^{y,u}}{\eta_C}, \frac{\alpha(M_{IB}^+)^y + (M_{IB}^-)^{y,u}}{\eta_B} \right] \quad (\text{C.1})$$

for interior joints, and

$$(M_j^+)^{y,u} = \min \left[\frac{(M_C^B)^{y,u} + (M_C^T)^{y,u}}{\eta_C}, \frac{\alpha(M_{EB}^+)^y}{\eta_B} \right] \quad (\text{C.2})$$

for the positive backbone, and

$$(M_j^-)^{y,u} = \min \left[\frac{(M_C^B)^{y,u} + (M_C^T)^{y,u}}{\eta_C}, \frac{(M_{EB}^-)^{y,u}}{\eta_B} \right] \quad (\text{C.3})$$

for the negative backbone; of exterior joints where $\eta_C = 1 - h_j/L_c$ and $\eta_B = 1 - b/L_b$ (subscripts *C*, *IB*, and *EB* refer to column, interior beam, and exterior beam; and superscripts *y* and *u* refer to yield and ultimate, and *B* and *T* refer to bottom and top, respectively).



13th World Conference on Earthquake Engineering
Vancouver, B.C., Canada
August 1-6, 2004
Paper No. 1464

SEISMIC PERFORMANCE OF OLDER BEAM-COLUMN JOINTS

Dawn LEHMAN¹, John STANTON²,
Meredith ANDERSON³, Daniel ALIRE⁴, Steve WALKER⁵

SUMMARY

Performance evaluation of a non-ductile reinforced concrete frame requires reliable estimates of the engineering response, including strength, stiffness, and damage states. Typically, the components that contribute to the response include beams, column, and joints. Although a significant number of studies have addressed the response of older beams and columns, few have evaluated the response of older beam-column joints. These older joints typically have no transverse reinforcement but in some cases may be subjected to high joint shear stress demands. The influence of the joint deformations on the response can be significant, but, in engineering practice, the joints are typically modeled as rigid elements and the effects of their deformations are neglected.

A research program was conducted to develop tools for the performance evaluation of joints in older reinforced concrete frame construction. Initially, eleven experimental specimens were tested. The specimens were designed to study joint behavior over a range of material strengths and joint shear stress demands. In addition, the influence of displacement history was investigated using nominally identical specimens. The results were used to quantify important response parameters including stiffness, strength, and damage. The measured response formed the basis of an advanced constitutive model for the joint shear-stress strain response. The model uses a tri-linear backbone curve with nonlinear branch curves and includes pinching in the response. In the experiments, degradation was noted in the stiffness, strength and pinching, specifically in cycles that exceeded a threshold strain. In the model, degradation relationships were developed to simulate this response. Mathematically, these relationships depend on the ratio of the current strain demand to the previous maximum strain (in the case of stiffness) or to the threshold strain (in the case of strength and pinching). The predicted response using the resulting model compared well with the measured response in both these experiments and those from an independent set conducted by others.

¹ Assistant Professor, University of Washington, Box 352700, Seattle WA 98195

² Professor, University of Washington, Box 352700, Seattle WA 98195

³ Former Graduate Student, University of Washington, Box 352700, Seattle WA 98195

⁴ Former Graduate Student, University of Washington, Box 352700, Seattle WA 98195

⁵ Former Graduate Student, Box 352700, Seattle WA 98195

INTRODUCTION

Reinforced concrete frames constructed prior to the 1970s are susceptible to damage under seismic loading. Joints in these frames may be subjected to high shear stresses. In current seismic design, limits on joint shear stresses play a dominant role in determining the column size in reinforced concrete frames, but this was not always the case. Prior to the pioneering experiments of Hanson and Connor (1967), codes did not specify limits on the joint shear stress or require joint transverse reinforcement, and as a result older joints have a wide range of shear stresses and typically do not contain transverse reinforcement. The mid 1970s saw the adoption of prescriptive rules for seismic design that resemble closely those in force today. However buildings constructed before that time were not detailed using modern codes and therefore the robustness of their seismic performance is open to question.

Seismic evaluation of these frames requires accurate estimates of the frame response and damage, which in turn requires analytical models for the elements, including the beams, columns, and beam-column joints. Although previous research has focused on damage to columns, most studies have neglected the beam-column joints. The joint flexibility is important because it increases the drift demand, which may lead to more non-structural damage and to structural instability through P-delta effects. However, practicing engineers usually ignore joint shear deformations in their analyses and the results of those analyses may therefore not be reliable. Although joint models exist, most are capable of simulating joints that meet the current code provisions and are subjected to monotonically increasing imposed cyclic deformation histories. Those models have limited applicability to older joints and more random cyclic deformation demands due to limitations in the calibration and validation data.

To better understand and model the seismic performance of joints in older frame buildings, a coordinated experimental and analytical study of older beam-column joints was undertaken. The joints studied in the experimental research simulated pre-1970s construction in that they contained no transverse reinforcement and were subjected to a wide range of joint shear stress demands. Eleven specimens were constructed and tested (Walker 2001, Alire 2002) to investigate the nature of shear resistance in older joints. The results provided insight into the influence of joint shear stress demand and concrete strength on joint performance, formed the basis for damage models that relate joint damage to local engineering parameters such as shear stress and strain.

Equally important, the experimental data were used to develop and calibrate a constitutive model that was developed to represent the joint shear-stress strain response of joints in older construction. The model is capable of simulating the response of reinforced concrete joints without transverse reinforcement to a wide variety of input motions. Here, key aspects of the model, including its primary parameters and its calibration and validation, are presented.

EXPERIMENTAL EVALUATION OF JOINT PERFORMANCE

Prior to planning the test program, a limited survey was conducted of reinforced concrete frame buildings constructed before 1973, which was the first year in which the UBC (Uniform 1997) incorporated ductile detailing requirements. A wide range of beam and column proportions was found, and the joints shear stress demands varied from 0.03 to $0.37f'_c$. The primary deficiencies were: column bar splices that were too short and that were located directly above the floors, lack of transverse reinforcement in the joints, inadequate transverse steel in the beams and columns, inadequate anchorage of the bottom beam bars in the column, and column/beam flexural strength ratios that were too low. Furthermore, the beam centerlines were in several cases offset from those of the columns. The scope of the project prevented all of these deficiencies from being studied, so the specimens were designed to focus on the joint shear behavior.

Test Program

The test program consisted of eleven specimens. The specimens all had the same geometry, which is shown in Figure 1. The column bars were continuous, to eliminate the possibility of premature splice failure, and the beams and columns were detailed in accordance with the principles of capacity design, as embodied in ACI 318-02. The joints contained no transverse reinforcement, and the joint shear stress demand was varied by suitable selecting suitable beam bars.

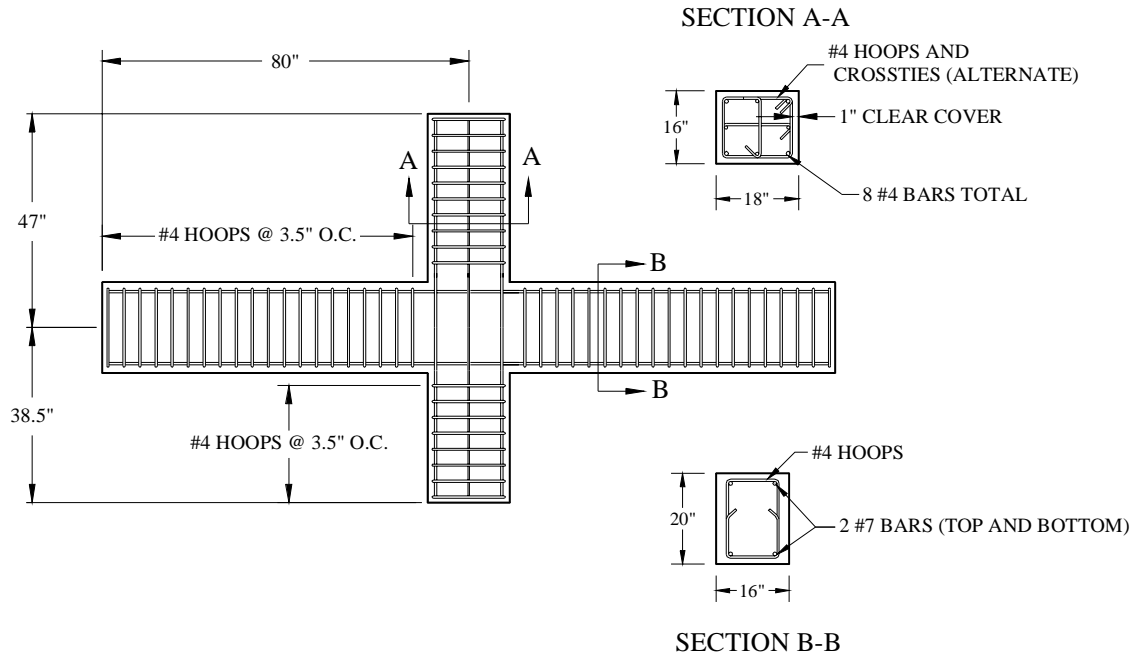


Figure 1 Test Specimen Dimensions (Reinforcement for PEER 0850 Shown)

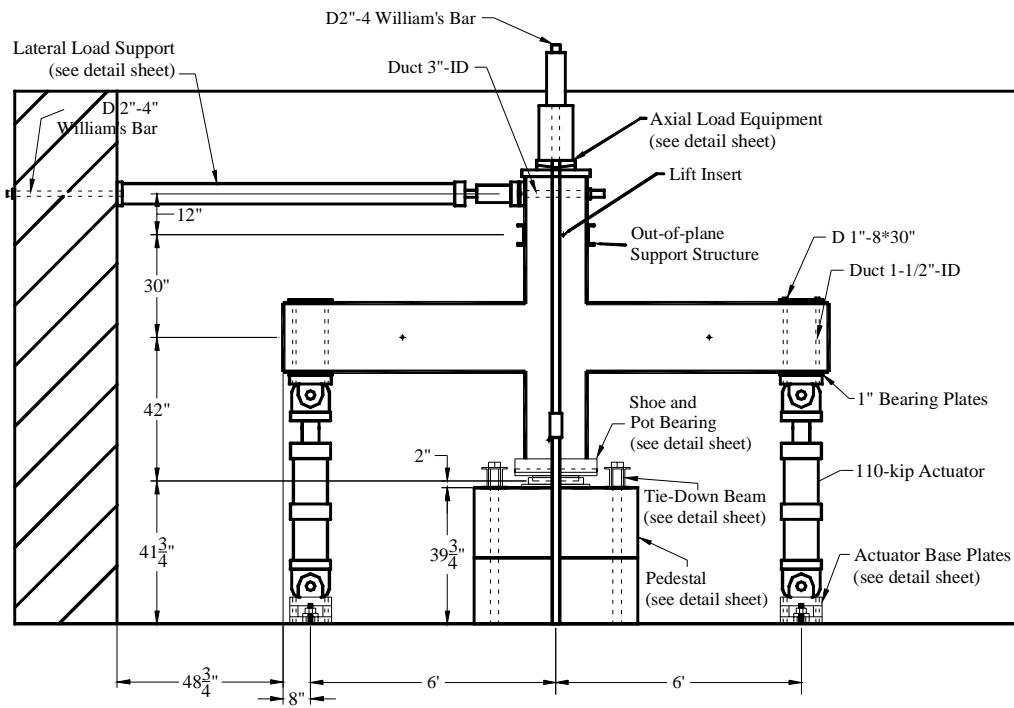


Figure 2 Test Setup

The specimens were set in a vertical plane for testing, as shown in Figure 2. Equal and opposite displacements were imposed at the beam ends by two servo-controlled actuators while the top and bottom of the column were fixed against translation and pinned against rotation. An axial load of $0.1f'_cA_g$ was applied to the column using a steel cross beam and high strength rods stressed to the strong floor. The principal instrumentation consisted of LVDTs at the beam tips, two joints shear strain rigs attached to threaded rods embedded in the joint concrete, and strain gages on the beam bars. Each joint shear strain rig consisted of six potentiometers, arranged in the sides and diagonals of a rectangle, from which the shear strain could be computed. The two rigs were attached on opposite faces of the column. The strain gages were attached, using a technique pioneered by Raynor (2000), in the bottom of slots milled along the bars. This method avoids the interruption to the bond that would otherwise be caused by the waterproofing over the gages when they are attached to the curved surface of the bar.

The test matrix is shown in Table 1, in which the test specimens are arranged in order of increasing amounts of normalized joint shear stress, $v_j/\sqrt{f'_c}$. The specimen naming system consists of the displacement history name (discussed below) followed by two digits that define the target shear stress demand as a fraction of f'_c , and two more digits that define f'_c . Thus, PEER 0850 has $v_{j,max} = 0.08f'_c$, and $f'_c = 5000$ psi.

Four displacement histories were used:

- **PEER**: sets of three equal cycles, with the amplitude of each set approximately 30% larger than the previous one. This was selected because such histories have been widely used in the past.
- **CD15**: 30 cycles with constant displacement amplitude of 1.5% drift ratio, followed by 12 cycles at 3%, then cycling at 5% drift ratio to failure. This was intended to simulate a distant, long-duration earthquake.
- **CD30**: 12 cycles with constant displacement amplitude of 3.0% drift ratio, followed by cycling at 5% drift ratio to failure.
- **PADH**: (*P*ulse *A*symmetric *D*isplacement *H*istory). A highly asymmetric history starting with a half-cycle to 5% drift. This was intended to simulate the effects of a near-source, pulse-type earthquake.

Table 1 Test Matrix

Phase	Specimen	Target f'_c (psi)	Target v_j (psi)	Target v_j/f'_c	Target v_j/f'_c	History
II	PEER 0850	5000	400	0.08	5.7	PEER
II	PEER 0995	9500	855	0.09	8.5	PEER
I	PEER-1450	5000	700	0.14	9.1	PEER
I	CD15-1450	5000	700	0.14	9.1	CD15
I	CD30-1450	5000	700	0.14	9.1	CD30
I	PADH-1450	5000	700	0.14	9.1	PADH
II	PEER 1595	9500	1425	0.15	14.4	PEER
I	PEER-2250	5000	1100	0.22	14.8	PEER
I	CD30-2250	5000	1100	0.22	14.8	CD30
I	PADH-2250	5000	1100	0.22	14.8	PADH
II	PEER 4150	5000	2050	0.41	28.3	PEER

The work was conducted in two phases. In Phase I, consisting of seven specimens (Walker 2001), the primary variables were the target joint shear demand (9 or $15\sqrt{f'_c}$ psi) and the displacement history. In Phase II, (Alire 2002), four more specimens with different joint shear stress demands and two different

concrete strengths, were tested. The goal was to study the effects of joint shear stress, both in the absolute and as a proportion of the concrete strength. The PEER load history was used in all four cases.

Experimental Performance

The experimental data were used to assess the seismic performance of beam-column joints in non-ductile reinforced concrete frame construction. Four aspects of joint performance are of great interest. First, the compressive strength of the joint must be sufficient to carry the gravity load on the column. This condition was satisfied in every test, even when the joint damage was so severe that the center of the joint was destroyed and a hole existed right through it. This result is, in fact, predictable. If the concrete in the joint loses all of its axial strength, but is still able to support the bars against buckling, an axial load of $P = \alpha f_y A_g$ can be supported by the bars alone, at a stress of f_y , if $\rho > \alpha f_y / f_c$, where ρ is the column longitudinal reinforcement ratio. The minimum permissible reinforcement in a column is 1%, so a column with $f_c = 5000$ psi can support a load of $0.12 f_c A_g$ on the bars alone. More heavily reinforced columns can carry a proportionately higher load.

The second behavioral feature of interest is the shear strength of the joint. The traditional viewpoint is that the joint has a certain strength in shear, often taken to be $12, 15$ or $20\sqrt{f_c}$ (psi), depending on the arrangement of beams framing into it, as specified by ACI318-02 for joints containing transverse reinforcement. The experiments showed that, for joints without transverse reinforcement, this description is not valid, and that the strength varies significantly with bar yielding and displacement history. For example, joints in specimens PEER-0850 and PEER-4150 were essentially identical, but were subjected to target joint shear demands of $5.7\sqrt{f_c}$ and $28.3\sqrt{f_c}$ (psi) respectively. Yet both reached peak loads defined by their joint shear demands, and both suffered major damage to the joint region. If the joint shear strength was a unique value (in this case at least equal to $28.3\sqrt{f_c}$ (psi)) then specimen PEER-0850 would have suffered no joint damage. Furthermore, the way in which failure progressed in the two specimens differed significantly. PEER-0850 underwent many cycles of beam yielding before suffering joint damage, while the beam bars in PEER-4150 had barely yielded when the joint failed in shear. This suggests that a joint shear stress demand of $5.7\sqrt{f_c}$ (psi) represents approximately the value that separates pure beam yielding failure from joint shear failure, and that $28.3\sqrt{f_c}$ (psi) is the joint shear demand above which beam yielding will not occur.

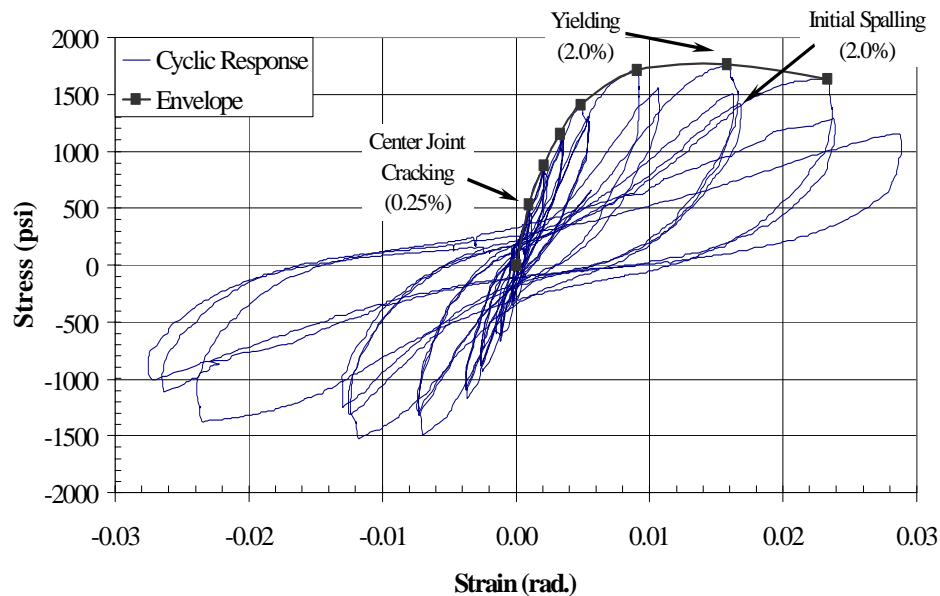


Figure 3. Joint Shear Stress vs. Strain for Specimen PEER 4150.

The third and fourth critical features of joint behavior are the joint stiffness and damage accumulation. They are related, because both change as the displacement history progresses. In the experiments, the stiffness of the beam and column changed little during the test, because they contained transverse reinforcement that complied with contemporary standards, but the joint stiffness dropped significantly as damage occurred. This can be seen in the joint shear stress vs. strain plots, such as the one for PEER 4150 shown in Figure 3. It can also be seen in a plot of the displacement components, such as shown in Figure 4 for Specimen PEER 1450. As can be seen, the joint deformation provided about 10% of the total at cycle 9 (to an applied drift ratio = 0.5%, which was the first cycle set after joint cracking) and and, at the end of the test, it provided 75% of the total drift. This finding shows that modeling the joints in a frame analysis as rigid is likely to lead to a significant underestimate of the lateral drift. The drift affects not only the damage to the non-structural components, but also the possibility of instability due to P- Δ effects.

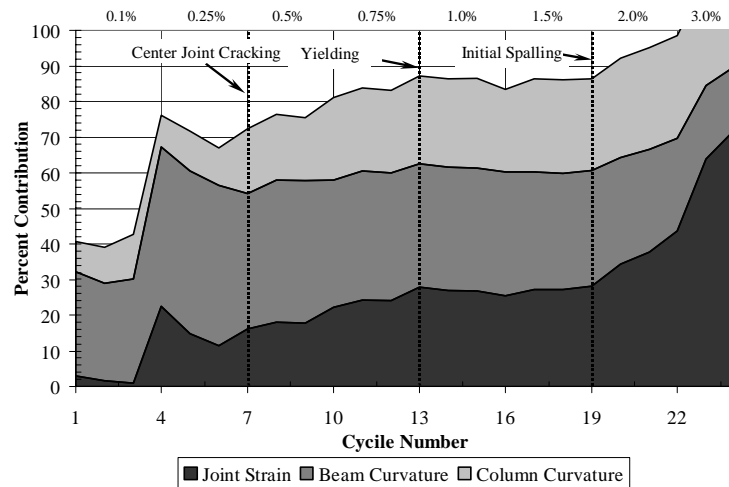


Figure 4 Components of Drift (Specimen PEER 0995)

The damage states identified were:

- Center joint cracking (first crack through the central region of the joint).
- Beam bar yielding.
- Initiation of joint spalling (first flaking of concrete in joint region).
- Extensive joint spalling (exposure of center column bar in joint region).

The sequence in which they occurred differed, depending on the specimen properties. Center Joint Cracking and Beam Bar Yielding are self-explanatory. Initiation of Spalling and Extreme Spalling are less obvious states. Examples are shown in figures 5a and b.

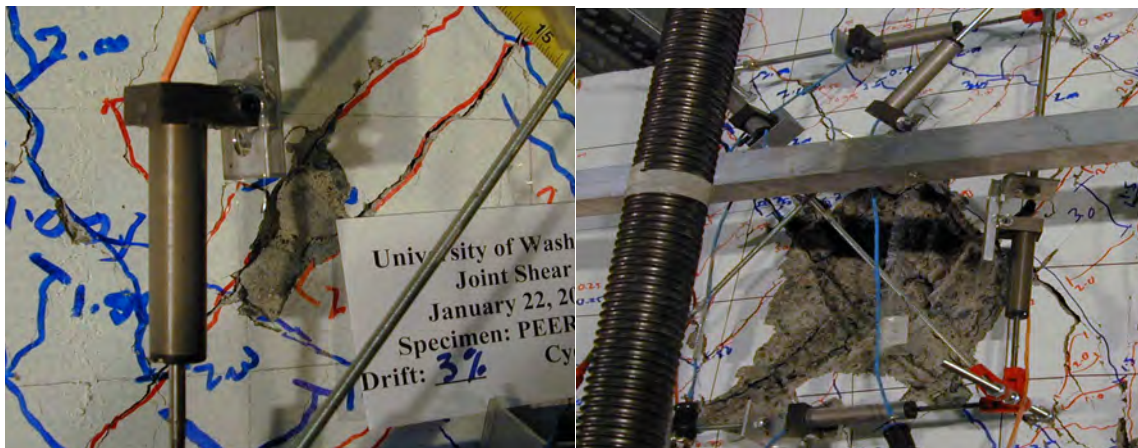


Figure 5 Initial Spalling (left) and Extensive Spalling (right).

Joint damage incurs repair costs, so it is of interest to relate the damage to some engineering parameter, such as drift or strain, so that it can be predicted from the results of a structural analysis. Damage was found to correlate best with joint strain. While it is not surprising that a local measure of deformation provides the best indicator of damage, it also emphasizes the need to include joint deformations in the analytical model. The damage cannot reliably be determined from a global parameter, such as drift, that would be the only choice if the joint shear deformations were not available. Furthermore, the prediction of damage is likely to be most reliable if the joint model reflects the degradation with cycling.

SIMULATION OF JOINT STRESS-STRAIN RESPONSE

A constitutive model was developed to simulate the response of the experimental specimens. The model has the ability to capture the degradation effects in the joint stiffness and strength as well as increase in pinching that result from cycling. The following provides a brief description of the model development and calibration. The model is currently being implemented in the OPENSEES structural analysis programming environment. A full description of the model development, operation, and implementation is provided in Anderson (2003).

Model Operation and Parameters

The proposed constitutive model was developed specifically to account for the important joint shear stress-strain curve characteristics demonstrated by the experimental results. Most importantly, the branch curves are controlled by relatively sophisticated rules to ensure that they reproduce correctly the wide range of observed behaviors. The key components of the model, illustrated in Figure 6, are:

- A tri-linear backbone curve, representing monotonic response
- Pre-yield and post-yield branch curves, to simulate cyclic deformation demands
- Functions to simulate degradation in strength and stiffness
- Pinched portions of the branch curves which degrade to represent the closing of increasingly wide cracks.

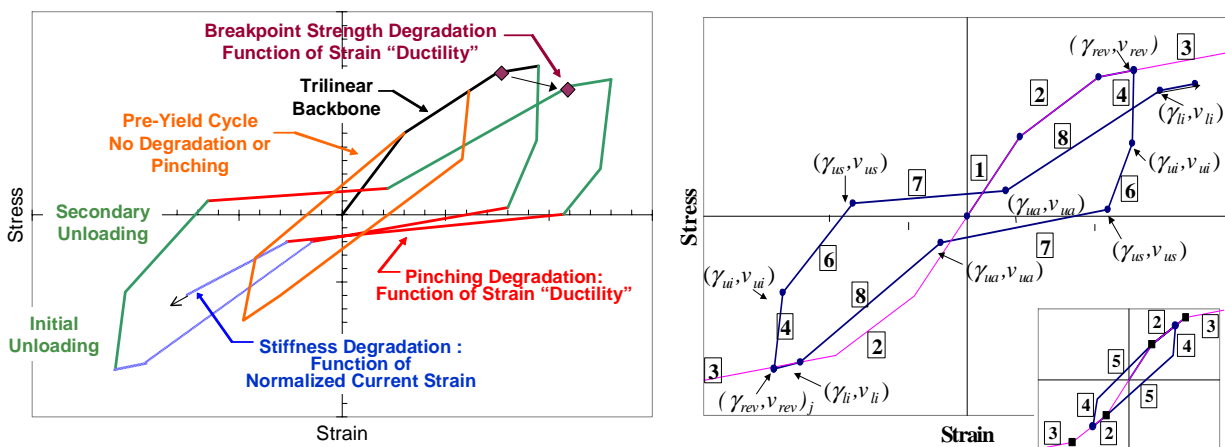


Figure 6: Characteristics of and Rules for Joint Shear Stress- Strain Constitutive Model

The backbone response is modeled using a tri-linear curve. For convenience, the breakpoints marking changes in stiffness are referred to as the ‘cracking’ and ‘yield’ points. However, they do not necessarily correspond to cracking of the joint core or yielding of the beam reinforcement.

The branch curves simulate the unloading and reloading responses, and their nonlinearity and degradation depend on the joint shear strain demand. The unloading or reloading portions of the branch curves are also tri-linear; the three segments are referred to as initial unloading, secondary unloading, and asymptotic unloading (Figure 6).

There are three categories of the joint response: pre-cracking, pre-yield, and post-yield response. The degree of inelastic action depends on the portion of the response curve in which the current strain lies. The response prior to cracking is modeled as elastic. The measured response indicates that cycling at strain levels below the threshold strain does not induce degradation. As such, in the model the pre-yield cycles result in inelastic loops that do not pinch or degrade (in the model the threshold strain is designated as the yield strain). Post-yield cycles induce pinching, stiffness and strength degradation.

In the three regions of the model, stress is obtained from strain using a series of hysteresis rules that are functions of input parameters and internal variables. The input parameters are constants supplied by the user and include stress and stiffness values that define the backbone curve as well as certain ratios that control cyclic behavior. Internal variables are used within the hysteresis rules and degradation functions, and their values change as loading progresses. In the following discussion, model input parameters are shown in bold and internal parameters are shown in italics. The input parameter and internal variable nomenclature is based on a system of main variables and primary and secondary subscripts. Main variables describe the type of parameter or internal variable; subscripts indicate the portion of the backbone or branch curve to which the parameter or variable applies. Outer subscripts are placed outside of parentheses and refer to the cycle number or direction.

Table 2 Hysteresis Rules

Rule	Segment	Label	Stiffness/Stress	Limits	Unloading	If Exceeded:
1	Pre-crack	cr	$G_{cr} = v_{cr}/\gamma_{cr}$	$\gamma_j < \gamma_{cr} < \gamma_{max}$	Rule 1	Rule 2
2	Pre-yield	yl	$G_{yl} = \frac{v_{yl} - v_{cr}}{\gamma_{yl} - \gamma_{cr}}$	$\gamma_{cr} < \gamma_j < \gamma_{yl} \leq \gamma_{max}$	Rule 4	Rule 3
3	Post-yield	py	$G_{py} = r_{G,py} * G_{sec,yl}$	$\gamma_{yl} < \gamma_j$	Rule 4	N/A
4	Initial Unloading	ui	$G_{ui} = r_{G,ui} * G_{sec,yl}$ $v_{ui} = r_{v,ui} * v_{rev,i}$			
	Pre-yield			$\gamma_{ui} < \gamma_j < \gamma_{rev} < \gamma_{yl}$	Rule 4	Rule 5
	Post-yield			$\gamma_{yl} < \gamma_{max} \quad \gamma_{ui} < \gamma_j < \gamma_{rev}$	Rule 4	Rule 6
5	Secondary Unloading Pre-yield	us	$G_{us} = \frac{v_{ui} - v_{cr}}{\gamma_{ui} - \gamma_{cr}}$	$(\gamma_{yl})_{opp} < \gamma_j < \gamma_{ui} \leq \gamma_{yl}$	Rule 4	Rule 2
6	Secondary Unloading Post-yield	us	$G_{us} = r_{G,us} * (G_{sec})_j$	$\gamma_{yl} < \gamma_{max}$ $\gamma_{us} < \gamma_j < \gamma_{ui}$	Rule 4	Rule 7
7	Asymptotic Unloading	ua	$G_{ua} = r_{G,ua} * G_{sec,yl}$	$\gamma_{yl} < \gamma_{max}$ $\gamma_{ua} < \gamma_j < \gamma_{us}$	Rule 4	Rule 8
8	Initial Loading Post-yield	li	$G_{li} = (G_{sec})_j = f(\alpha_{G, sec})$	$\gamma_{yl} < \gamma_{max}$ $\frac{\alpha_{v,yl} * v_{yl}}{(G_{sec})_j} < \gamma_j < \gamma_{ua}$	Rule 4	Rule 3

The monotonic backbone curve and the branch curves of the cyclic joint shear stress-strain response are defined by eight rules, as illustrated in Figure 6 and defined in Table 2. Three rules are used to define the backbone curve, two rules are needed for pre-yield branch curves, and an additional three rules are used to describe post-yield cycles. The stiffness rules are summarized in Table 2. The following provides a general description of the model components including model input and internal parameters and

associated main variables and subscripts. Recommended values for input parameters are provided in a later section.

Backbone Curve

A tri-linear backbone curve is used to model the monotonic response and envelope of the shear stress-strain response. The backbone curve is defined by two pairs of stress and stiffness input parameters (\mathbf{v}_{cr} , \mathbf{G}_{cr} and \mathbf{v}_{yl} , $\mathbf{G}_{sec,yl}$). Rules 1-3 are described in Table 2. The variables \mathbf{v}_{cr} and \mathbf{G}_{cr} are respectively the stress and secant stiffness to the cracking breakpoint. Similarly, \mathbf{v}_{yl} and $\mathbf{G}_{sec,yl}$ are the stress at yield and the secant stiffness from the origin to the yield point. This pair of variables defines the yield breakpoint. The yield strain, γ_{yl} is calculated as $\gamma_{yl} = \mathbf{v}_{yl} / \mathbf{G}_{sec,yl}$; strains larger than this induce degradation and pinching in the constitutive model. The input parameter $\mathbf{r}_{G,py}$ is a stiffness ratio (constant value) and is a multiplier on the yield secant stiffness $\mathbf{G}_{sec,y}$ to calculate the post-yield stiffness, G_{py} , as:

$$G_{py} = \mathbf{r}_{G,py} * \mathbf{G}_{sec,yl} \quad (1)$$

Pre-Yield Branch Curves

The branch curves are categorized as either pre-yield or post-yield, which determines the degree of degradation. Pre-yield branch curves consist of initial unloading and secondary unloading segments which are defined respectively by Rules 4 and 5 of Table 2. The initial unloading segment of the branch curve is the portion immediately following a reversal point (Segment 4 in Figure 6). The stiffness of the initial segment is designated as G_{ui} for an unloading segment. This stiffness is the product of an input stiffness ratio $\mathbf{r}_{G,ui}$ (recommended value of 20) and the yield secant stiffness $\mathbf{G}_{sec,yl}$, which results in an expression similar to that provided by Eq. 1. The stress at the breakpoint between the initial and secondary unloading segments is designated v_{ui} . This stress is the product of the input stress ratio $\mathbf{r}_{v,ui}$ (recommended value of 0.65) and the stress at the reversal point of the cycle $v_{rev,j}$. The secondary pre-yield unloading stiffness, G_{us} , is the slope of the line connecting the end of the initial unloading segment at v_{ui} to the cracking point in the opposite quadrant (γ_{cr} , \mathbf{v}_{cr}) (see Rule 5 in Table 2).

Post-Yield Branch Curves

Post-yield branch curves are defined using rules for initial unloading, secondary unloading, asymptotic unloading (or pinching) and the initial reloading portion of the branch curve. The post-yield initial unloading segment is also defined using Rule 4. The secondary unloading stiffness, G_{us} , is a ratio of the yield secant stiffness, $\mathbf{G}_{sec,yl}$, and a constant, $\mathbf{r}_{G,us}$, as given by Rule 6 (Eq. 2). Observations indicate that this ratio increases with an increase in the joint shear stress demand. The recommended expression is given by Eq. 2:

$$G_{us} = \mathbf{r}_{G,py} * \mathbf{G}_{sec,yl}; \quad \mathbf{r}_{G,py} = 0.2(v_j / (A_j \sqrt{f'_c})) + 0.59 \leq 3.5 \quad (2)$$

One of the primary differences between the pre- and post-yield branch curves is the use of degradation parameters to reduce the strength and stiffness. Figure 7 shows the measured response of Specimens CD30-1450 and PEER-2250. Figure 7a illustrates the secant stiffness (from the origin) of the ascending curves and shows that the stiffness degrades significantly with increases in the strain demand. Figure 7b shows the breakpoint (location of abrupt change in stiffness) of the ascending curves. Again, significant stress degradation occurs at large strain values. As a result, the proposed degradation relationships are functions of normalized strain demands (as indicated in Figure 6). Relative to other cyclic models, they are simpler to track in that they do not depend on counting cycles or tracking the dissipated energy.

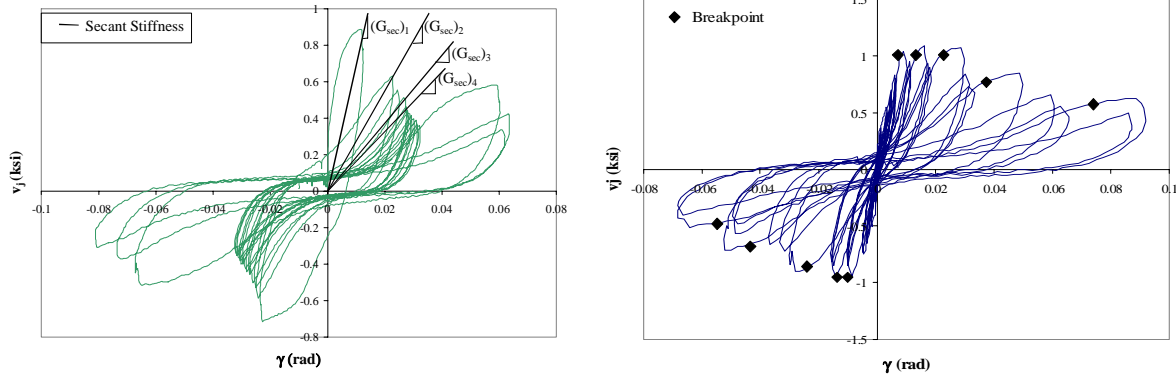


Figure 7 Influence of Strain Demand on (a) Stiffness and (b) Breakpoint Stress of Ascending Branch

Mathematical expressions were developed to model these two sources of degradation. Figure 6 illustrates both. The stiffness degrades only if the strain demand exceeds the current maximum strain reversal. Therefore, degradation in the secant stiffness of the ascending branch, $G_{j+1,sec}$ (for the $j+1$ cycle) is a nonlinear function of the strain demand for cycle j relative to the maximum reversal strain. If the strain limits are exceeded, the secant stiffness is calculated as:

$$G_{sec,j+1} = \alpha_{G,sec,j} * G_{sec,j} \quad (3)$$

For larger strain ratios, the multiplier, $\alpha_{G,sec}$, decreases. In addition, the stiffness degrades due to cycling in the opposite direction. This additional degradation is accounted for using a second multiplier (see Anderson 2002).

Degradation in the breakpoint stress occurred for strain demands that were large relative to the yield strain. Because the strain is normalized to the “yield” strain, this strain ratio is referred to as the strain ductility for convenience. Again, the multiplier on the breakpoint stress degrades with an increase in the strain ductility and with cycling in the opposite direction. Relations for each multiplier have been developed for the test specimens and are provided in Anderson (2002).

The experimental results indicate that pinching in the hysteresis curves becomes more severe with strain demands that exceed the yield strain. In the model, this response is represented analytically by a pair of degrading, pinching asymptotes. Each asymptote is defined by a number pair consisting of a stress intercept, $v_{ua,o}$, and secant stiffness values, G_{ua} . The pair of asymptote values is calculated using Equation 4, which degrades the stress and stiffness relative to the backbone yield values. The values of $r_{v,ua}$ and $r_{G,ua}$ are using degradation relations which are a function of the strain ductility values. The functions relating $r_{v,ua}$ and $r_{G,ua}$ to the strain ductility are tri-linear and decrease in value with an increase in the strain ductility. Calibrated functions are available in Anderson (2002), although the model is general and the functions may be defined by user input parameters. The breakpoint marking the initiation of pinching, v_{us} in Figure 6b, is the intersection of the secondary unloading leg of the branch curve and the unloading asymptote.

$$\begin{aligned} G_{ua} &= r_{G,ua} * G_{yl} \\ v_{ua} &= r_{v,ua} * v_{yl} \end{aligned} \quad (4)$$

The stiffness of the ascending branch of the curve that follows the pinching portion is referred to as initial loading and defined using Rule 8 in Table 2 (shown in Figure 6b) and Eq. 3. The breakpoint between the pinching asymptote and the initial loading segment, indicated by v_{ua} in Figure 6b, is the intersection of the unloading asymptote and the secant line defined by $G_{sec,j}$.

The previous discussion has summarized the operation of the constitutive model. Details and examples of model implementation are available in Anderson (2003).

Model Calibration and Validation

The experimental test data were used to calibrate the model parameters that determine the five model components. The calibration procedure was as follows: (1) Identify model parameters for each model component (as discussed in previous section). (2) Use measured trends to establish initial estimates of parameter relationship and values. (3) Minimize a local error measure to determine the best-fit expression and values for each model parameter. (4) Minimize a global error measure to refine the best-fit estimate. (5) Combine all best-fit expressions to develop a single recommended expression for each model parameter.

Individual best-fit expressions were developed for the data from each test series, since the model parameter may depend on the joint properties. For example, the monotonic response (or backbone response) curve depends on the joint shear stress demand but is independent of the displacement history. Therefore, all of the specimens within a test series (e.g., Test Series 1450) were used to develop a single best-fit calibration expression. The recommended expressions were derived using all of the best-fit expressions. Specific details on the calibration procedures, error measures, and the data-specific values may be found in the original reference (Anderson 2003).

The Walker-Alire experimental data were used to validate the constitutive model using the recommended expressions. The results indicate that the model is capable of approximating a range of joint shear stress demands and displacement histories, as shown in Figures 8 and 9. Figure 8 shows the measured and predicted responses of specimens PEER-1450 and PEER-2250, where PEER-1450 represents an average level of joint shear stress demand (and approximately equal to the ACI limit) and PEER-2250 represents a larger joint shear stress demand which may be found in existing construction (Mosier 2000). The results indicate that the model captures the cyclic responses of both specimens

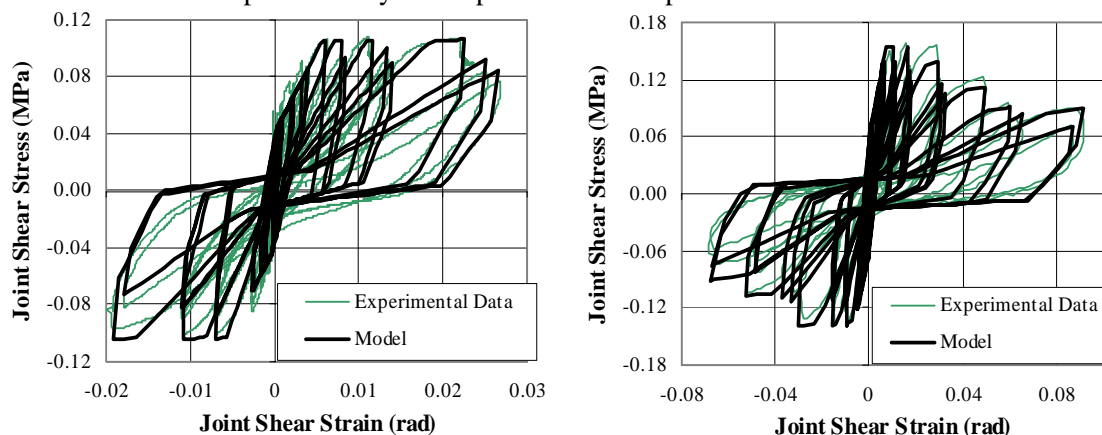


Figure 8 PEER-1450 and PEER-2250: Measured and Predicted Joint Shear Response

Previous research indicates that although other constitutive models may also effectively model standard deformation histories, few can adequately model unconventional histories (Anderson 2003). The proposed model is capable of modeling a wide range of shear strain histories, which represents a significant advancement. To illustrate this capability, the measured and predicted responses of specimens PADH-1450 and CD15-1450 are studied (Figure 9). The model is capable of predicting the slow degradation exhibited by CD15-1450 and the highly non-symmetric history of PADH-1450. The strength and stiffness of the final negative cycles of the PADH-1450 are over-predicted. However, these are cycles to 4% and 5% drift following a large 5% drift demand in the opposite direction and therefore modeling accuracy at

this large shear strain was sacrificed in order to permit better accuracy at the lower shear strain cycles (after the large pulse).

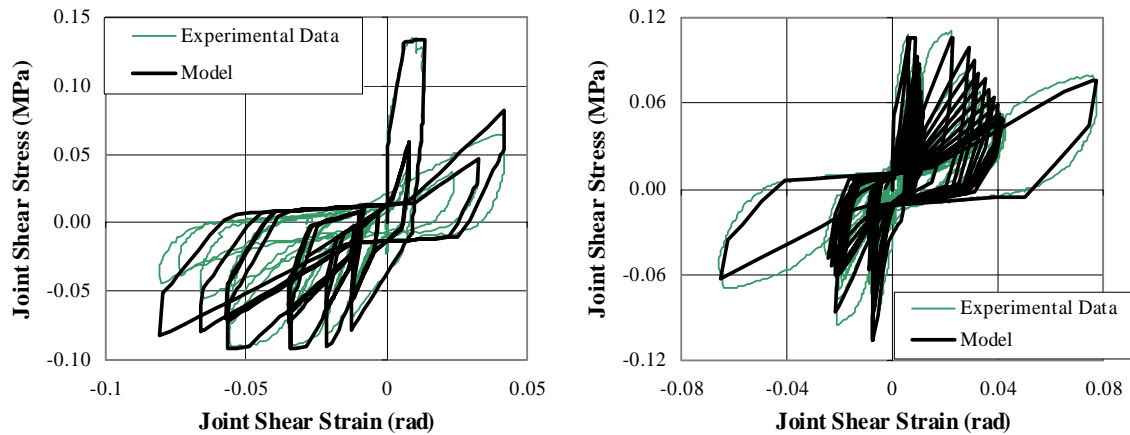


Figure 9 PADH-1450 and CD15-1450: Measured and Predicted Joint Shear Response

An independent experimental data set was used to further validate the model. For proper validation, the joint shear stress-strain data was needed and this is not always available. In addition, the specimen should model joints in non-ductile frame construction; few researchers have tested beam-column joints with little or no joint transverse reinforcement. Data from a specimen tested by Leon met the validation criteria (Leon 1990). The specimens had a peak joint shear stress demand of approximately $1.25\sqrt{f'_c}$ MPa ($15\sqrt{f'_c}$ (psi)) and a volumetric joint reinforcement ratio of approximately 0.6%. Figure 10 shows the measured and predicted responses of the specimen. The model predicts the cyclic response well, including degradation in the strength, stiffness, and pinching portion of the response.

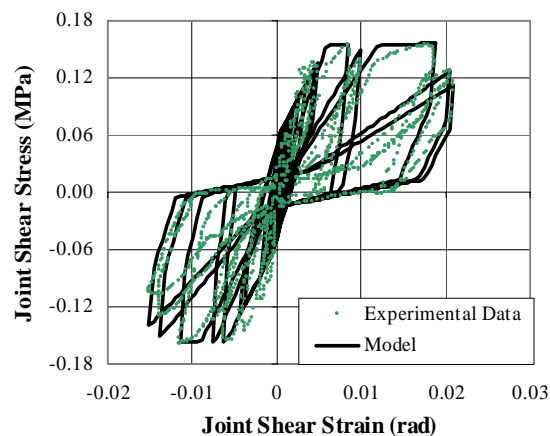


Figure 10 Measured and Predicted Response of Specimen BCJ2 (Leon 1990)

SUMMARY AND CONCLUSIONS

A test program was carried out to study the cyclic behavior of beam column joints in older reinforced concrete frames and designed to focus evaluating the joint shear behavior. The joints contained no transverse reinforcement, and the joint shear stress demand was varied by suitable selecting suitable beam bars. A primary study variable was the displacement history. Four different displacement histories were used which modeled the influence of asymmetric and constant-amplitude drift demands on the joint response. The experimental findings were used to evaluate the seismic performance of the specimen. Four aspects of joint performance were noted. First, the compressive strength of the joint must be sufficient to

carry the gravity load on the column and this condition was satisfied in every test. The second behavioral feature of interest showed that, for joints without transverse reinforcement the strength varies significantly with bar yielding and displacement history. The third and fourth critical features of joint behavior are the joint stiffness and damage accumulation, which both relate to the displacement history. During the course of the experiments, the joint stiffness dropped significantly as damage occurred which indicates that modeling the joints in a frame analysis as rigid is likely to lead to a significant underestimate of the lateral drift. The drift affects not only the damage to the non-structural components, but also the possibility of instability due to P- Δ effects. The primary damage states included cracking, yielding, joint spalling, and damage to the core concrete. Damage was found to correlate best with joint strain which also emphasizes the need to include joint deformations in the analytical model. Furthermore, a constitutive model for joint deformations should reflect the degradation with cycling.

The second phase of the research program was conducted to develop a constitutive model to simulate the degradation in the joint response and support performance evaluation of frames with joints without transverse reinforcement. To develop this model, measured joint shear strain data were used to establish general characteristics of the response in joints that represent pre-1970s construction. The proposed constitutive model was developed and calibrated using these observations. The model includes a backbone curve, to model the monotonic response, and unloading and reloading branch curves that consist of initial, secondary, and asymptotic (or pinching) segments. A series of expressions was developed for each component of the model. These expressions were calibrated using the experimental data and were simplified for general application of the model. Strength and stiffness degradation were explicitly included in the branch curves. The degradation expressions depend only on a characteristic of the previous strain history (e.g., the maximum reversal strain to date) rather than the entire strain history. In that respect, the model provides a unique method of accounting for cyclic degradation in that counting cycles or tracking energy is not required.

ACKNOWLEDGEMENTS

Funding for the experimental testing was provided by NSF under Award Number EEC-9701568 through the PEER center. The Department of Civil and Environmental Engineering at the University of Washington (UW) supported the graduate studies of Daniel Alire. The Valle Scholarship Program supported the graduate studies of Meredith Anderson. All sources of funding are gratefully acknowledged.

REFERENCES

- ACI Committee 318 (2002). "Building Code Requirements for Structural Concrete (ACI 318-02) and Commentary (ACI 318R-02). ACI, Farmington Hills, MI.
- Alire, D.A. (2002). "Seismic Evaluation of Existing Unconfined Reinforced Concrete Beam-Column Joints", MSCE Thesis, Dept. of Civil Engineering, University of Washington. 291 p.
- Anderson, M.A. (2003). "Analytical Modeling of Existing Reinforced Concrete Beam-Column Joints", MSCE Thesis, Civil and Environmental Engineering, University of Washington. 308 p.
- Durrani, A.J. and Wight, J.K. (1985). "Behavior of Interior Beam-to-Column connection Under Earthquake-Type Loading", *ACI Jo.*, Title No. 82-30, ACI, Farmington Hills, MI, May-June. pp. 343-350.
- Ehsani, M.R. and Wight, J.K. (1985). "Exterior R/C Beam-to-Column Connections Subjected to Earthquake-Type Loading", *ACI Jo.*, Title No. 82-43, ACI, Farmington Hills, MI, July-Aug. pp. 421-428.
- Hanson, N., Connor, H. (1967) "Seismic Resistance of Reinforced Concrete Beam-Column Joints". *Proc. ASCE, Jo. Str. Div.*, 93(ST5), Oct., pp. 533-560.

- Leon, R.T. (1990). "Shear Strength and Hysteretic Behavior of Interior Beam-Column Joints", *ACI Str. Jo.*, 87(1), Jan.-Feb. pp. 3-11
- Meinheit, D.F. and Jirsa, J.O. (1981). "Shear Strength of RC Beam-Column Connections". *Proc. ASCE, Jo. Str. Div.*, 107 (ST11), Nov. pp.
- Raynor (2000). "Bond Assessment of Hybrid Fiber Continuity Reinforcement". MSCE Thesis, Dept. of Civil Engineering, University of Washington. 248 p.
- "*Uniform Building Code*". (1997). International Conference of Building Officials, Whittier, CA.
- Walker, S.G. (2001). "Seismic Performance of Existing Reinforced Concrete Beam-Column Joints". MSCE Thesis, Dept. of Civil Engineering, University of Washington. 308 p.

SECTION B

THE ANALYSIS AND DESIGN OF AND THE EVALUATION
OF DESIGN ACTIONS FOR REINFORCED CONCRETE DUCTILE SHEAR WALL STRUCTURES

T. Paulay* and R.L. Williams**

ABSTRACT:

A comprehensive review of the state of the art in the design of earthquake resisting ductile structural walls is presented. The material has been compiled from the technical literature, the deliberations within the New Zealand National Society for Earthquake Engineering and research efforts at the University of Canterbury. The paper attempts a classification of structural types and elaborates on the hierarchy in energy dissipation. After a review of available analysis procedures, including modelling assumptions, a detailed description of capacity design procedures for both cantilever and coupled shear wall structures is given. The primary purpose of capacity design is to evaluate the critical design actions which can be used in the proportioning and reinforcing of wall sections. An approach to the estimation of structural deformation is suggested. To satisfy the ductility demands imposed by the largest expected earthquake, detailed design and detailing recommendations are given and the application of some of these is presented in an appendix.

INTRODUCTION:

The usefulness of structural walls in the planning of multistorey buildings has long been recognized. When walls are situated in advantageous positions in a building, they can become very efficient in lateral load resistance, while also fulfilling other functional requirements.

Because a large portion of the lateral load on a building, if not the whole amount, and the horizontal shear force resulting from it, are often assigned to such structural elements, they have been called shear walls. The name is unfortunate because shear should not be the critical parameter of behaviour.

The basic criteria that the designer will aim to satisfy when using structural walls in earthquake resistant structures are as follows:

- (a) To provide adequate stiffness so that during moderate seismic disturbances complete protection against damage, particularly in non-structural components, is assured.
- (b) To provide adequate strength to ensure that an elastic seismic response, generating forces of the order specified by building codes⁽¹⁾, does not result in more than superficial structural damage. Even though during such an event some non-structural damage is expected, it is unlikely that in buildings with well designed shear walls this will be serious.
- (c) To provide adequate structural ductility and capability to dissipate energy for the case when the largest disturbance to be expected in the region does occur. Extensive damage, perhaps beyond the possibility of repair, is accepted

under these extreme conditions, but collapse must be prevented.

- (d) The subsequent sections concentrate on those aspects of the design and response of structural walls that are relevant to this third design criterion. Consequently the inelastic response of structural walls, when subjected to simulated cyclic reversed loading, together with various parameters that must affect this response, will be examined in some detail for various types of structures. It will be assumed that in all cases adequate foundations can be provided so that rocking will not occur and that energy dissipation, when required, will take place in the structural wall above foundation level. A detailed discussion of concepts, relevant to the design of foundations for shear wall structures, is provided in Reference 5. Also it will be assumed that:
 - (i) Inertia forces at each floor can be introduced to the structural wall by adequate connections, such as collector beams or diaphragms and from the floor system, and that
 - (ii) The foundation for each wall does not significantly affect its stiffness relative to similar other walls in a building.

TYPES OF DUCTILE STRUCTURAL WALLS:

In this section the principles of the analyses and the design of earthquake resisting structural walls, in which significant amounts of energy can be dissipated by flexural yielding in the superstructure, are examined. The prerequisite in the design of such seismic walls is that flexural yielding in clearly defined plastic hinge zones must control the strength to be utilized during imposed inelastic seismic displacements. As a

* Professor of Civil Engineering, University of Canterbury, Christchurch

** District Structural Engineer, Ministry of Works & Development, Hamilton

corollary to this requirement, failure due to shear, inadequate anchorage or splicing of the reinforcement, instability of concrete components or compression bars and sliding along construction joints must be avoided, while large inelastic seismic displacements are sustained by the structure. Some of the failure modes mentioned are illustrated in figure 1.

In the evaluation of the equivalent lateral static design load, to be used in establishing the minimum seismic strength of a structure, the New Zealand Design and Loading Code⁽¹⁾ specifies structural type factors, S . These factors are intended to reflect the expected seismic performance of the structure. There are two aspects which are to be considered in the assessment of performance, one is the ability of the type of structure to dissipate energy in a number of inelastic displacement cycles, and the other is the degree of redundancy existing in the chosen structural system. A high degree of structural redundancy, involving a large number of localities where energy dissipation by flexural yielding can occur, is desirable.

Accordingly it is recommended that earthquake resisting ductile structural walls be classified as follows:

- (a) Two or more cantilever walls with a height, h_w , to horizontal length, l_w , ratio of not less than two are assigned a structural type factor of $S = 1.0$ (see figure 2a).
- (b) For two or more cantilever walls, each with an aspect ratio h_w/l_w not less than two, which are coupled by a number of appropriately reinforced ductile coupling beams that are capable of dissipating a significant portion of the seismic energy, the value of S is 0.8. This is in recognition of the high degree of redundancy and the fact that damage is likely to be small in the gravity load carrying elements.
- (c) Single cantilever walls, with $h_w/l_w > 2$, are to be designed with $S = 1.2$, to compensate for the lack of redundancy. (See figure 2b).
- (d) Squat cantilever walls with an aspect ratio of $h_w/l_w < 2$, in which shear effects are likely to be dominant, are not expected to produce as efficient energy dissipation due to flexural ductility as more slender structural walls. Shear deformations, particularly shear sliding, may cause significant pinching in the hysteresis loops exhibited by squat shear walls⁽²⁾, and thereby loss of energy dissipation will occur.

The significance of the coupling beams in energy dissipation is conveniently expressed by the contribution of the coupling beams to the total overturning moment that is produced by the code specified lateral loading at the base of the coupled shear wall structure. This is illustrated in figure 17. A suitable parameter which expresses this is the moment ratio

$$A = \frac{T\ell}{M_0} \quad (B-1)$$

where T = induced axial load in one of the two coupled shear walls at the base of the structure due to the code specified lateral static loading

ℓ = distance between axes of the two walls

M_0 = overturning moment due to the

load inducing T , about the base of the structure

These quantities may be seen in figure 17.

Depending on the contribution of the beams to the resistance of overturning moment and hence to total energy dissipation, the structural type factor, S , is made dependent on the moment ratio, A , thus

$$\text{when } 0.67 \geq A \geq 0.33 \quad (B-2)$$

$$\text{then } 0.8 \leq S = 0.8 + 0.6 \times (0.67 - A) \leq 1.0 \quad (B-3)$$

For intermediate values of A a linear interpolation of S may be made. The application of this is discussed in detail in section B.5.3.4.

Typically for a wall with deep coupling beams, illustrated in figure 17b, the appropriate S factor is likely to be 0.8. When walls are interconnected by slabs only, (figure 17c) as is often the case in apartment buildings, the value of A from Eq. (B-1) will usually be much less than 0.33 and hence $S = 1.0$. A comparison of the moment contribution of the ℓT component to the total overturning moment M_0 is shown in figure 18.

In order to reduce the displacement ductility demand on squat walls, the strength of the walls with respect to seismic loading should be increased. Hence for walls for which $1 \leq h_w/l_w < 2$, the structural type factor given above in (a), (b) and (c) should be multiplied by Z where

$$1 \leq Z = 2.2 - 0.6 h_w/l_w \leq 1.6 \quad (B-4)$$

It is to be noted that the use of higher structural type factors, i.e. $S = 1.6 \times 1.0 = 1.6$ or $S = 1.6 \times 1.2 = 1.92$, is expected only to reduce but not to eliminate the ductility demand on squat shear walls.

Squat walls will have a relatively low fundamental period ($T < 0.6$ sec). It is known that short period structures, designed to the requirements of the New Zealand loading code⁽¹⁾, are likely to be subjected to higher ductility demands than long period structures.

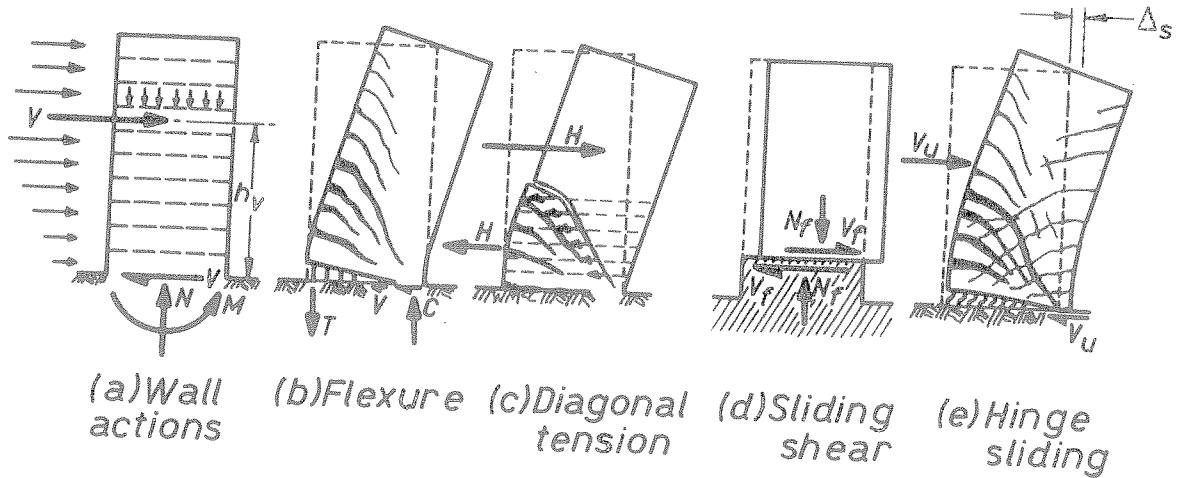


Fig. 1 - Possible Failure Modes in Cantilever Shear Walls

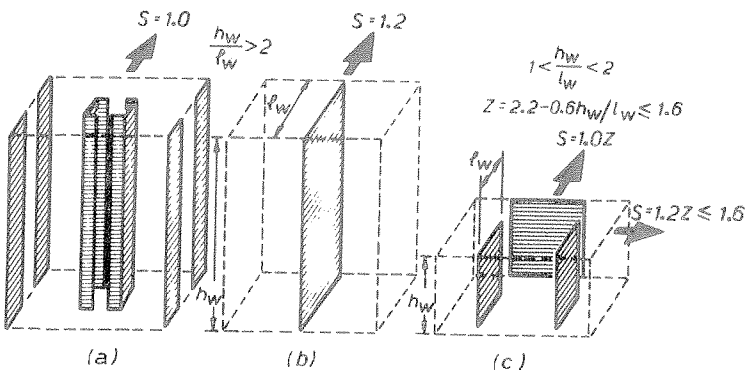


Fig. 2 - Types of Cantilever Shear Walls with Appropriate S Factors

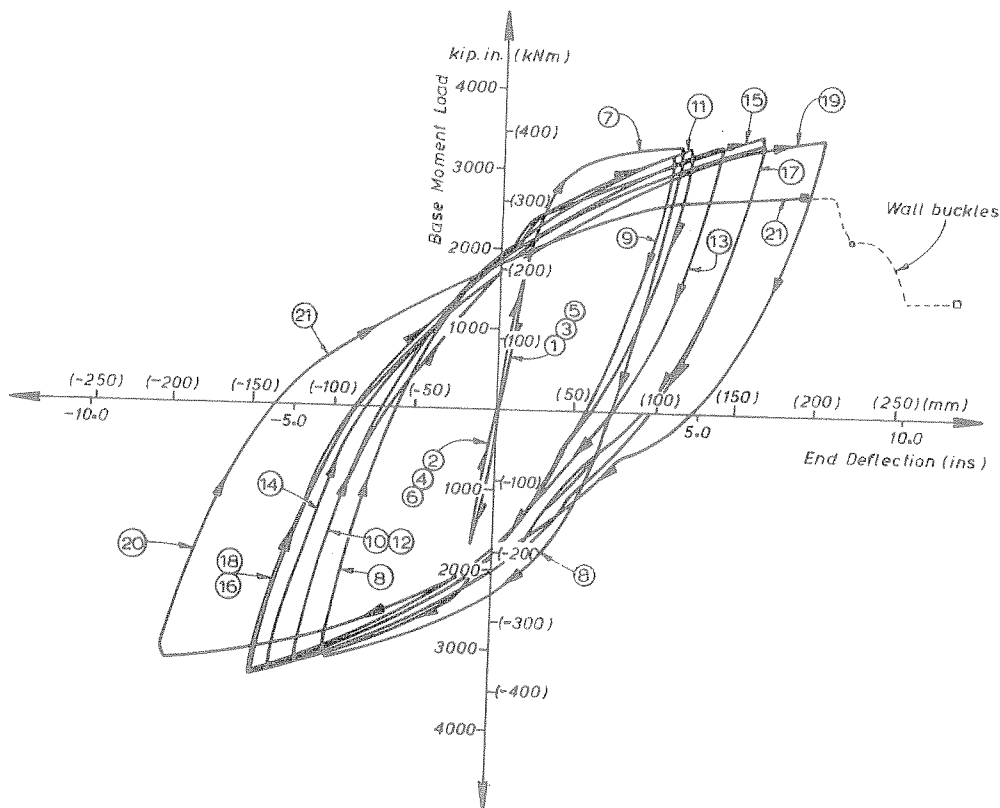


Fig. 3 - Load-Displacement Response to Cyclic Reversed Loading of a Ductile Shear Wall Structure (10)

Moreover, in a given earthquake, a short period squat shear wall is likely to be subjected to a greater number of excursions beyond yield than a long period structure. Therefore the cumulative ductility, which has some relevance to damage, is still high. These observations indicate that squat shear walls, such as shown in figure 2c, designed with a modified structural type factor, S , must also be ductile and hence they must be detailed accordingly.

Structural walls of different types are reviewed in Reference 3 and detailed procedures recommended for walls which cannot be made fully ductile are presented in Reference 4. The requirements for the design of foundations which can sustain inelastic superstructures when their maximum feasible seismic strength is being developed, are examined in Reference 5.

HIERARCHY IN ENERGY DISSIPATION:

It is generally accepted that for most situations energy dissipation by hysteretic damping is a viable means by which structural survival of large earthquake imposed displacements can be assured. This may involve very large excursions beyond yield. Such structures must therefore be ductile. To ensure the desired energy dissipation, the designer's primary aim will be to minimize the inevitable degradation in both stiffness and strength.

Flexural Yielding of Ductile Walls

An obvious source of hysteretic damping is the yielding of the principal flexural reinforcement. Yielding can be restricted to well defined plastic hinge zones, as shown in figure 1b. Therefore such areas deserve special attention. Concrete, being a relatively brittle material that shows rapid strength degradation, in both compression and shear, when subjected to repeated inelastic strains and multi-directional cracking, should not be considered in structural walls as a significant source of energy dissipation. To ensure the desired ductility, the major part of the internal forces in the potential plastic region of a shear wall should therefore be allocated to reinforcement. The desired response of a ductile shear wall structure manifests itself in well rounded load-displacement hysteresis loops, such as shown in figure 3.

Control of Shear Distortions

While shear resisting mechanisms in reinforced concrete, that rely on the traditional truss mechanism (figure 1c), can be made relatively ductile in shear during monotonic loading, they are generally unsuitable for inelastic cyclic shear loading. Shear resistance after inelastic shear displacements can be attained only when the subsequent imposed displacement is larger than the largest previously encountered displacement. Inelastic tensile strains in stirrup reinforcement can never be recovered and hence in such

cases the width of diagonal cracks also increases with progressive cyclic loading. Curves 3 and 4 in figure 4 show typical load displacement responses for one quadrant of a displacement cycle, which have been affected by significant shear displacements. In comparison curves 1 and 2 show the idealized elastic-plastic and the optimal response of a reinforced concrete member. In order to minimize the 'pinching' of hysteresis loops, i.e. the loss of energy dissipating capacity within restricted displacements, designers should endeavour to suppress inelastic shear distortions. In conventionally reinforced walls the detrimental effect of shear increases with the magnitude of the shear stress. For example figure 5 shows the hysteretic response of a cantilever shear wall in which, due to relatively large shear stresses, shear deformations have become increasingly significant with increased cycles of loading and the amplitude of the applied deflection at the top of the wall. It is also seen that in each cycle the stiffness of the wall decreased, even though the full capacity of the wall was attained. The envelope curve follows closely the load-displacement curve that is obtained during monotonic loading with the same displacement ductility. If several cycles with the same magnitude to top displacement are applied, for example to 4 in (10 cm) in each direction, (see figure 5), the load attained would have gradually decreased in each cycle. Such a wall is likely to fulfill the design criteria but its performance is clearly inferior to that demonstrated in figure 4.

The Desired Hierarchy in Strength

From the features considered above it becomes evident that the design procedure must endeavour to minimize the likelihood of a shear failure, even during the largest intensity shaking. This is achieved by evaluating the flexural capacity of a wall from the properties shown on the structural drawings. With proper allowance for various factors, to be examined in "Capacity Design Procedures", the likely maximum of the moment that can be extracted from a shear wall structure during an extreme seismic inelastic displacement can be readily evaluated. The shear force associated with the development of such a moment can then be estimated. This must be done using conservative estimates. Subsequently the wall can be reinforced so as to possess corresponding shear strength.

When the shear strength of a wall is not in excess of the flexural strength, a situation which commonly arises in squat shear walls, not only does stiffness degradation occur but the attainable full capacity of wall will also reduce with cyclic displacements. Such an undesirable response is shown in figure 6.

Similar procedures must be followed to ensure that other undesirable failure modes, such as due to bond and anchorage of the reinforcement or sliding along construction joints, will not occur while the maximum flexural capacity of the wall, usually at its base, is being developed

several times in both directions of the loading.

Capacity design procedures will ensure that the desired hierarchy in the energy dissipating mechanism can develop. The procedure is quantified and discussed in detail in "Capacity Design Procedures".

ANALYSIS PROCEDURES:

Modelling Assumptions

Modelling of member properties -

When, for the purpose of either a static or dynamic elastic analysis, stiffness properties of various elements of reinforced concrete shear wall structures need be evaluated, some approximate allowance for the effects of cracking should be made. In this, it is convenient to assume that reinforced concrete components exhibit properties that are similar to those of elements with identical geometric configurations but made of perfectly elastic, homogeneous and isotropic materials. For the sake of simplicity an approximate allowance for shear and anchorage deformations is also made.

These recommendations for modelling may be considered to lead to acceptable results when the primary purpose of the elastic analysis is the determination of internal structural actions that result from the specified lateral static loading or from dynamic modal responses. The estimates given below are considered to be satisfactory also for the purpose of predicting the fundamental period of the structure and for checking deflections in order to satisfy code specified limits for deflections or separations of non-structural components.

In ductile earthquake resisting structures significant inelastic deformations are expected. Consequently the allocation of internal design actions in accordance with an elastic analysis should be considered as one of several acceptable solutions which satisfy the unviolable requirements of internal and external equilibrium. As will be seen subsequently, deliberate departures in the allocation of design actions from the elastic solutions are not only possible, but they may also be desirable.

When it is necessary to make a realistic estimate of the deformations of an elastic wall system which is subjected to a relatively high intensity loading, the absolute value of the stiffness is required. Rather than specify a stiffness, an equivalent second moment of area of the wall section, I_e , will be defined in order to allow deflections to be estimated for various patterns of loading. The first loading of a wall up to and beyond first cracking is of little interest in design. In this recommendation only deformations of the wall, in which cracks have fully developed during previous cycles of elastic loading, will be considered.

In arriving at the equivalent stiffness of a wall section, flexural deformations of the cracked wall, anchorage deformations at the wall base and shear deformations after the onset of diagonal cracking should be considered. Detailed steps of these approximations are set out in Appendix I.

Deformations of the foundation structure and the supporting ground, such as tilting or sliding, are not considered in this study, as these produce only rigid body displacement for the shear wall superstructure. Such deformations should, however, be taken into account when the period of the structure is being evaluated or when the deformation of a shear wall is related to that of adjacent frames or walls which are supported on independent foundations(5).

Accordingly, for cantilever shear walls subjected predominantly to flexural deformations, the equivalent second moment of area may be taken as 60% of the value based on the uncracked gross concrete area of the cross section, with the contribution of reinforcement being ignored i.e.

$$I_e = 0.60 I_g \quad (B-5)$$

When elastic coupled shear walls are considered, where, in addition to flexural deformation, extensional distortions due to axial loads are also being considered, the equivalent moment of inertia and area may be estimated as follows:

(a) For a wall subjected to axial tension

$$I_e = 0.5 I_g \quad (B-6)$$

$$A_e = 0.5 A_g \quad (B-7)$$

(b) For a wall subjected to compression

$$I_e = 0.8 I_g \quad (B-8)$$

$$A_e = A_g \quad (B-9)$$

(c) For diagonally reinforced coupling beams

$$I_e = 0.4 I_g \quad (B-10)$$

(d) For conventionally reinforced coupling beams or coupling slabs

$$I_e = 0.2 I_g \quad (B-11)$$

In the above expressions the subscripts "e" and "g" refer to the "equivalent" and "gross" properties respectively.

When only slabs connect adjacent shear walls, the equivalent width of slab to compute I_g may be taken as the width of the opening between the walls or 8 times the thickness of the slab, whichever is less.

For cantilever walls with aspect ratios, h_w/ℓ_w , larger than 4, the effect of shear deformations upon stiffness may normally be neglected. When a combination of "slender" and "squat" shear walls provide the seismic resistance, the latter may be allocated an

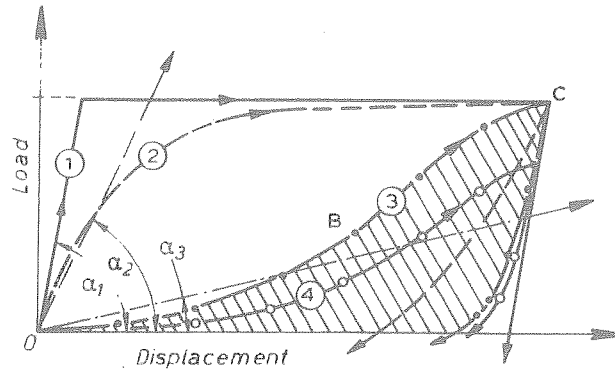


Fig. 4 - Load-Displacement Response for (1) Idealized, (2) Optimal, (3) (4) Repeated Shear Affected Conditions in Reinforced Concrete Members.

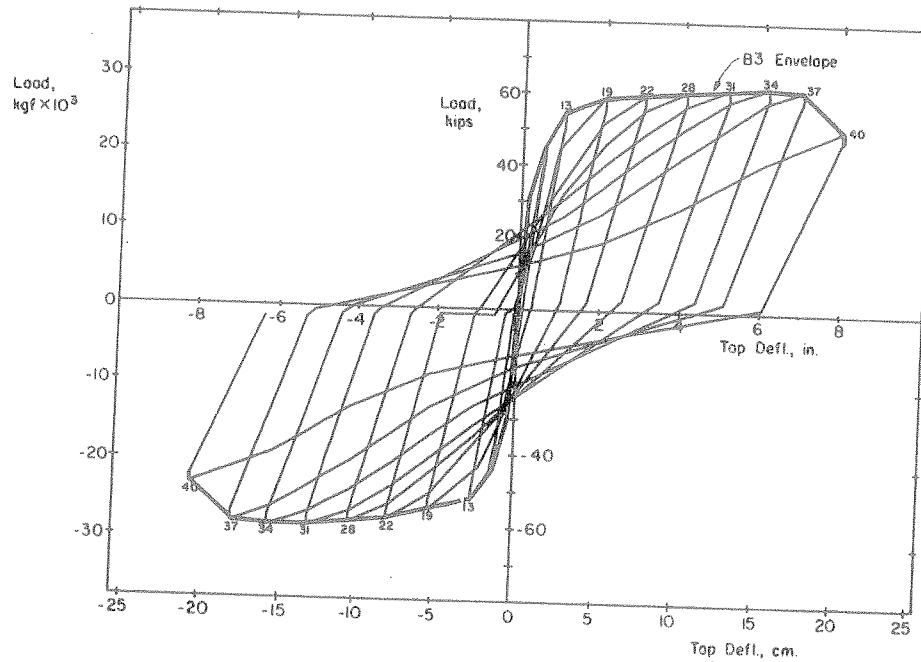


Fig. 5 - The Hysteretic Response of a Cantilever Shear Wall with Significant Shear Deformations (11)

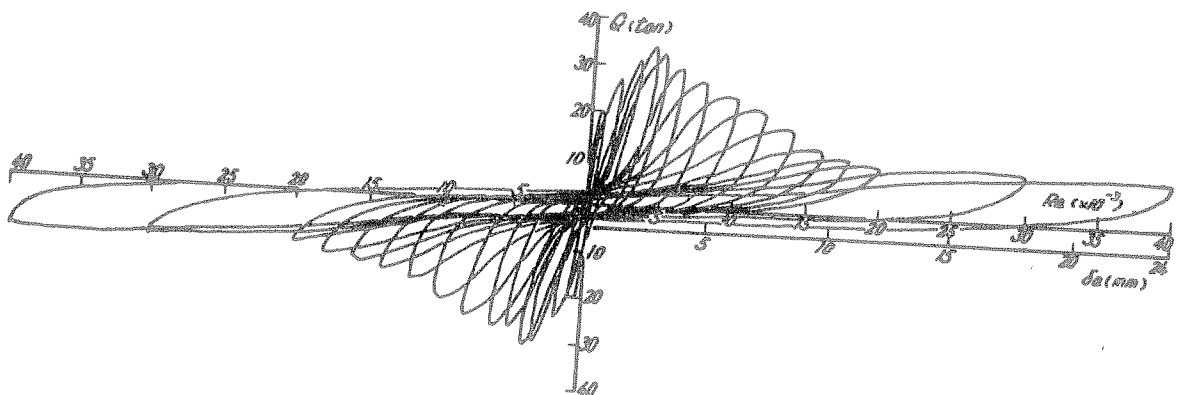
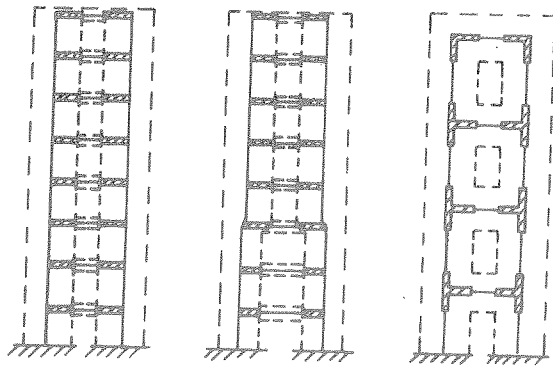


Fig. 6 - The Hysteretic Response of a Shear Wall in which Shear governs the strength.



WIDE COLUMN FRAME (a)

Fig. 7 The Modelling of Coupled Shear Walls for (a) Frame Analysis or (b) Laminar Analysis

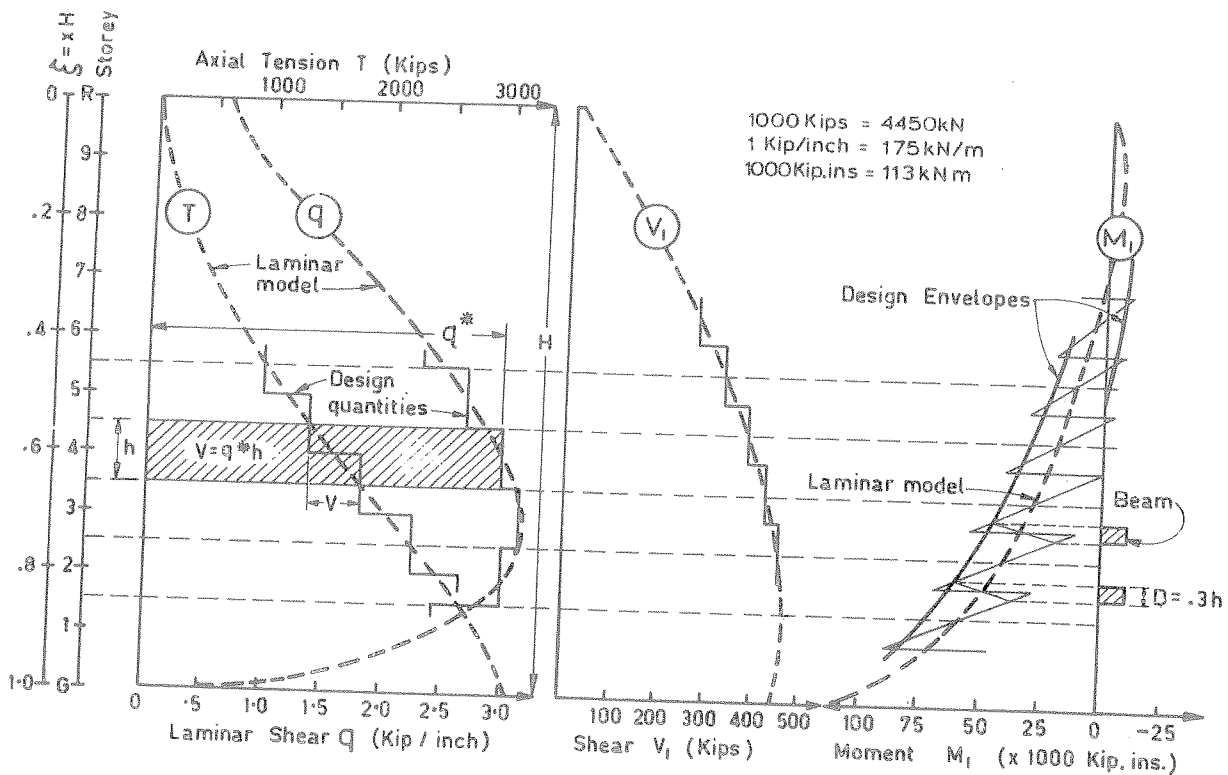
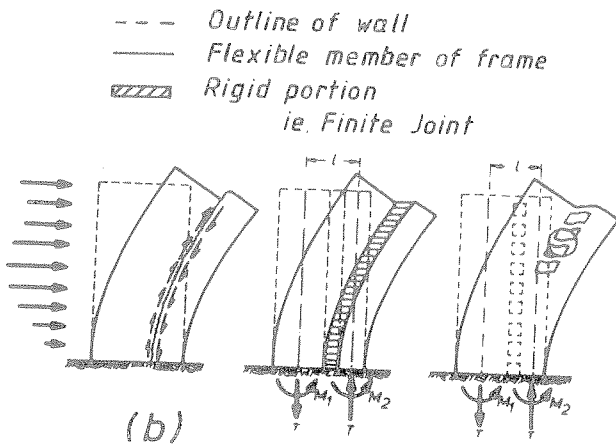


Fig. 8 - The Results of the Laminar Analysis of a Laterally Loaded Coupled Shear Wall Structure.

excessive proportion of the total load if shear distortions are not accounted for. For such cases, i.e. when $h_w/l_w < 4$, it may be assumed that

$$I_w = \frac{I_e}{1.2 + F} \quad (B-12)$$

$$\text{where } F = \frac{30 I_e}{h_w^2 b_w l_w} \quad (B-13)$$

A more accurate estimate of flexural deformations may be made if the ratio of the moment causing cracking to the maximum applied moment is evaluated and an improved value of I_e is used in Eqs. (B-12) and (B-13) thus

$$I_e = \left(\frac{M_{cr}}{M_a} \right)^3 I_g + \left(1 - \left(\frac{M_{cr}}{M_a} \right)^3 \right) I_{cr} \quad (B-14)$$

where b_w = web thickness of wall section
 l_w = horizontal length of wall
 h_w = height of wall
 M_{cr} = cracking moment according to Eq. (B-15)
 M_a = maximum moment at which deflection is computed
 I_{cr} = moment of inertia of cracked section transformed to concrete

$$M_{cr} = \frac{f_r I_g}{y_t} \quad (B-15)$$

where f_r = the modulus of rupture of concrete = $0.62 \sqrt{f_c}$ MPa
 y_t = distance from centroidal axis of gross section, neglecting the reinforcement, to extreme fibre in tension
 f_c = specified compressive strength of concrete, MPa
 I_g = second moment of area of the gross concrete section

In Eq. (B-12) some allowance has also been made for shear distortions and deflections due to anchorage (pull-out) deformations at the base of a wall, and therefore these deformations do not need to be calculated separately.

Deflections due to code⁽¹⁾ - specified lateral static loading may be determined with the use of the above equivalent sectional properties. However, for consideration of separation of non-structural components and the checking of drift limitations the appropriate amplification factor given in the code⁽¹⁾, must be used.

Geometric modelling -

For cantilever shear walls it will be sufficient to assume that the sectional properties are concentrated in the vertical centre line of the wall. This should be taken to pass through the centroidal axis of the wall section, consisting of the gross concrete area.

When cantilever walls are interconnected at each floor by a slab it is normally sufficient to assume that the floor will act as a rigid diaphragm. Thereby the positions of walls relative to each other will remain the same during the lateral loading of the shear wall assembly. By neglecting wall shear deformations and those due to torsion and restrained warping of an open wall section, the lateral load analysis can be reduced to that of a set of cantilevers in which flexural distortions only will control the compatibility of deformations. Such analysis, based on first principles, can properly allow for the contribution of each wall when it is subjected to deformations due to floor translations or torsion⁽²⁾. It is to be remembered that such an elastic analysis, however approximate it might be, will satisfy the requirements of static equilibrium, and hence it will lead to a satisfactory distribution of internal actions among the walls of an inelastic structure.

When two or more walls in the same plane are interconnected by beams, as is the case in coupled shear walls shown in figure 17, it will be necessary to account for more rigid end-zones where beams frame into walls. Such structures should be modelled as shown in figure 7a. Standard programs written for frame analyses^(6,7) may then be used. Alternatively coupled shear walls may be modelled by replacing the discrete coupling beams with a continuous set of elastic connecting laminae⁽²⁾ as shown in figure 7b. The internal actions resulting from such an analysis can be readily converted into discrete moments, shear or axial forces that develop in each floor level. The results of such an analysis are shown in figure 8. The continuous curves for beam shear, moment and axial load on the walls result from the mathematical modelling used in figure 7b. The stepped lines in figure 8 show the conversion of these quantities into usable design actions.

The analysis of wall sections

Because of the variability of wall section shapes, design aids, such as axial load-moment interaction charts for rectangular column sections, cannot often be used. The designer will have to resort to the working out of the required flexural reinforcement from first principles. Programs can readily be developed for minicomputers to carry out the section analysis. The manual section design usually consists of a number of successive approximation analyses of trial sections.

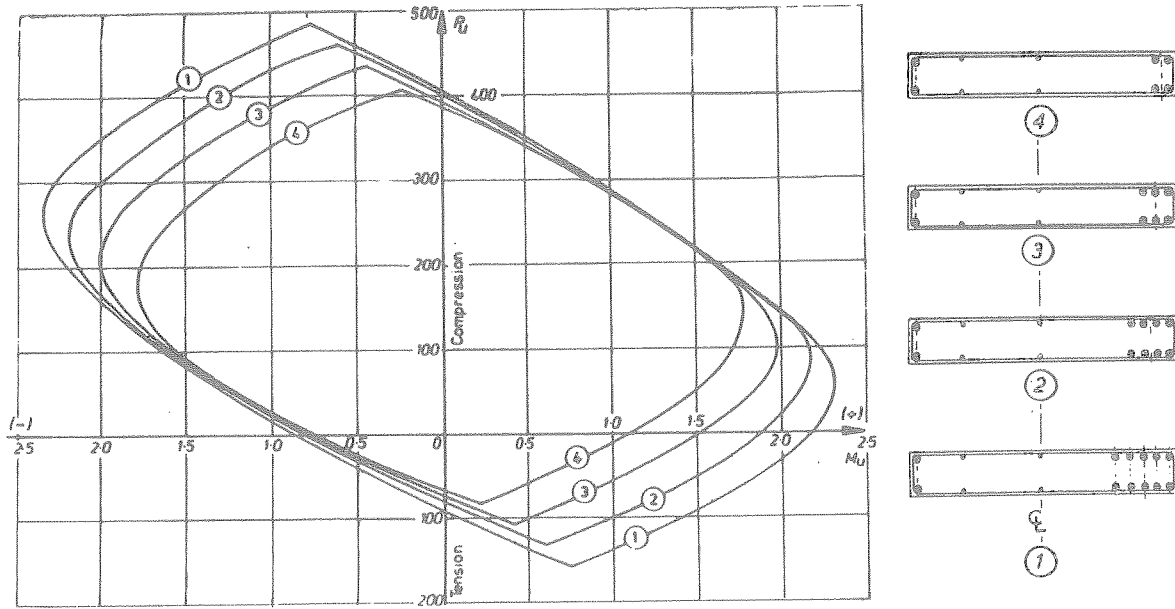


Fig. 9 - Axial Load-Moment Interaction Curves for an Unsymmetrical Shear Wall Section.

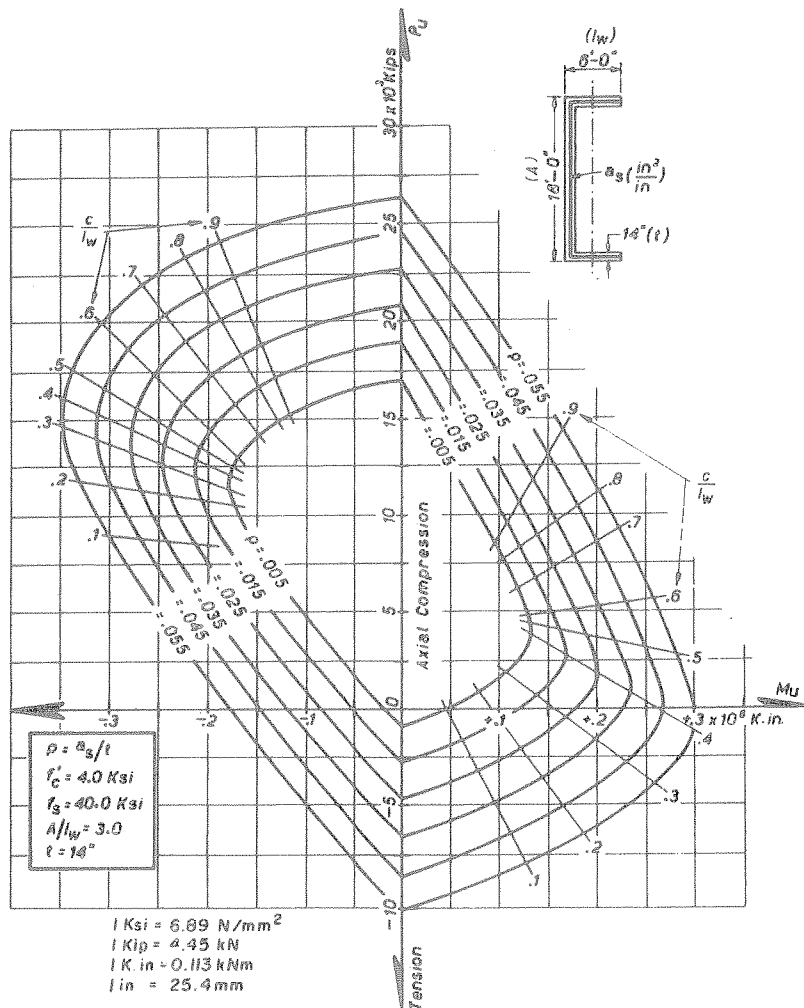


Fig. 10 - Axial Load-Moment Interaction Curves for a Channel Shaped Wall Section (2)

With a little experience convergence can be fast.

One of the difficulties that arises in the section analysis for flexural strength, with or without axial load, is the multi-layered arrangement of reinforcement. A very simple example of such a wall section is shown in figure 9. The four sections are intended to resist the design actions at four different levels of the structure. When the bending moment (assumed to be positive) causes tension at the more heavily reinforced right hand edge of the section, net axial tension is expected on the wall. On the other hand, when flexural tension is induced at the left hand edge of the section by (negative) moments, axial compression is induced in that wall. It is a typical loading situation in one wall of a coupled shear wall structure, such as shown in figure 7.

The moments are expressed with an eccentricity of the axial load, measured from the axis of the section, which, as stated earlier, is taken through the centroid of the gross concrete area rather than through that of the composite section. It is expedient to use the same reference axis also for the analysis of the cross section. It is evident that the plastic centroids in tension or compression do not coincide with the axis of the wall section. Consequently the maximum tension or compression strength of the section, involving uniform strain across the entire wall section, will result in axial forces that act eccentrically with respect to the axis of the wall. These points are shown in figure 9 by the peak values at the top and bottom meeting points of the four sets of curves. This representation enables the direct use of moments and forces, which have been derived from the analysis of the structural system, because in both analyses the same reference axis has been used.

Similar moment-axial load interaction relationships can be constructed for different shapes of wall cross section. An example for a channel shaped section is shown in figure 10. It is convenient to record in the analysis the neutral axis positions for various combinations of moments and axial forces, because these give direct indication of the curvature ductilities involved in developing the appropriate strengths, an aspect examined in "Limitations on Curvature Ductility".

Analyses for Equivalent Lateral Static Loads

The selection of load

The selection of the lateral static load, to determine the appropriate design actions which in turn lead to the desired strength, is in accordance with the earthquake provisions of the loadings code⁽¹⁾. Suitable structural type factors, S , which affect the total design base shear, have been suggested in "Types of Ductile Structural Walls" and elsewhere⁽³⁾.

To determine the magnitude of the basic seismic coefficient the period of the structure is required. This in turn involves the estimation of the structural stiffness at a state when, due to high intensity elastic dynamic excitation, the reinforced concrete components have extensively cracked. A suggested procedure for estimating stiffnesses for this purpose is outlined in "Modelling of member properties".

With this information the intensity of the lateral design loading and its distribution over the height can be determined because all other parameters (such as importance and risk factors) are specified in the loadings code⁽¹⁾. Using the appropriate model, described in the previous section, the analysis to determine all internal design actions may then be carried out.

Redistribution of actions in the inelastic structure

Because the structure is expected to be fully plastic when it develops its required strength, a departure from the elastic distribution of actions in walls linked together is acceptable as long as the total strength of the system is not reduced. For example the elastic analysis for the prescribed load may have resulted in bending moment patterns in three identically distorted shear walls, as shown in figure 11 by the full line curves. It is seen that these are proportional to the stiffnesses that were defined in "Modelling of member properties". It may be desirable to allocate more load to wall 3 because, for example in the presence of more axial compression, it could resist more moment with less flexural reinforcement (see figure 9). As the dashed curves show the design moments for wall 1 and wall 2 have been reduced and those of wall 3 have been increased by the same amount, so that no change in the total moment of resistance occurs.

In order to ensure that there will be no significant difference in the ductility demands when all three walls are required to develop plastic hinges, it is recommended that moment redistribution between walls should not change the maximum value of the moment in any wall by more than 30%. This is seen to be satisfied in the example shown in figure 11. When such redistribution is used in the design of walls, the floor diaphragms should also be designed to be capable of transferring the corresponding forces to each wall.

Similar consideration suggests that, if necessary, the maximum shear force indicated by the elastic analysis in coupling beams of shear walls could be reduced by up to 20% provided that corresponding increases in the shear capacities of beams at other floors are made. With reference to figure 8, this would mean a reduction of the shear forces at and in the vicinity of the 3rd storey with appropriate increases

in the lower and particularly upper storeys, so that the total area within curve "q" does not decrease.

These design quantities may then be used to proportion the wall sections so as to provide the required dependable strength in accordance with the Concrete Design Code⁽⁸⁾.

Dynamic Analyses

For most buildings in which reasonable uniformity in layout and stiffness prevails over the height of the structure, the derivation of design quantities from an elastic analysis for the code⁽¹⁾ specified lateral static loading is likely to assure as satisfactory a seismic performance as a more sophisticated dynamic analysis. However, when abrupt changes, such as setbacks or other discontinuities, occur, the dynamic response may expose features which may not be adequately provided for if the static analysis is used. For such situations the spectral modal dynamic analysis is recommended^(1,19). The results need to be scaled and if necessary the static load analysis may be suitably adjusted to provide the desired design quantities.

For unusual buildings or for special structures a time history dynamic analyses may be necessary. With the development of analysis programs^(6,9), in which the cyclic response of plastic hinges can be modelled with a high degree of sophistication, it is now possible to predict the response of a building to a selected ground excitation. In this, moments, shear and axial forces as well as inelastic deformations, deflections, storey drifts etc. are evaluated at every time step during the specified earthquake record. Maxima encountered during the entire duration of the excitations are also recorded. It is an analysis and not a design tool, and for this reason it may be used to check the performance of the structure as designed. In the definition of properties the probable strengths of the critical regions, discussed in "Probable Strength", should be used. The analysis may warrant certain changes to be made.

In the selection of earthquake records the designers should consider a representative excitation for the locality, which might test the design for its suitability in damage control. Such an analysis will reveal whether adequate stiffness has been provided. A viscous damping of 5% critical is suggested for such analyses.

Another study may be made for an earthquake record representing the largest credible excitation that would be expected in the locality during the probable life of the building. Thereby the inelastic deformations, such as plastic hinge rotations, and maximum actions, such as shear forces across inelastic regions of shear walls, can be predicted and hence compared with values that were envisaged in the design. For such a study a viscous damping of 8-10% of critical may

be used.

Torsion

As in all structures in seismic areas, symmetry in structural layout should be aimed at. This will reduce torsional effect due to the noncoincidence of the centre of rigidity, CR, (centre of stiffness) and the centre of gravity, CG, (centre of mass). Typical eccentricities with respect to the two principal actions of design loading, e_x and e_y , are shown for a set of shear walls of an apartment building in figure 12. Deliberate eccentricities should be avoided, if possible, because uneven onset of plastification during large excitations may aggravate eccentricity and this in turn may lead to excessive ductility demand in lateral load resisting elements situation far away from the centre of rotation.

An example of the unintended inelastic response of two ductile shear walls is illustrated in figure 13a. Because the centre of the mass, CG, is approximately at the centre of the plan, approximately one half of the induced earthquake load, E, will have to be resisted by each of the end walls at A and B. It may be difficult to prevent Wall A from having a lateral load carrying capacity considerably in excess of that on Wall B. Hence energy dissipation due to inelastic deformation may well be restricted to Wall B only which, as a result of this, could be subjected to a displacement, Δ , much larger than expected. Irrespective of the relative stiffness or strength of the two shear walls, structures in which only two principal planes of lateral resistance exist parallel to either major axes, are likely to be torsionally unstable during large inelastic seismic excitations.

The structural layout shown in figure 13b is symmetrical with respect to the earthquake loading E. It is seen that any eccentricity introduced during the inelastic response of the two end walls will result in torsion which is readily restricted by three walls acting in the perpendicular direction. These walls are likely to remain elastic and hence they will ensure a uniform inelastic translation of each floor, thereby reducing the ductility demand on each of the end walls at A and B.

The example structure shown in figure 13b also shows that, in spite of considerable eccentricity, it is likely to be much more tolerant with respect to horizontal earthquake loading, H, in the other direction. The very significant torsional resistance of the two end walls, at A and B, can ensure that the other three walls will dissipate seismic energy because of approximately equal inelastic wall displacements in the direction of the excitation H. Figure 13b thus shows a desirable, torsionally stable structural layout in which the full utilization of walls in one direction of seismic actions

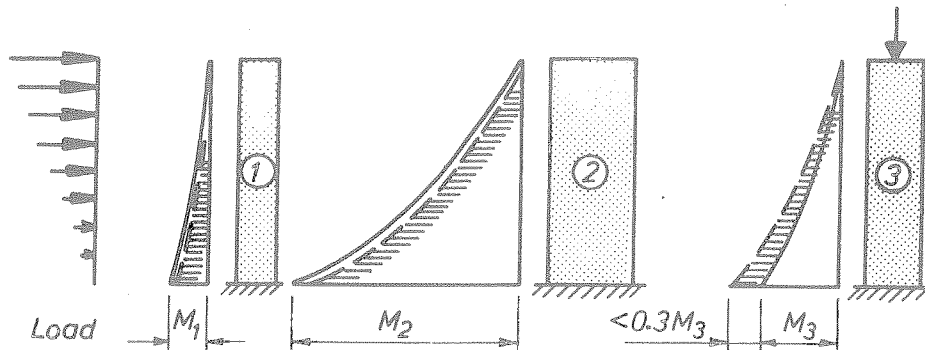


Fig. 11 - Load Redistribution between Three Inelastic Shear Walls.

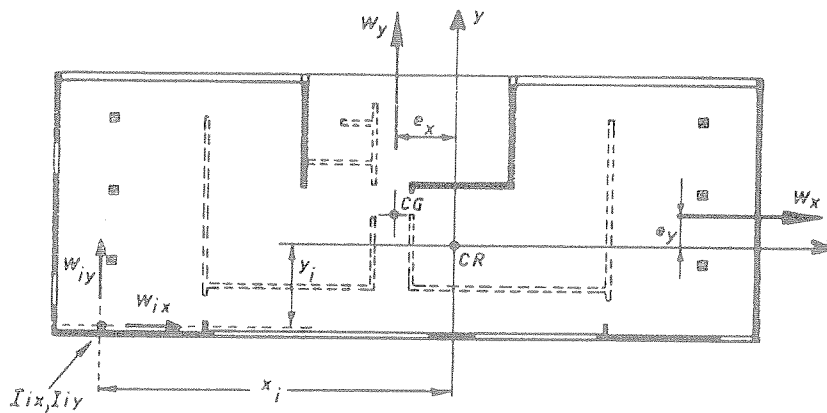


Fig. 12 - Shear Wall Layout for an Apartment Building (2)

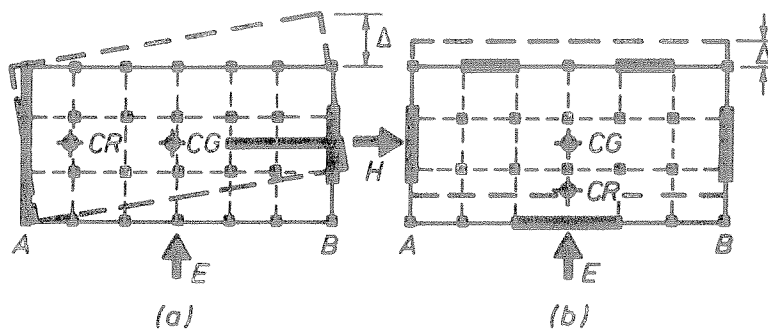


Fig. 13 - The layout of Shear Walls affects the Torsional Stability of the Lateral Load Resisting System.

is enhanced by (elastic) walls acting in the perpendicular direction by preventing inelastic storey twist.

Small single shear cores are particularly vulnerable to torsional instability.

CAPACITY DESIGN PROCEDURES:

The Definition of Strength

Before a hierarchy in the establishment of desirable energy dissipating mechanisms can be established, it is necessary to define the various strengths that might have to be quantified in the design. These have been studied in recent publications^(2,8) and for this reason only a brief summary of the definitions and their relative values are given here.

Ideal strength

The ideal or nominal strength of a section is obtained from established theory predicting failure behaviour of the section, based on assumed section geometry, the actual reinforcement provided and specified material strengths, such as f'_c and f_y .

Dependable strength

To allow for the variations in strength properties and the nature and consequence of the failure, only a fraction of the ideal strength is relied upon to meet the load demand specified by the loadings code⁽¹⁾. Therefore strength reduction factors, ϕ , are introduced⁽⁸⁾ to arrive at the dependable or reliable strength thus:

$$\text{Dependable Strength} = \phi \text{ Ideal Strength}$$

Probable strength

Routine testing of materials or components indicates the probable strength attainable by prototype components in the structure. The designer will seldom require this information. However, when the likely dynamic response of a shear wall structure during a selected ground excitation is to be studied analytically, as discussed in "Dynamic Analyses", it is more appropriate to consider the probable properties of materials at critical member sections.

Overstrength

The overstrength takes into account all the possible factors that may cause a strength increase above the ideal strength. These include steel strength higher than the specified yield strength and the additional strength due to strain hardening at large deformations, concrete strength higher than specified, section sizes larger than assumed in the initial design, increased axial compression strength in flexural members due to lateral confinement of the concrete, and participation of additional reinforcement such as that placed nearby for construction purposes.

Relationship between strengths

When using Grade 275 flexural reinforcement made in New Zealand the following relationships, based on the actual reinforcement provided, may be used to determine the flexural strengths of members -

- (i) Dependable Strength = 0.90 Ideal Strength
- (ii) Probable Strength = 1.15 Ideal Strength
- (iii) Overstrength = 1.25 Ideal Strength
- (iv) Overstrength = 1.39 Dependable Strength
- (v) Probable Strength = 0.90 Overstrength
- (vi) Probable Strength = 1.28 Dependable Strength

It is preferable, however, to determine these values from measured properties of the steel to be used.

It is recommended that wherever design actions, such as shear forces across shear walls, are derived from the flexural overstrength of the wall, the ideal strength be considered to be sufficient to resist it. Whereas in strength design the actions derived from factored loads, such as moment, M_u , or shear, V_u , need to be equal or smaller than the corresponding dependable strength provided, such as ϕM_i or ϕV_i , where M_i and V_i refer to ideal strengths of a section, in capacity design the criteria should be met:

$$M^O \leq M_i \quad \text{or} \quad V^O \leq V_i \quad (\text{B-16})$$

where M^O and V^O are the design actions at a particular section derived from capacity design procedures.

Cantilever Walls

The determination of the flexural and shear load on cantilever walls, taking into account moment redistribution as outlined in "Redistribution of actions in the inelastic structure", is a simple procedure.

The consideration of flexure and overstrength

When the appropriately factored gravity forces are also considered the required flexural reinforcement can be readily determined from the principles reviewed in 'The analysis of wall sections'. In this the designer should attempt to provide the minimum flexural reinforcement to just satisfy the dependable moment demand at the wall base. Apart from economy it should be the designer's aim to keep the overstrength of the wall to the minimum, otherwise demands for shear resistance and on the foundations might be unnecessarily compounded. In very lightly loaded walls, minimum requirement for wall reinforcement may override this criterion. The flexural overstrength is expressed by the "overstrength factor", ϕ_o , which is defined as follows:

$$\phi_0 = \frac{\text{overstrength moment of resistance}}{\text{moment resulting from code loading}} = \frac{M^0}{M_{\text{code}}} \quad (\text{B-17})$$

where both moments refer to the base section of the wall.

Even though in most walls Grade 380 reinforcement will be used, the flexural overstrength at the base may be assumed to be only 1.25 times the ideal flexural strength of that section. The reason for this is that cantilever walls will seldom be required to develop plastic hinge rotations involving excessive strain hardening of the tensile reinforcement. However, if wall configuration, slenderness or load demand indicate that tensile strains in excess of 10 times yield strain may be involved with Grade 380 reinforcement, it should be assumed that $\phi_0 = 1.6$. It should also be appreciated that in compression dominated wall sections the flexural resistance will be significantly larger if the concrete strength at the time of the earthquake is much in excess of the specified value f'_c .

Moment design envelopes

Once the flexural overstrength of a cantilever wall is determined at its base, it is necessary to define the reduction of moment demand at upper floors.

This used to be done by utilising the bending moment diagram. It is to be recognized, however, that the moment envelope that would be obtained from a dynamic analysis is quite different from the bending moment diagram drawn for the specified lateral static load. This has been identified from modal spectral analyses⁽¹²⁾ as well as from time history dynamic studies⁽¹³⁾. Typical bending moment envelopes for 20 storey cantilever shear walls with different base yield moment capacities, subjected to a particular ground excitation, are shown in figure 14. It is seen that there is an approximate linear variation of moment demand during dynamic excitations.

If the flexural reinforcement in a cantilever wall were to be curtailed according to the bending moment diagram, then flexural yielding (plastic hinges) could occur anywhere along the height of the building. This would be undesirable because potential plastic hinges do require special detailing, and hence more transverse reinforcement. Moreover, flexural yielding reduces the potential shear resisting mechanisms, and this again would require additional (horizontal) shear reinforcement at all levels where hinging might occur. This is discussed in "Control of Diagonal tension and compression".

For the reasons enumerated above it is recommended that the flexural reinforcement in a cantilever wall be curtailed so as to give a linear variation of moment of resistance. The recommendation is illustrated in figure 15. The linear envelope, shown by the dashed line, should be displaced by a distance equal to the horizontal length of the wall, l_w . This

allows for the fact that due to shear the internal flexural tension in a beam section at a section is larger than the bending moment at that section would indicate^(2,8). Accordingly the design envelope, indicating the minimum ideal moment of resistance to be provided, is obtained. Vertical flexural bars in the cantilever wall, to be curtailed must extend beyond the section indicated by the design envelope of figure 15, by at least the development length for such bar⁽⁸⁾.

Flexural ductility of cantilever walls

To ensure that a cantilever wall can sustain a substantial portion of the intended lateral load at a given displacement ductility ratio, μ_Δ , it is necessary that it can develop in its plastic hinge at the base a certain curvature ductility ratio, μ_ϕ . These ductility ratios are traditionally defined as follows:

Displacement ductility ratio:

$$\mu_\Delta = \frac{\Delta_u}{\Delta_y} \quad (\text{B-18})$$

Curvature ductility ratio:

$$\mu_\phi = \frac{\phi_u}{\phi_y} \quad (\text{B-19})$$

where Δ_u and Δ_y are the deflections at the top of the cantilever at the ultimate state and at the onset of yielding and ϕ_u and ϕ_y are the corresponding curvatures i.e. rotations of the section, at the base of the cantilever.

The relationship between the curvature ductility of the base section and the displacement ductility of the wall will depend on the length of the plastic hinge at the base⁽²⁾ and the wall height to horizontal length ratio, h_w/l_w . The variation of curvature ductility demand with h_w/l_w for various displacement demands is shown in figure 16. The dark bands represent the limits for the length of the plastic hinge, as obtained from two different proposed equations⁽¹⁴⁾. It is seen that for slender cantilever walls which are expected to be subjected to a displacement ductility demand of four, very considerable curvature ductility will need to be developed at the base. This will need to be taken into consideration when the detailing of the potential plastic hinge zone is being undertaken. (See "Satisfying Ductility Demands").

Shear strength of cantilever walls

It was emphasized in the previous sections that if a shear failure is to be avoided, the shear strength of a wall must be in excess of the maximum likely shear demand. Therefore the shear strength must be at least equal to the shear associated with the flexural overstrength of the wall i.e. $V_{\min} \geq \phi_0 V_{\text{code}}$

It has been demonstrated that during the inelastic dynamic response of a shear wall, with a given base hinge moment capacity,

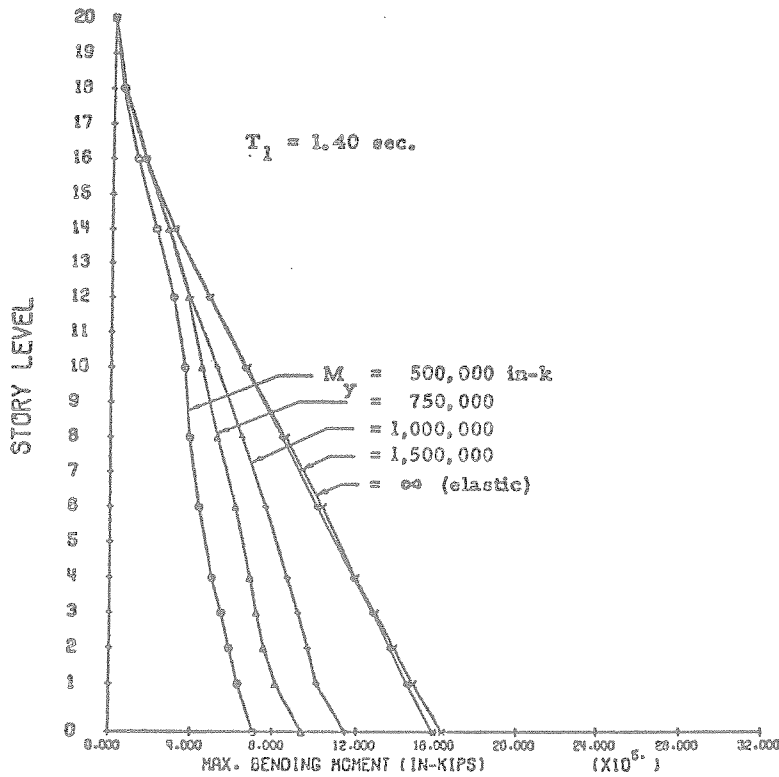


Fig. 14 - Dynamic Bending Moment Envelopes for a 20 Storey Shear Wall with different Base Yield Moment Capacities (13).

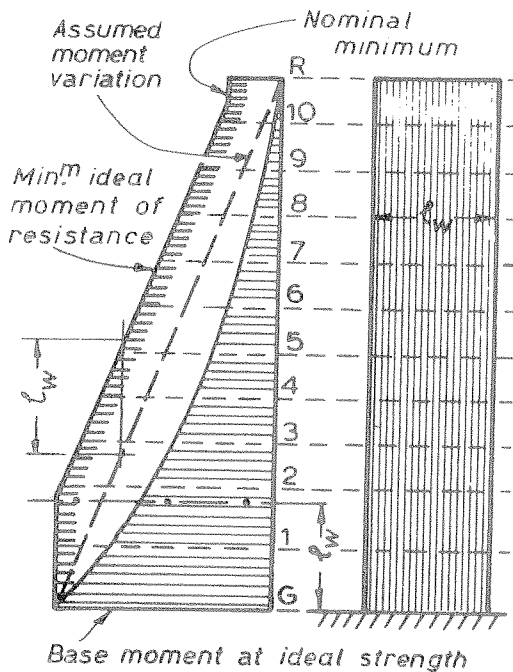


Fig. 15 - Recommended Design Bending Moment Envelope for Cantilever Shear Walls.

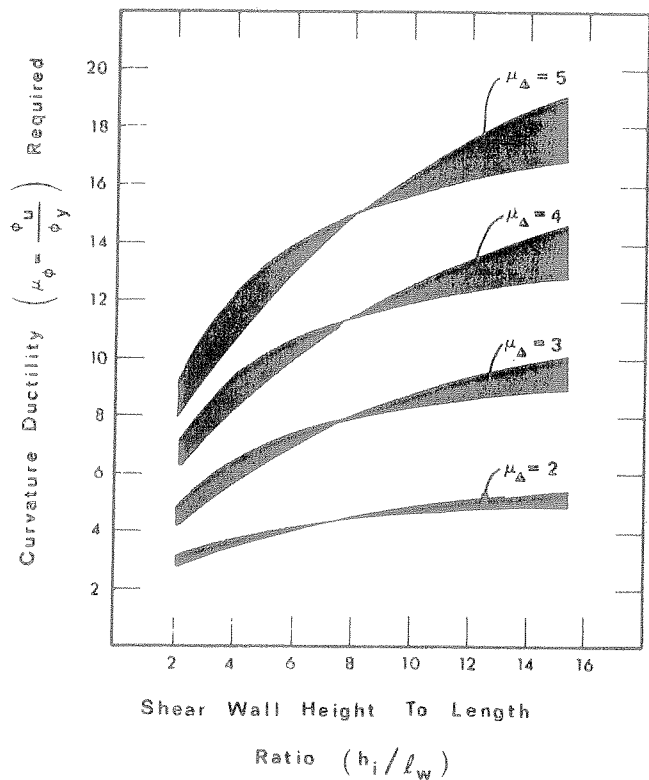


Fig. 16 - The Variation of Curvature Ductility at the base of Cantilever Shear Walls with the Aspect Ratio of the Walls and the Imposed Displacement Ductility Demand (14).

considerably larger shear forces can be generated than those predicted by static analysis⁽¹²⁾. For this reason the design shear forces must be magnified further. Therefore cantilever shear walls at all levels should possess an ideal shear capacity, V_i , of not less than

$$V_{wall} = \omega_v \phi_o V_{code} \quad (B-20)$$

where V_{code} is the shear demand derived from code⁽¹⁾ loading, ϕ_o was defined by Eq. (B-17) and the dynamic shear magnification factor is given by Eq. (B-21) for buildings up to 5 storeys high

$$\omega_v = 0.1N + 0.9 \quad (B-21)$$

where N is the number of storeys. For walls taller than 5 storeys the value of ω_v is given in Table B-1⁽¹²⁾. However, the ideal shear strength need not exceed

$$V_{wall} < (4/S) V_{code} \quad (B-22)$$

TABLE B-1

DYNAMIC SHEAR MAGNIFICATION FACTOR ω_v	
Number of Storeys	ω_v
1 to 5	Eq. (B-21)
6 to 9	1.5
10 to 14	1.7
15 and over	1.8

It may be that the flexural capacity provided at the base of the structure is so large that inelastic response of the shear wall will become unlikely. For such situations

Eq. (B-22) sets an upper limit whereby the product $\omega_v \phi_o$ need not be larger than 4/S. For example a single 8 storey cantilever shear wall need not possess an ideal shear strength in excess of $4/1.2 = 3.33$ times the code specified shear load, V_{code} .

The provisions to meet the design shear load V_{wall} from Eq. (B-20) are given in "Control of shear failure".

Coupled Shear Walls

In the following sections a recommended step by step capacity design procedure for coupled shear walls is outlined. When necessary reference should be made to figure 7 or figure 17.

Geometric review

Before the static analysis procedure commences the geometry of the structure should be reviewed to ensure that in the critical zones compact sections, suitable for energy dissipation, will result. Section configurations should satisfy criteria outlined in "Stability".

Lateral static load

The appropriate lateral static load, in accordance with the loadings code⁽¹⁾ is to be determined. To do this it might be necessary to estimate the probable value, S_p , of the structural type factor S , recommended in "Types of Ductile Structural Walls"(b).

Elastic analysis

With the evaluation of the lateral static load the complete analysis for the resulting internal structural actions, such as moments, forces etc. can be carried out. In this the modelling assumption of "Modelling Assumptions" should be observed. Typical results are shown in figure 8.

Confirmation of the structural type factor

Having obtained the moments and axial forces at the base of the structure the moment parameter

$$A = \frac{Tl}{M_o} \quad (B-1)$$

as discussed in "Types of Ductile Structural Walls"(b), can be determined. The significance of the parameter may also be seen in figure 18. With the use Eq. (B-3) the exact required value of the structural type factor, S can be found. If this differs from that assumed earlier i.e. S_p , all quantities of the elastic analysis are simply adjusted by the multiplier S/S_p .

Checking of foundation loads

To avoid unnecessary design computations, at this stage it should be checked whether the foundation structure for the coupled shear walls would be capable of transmitting at least 1.5 times the overturning moment, M_o , received from the superstructure (see figure 17), to the foundation material (soil). It is to be remembered that in a carefully designed superstructure, in which no excess strength of any kind has been allowed to develop, 1.4 times the overturning moment resulting from code loading M_o will be mobilized during large inelastic displacements. (See "Relationship between strengths"). Hence the foundation system must have a potential strength in excess of $1.4 M_o$, otherwise the intended energy dissipation in the superstructure may not develop.⁽⁵⁾

Design of coupling beams

Taking flexure and shear into account the coupling beams at each floor can be designed. Normally diagonal bars in cages⁽²⁾ should be used, preferably with Grade 275 reinforcement. A strength reduction factor of $\phi = 0.9$ is appropriate. Particular attention should be given to the anchorage of caged groups of bars and to ties which should prevent inelastic buckling of individual diagonal bars. (See "Detailing of Coupling Beams"). The beam reinforcement should match as closely as possible the load demand. Excessive coupling beam strength may lead to subsequent difficulties in the design of walls and foundations.

Determination of actions on the walls

In order to find the necessary vertical reinforcement in each of the coupled walls (figure 17) at the critical

base section, the following loading cases should be considered:

- i) $P_e = P_{eq} - 0.9P_D$ axial tension (or small compression) and M_1
- ii) $P_e = P_{eq} + P_D + P_{LR}$ axial compression and M_2

where P_e = axial design load including earthquake effects

P_{eq} axial tension or compression induced in the wall by the lateral static loading

P_D = axial compression due to dead load

P_{LR} = axial compression due to reduced live load L_R

M_1 = moment at the base developed concurrently with earthquake induced axial tension load (figure 17c)

M_2 = moment at the base developed concurrently with earthquake induced axial compression load (figure 17c)

- iii) If case (i) above is found to result in large demand for tension reinforcement or for other reasons, a redistribution of the design moments from the tension wall to the compression wall may be carried out in accordance with 'Redistribution of actions in the inelastic structure', within the following limits:

- (a) $M_1' > 0.7 M_1$
- (b) $M_2' = M_2 + M_1 - M_1' < 1.3 M_2$

where M_1' and M_2' are the design moments for the tension and compression walls respectively, after the moment redistribution has been carried out.

In the above three steps, which would complete the strength design of the structure, a capacity reduction factor of $\phi = 0.9$ may be used for all cases. The justification for this is considered to result from a subsequent requirement, according to which compression dominated wall sections specifically need to be confined to ensure sufficient curvature ductility.

Using these quantities the vertical flexural reinforcement for each wall, with Grade 275 or Grade 380 steel, can now be determined in accordance with "The analysis of wall sections".

Overcapacity of coupling beams

In order to ensure that the shear strength of the coupled shear wall structure will not be exceeded and that the maximum load demand on the foundation is properly assessed, i.e. to fulfill the intent of "Hierarchy in Energy Dissipation", the overstrength of the potential plastic regions must be estimated. Accordingly

the shear overcapacity, Q_i^O , of each coupling beam, as detailed, based on a yield strength of the diagonal reinforcement of $1.25 f_y \geq 345$ MPa is determined. Where slabs, framing into coupling beams, contain reinforcement parallel to the coupling beams which is significant when compared with the reinforcement provided within the beam only, the possible contribution of some of this the reinforcement to the shear capacity of coupling beams should also be considered in computing overstrength.

Earthquake induced axial loads

The maximum feasible axial load induced in one of the coupled walls would be obtained from the summation of all the coupling beam shear forces at overcapacity, Q_i^O , applied to the wall above the section that is considered. For structures with several storeys this may be an unnecessarily conservative estimate, and accordingly it is recommended that the wall axial load at overstrength be estimated with

$$P_{eq}^O = (1 - \frac{n}{80}) \sum_i^n Q_i^O \quad (B-23)$$

where n = number of floors above level i . The value of n in Eq. (B-23) should not be taken larger than 20.

The flexural overcapacity of the entire structure

In order to estimate the maximum likely overturning moment that could be developed in the fully plastic mechanism of the coupled shear wall structure, it is necessary to assume gravity loads that are realistic and consistent with such a seismic event. Accordingly, for this purpose only, the total overstrength axial loads to be sustained by the walls should be estimated as follows:

- i) For tension of minimum compression

$$P_1^O = P_{eq}^O - P_D$$

- ii) For compression

$$P_2^O = P_{eq}^O + P_D$$

It is now possible to estimate the flexural overstrength capacity of each wall section, as detailed, that may be developed concurrently with the above axial forces. The moments of resistance, which may be based on material strengths defined by $1.25f_y$ and $1.25f'_c$, so derived for the tension and compression walls respectively, are M_1^O and M_2^O . In similarity to Eq. (B-17) the overstrength factor for the entire coupled shear wall structure may be obtained from

$$\phi_O = \frac{M_1^O + M_2^O + P_{eq}^O \ell}{M_O} \quad (B-24)$$

In accordance with the assumed strength properties of "Relationship between strengths" the value of ϕ_O so obtained should not be less than 1.39. If it is, the design should be checked for the error.

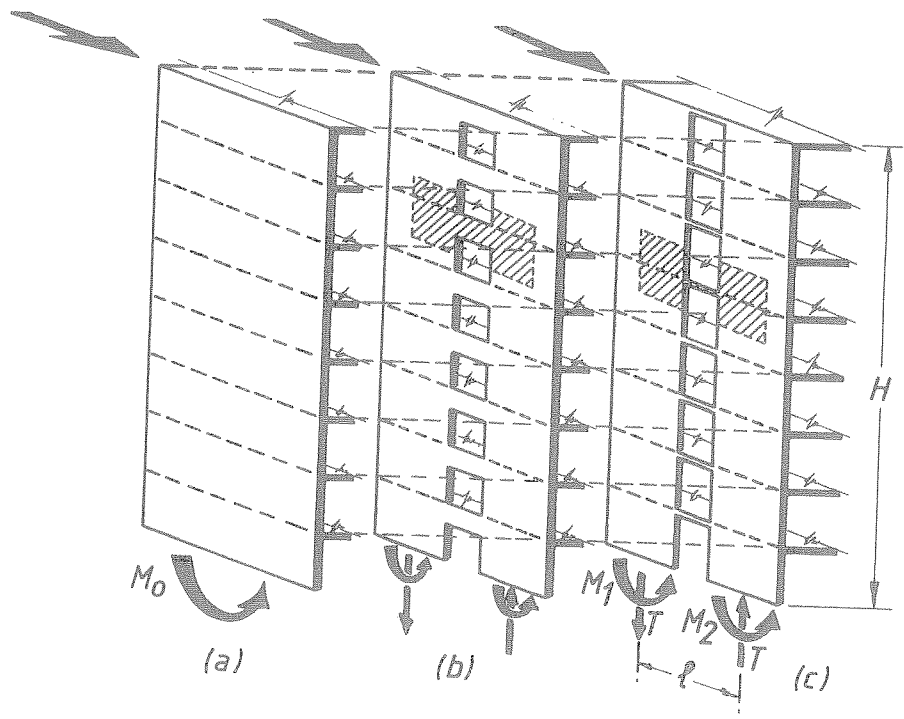


Fig. 17 - A Comparison of Ductile Walls (a) A Cantilever Wall (b) Wall Coupled by Strong Coupled Beams (c) Walls Coupled by Slabs Only

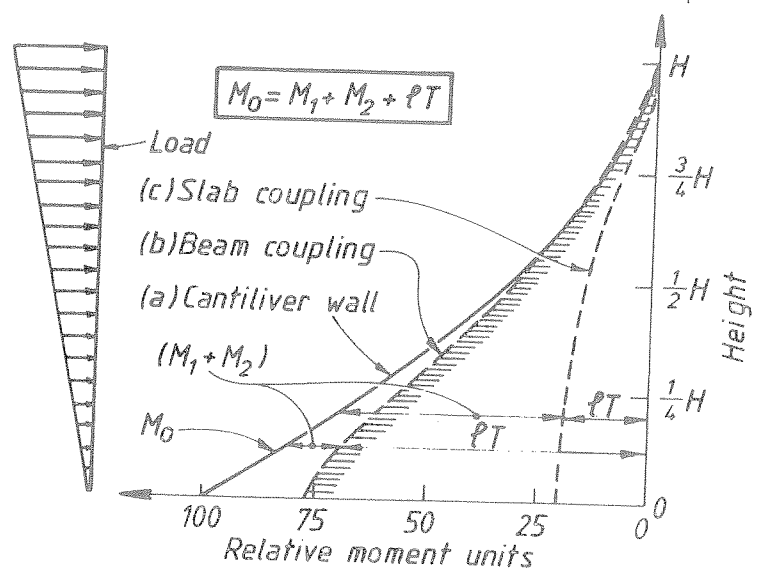


Fig. 18 - Contribution of Internal Coupling to the Resistance of Overturning Moments in Coupled Shear Walls.

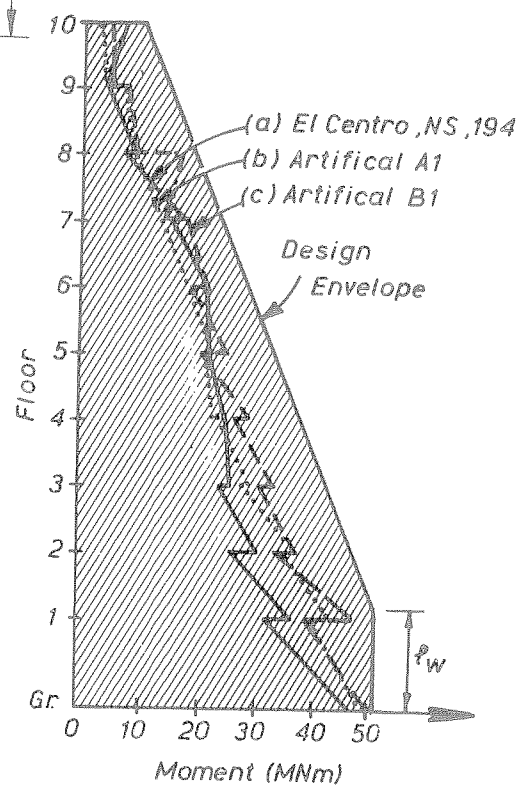


Fig. 19 - Bending Moment Envelopes for Coupled Shear Walls (a) Envelope Used in Design (b) Envelopes Observed in a Theoretical Study (15).

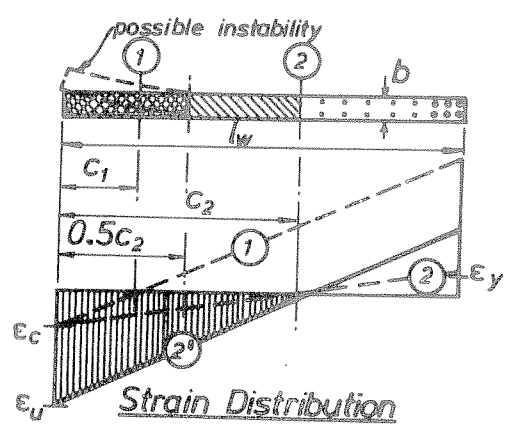


Fig. 20 - Strain Patterns for a Rectangular Wall Section Subjected to Flexure and Axial Load.

Wall shear forces

In similarity to the approach employed in the section "Shear strength of cantilever walls" for cantilever shear walls, the maximum shear force for one wall of a coupled shear wall structure may be obtained from

$$V_{i,wall} = \omega_v \phi_0 \left[\frac{M_i^0}{M_1^0 + M_2^0} \right] V_{code} ; i = 1, 2 \quad (B-25)$$

where ω_v = dynamic shear magnification factor in accordance with Eq. (B-20)

V_{code} = shear force on the entire shear wall structure at any level, derived by the initial elastic analysis for code loading⁽¹⁾ with the appropriate S factor.

$\omega_v \phi_0 \leq 4/S$ in accordance with Eq. (B-22)

The bracketed term in Eq. (B-25) makes an approximate allowance for the distribution of shear forces between the two walls, which, at the development of overstrength, is likely to be different from that established with the initial elastic analysis. It also takes into account the approximate redistribution of shear forces that may have resulted from the deliberate redistribution of design moments from the tension to the compression wall.

The required horizontal shear reinforcement may be determined now. In assessing the contribution of the concrete shear resisting mechanism, the effects of the axial forces P_1^0 and P_2^0 , as appropriate should be taken into account.

Confinement of wall sections

From the load combinations considered above the positions of the neutral axes relative to the compressed edges of the wall sections are readily obtained. From the regions of the wall section over which, in accordance with the section "Confinement of Wall Regions" anti-buckling and/or confining transverse reinforcement is required, this reinforcement can now be determined.

Curtailement of vertical flexural reinforcement

For the purpose of establishing the curtailement of the principal vertical wall reinforcement, a linear bending moment envelope along the height of each wall should be assumed, as shown in figure 19a. This is intended to ensure that the likelihood of flexural yielding due to higher mode dynamic responses along the height of the wall is minimized. Details for the justification of such an envelope

were examined in the section "Moment design envelopes". In a study, in which the inelastic dynamic response of a coupled shear wall was computed, the moment envelopes for responses to three different ground excitations, shown in figure 19, were obtained⁽¹⁵⁾.

Foundation design

The actions at the development of the overstrength of the superstructure, P_1^0 , P_2^0 , M_1^0 , M_2^0 and wall shear forces V_1 and V_2 , should be used as loading on the foundations. For ductile coupled shear walls, the foundation structure should be capable of absorbing these actions at its ideal strength capacity.

SATISFYING DUCTILITY DEMANDS

Stability

When part of a thin wall section is subjected to large compression strains, the danger of premature failure by instability arises. This is the case when a large neutral axis depth is required in the plastic hinge zone of the wall, as shown in figure 20, and the length of the plastic hinge is large i.e. one storey high or more. The problem is compounded when cyclic inelastic deformations occur. Instability should not be permitted to govern strength of ductile shear walls.

In the absence of information on the "compactness" of reinforced concrete wall sections, existing code rules⁽¹⁶⁾, relevant to short columns, are best considered. For such columns the effective height to width ratio, l_n/b , should not exceed 10⁽¹⁶⁾.

The relevance of such a code requirement to a shear wall may be studied with the aid of figure 20. For a certain load combination the computed neutral axis depth may be c_2 , so that a considerable portion of the wall section will be subject to compression. Near the extreme compression fibre, where, in accordance with accepted assumptions, the concrete strain at ideal flexural capacity is taken as $\epsilon_c = 0.003$, instability may occur unless this strain pattern is restricted vertically to a very short plastic hinge length. Moreover, the strain profile marked (2) in figure 20 shows that very limited curvature ductility would be available at the attainment of the ideal strength of the section. To satisfy the intended displacement ductility demand for the shear wall system, a strain profile shown by line (2') may need to be developed. Such large concrete compression strains, ϵ_u , could only develop if the concrete in this zone is confined, and this will be examined in a later section. The phenomenon is fortunately rare, but it emphasizes the need for considering instability. It occurs more commonly when a wall has a large tension flange, such as shown in figure 22 and figure 35.

In the absence of experimental evidence intuitive judgement was used to recommend that, with the exceptions to be

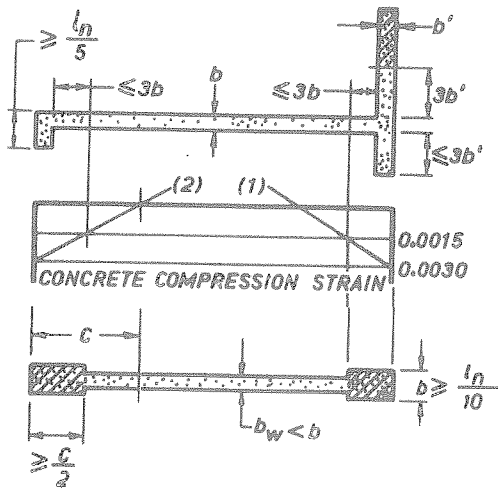


Fig. 21 - Parts of a Wall Section to be Considered for Instability and which Provides Lateral Support.

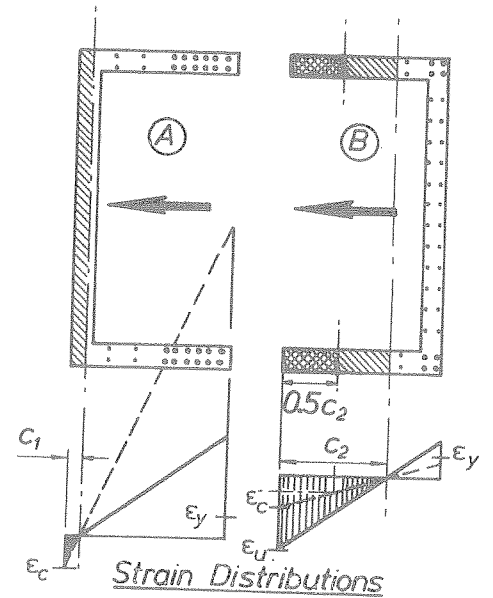


Fig. 22 - Strain Profiles for Channel Shaped Wall Sections.

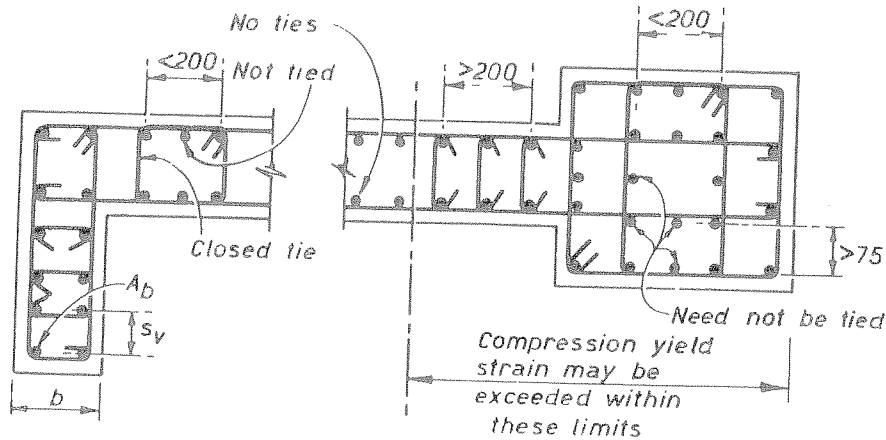


Fig. 23 - Transverse Reinforcement in Potential Yield Zones of Shear Wall Sections.

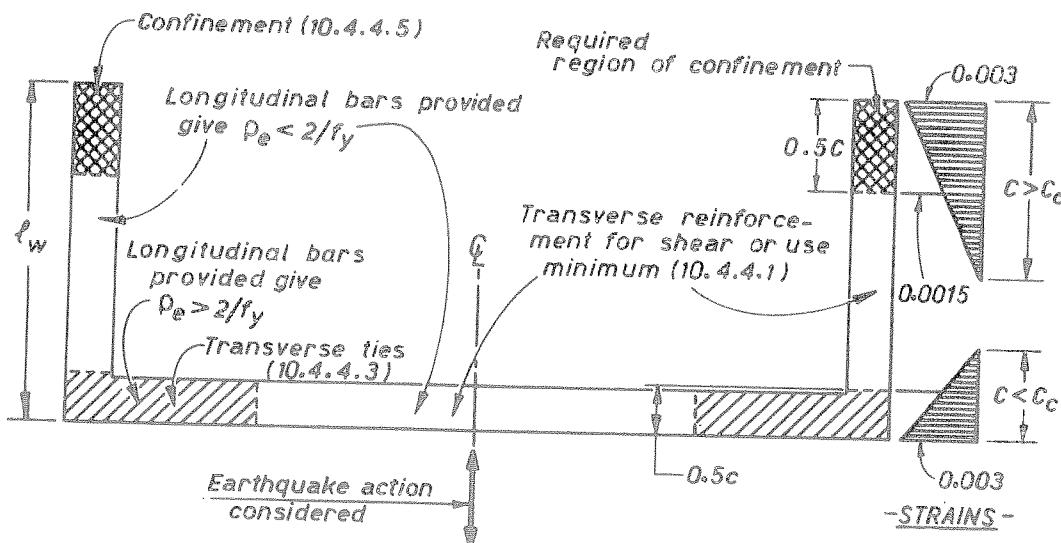


Fig. 24 - Regions of Different Transverse Reinforcement in a Shear Wall Section.

set out subsequently, in the outer half of the conventionally computed compression zone, the wall thickness b should not be less than one tenth of the clear vertical distance between floors or other effective lines of lateral support, l_n . Considering the strain pattern (2) in figure 20, this zone extends over a distance of $0.5c_2$, as shown with cross shading. This is an area over which the concrete compression strain will exceed 0.0015 when the strain in the extreme compression fibre of the section, consistent with the determination of the ideal flexural strength, attains its assumed maximum value of 0.003.

When the computed neutral axis depth is small, as shown by the strain distribution (1) in figure 20, the compressed area may be so small that adjacent parts of the wall will stabilize it. Accordingly, when the fibre of 0.0015 compression strain is within a distance of the lesser of $2b$ or $0.15 l_n$ from the compressed edge, the $b > l_n/10$ limit should not need to be complied with. In terms of neutral axis depth this criteria is met when $c \leq 4b$ or $c \leq 0.3 l_n$, whichever is less. The strain profile (1), which occurs commonly in lightly reinforced walls with small gravity load, clearly satisfies this condition.

It may be assumed that only in buildings 3 storeys or higher would the plastic hinge length at the base, extending toward the first floor, be large enough to warrant an examination of instability criteria.

Certain components of walls, such as shown in figure 21, provide continuous lateral support to adjacent compressed elements. Therefore it is considered that any part of a wall, subjected to computed strains larger than 0.0015, which is within a distance of $3b$ of such a line of support, should be exempted from slenderness limitation. Figure 2 shows a number of locations that are exempt. The shaded part of the flange is considered to be too remote to be effectively restrained by the web portion of the wall and hence it should comply with the $b > l_n/10$ slenderness limitation. In the absence of a flange, the width of which is at least $l_n/5$, a boundary element may be formed that satisfies the slenderness limit. These latter two cases are also shown in figure 21.

Limitations on Curvature Ductility

By simple limitations of the amount of flexural tension reinforcement⁽⁸⁾ in beam sections, it can be ensured that adequate curvature ductility, to meet the intents of seismic design, will be available. Because of the variety of cross sectional shapes and arrangements of reinforcements that can be used, and the presence of some axial load, the availability of ductility in shear walls cannot be checked by the simple process that is used for rectangular beams or sections.

In the analysis of wall sections for flexure and axial load, the neutral axis depth, c , is always determined. Hence the ratio of c/l_w , an indicator of the curvature ductility required at the development of the ideal strength, (figure 21) can be readily found. Various strain profiles, associated with a maximum assumed concrete compression strain of $\epsilon_c = 0.003$ are shown by dashed lines in figures 20 and 22. It is seen that different neutral axis depths, c_1 and c_2 , for different wall configurations can give very different curvature ductilities.

The curvature ductility demand in the plastic hinge zone of cantilever walls was related to the displacement ductility in 'Flexural ductility of cantilever walls'. Typical relationships were also presented in figure 16. It will be seen that in a relatively slender shear wall with $h_w/l_w = 8$, a curvature ductility of approximately 11 is required if the displacement ductility is to be 4. The yield curvature of a section may be approximated by $\phi_y = (\epsilon_y + \epsilon_{ce})/l_w = 0.0025/l_w$ where ϵ_y and ϵ_{ce} are the steel and concrete strains at the extreme edges when the yield strain of the reinforcement is just reached. Hence the desired ultimate curvature will be $\phi_u = 11\phi_y = 0.0275/l_w$. Current strength computations are based on the conservative assumption that $\epsilon_c = 0.003$. It is found, however, that a strain of 0.004 can be readily attained in the extreme compression fibre of a section before crushing of the concrete commences⁽²⁾. By assuming that the maximum concrete strain will reach the value of 0.004 it is found that the neutral axis depth at this curvature needs to be $c = 0.004 l_w / 0.0275 = 0.145 l_w$. As figure 16 shows however, for h_w/l_w ratios less than 8 lesser curvature ductilities will suffice.

The above discussion was based on cantilevers, for which a structural type factor of $S = 1$ is relevant, and for which a displacement ductility demand of 4 might arise when the intended base overstrength, corresponding with $\phi_o = 1.39$, is developed. For walls with larger S factors or larger unintended overstrength (i.e. when $\phi_o > 1.39$), the displacement ductility requirement may be assumed to be proportionally reduced. Consequently the critical neutral axis depth can be conservatively assumed to be

$$c_c = 0.10 \phi_o S l_w \quad (B-26)$$

If desired, the designer could carry out a more refined analysis, using Eq. (B-27) which may show that a larger neutral axis depth would provide the desired curvature ductility.

$$c_c = \frac{8.6 \phi_o S l_w}{(4 - 0.7S)(17 + h_w/l_w)} \quad (B-27)$$

Whenever the computed neutral axis depth for the design loading on the given section exceeds the critical value c_c , given by Eq. (B-26), it will be necessary to assume that increased ductility can be attained only at the expense of increased concrete compression strains.

It is seen on the left hand side of figure 22, showing the channel shaped cross section of a single cantilever wall, that, because of the large available concrete compression area, very large curvature ductility is associated with the development of the flexural strength. A given displacement ductility, however, may require only a strain pattern shown by the heavy line. It is evident that this curvature could only be attained in the other wall section, shown on the right in figure 22, if the concrete compression strains increase considerably. The same relationship can be seen between the strain patterns (1) and (2') shown in figure 20. Excessive compression strains would lead to failure of the section unless the concrete in the core of the compression zone is suitably confined. This aspect of the design is examined in the next section.

Confinement of Wall Regions

From the examination of curvature relationships in the simple terms of c/ℓ_w ratio, it is seen that in cases when the computed neutral axis is larger than the critical value c_c , given by Eq. (B-26) or Eq. (B-27), the compression region of the wall needs to be confined. It does not seem necessary to confine the entire compression zone. It is suggested, however, that the outer half of it be confined. Accordingly the following simple rules are suggested.

Region of confinement

When the neutral axis depth in the potential yield regions of a wall, computed for the most adverse combination of design loadings, exceeds

$$c_c = 0.10 \phi_o S \ell_w \quad (B-26)$$

the outer half of the compression zone, where the compression strain, computed when the ideal flexural strength of the section is being determined, exceeds 0.0015, should be provided with confining reinforcement. This confining transverse reinforcement should extend vertically over the probable plastic hinge length, which for this purpose should be assumed to be equal to the length of the wall ℓ_w , as shown in figure 15 and figure 19.

Confining reinforcement

The principles of concrete confinement (2) to be used are those relevant to column sections, with the exceptions that very rarely will the need arise to confine the entire section of a shear wall. Accordingly it is recommended that rectangular or polygonal hoops and supplementary ties, surrounding the longitudinal bars in the region to be confined, should be used so that

$$A_{sh} = 0.3 s_h h'' \left(\frac{A_g^*}{A_c^*} - 1 \right) \frac{f'_c}{f_{yh}} \left(0.5 + 0.9 \frac{c}{\ell_w} \right) \quad (B-28)$$

$$A_{sh} = 0.12 s_h h'' \frac{f'_c}{f_{yh}} \left(0.5 + 0.9 \frac{c}{\ell_w} \right) \quad (B-29)$$

whichever is greater, where the ratio c/ℓ_w need not be taken more than 0.8.

In the above equations:

A_{sh} = total effective area of hoops and supplementary cross ties in direction under consideration within spacing s_h , mm^2

s_h = vertical centre to centre spacing of hoop sets, mm

A_g^* = gross area of the outer half of wall section which is subjected to compression strains mm^2

A_c^* = area of concrete core in the outer half of section which is subjected to compression strains, measured to outside of peripheral hoop legs, mm^2

f'_c = specified compression strength of concrete, MPa

f_{yh} = specified yield strength of hoop or supplementary cross tie steel, MPa

h'' = dimension of concrete core of section measured perpendicular to the direction of the hoop bars, mm

These equations are similar to those developed by Park⁽¹⁷⁾ for columns. The area to be confined is thus extending to $0.5c$, from the compressed edge as shown by cross hatching in the examples of figures 20 and 22.

For the confinement to be effective the vertical spacing of hoops or supplementary ties, s_h , should not exceed 6 times the diameter of vertical bars in the confined part of the wall section, one third of the thickness of the confined wall or 150 mm, whichever is less.

An application of this procedure is given in Appendix II.

Confinement of longitudinal bars

A secondary purpose of confinement is to prevent the buckling of the principal vertical wall reinforcement where the same may be subjected to yielding in compression. It is therefore recommended that in regions of potential yielding of the longitudinal reinforcement within a wall with two layers of reinforcement, where the longitudinal reinforcement ratio ρ_l , computed from Eq. (B-31), exceeds $2/f_{yv}$, transverse tie reinforcement, satisfying the following requirements, should be provided:

- (a) Ties suitably shaped should be so arranged that each longitudinal bar or bundle of bars, placed close to the wall surface, is restrained against buckling

by a 90° bend or at least a 135° standard hook of a tie. When two or more bars, at not more than 200 mm centres apart, are so restrained, any bars between them should be exempted from this requirement.

- (b) The area of one leg of a tie, A_{te} , in the direction of potential buckling of the longitudinal bar, should be computed from Eq. (B-30) where ΣA_b is the sum of the areas of the longitudinal bars reliant on the tie including the tributary area of any bars exempted from being tied in accordance with (a) above.

$$A_{te} = \frac{\Sigma A_b f_y s_h}{16 f_{yh}} \quad (B-30)$$

Longitudinal bars centered more than 75 mm from the inner face of stirrup ties need not be considered in determining the value of ΣA_b .

- (c) The spacing of ties along the longitudinal bars should not exceed six times the diameter of the longitudinal bar to be restrained.
- (d) Where applicable, ties may be assumed to contribute to both the shear strength of a wall element and the confinement of the concrete core.
- (e) The vertical reinforcement ratio that determines the need for transverse ties should be computed from

$$\rho_l = \frac{\Sigma A_b}{bs_v} \quad (B-31)$$

where the terms of the equation, together with the interpretation of the above requirements are shown in figure 23. The interpretation of Eq. (B-31) with reference to the wall return at the left hand end of figure 23 is as follows: $\rho_l = 2A_b/bs_v$.

The requirements of transverse reinforcement in a shear wall section are summarized in figure 24 as follows:

- (a) For the direction of loading the computed neutral axis depth c exceeds the critical value c_c , given by Eq. (26) or Eq. (27), hence confining reinforcement over the outer half of the compression zone, shown by cross hatching, should be provided in accordance with "Confining reinforcement".
- (b) In the web portion of the channel shaped wall, within the outer half of the computed neutral axis depth, vertical bars need be confined (using antibuckling ties) in accordance with "Confinement of longitudinal bars" only if $\rho_l > 2/f_y$. The affected areas are shaded.
- (c) In all other areas, which are unshaded

the transverse (horizontal) reinforcement need only satisfy the requirements for shear and its ratio to the concrete area should not be less than 0.0025.

Longitudinal Wall Reinforcement

For practical reasons the ratio of longitudinal i.e. vertical reinforcement, ρ_l , (Eq. (B-31)) over any part of wall should not be less than $0.7/f_y$ nor more than $17/f_y$.

In walls which are thicker than 200 mm or when the design shear stress exceeds $0.3 \sqrt{f_c}$ MPa, at least two layers of reinforcement should be used, one near each side of the wall.

The diameter of bars used in any part of a wall should not exceed one tenth of the thickness of the wall. The spacing between longitudinal bars should not exceed twice the thickness of the wall nor 400 mm.

In regions where the wall section is required to be confined the spacing of vertical bars should not exceed 200 mm.

Control of Shear Failure

Shear forces and shear stresses

The derivation of the design shear forces, using the principles of capacity design, have been outlined previously for cantilever walls ("Shear strength of cantilever walls") and in "Wall shear forces" for coupled shear wall structures. Shear strength provided in accordance with these shear forces is expected to ensure ductile flexural response of walls with an acceptable amount of reduction in energy dissipation during hysteretic response. For convenience and in keeping with traditional practice these forces may be converted into stresses thus

$$v_i = \frac{V_{wall}}{b_w d} \quad (B-32)$$

where the effective depth need not be taken less than $0.8 l_w$. Eq. (B-32) should be considered as an index rather than an attempt to quantify a stress level at any particular part of the wall section. From observed behaviour of walls, using this expression, certain limits have been set to ensure satisfactory performance.

Shear may lead to different types of failure, such as diagonal tension, diagonal compression and sliding, each of which are examined subsequently. In general the principles relevant to the design of ordinary reinforced concrete beams⁽²⁾ are also applicable to structural walls.

Control of diagonal tension and compression

Two areas within a wall must be distinguished for which the design procedures

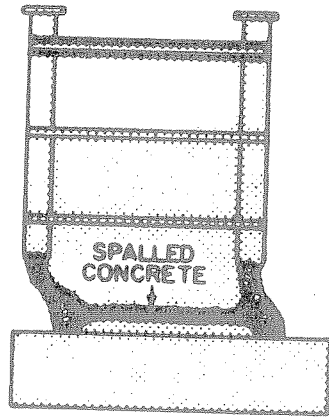


Fig. 25 - Sliding Shear Failure Initiated by Web Crushing.

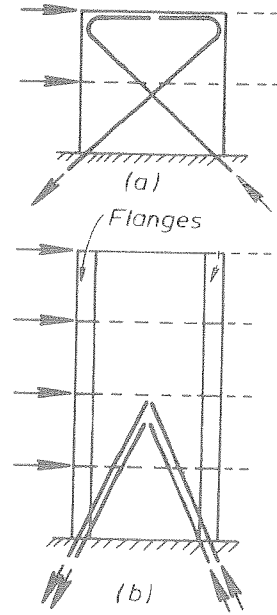


Fig. 26 - Suggestions for the Arrangement of Diagonal Reinforcement to Control Sliding Displacement at the Base.

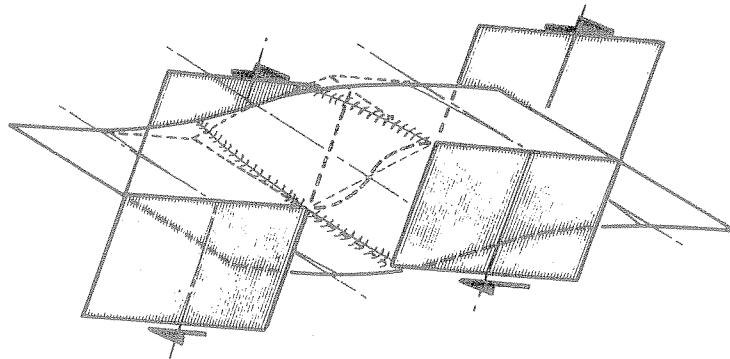


Fig. 27 - The Inelastic Deformations of a Slab Interconnecting two Laterally Loaded Shear Walls.

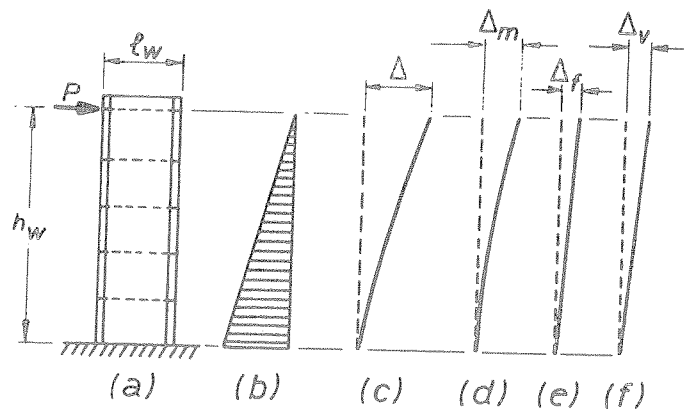


Fig. 28 - A Cantilever Wall and its Distortions.

are different. These are the potential plastic hinge zone and the remainder of the wall, which is expected to remain free of significant flexural yielding during any kind of dynamic excitation. In the design to control diagonal tension, one part of the shear strength is assumed to be provided by the shear reinforcement (v_s) and the other by mechanisms collectively designated as the contribution of the concrete (v_c). Accordingly

$$v_i = v_c + v_s \quad (B-33)$$

In this the contribution of the "concrete" to shear resistance, v_c , is assumed to be zero in the potential plastic hinge zone, unless the minimum design axial load, N_u , produces an average compression stress of $0.1 f'_c$ or more over the gross concrete area, A_g , including flanges, in which case

$$v_c = \frac{2}{3} \sqrt{\frac{N_u}{A_g} - \frac{f'_c}{10}} \quad (B-34)$$

The value of v_c outside the potential plastic hinge zone may be taken as that specified for beams⁽⁸⁾ subjected to gravity (non-seismic) loading only. This will normally result in significant reduction in the web reinforcement in the upper parts of a shear wall.

Web reinforcement, consisting of horizontal bars, fully anchored at the extremities of the wall section, must be provided so that

$$A_v = \frac{v_s b_w s}{f_y} = \frac{(v_i - v_c) b_w s}{f_y} \quad (B-35)$$

These provisions should ensure that diagonal tension failure across the wall will never occur. To guard against diagonal compression failure, which may occur in flanged walls, that are over-reinforced for shear, codes^(8, 16) set an upper limit for the value of v_i . These values were based on tests with monotonic loading. Recent tests by the Portland Cement Association⁽¹¹⁾ and the University of Berkeley⁽¹⁸⁾ have demonstrated, however, that web crushing in the plastic hinge zone may occur after only a few cycles of reversed loading involving displacement ductilities of 4 or more. When the imposed ductilities were only 3 or less, the shear stresses stipulated by existing codes⁽¹⁶⁾ could be repeatedly attained. Web crushing may eventually lead to apparent sliding shear failure, as shown in figure 25. To prevent such failure the ideal shear strength of the wall should be such that

$$v_{i,max} \leq (0.3 \phi_o S + 0.16) \sqrt{f'_c} \leq 0.8 \sqrt{f'_c} \text{ (MPa)} \quad (B-36)$$

It is seen that for cantilever shear walls with $\phi_o = 1.39$ and a structural type factor of $S = 1.6$, in which limited

displacement ductility demand is expected, the design shear stress will attain the maximum value considered for all structures i.e. $0.8 \sqrt{f'_c}$ MPa. On the other hand for a coupled shear wall structure with $\phi_o = 1.39$ and $S = 0.8$, $v_{i,max} = 0.49 \sqrt{f'_c}$.

Control of sliding shear

It is likely that sliding in the plastic hinges of walls is better controlled by conventional reinforcement than it is in beams where sliding, resulting from high intensity reversed shear loading, can significantly affect the hysteretic response (see figure 4). The reasons for this are that most shear walls carry some axial compression due to gravity and this assists in closing cracks across which the tension steel yielded in the previous load cycle, and that the more uniformly distributed and embedded vertical bars across a potential sliding plane provide better dowel shear resistance.

Also, more evenly distributed vertical bars across the wall section provide better crack control. In beams several small cracks across the flexural reinforcement may merge into one or two large cracks across the web, thereby forming a potential plane of sliding. Because of the better crack control and the shear stress limitation imposed by Eq. (B-36), it does not appear to be necessary to provide diagonal steel across the potential sliding planes of the plastic hinge zone, as it has been suggested⁽⁸⁾ for beams. However, it is recommended that in low rise shear walls some of the shear should be resisted by diagonal bars, placed in the middle of the wall thickness, particularly when the minimum axial compression stress on such walls is less than $0.1 f'_c$ and the shear stress exceeds $0.4 \sqrt{f'_c}$. Suggested arrangements are shown in figure 26. Such bars should be included in the evaluation of the flexural resistance and may be included in the resistance to diagonal tension.

Construction joints represent potential weaknesses where sliding shear displacement can occur. Therefore it is recommended that the design for shear transfer across construction joints be based on the shear friction mechanism⁽²⁾. Accordingly where shear is resisted at a construction joint by friction between carefully roughened surfaces and by dowel action of the vertical reinforcement, the ratio of reinforcement that crosses at right angles to the construction joint should not be less than

$$\rho_{vf} = (V_{wall} - \frac{N_u}{A_g}) \frac{1}{f_y} > 0.0025 \quad (B-37)$$

where N_u is the minimum design compression force on the wall. For tension, N_u should be taken as negative. V_{wall} is obtained from Eq. (B-20) or Eq. (B-25).

Detailing of Coupling Beams

The ductility demand on coupling beams of coupled shear walls, such as examined in "Coupled Shear Walls", can be large.

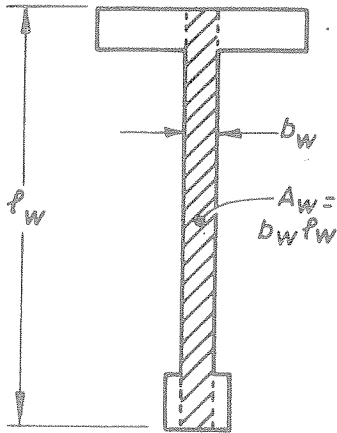


Fig. 29 - Effective Shear Area of a Flanged Wall Section.

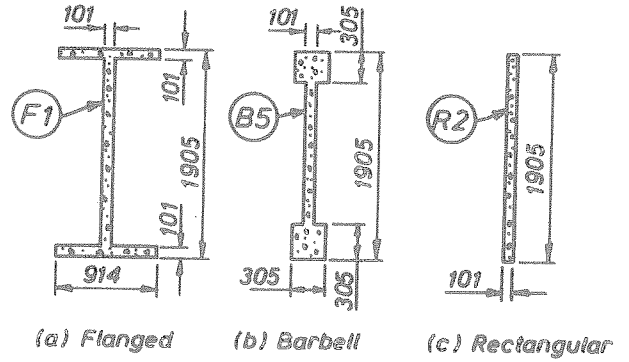


Fig. 30 - Nominal Cross Sectional Dimensions of the PCA Test Specimens (11).

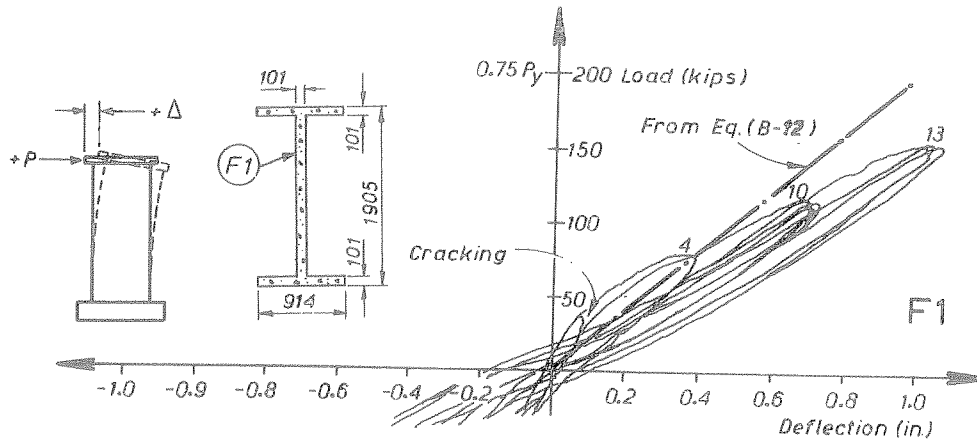


Fig. 31 - Continuous Load-Deflection Plot for Initial Cycles for the Flanged Wall Specimen F1.

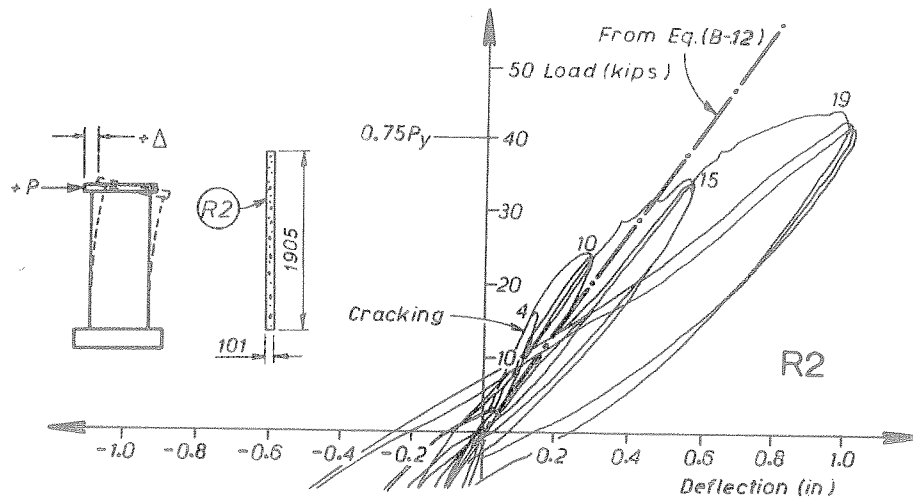


Fig. 32 - Continuous Load-Deflection Plot for Initial Cycles for the Rectangular Wall Specimen R2.

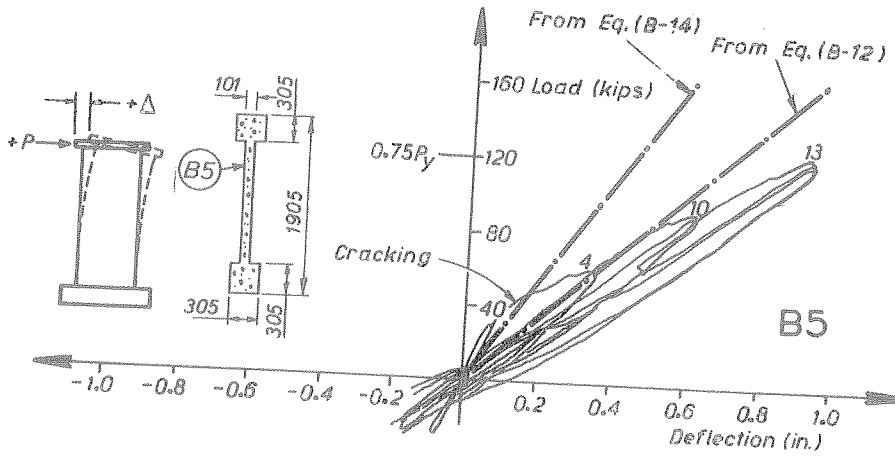


Fig. 33 - Continuous Load-Deflection Plot for the Initial Cycles for Specimen B5.

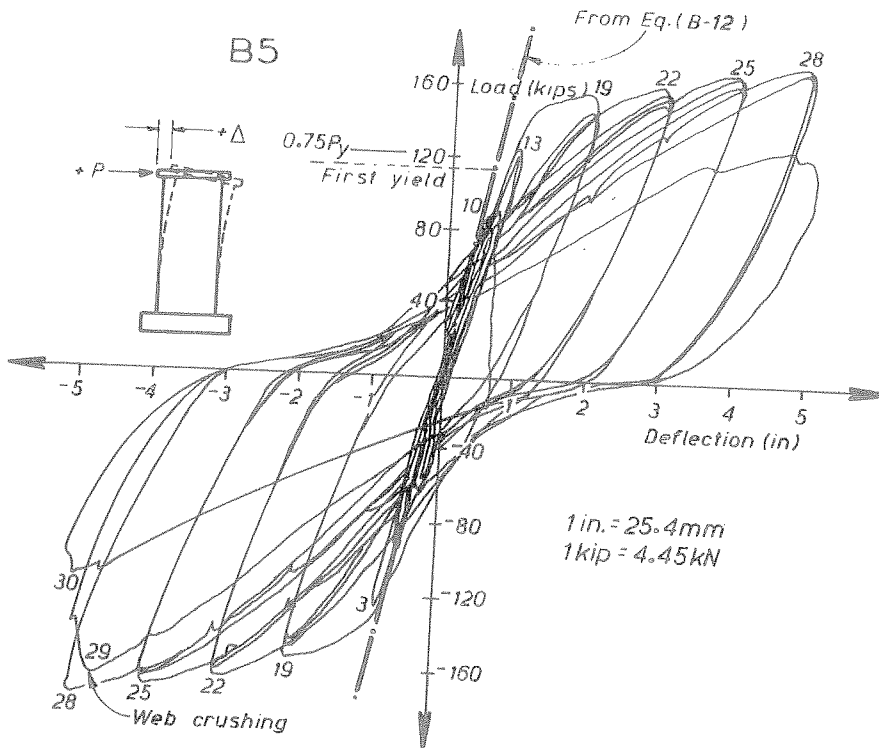


Fig. 34 - Continuous Load-Deflection Plot for all Cycles for Specimen B5

(See figure 7b). To preserve the energy dissipating properties of such beams, which are often relatively deep, diagonal reinforcement should be utilized(2) to resist simultaneously both the moments and the shear. Diagonal bars in cages should be confined to ensure that buckling of diagonal bars cannot occur. For this purpose Eq. (B-30) and the rules listed in 'Confinement of longitudinal bars' should be followed. However neither the spacing of ties nor the pitch of rectangular spirals should exceed 100 mm.

When coupling beams are as slender as normal beams, which are used in ductile frames, distinct plastic hinges will form at the ends and these can be detailed as for beams. The danger of sliding shear failure and the inhibition of flexural ductility increases with increased depth to span ratio, h/ℓ , and with increased shear stresses. Therefore it is recommended that in coupling beams of shear walls the entire seismic design shear and flexure should be resisted by diagonal reinforcement in both directions unless the earthquake induced shear stress is less than

$$v_i = 0.1 \frac{\ell}{h} \sqrt{F_c} \quad (\text{B-38})$$

It should be noted that this severe limitation is recommended because coupling beams can be subjected to much larger rotational ductility demands than spandrel beams of similar dimensions in frames. There is no limitation on the inclination of the diagonal bars.

Slab Coupling of Walls

When walls are interconnected by slabs only, as shown in figure 17c, the stiffness and strength of the coupling between the two walls becomes difficult to define. In the elastic range of displacement a considerable width of the slab will participate in load transfer. However, when inelastic deformations occur in the doorway, as illustrated in figure 27, a dramatic loss of stiffness can be expected(15). Even when the flexural reinforcement is placed in a narrow band, with a width approximately equal to that of the doorway, and the band is confined by stirrup-ties enclosing the top and bottom slab bars in the band, it is difficult to control punching shear around the toes of the walls. From preliminary studies(15) it appears that the hysteretic response of slab coupling is poor and that this system does not provide good energy dissipation with reversed inelastic cyclic loading. As figure 18 indicates, the contribution of slab coupling to the total moment of resistance is not likely to be significant. For this reason its contribution to seismic strength should be neglected in most cases.

When shallow beams, projecting below the slab, are provided across doorways, it must be expected that they will fail in shear, unless the very significant contribution of the slab reinforcement, placed parallel to the coupled walls, is

included in the evaluation of the flexural overcapacity of the relevant beam hinge, and thus in the evaluation of the imposed shear.

NOTATION:

- A = moment parameter used for coupled shear walls
- A_b = area of one bar, mm^2
- A_c^* = area of concrete core in the outer half of section which is subjected to compression strains, measured to outside of peripheral hoop legs, mm^2
- A_e = effective area of the cross section of a wall subjected to axial load
- A_g = gross area of section, mm^2
- A_g^* = gross area of the outer half of wall section which is subject to compression strains, mm^2
- A_{sh} = total effective area of hoop bars and supplementary cross ties in directions under consideration within spacing s_h , mm^2
- A_{te} = area of one leg of stirrup or stirrup tie, mm^2
- A_v = area of shear reinforcement within a distance s , mm^2
- A_w = effective web area of wall cross section, mm^2
- b = width of compression face of member or thickness of rectangular wall section
- b_w = web width or wall thickness
- c = computed distance of neutral axis from compressive edge of the wall section
- c_c = critical value of c
- d = distance from extreme compression fibre to centroid of tension steel
- e_x, e_y = eccentricity of centre of mass in x and y directions respectively
- E_c = modulus of elasticity of concrete, MPa
- f = form factor considered with shear deformation
- f'_c = specified compressive strength of concrete, MPa
- f_r = modulus of rupture of concrete, MPa
- f_y = specified yield strength of steel reinforcement, MPa
- f_{yh} = specified yield strength of hoop or supplementary cross tie steel, MPa
- G_c = modulus of rigidity of concrete, MPa
- h = overall thickness of member or depth of beam, mm

h_w	= overall height of wall of horizontal length l_w , mm	P_e	= maximum design axial load due to gravity and seismic loading acting on the member during an earthquake, N
h''	= dimension of concrete core of section measured perpendicular to the direction of the hoop bars, mm	P_{eq}	= axial load on member due to design earthquake loading only
I	= importance factor	P_{LR}	= axial load on member due to reduced live load
I_{cr}	= moment of inertia of cracked section transformed to concrete	P_{eq}^O	= maximum axial load on member due to earthquake only at the development of flexural overcapacity
I_e	= effective moment of inertia for computation of flexural and shear deflections	P_1^O, P_2^O	= design axial tension and compression force acting on wall at the development of the flexural overstrength capacity of the structure
I_g	= moment of inertia of gross concrete section about centroidal axis	Q_i^O	= shear overcapacity of a coupling beam
I_w	= equivalent moment of inertia of wall section neglecting the reinforcement for computing total deflections	s	= spacing of stirrups, mm
l	= distance between axes of shear walls	s_h	= vertical spacing of horizontal reinforcement, mm
l_n	= length of clear span or distance, measured face to face of support	s_v	= horizontal spacing of vertical reinforcement along length of wall, mm
l_w	= horizontal length of wall	S	= structural type factor
M_a	= maximum moment in member at stage for which deflection is being computed	T	= tension force or period of vibration, seconds
M_{cr}	= cracking moment	v_c	= nominal permissible shear stress carried by concrete, MPa
M_{code}	= moment induced by code specified static loading	v_i	= ideal shear stress, MPa
M_i	= ideal flexural strength of wall section	v_s	= nominal shear stress allocated to resistance of web reinforcement, MPa
M_o	= overturning moment at the base of a shear wall structure due to code load	V_{code}	= shear demand derived from code loading
M^O	= moment developed at flexural overcapacity of member	V_i	= ideal shear capacity of wall
M_2	= moments due to code loading developed at the base of the wall concurrently with earthquake induced axial tension or compression respectively	V_{wall}	= design shear force for a wall at the development of the flexural overcapacity of the structure
M_1^O, M_2^O	= flexural overcapacity developed in the tension and compression wall respectively	V^O	= shear force developed at flexural overcapacity
M_1^1, M_2^1	= design moments at the base after moment redistribution in the tension and compression walls respectively	y_t	= distance from centroidal axis of gross section, neglecting the reinforcement, to the extreme fibre in tension
n	= number of floors above the section of wall being considered	Z	= modifier of structural type factor
N	= number of storeys in a shear wall structure	Δ_f	= wall deflection due to anchorage deformations only
N_u	= design axial compression load normal to cross section occurring simultaneously with the design shear force, N	Δ_m	= wall deflection due to flexural deformations only
P_D	= axial load on member due to dead load only	Δ_u	= deflection at top of shear wall at ultimate state
		Δ_v	= wall deflection due to shear deformations only
		Δ_y	= deflection at top of shear wall at first yield

- ϕ = strength reduction factor
- ϕ_u = curvature at maximum displacement ductility
- ϕ_y = curvature at first yield
- ϕ_o = overstrength factor
- ϵ_c = specified compression strain at extreme concrete fibre, 0.003
- ϵ_{ce} = compression strain at extreme concrete fibre at first yield of tension steel
- ϵ_u = compression strain at extreme concrete fibre at development of a maximum curvature
- ϵ_y = yield strain of reinforcement
- μ_Δ = displacement ductility factor
- μ_ϕ = curvature ductility factor
- ω_v = dynamic shear magnification factor
- ρ_l = ratio of vertical tension reinforcement in wall spaced at s_v
- ρ_{vf} = ratio of reinforcement crossing unit area of construction joint
7. "ICES-STRU DL-II", Engineering Users' Manual, Vol. 1, 1967, Vol. 2, 1969, Vol. 3, 1970, Massachusetts Institute of Technology.
8. DZ 3101 : Part 1 and Part 2, Draft New Zealand Standard Code of Practice for the Design of Concrete Structures, Standards Association of New Zealand, 1978.
9. Sharpe, R.D., "The Seismic Response of Inelastic Structures", Ph.D. thesis, University of Canterbury, Christchurch, New Zealand, Nov. 1974, 126 pp.
10. Paulay, T. and Spurr, D.D., "Simulated Seismic Loading on Reinforced Concrete Frame - Shear Wall Structures", 6th World Conference on Earthquake Engineering, New Delhi, 1977, Preprints 3, pp. 221-226.
11. Oesterle, R.G., Fiorato, A.E., Johal, L.S., Carpenter, J.E., Russell, H.G. and Corley, W.G., "Earthquake Resistant Structural Walls - Tests of Isolated Walls," Report to National Science Foundation, Portland Cement Association, Nov. 1976, 44 pp. (Appendix A, 38 pp. Appendix B, 233 pp.)
12. Blakeley, R.W.G., Cooney, R.C. and Megget, L.M., "Seismic Shear Loading at Flexural Capacity in Cantilever Wall Structures", Bulletin of the New Zealand National Society for Earthquake Engineering, Vol. 8, No. 4, December 1975, pp. 278-290.
13. Fintel, M., Derecho, A.T., Freskakis, G.N., Fugelso, L.E. and Gosh, S.K., "Structural Walls in Earthquake Resistant Structures", Progress Report on the National Science Foundation, (RANN) Portland Cement Association, Skokie, Aug. 1975, 261 pp.
14. Paulay, T. and Uzumeri, S.M., "A Critical Review of the Seismic Design Provisions for Ductile Shear Walls of the Canadian Code and Comments", Canadian Journal of Civil Engineering, Vol. 2, Dec. 1975, pp. 592-601.
15. Taylor, R.G., "The Nonlinear Seismic Response of Tall Shear Wall Structures", Ph.D. thesis, Research Report 77/12, Department of Civil Engineering, University of Canterbury, Christchurch, New Zealand, 1977, 234 pp.
16. ACI Committee 318, "Building Code Requirements for Reinforced Concrete, (ACI 318-77)", American Concrete Institute, Detroit, 1977, 102 pp.
17. Park, R., "Columns Subjected to Flexure and Axial Load", Bulletin of the New Zealand National Society for Earthquake Engineering, Vol. 10, No. 2, June 1977, pp 95-105.
18. Bertero, V.V., Popov, E.P., Wang, T.Y. and Vallenias, J., "Seismic Design Implications of Hysteretic Behaviour of Reinforced Concrete Structural Walls", 6th World Conference on

REFERENCES:

1. NZS 4203 : 1976 "Code of Practice for General Structural Design and Design Loadings for Buildings", Standards Association of New Zealand, 80 pp.
2. Park, R. and Paulay, T., "Reinforced Concrete Structures", John Wiley and Sons, New York, 1975, 769 pp.
3. Taylor, R.G., "Introduction to and Aims in the Design of Earthquake Resisting Shear Wall Structures", Section A of the Shear Wall Study Group of the New Zealand National Society for Earthquake Engineering, The Bulletin of the New Zealand National Society for Earthquake Engineering, Vol. 13, No. 2, 1980.
4. Robinson, L.M., "Shear Walls of Limited Ductility", Section C of the Shear Wall Study Group of the New Zealand National Society for Earthquake Engineering, The Bulletin of the New Zealand National Society for Earthquake Engineering, Vol.13, No. 2, 1980
5. Binney, J. and Paulay, T., "Foundations for Shear Wall Structures", Section F of the Shear Wall Study Group of the New Zealand National Society for Earthquake Engineering, The Bulletin of the New Zealand National Society for Earthquake Engineering, Vol. 13, No. 2, 1980.
6. Powell, G.H., "DRAIN - 2D Users Guide", Report EERC 73-22, Earthquake Engineering Research Centre, University of California, Berkeley, April 1973.

Earthquake Engineering, New Delhi, 1977, Preprints 5, pp. 159-165.

19. Clough, R.W. and Penzien, J., "Dynamics of Structures", Chapter 27, Mcgraw Hill, 1975, 634 pp.

$$I_e = \left(\frac{M_{cr}}{M_a} \right)^3 I_g + \left[1 - \left(\frac{M_{cr}}{M_a} \right)^3 \right] I_{cr} \quad (B-14)$$

The moment assumed to cause cracking is from first principles⁽²⁾

$$M_{cr} = \frac{f_r I_g}{y_t} \quad (B-15)$$

It is seen that the relationship between the second moment of area and the moments are such that $I_g \gg I_e \gg I_{cr}$ where $l > (M_{cr}/M_a) > 0$.

For beams and columns of normal proportions and reinforcement contents it is found that usually $0.4 < I_{cr}/I_g < 0.6$, and hence the equivalent moment of inertia is such that $0.5 < I_e/I_g < 0.7$. Consequently in the elastic analysis of frames customarily the "gross moment of inertia", I_g of members is used, and this is reduced by 30 to 50% to allow for the effects of cracking.

In structural walls usually considerably less flexural reinforcement is being used than in beams of ductile earthquake resisting frames. The flexural tension steel content, $\rho = A_s/bd$, to be considered in the evaluation of flanged transformed wall sections can be as small as 0.05%. Consequently in such walls the "transformed moment of inertia", I_{cr} will be a smaller fraction of the "gross moment of inertia", I_g . Cracking has thus a more profound effect on the stiffness of normal walls than on that of beams.

The flexural deformation, shown in figure 28d can therefore be obtained thus

$$\Delta_m = \frac{Ph_w^3}{3E_c I_e} \quad (I-2)$$

Anchorage Deformations

The analytical model commonly used is a cantilever. This is fully fixed against rotations at its base. (figure 28a). Under lateral load the vertical wall reinforcement is at its highest stress at the base. Consequently tensile strains along the flexural bars will only gradually decay in the foundation structure. The elongation of the vertical bars within the foundation structure and the slip due to high local bond stresses along the development length will result in an apparent "pull out" of such bars at the base of the wall. This can significantly increase the wall deflection, as shown in figure 28e. Based on the relative magnitudes of observed "pull out" deformations, it is suggested that its magnitude be estimated as

$$\Delta_f = 0.2 \Delta_m \quad (I-3)$$

Shear Deformations

It is well known that shear deformations

APPENDIX I

THE ESTIMATION OF DEFLECTIONS OF CRACKED REINFORCED CONCRETE CANTILEVER WALLS

Assumptions

Deflection estimates generally used in seismic design should reflect the behaviour of the structure after the development of extensive cracking at a load level which, as yet, does not result in inelastic deformations. Therefore for the purpose of the derivations that follow, wall behaviour at 75% of the theoretical yield load will be considered. The yield load is that which causes the in part of the flexural reinforcement, placed in boundary regions of walls, such as flanges, to yield. If for example the main flexural reinforcement in a wall section consists of seven layers of D28 bars, the yield load is that attained at the onset of yielding in the innermost (i.e. seventh layer of these D28 bars). This load will be close to the ideal flexural capacity.

In order to define the stiffness of any elastic member with given boundary conditions, a certain unit deformation must be related to a certain load pattern. For the purpose of this study the structure and the load on it are those shown in figure 28a and figure 28b, and the deformation to be determined is the lateral deflection at roof level, Δ , as shown in figure 28c.

The symbols used in the subsequent derivation are fully defined in the text or the list of symbols.

Flexural Deformations

The flexural deformations, being dominant, are normally the only ones that are considered in the design of flexural members. Accordingly the roof deflection for a homogeneous elastic cantilever wall of figure 28a is

$$\Delta = \frac{Ph_w^3}{3E_c I_g} \quad (I-1)$$

The most appropriate approach to the estimation of cracking is to allow for a loss of effective resisting area in the cross section. The effective moment of inertia of the section, I_e , will be between that based on the uncracked section, I_g , and that obtained from the fully cracked section in which the steel area is transformed to concrete area, I_{cr} . An interpolation for I_e between the above limits has been developed by Branson and it has been adopted by the American Concrete Institute⁽¹⁶⁾. Its background is examined elsewhere^(2, 8). This is

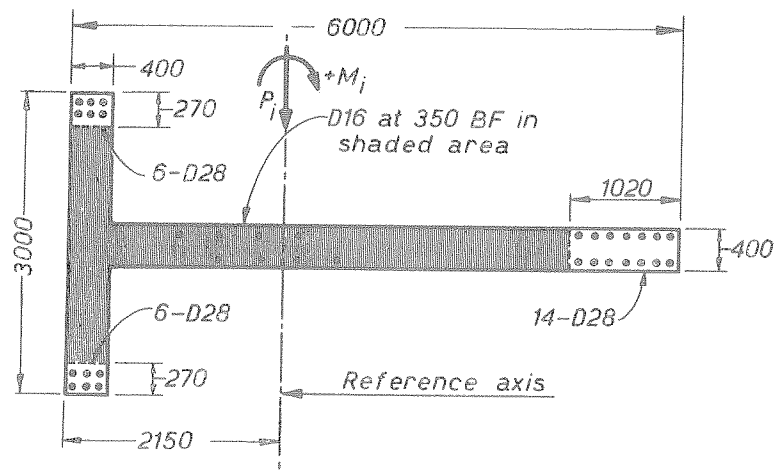


Fig. 35 - Sectional Properties of an Example Shear Wall Section.

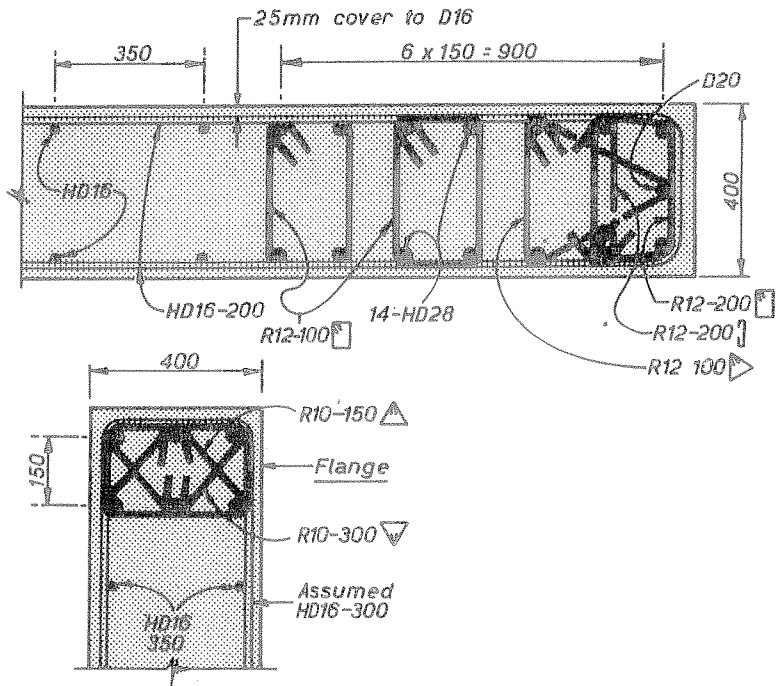


Fig. 36 - Arrangement of Transverse Reinforcement in the Critical Regions of the Example Shear Wall Section.

in slender flexural members are negligibly small in comparison with those due to flexure. Walls, however, may belong to the family of "deep beams", in which shear deformations are likely to be significant. Therefore shear deformations should be considered.

The shear deflection of a homogeneous elastic wall at roof level, shown in figure 28f, is known to be

$$\Delta_v = \frac{fPh_w}{G_c A_w} \quad (I-4)$$

The area of the wall, effective in shear, A_w , is defined in figure 29. It will be assumed that $A_w = b_w l_w$ for the common type of walls used.

It has been found that in members in which diagonal cracks have developed as a result of shear stresses, the relative contribution of shear deformations is considerably larger than what Eq. (I-4) would predict. It will be appreciated that after the development of diagonal cracking a new form of shear transfer begins to operate i.e. the truss mechanism. In this new mechanism the web reinforcement (stirrups) contributes to large shear strains. It has been shown⁽²⁾ that the shear stiffness of diagonally cracked beams is only 10-30% of that of uncracked beams, depending on the contribution of web reinforcement.

The estimation of shear deformation in a shear wall is complicated by the fact that the shear force in a real wall will decrease from a minimum at the top of the wall to a maximum of the base. Moreover, in the lower portions of the wall more extensive flexural and shear cracking will occur, and it can be expected that in these more heavily cracked zones the shear deformations will be larger. Taking these considerations into account it is suggested that the contributions of shear deformations along the height of a cantilever wall be estimated from the following simple expression:

$$\Delta_v = \frac{1.2 Ph_w}{0.4 E_c 0.3 A_w} = \frac{10 Ph_w}{E_c A_w} \quad (I-5)$$

Combined Deformations

It is seen from figure 28 that the roof deflection of the cracked cantilever wall due to flexural, anchorage pull-out and shear deformations is $\Delta = \Delta_m + \Delta_f + \Delta_v$. Substituting from Eqs. (I-2), (I-3) and (I-5) we obtain

$$\Delta = \frac{Ph_w^3}{3E_c I_e} + \frac{0.2 Ph_w^3}{3E_c I_e} + \frac{10 Ph_w}{E_c A_w} \quad (I-6)$$

It is convenient to express the deflection in terms of flexural deformations and an equivalent wall moment of inertia, I_w , so that

$$\Delta = \frac{Ph_w^3}{3E_c I_w} \quad (I-7)$$

By equating the above two equations the equivalent wall moment of inertia, I_w , is obtained thus

$$I_w = \frac{I_e}{1.2 + F} \quad (B-12)$$

where value of I_e is given by Eq. (B-14) and

$$F = \frac{30 I_e}{h_w^2 b_w l_w} \quad (B-13)$$

A Comparison with Experiments

Recently the Portland Cement Association in Skokie (US) carried out extensive testing with cantilever shear walls⁽¹¹⁾. Some observed results of this programme are compared with values obtained from Eq. (B-12) and Eq. (B-14). All the walls reported have the same aspect ratio of $h_w/l_w = 2.4$. This is in the range where shear deformations are likely to be significant.

The basic dimensions of the cross sections used for the 4752 mm high wall specimens are shown in figure 30. A comparison of predicted deflections with observed ones was made for all seven specimens reported. However, representative results for only three of the cases are presented here.

Figure 31 shows the initial cycles of the load displacement relationship for the flanged wall specimen (figure 30), when the load did not exceed approximately 60% of the yield load P_y . The straight line shows the idealized^y relationship that would have resulted from Eq. (B-12).

A similar relationship is shown in figure 32 for a wall with a rectangular cross section. In the response shown the maximum load reached approximately 83% of the yield load, P_y .

Finally a comparison is made for a wall with a rectangular boundary element (barbell), B-5, in figure 33. Here Eqs. (B-12) and (B-14) are compared. It is seen that Eq. (B-14) generally recommended⁽⁸⁾ for the prediction of beam deflection, overestimates the wall stiffness. The differences in deflections, as predicted by the two equations, result from the considerations of shear and anchorage deformations, which have been incorporated into Eq. (B-12). The full response, including the inelastic cycles, of this wall specimen, is shown in figure 34.

With respect to the PCA experiments used here, it may be said that the suggested deflection estimate procedure should be acceptable for design purposes.

APPENDIX II

DESIGN OF A CANTILEVER SHEAR WALL

Design Requirements and Properties

Preliminary design has indicated that one of several symmetrically arranged canti-

lever shear walls of a 11 storey Class III building, resisting the required seismic loading, may be dimensioned and reinforced at ground floor level as shown in figure 35. In this study seismic actions in the longitudinal direction of the wall sections are considered only. The first storey is 3.50 m high and the upper 10 storeys are 3.25 m each.

The strength properties to be used are as follows:

Concrete	$f'_c = 25\text{MPa}$
Vertical wall reinforcement	$f_y = 380\text{MPa}$
Horizontal wall shear reinforcement	$f_y = 380\text{MPa}$
Horizontal hoops and ties	$f_y = 275\text{MPa}$

The total loading at ground floor level from all the tributary areas of the upper floors is as follows:

Dead load	7000 kN
Reduced live load	3000 kN

The centre of the lateral static load, used in the preliminary design, was located at 23 m above ground floor. At ground level the wall is assumed to be fully fixed against rotations.

Minimum requirements with respect to

- i) Section "Stability" i.e. $\lambda_n/b < 3500/400 = 8.75 < 10$
 - ii) Section "Longitudinal Wall Reinforcement" i.e. $\rho_{l,min} = 0.7/380 < 2 \times 201/(400 \times 350) = 0.004$
- and
- iii) Bars spacing requirements are all satisfied

Flexural Capacities

The flexural capacities are to be evaluated for each direction of loading. The maximum axial compression to be considered for the evaluation of the available ideal flexural strength is from (1)

$$U_{ideal} = (D + L_R)/\phi = (7000 + 3000)/0.9 = 11,100 \text{ kN}$$

Loading causing compression in the flange

$$P_i = 11,100 \text{ kN} \quad M_i = ?$$

Using a trial and error process, the neutral axis depth will be estimated so that the internal compression forces less the tensile forces will give a compression resultant of approximately 11 MN. Then the moment about the reference axis (the centroid of the gross concrete section) will be computed.

$$\text{Assume first } c = 0.05 \times 6000 = 300 \text{ mm}$$

The D16 bars provide $(2 \times 201)380/(0.35 \times 10^6) = 0.44 \text{ MN force per meter wall length.}$

Ignore contribution of reinforcement in the flange and the reduction of steel flexural contribution in the elastic core of the section then:

$$\begin{aligned} \text{Compression } C_c &= (0.85 \times 300)3000 \times (0.85 \times 25)/10^6 = 16.3\text{MN} \\ \text{Tension } T_{28} &= 14 \times 615 \times 380/10^6 = 3.27 \\ T_{16} &= (6.0 - 0.4 - 1.02) \times 0.44 = 2.01 \\ \text{Total tension } T &= 5.28 = 5.3\text{MN} \end{aligned}$$

$$\begin{aligned} \text{Therefore } C_c - T &= P_i = 11.0\text{MN} \\ M_i &= 16.3(2.15 - 0.5 \times 0.85 \times 0.3) = 33.0\text{MNm} \\ &= 3.27(6.00 - 2.15 - 0.5 \times 1.02) = 10.9\text{MNm} \\ &= 2.01(0.5 \times 4.58 + 0.4 - 2.15) = 1.1\text{MNm} \end{aligned}$$

No new trial for c is required. Therefore $M_i = 45.0\text{MNm}$

Loading causing tension in the flange

$$P_i = 11.1 \text{ MN} \quad M_i = ?$$

$$\text{Assume first } c = 0.35 \times 6000 = 2100 \text{ mm}$$

$$\begin{aligned} \text{Compression } C_c &= (0.85 \times 2100)400(0.85 \times 25)/10^6 = 15.2\text{MN} \\ C_{28} &= 14 \times 615 \times 380/10^6 = 3.3\text{MN} \\ C_{16} &= \text{neglect} = - \\ \text{Total compression } C &= 18.5\text{MN} \end{aligned}$$

$$\begin{aligned} \text{Tension } T_{28} &= (6 \times 615)380/10^6 = 1.4\text{MN} \\ \text{in the flange } T_{16} &= (3.0 - 2 \times 0.27)0.44 = 1.1\text{MN} \\ \text{in the web } T_{16} &= (6.0 - 0.4 - 2.1)0.44 = 1.5\text{MN} \\ \text{Total tension } T &= 4.0\text{MN} \end{aligned}$$

$$\text{Net compression } P_i = 11.1 < 14.5\text{MN}$$

$$\text{Reduce } a \text{ by } \Delta a = (14.5 - 11.1)10^6 / (0.85 \times 25 \times 400) = \text{say } 370 \text{ mm}$$

$$\text{Hence } c = 2100 - 370/0.85 = 1664 \text{ mm}$$

by proportion

$$\begin{aligned} C_c &= 1664 \times 15.2/2100 = 12.0\text{MN} \\ C_{28} &= \text{as before} = 3.3\text{MN} \\ C_{16} &= \text{as before} = - \\ &= 15.3\text{MN} \\ T_{28} &= \text{as before} = 1.4\text{MN} \\ \text{in the flange } T_{16} &= \text{as before} = 1.1\text{MN} \\ \text{in the web } T_{16} &= (6.0 - 0.4 - 1.66)0.44 = 1.7\text{MN} \\ &= 4.2\text{MN} \\ P_i &= 11.1 = 11.1\text{MN} \end{aligned}$$

$$\begin{aligned}
 M_i &= 12.0(6.0-2.15-0.85 \times 1.66 \times 0.5) = 37.7 \text{ MNm} \\
 &+ 3.3(6.0-2.15-0.5 \times 1.02) = 11.0 \text{ MNm} \\
 &+ (1.4+1.1)(2.15-0.5 \times 0.4) = 4.9 \text{ MNm} \\
 &+ 1.7 \{ -(6.0-0.4-1.66)0.5+2.15-0.4 \} \\
 &= 0.4 \text{ MNm}
 \end{aligned}$$

Hence moment of resistance
is $M_i = 53.2 \text{ MNm}$

Design for Shear

As the ideal moment capacity for the most adverse load combination is 53.2 MN, the code required shear is close to $0.9 \times 53.2 / 23 = 2.08 \text{ MN}$.

For a 11 storey building the dynamic shear magnification from Table B-I is $\omega_v = 1.7$. With a flexural overstrength of 125% of ideal strength, the design shear force for the wall is obtained from Eq. (B-18).

$$V_{\text{wall}} = 1.7 \times 1.25 \times 2.08 = 4.42 \text{ MN}$$

Hence from Eq. (B-32)

$$v_i = 4.42 \times 10^6 / (400 \times 0.8 \times 6000) = 2.30 \text{ MPa}$$

From Eq. (B-36) the maximum allowable shear stress is

$$v_{i,\text{max}} = \frac{0.3 \times 1.39 \times 1.0 + 0.16}{\sqrt{25}} = 2.89 > 2.30 \text{ MPa}$$

$$N_u / A_g = 11.1 \times 10^6 / \{ 6000 \times 400 + (3000 - 400) 400 \} = 3.23 \text{ MPa}$$

From Eq. (B-34)

$$v_c = 0.25(1 + 25/25) \sqrt{3.23 - 25/10} = 0.43 \text{ MPa}$$

From Eq. (B-33)

$$v_s = v_i - v_c = 2.30 - 0.43 = 1.87 \text{ MPa}$$

From Eq. (B-35)

$$s = 1.87 \times 400 \times 380 / 380 = 1.97 \text{ s}$$

Assume two legs of HD16 bars, $A_v = 402 \text{ mm}^2$

$$s = 402 / 1.97 = 204 \approx 200 \text{ mm}$$

Use HD16 at 200 mm crs for horizontal shear (stirrup) reinforcement

Confinement

It is evident that no confinement is required when the flange is in compression as the section is extremely ductile with $c/l_w = 0.05$. However, when the flange is in tension the stem of the section will need to be confined. For this it was found in "Loading causing tension in the flanges", that $c = 1664 \text{ mm}$.

From Eq. (B-26) with $\phi_o = 1.4$

$$c_c = 0.10 \times 1.4 \times 1.0 \times 6000 = 840 \approx 1664$$

Hence provide confinement over a length of $0.5 \times 1664 = 832 \text{ mm}$

For Eqs. (B-28) and (B-29) to be used take the following values

$$\begin{aligned}
 h'' &= 832 - 41 + 0.5 \times 12 = 797 \approx 800, \\
 A_g^* &= 400 \times 832 = 333000 \text{ mm}^2, \text{ Assume R12 ties,}
 \end{aligned}$$

Assume cover to HD stirrups = 25 mm and to main bars 41 mm, hence

$$A_c^* = (400 - 2 \times 41 + 2 \times 12)(832 - 41 + 12) = 275000 \text{ mm}^2$$

$$(A_g^* / A_c^* - 1) = (333 / 275 - 1) = 0.21$$

$0.3 \times 0.21 = 0.063 < 0.12$ hence Eq. (B-29) governs

From Eq. (B-29)

$$A_{sh} = 0.12 s_h 800 \times (25/275)(0.5 + 0.9 \times 1664/6000) = 6.54 s_h$$

With 6 R12 legs over 800 mm length

$$s_h = 6 \times 113 / 6.54 = 104 \text{ mm}$$

From the spacing requirements stated in "Confining reinforcement"

$$s_{h,\text{max}} = 6 \times 28 = 168 \text{ or } 400/3 = 133 \text{ or } 150 \text{ mm}$$

Hence use R12 hoops and ties at 100 mm crs and for practical reason confine all 14 HD28 bars.

For the confinement in the longitudinal direction $h'' = 400 - 2 \times 41 + 12 = 330 \text{ mm}$

As the distance between the 2 HD28 bars is more than 200 mm, it will be necessary to place in the confined region an intermediate (nominal) bar in between them. A D20 bar will enable another tie to be placed over the 400 mm width of the section. Hence by proportion from the above derivation of A_{sh} and $s_h = 100$

$$A_{sh} = (330/800) 5.90 \times 100 = 243 \text{ mm}^2$$

R10 legs could be used, but for the sake of uniformity R12 ties will be provided as shown in figure 36.

To confine the HD28 bars against buckling at the ends of the flange, ties are required in accordance with 'Confinement of longitudinal bars' and Eq. (B-30)

From Eq. (B-31)

$$\rho_l = 3 \times 615 / 400 \times 150 = 0.0308 > 0.0075$$

Hence

$$A_{te} = \frac{615}{16} \frac{380}{275} \frac{s_h}{100} = 0.53 s_h$$

The max^m spacing is $6 \times 28 = 168 \text{ mm}$

R10 ties may be used, thus

$$s_h = 78.5 / 0.53 = 148 \text{ mm}$$

Use R10 ties at 150 mm crs as shown in figure 36

The confining reinforcement as computed should extend, in accordance with figure 15, to a height of $l_w = 6000 \text{ mm}$, i.e. up to the 2nd floor of this structure.

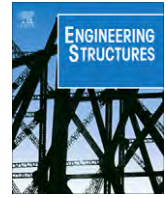
Note that a more rigorous analysis, using Eq. (B-27) would have given the critical value for the neutral axis depth as follows:

With $S = 1.0$, $l_w = 6000$ and $h_w =$

$$3.5 + 10 \times 3.25 = 36 \text{ m}$$

$$c_c = \frac{8.6 \times 1.4 \times 1 \times 6000}{(4 - 0.7 \times 1)(17 + 36/6)} = 952 \text{ mm} > 840 < 1664$$

Hence confinement is to be provided as computed above.



Parameters for shear strength prediction of exterior beam–column joints without transverse reinforcement

Sangjoon Park, Khalid M. Mosalam *

Department of Civil and Environmental Engineering, University of California, Berkeley, United States

ARTICLE INFO

Article history:

Received 29 October 2010

Revised 11 October 2011

Accepted 11 November 2011

Available online 5 January 2012

Keywords:

Beam–column joints

Earthquake engineering

Non-ductile reinforced concrete

Shear strength model

ABSTRACT

The paper presents key parameters to determine the shear strength of exterior beam–column joints without transverse reinforcement in the joint region (referred to as unreinforced exterior joints). A large experimental data set of these joints is collected from published literature based on consistent criteria for data selection. The parametric study from the database indicates that the shear strength of unreinforced exterior joints is mainly influenced by two parameters: (1) joint aspect ratio which is defined as the ratio of beam to column cross-section heights and (2) joint shear index which is dependent on the beam longitudinal tension reinforcement ratio and its strength. The effect of these two parameters on the joint shear strength is investigated using proposed equations that are verified by comparison with the database. Using the parametric equations of the two key parameters, an empirical shear strength model is proposed in this study and validated by accurate shear strength predictions of the test specimens collected in the database. The proposed shear strength model can be adopted to assess the seismic performance of non-ductile reinforced concrete buildings with deficient seismic details in the joint region.

Published by Elsevier Ltd.

1. Introduction

Many reinforced concrete (RC) buildings constructed without transverse reinforcement in the beam–column joint region (referred to as unreinforced joint) still widely exist in seismically active regions, e.g. western USA, Japan and New Zealand, since the transverse reinforcement requirements for the design of beam–column joints (referred to hereafter as “joints”) were not addressed in earlier code provisions prior to the 1970s. Such unreinforced joints are considered vulnerable to brittle shear failure under earthquake shaking due to insufficient shear reinforcement in the joint region. In practice, many tests have proven the poor seismic performance of unreinforced joints, especially exterior joints. Several shear strength models of unreinforced exterior joints have been proposed and available in the literature. Some empirical models [1–3] have been developed based on statistical regression analysis with large scatter or small size of experimental data sets. More sophisticated models based on the strut-and-tie (SAT) idealization [4–6] have some conceptual limitations for direct application to unreinforced joints [7]. Thus, an accurate shear strength model for unreinforced joints is still needed.

There are some differences in the design of joints between USA, Japan, and New Zealand codes. The main difference is whether a truss mechanism due to joint transverse reinforcement and intermediate column bars is taken into account or ignored. The unreinforced joints are free from this disagreement because a truss mechanism is hardly developed and the joint shear forces are directly resisted by the compressive strength of a diagonal strut developed in the joint as considered in the USA [8,9] and Japan codes [10].

Traditionally, the shear strength of concrete has been expressed in terms of the square root of the concrete standard compressive strength, $\sqrt{f'_c}$, in the USA codes [9]. The ACI 352-02 [8] follows the same expression for the shear strength of joints. Unlike the USA codes, the New Zealand code [11] specifies that the horizontal shear stress should not exceed $0.2f'_c$ to avoid the diagonal compression failure by crushing. Some of existing empirical models [1,2] use a function of $\sqrt{f'_c}$ as the USA codes suggests, whereas other models [3,12] employ a function of $\sqrt[3]{f'_c}$. In the present study, it is assumed that the joint shear strength is proportional to $\sqrt{f'_c}$. The effects of three parameters, namely (1) joint aspect ratio, (2) beam longitudinal reinforcement ratio, and (3) column axial load, on the joint shear strength are investigated from the experimental test database of unreinforced exterior joints. Based on the results of the parametric study, this research subsequently proposes a shear strength model using a rational mechanistic approach.

* Corresponding author. Address: Department of Civil and Environmental Engineering, University of California, 733 Davis Hall, Berkeley, CA 94720-1710, United States. Tel.: +1 510 643 4805; fax: +1 510 643 8928.

E-mail address: mosalam@ce.berkeley.edu (K.M. Mosalam).

2. Investigation of main parameters

2.1. Database of unreinforced exterior joints

A large database of tests on unreinforced exterior (and corner) joints are collected from published literature and analyzed in this section. To focus on the joints vulnerable to shear failure, only exterior joints without or with one lateral beam (Fig. 1(b)) are included, whereas interior joints of exterior frames (Fig. 1(a)) and exterior joints of internal frames (Fig. 1(c)) are excluded. This distinction is made because crushing along the joint diagonal occurred in the joints without lateral beams or with a lateral beam on one side only, and the shear capacity of joints with lateral beams on two sides increased significantly compared to the two other cases [13,14]. In addition, the hook anchorage details are considered as one of the criteria for data selection. There are several types of hook anchorage details in the joint region, which were used in gravity load designed RC buildings. Fig. 2 shows the selected anchorage details that can develop at least one strut mechanism under lateral loading. It is to be noted that the test specimens designed with wide beam, i.e. with a beam width greater than the column width, are not included in the database due to different confinement condition around the joint region. Moreover, exterior joint tests affected by column or beam shear failure are excluded from the database.

Based on the discussion above, 62 tests of unreinforced exterior joints satisfying the selection requirements of the database candidates are identified and summarized in Table 1. The information of each test is extracted from the published literature and consistent assumptions are made for shear strength calculation when available data are incomplete. The joint shear strength is expressed as $\gamma_n = V_n / (b_j h_c \sqrt{f'_c})$ to be compared to the criteria of the current USA code provisions. The effective joint width, b_j , is taken as $(b_b + b_c) / 2$ which gives a reasonable equivalent strut [14]. Note that V_n is the maximum horizontal shear force (V_{jn}) in the joint, h_c is the total height of column cross-section in the loading direction, b_c and b_b are the respective widths of the column and beam cross-sections. Six types of specimen failure are observed as

follows: (1) joint shear failure without beam reinforcement yielding (J), (2) joint shear failure with beam reinforcement yielding (BJ), (3) beam flexural failure (BF), (4) column flexural failure (CF), (5) beam reinforcement pull-out failure (P), and (6) beam reinforcement 90° hook anchorage failure (A).

2.2. Effect of joint aspect ratio

The effect of the joint aspect ratio on the joint shear strength has been investigated experimentally by several researchers. For the case of reinforced joints, Kim and LaFave [15] reported that the increase of the joint aspect ratio (h_b/h_c) ranging from 1.0 to 1.6 had little influence on the joint shear strengths and shear strains for the case of J type failure but slightly reduced the joint shear strength for the case of BJ failure. Note that h_b is the total cross-section height of the beam framing into the joint. Wong [5,16] tested unreinforced exterior joints having the three joint aspect ratios of 1.0, 1.5, and 2.0. These test results showed that the joint strength is inversely proportional to the joint aspect ratio. Vollum and Newman [1] and Bakir and Boduroğlu [2] made the same observations from published test results. Each of these studies developed a joint strength model considering this adverse effect of the joint aspect ratio.

The effect of the joint aspect ratio on the joint shear strength can be explained by the SAT approach where a steeper diagonal strut is developed in high aspect ratio of a joint region if there is no transverse reinforcement in the joint region. Consequently, the steeper diagonal strut results in less effective shear resistance to equilibrate the horizontal joint shear force as illustrated in Fig. 3(a). Hence, the shear strength of unreinforced exterior joints decreases with increase of the joint aspect ratio. This hypothesis is supported by the plot of the database findings shown in Fig. 3(b). The adverse effect of the joint aspect ratio on the joint shear strength is more evident for the case of J type failure. It is worth mentioning that the joint shear strengths for J failure types are greater than those for other joint failure types, except for the pull-out (P) failure and for the rare cases of high column axial load specimens.

2.3. Effect of beam longitudinal reinforcement

Tests on unreinforced interior joints [17,18] showed that joints failed in shear at different levels of joint shear demand (attributed to different beam longitudinal reinforcement) although all tests were conducted for the same concrete geometry and column axial load. Based on this observation, Anderson et al. [19] claimed that joint shear strength is not a single number and beyond a certain threshold, joint shear failure can occur at joint shear demand related to the beam reinforcement strength and the specimen geometry. Wong [5] tested unreinforced exterior joints with two different beam longitudinal reinforcement ratios. The results of these tests [5] show that the specimens having high beam longitudinal reinforcement ratio showed J type failure, i.e. joint shear failure prior to beam reinforcement yielding, while the specimens having low beam longitudinal reinforcement ratio experienced BJ type failure, i.e. joint shear failure with beam reinforcement yielding. Bakir and Bouroğlu [2] concluded that the joint shear strength is related to the beam longitudinal reinforcement ratio from the investigation of the tests [20] which had three different beam reinforcement ratios.

For the unreinforced joints, the increase of joint shear strength with increase of the beam longitudinal reinforcement ratio can be explained as follows: (1) increasing the beam longitudinal reinforcement ratio leads to the increase of the horizontal joint shear force without yielding of the beam longitudinal bars, i.e. larger horizontal joint shear force is imposed with less deterioration of

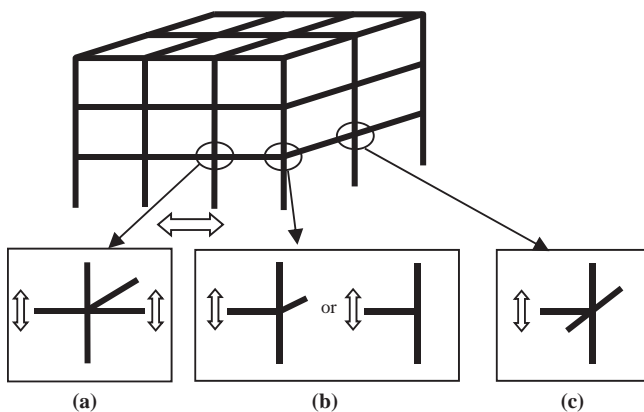


Fig. 1. Beam-column joint types: (a) interior joint, (b) exterior joint without or with one lateral beam (selected in this study), (c) exterior joint with two side lateral beams.

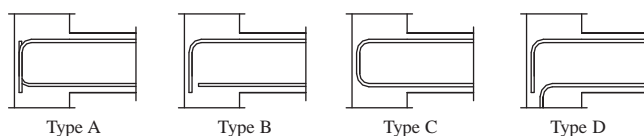


Fig. 2. Anchorage details selected in the joints database.

Table 1
Experimental database.

References	Specimen	f'_c (MPa)	$f_{y,beam}$ (MPa)	A_s (mm ²)	b_j (mm)	h_c (mm)	h_b (mm)	$P/f'_c A_g$	V_n (kN)	γ_n (MPa ^{0.5})	Failure type
[39,40]	V	22.8	352	4.0	342.9	381	508	0.86	615.7	0.99	J
	7	39.3	352	4.0	342.9	381	508	0.50	844.1	1.03	BJ
[41]	OT0	67.3	435	3.16	370	420	450	0.02	997	0.78	BJ
[42]	SP1	30.8	347	3.0	342.9	381	508	0.41	626.8	0.87	BJ
	SP2	31.1	349	3.0	342.9	381	508	0.41	609.0	0.84	BJ
	SP5	31.9	348	3.0	381	381	508	0.43	608.1	0.74	BJ
[5]	BS-L	30.9	520	1.46	280	300	450	0.15	315.5	0.68	J
	BS-U	31.0	520	1.46	280	300	450	0.15	341.2	0.73	J
	BS-L-LS	31.6	520	1.46	280	300	450	0.15	344.9	0.73	J
	BS-L-300	34.1	520	1.46	280	300	300	0.15	505	1.03	BJ
	BS-L-600	36.4	520	1.46	280	300	600	0.15	283.9	0.56	J
	BS-L-V2T10	32.6	520	1.46	280	300	450	0.15	398.8	0.83	J
	BS-L-V4T10	28.3	520	1.46	280	300	450	0.15	402.9	0.90	J
	JA-NN03	44.8	75.4	0.97	280	300	400	0.03	304.2	0.54	BJ
	JA-NN15	46.0	520	0.97	280	300	400	0.15	325.1	0.57	BJ
	JB-NN03	47.4	520	0.97	280	300	300	0.03	317	0.55	BJ
[31]	01	33.1	459	4.0	406.4	406.4	406.4	0.10	859.4	0.90	J
	02	33.1	459	4.0	406.4	406.4	406.4	0.25	798.8	0.88	J
	03	34.0	459	4.0	406.4	406.4	406.4	0.10	815.9	0.85	J
	04	34.0	459	4.0	406.4	406.4	406.4	0.25	901.9	0.97	J
	05	31.7	459	4.0	406.4	406.4	406.4	0.10	857.0	0.92	J
	06	31.7	459	4.0	406.4	406.4	406.4	0.25	862.8	0.94	J
[32]	02	46.2	454	4.0	304.8	457.2	406.4	0.10	951.7	1.00	J
	06	41.0	454	4.0	304.8	457.2	406.4	0.10	940.5	1.05	J
	04	37.0	454	4.0	304.8	457.2	406.4	0.25	929.4	1.10	J
	05	40.1	454	4.0	304.8	457.2	406.4	0.25	982.5	1.11	J
[43]	BCJ1	34.0	720	1.24	200	300	400	0	306	0.87	J
	BCJ3	33.0	720	1.24	200	300	400	0	322	0.93	J
	BCJ5	38.0	720	1.24	200	300	400	0.08	314	0.85	J
	BCJ6	35.0	720	1.24	200	300	400	0.09	315	0.89	J
[22]	C4ALN0	42.4	522	0.62	130	150	210	0.05	110.5	0.87	P
	C4ALH0	104.0	522	0.62	130	150	210	0.02	188.2	0.95	P
	C6LN0	51.0	522	0.62	130	150	210	0.04	104.1	0.75	J
	C6LH0	101.0	522	0.62	130	150	210	0.02	157.3	0.80	J
[21]	4a	39.0	570	1.52	275	300	500	0	198.6	0.39	CF
	4b	39.0	570	1.52	275	300	500	0.09	232.3	0.45	J
	4c	39.0	570	1.52	275	300	500	0.16	286.1	0.55	J
	4d	39.0	570	1.52	275	300	500	0	252.4	0.49	J
	4e	39.0	570	1.52	275	300	500	0.09	269.3	0.52	J
	4f	39.0	570	1.52	275	300	500	0.17	308.0	0.60	J
[44]	U40L	24.3	387	1.76	280	300	380	0	266.2	0.64	J
	U20L	26.7	387	0.88	280	300	380	0	188.7	0.44	A
	B101	31.9	392	1.76	280	300	380	0	348.4	0.73	J
[45]	T-1	30.8	425	1.85	250	400	400	0.19	503.8	0.91	BJ
	T-2	30.8	425	1.85	250	400	400	0.10	503.8	0.91	BJ
[12]	EX-2	52.5	520	0.88	154.5	272	305	0.13	176.3	0.58	BJ
[46]	J1	32.0	520	1.04	154	300	300	0.30	261.9	1.00	J
[47]	Model 5	26.5	385	0.44	167	167	200	0	72.1	0.50	BJ
[48]	RC-1	19.4	324	0.66	215	230	330	0	130.5	0.60	BJ
[49]	SP1-NS	25.8	315	2.64	330.5	356	508	0.02	362.2	0.61	CF
	SP1-EW	25.8	315	2.64	330.5	356	508	0.02	401.9	0.67	CF
	SP2-NS	34.6	315	2.64	330.5	356	508	0.02	408.0	0.59	J
	SP2-EW	34.6	315	2.64	330.5	356	508	0.02	431.0	0.62	J
[24]	RCNH1	30.0	525	0.22	125	200	300	0.13	48.4	0.35	BF
[50]	T0	30.6	425	1.95	200	400	400	0.20	393.1	0.71	BJ
[23]	A0	31.6	580	0.22	200	200	300	0.05	81.2	0.36	BJ
	B0	31.6	580	0.66	200	300	300	0.05	197.6	0.59	BJ
	C0	31.6	580	0.70	200	300	300	0.05	204.3	0.61	BJ
[51]	C-1	19.5	585	0.72	200	200	300	0.06	108.6	0.61	J
	C-2	23.7	585	0.72	200	200	300	0.05	107.7	0.55	J
	T-C	24.6	585	0.72	200	200	300	0.05	124.9	0.63	J
[52]	ED1	31.1	349	3.0	342.9	381	508	0	596.4	0.82	BJ

bond resistance around the beam longitudinal bars in the joint region; (2) this more stable bond resistance produces a wider diagonal strut which can carry the larger horizontal joint shear force.

The joint shear strengths of the test specimens in the database are plotted in Fig. 4 against the subsequently derived joint shear index (S_j) which is dependent on the beam longitudinal reinforcement ratio and its strength. The joint shear index is derived based on global equilibrium, as discussed in Section 3.2. For clarity of the trend, the data of low ($0.89 \leq h_b/h_c \leq 1.33$) and high ($1.4 \leq h_b/h_c \leq 2.0$)

joint aspect ratios are separately plotted in Fig. 4. For the low joint aspect ratio, the joint shear strength increases with the increase of the joint shear index within an approximate range of 0.4–1.0 and beyond the value of 1.0, the joint shear strength does not increase as shown in Fig. 4(a). For the high joint aspect ratio, there are few experimental data to demonstrate the variation of the joint shear strength. Among these limited data points, the joint shear strengths for a specific aspect ratio of $h_b/h_c = 1.5$ are compared. The minimum joint shear strength for this aspect ratio is $0.35 \sqrt{f'_c} b_j h_c$ from

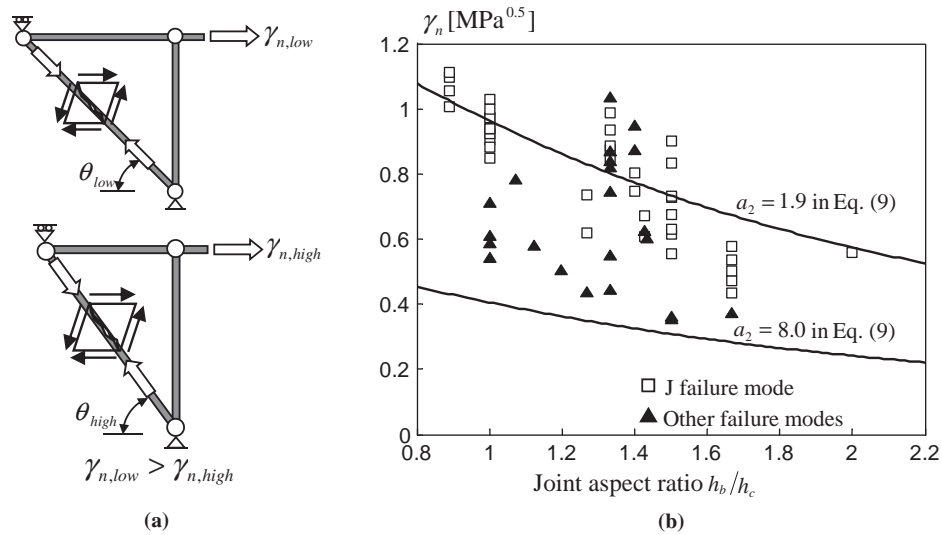


Fig. 3. Effect of the joint aspect ratio: (a) SAT idealizations for two joint aspect ratios, (b) Evaluation of the database against joint aspect ratio.

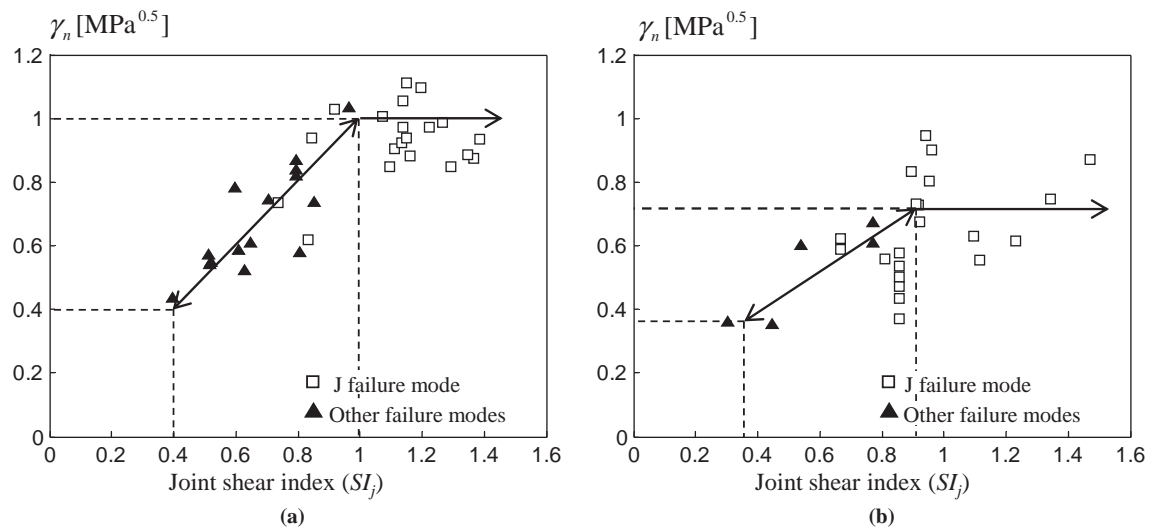


Fig. 4. Effect of the beam longitudinal reinforcement: (a) low joint aspect ratio, $0.89 \leq h_b/h_c \leq 1.33$, (b) high joint aspect ratio, $1.4 \leq h_b/h_c \leq 2.0$.

specimens A0 [23] and RCNH1 [24] whose beam longitudinal reinforcement yielded, whereas the maximum joint shear strength is $0.72\sqrt{f'_c}b_jh_c$ by averaging the shear strengths of specimens BS-L, BS-U, and BS-L-LS from [5] where beam longitudinal reinforcement did not yield. Using these findings, it is suggested that the variation of the joint shear strength for high aspect ratio ranges from 0.35 to 0.72 as plotted in Fig. 4(b). The four approximate values, 1.0, 0.72, 0.4 and 0.35 are also supported by the following: (1) the values of 1.0 and 0.72 are close to the upper bound of the joint shear strength for J failure having joint aspect ratio of 1.0 and 1.5, respectively, as shown in Fig. 3, and (2) the values of 0.4 and 0.35 are close to the minimum joint shear strength of unreinforced exterior joints suggested by Moehle et al. [25] and Hakuto et al. [26].

From the above analysis of the database with respect to the joint shear index, it is found that the joint shear strength is proportional to the joint shear index up to a certain limit and beyond this limit, the joint shear strength does not increase with the increase of the joint shear index.

2.4. Effect of column axial load

The effect of column axial load on the joint strength is not completely understood. Some researchers concluded that the joint shear strength is little influenced by the column axial load [27–29]. On the contrary, other researchers reported that the high axial load on column increased the joint shear strength in their tests [30–32]. In the case of weak column and strong beam design, increasing the column axial load up to the column cross-section balanced point improves the joint shear strength because the column moment capacity is improved by the high compressive axial load. In the case of strong column and weak beam design, which is the case of most tests in the database, high column axial load might give both beneficial and detrimental effects to the joint shear strength. The plot of the test results in the database shown in Fig. 5 also illustrates that the joint shear strength is not clearly affected by the column axial load up to $0.2f'_cA_g$ where $A_g = h_cb_c$ is the gross area of the column cross-section. More test data for high-

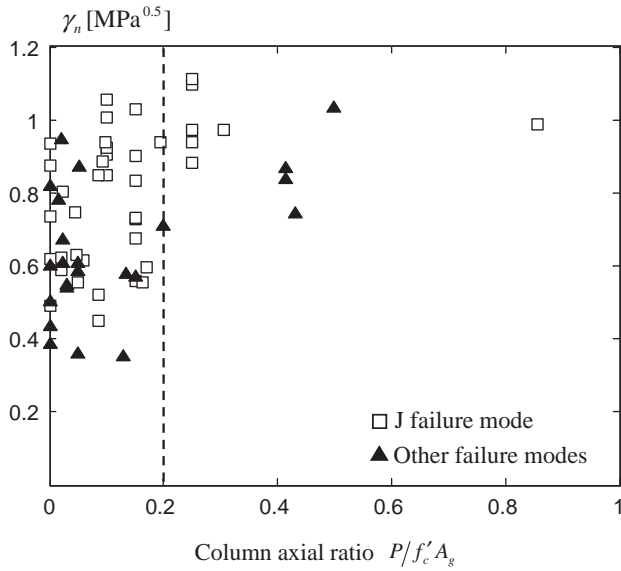


Fig. 5. Complex effect of the column axial load ratio.

er column axial load are needed to clarify the effect of column axial load on the joint shear strength.

The principal tensile strain in Eq. (1) derived by Pantazopoulou and Bonacci [29] has been used to explain the detrimental effect of the high column axial load.

$$\varepsilon_1 = \frac{\varepsilon_x - \varepsilon_y \tan^2 \beta}{1 - \tan^2 \beta} \quad (1)$$

where ε_x and ε_y are the average joint transverse (horizontal) and longitudinal (vertical) strains, respectively, and β is the angle of inclination (from the horizontal axis) of the principal tensile strain. Note that positive sign represents tensile strain in this study. Pantazopoulou and Bonacci [29] concluded that the principal tensile strain (ε_1) increases as the average compressive (negative) longitudinal strain (ε_y) increases due to the high compressive column axial load. This conclusion is based on the assumption that the principal tensile strain direction, i.e. the angle β , is fixed while the column axial load changes. However, the shear strain has to significantly increase in order to keep the principal tensile strain

direction fixed, Fig. 6(a), which is unrealistic based on the shear strain measurements from [31,32]. Eq. (2a) indicates that if the variation of shear strain (γ_{xy}) is small, the principal tensile strain slightly changes although the average compressive longitudinal strain (ε_y) may substantially increase to large negative value. This is more apparent if the average transverse strain (ε_x) is assumed to be zero, as shown in Eq. (2b), refer to Fig. 6(b).

$$\varepsilon_1 = \frac{\varepsilon_x + \varepsilon_y}{2} + \frac{1}{2} \sqrt{(\varepsilon_x - \varepsilon_y)^2 + \gamma_{xy}^2} \quad (2a)$$

$$\text{If } \varepsilon_x = 0 \Rightarrow \varepsilon_1 = \frac{\varepsilon_y}{2} + \frac{1}{2} \sqrt{\varepsilon_y^2 + \gamma_{xy}^2} \quad (2b)$$

Furthermore, if the column axial load is small, i.e. less than $0.2f'_c A_g$ as most of the previous joint tests, the average compressive longitudinal strain becomes negligible. Therefore, the principal tensile strain in the joint panel is close to half of the joint shear strain, i.e. $\varepsilon_1 \approx \gamma_{xy}/2$.

3. Derivation of the semi-empirical shear strength model

The joint aspect ratio and beam longitudinal reinforcement ratio are selected as key parameters to derive a shear strength equation. The effect of the column axial load parameter is not considered due to its unclear influence as discussed in the previous section.

3.1. Joint aspect ratio parameter

Assuming that a single diagonal strut resists the whole horizontal shear force in the joint panel, Fig. 7, the equilibrium equation is derived as follows,

$$V_{jh} = c_0 D \cos \theta, \quad \theta = \tan^{-1}(h_b/h_c) \text{ and } D = \sigma_d b_j h_s \quad (3)$$

where $c_0 \leq 1.0$ is a constant to be determined from the database, D is the compressive force in the diagonal strut, σ_d is concrete strength of the diagonal strut based on a softening concrete strength model, and h_s is the width of the diagonal strut at the C-C-T nodal zone, Fig. 7. To express the joint shear strength in terms of $\sqrt{f'_c}$, a practical softening concrete strength model proposed by Vollum and Newman [1] is adopted to develop a relevant model for the concrete panel of unreinforced joints, i.e.

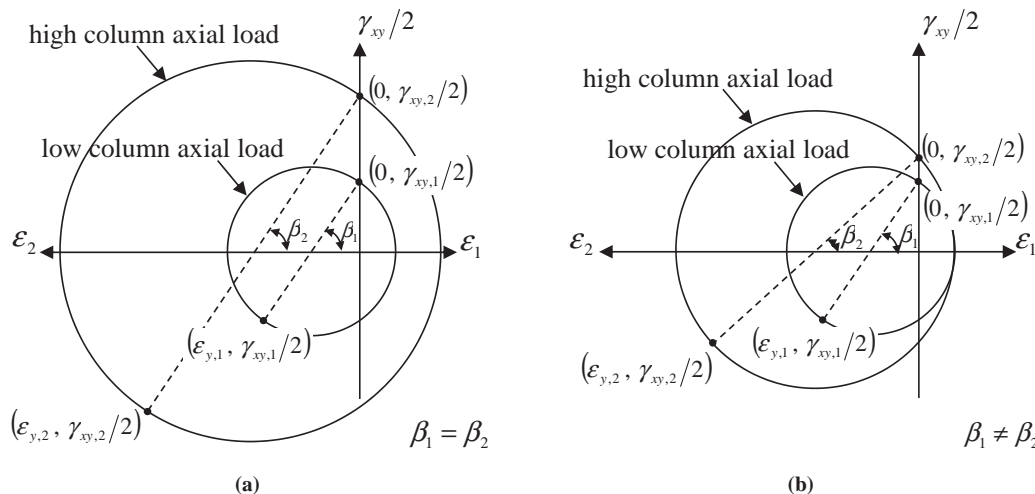


Fig. 6. Change of the principal tensile strain due to the column axial load ratio: (a) fixed principal directional angle, (b) varying principal directional angle. Note: ε_x is assumed to be zero because of negligible axial load in the beam.

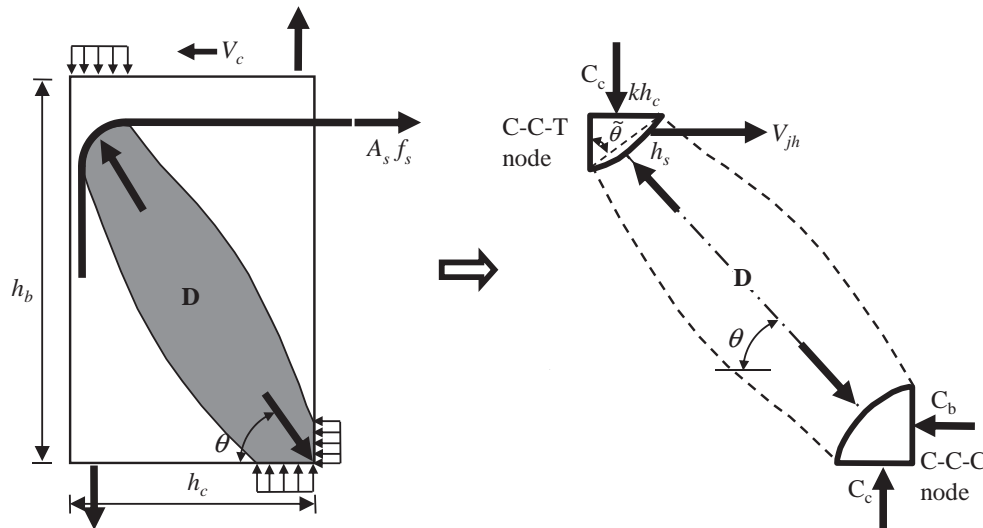


Fig. 7. Single strut mechanism.

Table 2
Comparison of softening concrete strength models.

f'_c (MPa)	$\varepsilon_1 = 0.0030$		$\varepsilon_1 = 0.0035$		$\varepsilon_1 = 0.0040$	
	σ_{Vollum}^a	σ_{Zhang}^b	σ_{Vollum}	σ_{Zhang}	σ_{Vollum}	σ_{Zhang}
20	20	20	19	19	18	18
30	25	24	23	23	22	22
40	29	28	27	27	25	26
50	32	31	30	30	28	29
60	35	34	33	33	31	32
70	38	37	36	35	33	34
80	40	39	38	38	36	37
90	43	42	40	40	38	39
100	45	44	42	42	40	41

^a Strain-softened concrete compressive strength using Vollum and Newman [1] (Eq. (4)).

^b Strain-softened concrete compressive strength using Zhang and Hsu [33] (Eq. (5)).

$$\sigma_d = \frac{a_1 \sqrt{f'_c}}{0.8 + 170\varepsilon_1} \quad (4)$$

where a_1 is an empirical constant with a value of 5.9 [MPa units]. Eq. (4) is compared to another widely used softening concrete strength model, Eq. (5), proposed by Zhang and Hsu [33] in Table 2. The comparison shows that the two models are almost identical within the range $0.003 \leq \varepsilon_1 \leq 0.004$ where the joint shear failure is expected as subsequently discussed.

$$\sigma_d = \frac{\tilde{a}_1 \sqrt{f'_c}}{\sqrt{1 + 250\varepsilon_1}} \quad (5)$$

where \tilde{a}_1 is an empirical constant with a value of 5.8 [MPa units].

In the existing analytical models [4,5], average strain compatibility equations in the joint are adopted to determine ε_1 , assuming that the principal tensile direction is simply orthogonal to the assumed diagonal strut. The average strain compatibility equations are generally valid for the membrane element having longitudinal and transverse reinforcement but may not be applicable to unreinforced joints in the same way because there is no longitudinal and transverse reinforcement in the joint region. For example, Hwang and Lee [4] used tensile yield strains of the beam and column longitudinal bars as the horizontal and vertical strains, respectively, of the unreinforced joint panel to calculate the principal tensile strain. However, the yield strains of the beam and column bars do not rep-

Table 3
Strength reduction factor for a C-C-T node.

References	η where $f_{c,node} = \eta f'_c$
(a) Collins and Mitchell [53]	0.75
(b) Schlaich and Schäfer [54]	0.68
(c) MacGregor [55]	$0.85\eta_1, \eta_1 = 0.55 + \eta_2/\sqrt{f'_c}$
(d) Jirsa et al. [56]	0.80
(e) ACI-318-08 Appendix A [9]	0.68
(f) AASHTO [57]	0.75
(g) CEB-FIP 1990 [58]	$0.60(1 - f'_c/\eta_3)^b$
(h) DD ENV 1992-1-1 [59]	0.70
(i) CAN A23.3M94 [60]	0.75
(j) NZS 3101:Part 2 [11]	0.55

^a $\eta_2 = 1.25$ for $\sqrt{f'_c}$ in MPa^{0.5}.

^b $\eta_3 = 250$ for $\sqrt{f'_c}$ in MPa.

resent the average horizontal and vertical strain of the unreinforced joint panel, especially if the reinforcement does not yield.

In this study, the principal tensile strain is approximated by the following two approaches instead of using the average strain compatibility equations. The first approach is to compare the strength reduction calculated using the softening concrete strength model, i.e. Eq. (4), to the strength reduction factors (Table 3) for a C-C-T node from literature and code provisions as shown in Fig. 8, where code safety factors are excluded in this comparison. The selection of the C-C-T node shown in Fig. 7 is supported by the following published experimental results: (1) the joint shear failure was initiated adjacent to the top node when the beam top reinforcement was in tension [34], and (2) the joint crack morphology implied that the crack opening was greatest at the C-C-T node which led to the reduction of the strength of the diagonal strut. The second approach is to calculate the principal tensile strain using the joint shear strains measured from Clyde et al. [31], Pantelides et al. [32], and Park and Mosalam [35] as presented in Table 4. From the results of these two approaches, the principal tensile strain at joint shear failure is approximated to be 0.0035 for joint aspect ratio of 1.0, which is close to the value of 0.003 proposed in Vollum [34]. In addition, the principal tensile strain is assumed to be slightly greater for a higher joint aspect ratio based on the joint shear strains measured in tests from [35], Table 4. For simplicity, the principal tensile strain is proposed to vary linearly from 0.0035 for $h_b/h_c = 1.0$ and 0.0040 for h_b/h_c , i.e.

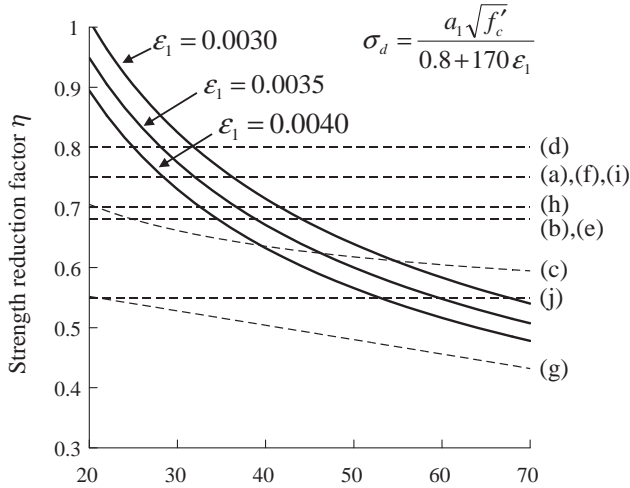


Fig. 8. Comparison of strength reduction factors at C-C-T node (refer to Table 3 for (a)–(j) designations).

Table 4
Measured joint shear strain and approximation of the principal tensile strain.

Specimen	h_b/h_c	$P/A_g f'_c$	Shear strain γ_{xy}	$\varepsilon_1 \approx \gamma_{xy}/2$
Clyde ^a -#2	0.89	0.10	7.18×10^{-3}	3.59×10^{-3}
Clyde ^a -#6	0.89	0.10	4.81×10^{-3}	2.41×10^{-3}
Clyde ^a -#4	0.89	0.20	8.45×10^{-3}	4.23×10^{-3}
Clyde ^a -#5	0.89	0.25	4.84×10^{-3}	2.42×10^{-3}
Pantelides ^b -#3	1.00	0.10	8.08×10^{-3}	4.04×10^{-3}
Pantelides ^b -#4	1.00	0.25	4.73×10^{-3}	2.37×10^{-3}
Pantelides ^b -#5	1.00	0.10	6.10×10^{-3}	3.05×10^{-3}
Pantelides ^b -#6	1.00	0.25	6.54×10^{-3}	3.27×10^{-3}
SP1-EW ^c	1.00	0.01	5.59×10^{-3}	2.80×10^{-3}
SP2-EW ^c	1.00	0.10	7.18×10^{-3}	3.59×10^{-3}
SP3-EW ^c	1.67	0.07	6.68×10^{-3}	3.34×10^{-3}
SP4-EW ^c	1.67	0.08	7.59×10^{-3}	3.80×10^{-3}
Mean				3.24×10^{-3}
Standard deviation				0.61×10^{-3}
COV				0.19

^a From Clyde et al. [31].

^b From Pantelides et al. [32].

^c From Park and Mosalam [35].

$$\varepsilon_1 = 0.0030 + 0.0005 (h_b/h_c) \quad (6)$$

The horizontal length of the C-C-T node, Fig. 7, is expressed using a constant k as follows,

$$h_s \sin \tilde{\theta} = kh_c \quad (7)$$

where $\tilde{\theta}$ is the angle of C-C-T node. Substituting Eqs. (4), (6), and (7) into Eq. (3) and changing horizontal shear force, V_{jh} , into the maximum, V_n , the equilibrium equation becomes

$$V_n = c_0 \left[\frac{a_1 b_j k h_c \sqrt{f'_c}}{(0.8 + 170\varepsilon_1) \sin \tilde{\theta}} \right] \cos \theta \quad (8)$$

Dividing both sides by $(b_j h_c \sqrt{f'_c})$, Eq. (8) becomes

$$\gamma_n = \frac{V_n}{b_j h_c \sqrt{f'_c}} = a_2 \frac{\cos \theta}{1.31 + 0.085(h_b/h_c)} \quad (9)$$

where $a_2 = c_0 a_1 k / \sin \tilde{\theta}$ is a constant determined in the following manner. For the upper bound of the shear strength of unreinforced joints, a_2 is selected as 1.9 [MPa units] so as to be bounded by the shear strength of transversely reinforced joints as suggested by Moehle et al. [25] for joint aspect ratio $h_b/h_c = 1.0$. This value is also

obtained by selecting the coefficients as follows: (1) the maximum value of $c_0 = 1.0$, (2) original value of a_1 , i.e. 5.9 [MPa units] according to Vollum and Newman [1], (3) $k = 0.325$ as the mean value of minimum, 0.25, and maximum, 0.4, values from Hwang and Lee [4] and Vollum [34], respectively, and (4) $\sin \tilde{\theta} = 1$ as assumed by Hwang and Lee [4]. For the lower bound of the shear strength of unreinforced joints, a_2 is selected as 0.8 [MPa units] based on the comparison with the experimental database as well as the recommendations by Moehle et al. [25] and Hakuto et al. [26]. The curves of Eq. (9) for the proposed two values of a_2 are plotted on the experimental database for $0.8 \leq h_b/h_c \leq 2.2$ in Fig. 3 where it is shown that Eq. (9) and the above two values of a_2 represent the upper and lower bounds of the joint shear strength from the database for different values of the joint aspect ratio with reasonable accuracy.

3.2. Beam longitudinal reinforcement ratio parameter

From Fig. 9, the global equilibrium equation is presented as follows,

$$M_b = V_b \times L = A_s f_s \times j d_b \quad (10)$$

$$V_c = \frac{L + h_c/2}{H} V_b \quad (11)$$

where V_b and V_c are the beam and column shear forces, respectively, L is the length from the beam inflection point to the column face, H is the height between upper and lower column inflection points, A_s and f_s are the area and stress of beam longitudinal reinforcement in tension, respectively, d_b is the effective depth of the beam, and $j d_b$ indicates the internal moment arm of the beam cross-section at the column face.

Accordingly, the horizontal shear force of the joint panel is calculated as follows,

$$V_{jh} = A_s f_s - V_c = A_s f_s \left(1 - \frac{L + h_c/2}{H} \frac{j d_b}{L} \right) \quad (12)$$

It is assumed that the beam longitudinal reinforcement ratio affects the joint shear strength for BJ failure only. This assumption is based on the previous observation that the joint shear strength for J failure does not increase with joint shear index beyond a certain limit, as presented in Fig. 4. Therefore, $f_s = f_y$ can be used

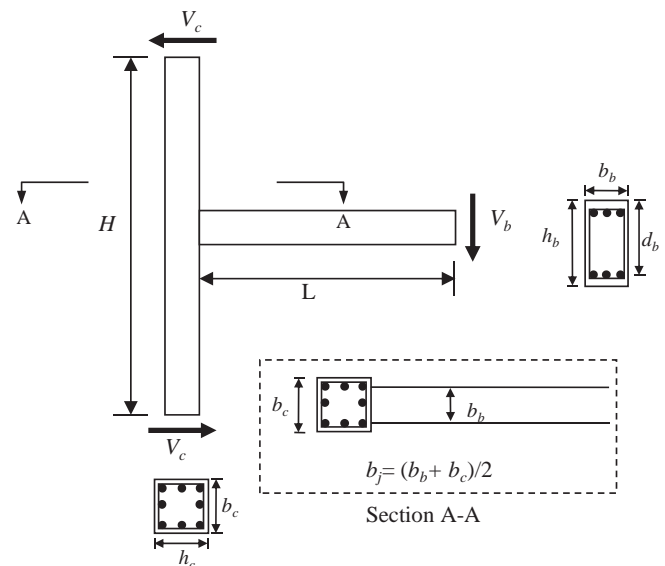


Fig. 9. Global equilibrium of an exterior beam-column joint.

in Eq. (12) assuming that the beam longitudinal reinforcement yields. Dividing Eq. (12) by $(b_j h_c \sqrt{f'_c})$, the following equation is obtained,

$$\frac{V_{jh}}{b_j h_c \sqrt{f'_c}} = \left(\frac{A_s f_y}{b_j h_c \sqrt{f'_c}} \right) \left(1 - \frac{L + h_c/2 j d_b}{H} \right) \quad (13)$$

In section analysis, an internal moment arm at yielding of beam longitudinal bars is generally close to 0.87 times the effective depth of beam cross-section, i.e. $j d_b = 0.87 d_b$, based on $j d_b = d_b - \kappa d_b/3$ where κ is estimated as 0.4 [36]. Then, the effective depth is conservatively approximated as 0.9 times the total height of the beam cross-section, i.e. $d_b = 0.9 h_b$, considering that cover depth is close to 10% of the total height in practical beam cross-section. Therefore, the internal moment arm is estimated as 0.8 times the total height, i.e. $j d_b = 0.8 h_b$. Accordingly, the following approximation can be made as

$$j d_b = 0.8 h_b \Rightarrow \frac{L + h_c/2 j d_b}{H} = \frac{L + h_c/2 \cdot 0.8 h_b}{H} \approx 0.85 \frac{h_b}{H} \quad (14)$$

Finally, Eq. (13) can be simplified as follows,

$$\frac{V_{jh}}{b_j h_c \sqrt{f'_c}} \approx \left(\frac{A_s f_y}{b_j h_c \sqrt{f'_c}} \right) \left(1 - 0.85 \frac{h_b}{H} \right) = S I_j \quad (15)$$

where the non-dimensional parameter $S I_j$ is previously referred to as the joint shear index and represents the joint shear demand at the onset of beam longitudinal reinforcement yielding.

3.3. Semi-empirical shear strength model

To develop a semi-empirical model, two basic concepts are assumed as follows: (1) the upper and lower bounds of the joint shear strength are affected by the joint aspect ratio only, and (2) between the upper and lower bounds of the joint shear strength for a certain joint aspect ratio, the joint shear strength is proportional to the joint shear index. Regarding the first assumption, the upper and lower bounds of the joint shear strength dependency on the joint aspect ratio is justified by the SAT idealization and the trends of the experimental database as shown in Fig. 3. The second assumption is based on the observations from the

low joint aspect ratio data, Fig. 4(a). For the case of high joint aspect ratio, the same assumption is also made based on the previous discussion related to Fig. 4(b).

In the proposed semi-empirical model, the upper and lower bounds of the joint shear strength are determined by Eq. (9). When the joint shear index is between the upper and lower bounds, the joint shear strength is determined as the joint shear index multiplied by an over-strength factor, $\Phi \geq 1.0$, to consider the increase of beam reinforcement tensile stress due to strain hardening after beam reinforcement yielding. The over-strength factor is larger for smaller joint shear index because larger plastic strain is expected. For simplicity, Φ is assumed to be 1.25, i.e. $f_s = 1.25 f_y$, at the lower bound of the joint shear strength and decreases linearly to $\Phi = 1.0$, i.e. $f_s = f_y$ at the upper bound of the joint shear strength, Fig. 10. It is to be noted that the over-strength factor 1.25 is selected from [37]. Finally, a shear strength equation is proposed in [MPa units] as follows:

$$\gamma_n = \frac{V_n}{b_j h_c \sqrt{f'_c}} = \Phi \left[\left(\frac{A_s f_y}{b_j h_c \sqrt{f'_c}} \right) \left(1 - 0.85 \frac{h_b}{H} \right) \right] \quad (16a)$$

$$0.8 \frac{\cos \theta}{1.31 + 0.085(h_b/h_c)} \leq \frac{V_n}{b_j h_c \sqrt{f'_c}} \leq 1.9 \frac{\cos \theta}{1.31 + 0.085(h_b/h_c)} \quad (16b)$$

The procedure to predict the joint shear strength by the proposed model is summarized as follows:

- (1) Input the joint geometry, concrete strength, and joint aspect ratio.
- (2) Determine X_1 at the lower bound, Y_{\min} , and X_2 at the upper bound, Y_{\max} , as shown in Fig. 10.
- (3) Calculate the joint shear index ($S I_j$) using Eq. (15).
- (4) If $X_1 \leq S I_j \leq X_2$, calculated the over-strength factor, Φ , by interpolation as shown in Fig. 10.
- (5) Calculate the joint shear strength by Eq. (16).

4. Evaluation of the proposed shear strength model

For verification of the proposed shear strength model, the shear strengths of the test specimens in the database are predicted. The predictions show good agreement with the experimental data with a mean value of 0.95 for the ratio of the test results to the model

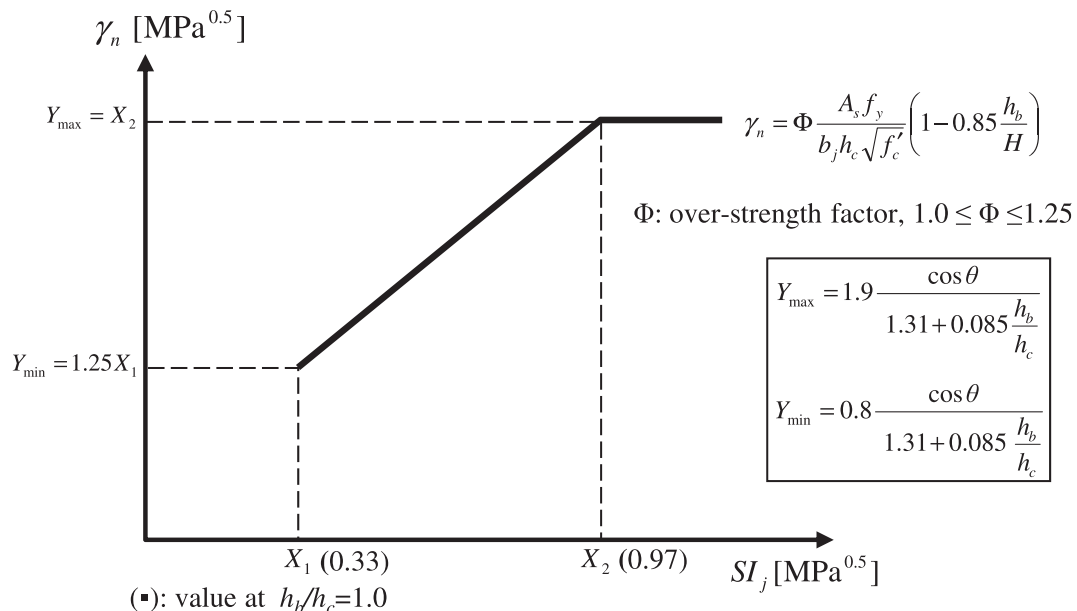


Fig. 10. Illustration of the proposed semi-empirical model.

predictions and a corresponding coefficient of variation (COV) of 0.16, Fig. 11(a). Excluding the six tests by Parker and Bullman [21] whose results are questionable due to low joint shear strength as discussed in Vollum [34], the accuracy of the proposed model is improved to a mean value of 0.97.

The proposed model predictions are compared with those from existing five strength models proposed by Vollum and Newman [1], Bakir and Bodurođlu [2], Hegger et al. [3], Hwang and Lee [4], and Tsonos [6]. These five models have been validated using exterior joint tests collected in each of these studies. This study uses the same tests if the specimens were not transversely reinforced in the joint region. However, it is noted that the majority of the past test specimens collected in each of these studies [1–4,6] corresponded to joints with small amount of transverse reinforcement which are not of interest in this study. Detailed review

of these five models is presented in [7]. Except the model by Hwang and Lee [4] which requires an iterative procedure, the joint shear strength calculations of these models are as follows:

Vollum and Newman [1]:

$$V_n = 0.642\zeta[1 + 0.552(2 - h_b/h_c)]b_j h_c \sqrt{f'_c} \quad (17a)$$

Bakir and Bodurođlu [2]

$$V_n = \frac{0.71\zeta(100\rho_b)^{0.4289}}{(h_b/h_c)^{0.61}} b_j h_c \sqrt{f'_c} \quad (17b)$$

Hegger et al. [3]:

$$V_n = 2\zeta(1.2 - 0.3h_b/h_c) \left(1.0 + \frac{\rho_c - 0.5}{7.5}\right) b_j h_c \sqrt[3]{f'_c} \quad (17c)$$

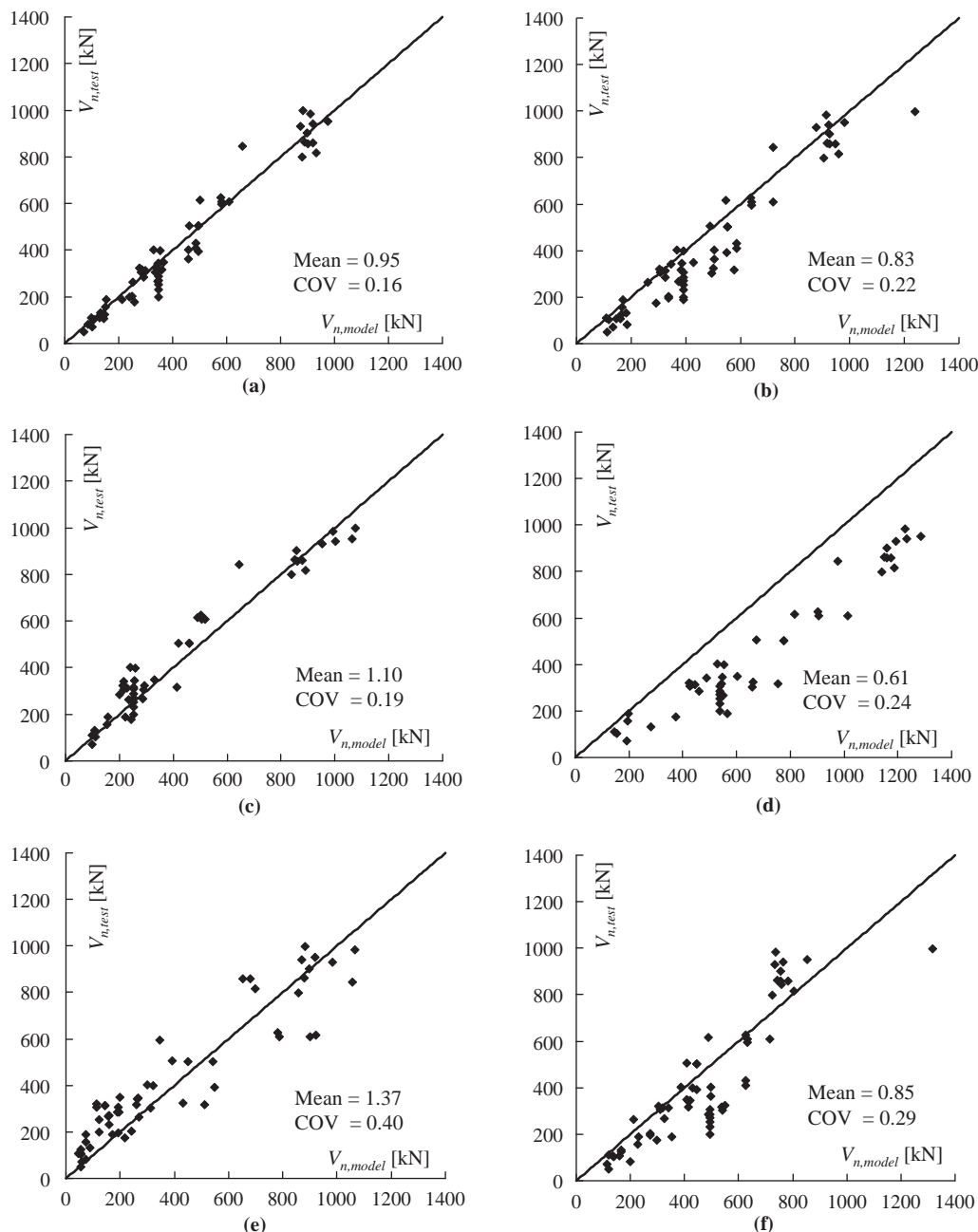


Fig. 11. Comparison of evaluation results: (a) proposed model, (b) Vollum and Newman model [1], (c) Bakir and Bodurođlu model [2], (d) Hegger et al. model [3], (e) Hwang and Lee model [4], and (f) Tsonos model [6]. Note: Mean and COV=Coefficient of Variation for $V_{n, test}/V_{n, model}$

Tsonos [6]:

$$\left[\frac{\gamma_n (h_b/h_c)}{2\sqrt{f'_c}} \left(1 + \sqrt{1 + \frac{4}{(h_b/h_c)^2}} \right) \right]^5 + \frac{5\gamma_n (h_b/h_c)}{\sqrt{f'_c}} \left(\sqrt{1 + \frac{4}{(h_b/h_c)^2}} - 1 \right) = 1 \quad (17d)$$

where ζ represents the effect of anchorage detail: for Type A and Type C in Fig. 2, $\zeta = 1.0$ and 0.9 , respectively, in Vollum and Newman [1], $\zeta = 1.0$ and 0.85 , respectively, in Bakir and Boduroğlu [2], $\zeta = 0.95$ and 0.85 , respectively, in Hegger et al. [3], and ρ_b and ρ_c represent the longitudinal reinforcement ratio of the beam and the column, respectively.

Vollum and Newman model [1] includes the detrimental effect of the joint aspect ratio in Eq. (17a) but this model does not consider the variation of the joint shear strength with the joint shear index. Therefore, this model overestimates the joint shear strength for specimens with BJ failure, while accurate predictions are obtained for specimens with J failure, which are negligibly affected by the joint shear index. The evaluation results using this model are shown in Fig. 11(b).

Bakir and Boduroğlu model [2] includes the parameters of beam longitudinal reinforcement ratio and joint aspect ratio in Eq. (17b). The evaluation results (Fig. 11(c)) show good correlation with test data due to the inclusion of these two parameters. However, this model has the defect that the effect of beam reinforcement ratio is included by the exponential term with the exponent 0.4289, which is determined by a statistical regression analysis using only three beam reinforcement ratios from the collected test data with large scatter.

Hegger et al. [3] developed an empirical model including the parameters of column reinforcement ratio and joint aspect ratio in Eq. (17c). The evaluation results (Fig. 11(d)) show consistent overestimation of the joint shear strength. This overestimation is attributed to the column reinforcement ratio parameter derived by best fitting of test data with large scatter from reinforced exterior joints. Based on this observed overestimation of the model, the column reinforcement ratio may not be an influencing parameter in predicting the shear strength of unreinforced joints.

Hwang and Lee [4] developed an analytical joint shear strength model for transversely reinforced joints based on SAT idealization. In this model, the joint shear strength is determined by an iterative procedure to solve the equations of equilibrium, compatibility, and softened constitutive law of concrete for the diagonal strut. Hwang and Lee [4] insisted that their model is applicable to predict the shear strength of unreinforced joints, but this application is inappropriate because of the following reasons: (1) the average strain compatibility equations are not applicable to unreinforced joints as previously discussed, (2) intermediate column bars do not function as tension ties because steep inclination angles of the struts are not feasible, (3) only beneficial effect of column axial load on the joint shear strength is included where the width of the diagonal strut is increased as follows $h_s = (0.25 + 0.85P/f'_c A_g)h_c$, and (4) this model highly depends on the estimate of the diagonal strut width [38]. The evaluation results using this model are shown in Fig. 11(e).

Tsonos [6] proposed a new formulation to predict the shear strength of joints based on the SAT mechanism. The main difference between this model and other SAT models is assuming biaxial concrete strength equation as a fifth-degree polynomial and using it with average horizontal and vertical stresses in the joint. This model overestimates the unreinforced joint shear strength and this overestimation results from use of overly simplified average stress equilibrium equation and the increase of the joint shear strength with increasing joint aspect ratio, which is opposite to the trend observed from database. This model was originally developed for transversely reinforced joints. Therefore, this model is inappropriate

for predicting the shear strength of unreinforced joints. The evaluation results using this model are shown in Fig. 11(f).

From the above validation, the proposed semi-empirical model is shown to be more accurate compared to the existing models. It is worth mentioning that the proposed model shows this better accuracy for concrete strength in the range 25–70 MPa in which the proposed model is therefore recommended. This model can be easily implemented in many existing nonlinear structural analysis programs to evaluate the seismic response of non-ductile RC frames having unreinforced joints.

5. Conclusions

From the extensive database of unreinforced exterior beam-column joint tests, parametric studies are performed and influencing parameters are determined. The parametric equations to reflect the effect of these parameters are derived using a mechanistic approach and a shear strength model is developed for unreinforced exterior joints. The main conclusions from this study are as follows:

- (1) The test data from literature show that the shear strength of unreinforced exterior joints reduces with increase of the joint aspect ratio, i.e. the ratio of the beam to column cross-section heights. This negative effect of the joint aspect ratio can be explained by the strut-and-tie idealization where a steeper diagonal strut is developed in high joint aspect ratio, which is therefore less effective to equilibrate the horizontal joint shear force.
- (2) The upper and lower bounds of the shear strength of unreinforced exterior joints are determined by the joint aspect ratio. Between these upper and lower bounds for a specific joint aspect ratio, the shear strength of unreinforced exterior joints is proportional to the joint shear index, which is dependent on the beam longitudinal tension reinforcement ratio and its strength.
- (3) The shear strength of unreinforced exterior joints is not systematically affected by the compressive column axial load ($P \leq 0.2f'_c A_g$) under which most of the previous tests were conducted. Therefore, it is postulated that column axial load is not an influencing parameter for characterizing the shear strength of unreinforced exterior beam-column joints.
- (4) Two terms are derived as $\frac{\cos \theta}{1.31+0.085(h_b/h_c)}$ and $\frac{A_s f_y}{b_j h_c \sqrt{f'_c}} \left(1 - 0.85 \frac{h_b}{H} \right)$ to reflect the effect of the joint aspect ratio and the beam longitudinal reinforcement ratio, respectively, on the shear strength of unreinforced exterior beam-column joints. Using these two terms, a semi-empirical equation is proposed to predict the shear strength of unreinforced exterior joints. The proposed model predicts the shear strength of many test specimens from the literature with high accuracy compared to several existing models.

Acknowledgments

This study was supported by the NSF award #0618804 (J.P. Moehle, PI) through PEER, University of California, Berkeley. NSF financial support is gratefully acknowledged. Opinions, findings or recommendations expressed in this paper are those of the authors and do not necessarily reflect those of the NSF.

Appendix A. Numerical example

It is assumed that an unreinforced exterior beam-column joint is given the following properties:

$f'_c = 40$ MPa, $f_y = 415$ MPa, $A_s = 1548.4$ mm² (4-D22), $h_b = 450$ mm, $b_b = 400$ mm, $h_c = 450$ mm, $b_c = 450$ mm, $H = 3000$ mm, and $L = 2400$ mm.

The shear strength of the given exterior joint can be predicted by the proposed semi-empirical model following these steps:

(1) Calculate joint geometry and joint aspect ratio:

$$B_j = (400 + 450)/2 = 425 \text{ mm}, h_b/h_c = 1.0 \Rightarrow \theta = 45^\circ.$$

(2) Determine X_1 and X_2 from Y_{\min} and Y_{\max} :

$$Y_{\min} = 0.8 \frac{\cos \theta}{1.31 + 0.085 \left(\frac{h_b}{h_c}\right)} = 0.41 \Rightarrow X_1 = 0.41/1.25 = 0.33$$

$$Y_{\max} = 1.9 \frac{\cos \theta}{1.31 + 0.085 \left(\frac{h_b}{h_c}\right)} = 0.97 \Rightarrow X_2 = 0.97$$

(3) Calculate the joint shear index:

$$\frac{A_s f_y}{b_j h_c \sqrt{f'_c}} \left(1 - 0.85 \frac{h_b}{H}\right) = 0.46$$

(4) Check if the joint shear index is between X_1 and X_2 . If so, calculate the over-strength factor by linear interpolation from 1.25 to 1.00:

$$X_1 < \frac{A_s f_y}{b_j h_c \sqrt{f'_c}} \left(1 - 0.85 \frac{h_b}{H}\right) < X_2 \Rightarrow \Phi$$

$$= 1.00 + (1.25 - 1.00) \times \frac{0.97 - 0.46}{0.97 - 0.33} = 1.20$$

(5) Determine the shear strength, γ_n :

$$\gamma_n = \frac{V_{jh}}{b_j h_c \sqrt{f'_c}} = \Phi \frac{A_s f_y}{b_j h_c \sqrt{f'_c}} \left(1 - 0.85 \frac{h_b}{H}\right) = 1.20 \times 0.46 = 0.55$$

References

- [1] Vollum RL, Newman JB. Strut and tie models for analysis/design of external beam-column joints. *Mag Concr Res* 1999;51(6):415–25.
- [2] Bakir PG, Boduroglu HM. A new design equation for predicting the joint shear strength of monotonically loaded exterior beam-column joints. *Eng Struct* 2002;24(8):1105–17.
- [3] Hegger J, Sherif A, Roeser W. Nonseismic design of beam-column joints. *ACI Struct J* 2003;100(5):654–64.
- [4] Hwang SJ, Lee HJ. Analytical model for predicting shear strength of exterior reinforced concrete beam-column joints for seismic resistance. *ACI Struct J* 1999;96(5):846–58.
- [5] Wong HF. Shear strength and seismic performance of non-seismically designed reinforced concrete beam-column joints. PhD thesis. Hong Kong University of Science and Technology; 2005.
- [6] Tsonos AG. Cyclic load behavior of reinforced concrete beam-column subassemblages of modern structures. *ACI Struct J* 2007;104(4):468–78.
- [7] Park S, Mosalam KM. Shear strength models of exterior beam-column joints without transverse reinforcement. PEER report 2009/106. Berkeley: Pacific Earthquake Engineering Research Center. University of California; 2009.
- [8] Joint ACI-ASCE Committee 352. Recommendations for design of beam-column connections in monolithic reinforced concrete structures (ACI 352R-02). Farmington Hills, Michigan; 2002.
- [9] ACI 318M-08. Building code requirements for reinforced concrete. Detroit (Michigan): American Concrete Institute; 2008.
- [10] AIJ. Structural design guidelines for reinforced concrete buildings. Architectural Institute of Japan; 1994.
- [11] NZS 3101. Design of concrete structures, vols. 1 and 2. Wellington: Standards Association of New Zealand; 1995.
- [12] Sarsam KF, Phipps ME. The shear design of in situ reinforced beam-column joints subjected to monotonic loading. *Mag Concr Res* 1985;37(130):16–28.
- [13] Ohwada Y. A study on effect of lateral beams on reinforced concrete beam-column joints. In: Conference of AIJ; 1977.
- [14] Zhang L, Jirsa JO. A study of shear behavior of reinforced concrete beam-column joints. PMFSEL Report No. 82-1. University of Texas at Austin; 1982.
- [15] Kim J, LaFave JM. Key influence parameters for the joint shear behavior of reinforced concrete (RC) beam-column connections. *Eng Struct* 2007;29(10):2523–39.
- [16] Wong HF, Kuang JS. Effects of beam-column depth ratio on joint seismic behavior. *Struct Build* 2008;161(SB2):91–101.
- [17] Walker SG. Seismic performance of existing reinforced concrete beam-column joints. MSCE thesis. University of Washington; 2001.
- [18] Alire DA. Seismic evaluation of existing unconfined reinforced concrete beam-column joints. MSCE thesis. University of Washington; 2002.
- [19] Anderson M, Lehman D, Stanton J. A cyclic shear stress-strain model for joints without transverse reinforcement. *Eng Struct* 2008;30(4):941–54.
- [20] Scott RH. The effects of detailing on RC beam column connection behavior. *Struct Eng* 1992;70(18):318–24.
- [21] Parker DE, Bullman PJM. Shear strength within reinforced concrete beam-column joints. *Struct Eng* 1997;75(4):53–7.
- [22] Scott RH, Hamil SJ. Connection zone strain in the reinforced concrete beam column connections. In: Proceedings of the 11th international conference on experimental mechanics. Oxford, UK; 1998. p. 65–9.
- [23] Karayannis CG, Chalioris CE, Sirkelis GM. Local retrofit of exterior RC beam-column joints using thin RC jackets – an experimental study. *Earthquake Eng Struct Dyn* 2007;37:727–46.
- [24] Gencoglu M, Eren I. An experimental study on the effect of steel fiber reinforced concrete on the behavior of the exterior beam-column joints subjected to reversal cyclic loading. *Turk J Eng Environ Sci* 2002;26:493–502.
- [25] Moehle JP, Lehman D, Lowes L. Beam-column connections. New information on the seismic performance of existing buildings, EERI Technical Seminar; 2006.
- [26] Hakuto S, Park R, Tanaka H. Seismic load tests on interior and exterior beam-column joints with substandard reinforcing details. *ACI Struct J* 2000;97(1):11–25.
- [27] Meinheit DF, Jirsa JO. The shear strength of reinforced concrete beam-column joints. CESRL report no. 77-1. University of Texas at Austin; 1977.
- [28] Kurose Y, Guimaraes G, Liu Z, Kreger M, Jirsa JO. Study of reinforced concrete beam-column joints under uniaxial and biaxial loading. PMFSEL report no. 88-2. University of Texas at Austin; 1988.
- [29] Pantazopoulou S, Bonacci J. Consideration of questions about beam-column joints. *ACI Struct J* 1992;89(1):27–37.
- [30] Beres A, White RN, Gergely P. Seismic performance of interior and exterior beam-to-column joints related to lightly reinforced concrete frame buildings: detailed experimental results. Structural Engineering Report 92-7. Cornell University; 1992.
- [31] Clyde C, Pantelides CP, Reaveley LD. Performance-based evaluation of exterior reinforced concrete building joints for seismic excitation. PEER Report 2000/05. Berkeley: Pacific Earthquake Engineering Research Center. University of California; 2000.
- [32] Pantelides CP, Hansen J, Nadauld J, Reaveley LD. Assessment of reinforced concrete building exterior joints with substandard details. PEER Report 2002/18. Berkeley: Pacific Earthquake Engineering Research Center. University of California; 2002.
- [33] Zhang LX, Hsu TC. Behavior and analysis of 100 MPa concrete membrane elements. *J Struct Eng ASCE* 1998;124(1):24–34.
- [34] Vollum RL. Design and analysis of exterior beam column connections. PhD thesis. Imperial College of Science Technology and Medicine-University of London; 1998.
- [35] Park S, Mosalam KM. Analytical and experimental study on RC exterior beam-column joints without transverse reinforcement. In: 7th International conference on Urban earthquake engineering and 5th international conference on earthquake engineering, Tokyo, Japan; 2010. p. 803–11.
- [36] Hakuto S, Park R, Tanaka H. Effect of deterioration of bond of beam bars passing through interior beam-column joints on flexural strength and ductility. *ACI Struct J* 1999;96(5):858–64.
- [37] French, CW, Moehle, JP. Effect of floor slab on behavior of slab-beam-column connections. SP-123. Farmington Hills (MI): American Concrete Institute; 1991. p. 225–58.
- [38] Hwang SJ, Lee HJ. Strength prediction for discontinuity regions by softened strut-and-tie model. *J Struct Eng ASCE* 2002;128(12):1519–26.
- [39] Hanson NW, Conner HW. Seismic resistance of reinforced concrete beam-column joints. *J Struct Div ACSE* 1967;93(5):533–60.
- [40] Hanson NW, Conner HW. Tests of reinforced concrete beam-column joints under simulated seismic loading. Portland Cement Association Research and Development Bulletin; 1972.
- [41] Hwang SJ, Lee HJ, Liao TF, Wang KC, Tsai HH. Role of hoops on shear strength of reinforced concrete beam-column joints. *ACI Struct J* 2005;102(3):445–53.
- [42] Uzumeri SM. Strength and ductility of cast-in-place beam-column joints. SP-53. Farmington Hills (MI): American Concrete Institute; 1977. p. 293–350.
- [43] Ortiz IR. Strut-and-tie modeling of reinforce concrete short beams and beam-column joints. PhD thesis. University of Westminster; 1993.
- [44] Kanada K, Kondo G, Fujii S, Morita S. Relation between beam bar anchorage and shear resistance at exterior beam-column joints. *Trans Jpn Concr Inst* 1984;6:433–40.
- [45] Ghobarah A, Said A. Shear strengthening of beam-column joints. *Eng Struct* 2002;24(7):881–8.
- [46] Wilson ID. SIFCON joints in pre-cast concrete structures. In: Proceedings of the 8th BCA annual conference on higher education and the concrete industry. Southampton, UK; 1998. p. 227–39.
- [47] Woo SW. Seismic performance of RC frames in a low to moderate seismicity region. PhD thesis. Korea University; 2003.
- [48] Liu C. Seismic behavior of beam-column joint assemblies reinforced with steel fibers. MSCE thesis. University of Canterbury; 2006.
- [49] Engindeniz M, Kahn LF, Zureick AH. Performance of an RC corner beam-column joint severely damaged under bidirectional loading and rehabilitated

- with FRP composites. SP-258. Farmington Hills (MI): American Concrete Institute; 2008. p. 19–36.
- [50] El-Amoury T, Ghobarah A. Seismic rehabilitation of beam–column joints using GFRP sheets. *Eng Struct* 2002;24(11):1397–407.
- [51] Antonopoulos CP, Triantafillou TC. Experimental investigation of FRP-strengthened RC beam–column joints. *J Compos Constr ACSE* 2003;7(1):39–49.
- [52] Sagbas G. Nonlinear finite element analysis of beam–column subassemblies. Master of Applied Science thesis. University of Toronto; 2007.
- [53] Collins MP, Mitchell D. A rational approach to shear design – the 1984 Canadian code provisions. *ACI Struct J* 1986;83(6):925–33.
- [54] Schlaich J, Schäfer K. Design and detailing of structural concrete using strut-and-tie models. *Struct Eng* 1991;69(6):113–25.
- [55] MacGregor JG. Reinforced concrete mechanics and design. Englewood Cliffs, New Jersey: Prentice-Hall; 1997.
- [56] Jirsa JO, Breen JE, Bergmeister K, Barton D, Anderson R, Bouadi H. Experimental studies of nodes in strut-and-tie models. Report of the IABSE colloquium on structural concrete. Stuttgart, Germany; 1991. p. 525–32.
- [57] AASHTO. Standard specifications for highway bridges. American Association State and Highway Transportation Officials Washington, DC; 1996.
- [58] Comité Euro-International du Béton. Bulletin d'information No. 213/214 CEB-FIP Model Code 1990. London, UK: Thomas Telford; 1993.
- [59] Eurocode 2. Design of concrete structures, Part 1: general rules and rules for buildings (DD ENV 1992-1-1: 1992). Commission of the European Communities; 1992.
- [60] Canadian Standard Association. Design of concrete structures (CAN3-A23.3M94). Structural Design. Roxdale, Canada; 1994.

CTV Non-linear Time-History Analyses Report

Appendix D. Curriculum Vitae - Athol J. Carr

CURRICULUM VITAE

NAME: **ATHOL JAMES CARR**

PLACE OF BIRTH: Methven, New Zealand

ACADEMIC QUALIFICATIONS:

1. 1964 Bachelor of Engineering (Civil)(1st Class Honours) University of Canterbury. N.Z.
2. 1966 Master of Science in Engineering, University of California, Berkeley, U.S.A.
3. 1967 Doctor of Philosophy, University of California, Berkeley, U.S.A.

PROFESSIONAL QUALIFICATIONS:

1. Member, American Society of Civil Engineers
2. Fellow, Institution of Professional Engineers New Zealand
3. Life Member, New Zealand National Society for Earthquake Engineering

UNIVERSITY EXPERIENCE:

1. 1964–1966 Teaching Assistant, Department of Civil Engineering, Div. SESM, University of California, Berkeley, U.S.A.
2. 1968–1971 Lecturer, Department of Civil Engineering, University of Canterbury.
3. 1972–1986 Senior Lecturer, Department of Civil Engineering, University of Canterbury.
4. 1987–2006 Reader, Department of Civil Engineering, University of Canterbury.
5. 2007–2010 Professor, Department of Civil Engineering, University of Canterbury.
6. 2010- Professor Emeritus, Department of Civil and Natural Resources Engineering, University of Canterbury.
7. 1975 Visiting Professor, Institutt for Statikk, Norges Tekniske Høgskole, Universitet i Trondheim, Norge.
8. 1982 Visiting Professor, Institutt for Statikk, Norges Tekniske Høgskole, Universitet i Trondheim, Norge.
8. 1989 Visiting Professor, Institutt for Konstruksjonsteknikk, Norges Tekniske Høgskole, Universitet i Trondheim, Norge
9. 2001 Visiting Professor, Department of Structural Engineering, University of California, San Diego, La Jolla, California, USA.

10. 2001 Visiting Professor, Section of Structural Mechanics, Faculty of Civil Engineering and Geosciences, Technical University of Delft, Delft, The Netherlands.
11. 2001 Visiting Professor, Earthquake Engineering Research Centre, University of Iceland, Selfoss, Iceland.
12. 2005- Appointed Member of Faculty of the Rose School (Advanced Studies in Reduction of Seismic Risk) at the University of Pavia, Pavia, Italy
Teach a course on 'Non-linear dynamic analysis', 2005,2008,2011
13. 2009- Adjunct Professor, Earthquake Engineering Research Centre, University of Iceland.

AWARDS:

- 1964 "The Travelling Scholarship in Engineering"
- 1964 Fulbright Travel Award for study at the University of California
- 1966 University Fellowship, University of California, Berkeley
- 1983 Otto Glogau Award, presented by the New Zealand National Society for Earthquake Engineering (as a member of the Bridge Study Group)
- 1985 Otto Glogau Award, presented by the New Zealand National Society for Earthquake Engineering (with B. Wood and P. Boardman for Paper "Union House – A Cross Braced Structure with Base Isolation")
- 1985 Freyssinet Award, presented by IPENZ (with B. Wood and P. Boardman for Paper "Union House – A Cross Braced Structure with Base Isolation").
- 1995 Structural Award, presented by IPENZ for the paper "Dynamic Analysis of Structures" published in the Bull. N.Z.National Society for Earthquake Engineering. v27, no2, June 1994.
- 2004 Erskine Grant to visit the USA, Germany, Norway and Iceland to discuss developments in the teaching of structural dynamics and mechanics.
- 2005 Japanese Society for the Promotion of Science (JSPS) Fellowship to spend 8 weeks in Japan to collaborate with Japanese researchers in earthquake engineering. This Fellowship was taken in January-February 2007, mostly at University of Ryukus, Okinawa,.
- 2010 Awarded Life Membership of the New Zealand Society for Earthquake Engineering.

UNIVERSITY COMMITTEES:

1971–1973	School of Engineering Computer Centre Liaison Committee
1972–1974	Faculty of Engineering Timetable Committee
1973–1974	Computer Centre Liaison Officer, Department of Civil Engineering
1976–1981	Computer Centre Liaison Officer, Department of Civil Engineering
1983–1988	Computer Centre Liaison Officer, Department of Civil Engineering
1976–1977	Committee, Sixth Australasian Conference on the Mechanics of Structures and Materials (held at University of Canterbury, August 1977)
1978–1979	Faculty of Engineering Timetable Committee
1981	Chairman, Faculty of Engineering Subcommittee on Computer Aided Design
1983–1988	Chairman, Faculty of Engineering Subcommittee on Computer Aided Design
1983–1988	Chairman, Faculty of Engineering Computer Committee
1990-2005	Faculty of Engineering, Committee on Computer Aided Design, Deputy Chairman, 1997 – Chairman
1991-2000	Academic Board, Civil Engineering Department representative
1997-2005	Faculty of Engineering, Associate Dean (Computing)
1997–1998	Faculty of Engineering, Statutes and Prescriptions Committee representative
1999--2000	Member Information Technology Services Committee Chairman, Electronics and Telecommunications Sub-committee Chairman, Working Party on Network Reliability
2001-2005	Chair, Department of Civil Engineering, Research Committee.
2002-2003	Chair, University of Canterbury IT Committee
2003-2007	Chair, University of Canterbury IT Advisory Committee
2003-2009	Chair, College of Engineering IT Committee
2006	Acting Chair, Department of Civil Engineering Postgraduate Committee
2006-2007	Department of Civil Engineering Executive Committee

EXTENSION STUDIES SEMINARS:

The Finite Element Method in Structural Mechanics, University of California, Berkeley, March 20–24, 1967. *Refined Shell Analysis and Dynamic Response*.

Use of Digital Computer in Civil Engineering, University of Canterbury, July 8–12, 1969. *Communication with the Computer*, and *The Computer in Structural Engineering and Structural Mechanics*.

Matrix Methods in Engineering Analysis. University of Auckland, September 2–5, 1970. *Stress Analysis Problems*. Faculty member in charge of Seminar.

Analysis of Shells, University of Canterbury, May 21–23, 1969. *Finite Element Analysis of Shells*, and *Hanging Roofs*.

Engineering Seismology and Fundamentals of Seismic Design of Earth Structures. University of Canterbury, May 8–9, 1978. *Site Effects*.

Dynamics of Structures, University of Auckland (with I.G. Buckle and B.J. Davidson), Part I, 6 weekly lectures from 16 July, 1980; Part II, 21–23 August, 1980.

Fundamentals of Earthquake Engineering, University of Canterbury, 6 May 1993. *Linear Seismic Responses of Multi-storey Structures*, and *Nonlinear Seismic Response of Multi-storey Structures*.

Earthquake Engineering, Concepts and Structural Modelling, June 20–22, 2001, Technical University of Delft, Delft, The Netherlands.

SHORT COURSES given by Athol J. Carr

“Non-linear Seismic Analysis of Reinforced Concrete Buildings”. Five evening course given for ACHISINA Asociación Chilena de Sismología e Ingeniería Antisísmica, Santiago, Chile, 2–6 June 2008.

“Earthquake Engineering”. A Joint Five afternoon Course of Reykjavik University and University of Iceland. Reykjavik, Iceland, August 2009

PROFESSIONAL COMMITTEES:

- 1972–1975 University of Canterbury representative:
Long Span Bridges Research Coordinating Subcommittee of TC4 of the Road Research Unit of the National Roads Board.
- 1976–1977 University of Canterbury representative:
Bridge Dynamics Research Coordinating Subcommittee of TC4 of the Road Research Unit of the National Roads Board.
- 1976–1977 Member Organising Committee, 1977 Annual Conference of the New Zealand Institution of Engineers, February 1977 – Convener Registration Subcommittee.
- 1978–1980 Member, Discussion Group on Seismic Design of Bridges, The New Zealand National Society for Earthquake Engineering. On Subcommittee on Soil-Structure Interaction, Special Structures.
- 1978–1988 University of Canterbury representative:
Substructures Research Coordinating Subcommittee of TC4 of the Road Research Unit of the National Roads Board.
- 1986 Member, Discussion Group on Structures of Limited Ductility. The New Zealand National Society for Earthquake Engineering.
- 1991–1994 Member, Study Group on Dynamic Analysis. The New Zealand National Society for Earthquake Engineering.
- 1997 Standards New Zealand. Joint Earthquake Loading Standard, Sub-committee BD/6/4 Earthquake Loads.

INVITED LECTURES:

Earthquake Engineering. Address given to Norwegian Society for Earthquake Engineering, Oslo, 26 April 1989.

Earthquake Engineering in New Zealand. Lecture given, Division of Structural Mechanics, Luleå University of Technology, Sweden, 12 November 1989.

Three Decades of Earthquake Engineering Research at the University of Canterbury. Invited by The New Zealand Society for Earthquake Engineering to give an address at the 8th National Conference on Earthquake Engineering, held in San Francisco, 17-22 April 2006 to celebrate the 10th anniversary of the 1906 San Francisco earthquake.

KEYNOTE ADDRESSES:

Control of Deformation Under Seismic Excitation. *Fifth World Conf. Habitat and the High Rise*. Council on Tall Buildings and Urban Habitat, Amsterdam, 14–19 May 1995:

Structural Engineering in New Zealand – Trends in Practice and Recent and Current Research, *XXXIII Jornadas Sudamericanas di Ingenieria Estructural*, Santiago, Chile, 26-29 May 2008.

The Darfield and Christchurch Earthquakes. *International Symposium on Stron-motion Earthquake Effects, ISSEE2011*, University of Iceland, Reykjavik, Iceland. April 29, 2011.

PROFESSIONAL SEMINARS:

Seminar on Bridge Design and Research, *Elastic Soil-Structure Interaction* (with P.J. Moss). National Roads Board, Bridges and Structures, Wellington, October 3–4, 1974.

Civil Engineering – A Survey of New Developments. A joint seminar by NZIE and University of Canterbury Extension Studies, October 11–13, 1978. *Computers II – Structural Uses*.

Earthquake Engineering - Seminar presented at Det Norske Veritas, Høvik, Oslo, Norway, June 28–29, 1982.

Earthquake Engineering Seminar. (with Rajesh Dhakal) IPENZ one day course on earthquake engineering..

22nd August 2011: New Plymouth

23rd August 2011: Taupo

24th August 2011: Dunedin

29th August 2011: Auckland

30th August 2011: Wellington

31st August 2011: Christchurch

15th November 2011: Auckland

16th November 2011: Wellington

18th November 2011: Christchurch

ENGINEERING STRUCTURES:

In 1983 was invited to join the International Editorial Board for the new journal, *Engineering Structures*, published by IPC Science and Technology Press Ltd, Guildford, England. Resigned from Editorial Board 2000.

RESEARCH COUNCIL of NORWAY

Since 2004 I have been asked by the Research Council of Norway to review some of the applications from researchers in Norway for funding from the Research Council of Norway.

INTERNATIONAL CONFERENCE COMMITTEES:

- 1993 APVC '93 Asia Pacific Vibration Conference, Kitakyohu, Japan, Nov. 1993, International Steering Committee.
- 1996 XXV General Congress of European Seismological Commission, Reykjavik, Iceland, Sept. 9–14, 1996, International Steering Committee.
- 1997 APVC'97 Asia Pacific Vibration Conference, Kjongju, Korea, Nov. 1997, International Steering Committee.
- 1999 APVC '99 Asia Pacific Vibration Conference, Singapore, Nov. 1999, International Steering Committee.
- 1999 Civil and Environmental Engineering Conference New Frontiers and Challenges, Bangkok, Thailand, Nov. 1999, International Technical Committee.
- 2003 APVC '03 Asia Pacific Vibration Conference, Gold Coast, Australia, Nov. 2003, International Steering Committee.
- 2005 APVC '05 Asia Pacific Vibration Conference, Langkawi, Malaysia, Nov. 2005, International Steering Committee.
- 2007 APVC '07 Asia Pacific Vibration Conference, Sapporo, Japan, Aug. 2007, International Steering Committee.
- 2009 APVC'09 Asia Pacific Vibration Conference, Christchurch, New Zealand, Nov. 2007, Chairman, Conference Organizing Committee, International Steering Committee.

PROFESSIONAL EXPERIENCE:

- 1963–1964 Design engineer, Bill Lovell-Smith, Consulting Engineer, Christchurch.
- While a postgraduate student and since joining the University of Canterbury, I have carried out specialised computer consulting for:
- 1966–1967 State of California, Division of Water Resources, Analysis of pipe manifolds, Tehacaphi mountain pumping stations water project for Southern California (with Prof. R.W. Clough).
- 1966–1967 United States Steel Corporation. Analysis of ship hull vibration (with Prof. R.W. Clough)
- 1969 Edwards Clendon and Partners, Consulting Engineers, Wellington, to advise on choice of computer hardware and computational facilities for a proposed engineering computer bureau.
- 1969–1973 Engineers Computer Bureau, Wellington, structural analysis program development and modification, analysis of particularly difficult structures.
- 1969 A.E. Tyndall, Consulting Engineer, Christchurch. Analysis of frames for Timaru Hospital and multistorey hotel for Queenstown.
- 1970–1971 Marine Department. Analysis of a series of ferro-cement trawlers to facilitate a code of practice for the design of such vessels (with Dr J.C. Scrivener).
- 1971 Christchurch City Council, to set up traffic signal timing sequence design program on the University of Canterbury Computer.
- 1971 Holmes, Wood and Poole, Consulting Engineers, Christchurch, Shear wall finite element analysis for Queenstown hotel.
- 1972 Royds, Sutherland and McLeay, Consulting Engineers, Christchurch. Analysis of Waiiau Ferry Bridge to facilitate strengthening without changing its appearance.
- 1972 Hardie and Anderson, Consulting Engineers, Christchurch. Floor slab analyses for Lincoln College.
- 1974 Edwards, Clendon and Partners. Inelastic seismic analysis of the Maui A offshore platform. Verification of ductile response characteristics. (with P.J. Moss).
- 1974 Dunedin City Corporation. Cumberland Street Overpass box girder bridge analysis.
- 1974 Beca, Carter, Hollings and Ferner, Consulting Engineers, Auckland. Seismic behaviour of North Rangitikei and Kawhatu Railway viaduct sites (with P.J. Moss).

- 1976–1977 Shell, BP, Todd Oil Services, New Plymouth. Pressure vessel seismic analysis. This included devising a method of analysis, justifying it against conventional “code” analyses, and training their engineers in the use of the finite element method.
- This eventually resulted in their purchase of a license for the computer program from the University of Canterbury.
- 1976 Beca, Carter, Hollings and Ferner. Review of program capability and manuals for the large EAC/EASE2 finite element program and for the analysis of new NAC hangar (Christchurch) for seismic analysis and analysis of box girder over doors.
- 1976 National Roads Board. Analysis of box girder bridge.
- 1976 Hardie and Anderson. Analysis of stainless steel standard “container” tanks (with P.J. Moss)
- 1977 Halliday, O’Loughlin and Associates, Consulting Engineers, Christchurch. Analysis of multi-storey bank building for Christchurch.
- 1977 Wilkins and Davies. Review of seismic aspects of a feasibility study for a concrete offshore production platform (with D.G. Elms).
- 1978 Brickell, Moss, Rankine and Hill, Consulting Engineers, Wellington. Dynamic analysis of twin tower building Britannic House.
- 1978 Holmes, Wood, Poole and Johnstone, Consulting Engineers, Christchurch. Establishment of suite of computer programs for analysis of multistorey framed structures.
- 1978–1982 Central Otago Electric Power Board. Finite element analysis of two concrete arch dams for the Teviot River hydroelectric power scheme (with P.J. Moss)
- 1980 Beca, Carter, Hollings and Ferner. Floor slab analyses for ANZ tower building in Wellington, (with T. Paulay).
- 1980 Beca, Carter, Hollings and Ferner. Todd Motors Ltd. Hyperbolic-paraboloid umbrella shell roof analyses (with M.J.N. Priestley).
- 1980 N.Z. National Society for Earthquake Engineering. To comment on the International Electro-Technical Commission Draft Document for N.Z. comment, guide for equivalent testing procedures (50A (Secretariat) 17 September 1979).
- 1981–1983 Holmes, Wood, Poole and Johnstone. Analysis of Union House, base isolated building, Auckland.

- 1982 SINTEF, AVD 71, Trondheim, Norway. Spherical tank support for LNG tanks. Review for Kvaerne, Moss Rosenborr F. Selmer. Joint venture tender proposal, Statoil Project E002.
- 1983 Edward Clendon and Partners. Analysis of hyperbolic paraboloid cooling towers.
- 1983 Holmes, Wood, Poole and Johnstone. Seismic analysis of silo structures.
- 1984 Frame, Harvey and West, Consulting Engineers, Boroko, Papua New Guinea. Dynamic analysis of a multi-storey apartment house for Port Moresby.
- 1984 Canterbury Frozen Meat. Dynamic analyses of stacked meat carcass pallets to investigate rocking stability during possible seismic excitation.
- 1984 New Zealand Electricity Department. Dynamic testing of switchgear support systems (with P.J. Moss).
- 1985 ACADS Melbourne. Review of proposed recommendations for standards of engineering software using FORTRAN 77.
- 1986 Holmes, Wood, Poole and Johnstone. Dynamic testing, laundry floor, Sunnyside Hospital.
- 1988 Holmes Consulting. Dynamic analyses of multi-storey buildings.
- 1988–1990 KRTA, Consulting Engineers, Wellington. Dynamic analyses for proposed base-isolated multi-storey structure for Prince's Wharf, Auckland.
- 1991 Duffill, Watts and King, Consulting Engineers, Dunedin. Review of analyses and dynamic analyses of spillway structure for Roxborough Dam.
- 1994–1995 Beca Carter Hollings and Ferner. Expert advisor on the dynamic analyses for the *Sky-Tower*, Auckland.
- 2000 AC Power Group, Consulting Engineers, Wellington. Generation of suite of synthetic earthquake accelerograms for the analysis and design of electrical equipment.
- 2001 Nýverk, Consulting Engineers, Reykjavik, Iceland. With Ragnar Sigbjornsson of the University of Iceland. Advice on how to strengthen a 1970 lift-slab building to better resist earthquake excitation. The existing structure has poor quality welded connections between the slabs and precast wall panels and which were meant to provide resistance to lateral forces.

- 2010 Aurecon Ltd., Consulting Engineers, Wellington. Advice on problems in the earthquake analyses for a structure in the Hutt Valley that has to be fully operational in a 2500 return period earthquake. Under the strong horizontal shaking the base-isolated structure shows significant vertical floor accelerations as a consequence of a rocking motion on the isolation bearings and these accelerations are greater than those acceptable for the control systems in the structure.
- 2011 Royal Commission into the Christchurch Earthquakes - Asked to provide in-elastic response spectra for the 4th September 2010 Darfield earthquake and the 22nd February 2011 and 13th June 2011 earthquakes.
- 2011-2012 Dunning Thornton Consultants, Consulting Structural Engineers, Wellington, Victoria University of Wellington: Easterfield Seismic Retrofit Structural Engineering Peer Review. (With Greg MacRae)
- 2012 Royal Commission into the Christchurch Earthquakes - In-elastic analyses of the Hotel Grand Chancellor to investigate behavioural characteristics missed by the Expert panel and the Engineers reports on the building failure.
- 2012 Royal Commission into the Christchurch Earthquakes - In-elastic analyses of a six storey building with marked torsional responses.
- 2012 Royal Commission into the Christchurch Earthquakes - Expert witness to the Non-Linear Time-History Analyses (NLTHA) performed by consulting engineers for the Department of Building and Housing. To be presented to the Royal Commission hearings in June 2012.

Athol J. Carr

PUBLICATIONS:

1. Books (sole/joint author)

1. Bell, K., Carr, A.J. and Syvertsen, T. A. Handbook of Computer Programming, *SINTEF*, Trondheim, June 1983, ISBN 82-595-2874-6, 315p.
2. Carr, A.J. RUAUMOKO. Non-linear Dynamic Analysis of Framed Structures. *Department of Civil Engineering. University of Canterbury.* October 2004, 3 Volumes:
 Volume 1. Theory and User Guide to Associated Programs.173p.
 Volume 2. User Manual for 2-Dimensional version, Ruaumoko2D. 161p.
 Volume 3. User Manual for 3-Dimensional version, Ruaumoko3D. 1813p.

2. Articles/papers in refereed scholarly journals

1. Shepherd, R. *et al.* "The 1968 Inangahua Earthquake". *Bulletin of the Seismological Society of America*, v60 no5, October 1970: 1561–1605.
2. Moss, P.J. and Carr, A.J. "Aspects of the Analysis of Frame–panel Interaction". *Bulletin N.Z. Society Earthquake Engineering*, v4 no1, March 1971: 126–44
3. Carr, A.J. and Moss, P.J. "Elastic Soil Structure Interaction". *Bulletin of N.Z. Society Earthquake Engineering*, v4 no2, April 1971: 258–69.
4. Moss, P.J. and Carr, A.J. "The Use of Computers in Civil Engineering Education and Research". *N.Z. Engineering*, v27, Aug. 1972.
5. Sharpe, R.D. and Carr A.J. "The Seismic Response of Inelastic Structures". *Bulletin N.Z. Society for Earthquake Engineering*. v8 no3, September 1975: 192–203.
6. Carr, A.J. and Moss, P.J. "Maui Platform Analysis". *The Consulting Engineer*. London, August, 1976: 27–33.
7. Priestley, M.J.N., Crosbie, R.L. and Carr, A.J. "Seismic Forces in Base-Isolated Masonry Structures". *Bulletin of N.Z. National Society for Earthquake Engineering*. v10 no2, June 1977: 55–68.
8. Priestley, M.J.N., Evison, R.J. and Carr, A.J. "Seismic Response of Structures Free to Rock on Their Foundations". *Bulletin of the N.Z. National Society for Earthquake Engineering*, v11 no3, September 1978: 141–50.
9. Moss, P.J., Carr, A.J. and Cree-Brown, N.C. "Large Deflection Nonlinear Behaviour of Layered Timber Cylindrical Shells". *Proc. Struct. Div. ASCE*, October 1979: 2019–34.
10. Moss, P.J., Carr, A.J. and Cree-Brown, N.C. "Large Deflection Non-Linear Behaviour of Nailed Layered Timber Hyperbolic Paraboloid Shells". *Proc. I.C.E. Part 2*, v69, March 1980: 33–47.

11. Paulay, T., Carr, A.J. and Tompkins, D.N. "Response of Ductile Reinforced Concrete Frames Located in Zone C". *Bulletin of the N.Z. National Society for Earthquake Engineering*, v13 no3, Sept. 1980: 209–25.
12. Edmonds, F.D. *et al.* Seismic Design of Bridges – Section 4 – Bridge Foundations. *Bulletin of the N.Z. National Society for Earthquake Engineering*, v13 no3, Sept. 1980: 248–61.
13. Priestley, M.J.N., Stanford, P.R. and Carr, A.J. "Seismic Design of Bridges – Section 11 – Bridges Requiring Special Studies". *Bulletin of the N.Z. National Society for Earthquake Engineering*, v13 no4, Sept. 1980: 302–7.
14. Moss, P.J. and Carr, A.J. "The Effects of Large Displacements on the Earthquake Response of Tall Concrete Frame Structures". *Bulletin of the N.Z. Society for Earthquake Engineering*, v13 no4, Dec. 1980: 317–28.
15. Moss, P.J., Carr, A.J. and Cree-Brown, N.C. "The Influence of Planking Direction on the Behaviour of Nailed Layered Timber Hyperbolic Paraboloid Shells". *Bulletin of the International Association of Shell and Spatial Structures*, No. 75, April 1981: 19–34.
16. Moss, P.J., Carr, A.J. and Cree-Brown, N.C. "The Effects of Material Properties and Mesh Refinement on the Analysis of Timber Hyperbolic Shells". *Bulletin of the International Association of Shell and Spatial Structures*, No. 76, August 1981: 27-46.
17. Kivell, B.T. Moss, P.J. and Carr, A.J. "Hysteretic Modelling of Moment-Resisting Nailed Timber Joints". *Bulletin of the N.Z. National Society for Earthquake Engineering*, v14 no4, Dec. 1981: 233–43.
18. Kivell, B.T., Moss, P.J. and Carr, A.J. "The Cyclic Load Behaviour of Two Moment Resisting Nailed Timber Joints". *Trans. IPENZ*, v9, No. 2/CE, July 1982: 45–55.
19. Moss, P.J., Carr, A.J. and Pardoen G.C. "Vibrational Behaviour of Three Composite Beam-Slab Bridges". *Engineering Structures*, v4 no4, Oct. 1982: 277–88.
20. Boardman, P.R., Wood, B.J. and Carr, A.J. "Union House – A Cross Braced Structure with Base Isolation". *Bulletin N.Z. Nat. Soc. Earthquake Engineering*, v16 no2, June 1983: 83–97.
21. Moss, P.J., Carr, A.J. and Pardoen, G.C. "Inelastic Analysis of the Imperial County Services Building". *Bulletin N.Z. Nat. Soc. Earthquake Engineering*. v16 no2, June 1983: 141–55.
22. Goodsir, W.J., Paulay, T. and Carr, A.J. "A Study of the Inelastic Seismic Response of Reinforced Concrete Coupled Frame-Shear Wall Structures". *Bulletin. N.Z. Nat. Soc. Earthquake Engineering*, v16 no3, Sept. 1983: 185–200.
23. Pardoen, G.C., Moss, P.J. and Carr, A.J. "Elastic Analysis of the Imperial County Services Building". *Bulletin Seismological Soc. America*, v73 no6, Dec. 1983: 1903–16.
24. Van Luijk, C.J., Carr, A.J. and Carnaby, G.A. "Finite-Element Analysis of Yarns, Part I: Yarn Model and Energy Formulations". *J. Text. Inst.*, v75 no5, 1984: 342–53.
25. Van Luijk, C.J., Carr, A.J. and Carnaby, G.A. "Finite-Element Analysis of Yarns, Part II: Stress Analysis". *J. Text. Inst.*, v75 no5, 1984: 354–62.
26. Van Luijk, C.J., Carr, A.J. and Carnaby, G.A. "The Mechanics of Staple-Fibre Yarns, Part I: Modelling Assumptions". *J. Text. Inst.*, v76 no1, 1985: 11–18.

27. Van Luijk, C.J., Carr, A.J. and Carnaby, G.A. "The Mechanics of Staple-Fibre Yarns, Part II: Analysis and Results". *J. Text. Inst.*, v76 no1, 1985: 19–29.
28. Dean, J.A., Stewart, W.G. and Carr, A.J. "The Seismic Behaviour of Plywood Sheathed Walls". *Bulletin of the N.Z. National Society for Earthquake Engineering*, v19 no1, March 1986: 48–63.
29. Moss, P.J., Carr, A.J. and Buchanan, A.H. "Seismic Response of Low Rise Buildings". *Bulletin of the N.Z. National Society for Earthquake Engineering*, v19 no3, Sept. 1986: 180–99.
30. Moss, P.J., Carr, A.J., Cooke, N. and Tan, F.K. "The Influence of Bridge Geometry on the Seismic Behaviour of Bridges on Isolating Bearings". *Bulletin of the N.Z. National Society for Earthquake Engineering*, v19 no4, Dec. 1986: 255–62.
31. Cooke, N., Carr, A.J., Moss, P.J. and Tan, F.K. "The Influence of Non-Geometric Factors on the Seismic Behaviour of Bridges on Isolating Bearings". *Bulletin of the N.Z. National Society for Earthquake Engineering*, v19 no4, Dec. 1986: 263–71.
32. Turkington, D.H., Cooke, N., Moss, P.J. and Carr, A.J. "Development of a Design Procedure for Bridges on Lead-Rubber Bearings". *Jnl. of Engrg Struct.*, v11 no1, Jan. 1989: 2–8.
33. Bhimaraddi, A., Carr, A.J. and Moss, P.J. "A Shear Deformable Finite Element for the Analysis of General Shells of Revolution". *Comp. & Struct.*, v31 no3, 1989: 299–308.
34. Bhimaraddi, A., Carr, A.J. and Moss, P.J. "Generalised Finite Element Analysis of Laminated Curved Beams with Constant Curvature". *Comp. & Struct.*, v31 no3, 1989: 309–17.
35. Bhimaraddi, A., Moss, P.J. and Carr, A.J. "Out-of-Plane Vibrations of Thick Rings". *Thin-Walled Structures*, v8 no1, 1989: 73–79.
36. Bhimaraddi, A., Carr, A.J. and Moss, P.J. "Finite Elements Analysis of Laminated Shells of Revolution with Laminated Stiffeners". *Computers and Structures*, v33 no1, 1989: 295–305.
37. Bhimaraddi, A., Moss, P.J. and Carr, A.J. "Finite Elements Analysis of Orthogonally Stiffened Annular Sector Plates". *Proc. American Society of Civil Engineers, Jnl. of Engrg Mech.*, v115 no9, Sept. 1989: 2074–88.
38. Turkington, D.H., Carr, A.J., Cooke, N. and Moss, P.J. "Seismic Design of Bridges on Lead-Rubber Bearings". *Jnl. of Struct. Engrg, American Society of Civil Engineers*, v115 no12, Dec. 1989: 1000–16.
39. Turkington, D.H., Carr, A.J., Cooke, N. and Moss, P.J. "Design Method for Bridges on Lead-Rubber Bearings". *Jnl. of Struct. Engrg, American Society of Civil Engineers*, v115 no12, Dec. 1989: 3017–30.
40. Tjondro, J.A., Moss, P.J. and Carr, A.J. "{P-Delta Effects in Medium Height Moment Resisting Steel Frames Under Seismic Loading". *Bull. of the N.Z. Nat. Soc. for Earthq. Engrg*, v23 no4, Dec. 1990: 305–21.
41. Bhimaraddi, A., Moss, P.J. and Carr, A.J. "Free-Vibration Response of Column-Supported Ring Stiffened Cooling Tower". *J. Eng. Mech. ASCE.*, v117 no4, Apr. 1991: 770–88.

42. Andriono, T. and Carr, A.J. "Reduction and Distribution of Lateral Seismic Forces on Base Isolated Multistorey Structures". *Bull. of the New Zealand Nat. Soc. for Earthq. Engrg*, v24 no3, Sept. 1991: 225–37.
43. Andriono, T. and Carr, A.J. "A Simplified Earthquake Resistant Design Method for Base Isolated Multistorey Structures". *Bull. of the New Zealand Nat. Soc. for Earthq. Engrg*, v24 no3, Sept. 1991: 238–50.
44. Tjondro, J.A., Moss, P.J. and Carr, A.J. "Seismic P-Ä Effects in Medium Height Resisting Steel Frames". *Engineering Structures*, v14 no2, 1992: 75–90.
45. Wijanto, L.S., Moss, P.J. and Carr, A.J. "The Behaviour of Cross-Braced Steel Frames". *Earthq. Engrg & Struct. Dynamics*, v21, Apr. 1992: 319–40.
46. Djaja, R.G., Moss, P.J., Carr, A.J., Carnaby, G.A. and Lee, D.H. "Finite Element Modelling of An Oriented Assembly of Continuous Fibers". *Textile Research Journal*, v62 no8, Aug. 1992: 447–57.
47. Carr, A.J. and Moss, P.J. "Impact Between Buildings During Earthquakes". *Bull. N.Z. Nat. Soc. Earthq. Engrg*, v27 no2, June 1994: 107–13.
48. Carr, A.J. "Dynamic Analysis of Structures". *Bull. N.Z. Nat. Soc. Earthq. Engrg*, v27 no2, June 1994: 129–46.
49. Thomas, G.C., Buchanan, A.H., Carr, A.J., Fleischmann, C and Moss, P.J. "Light Timber-Framed Walls Exposed to Compartment Fires". *J. of Fire Protection Engrg*, v7 no1, 1995: 15–25.
50. Mori, A., Carr, A.J., Cooke, N. and Moss, P.J. "The Compression Behaviour of Bridge Bearings Used for Seismic Isolation". *J. Engineering Structures*, v18 no5, 1995: 351–62.
51. Zhao, J.X., Carr, A.J. and Moss, P.J. "Calculating the Dynamic Stiffness Matrix of 2-D Foundations by Discrete Wave Number Indirect Boundary Element Method". *Earthquake Engineering and Structural Dynamics*, v26 no1, 1997: 115–33.
52. Mori, A., Moss, P.J., Carr, A.J. and Cooke, N. "Behaviour of Laminated Elastomeric Bearings", *Structural Engineering and Mechanics*, v5 no4, 1997: 451–69.
53. Munro, W.A., Carnaby, G.A., Carr, A.J. and Moss, P.J. "Some Textile Applications of Finite-Element Analysis. Part I: Finite Elements for Aligned Fibre Assemblies". *The Journal of the Textile Institute*, v88 no4, 1997: 325–38.
54. Munro, W.A., Carnaby, G.A., Carr, A.J. and Moss, P.J. "Some Textile Applications of Finite-Element Analysis Part II: Finite Elements for Yarn Mechanics". *The Journal of the Textile Institute*, v88 no4, 1997: 339–51.
55. Mori, A., Moss, P.J. Carr, A.J. and Cooke, N. "Behaviour of Lead-Rubber Bearings". *Structural Engineering and Mechanics*, v6 no1, Jan. 1998: 1–15.
56. Mori, A., Moss, P.J., Cooke, N. and Carr, A.J. "The Behaviour of Bearings Used for Seismic Isolation Under Shear and Axial Load". *Earthquake Spectra*, v15 no2, May 1999: 199–224.
57. Mori, A., Moss, P.J., Cooke, N. and Carr, A.J. "The Behaviour of Bearings Used for Seismic Isolation Under Rotation and Axial Load". *Earthquake Spectra*, v15 no2, May 1999: 225–44.

58. Crisafulli, F.J., Carr, A.J. and Park, R. "Analytical Modelling of Infilled Frame Structures" *Bull. NZ Society for earthquake Engineering, Vol 33, No1, 2000, pp 30-47.*
59. Rodriguez, M.E., Restrepo, J.I. and Carr, A.J. "Earthquake Induced Horizontal Accelerations in Buildings". 22p. *J. Earthquake Engineering and Structural Dynamics.* v31, 2002: 693-718
60. Lee, B.K., Carr, A.J., Lee, T.E. and Ahn,D.S. "Elasticas and Buckling Loads of Shear Deformable Tapered Columns". *Int. J. Structural Stability and Dynamics.* v5, no3, September 2005: 317-35
61. Lee, Byoung Koo, Carr, Athol J., Lee, Tae Eun and Kim, Il Jung. "Buckling Loads of Columns with Constant Volume". *J. Sound and Vibration*, 294, (2006) 381-7.
62. Rodgers, GW, Mander, JB, Chase, JG, Mulligan, KJ, Deam, BL and Carr, AJ (2007). "Re-Shaping Hysteretic Behaviour - Spectral Analysis and Design Equations for Semi-Active Structures," *Earthquake Engineering & Structural Dynamics (EESD)*, online 2006, Vol 36(1), pp. 77-100, ISSN: 0098-8847.
63. Carey, MW, Chase, JG, Carr, AJ and Kowarz, MW (2004). "Dynamic analysis of bifurcating, non-linear thin film micro structures," *Engineering Structures*, Vol 26(12), pp. 1821-1831, ISSN: 0141-0296.
64. Schreiber,K.U., Velikoseltev,A., Carr,A.J. and Franco-Anaya,R.,(2009) "The Application of Fiber Optic Gyroscopes for the Measurement of Rotation in Structural Engineering". *Bulletin Seisomological Society of America*,. Vol 99, No.2B, Supplement.May 2009. pp1207-1213.
65. Mulligan, K.J., Chase, J.G., Mander, J.B., Rodgers, G.W., Elliot,R.B., Franco-Anaya, R. and Carr,A.J. "Experimental Validation of Semi-active Resettable Actuators in a 1/5th Scale Test", *Earthquake Engineering and Structural Dynamics*, Vol 38 No 4, 2009. pp 517-536
66. Toranzo, L., Restrepo, J.I., Mander, J.B. and Carr, A.J. "Shake-Table Tests of Confined-Masonry Rocking Walls with Supplementary Hysteretic Damping", *Journal of Earthquake Engineering*, Published Online on 21 July 2009,
67. Chey, MH, Chase, JG, Mander, JB and Carr, AJ (2010). "Semi-active tuned mass damper building systems: Application," *Earthquake Engineering & Structural Dynamics (EESD)*, Vol 39(1), pp. 69-89, ISSN: 0098-8847
68. Chey, MH, Chase, JG, Mander, JB and Carr, AJ (2010). "Semi-active tuned mass damper building systems: Design," *Earthquake Engineering & Structural Dynamics (EESD)*, Vol 39(2), pp. 119-139, ISSN: 0098-8847
69. Moghaddasi, M., Cubrinovski, M, Chase, J.G., Pampanin,S and, Carr, A. " Probabilistic evaluation of soil–foundation–structure interaction effects on seismic structural response". *Earthquake Engng Struct. Dyn.* (2010) Published online in Wiley InterScience (www.interscience.wiley.com). DOI: 10.1002/eqe.1011
70. Kam, W.Y., Pampanin, S., Palermo, A. and Carr, A. (2010) Self-centering structural systems with combination of hysteretic and viscous energy dissipations. *Earthquake Engineering & Structural Dynamics*, early view <http://dx.doi.org/10.1002/eqe.983>.

71. Cole, G., Dhakal, R.P., Carr, A. and Bull, D. (2011) "An Investigation of the Effects of Mass Distribution on Pounding Structures". *Earthquake Engineering and Structural Dynamics*, 40(6), 641-659 <http://onlinelibrary.wiley.com/doi/10.1002/eqe.1052/full>
72. Moghaddasi, M., Cubrinovski, M., Chase, G.J., Pampanin, S. and Carr, A. (2011) "Probabilistic evaluation of soil-foundation-structure interaction effects on seismic structural response" *Earthquake Engineering and Structural Dynamics*, 40(2), 135-154 <http://dx.doi.org/10.1002/eqe.1011>
73. Moghaddasi, M., Cubrinovski, M., Chase, J.G., Pampanin, S. and Carr, A. (2011) "Effects of soil-foundation-structure interaction on seismic structural response via robust Monte Carlo simulation. *Engineering Structures*, 33(4), 1338-1347. <http://dx.doi.org/10.1016/j.engstruct.2011.01.011>.
74. Peng, H.H.S., Dhakal, R.P., Fenwick, R.C., Carr, A. and Bull, D. (2011) "Elongation of plastic hinges in ductile RC members: Model development". *Advanced Concrete Technology*, 9(3), 315-326. <http://www.j-act.org/4-27.html>
75. Peng, H.H.S., Dhakal, R.P., Fenwick, R.C., Carr, A. and Bull, D. (2011) "Elongation of plastic hinges in ductile RC members: Model verification." *Advanced Concrete Technology*, 9(3), 327-338. <http://www.j-act.org/4-27.html>.
76. Smyrou, E., Priestley, M.J. and Carr, A.J. "Modelling of Elastic Damping in Non-linear Time-History Analyses of Cantilever R.C. Walls". *Bull. Earthquake Engineering*. Published on-line 31 May 2011.

3. Chapters in books and books edited

1. Paulay, T. and Carr, A.J. Chapter 26 — New Zealand, International Handbook of Earthquake Engineering, Ed. Mario Paz, Chapman & Hall, N.Y. 1994, 361–76 plus 997 line program on disk.

4. Papers published in refereed conference proceedings

1. Carr, A.J. and Clough, R.W. "Finite Element Analysis of Dynamic Shell Behaviour". *Proc. Engineering Mechanics Division A.S.C.E. Specialty Conference*, Raleigh, North Carolina, Nov. 1967.
2. Carr, A.J. and Clough R.W. "Dynamic Earthquake Behaviour of Shells". *Proc. 4th World Conference on Earthquake Engineering*, Santiago, Chile, Jan. 1969. v2,171–85.
3. Moss, P.J. and Carr, A.J. "The Application of a Finite Element Computer Program to the Analysis of General Three Dimensional Structures". *Proc. 3rd Australasian Conference on the Mechanics of Structures and Materials*, Auckland, Aug. 1971: A3.1–A3.23.
4. Scrivener, J.C. and Carr, A.J. "Ferro-Cement Boat Hulls Analysed by Finite Element Method". *Proc. Symposium on Design and Construction of Ferro-Cement Fishing Vessels*, FAO Wellington, Oct. 1972. 17p.
5. Carr, A.J. and Moss, P.J. "The Dynamic Behaviour of Structures as Influenced by Soil Structure Interaction". *Proc. 5th World Conference on Earthquake Engineering*, Rome, June 1973: 2058–60.

6. Sharpe, R.D. and Carr A.J. "A Stable Integration for Non-Linear Dynamic Analysis". *Proc. Texas Institute for Computational Mechanics International Conference on Computational Methods in Non-Linear Mechanics*, Austin, Texas, Sept. 1974: 777–86.
7. Sharpe, R.D. and Carr A.J. "The Inelastic Seismic Response of Bridge Structures". *Proc. International Symposium on Earthquake Engineering*, St. Louis, Aug. 1976: 91–105.
8. Moore, T.A. and Carr A.J. "Finite Element Analyses of Box and Plate Girder Bridges". *Proc. 1976 International Conf. on Finite Element Methods in Engineering*, Adelaide, December 1976: 5.1–5.15.
9. Moss, P.J. and Carr, A.J. "The Dynamic Soil-Structure Interaction on Bridge Sites". *Proc. International Symposium on Soil-Structures Interaction*. Roorkee, India, Jan. 1977: 145–49.
10. Moss, P.J. and Carr, A.J. "The Seismic Behaviour of River Valleys". *Proc. 6th World Conference on Earthquake Engineering*. New Delhi, India, Jan. 1977: 2274–79.
11. Moss, P.J. and Carr, A.J. "Inelastic Stability Analyses of Tubular Beam-Columns". *Proc. 6th Australasian Conference on the Mechanics of Structures and Materials*. Christchurch, Aug. 1977: 215–22.
12. Van Luijk, C.J., Carr, A.J., Carnaby, G.A. and Moss, P.J. "Finite Element Analysis of Wool Yarns". *Proc. 3rd International Conference in Australia on Finite Element Methods*, University of New South Wales, Sydney, July 1979: 787–802.
13. Carr, A.J. and Moss, P.J. "The Effects of Large Displacements on the Earthquake Response of Tall Structures". *Proc. 7th World Conference on Earthquake Engineering*. Istanbul, Turkey, September 1980, v5, 113–20.
14. Park, R. et al. "Progress Report of Earthquake Engineering Research at the University of Canterbury". *Proc. 7th World Conference on Earthquake Engineering*. Istanbul, Turkey, Sept. 1980, v9, 33–48.
15. Pardoen, G.C., Carr, A.J. and Moss, P.J. "Bridge Model Identification Problems". *Proc. 2nd ASCE/EMD Specialty Conference on Dynamic Response of Structures*. Atlanta, U.S.A., Jan. 1981.
16. Wilby, G.W., Park, R. and Carr, A.J. "Static and Dynamic Loading Tests on Two Small Three-Dimensional Reinforced Concrete Frames". *Dynamic Modelling of Concrete Structures*, SP.-73, American Concrete Institute, Detroit, 1982: 35–63.
17. Goodsir, W.J., Paulay, T. and Carr, A.J. "A Study of the Inelastic Seismic Response of Reinforced Concrete Coupled Frame-Shear Wall Structures". *Proc. 3rd South Pacific Regional Conference in Earthquake Engineering*, Wellington, May 1983: 227–48.
18. Moss, P.J., Carr, A.J. and Pardoen, G.C. "Inelastic Analysis of the Imperial County Services Building". *Proc. 3rd South Pacific Regional Conference in Earthquake Engineering*. Wellington, May 1983: 451–69.
19. Boardman, P.R., Wood, B.J. and Carr, A.J. "Union House – A Cross Braced Structure with Base Isolation". *Proc. 3rd South Pacific Regional Conference in Earthquake Engineering*, Wellington, May 1983: 525–44.
20. Moss, P.J., Carr, A.J. and Buchanan, A.H. "Seismic Design Loads for Low-Rise Buildings". *Proc.*

Pacific Structural Steel Conference, Auckland, 5–7 Aug. 1986: 149–65.

21. Tan F. K., Moss, P.J., Carr, A.J. and Cooke, N. "The Seismic Behaviour of Bridges on Isolating Bearings". *Proc. 10th Australasian Conference on the Mechanics of Structures and Materials*, Adelaide, 20–22 Aug. 1986: 617–22.
22. MacRae, G.A. and Carr, A.J. "Capacity Design of Steel Moment Resisting Frames". *Proceedings of the Pacific Conference on Earthquake Engineering*, Wairakei, New Zealand, 5–8 Aug. 1987, v2, 47–58.
23. Turkington, D.H., Carr, A.J., Cooke, N. and Moss, P.J. "Seismic Design of Bridges on Lead-Rubber Bearings". *Proc. Pacific Conf. on Earthq. Engrg*, Wairakei, N.Z., v2, Aug. 1987: 389–400.
24. Moss, P.J. and Carr, A.J. "Seismic Response of Low-Rise Timber Buildings". *Proc. Pacific Conf. on Earthq. Engrg*, Wairakei, N.Z. v2, Aug. 1987: 153–64.
25. Dean, J.A., Stewart, W.G. and Carr, A.J. "The Seismic Design of Sheathed Timber Frame Shear-Walls". *Proc. Pacific Conf. on Earthq. Engrg*, Wairakei, N.Z., Aug. 1987: 165–75.
26. Whittaker, D., Park, R. and Carr, A.J. "Experimental Tests on Hollow Circular Concrete Columns for Use in Offshore Concrete Platforms". *Proc. Pacific Conf. on Earthq. Engrg*, v1, Wairakei, N.Z., Aug. 1987: 213–24.
27. Andriono, T. and Carr, A.J. "Seismic Performance of Base-Isolated Multistorey Structures". *Proc. Pacific Conf. on Earthq. Engrg*, v1, Wairakei, N.Z. Aug. 1987: 309–20.
28. Moss, P.J., Carr, A.J., Cooke, N. and Tan, F.K. "The Influence of Bridge Geometry on the Seismic Behaviour of Bridges on Isolating Bearings". *Proc. Pacific Conf. on Earthq. Engrg*, Wairakei, N.Z., v2, Aug. 1987: 341–51.
29. Carr, A.J., Moss, P.J. and Carnaby, G.A. "The Tangent Compliance Matrix of Wool Fibre Assemblies". *Proc. the Advanced Workshop on the Application of Mathematics and Physics in the Wool Industry*, Lincoln, N.Z., Feb. 1988: 193-203.
30. Zhao, X., Carr, A.J. and Moss, P.J. "Soil Structure Interaction Using Boundary Elements in the Time Domain". *Proc. of the 11th Australasian Conf. on the Mech. of Struct. and Materials*. Auckland, Aug. 1988: 27–32.
31. Bhimaraddi, A., Carr, A.J. and Moss, P.J. "Finite Element Analysis of Shells of Revolution of Moderate Thickness". *Proc. of the 11th Australasian Conf. on the Mech. of Struct. & Materials*, Auckland, Aug. 1988: 389–94.
32. Bhimaraddi, A., Moss, P.J. and Carr, A.J. "Finite Element Analysis of Curved Beams of Rectangular Cross-Section". *Proc. of the 11th Australasian Conf. on the Mech. of Struct. & Materials*, Auckland, Aug. 1988: 431–35.
33. Andriono, T., and Carr, A.J. "Simplified Method of Analysis for Seismic Resistant Design of Base-Isolated Multistorey Structures". *Proc. 2nd East Asia – Pacific Conf. on Struct. Engrg and Construction*, Chaing Mai, Thailand, Jan. 11-13 1989: 1671–76.
34. MacRae, G.A., Walpole, W.R. and Carr, A.J. "Cyclic Bending of Steel I-Shaped Beam-Columns". *Proc. Pacific Struct. Steel Conf.*, Gold Coast, Queensland, Australia, May 1989: 320–32.
35. MacRae, G.A., Carr, A.J. and Walpole, W.R. "Inelastic I-Shaped Beam-Columns in Earthquake

- Resistant Structures". *Proc. Pacific Struct. Steel Conf.*, Gold Coast, Queensland, Australia, May 1989: 309–19.
36. Moss, P.J. and Carr, A.J. "Finite Element Modelling with the Unit Cell of Wool Fibres". *Proc. 8th Int. Wool Textile Research Conf.*, Christchurch, N.Z., Feb. 1990, v5: 11–33.
 37. Cooke, N., Turkington, D.H., Moss, P.J. and Carr, A.J. "Seismic Response of Bridges Supported on Lead-Rubber Bearings", *Third Int. Conf. on Short and Medium Span Bridges*, Canadian Society for Civil Engineering, Toronto, Canada, v2 Aug. 7–10, 1990: 459–70.
 38. MacRae, G.A., Carr, A.J. and Walpole, W.R. "The Dynamic Behaviour of Multistorey Steel Frames". *Proc. 8th Japanese Symposium on Earthq. Engrg*, Tokyo, Japan, Dec. 1990: 1599–1604.
 39. MacRae, G.A., Walpole, W.R. and Carr, A.J. "Behaviour and Design of Moment-Resisting Steel Frames". *Proc. Pacific Conf. on Earthq. Engrg*, Auckland, v3, Nov. 1991: 103–12.
 40. Mori, A., Moss, P.J., Carr, A.J., and Cooke, N. "The Behaviour of Rubber Bearings for Base Isolation". *Proc. Pacific Conf. on Earthq. Engrg*, Auckland, v2, Nov. 1991: 233–44.
 41. Carr, A.J., Moss, P.J. and Mori, A. "The Experimental and Analytical Investigations of the Behaviour of Seismic Isolation Bearings". *Proc. 2nd European Conf. on Struct. Dynamics: EURODYN '93*, Trondheim, Norway, 21–23 June 1993: 237–44.
 42. Carr, A.J. and Tabuchi, M. "The Structural Ductility and the Damage Index for Reinforced Concrete Structures Under Seismic Excitation". *Proc. 2nd European Conf. on Struct. Dynamics: EURODYN '93*, Trondheim, Norway, 21–23 June 1993: 169–76.
 43. Mori, A., Moss, P.J. and Carr, A.J. "The Behaviour of Seismic Isolation Bearings". *Proc. Asia-Pacific Vibration Conf. '93*, Kitakyushu, Japan, v3, Nov. 1993: 1389–94.
 44. Moss, P.J. and Carr, A.J. "Structural Damping Models for Non-Linear Seismic Analysis". *Proc. NZNSEE Tech. Conf.*, Taupo, 1994: 86–95.
 45. Zhao, J.X., Carr, A.J. and Moss, P.J. "Calculating Green's Functions for In-Plane Motion in A Horizontally Layered Half Space". *Proc. Int. Conf. on Computational Methods in Structural and Geotechnical Engineering*, Hong Kong, Dec. 1994: 1059–64.
 46. Carr, A.J., Cooke, N., Mori, A., and Moss, P.J. "The Axial and Shear Load Behaviour of Seismic Isolation Bearings". *Proc. Annual Tech. Conf. N.Z. Nat. Soc. Earthq. Engrg*, Rotorua, Mar.–Apr. 1995: 77–84.
 47. Carr, A.J., Moss, P.J. and Filiatrault, A. "Pounding of Adjacent Structures During Earthquakes: A Review of the Current State of Knowledge". *Proc. Annual Tech. Conf. N.Z. Nat. Soc. Earthq. Engrg*, Rotorua, Mar.–Apr. 1995.
 48. Carr, A.J. "Control of Deformation Under Seismic Excitation". *Proc. Fifth World Conf. Habitat and the High Rise*. Council on Tall Buildings and Urban Habitat, (Lehigh Univ. PA), Amsterdam, 14–19 May 1995: 961–84.
 49. Carr, A.J., Moss, P.J. and Filiatrault, A. "Pounding of Adjacent Structures During Earthquakes: A Review of the Current State of Knowledge". *Proc. 7th Canadian Conf. on Earthq. Engrg*, Montreal, 5–7 June 1995: 221–28.
 50. Carr, A.J., Cooke, N., Mori, A. and Moss, P.J. "The Shear and Axial Load Behaviour of Seismic

- Isolation Bearings". *Proc. 7th Canadian Conf. on Earthq. Engrg*, Montreal, 5–7 June 1995: 673–80.
51. Carr, A.J. and Widodo. "Damage Parameters of Rocking Reinforced Concrete Frame-Wall Structures". *Proc. of the Pacific Conf. on Earthquake Engrg*, Melbourne, v2, Nov. 1995: 135–44.
 52. Crisafulli, F.J., Carr, A.J. and Park, R. "Shear Strength of Unreinforced Masonry Panels". *Proc. of the Pacific Conf. on Earthquake Engrg*, Melbourne, v3, Nov. 1995: 77–86.
 53. Mori, A., Moss, P.J., Carr, A.J. and Cooke, N. "The Performance of Seismic Isolation Bearings". *Proc. Pacific Conf. on Earthquake Engrg*, Melbourne, Australia, v1, Nov. 1995: 111–20.
 54. Thomas, G.C., Buchanan, A.H., Carr, A.J., Fleischmann, C. and Moss, P.J. "The Behaviour of Timber Walls Exposed to Fire". *Proc. 14th Australasian Conf. on the Mechanics of Structures and Materials*, Hobart, v1, Dec. 1995: 100–5.
 55. Carr, A.J., Moss, P.J. and Fathalla, A.M. "Impact Between Buildings and the Influence of Foundation Compliance". *Proc. Tech. Conf. of New Zealand National Society for Earthquake Engrg*, New Plymouth, Arch 1996: 152–60.
 56. Mori, A., Moss, P.J., Carr, A.J. and Cooke, N. "The Seismic Behaviour of Elastomeric and Lead-Rubber Bearings". *Proc. 11th World Conf. on Earthquake Engrg*, Acapulco, Mexico, 1996.
 57. Carr, A.J. "Passive Control of Deformations Under Seismic Excitation". *Proc. ESC XXV General Assembly, Seismology in Europe*, Reykjavik, Iceland, 9–14 Sept. 1996: 526–31.
 58. Charng, P-H., Carr, A.J. and Moss, P.J. "Base Isolation for Building Structures". *Proc. Tech. Conf. N.Z. National Society for Earthquake Engrg*, Wairakei, March 1997: 153–59.
 59. Pradono, M.H., Moss, P.J. and Carr, A.J. "Earthquake Response of Coupled Structural Walls". *Proc. Tech. Conf. N.Z. National Society for Earthquake Engrg*, Wairakei, March 1997: 213–7.
 60. Rahman, A.M., Carr, A.J. and Moss, P.J. "Impact Between Buildings During Earthquakes and the Influence of Foundation Compliance". *2nd Asia-Pacific Conference on Shock and Impact Loads on Structures*, Melbourne, Australia, 1997: 441–8.
 61. Pradono, M.H., Moss, P.J. and Carr, A.J. "Earthquake Response of Coupled Structural Walls". *Proc. 15th Australasian Conference on Mechanics of Structures and Materials*, Melbourne, Australia, 1997: 357–62.
 62. Carr, A.J. "Damping Models for Inelastic Analyses". *Proc. Asia-Pacific Vibration Conference '97*, Kyongju, Korea, Nov. 1997: 42–8.
 63. Charng, P-H., Carr, A.J. and Moss, P.J. "Base Isolation for Segmented Building Structures". *Proc. 15th Australasian Conf. On Mechanics of Structures and Materials*, Melbourne, Australia, 1997: 363–8.
 64. Lin, Z., Moss, P.J. and Carr, A.J. "Analysis and Seismic Design of Building Structures with Supplemental Lead Dampers". *Proc. N.Z. National Society for Earthquake Engineering Technical Conference*, Taupo, N.Z., 1998: 167–74.
 65. Zhaglool, B., Carr, A.J. and Moss, P.J. "Three Dimensional Behaviour of Structures Under Concurrent Orthogonal Seismic Excitations". *Proc. N.Z. National Society for Earthquake Engineering Technical Conference*, Taupo, N.Z., 1998: 119–22.

66. Satyarno, I., Carr, A.J. and Restrepo, J. "Refined Pushover Analysis for the Assessment of Older Reinforced Concrete Buildings". *Proc. N.Z. National Society for Earthquake Engineering Technical Conference, Wairakei, N.Z., Mar. 1998: 75–82.*
67. Cho, J.H., Moss, P.J. and Carr, A.J. "Assessment of P-delta Effects in Framed Structures Subjected to Earthquake Motions". *Proc. Australasian Structural Engineering Conference, Auckland, Sept.-Oct. 1998: 705–12.*
68. Rahman, A.M., Carr, A.J. and Moss, P.J. : "Impact Between Buildings During Earthquakes and the Influence of Foundation Compliance". *Proc. Australasian Structural Engineering Conference, Auckland, Sept.-Oct. 1998: 743–50.*
69. Lin, X., Moss, P.J. and Carr, A.J. "Seismic Analysis and Design of Building Structures with Supplemental Dampers". *Proc. Australasian Structural Engineering Conference, Auckland, Sept.-Oct. 1998: 735–42.*
70. Murakami, M., Moss, P.J., Carr, A.J. & Inayama, M. "Formulae to Predict Non-linear Behaviour of Sheathed Walls with any Nailing Arrangement Pattern". *Proc. PTEC'99 Pacific Timber Engineering Conf., v3, (Forest Research Bull. 212), Mar. 1999: 189–96.*
71. Carr, A.J., Moss, P.J. & Rahman, A.M. "Structural Pounding of Adjacent Multi-storey Structures Considering Soil Flexibility Effects". *Proc. 12th World Conference on Earthquake Engineering, Auckland, NZ, Feb 2000. CD Rom, #1175, 2000: 8p.*
72. Zhang, Jianjing, Carr, A.J., & Moss, P.J., "Nonlinear Seismic Soil-structure Interaction by Using a Be-Fe Method in the Time Domain". *Proc. 12th World Conference on Earthquake Engineering, Auckland, NZ, Feb 2000. CD Rom, #1397, 2000: 8p.*
73. Lin, Xi, Moss, P.J. & Carr, A.J. "Seismic Analysis and Design of Building Structures with Supplemental Lead Dampers". *Proc. 12th World Conference on Earthquake Engineering, Auckland, NZ, Feb 2000. CD Rom, #1417, 2000: 8p.*
74. Murakami, M, Moss, P.J. Carr, A.J. & Inayama, M. "The Effect of Flexible Horizontal Diaphragms on the Seismic Torsional Resistance of Systems with Ductile Walls". *Proc. 12th World Conference on Earthquake Engineering, Auckland, NZ, Feb 2000. CD Rom, #0074, 2000: 7p.*
75. Zaghlool, B., Carr, A.J. & Moss, P.J. "Inelastic Behaviour of Three-dimensional Structures Under Concurrent Seismic Excitations". *Proc. 12th World Conference on Earthquake Engineering, Auckland, NZ, Feb 2000. CD Rom, #2001, 2000: 8p.*
76. Crisafulli, F.J., Carr, A.J. and Park, R. "Capacity Design of Infilled Framed Structures". *Proc. 12th World Conference on Earthquake Engineering, Auckland, NZ, Feb 2000. CD Rom, #0221, 2000: 8p.*
77. Toranzo, L., Restrepo, J.I. and Carr, A.J. Improvement of Traditional Masonry Wall Construction for use in Low-rise / Low-wall-density Buildings in Seismically Prone Regions. *Proc. NZSEE Technical Conference, Wairekei, March 2001. 10p.*
78. Toranzo, L., Carr, A.J. and Restrepo, J.I. " Displacement Base Design of Rocking Walls Incorporating Hysteretic Energy Dissipators", *7th International Seminar on Seismic Isolation, Passive Energy Dissipation and Active Control. Assisi, Italy, Oct. 2001.*

79. Castillo, Rolando, Paulay, Tom and Carr Athol J., Design Concepts for Ductile Single Mass Asymmetric Systems. *Proc, Third European Workshop on the Seismic Behaviour or Irregular and Complex Structures*. Florence, Italy, September 17-18, 2002 Cdrom, 17p
80. Wang, J., Carr, A.J., Cooke,N.and Moss, P.J. "Wave-passage Effect on the Seismic Response of Long Bridges". *Proc. 2003 Pacific Conference on Earthquake Engineering*, Christchurch, 13-15 Feb. 2003. cdrom paper 050, 9p.
81. Dong, P., Moss,P.J. and Carr, A.J.. "Seismic Structural Assessment of Reinforced Concrete Framed Structures". *Proc. 2003 Pacific Conference on Earthquake Engineering*, Christchurch, 13-15 Feb. 2003. cdrom paper 075, 79.
82. Wang, J.,Carr, A.J., Cooke,N.and Moss, P.J. "A Simple Method for Stochastic Dispersion of Earthquake Waves". *Proc. 2003 Pacific Conference on Earthquake Engineering*, Christchurch, 13-15 Feb. 2003. cdrom paper 051, 7p.
83. Liu, A., Carr, and Park, R. "A Proper Member Model for Member Flexural Behaviour at the Fixed-ends". *Proc. 2003 Pacific Conference on Earthquake Engineering*, Christchurch, 13-15 Feb. 2003. cdrom paper 047, 8p.
84. Carr, A.J. "The Generation of Inelastic Response Spectra for Earthquake Acceleration Records". *Proc. 2003 Pacific Conference on Earthquake Engineering*, Christchurch, 13-15 Feb. 2003. cdrom paper 076, 8p.
85. Zhang, J.J., Moss,P.J. and Carr, A.J. "Non-linear Local Site Amplification and its Effects on Structural Response". *Proc. 2003 Pacific Conference on Earthquake Engineering*, Christchurch, 13-15 Feb. 2003. cdrom paper 078, 9p..
86. Carey, M.W., Chase, J.G., Carr,A.J. and Kowarz, M.W. "Bifurcation Dynamics of Conformal Non-linear Thin Film Michromechanical Structures". *Proc. 10th Asia-Pacific Vibration Conference*, Gold Coast, 12-14 Nov. 2003 pp 31-36.
87. Carr, A.J. "Inelastic Earthquake Response Spectra". *Proc. 10th Asia-Pacific Vibration Conference*, Gold Coast, 12-14 Nov. 2003 pp 37-42.
88. Speith, H.A., Arnold, D., Davies, M., Mander, J.B. and Carr. A.J. "Seismic Performance of Post-tensioned Precast Concrete beam to Column Connections with Supplementary Energy Dissipation". *Proc. 2004 New Zealand National Society for Earthquake Engineering Conference*, Rotorua, 19-21 March 2004. cdrom 8p.
89. Dong, P., Carr, A.J. and Moss, P.J. "Earthquake Scaling for Inelastic Dynaminc Analysis of Reinforced Concrete Ductile Framed Structures". *Proc. 2004 New Zealand National Society for Earthquake Engineering Conference*, Rotorua, 19-21 March 2004. cdrom 11p.
90. Speith, H.A., Carr, A.J. Murahidy, A.G., Arnold, D., Davies, M., and Mander, J.B. "Modelling of Post-tensioned Precast Reinforced Concrete Frame Structures with Rocking Beam-Column Connections". *Proc. 2004 New Zealand National Society for Earthquake Engineering Conference*, Rotorua, 19-21 March 2004. cdrom 9p.
91. Murahidy, A.G., Carr, A.J., Mander, J.B. and Bull, D.K. "Design, Construction and Dynamic Testing of Post-Tensioned Precast Reinforced Concrete Frame Building with Rocking Beam-Column Connections and ADAS Elements". *Proc. 2004 New Zealand National Society for Earthquake Engineering Conference*, Rotorua, 19-21 March 2004. cdrom 10p.

92. Toranzo-Dianderas, L.A., Restrepo, J.I., Carr A.J. and Mander J.B. "Rocking Confined Masonry Walls with Hysteretic Energy Dissipation and Shake-Table Validation". *Proc. 13th World Conference on Earthquake Engineering*, Vancouver, B.C. Canada, August 1-6, 2004, cdrom paper 248, 11p.
93. Snæbjornsson, J.T., Carr A.J. and Sigbjornsson, R. "Analysing and Modelling Recorded Earthquake Induced Structural Response". *Proc. 13th World Conference on Earthquake Engineering*, Vancouver, B.C. Canada, August 1-6, 2004, cdrom paper 445, 15p.
94. Wang, J., Carr, A., Cooke, N, and Moss, P. "Inelastic Responses of Long Bridges to Asynchronous Seismic Inputs". *Proc. 13th World Conference on Earthquake Engineering*, Vancouver, B.C. Canada, August 1-6, 2004, cdrom paper 638, 11p.
95. Wang, J., Carr, A., Cooke, N, and Moss, P. "Effects of Spatial Variation of Seismic Inputs on Bridge Longitudinal Response". *Proc. 13th World Conference on Earthquake Engineering*, Vancouver, B.C. Canada, August 1-6, 2004, cdrom paper 640, 13p.
96. Palermo, A., Pampanin, S. and Carr, A. (2005) "Efficiency of Simplified Alternative Modelling Approaches to Predict the Seismic Response of Precast Concrete Hybrid Systems". *fib Symposium 2005: "Keep Concrete Attractive"*, Budapest, Hungary., 23-25 May 2005. Paper no. 1503.
97. Carr, Athol J. "Damping Models for Time-history Structural Analyses". *Proc. 11th Asia-Pacific Vibration Conference APVC-05*, Langkawi, Malaysia, November 25-27 2005. pp287-293.
98. Browne, M, Carr A.J. and Bull D.K. "The Analysis of reinforced Concrete Rocking Wall Behaviour". *Proc. 2006 NZSEE Conference*, Napier, New Zealand, March 10-12. 2006. cdrom, paper 15, 8p
99. Pender, M.J., Wotherspoon, L.M., Ingham, J.M. and Carr, A.J. "Shallow Foundation Stiffness: Continuous Soil and Discrete Spring Models Compared". *Proc. 2006 NZSEE Conference*, Napier, New Zealand, March 10-12. 2006. cdrom, paper 27, 7p
100. Carr, Athol J., Ingham, Jason and Pender, Michael. "Approach to Design of Shallow Foundations for Low-Rise Framed structures". *Proc. 8th National Conference on Earthquake Engineering*, San Francisco, Ca, USA. April 17-20 2006, cdrom paper 8NCEE-001063, 10p.
101. Carr, Athol, Sigbjornsson, Ragnar and Snæbjornsson, Jonas. "Long Term Dynamic Behaviour of a Multi-storey R-C Building in Seismic and Windy Environment". *Proc. 8th National Conference on Earthquake Engineering*, San Francisco, Ca, USA. April 17-20 2006, cdrom paper 8NCEE-000883, 10p.
102. Rodgers, G.W., Mander, J.B., Chase, J.G., Mulligan, K.J., Deam, B.L. and Carr, A.J.. "Reshaping Hysteretic Behaviour Using Resettable Devices to Customise Structural Response and Forces". *Proc. 8th National Conference on Earthquake Engineering*, San Francisco, Ca, USA. April 17-20 2006, cdrom paper 8NCEE-001034, 10p.
103. Carr, Athol, Fenwick, Richard and Ruiz, Jose. "Seismic Design of Reinforced Concrete Buildings in New Zealand". *Proc. 8th National Conference on Earthquake Engineering*, San Francisco, Ca, USA. April 17-20 2006, cdrom paper 8NCEE-001192, 11p.
104. Carr, A.J. "Three Decades of Earthquake Engineering Research at the University of Canterbury".

8th National Conference on Earthquake Engineering, San Francisco, 17-22 April 2006.

- 105 Kam, W.Y., Pampanin, S., Palermo, A. and Carr, A. (2006) "Advanced Flag-Shape Systems For High-Seismic Performance". *Proc. First European Conference on Earthquake Engineering and Seismology (ECEES)*, Geneva, Switzerland: 3-8 Sep 2006. Paper 991, 10pp.
106. Uma, S.R., Pamapanin, S., and Carr, A. " Formulation of Integrated Beam-Column-Joint Model for Seismic Non-conforming R-C Frame Systems.*Proc. First European Conference on Earthquake Engineering and Seismology (ECEES)*, Geneva, Switzerland: 3-8 Sep 2006. Paper 716.
- 107 Gunasekaren, U., MacRae, G., Fenwick, R. and Carr, A. " Slab Effects on Building Seismic Performance.*Proc. First European Conference on Earthquake Engineering and Seismology (ECEES)*, Geneva, Switzerland: 3-8 Sep 2006.
- 108 Rodgers, G.W, Mulligan, K.J, Chase, J.G, Mander, J.B, Deam, B.L and Carr, A.J. "Off-Diagonal 2-4 Damping Technology Using Semi-Active Resetable Devices," *19th Australasian Conference on Mechanics of Structures and Materials (ACMSM)*, 29 November-1 December, 2006, Christchurch, New Zealand, pp. 421-427, ISBN13 978-0-415-42692-3.
- 109 Mulligan, K.J, Miguelgorry, M, Novello, V, Chase, J.G, Horn, B, Mander, J.B, Rodgers, G.W, Carr, A.J, and Deam, B.L.. "Semi-active Tuned Mass Damper Systems," *19th Australasian Conference on Mechanics of Structures and Materials (ACMSM)*, 29 November-1 December, 2006, Christchurch, New Zealand, pp. 337-342, ISBN13 978-0-415-42692-3.
- 110 Gunasekaran, U., MacRae, G.A., Fenwick, R. and Carr, A.J. (2006) "Slab effects on building seismic performance". *19th Australasian Conference on Mechanics of Structures and Materials (ACMSM19)* Christchurch, New Zealand:, 30 Nov-1 Dec 2006. In Progress in Mechanics of Structures and Materials, 289-294.
- 111 Franco-Anaya, R, Carr, A.J, Mander, J B. Chase, J.G, and Mulligan, K J. "Seismic Protection of a Model Structure Using Semi-Active Resetable Devices," *19th Australasian Conference on Mechanics of Structures and Materials (ACMSM)*, 29 November – 1 December, 2006, Christchurch, New Zealand, pp. 379-384, ISBN13 978-0-415-42692-3.
- 112 Chey, M.H, Mander, J.B, Carr, A.J and Chase, J.G. "Multi-Story Semi-Active Tuned Mass Damper Building System," *19th Australasian Conference on Mechanics of Structures and Materials (ACMSM)*, 29 November – 1 December 2006, Christchurch, NZ, pp. 371-377, ISBN13 978-0-415-42692-3.
- 113 Franco-Anaya, R, Carr, A.J., Mander, J., Chase, G., Mulligam, K., and Rodgers, G., "Seismic Testing of a Model Structure with Semi-Active resetable Devices", *Proc. New Zealand Society of Earthquake Engineering 2007 Conference (NZSEE 2007)*, Palmerston North, New Zealand: New Zealand , 30 Mar-1 Apr 2007.
- 114 Kam, W.Y., Pampanin, S., Carr, A.J.. and Palermo, A., " Advanced Flag-Shaped Systems for High Seismic Performance Including Near-Fault Effects".*Proc. New Zealand Society of Earthquake Engineering 2007 Conference (NZSEE 2007)*, Palmerston North, New Zealand: New Zealand , 30 Mar-1 Apr 2007
- 115 Amaris, A.D., Pampanin, S., Bull, D.K. and Carr, A.J. (2007) "Development of a Non-Tearing Floor Solution for Jointed Precast Frame Systems". *Proc. New Zealand Society of Earthquake Engineering 2007 Conference (NZSEE 2007)*, Palmerston North, New Zealand: New Zealand , 30

Mar-1 Apr 2007.Paper 14.

- 116 Peng, B.H.H., Dhakal, R.P., Fenwick, R.C., Carr, A.J. and Bull, D.K, " Analytical Model on Beam Elongation Within the Reinforced Plastic Hinges", *Proc. New Zealand Society of Earthquake Engineering 2007 Conference (NZSEE 2007)*, Palmerston North, New Zealand: New Zealand , 30 Mar-1 Apr 2007
- 117 Franco-Anaya, R., Carr, A.J. and Chase, J.G. (2007) "Experimental Investigation of Semi-Active Resetable Devices for Seismic Protection of Structures". *Proceedings of the 12th Asia Pacific Vibration Conference (APVC 2007)*, Sapporo, Japan: 6-9 Aug 2007. In, 9pp.
- 118 Chey, M.H., Carr, A.J., Chase, J.G. and Mander, J.B. (2007) "Design of Semi-Active Tuned Mass Damper Building Systems using Resetable Devices". *Proceedings of 8th Pacific Conference On Earthquake Engineering (8PCEE)*, Singapore: 5-7 Dec 2007. In, Paper 66.
- 119 Chase, J.G., Mulligan, K.J., Elliott, R.B., Rodgers, G.W., Mander, J.B., Carr, A.J. and Anaya, R.F. (2007) "Re-Shaping Hysteresis: Seismic Semi-Active Control Experiments for a 1/5th Scale Structure". *Proceedings of 8th Pacific Conference On Earthquake Engineering (8PCEE)*, Singapore: 5-7 Dec 2007. Paper 71
- 120 Peng, B.H.H., Dhakal, R.P., Fenwick, R.C., Carr, A.J. and Bull, D.K. (2007) "Flexural, axial load and elongation response of plastic hinges in reinforced concrete member". *Proceedings of 8th Pacific Conference On Earthquake Engineering (8PCEE)* Singapore: 5-7 Dec 2007., Paper 30. .
- 121 Gardener, D.R., Bull, D.K. and Carr, A.J. " Internal Forces of Concrete Floor Diaphragms in Multi- Storey Buildings", *Proceedings New Zealand Society for Earthquake Engineering Conference, Engineering an Earthquake Resilient New Zealand*. Wairakei, New Zealand, 11-13 April, 2008.
- 122 Amaris, A., Pampanin, S., Bull, D., and Carr A., " Experimental Investigation on a Hybrid Jointed Precast Frame with Non-tearing Floor Connections." *Proceedings New Zealand Society for Earthquake Engineering Conference, Engineering an Earthquake Resilient New Zealand*. Wairakei, New Zealand, 11-13 April, 2008.
- 123 Kam, W.Y., Pampanin, S., Palermom, A., and Carr, A., "Design Procedure and Behaviour of the Advanced Flag-Shape (AFS) Systems for Moment-Resisting Frame Structures". *Proceedings New Zealand Society for Earthquake Engineering Conference, Engineering an Earthquake Resilient New Zealand*. Wairakei, New Zealand, 11-13 April, 2008.
- 124 Franco-Anaya, R., Carr, A, and Schreiber, U., "Qualification of Fibre-Optic Gyroscopes for Civil Engineering Applications", *Proceedings New Zealand Society for Earthquake Engineering Conference, Engineering an Earthquake Resilient New Zealand*. Wairakei, New Zealand, 11-13 April, 2008.
- 125 Carr, A.J., " Structural Engineering in New Zealand - Trends in Practice and Recent and Current Research" *Keynote address, XXXIII Jornadas Sudamericanas De Ingenieria Estructural*, Santiago, Chile, 26-30 May 2008. 14pp.
- 126 Chey, M.H., Carr, A.J., Chase, J.G. and Mander, J.B. (2008) "Resetable Tuned Mass Damper and Its Application to Isolated Stories Building System". *14th World Conference on Earthquake Engineering*, Beijing, China: 12-17 Oct 2008.
- 127 Franco-Anaya, R., Carr, A.J. and Chase, J.G. (2008) "Semi-Active Resettable Devices for Seismic Protection of Civil Engineering Structures *14th World Conference on Earthquake*

Engineering, Beijing, China: 12-17 Oct 2008

- 128 Peng, B.H.H., Dhakal, R.P., Fenwick, R.C., Carr, A.J. and Bull, D.K. (2008) "Experimental Investigation on the Interaction of Reinforced Concrete Frames with Precast-Prestressed Concrete Floor Systems". *14th World Conference on Earthquake Engineering*, Beijing, China, 12-17 Oct 2008.
- 129 Pettinga, D., Pampanin, S., Christopoulos, C., Carr, A.J, Castillo-Barahona, R., "Experimental Investigation into Residual Displacements due to Inelastic Torsional Response". *14th World Conference on Earthquake Engineering*, Beijing, China, 12-17 Oct 2008.
- 130 Amaris, A., Pampanin, S., Bull, D., and Carr, A., " Experimental performance of Hybrid Frams Systems with Non-Tearing Floor Connections". *14th World Conference on Earthquake Engineering*, Beijing, China, 12-17 Oct 2008.
- 131 Liu, A., and Carr, A., "Seismic Assessment of a Pre-1970s reinforced Concrete Frame Building with Plain Round Reinforcing Bars". *14th World Conference on Earthquake Engineering*, Beijing, China, 12-17 Oct 2008.
- 132 Kam, W.Y., Pampanin, S., Palermo, A., and Carr, A.J., "Implementation of Advanced Flag-shaped (AFS) Systems for Moment-resisting Frame Structures". *14th World Conference on Earthquake Engineering*, Beijing, China, 12-17 Oct 2008.
- 133 Peng, B.H.H., Dhakal, R.P., Fenwick, R.C., Carr, A.J. and Bull, D.K. (2008) "Analytical model of ductile reinforced concrete members allowing for elongation of plastic hinges". *11th East-Asia and Pacific Conference on Structural Engineering and Construction*, Taipei, Taiwan: 19-21 Nov 2008.
- 134 Moghaddasi K. M., Cubrinovski, M., Pampanin, S., Carr, A., and Chase G. (2009) "Monte Carlo Simulation of SSI Effects Using Simple Rheological Soil Model". *Proceedings NZSEE Conference* Christchurch, New Zealand: 2009, 3-5 April 2009.
- 135 Peng, B.H.H., Dhakal, R.P., Fenwick, R.C., Carr, A.J. and Bull, D.K. "Modelling of RC Moment Resisting Frames with Precast-prestressed Flooring System". *Proceedings, New Zealand Society for Earthquake Engineering Conference - Why Do We Still Tolerate Buildings That Are Unsafe in Earthquakes?*. Christchurch, New Zealand, 3-5 April 2009.
- 136 Amaris, A.D., Pampanin, S., Bull, D.K., and Carr, A.J., "Numerical Investigations on the Seismic Response of Multi-storey Hybrid Post-Tensioned Precast Concrete Frames with Non-tearing Floor Connections". *Proceedings, New Zealand Society for Earthquake Engineering Conference - Why Do We Still Tolerate Buildings That Are Unsafe in Earthquakes?*. Christchurch, New Zealand, 3-5 April 2009.
- 137 Franco-Anaya, R, Carr, A.J. and Chase, J.G. "Seismic Response Reduction of a 12-storey Reinforced Concrete Structure Using Semi-active Resettable Devices". *Proceedings, New Zealand Society for Earthquake Engineering Conference - Why Do We Still Tolerate Buildings That Are Unsafe in Earthquakes?*. Christchurch, New Zealand, 3-5 April 2009..
138. Chey, M.H., Chase, J.G., Mander J.B. and Carr, A.J. " Semi-active Control of Mid-storey Isolation Building System". *2009 Asia-Korean Conference on Advanced Science and Technology*, Yanji, China. 28-29 Aug, 2009
- 139 Cole, G., Dhakal, R.P., Carr, A.J., and Bull, D.K. "The Significance of Lumped or Distributed Mass Assumptions on the Analysis of Pounding Structures". *Proceedings 13th Asia-Pacific*

Vibration Confernce, APVC'09. Christchurch, New Zealand, 22-25 November 2009.

- 140 Gardener, D., Bull, D.K., and Carr, A.J. "Investigation of the Distribution of Inertial Forces in Floor Diaphragms During Seismic Shaking". *Proceedings 13th Asia-Pacific Vibration Confernce, APVC'09*. Christchurch, New Zealand, 22-25 November 2009.
- 141 Chase, J.G., Chey, M-H, MacRae, G., Carr, A.J. and Rodgers, G.W., " Analytical Modelling and MDOF Response Considerations for Semi-Active Tuned mass Damper Building Systems Subjected to Earthquake Excitation". *Proceedings 13th Asia-Pacific Vibration Confernce, APVC'09*. Christchurch, New Zealand, 22-25 November 2009.
- 142 Moghaddasi M.K., Cubrinovski M., Pampanin S., Carr., A. and Chase G. (2009) "A robust probabilistic simulation to elucidate soil-shallow foundation-structure interaction effects on structural response". *Proceedings International Workshop on Soil-Foundation-Structure-Interaction*, Auckland, NZ: 26-27 November 2009.
143. Cole, G., Dhakal, R., Carr, A. and Bull, D. " Building Pounding State of the Art: Identifying Structures Vulnerable to Pounding Damage". *Proc. NZSEE 2010 Conference -Earthquake Prone Buildings, How Ready Are We?*, Wellington, NZ, 26-28 March 2010., paper 11.
144. Moghaddasi,M., Cubrinovski,M., Pampanin,S., Carr,A.J. and Chase, J.G. " Soil-structure Interaction Effects on Non-linear Seismic Demand of Structures". *Proc. NZSEE 2010 Conference - Earthquake Prone Buildings, How Ready Are We?*, Wellington, NZ, 26-28 March 2010., paper 17.
145. Quintana,P., Pampanin,S., Carr,A.J. and Bonelli,P. " Shake-table Tests of Under-designed RC Frames for the Seismic Retrofit of Buildings - Design and Similitude Requirements of the Benchmark Specimen". *Proc. NZSEE 2010 Conference - Earthquake Prone Buildings, How Ready Are We?*, Wellington, NZ, 26-28 March 2010., paper 39.
146. Cole,G., Dhakal,R., Carr, A. and Bull,D. "Building Pounding and the Effects of Mass Distribution". *Proc. NZSEE 2010 Conference - Earthquake Prone Buildings, How Ready Are We?*, Wellington, NZ, 26-28 March 2010., poster 11.
- 147, Gardiner,D., Bull,D. and Carr,A. " Inertial Force Paths Within Floor Diaphragms Due to Seismic Shaking". *Proc. NZSEE 2010 Conference - Earthquake Prone Buildings, How Ready Are We?*, Wellington, NZ, 26-28 March 2010., poster 17.
148. Moghaddasi, M., Cubrinovski, M., Pampanin, S., Carr, A.J. and Chase, J.G. Soil-Foundation-Structure Interaction Effects on Nonlinear Seismic Demand of Structures. *Proc. NZSEE 2010 Conference - Earthquake Prone Buildings, How Ready Are We?*, Wellington, NZ, 26-28 March 2010., Paper 17 9pp.
149. Gallo, P.Q., Pampanin, S. and Carr, A.J. (2010) Experimental design and analytical modeling of 1/2.5 scale under-designed reinforced concrete frame subassemblies with masonry infills. *Proc. NZSEE 2010 Conference - Earthquake Prone Buildings, How Ready Are We?*, Wellington, NZ, 26-28 March 2010.
150. Cole, G., Dhakal, R.P., Carr, A.J. and Bull, D. (2010) Distributed mass effects on building pounding analysis. *9th US National and 10th Canadian Conference on Earthquake Engineering*, Toronto, Canada: 25-29 Jul 2010.
151. Cole, G., Dhakal, R.P., Carr, A. and Bull, D. (2010) Abilities of existing contactelements to model critical pounding problems. *3rd Asia Conference on Earthquake Engineering*

(ACEE 2010) Bangkok, Thailand:, 1-3 Dec 2010.

152. Puthanpurayil, A.M., Dhakal, R.P. and Carr, A.J. Modelling of In-Structure Damping: A Review of the State-of-the-art. *Proceedings of the Ninth Pacific Conference on Earthquake Engineering -Building an Earthquake-Resilient Society*. Auckland, New Zealand. 14-16 April 2011
153. Cole, G.L. Dhakal, R.P. Carr, A.J. and Bull, D.K. Case Studies of Observed Pounding Damage During the 2010 Darfield Earthquake. *Proceedings of the Ninth Pacific Conference on Earthquake Engineering -Building an Earthquake-Resilient Society*. Auckland, New Zealand. 14-16 April 2011
154. Quintana Gallo, Akguzeal, U, Pampanin, S. Carr, A.J. and Bonelli, P. Shake Table Tests of Non-Ductile RC Frames Retrofitted with GFRP Laminates in Beam Column Joints and Selective Weakening in Floor Slabs. *Proc. NZSEE 2012 Conference.- Implementing Lessons Learnt*, Christchurch, New Zealand, 13 -15 April 2012.
155. Cole, G.L. Dhakal, R.P., Carr, A.J. and Bull, D.K. The Influence on Member Demands in Low Rise Buildings. *Proc. NZSEE 2012 Conference.- Implementing Lessons Learnt*, Christchurch, New Zealand, 13 -15 April 2012.
156. Bonelli, P. Quintana Gallo, P. Restrepo, J, Pampanin, S. and Carr, A.J. Improvements for the Seismic Design of Reinforced Concrete Walls in Chile and Suggestions for the Refinement of ACI318 Seismic Provisions. *Proc. NZSEE 2012 Conference.- Implementing Lessons Learnt*, Christchurch, New Zealand, 13 -15 April 2012.
157. Masoud, M, Carr, A.,Cubrinovski, M., Pampanin, S. Chase, J.G. Chatzogogo, C.T. and Pecker, A. The Effects of Soil-Foundation Interface Nonlinearity on Seismic Soil-Structure Interaction Analysis. *Proc. NZSEE 2012 Conference.- Implementing Lessons Learnt*, Christchurch, New Zealand, 13 -15 April 2012

5. Papers in un-refereed journals, professional publications and conference proceedings

1. Shepherd, R. *et al.* The 1968 Inangahua Earthquake. Report of the University of Canterbury Survey Team, *Canterbury Engineering Journal*, no1, June 1970.
2. Scrivener, J.C. and Carr, A.J. An Analysis of Ferro-Cement Boat Hulls. *Proc. Pacific Symposium on Hydrodynamically Loaded Shells – Part I*, Honolulu, Oct. 1971.
3. Moss, A.J. and Carr, A.J. Vibration Tests on the Timaru Port Access Bridge. *N.Z. Engineering*. v31 no7, July 1976.
4. Carr, A.J. and Moss, P.J. The Analysis of Cylindrical Shells Under Local Loadings. *Research Report No.77/6*, Department of Civil Engineering, University of Canterbury, March 1977. 34p.
5. Priestley, M.J.N., Crosbie, R.L. and Carr, A.J. Seismic Forces in Base-Isolated Masonry Structures. *Masonry Industry*, Pt 1, Feb. 1978, Pt 2, March 1978.
6. Carr, A.J., Moss, P.J. and Pardoen, G.C. Imperial County Services Building Elastic and Inelastic Responses Analyses. *Research Report No. 79/15*, Department of Civil Engineering, University of Canterbury, December 1979. 91p.
7. Moss, P.J. and Carr, A.J. Vibration Tests on the Buller Bridge at Westport. *Research Report 79/16*, Department of Civil Engineering, University of Canterbury, Dec. 1979. 33p.
8. Pardoen, G.C., Carr, A.J. and Moss, P.J. Vibration Tests on the Toe Toe Stream Bridge (S.H.1). *Research Report 80/14*, Department of Civil Engineering, University of Canterbury, June 1980. 39p.
9. Moss, P.J., Carr, A.J. and Pardoen, G.C. Further Vibration Tests on the Buller River Bridge at Westport. *Research Report 80/16*, Department of Civil Engineering, University of Canterbury, June 1980. 34p.
10. Moss, P.J., Carr, A.J. and Pardoen, G.C. Vibration Tests on the Grey River Bridge at Stillwater. *Research Report 80/17*, Department of Civil Engineering, University of Canterbury, June 1980. 37p.
11. Moss, P.J., Carr, A.J. and Pardoen, G.C. Vibration Tests on the Cobden Bridge over the Grey River at Greymouth. *Research Report 80/18*, Department of Civil Engineering, University of Canterbury, June 1980. 42p.
12. Moss, P.J., Carr, A.J. and Pardoen, G.C. The Vibrational Behaviour of Three Composite Beam-Slab Bridges. *Research Report 81/5*. Department of Civil Engineering, University of Canterbury, June 1981.
13. Carr, A.J. and Moss, P.J. Review of Impact Factors for Design of Highway Bridges. *Research Report 82/14*, Department of Civil Engineering, University of Canterbury, May 1982. 14p.
14. Carr, A.J. Assessment of Earthquake Analysis for Concrete Container and Support Structure for Spherical Tank at Karstø. *SINTEF Report STF 71 F82008*, SINTEF AVD 71, Norges Tekniske Høgskole, Trondheim, Norway. June 1982. 7p.

15. Carr, A.J. Earthquake Design of Support Structure for Spherical Tank – Revised Design Spectra and Damping Capacity. *SINTEF Report STF 71 F82009*, SINTEF, AVD 71, Norges Tekniske Høgskole, Trondheim, Norway. June 1982. 5p.
16. Boardman, P.R., Wood, B.J. and Carr, A.J. Tectonic Isolation. *Monier Rocla Piper*. Sydney. Dec. 1983: 9–11.
17. Dean, J.A., Stewart, W.G. and Carr, A.J. The Seismic Performance of Plywood Sheathed Shearwalls. *Proc. Pacific Timber Engineering Conference*, Auckland, May 1984: 486-95.
18. Phillips, M.H. and Carr, A.J. Impact Factors and Stress Histograms for Bridges. *National Roads Board 1984 Bridge Design and Research Seminar*, Auckland, RRU Bulletin 73, 1984: 151–55.
19. Moss, P.J., Carr, A.J. and Buchanan, A.H. Seismic Design Loads for Low Rise Timber Buildings. *Proc. Timber Design Group, IPENZ Conference*, Auckland, Feb. 1986. 17p.
20. Dean, J.A., Stewart, W.G. and Carr, A.J. The Seismic Design of Plywood Sheathed Shear Walls. *Proc. Timber Design Group, IPENZ Conference*, Auckland, Feb. 1986, 27p.
21. Moss, P.J., Carr, A.J. and Buchanan, A.H. Seismic Design of Low-Rise Buildings. *Research Report 86/15*, Department of Civil Engineering, University of Canterbury, June 1986. 109p.
22. Park, R. *et al.* Current Research Projects in Earthquake Engineering in the Department of Civil Engineering at the University of Canterbury, *Proc. Annual Conf. of IPENZ*. v1 Civil, May 1987: 62–5.
23. Turkington, D.H., Cooke, N., Carr, A.J. and Moss, P.J. Development of Revised Design Procedures for Bridges on Lead-Rubber Bearings. *Proc. Japan–N.Z. Workshop on Base-Isolation of Highway Bridges*. Tech. Res. Ctr. for Nat. Land Dev., Dec. 1987: 132–41.
24. Buchanan, A.H., Carr, A.J. and Munukutla, R. Modelling Fire Performance of Concrete Walls. *Proc. Pacific Conc. Conf.*, Auckland, Nov. 1988: 229–40.
25. Astley, R.J. and Carr, A.J. Finite Elements At the University of Canterbury, New Zealand. *Finite Element News*, No.6, 1988: 13–17.
26. Wijanto, L.S., Moss, P.J. and Carr, A.J. Seismic Behaviour of Low-Rise Braced Steel Structures. *Research Report 88/12*. Department of Civil Engineering, University of Canterbury, Dec. 1988. 114p.
27. Tjondro, J.A., Moss, P.J. and Carr, A.J. Analytical Investigation of P-Delta Effects in Medium Height Steel Moment resisting Frames Under Seismic Loading. *Research Report 88/13*, Department of Civil Engineering, University of Canterbury. Dec. 1988. 139p.
28. Djaja, R.G., Carnaby, G.A., Moss, P.J., Carr, A.J. and Lee, D.H. A Tangent Compliance Matrix for An Oriented Assembly of Fibres, *WRONZ Communication*, No. C111, Wool Research Organisation of New Zealand, Lincoln, July 1989.
29. Lee, D.H., Carnaby, G.A., Carr, A.J., and Moss, P.J. A Review of Current Micromechanical Models of the Unit Fibrous Cell. *WRONZ Communication No. 113*, June 1990.
30. Carr, A.J. and Tabuchi, M. Potential Problems in Design for Maximum Flexibility. *Proc. The Tom Paulay Symposium: Recent Developments in Lateral Force Transfer in Buildings*. La Jolla, California, 20–22 Sept. 1993: 169–87.

31. Thomas, G.C., Buchanan, A.H., Carr, A.J., Fleischmann, C.M. and Moss, P.J. Light Timber Framed Walls Exposed to Compartment Fires. *Proc. Pacific Timber Engrg. Conf.*, Gold Coast, Australia, v2, 1994: 531–38.
32. Tanaka, H., Komuro, T., Carr, A.J. and Park, R. Reinforced Concrete Bridge Columns with Mixed Grade Longitudinal Reinforcement. *Proc. of the Second International Workshop on the Seismic Design and Retrofitting of Reinforced Concrete Bridges*, Queenstown, New Zealand, Aug. 1994: 345–63.
33. Carr, A.J. RUAUMOKO Users Manual, Department of Civil Engineering, University of Canterbury, March 1995, 133 p.
34. Crisafulli, F.J., Carr, A.J., Park, R. and Restrepo, J.I. Evaluation of the Compressive Strength of Masonry. *Proc. of 4th Australasian Masonry Conf.*, Sydney, Nov. 1995: 218–27.
35. Crisafulli, F.J., Carr, A.J. and Park, R. Shear Strength of Unreinforced Masonry Panels. *Proc. Third N.Z. Conf. of Postgraduate Students in Engineering and Technology*, Christchurch, 1–2 July 1996: 401–5.
36. Fathalla, A.M., Carr, A.J. and Moss, P.J. Impact Between Buildings During Earthquakes and the Influence of Foundation Compliance. *Proc. Third N.Z. Conf. of Postgraduate Students in Engineering and Technology*, Christchurch, 1–2 July 1996: 366–71.
37. Charng, P-H., Carr, A.J. and Moss, P.J. Base Isolation for Building Structures. *Proc. Third N.Z. Conf. of Postgraduate Students in Engineering and Technology*, Christchurch, 1–2 July 1996: 353–57.
38. Rodriguez, M., Restrepo, J.I. and Carr, A.J. Earthquake Resistant Precast Concrete Buildings: Floor Accelerations in Buildings. *Department of Civil Engineering, University of Canterbury, Research Report 2000-6*, Christchurch, N.Z. August 2000, 82p +appendices.
39. Carr, A.J. RUAUMOKO 3-Dimensional version, Users manual, The Department of Civil Engineering, University of Canterbury. April 2001. 242p.
40. Carr, Athol J. Analysis of Rådhus in Selfoss. Report to Earthquake Engineering Research Center, University of Iceland, Selfoss, Iceland. October 2001, 42p.
41. Carr, Athol J. Inelastic Response Spectra for the Christchurch Earthquake Records. *Report to the Royal Commission on the Canterbury Earthquakes*. September 2011, p150.

Research Student Supervision

Master of Engineering Students.

1. Climo, N.A. *Finite Element Modelling of Soil Continua.* 1972
2. Sinclair, P.J. *Finite Element Analysis of Steady State Seepage with a Free Surface.* 1972
3. Gormack, P.J. *Non-linear Finite Element Analysis of Shear Walls and two Dimensional Reinforced Concrete Structures.* 1974
4. Cameron, A.J. *The Response of Reinforced Concrete Bridge Piers to Seismic Motion.* (with R. Park) 1975
5. Lim, Chin Pau. *The Effects of Temperature on Reinforced Concrete Joints.* (with R. Park) 1975
6. Lindup, G.H. *Seismic Demands on Columns of Reinforced Concrete Multistorey Frames.*(with T. Paulay) 1975
7. Macdonald, A. *Non-linear Finite Element Analysis of Reinforced Concrete Structures Subject to Cyclic Loading.* 1975
8. Cree Brown, N.C. *Non-linear Finite Element Analysis of Layered Shells.* (with P. Moss) 1977
9. Evison, R.J. *Rocking Foundations.* (with N. Priestley) 1977
10. Crosbie, R.L. *Base Isolation for Brick Masonry Shear Wall Structures.* (with N. Priestley) 1977
11. Jury, R.D. *Seismic Load Demands on Columns of Reinforced Concrete Multi-storey Frames.* (with T. Paulay) 1978
12. Carter, B.H.P. *The Seismic Behaviour of Reinforced Concrete Frame-Shear Wall Structures.* (with T. Paulay) 1980
13. Crisp, D.J. *Damping Models for Inelastic Structures.* (with P. Moss) 1980
14. Tompkins, D.M. *The Seismic Response of Reinforced Concrete Multi-storey Frames.* (with T. Paulay) 1980
15. Kivell, B.T. *Hysteretic Modelling of Moment Resisting Nailed Timber Joints.* (with P. Moss) 1981
16. Goodsir, W.J. *The Response of Coupled Shear Walls and Frames.* (with T. Paulay) 1982
17. Lowe, P.J. *Non-linear Finite Element Analysis of Shell Structures.* (with P. Moss) 1982
18. Clendon, J.E. *Alternative Damping Models.* (with P. Moss) 1985
19. Smith, D.B.M. *The Response of Buildings with Coupled Shear Walls.* (with T. Paulay) 1985
20. Cooper, A.C. *Finite Element Analysis of Shell Structures Using Triangular Layered Elements.* (with P. Moss) 1986
21. Mallaly, K.W. *Gravity Dominated Reinforced Concrete Framed Buildings.* (with T. Paulay) 1986
22. Papakyriacou, M.A. *The Seismic Response of Coupled Shear walls.* (with T. Paulay) 1986
23. Tan, Fun Kwai. *Seismic Behaviour of Bridges on Isolating Bearings.* (with P. Moss) 1986
24. Turkington, D. *Seismic Design of Bridges on Lead-Rubber Bearings.* (with N. Cooke and P. Moss) 1987

25. Tjondro, J.A. *Analytical Investigation of P-Delta Effects in Medium Height Steel Moment Resisting Frames.* (with P. Moss) 1988
26. Wijanto, L.S. *Seismic Behaviour of Low-Rise Braced Steel Structures.* (with P. Moss) 1988
27. Chew, A.S. *Seismic Response of Timber Structures.* (with P. Moss) 1989
28. Djaja, R.G. *Finite Element Modelling of Fibrous Assemblies.* (with P. Moss and G. Carnaby (WRONZ)) 1989
29. Lee, Poh Chuan. *Seismic Response of Six Storey Braced Steel Frames.* (with P. Moss) 1989
30. Thomson, E.D. *P-Delta Effects in Ductile Reinforced Concrete Frames Under Seismic Loading.* (with P. Moss) 1991
31. Sinclair, K.M. *The Response of Multi-storey Frames to Seismic Pounding.* (with P. Moss) 1993
32. Stewart, N.L. *An Analytical Study of the Seismic Response of Reinforced Concrete Frame-Shear Wall Structures.* (with D. Bull) 1995
33. Cho, J.H. *Non-linear Geometric Effects in Framed Structures.* (with P. Moss) 1997
34. Rashidi, A.B. *The Behaviour of Imperfect Shear Walls Under Earthquake Loading.* (with P. Moss) 1997
35. Chambers, D.J. *A Distributed Spring Soil Model for Dynamic Soil-Structure Interaction Analysis.* 1998
36. Kao, Grace C. *Design and Shaking Table Tests of a Four Storey Miniature Structure Built With Replaceable Plastic Hinges.*(with J. Restrepo) 1998
37. Pradono, M.H. *Dynamic Amplification of Static Design Forces at Flexural Overstrength of Coupled Wall Structures.* (with P. Moss) 1998
38. Bishay-Girges, N.W. *Damping Models for Inelastic Structures.* (with P Moss) 1999
39. Dong, Ping. *Effects of Different Choice of Hysteresis Models on the Response of Framed Structures of Reinforced Concrete Subjected to Earthquake Excitation.* (with P. Moss) 1999
40. Chey, Min Ho. *Parametric Control of Structures Using a Tuned Mass Damper System Under Earthquake Excitation.* (with P. Moss) 2000
41. Hou, Ming. *Dynamic Behaviour of Bridges with Energy Absorbing Bearings.* (with P. Moss) 2000
42. Thompson, N.S. *Curved Reinforced Concrete Shells.* (with P. Moss) 2000
43. Beyer, K. *Re-examination of the Seismic Behaviour of Ductile Coupled Walls* (with T. Paulay and H.Bachmann) 2001
44. Chu, K.H. *Soil-Structure Interaction of Masonry In-filled Frames with Openings.* 2002
45. Robertson, K. *Probabilistic Seismic Design and assessment Methodologies for the New Generation of damage Resistant Structures.* (with J Mander) 2006
46. Hertanto, Eric. *Seismic Assessment of pre-1970s Reinforced Concrete Structures* (with S. Pampanin) 2006
47. Alistair Waller. *The Effect of Mass Irregularity on the Response of Drift and Acceleration for Isolated and Un-isolated Structures,* (with Bruce Deam) 2010

Doctor of Philosophy Students.

1. Sharpe, R.D. *The Seismic Response of Inelastic Structures.* 1974
2. Moore, T.A. *Finite Element Analysis of Box-Girder Bridges.* 1975
3. Wilby, G.K. *Response of Concrete Structures to Seismic Motion.*
(with R. Park) 1975
4. Taylor, R.G. *The Non-linear Seismic Response of Tall Shear Wall Structures.*
(with T. Paulay) 1977
5. van Luijk, C.J. *Structural Analysis of Wool Yarns.*
(with P. Moss and G. Carnaby(WRONZ)) 1981
6. Goodsir, W.J. *The Design of Coupled Frame-wall Structures for Seismic Actions.*
(with T. Paulay) 1985
7. Whittaker, D. *Seismic Performance of Offshore Concrete Gravity Platforms.*
(with R. Park) 1987
8. Andriono, T. *Seismic Resistant Design of Base Isolated Multi-storey Structures.*
1989
9. MacRae, G.A. *The Seismic Response of Steel Frames.*
(with W. Walpole) 1989
10. Zhao, X. *Seismic Soil Structure Interaction.*
(with P. Moss) 1990
11. Mori, A. *Investigation of the Behaviour of Seismic Isolation Systems for
Bridges.* (with P. Moss) 1993
12. Munro, W.A. *Finite Elements for Yarn Mechanics.*
(with P. Moss and G. Carnaby(WRONZ)) 1995
13. Widodo. *Rocking of Multi-storey Buildings.* 1995
14. Crisafulli, F.J. *Seismic Behaviour of Reinforced Concrete Structures with Masonry
Infills.* (with R. Park) 1997
15. Charng, P.S. *Base isolation for Multi-storey Building Structures.*
(with P. Moss) 1998
16. Rahman, A.M. *Seismic Pounding of Adjacent Multiple-Storey Buildings Considering
Soil-Structure Interaction and Through-Soil Coupling.*
(with P. Moss) 1998
17. Xi Lin. *Analysis and Design of Building Structures with Supplemental Lead
Dampers Under Earthquake and Wind Loads.*
(with P. Moss) 1999
18. Satyarno, I. *Adaptive Pushover Analysis for the Seismic Assessment of Older
Reinforced Concrete Buildings.* (with J. Restrepo) 2000
19. Zhang, J.J. *Seismic Soil-Structure Interaction in the Time-Domain.*
(with P. Moss) 2000
20. Liu, Aizhen. *Seismic Assessment and Retrofit of Pre-1970s Reinforced Concrete
Frame Structures.* (with R. Park) 2002
21. Bishay-Girges, Nagui. *Seismic Protection of Structures Using Passive Control Systems.*
(with P. Moss) 2004
22. Castillo-Barahona, Rolando. *Torsional Response of Ductile Structures.*
(with T. Paulay) 2004
23. Dong, Ping. *Effect of Different Choice of Hysteresis Models and Damage Models
on Seismic Damage Analysis for Reinforced Concrete Ductile Framed
Structures.* (with P Moss) 2003
24. Saunders, Dean. *Refined Pushover Analysis for the Assessment of Reinforced Concrete
Frames Inelastic Performance Under Seismic Attack and Investigation
into the Performance of the Structural Mechanisms of the Civil Office
Building, Christchurch.* (with J. Mander) 2005

25. Zaghlool, Baher. *Energy Modelling and Behaviour of Multi-storey Structures Under Concurrent Orthogonal Seismic Excitation.*
(with J. Mander) 2007
26. Chey, Min Ho. *Inelastic 3-Dimensional Analysis of Structures with Semi-active Non-linear Tuned Mass Dampers Under Earthquake Excitations.*
(with J. Mander and G.Chase) 2007
27. Wijanto, L. Sugeng. *Seismic Assessment and Performance of Historical Un-reinforced Masonry Buildings Built in Indonesia.*
(with J. Restrepo (UCSD)) 2008
28. Franco-Anaya, Roberto *Use of Semi-Active Devices to Control Deformation of Structures subjected to Seismic Excitation.*
(with J. Mander and G. Chase) 2008
29. Peng,Brian H.H. *Seismic Performance Assessment of Reinforced Concrete Buildings with Precast Concrete Floor Systems.*
(with R. Dhakal, R.Fenwich, D.Bull) 2009
30. Alejandro Amaris Mesa. *Developments of Advanced Solutions for Seismic Resisting Precast Concrete Frames.*
(with Stefano Pampanin, Des Bull and Alessandro Palermo) 2010
31. Kam Weng Yuen. *The development of selective retrofit strategy and techniques for reinforced concrete structures within a performance-based approach*
(with Stefano Pampanin and Des Bull) 2010
32. Iqbal. Asif *“Seismic Response and Design of Subassemblies for MultiStorey Prestressed Timber Buildings”*
(with Stefano Pampanin) 2011
33. Umat Akguzel *Seismic Assessment and Retrofit of Pre-1970s Reinforced Concrete Structures with Masonry Infill*
(with S. Pampanin and Constantin Christopoulos (University of Toronto)) 2011
34. Debra Gardiner *Development of design recommendations for the internal forces in concrete floor diaphragms*
(with Des Bull) 2012

BE(Hons) Research Project Students

1. Hills, Ian and Greenfield, Richard. *Structural Behaviour of Centreboard Yachts*. 1995
(with John Dean)
2. Williams, Alan. *Behaviour of Reinforced Concrete Beam-Column Joints and Their Effects of the Behaviour of Frames under Seismic Excitation*. 2005
(with Stefano Pampanin)
3. Gardiner, Debra. *The Forces in Floor Diaphragms under Earthquake Excitation*. 2006 (with Des. Bull)

Current Doctor of Philosophy Students.

1. K.Masoud.Moghaddasi *Performance-based seismic design and assessment of structures including SSI effects*
(with Misko Cubrinovski, Stefano Pamapanin and Goeffrey.Chase)
2. Greg Cole *Quantifying the effects of building pounding*
(with Rajesh Dhakal and Des Bull)
3. Patricio Quintana-Gallo *Performance-based retrofit and assessment of under-designed reinforced concrete frame buildings - a dynamic investigation*
(with S.Pampanin and P.Bonneli (University Santa Maria, Valparaiso Chile))
4. Arun Puthanpurayil. *Development of optimal performance-based passive building control strategies for earthquakes.*
(with Rajesh Dhakal and Greg Macrae)
5. Simona Giorgini *Non-linear Dynamic Soil-Foundation-Structure Interaction*
(with Misko Cubrinovski and Stefano Pampanin)